Nouvelle approche pour le Suivi et la Modélisation du comportement au Fluage et du Retrait de Pâtes de Ciment, Mortiers et Bétons depuis la Prise

Brice Delsaute

PhD Thesis

Université Libre de Bruxelles, BATir, Belgium
Université Paris-Est, Ifsttar, France

New approach for Monitoring and Modelling of the Creep and Shrinkage behaviour of Cement Pastes, Mortars and Concretes since Setting Time

Brice Delsaute

M. Farid Benboudjema	LMT, École Nationale Supérieure de Cachan, France	Rapporteur
M. Bernard Espion	BATir, Université Libre de Bruxelles, Belgium	Chair of the Jury
M. Robert Le Roy	Ecole Nationale des Ponts et Chaussées, Université Paris-Est, France	Examiner
M. Thierry J. Massart	BATir, Université Libre de Bruxelles, Belgium	Secretary of the Jury
M Bernhard Pichler	IMWS, TUWien, Austria	Rapporteur
Mrs Stéphanie Staquet	BATir, Université Libre de Bruxelles, Belgium	Thesis supervisor
M. Jean-Michel Torrenti	Ifsttar, Université Paris-Est, France	Thesis supervisor

Academic year 2016-2017

ACKNOWLEDGEMENT

First of all, I would like to thank my supervisor, Stéphanie Staquet, who gave me the opportunity to perform this research. She has been always available throughout the whole duration of this PhD thesis. She trusted me and gave me her support for the realization of the heavy and complex experimental works. Moreover, I had the opportunity to meet a lot of researchers from several laboratories thanks to her. Indeed, it is thanks to her if I could collaborate with several teams (Ifsttar, EC Nantes, UMinho) and started a joint PhD with Ifsttar.

On the Ifsttar side, I am also very grateful to my other supervisor, Jean-Michel Torrenti, who, despite a busy schedule, agreed to supervise this thesis. Even if we did not often have the opportunity to meet, he remained available as soon as necessary and this was reflected in each case by fruitful discussions and constructive suggestions. His advices and criticism have been a great stimulation.

I would like to thank the members of the jury for their interest in this work, namely Farid Benboudjema and Bernhard Pichler, who have done me the honour of reporting this thesis work and Robert Le Roy who has accepted to be a member of this jury.

I am also very grateful to Bernard Espion for the continuous feedback provided throughout this work, to have been the president of my thesis advancement committee and of my thesis jury. I would like to thank Thierry Massart for being part of my thesis advancement committee, for his interesting remarks and for agreeing to serve as secretary of my thesis jury.

In particular, I would like to show my gratitude to Claude Boulay with whom I was lucky to discuss specific points of this research since the earliest steps.

I would also like to warmly thank Florent Baby, Sandrine Ramanich and Jean-Claude Renaud for their valuable insights regarding the experimental work performed at Ifsttar.

This thesis would not have been possible without the continuous technical support and day to day management of the laboratory by Olivier Leclercq and Gilles Van Hooren at the laboratory of civil engineering.

I am also very appreciative for the experimental help of Master students Ruben Simonart, Anh Chi Nguyen, Cédric Buyssens, Peter Favreau, Manon Blazy, Coralie Van Luchene, Matthieu Wauters, Mohamed Saleh and Jérôme Couck.

I am definitely very thankful to colleagues Jérôme Carette, Cédric Dumoulin, Ameur Hamami for the countless discussions that we had about everything and nothing, for the punctual help with the heavy experimental work, and for contributing to the daily interest of working in a research environment. I'm also very grateful to my other BATir colleagues for the different moment shared at Pickwick.

I would like to thank my roommates and my friends who had to endure my daily stories of concrete!

Por último, quisiera expresar mi gratitud y sincero agradecimiento a Sonia Caso de los Cobos Perrotta por su paciencia ilimitada, comprensión, ánimo y amor durante los ultimos tres años y medio. Sin su apoyo continuo este trabajo no habría sido completado.

Acknowledgement

ABSTRACT

English - *For usual concrete structure built in several phases, concrete deformations are restrained during the hardening process. When shrinkage is restrained, tensile stresses are induced and a cracking risk occurs. Modelling the evolution of an early age set of parameters on concrete is necessary to predict the early age behaviour of concrete structures. The difficulty lies in the fact that the modelling of concrete properties must be based on experimental data at early age and this data must be obtained automatically because the hardening process of the concrete takes place rapidly during the first hours and also the first days. The thesis deals with experimental and numerical study of the early age properties of cement based materials and more specifically the development of the autogenous deformation, the coefficient of thermal expansion, the E-modulus and the basic creep in compression and tension. For this purpose, a comprehensive work was carried out at ULB and Ifsttar involving the development of a new approach with new test procedures and the design of new testing devices to generate experimental data since the setting of the material. The methodology is based on two repeated testing methods. For the characterization of the viscoelastic behaviour of a concrete since setting, a permanent loading coupled to a test with repeated minute-long loadings is needed. Whereas, the autogenous strain, the coefficient of thermal expansion and the setting are characterized with repeated thermal variations on a concrete sample. The new approach was defined on an ordinary concrete and then extended to the study of the following parameters: the water-cement ratio, the restrained effect of aggregate on the cement paste in the development of concrete properties at early age, the substitution of cement by mineral addition and the difference of behaviour in tension and in compression. Based on these experimental results, new models were developed for the characterization of the early age properties of cement based materials since setting time. An adapted version of the Model Code 2010 for modelling of basic creep is also proposed.*

Français - *Lors de la construction de structure réalisée en plusieurs phases de bétonnage, les déformations du béton sont entravées durant son durcissement. Quand le retrait est entravé, des contraintes de traction sont induites dans le matériau et un risque de fissuration est présent. Il est alors nécessaire de modéliser l'évolution des propriétés au jeune âge afin de prédire le comportement de la structure durant le jeune âge du béton. La difficulté réside dans le fait que la modélisation des propriétés du béton doit être basée sur des données expérimentales au jeune âge et que ces données doivent être obtenues automatiquement car le durcissement du béton se produit rapidement pendant les premières heures et les premiers jours. La thèse porte sur l'étude expérimentale et numérique des propriétés au jeune âge des matériaux à base de ciment et plus particulièrement sur le développement des déformations endogènes, le coefficient de dilatation thermique, le module d'élasticité et le fluage propre en compression et en traction. A cet effet, un travail complet a été réalisé à l'ULB et à l'Ifsttar impliquant le développement d'une nouvelle approche avec de nouvelles procédures d'essai et la conception de nouveaux dispositifs d'essai pour générer des données expérimentales depuis la prise du matériau. La méthodologie est basée sur deux méthodes d'essai répété. Pour la caractérisation du comportement viscoélastique d'un béton depuis sa prise, un essai de chargement permanent couplé à un essai avec des chargements répétés de plusieurs minutes est nécessaire. Les déformations endogènes, le coefficient de dilatation thermique et la prise sont caractérisés avec des variations thermiques répétées sur un échantillon de béton. Cette nouvelle approche a été définie sur un béton ordinaire et ensuite étendue sur l'étude de 4 paramètres pertinents : le rapport eau-ciment, l'effet de restriction de l'agrégat sur la pâte de ciment dans le développement des propriétés du béton au jeune âge, la substitution du ciment par des additions minérales et la différence de comportement en*

traction et en compression. Sur la base de ces résultats expérimentaux, de nouveaux modèles ont été développés pour la caractérisation des propriétés au jeune âge de matériaux cimentaires depuis le temps de prise. Une version adaptée de la modélisation du fluage propre dans le Code modèle 2010 est également proposée.

TABLE OF CONTENT

LIST OF SYMBOLS

A	[/]	Amplitude creep factor	$a_{E,\alpha}$	[/]	Kinetic parameter of the elastic modulus (model using α)
A_{GS}	[/]	Amplitude parameter of the amplitude creep factor (model using GS)	$a_{E,\xi}$	[/]	Kinetic parameter of the elastic modulus (model using ξ)
A_{sd}	[/]	Amplitude of the autogenous shrinkage deformation (model using t_{eq})	$a_{f,\alpha}$	[/]	Kinetic parameter of the compressive strength (model using α)
A_{sw}	[/]	Amplitude of the autogenous swelling deformation (model using t_{eq})	$a_{f,\xi}$	[/]	Kinetic parameter of the compressive strength (model using ξ)
$A_{t,1}$	[/]	Parameter of the amplitude creep factor (model using t_{eq})	B_{sd}	[/]	Amplitude of the autogenous shrinkage deformation (model using α)
$A_{t,2}$	[/]	Parameter of the amplitude creep factor (model using t_{eq})	B_{sw}	[/]	Amplitude of the autogenous swelling deformation (model using α)
A_{α}	[/]	Amplitude parameter of the amplitude creep factor (model using α)	C	[MPa^{-1}]	Specific creep function
A_{ξ}	[/]	Amplitude parameter of the amplitude creep factor (model using ξ)		[MPa]	Or amplitude creep parameter of the adapted Model Code 2010
$a_{A,\alpha}$	[/]	Kinetic parameter of the amplitude creep factor (model using α)	C_{IST}	[MPa^{-1}]	Specific initial short term creep function
$a_{A,\xi}$	[/]	Kinetic parameter of the amplitude creep factor (model using ξ)	C_{LT}	[MPa^{-1}]	Specific long term creep function
a_{sd}	[/]	Kinetic parameter of the autogenous shrinkage (model using α)	C_{ST}	[MPa^{-1}]	Specific solidification term creep function
a_{sw}	[/]	Kinetic parameter of the autogenous swelling (model using α)	c_{α}	[/]	Kinetic parameter of the CTE during the decrease of the CTE (model using α)

J	[MPa^{-1}]	Creep compliance	R	[J/mol/K]	Universal gas constant (= 8.314 J/mol/K)
K	[/]	Kinetic creep factor		[MPa]	Or specific relaxation function
$K_{t,1}$	[/]	Parameter of the kinetic creep factor (model using t_{eq})	r_1	[/]	Kinetic parameter of the CTE during the decrease of the CTE (model using t_{eq})
$K_{t,2}$	[/]	Parameter of the kinetic creep factor (model using t_{eq})	r_2	[/]	Kinetic parameter of the CTE during the increase of the CTE (model using t_{eq})
K_α	[/]	Parameter of the kinetic creep factor (model using α)	r_E	[/]	Kinetic parameter of the elastic modulus (model using t_{eq})
K_ξ	[/]	Parameter of the kinetic creep factor (model using ξ)	r_{sw}	[/]	Kinetic parameter of the autogenous swelling (model using t_{eq})
P	[/]	Parameter of the kinetic creep factor (model using α and ξ)	$r_{\nu,f}$	[/]	Kinetic parameter of the Poisson's ratio when the material is considered as a fluid (model using t_{eq})
p_E	[h]	Kinetic parameter of the elastic modulus (model using t_{eq})	$r_{\nu,s}$	[/]	Kinetic parameter of the Poisson's ratio when the material is considered as a solid (model using t_{eq})
p_f	[h]	Kinetic parameter of the compressive strength (model using t_{eq})	s_A	[/]	Kinetic parameter of the amplitude creep factor (model using GS)
p_{sd}	[h]	Kinetic parameter of the autogenous shrinkage (model using t_{eq})	s_E	[/]	Kinetic parameter of the elastic modulus (model using GS)
p_{sw}	[h]	Kinetic parameter of the autogenous swelling	T	[°C]	Temperature
p_α	[h]	Kinetic parameter of the CTE during the increase of the CTE	t_{eq}	[h]	Equivalent time
q	[J/g/h]	Heat released	t_i	[h]	Initial setting time
Q	[J/g]	Cumulated heat released	t_f	[h]	Final setting time
Q_∞	[J/g]	Cumulated heat released at an infinite time	V_P	[m/s]	P-wave velocity

V_S	[m/s]	S-wave velocity	$\nu_{t,f}$	[/]	Poisson's ratio when the material is considered as fluid (model using t_{eq})
α	[/]	Advancement degree of reaction	$\nu_{t,s}$	[/]	Poisson's ratio when the material is considered as fully hydrated (model using t_{eq})
α_0	[/]	Advancement degree of reaction at final setting	ν_α	[/]	Poisson's ratio when the advancement degree of reaction is equal to 1
α_c	[°C^{-1}]	Coefficient of Thermal Expansion (CTE)	ν_ξ	[/]	Poisson's ratio when the hydration degree is equal to 1
α_{t1}	[°C^{-1}]	Amplitude parameter of the CTE related to the decrease of the CTE (model using t_{eq})	ξ	[/]	Hydration degree
α_{t2}	[°C^{-1}]	Amplitude parameter of the CTE related to the decrease of the CTE (model using t_{eq})	ξ_0	[/]	Hydration degree at final setting
$\alpha_{\alpha1}$	[°C^{-1}]	Amplitude parameter of the CTE related to the increase of the CTE (model using α)	ξ_∞	[/]	Final hydration degree
$\alpha_{\alpha2}$	[°C^{-1}]	Amplitude parameter of the CTE related to the decrease of the CTE (model using α)	ρ	[kg/m^3]	Density
β	[/]	Kinetic parameter of the autogenous swelling (model using α)	σ	[MPa]	Stress
γ	[/]	Kinetic parameter of the autogenous swelling (model using α)	τ	[h]	Aging factor of the adapted Model Code 2010
ε_{au}	[/]	Autogenous strain	φ_c	[/]	Creep coefficient
ε_{cr}	[/]	Creep strain	φ_{IST}	[/]	Initial short term creep coefficient
ε_{el}	[/]	Elastic strain	φ_{LT}	[/]	Long term creep coefficient
ε_{th}	[/]	Thermal strain	φ_{ST}	[/]	Solidification term coefficient
ε_{tot}	[/]	Total strain	Ψ_r	[/]	Relaxation coefficient
ν	[/]	Poisson's ratio			
ν_{dyn}	[/]	Dynamic Poisson's ratio			

CHAPTER 1:
GENERAL INTRODUCTION

SECTION 1.1 – BACKGROUND

Concrete, general description

Through the several materials used in the construction sector, concrete has a major importance. Its worldwide consumption represents around 6 billion of m³/year. According to the country, the consumption of concrete is 5 to 10 times higher than steel and 10 to 30 times higher than cardboard and plastic. The average annual consumption of cement in Belgium is 574 kg/year/person and in France is 297 kg/year/person in 2014 [1]. It makes concrete the second most used material in the world after water. The use of concrete is not new and goes back to the Ancient Rome. However the concrete as it stands today has significantly evolved due to the composition of its binder. Currently, classical concretes are composed by sand, aggregate, water and Portland cement. During the 19th and 20th century its use increased strongly thanks to the many advantages of concrete in comparison with other structural materials such as wood, brick and steel. Among these advantages there are the possibility to realize structures with complex shapes, a high compressive strength, a non-combustible material which makes it fire-proof, a low maintenance requirement and a generally good behaviour under severe environment. Therefore concrete is an economical solution. However concrete has two main drawbacks in comparison to other building materials. From a mechanical point of view, concrete has a low ductility, a low strength-to-weight ratio and a low tensile strength which makes it susceptible to cracking. From an environmental point of view, the cement production has a significant carbon footprint with its contribution to the CO_2 emission. It is estimated that between 4 and 7% of the CO_2 emission comes from the production of cement. In addition, the aggregates, which constitute the inert skeleton of concrete, are unequally shared and are hardly inexhaustible resources.

Environmental issues

During the last decades, a lot of research has been performed in order to reduce the environment impact of the concrete industry. Several parameters were optimized such as the efficiency of the cement production chain, optimizing the compressive strength, recycling concrete obtained from concrete structure demolition and the substitution of cement with by-product of various industries. Recent studies have shown that the use of recycled element from concrete structure has a double advantage. The volume of waste coming from the demolition increases and will become critical in the near future. Therefore, a partial use of such element in concrete structure is a relevant solution. Moreover, when exposed to the ambient air, the recycled aggregates entrap the CO_2 in the air by carbonation and this carbonation improves the microstructural and mechanical properties of the concrete. However more works are still needed to extend industrially the substitution of natural aggregate by recycled aggregate in high quantity. Presently, the substitution of Portland cement is limited to a certain percentage which varies according to the country. One of the primary causes of this limitation is the lack of knowledge on the effect of high substitution of cement by mineral additions (blast furnace slag, fly ash, limestone filler…) in the behaviour of concrete. Nevertheless, to reduce the carbon footprint of cement based materials, such substitution is inevitable and will occur in a close future in order to respect several objectives as the European directive 2008/98/CE. For long term objectives, a complete substitution of Portland cement by material with very low environmental impact must be realized. Recent works have shown interesting perspective in this frame with the use of geopolymer and sulfoaluminate clinker which allow substituting completely the Portland cement. But more works are still needed for a correct understanding of this new material and their effect on the performance of cement based materials.

Mechanical issues

New advances were also performed in order to decrease the cracking risk of cement based materials or to improve its control. A first solution is the incorporation of fibres which can increase the ductility of concrete. This increase allows improving the distribution of cracking on the concrete structure. So, not one wide crack occurs, but several very small cracks are formed which has for advantage to avoid contact between steel reinforcement and air, and thus to protect steel from corrosion. Several types (metallic, organic, ceramic…), dimensions and geometries of fibre exist and lead to a different behaviour of the concrete. A second solution consists to heal the crack by using self-healing concrete. The main idea of this method is to plug and grout the crack with the activation of elements when they are in contact with the environment. Several self-healing methods were developed and use new materials (superabsorbent polymers, calcium carbonate precipitating micro-organisms, encapsulated polymers, alkali-activators…). These technologies are not yet fully mastered and are thus under development.

Actual standards are based on classical concrete and are not yet able to consider the effect of these new materials on the properties of cement based materials. Therefore new recommendations and standards are needed for the design of concrete structures using these new materials.

An aging material

Building materials are generally used when their properties do not evolve anymore with the time (when no external activity occurs). Concrete has the particularity to be a complex material for which its properties continuously change. It evolves from a nearly liquid state to a viscoplastic material within a few hours, followed by the setting of the concrete. Then the mechanical properties start to develop and the material exhibits a viscoelastic behaviour. During the first days after mixing, the evolution of the concrete properties is very intense. This period is called the early age. Finally, the concrete properties continue to evolve on a period counted in years.

Concrete has also another important specificity coming from its time-dependent properties. The structural behaviour is strongly dependent of these properties such as shrinkage, creep and its associated stress relaxation. On one side, their effects are unfavourable when the time-dependent deformations cause a loss in pre-stress, excessive deformations of the structure (e.g. deflections) or stressing of non-load bearing members which may affect the service-life of a concrete structure. On the other side, they can be beneficial in terms of reduction of eigenstresses (e.g. due to shrinkage) or reduction of stresses due to a restraint of the displacement of the structure, particularly for early age concrete.

Restrained shrinkage

For general concrete structures built in several phases, the evolution of the restrained strains is similar and is composed of two periods: a heating period followed by a cooling one (Figure 1a). The heating period begins just after the final setting when the mechanical properties of concrete start to develop. During and after the setting, the heat flow of the cement is very intense which leads to an increase of the temperature inside the concrete element and as a result to an increase of the thermal strain. In the meantime, autogenous strain starts to develop. No systematic tendency can be given for the autogenous strain, because during the heating period, autogenous deformation results in swelling or shrinkage according to the mixtures proportions and content [2]. However thermal strains are generally higher than autogenous strain (especially for massive structures) and thus a general swelling of the concrete occurs during the heating period. The cooling period starts when the heat flow of the

cement decreases strongly or when the formwork is removed (according to the massivity). During this period, both autogenous and thermal strains decrease. As a result of the restriction of the strains of concrete, stresses are induced (Figure 1b). During the heating period, concrete element is in compression and inversely during the cooling period the concrete is submitted to tension.

The impact of creep properties at very early age in case of restrained deformation is highlighted on Figure 1b (red curve, viscoelastic stress). In a general view, no consideration of creep/relaxation leads to a global overestimate of the stress. Thus creep/relaxation seems to play a general positive role for the design of concrete structures at early age. However, at very early age, the creep/relaxation amplitude is very significant and reduces strongly the compressive stresses. Then, during the cooling period, stresses switch rapidly in tension. During this period, an underestimation of the creep/relaxation phenomenon leads to an underestimation of the tensile stresses which can cause cracking in the concrete structure. Hence it is important to model correctly the basic creep since final setting time.

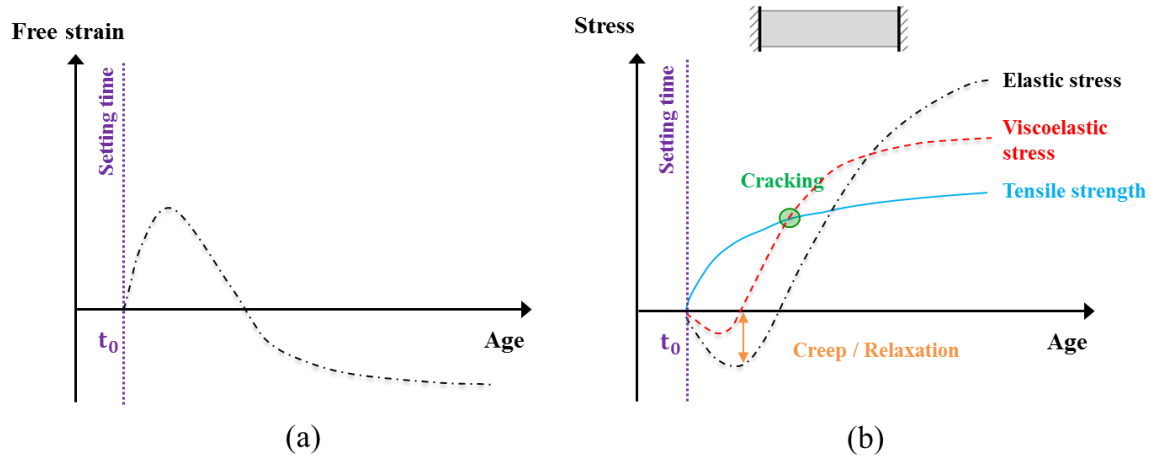

Figure 1 - (a) Free strain inside concrete element. (b) Stress induced by restriction of the concrete displacement.

For thin concrete structure, the development of the free strain differs. The amplitude of the swelling is largely lower and the stresses change faster in tension. In that case, the creep/relaxation phenomenon plays an important positive role by decreasing the tensile stresses which reduces the cracking risk or the magnitude of the opening of the cracking.

The calculation of stresses depend also on many parameters such as the boundary conditions of the concrete elements, the interface between steel reinforcement and concrete, energy release due to cracking, coupling between creep and damage, the self-healing (especially at early age).

Multiscale problem

Restrained shrinkage occurs at different scales (Figure 2). From a structural view, the displacement of concrete element can be restrained by the different boundary conditions of the structure (Figure 2d). When looking in the concrete element, the concrete surrounding the reinforcement is also restrained due to the bonding between both (Figure 2c). As mentioned in the first paragraph, concrete is generally composed of aggregate, sand, cement and water which makes it a heterogeneous material. Each phase has a specific behaviour. Therefore, restrained shrinkage occurs in the concrete itself. At

this interface between mortar and aggregate, the displacement of the mortar is restrained by the aggregate (Figure 2b). The same kind of restriction takes place at the interface between the cement paste and the sand (Figure 2a). This analysis can be extended to the cement paste.

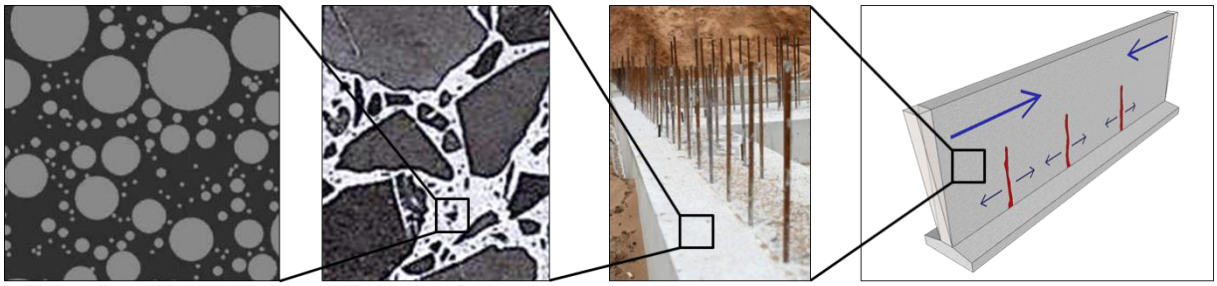

(a) (b) (c) (d)

Figure 2 – Restrained shrinkage at different scales. Left to right: the cement paste around the sand has its displacement restrained – the displacement of mortar is restrained around the aggregate – the displacement of the concrete is restrained around the reinforcement bar – the concrete element is restrained by other concrete elements and or boundary conditions.

Testing concrete since setting

Nowadays, the construction phases of modern concrete structures become more and more complex. Consequently, for the design of concrete structures it is important to have in depth knowledge of the early age behaviour of concrete, which will influence all the service life of the concrete structures. Even though the mechanical behaviour of hardened concrete can usually be correctly predicted; it is not always the case for the early age behaviour of concrete, when the mechanical properties change rapidly in function of the advancement of the hydration reaction. However, several multiscale models are able to estimate the evolution of concrete properties such as the elastic modulus [3] or the basic creep [4]. Monitoring the evolution of early age properties of concrete is necessary to provide input data to the models of prediction of the behaviour of concrete structures since setting time. The experimental challenge lies in the fact that this monitoring must be fully automatic since the earliest age because the hardening process of the concrete takes place continuously over a period counted in hours and even in days after the casting time.

Among all the usual parameters (strength values, E-modulus…) needed for the design of the concrete structures, creep and relaxation in tension and in compression should also be taken into account. For example, in the design of a concrete dam, Slowik, *et al*. [5] showed that at early age, the relaxation phenomenon is responsible for a decrease of 70% of the thermally induced stresses in the structure. Different investigations were carried out for a good understanding of the physical mechanisms of basic and drying creep. Currently, there is no consensus on all these physical mechanisms which occur in a hardened concrete and even less in a hardening concrete. More investigations have to be carried out to predict with more accuracy the behaviour of concretes at early age.

Modelling concrete

Several models were developed in the past for the characterization of the evolution of the properties of concrete. These models are based on a large data base of experimental results. A large part of these results are related to concrete in a hardened state. During the hardening process, models are not yet able to predict correctly the evolution of properties such as the E-modulus, the Poisson's ratio, the

coefficient of thermal expansion, the autogenous deformation and creep properties. Models were more developed on the basis of fitting than in an understanding of the physical mechanisms which govern the evolution of these properties. It is therefore questionable if such models are able to consider correctly the evolution of properties of new concrete coming onto the market particularly at early age. A more physical approach is needed for the creation of new standards and recommendations.

In addition, the evolution of several concrete properties is strongly dependent on many parameters. Among all parameters, the composition of the concrete (e.g. nature of the binder, water-cement ratio, aggregate content…), the boundary conditions of the structure (e.g. the external environment in contact with concrete, the restriction of the displacement) and the size of the concrete elements (hydration temperature) play an important role in the development of the early age properties of cement based materials. This makes concrete a very complex and challenging material to test and model.

SECTION 1.2 – OBJECTIVES AND SCOPE OF THE THESIS

The aim of this thesis is to extend the present knowledge about the development of the early age properties of cement based materials. It is intended that this knowledge should contribute to better characterization of the development of the early age properties of cement based materials. The thesis is focused on the development of the following properties: the setting, the autogenous deformation, the coefficient of thermal expansion, the elastic modulus and the basic creep. This work is composed of an experimental and a numerical work.

The experimental work is meant to identify and quantify how the properties of cement based materials in sealed conditions since very early age evolve. As the early age properties evolution occurs very fast, the characterization of these properties must be automatic. For that purpose, new testing methods aim at monitoring the early age properties of cement based materials are needed. Since experimental testing of several properties such as creep at early ages is very complicated and time consuming, the necessary number of tests to find parameters related to the model has to be limited. The first part of the experimental work focuses on the development of new testing methods. For the understanding of the physical mechanisms which occur during the hydration process, several parameters should be tested. In that frame, the following parameters are studied: the water-cement ratio, the nature of the binder (with eco-concrete for which 75% of the cement is substituted by slag and limestone filler) and the scale effect.

Models for the prediction of stress development due to restrained deformation of cement based materials suffer from serious lack of experimental data about the development of the early age properties. The modelling part aims to reproduce experimental results with models based on physical mechanisms that were observed on the experimental work. Comparison with actual standards is carried out and improvement of these standards is proposed.

The ultimate goal and perspective of this thesis is to integrate these new models in a finite element code allowing the use of the models for the study of concrete structures.

SECTION 1.3 – ORGANIZATION OF THE THESIS

The thesis is organized in 10 chapters. A literature review of existing knowledge about the development of the early age properties of cement based materials is given in chapter 2.

Chapter 3 presents the different compositions studied in the experimental work as well as their related mixing procedure and basic mechanical properties. In addition, existing measuring devices and existing testing procedure and the experimental program are described.

The description of the new developed experimental equipment (tensile creep rig) and the new adaptation carried out on experimental equipment (compressive creep rig, autoshrink, hydrostatic weighing and TSTM) are shown in chapter 4. Moreover the development of a new experimental strategy for the monitoring and the modelling of cement based materials is shown. All results presented in Chapter 4 are obtained on an ordinary concrete.

The chapter 5 presents a new methodology for the monitoring of the setting of cement paste. This methodology is based on the combined monitoring of ultrasonic pulse transmission of P- and S-wave.

The effect of the water-cement ratio on concrete is studied in chapter 6. This chapter is separated in 2 parts. The first part is related to the monitoring and the modelling of the autogenous strain and the coefficient of thermal expansion. The second part is related to the study of the development of the mechanical properties with a focus on the development of the short and long term creep.

The chapter 7 is an extension of the chapter 6. It presents a multiscale study (on cement paste, mortar and concrete) on the development of the autogenous strain, the coefficient of thermal expansion and the short term viscoelastic properties.

The effect of the substitution of cement by slag and limestone filler is studied in chapter 8. Tests of short and long duration creep are presented. An extension of the model developed in chapter 4 is shown. Results and modelling of a very high performance self-compacting concrete is also shown.

The chapter 9 presents a comparison between tensile and compressive creep on several compositions. For this comparison, the effect of the stress level is studied on compressive creep.

Finally, the main conclusions of the thesis are presented in Chapter 10.

REFERENCES

[1] Infociments, INFOCIMENTS 2016 L'essentiel, 2015. http://www.infociments.fr/publications/industrie-cimentiere/statistiques/st-g08-2015.

[2] A. Bentur, Terminology and definitions, in: A. Bentur (Ed.), Early Age Crack. Cem. Syst. - Rep. RILEM Tech. Comm. 181-EAS - Early Age Shrinkage Induc. Stress. Crack. Cem. Syst., RILEM Publications SARL, 2003: pp. 13–15. doi:10.1617/2912143632.002.

[3] O. Bernard, F.-J. Ulm, E. Lemarchand, A multiscale micromechanics-hydration model for the early-age elastic properties of cement-based materials, Cem. Concr. Res. 33 (2003) 1293–1309. doi:10.1016/S0008-8846(03)00039-5.

[4] T. Honorio, B. Bary, F. Benboudjema, Multiscale estimation of ageing viscoelastic properties of cement-based materials: A combined analytical and numerical approach to estimate the behaviour at early age, Cem. Concr. Res. 85 (2016) 137–155. doi:10.1016/j.cemconres.2016.03.010.

[5] V. Slowik, Schmidt D., Nietner L., Effect of stress relaxation on thermal stresses, in: Concreep 7, 2005: pp. 411–416.

CHAPTER 2:
PROPERTIES OF EARLY AGE CONCRETE

Concrete has the particularity to be a complex material for which its properties continuously change. It evolves from a nearly liquid state to a viscoplastic material within a few hours, followed by the setting of the concrete. Then the mechanical properties start to develop and the material exhibits a viscoelastic behaviour. During the first days after mixing, the evolution of the concrete properties is very intense. This period is called the early age. Finally, the concrete properties continue to evolve on a period counted in years.

During the hardening of cement based materials, volume changes occur due to the hydration of cement. If the displacement of the concrete is restrained, stresses are induced in the concrete. When this displacement corresponds to a contraction of the material, concrete is in tension and per consequent a cracking risk exists. There is a need for an understanding of the mechanisms involved and the factors influencing the risk of cracking and particularly for concrete with a low water-cement ratio. Among all the properties evolving at early age, the autogenous strains, the coefficient of thermal expansion (CTE), the elastic modulus and the creep play a major role in the calculation of stresses in case of restrained shrinkage.

The purpose of this chapter is to give a short review of the existing knowledge about the evolution of the properties of cement based materials during the early age of the material.

SECTION 2.1 – HARDENING PROCESS

The life-cycle of concrete can be separated in three states:

- The fresh state
- The hardening state
- The hardened state

It is generally accepted that, just after the casting of a concrete, a first period exists during which the material can be transported and cast into a mould where it can be vibrated and where it can flow to fill the mould (period of workability). This period corresponds to the fresh state of the material. Just after casting, the aggregates can move slowly under the effect of the gravity and, eventually, a bleeding can appear. Cracking is then possible under the effects of these movements, especially when reinforcement bars are present. A second period, or period of the setting, commonly defined after the results of penetration tests on cement pastes or mortars, corresponds to a progressive coalescence of a continuous path of hydrates. At the beginning of this period, the concrete stiffness is almost inexistent while, at the end of this period (t_0), the concrete starts to stiffen [1]. In a third period, after t_0, stiffness, thermal and autogenous deformations evolve rapidly so that risks of cracking become critical, especially when deformations are restrained. It is then considered that the material behaves like a solid. Therefore the hardening state of the material starts at the setting. For the sake of predictions of structural behaviour, measurements of these parameters at early age are of a great interest [2,3]. However one question remains on how to determine t_0?

A first attempt for the determination of t_0 was based on the monitoring of the strain rate of the autogenous shrinkage on concrete. It has been shown [4] that this parameter is not as reliable as it is in tests performed on cement pastes. Penetration tests provide reliable information about setting of cement pastes and mortars. For example, [5] proposed relations between the results of such tests and mechanical properties like yielding stress and thus shear modulus and ultrasonic measurements. But, as penetration tests are not well suitable for concrete, other methods have to be found. A steel bar wrenching device could be used according to the Belgian standard NBN B15-204 [6] but it does not give a stiffness evolution. A new promising technique, using natural vibrations, has been described recently [7]. It consists to monitor the first flexural frequency of a concrete beam cast inside an acrylic tube submitted to ambient vibrations.

Ultrasonic measurements seem to be good candidates for the determination of t_0 and elastic properties. Ultrasonic testing is used since a long time and recent applications, using P- or S-waves (primary and secondary waves respectively moving in compressional or in shear motion), aimed at the detection of the setting, at high or low frequencies, can be found in the literature [8–14]. Initial and final setting times have been discussed in previous works [8], [15] and it seems that the former is unambiguous while the later is more controversial as there is no clear event in the recordings indicating that a threshold has been crossed. Another ambiguity comes from the fact that the ultrasonic pulse velocity (UPV) of P-waves, measured in fresh concrete, is almost equal to the velocity in the air even if, for hardened concrete, results are more expectable. This phenomenon has been attributed to the entrapped air [14]. De-aeration of concrete is not really feasible in field applications even if, special mixers exist for such a purpose. However, the flexibility of ultrasound measurements is undeniable. Recently, Carette, *et al.* [16,17] have developed new criteria for the determination of the initial and final setting. These new criteria are based on the monitoring of the p- and s-waves. The initial setting corresponds to the time when the maximum of the derivative of the s-wave velocity is reached. The final setting is obtained with the maximum of the derivative of the dynamic E-modulus. Whereas Kruger, *et al.* [18]

use threshold values of the dynamic shear and elastic modulus for the characterization of the initial and final setting. However the physical meaning of such criteria is questionable. It is necessary to raise the question of why the maximum of the rate evolution of one particular parameter should correspond at the initial or final setting time of a cement based material. It is true that such events occur in a small time window but no direct physical link connects them. The use of threshold value suggests that each cement based material reaches a same stiffness or more generally a same material property at setting. However the initial and final setting time are highly dependent on the quantity of the solid phase [19,20] and thus to the aggregate content and nature. It is therefore expected that threshold criterion is only valid for concrete composition with small changes in the solid phase (limited variation in the nature of the binder, small variation in the water/cement ratio…) or the threshold value should depend on the material parameters.

SECTION 2.2 – EARLY AGE VOLUME CHANGES

2.2.1. General scheme

When concrete is not subjected to a restraint of its displacement or a loading, only free deformations occur. At early age, the free deformations are mainly related to the hydration of the cement, the size of the concrete element and the environment in contact with the concrete. However, in practice, the movements of a concrete structure are generally always partially or fully restrained, and per consequent stresses are induced. For the stresses calculation at early age, it is needed to divide correctly the total strain ε_{tot} according to their associated physical mechanisms.

At early age, the free deformations are divided in three categories:

- The thermal deformations ε_{th}
- The hydration deformations,
- The drying deformation.

The development of the thermal deformations is due to the heat release occurring during the hydration of the cement paste and to the evolution of the temperature around the concrete element. The thermal deformations are computed with the consideration of the coefficient of thermal expansion and the thermal variations inside the concrete. The thermal variations inside the concrete are defined with the consideration of the thermal conductivity of the concrete and other elements inside the concrete element (e.g. reinforcement), the heat release of the cement paste and the thermal variation around the concrete element. The distribution of the thermal deformations is non-uniform because of the thermal gradients inside the concrete element.

The hydration deformations are divided in two parts: the chemical shrinkage and the autogenous deformations. The chemical shrinkage occurs before setting and the autogenous strains take place after setting. Both deformations are related to the hydration process and do not consider any drying or thermal effect. For that reason, tests used for their characterization are performed in sealed condition and under a constant temperature (generally 20°C).

The development of the drying deformations is due to the exchange of water between the concrete and the environment. Generally the relative humidity of the environment is lower than the one of concrete. Therefore, when exposed to the ambient air, water in concrete is lost by evaporation and a contraction of the concrete occurs. The distribution of the drying deformations is non-uniform because the drying phenomenon takes places mainly in the surface of the concrete element and particularly at early age. For massive structure, some standards [21] accept to neglect the effect of drying. As the hydration deformation, drying deformations are divided in two parts. The plastic shrinkage occurs before setting and the drying shrinkage take places after setting.

When a load is applied, the viscoelastic behaviour of the concrete is considered for the determination of the mechanical deformations and the stresses. The mechanical deformations are divided in three categories:

- The elastic deformation defined with the elastic modulus of the concrete;
- The basic creep deformation defined with the basic creep compliance;
- The drying creep deformation defined with the drying creep compliance.

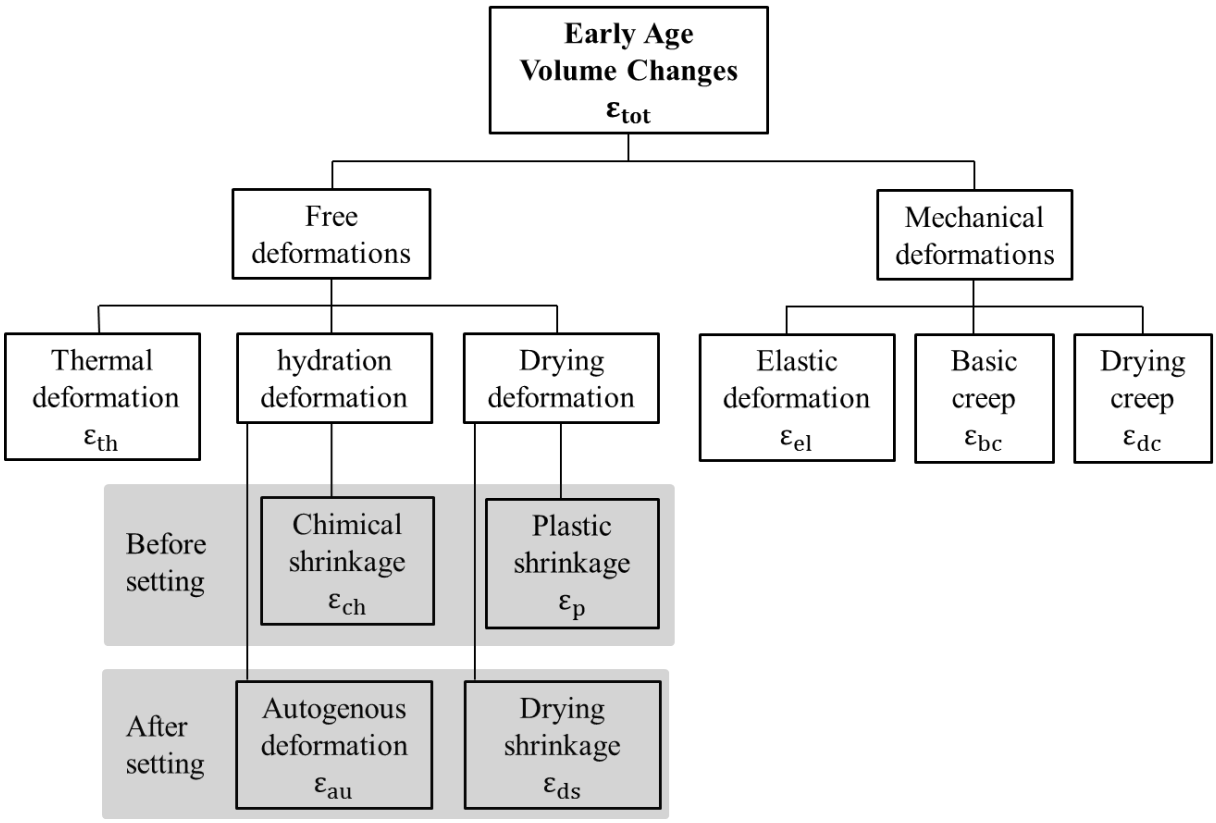

Figure 1 - General scheme of the early age volume change.

The general scheme of the volume changes in a cement based material is presented in Figure 1. This thesis is limited to the study of concrete under sealed condition and, per consequent, the drying phenomenon will not be studied. In addition, the deformations occurring before setting are not studied also and concrete is considered as a viscoelastic material. Results presented in this work focus on the thermal, autogenous, elastic and basic creep deformations. By using the superposition principle, it is therefore assumed that the total strain ε_{tot} of a loaded concrete sample is a sum of the elastic strain ε_{el}, the creep strain ε_{cr}, the autogenous strain ε_{au} and the thermal strain ε_{th} as expressed in Equation 1. For a constant uniaxial stress σ, the uniaxial mechanical strain can be defined as in Equation 1 and 2 where t is the age of the concrete, t' the age of the concrete at loading, J(t,t') is the compliance function, E(t') is the elastic modulus and C(t,t') is the specific creep. In Equation 2, the behaviour of concrete is considered as linear (independent of the stress level) and viscoelastic.

$$\varepsilon_{tot} = \varepsilon_{el} + \varepsilon_{cr} + \varepsilon_{au} + \varepsilon_{th} \quad (1)$$

$$\varepsilon_{el}(t') + \varepsilon_{cr}(t,t') = \sigma.J(t,t') = \sigma.\left(\frac{1}{E(t')} + C(t,t')\right) \quad (2)$$

2.2.2. Maturity

For consideration of the aging and the main temperature effect, concrete properties are expressed in function of the equivalent time t_{eq}, the advancement degree of reaction α or the hydration degree ξ.

► EQUIVALENT TIME

Equation 3 defines the equivalent time which is based on the Arrhenius equation and which is function of the age of the material t, the evolution of the temperature T (°C), a reference temperature T_r (generally 20°C), the universal gas constant R (=8.314 J/mol/K) and the apparent activation energy E_a expressed in J/mol.

$$t_{eq}(t,T) = \int_0^t \exp\left(\frac{E_a}{R}.\left(\frac{1}{273+T(s)} - \frac{1}{273+T_r}\right)\right).ds \quad 3$$

► ADVANCEMENT DEGREE OF REACTION

The advancement degree of reaction is defined according to Equation 4 where Q is the cumulated heat released and Q_∞ is the cumulated heat release for an infinite time. In the frame of this thesis, the heat released is measured with an isothermal calorimeter.

$$\alpha = \frac{Q(t)}{Q_\infty} \quad 4$$

► DEGREE OF HYDRATION

The degree of hydration corresponds to the fraction of the cement that has reacted. A complete hydration of all the cement gives a degree of hydration equal to 1. If the cement is fully hydrated, the degree of hydration is equal to the advancement degree of reaction. Generally, only a part of the cement reacts. In that case, the hydration degree corresponds to the advancement degree of reaction multiplied by the final hydration degree ξ_∞. Waller [22] proposed a relation between ξ_∞ and the effective water-cement ratio W_{eff}/C (Equation 5) where W_{eff} is the effective water content (water content without any allowance for the water demand of the aggregate) and C is the cement content. However this equation is limited to Portland cement.

$$\xi_\infty = 1 - \exp(-3.3.W_{eff}/C) \quad 5$$

2.2.3. Free deformations

The development of the autogenous deformation and the coefficient of thermal expansion is mainly related to the hardening and the internal variation of relative humidity in the microstructure of the cement paste.

► AUTOGENOUS DEFORMATION

The autogenous deformation occurs under isothermal conditions and without water exchange with the external environment. The autogenous deformations are the results of the combination of three phenomena:

- The chemical shrinkage (also called “Le Chatelier” contraction)
- The self-desiccation
- The swelling

The first volume change is the chemical shrinkage which is related to the reduction in volume between the hydration products (CSH, portlandite…) and the anhydrous grains and water combined. The chemical shrinkage starts when cement particles are in contact with water. When the material sets, an increase of the mechanical properties occurs. As the stiffness of the skeleton of the cement paste increases, a restriction of the chemical shrinkage takes places [23]. Then, chemical shrinkage is

not transformed in volumetric deformation due to the formation of a gaseous volume phase in the pore (because to the water consumption by the hydration reaction). At this stage, a progressive desaturation of the capillarity pores and per consequent a decrease of the internal relative humidity takes place in the cement paste. A capillarity pressure appears due to the superficial tension at the gas-liquid interphase. This leads to a global contraction of the cement paste and is called the self-desiccation. According to its composition, concrete can present an early age swelling. Several studies aimed at understanding the origin of the swelling were carried out in the past. However, there is still no general consensus on the mechanisms related to the swelling. A first mechanism is linked to the water absorption of cement paste which cancels the self-desiccation phenomena [24]. The excess of water can either come from bleeding or from the aggregate. However this parameter alone cannot explain swelling but can only explain a decrease of the amplitude of the self-desiccation phenomenon during the very early age. In [25], an opposite observation is carried out. For identical water content, concrete with initially dry aggregates shows swelling whereas no such behaviour is observed with initially saturated aggregates. Swelling is also linked to the formation and growth of portlandite crystals [26,27] and ettringite [28]. The formation of both elements will lead to a crystallization stress. These stresses depend on many factors such as the size of the elements and their growth direction [29,30], porosity (size distribution and quantity), the E-modulus and the creep of the cement paste [31]. Another source of swelling comes from measurement artifacts. The removal of the thermal deformation needs an accurate knowledge of the evolution of the coefficient of thermal expansion during the whole hydration process which is generally not the case [24]. Secondly, round-robin testing [24] have shown quite important dispersion between results from different laboratory and different test rigs [24]. This can be due to differences between volumetric and linear measurements, between vertical and horizontal measurements, or between rigid and flexible mould measurements [32,33]. Therefore the main influencing parameters of the autogenous deformations are the nature of the binder (chemical composition and morphology [34,35], the fineness of cement [36] and the adding of mineral addition [37,38]), the water-cement ratio [39,40], the aggregate nature and their content [41–43] and the temperature [44,45].

► THERMAL DEFORMATION

Thermal deformation of cement based materials is defined according to Equation 6 where α_c is the coefficient of thermal expansion (CTE) [µm/m/°C], T is the temperature [°C] and ε_{th} is expressed in [µm/m]. Several authors [46–51] assume constant value of CTE over time and thus Equation 6 becomes Equation 7.

$$\varepsilon_{th}(t) = \int_0^t \alpha_c(\tau).\dot{T}(\tau).d\tau \quad (6)$$

$$\varepsilon_{th}(T, T_0) = \int_{T_0}^{T} \alpha_c.dT \quad (7)$$

The thermal variations are also function of several material properties (thermal conductivity, heat capacity, heat release) and the exchange of heat with the environment. These properties were not studied during this thesis and thus are not discussed.

COEFFICIENT OF THERMAL EXPANSION

The coefficient of thermal expansion depends mainly of the relative humidity in the cement paste and of the nature of the aggregate [52–54]. During the hardening process, 3 stages occur [55,56]. First the value of the CTE is very high due to the contribution of water when the cement paste is still in a plastic phase. When the cement paste sets, a sudden decrease of the CTE is observed till a value

corresponding to the CTE of the solid skeleton. Then a small increase of the CTE is observed and is due to the decrease of the relative humidity in the cement paste. Therefore the CTE has a minimum value around the setting time. For low water-cement ratio, a factor 2 can be observed between this minimum and the value of the CTE obtained after several weeks [55].

2.2.4. Mechanical deformation

The modelling of the viscoelastic properties is based on the decomposition of the total strain ε_{tot} of a loaded concrete sample in a sum of the elastic strain ε_{el}, the creep strain ε_{cr}, the autogenous strain ε_{au} and the thermal strain ε_{th} as expressed in Equation 1. Here drying effect is not considered. For a constant uniaxial stress σ, the uniaxial mechanical strain can be defined as in Equation 2. Generally authors use the creep deformation, the creep compliance, the specific creep or the creep coefficient $\varphi(t,t')$ to model creep. The link between these three last parameters is given in Equation 8.

$$J(t,t') = \frac{1}{E(t')} + C(t,t') = \frac{1+\varphi(t,t')}{E(t')} \qquad 8$$

► ELASTIC MODULUS

How evolves concrete E-modulus since casting and along hydration process is very important for the prediction of stress development in hardening concrete at early ages. The volumetric change due to thermal and autogenous shrinkage phenomena is generally responsible of the stress development at very early age. For this purpose, different devices and technics were developed for the study of the elastic modulus at early age. These techniques can be divided in two parts: dynamic and static. Section 5 of chapter 4 presents several technics aimed at monitoring the E-modulus since casting or since setting. However, the measurement of the static elastic modulus is generally carried out with an extensometer. The static E-modulus is given by the slope of the stress-strain curve for concrete under uniaxial load. As this curve is non-linear, three methods were defined in order to compute it: the tangent modulus, the secant modulus and the chord modulus. The main difference between these three methods comes from the data considered for the computation of the E-modulus. The tangent modulus is the slope of the stress-strain curve at one point. The secant modulus is defined with the stress-strain measurement till a load corresponding to 40% of the strength. The chord modulus is defined between a point corresponding to a strain of 50µm/m and a point corresponding to a stress representing 40% of the strength. The protocol of loading is also important and two parameters must be considered: the amplitude of the loading/strain and the rate of loading/strain. For practical reason, it is generally preferred to refer to a criterion in stress than in displacement which needs to control the device according to the longitudinal displacement of the sample. Due to the non-linearity of the stress-strain curve, the magnitude of the loading has an importance for the determination of the tangent modulus. Higher is the loading lower is the E-modulus computed. The loading must be applied as fast as possible in order to reduce creep strain occurring when the load is applied. The E-modulus of concrete is also influenced by its composition with the distribution and the stiffness of its components (binder, sand and aggregate). The interfacial transition zone (ITZ) between the aggregate and the cement paste plays an important role in the value of the E-modulus. In general, microcracks, capillarity voids and calcium hydroxide crystals are very present in this zone. Figure 2 presents the different factors which influence the modulus of elasticity [57].

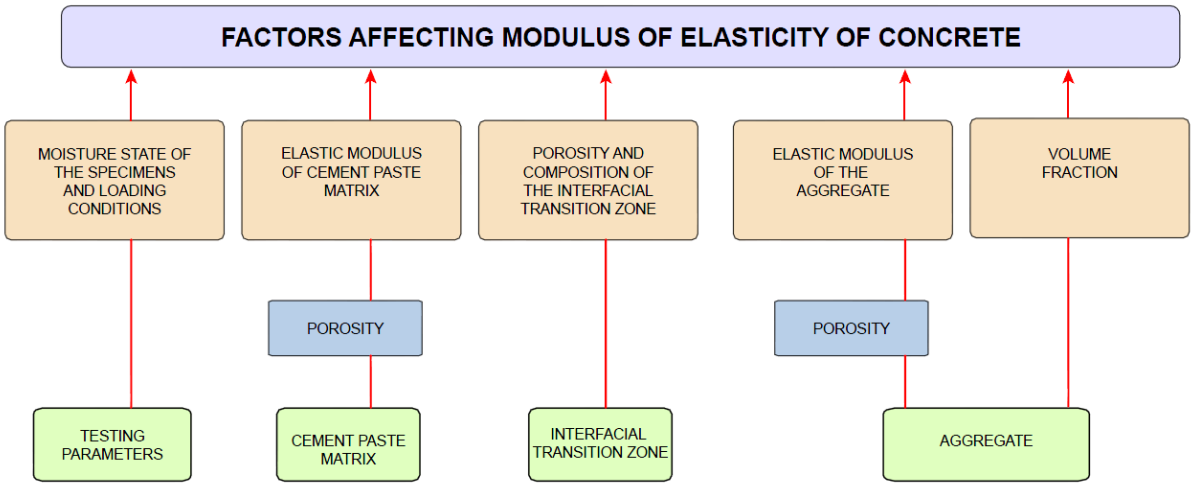

Figure 2 - Various parameters influencing the modulus of elasticity of concrete [57].

Currently, the tensile modulus of elasticity of concrete is considered as equal to the compressive modulus. This consideration is certainly due to a lack of data on this subject which is related to the technical difficulties to test concrete in tension. However, this parameter is important for the estimation of the tensile stresses and the risk of early age cracking that are generated with restrained shrinkage. The difference of the elastic modulus in tension and in compression has already been observed by different authors. These results were obtained from direct tension tests [58–61] or tensile creep tests [62–64] according to [61] and [65]. Results of Atrushi *et al.*, Hagihara *et al.*, Bissonnette *et al.* and Yoshitake *et al.* were carried out at early age. **According to the literature, the elastic modulus seems to be higher in tension than in compression**. This difference varied between 9 and 15% generally. Atrushi *et al.* found a difference of 11% for high performance concrete (HPC) for tests performed at 1, 2, 3, 4, 6 and 8 days. Hagihara *et al.* found a difference of 15 % for high-strength concrete. Aoki *et al.* found a difference of 9-12% for mature concrete containing ground granulated blast furnace slag and pulverized fuel ash. Recently, Yoshitake *et al.* carry out several direct tension tests on different concretes with a different W/C ratio. The results are shown in Figure 3. **The ratio between the elastic modulus in tension and in compression seems to be very influenced by the W/C ratio**. Concretes with a lower W/C ratio have a higher difference as for the HPC. A possible explanation of **this difference in tension and in compression comes from the development of microcracking in the cement paste induced by the restrained of the autogenous shrinkage due to the presence of the sand and the aggregate** (Figure 4). This phenomenon can be better explained by the difference observed between concrete with high and low W/C ratio. More the W/C ratio is high more the autogenous shrinkage is low. Then a link between the shrinkage of the cement paste and the development of the microcracking can be used for the determination of the possible evolution of this difference in tension and in compression. Atrushi *et al.* mentioned that the difference might have also several other reasons: different σ-ε relation in tension and compression, beyond the initial tangent relation; different load magnitudes imposed to the concrete in the different directions; test procedure. Other parameters should be also considered in this difference of behaviour in tension and in compression such as the incertainties in the measurement of the displacement and the force and the difference in the mechanism of closing of microcracking.

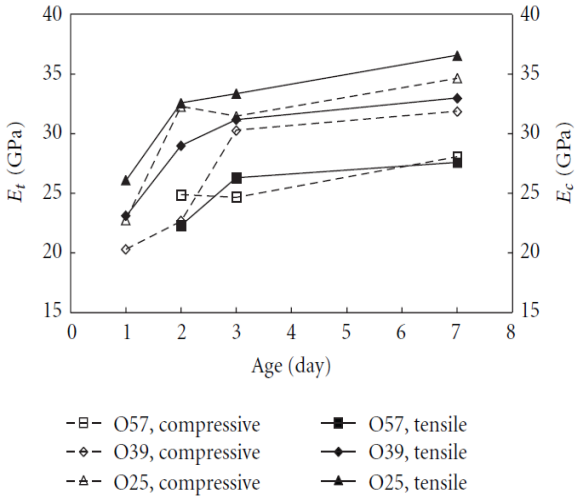

Figure 3 – Elastic modulus in tension and in compression versus age of concrete with water-cement ratio of 0.25, 0.39 and 0.57 [61].

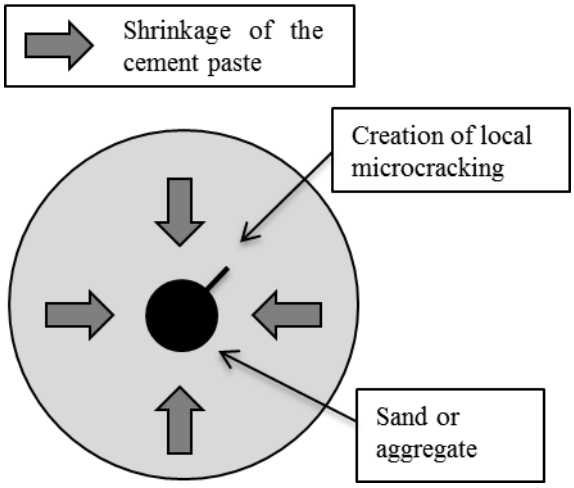

Figure 4 – Microcracking induced by restrained shrinkage of the cement paste by aggregate or sand.

Currently, no information is given about how evolves the ratio between the tensile and compressive elastic modulus with time. This property seems to be considered as constant. More investigation has to be done on this dissymmetry and the physical mechanisms which induce this difference.

According to results of Switek, *et al.* [66] on an UHPFRC, the stress level (from 19 to 90% of the tensile strength) has no influence on the E-modulus in tension is not dependent on the stress level. This means that the elastic stress-strain relation in tension is linear.

To compare results, it is very important to define the same protocol of loading for each laboratory which allows good repeatability of results. But **the protocol of loading for the measurement of elastic modulus is not yet imposed for a hardening concrete**. A new methodology has to be defined for the measurement of the elastic modulus in compression of concrete material at early age. No information is neither given for the measurement in tension of the elastic modulus for hardened and hardening concrete. More investigation has to be done on this subject.

Several models exist for the modelling of the elastic modulus. They differ, between others, by the main time-dependent variable that is used to express the evolution of the elastic modulus:

- the **equivalent time:** [62,67] (Equation 9), [68] (Equation 10) and [69] (Equation 11),

- the **advancement degree of reaction:** [70] (Equation 12),

- the **hydration degree** [71,72] (Equation 13) and [73] (Equation 14).

In each model, different parameters depend on the concrete composition. These models are detailed hereafter.

$$E_c(t) = E_{28}.\left\{exp\left[s\left(1-\sqrt{\frac{28}{t-t_0}}\right)\right]\right\}^n \qquad 9$$

Where : $E_c(t)$: the elastic concrete modulus at age t
E_{28} : elastic modulus at 28 days
t : equivalent time
t_0 : setting time
s : constant related to cement type
n : material fitting parameter

$$E_c(t) = 0.04326.\sqrt{\rho^3.f_{cm}\left(\frac{t}{a+b.t}\right)} \quad (10)$$

Where : a,b : constants related to cement type and curing conditions
ρ : density of the concrete
f_{cm} : mean value of the strength measured on cylinders

$$E_c(t) = a.e^{-\left(\frac{b}{t}\right)^c} \quad (11)$$

Where : a,b,c : material fitting parameters

$$E_c(\alpha) = E_\infty\left(\frac{\alpha(t)-\alpha_0}{1-\alpha_0}\right)^a \quad (12)$$

Where : E_∞ : elastic modulus at the end of hydration
a : material fitting parameter
$\alpha(t)$: advancement degree of the reaction at age t
α_0 : advancement degree of reaction at the setting time

$$E_c(\xi) = E_\infty.\frac{1+1{,}37.f_{c,\infty}^{2{,}204}}{1+(f_c(\xi))^{2{,}204}}\left(\frac{f_c(\xi)}{f_{c,\infty}}\right) \quad (13)$$

Where : ξ : hydration degree

$$E_c(\xi) = E_\infty\left(\frac{\xi(t)-\xi_0}{1-\xi_0}\right)^a \quad (14)$$

Where : $\xi(t)$: hydration degree at age t
ξ_0 : hydration degree at setting time

According to the litterature, the elastic modulus seems to be higher in tension than in compression.
The lower the W/C ratio, the higher the autogenous shrinkage, the higher the restrained shrinkage induces by the presence of the aggregate and sand, the higher the development of microcracking and the higher the difference in tension and in compression of the elastic modulus.
No protocol of loading exists for the measurement of the elastic modulus in compression for a hardening concrete and in tension for a hardened and a hardening concrete.

Through this state of art, different questions have to be answered:

- How can we measure the static elastic measurement at very early age?

- What is the difference of the elastic modulus in tension and in compression?
- How evolves the difference between the elastic modulus in tension and in compression?
- Which physical mechanisms explain the difference between the elastic modulus in tension and in compression for hardened and hardening concrete?
- Which protocol of loading can define correctly the elastic modulus at very early age in compression?
- Which protocol of loading can define correctly the elastic modulus in tension and especially at early age?
- Which model can correctly predict the elastic modulus at very early age in tension and in compression?

► BASIC CREEP

This work is limited to the study of concrete in sealed conditions. Each time that the creep is mentioned, it is referred to the basic creep. The drying creep is not studied in this work.

Creep and relaxation have not been thoroughly investigated at early age especially in tension. The knowledge of these properties is essential for assessing the long term performance but also the early age performance. Several authors tried to explain the physical mechanism of the creep and the relaxation. No theories of the basic creep are commonly accepted by the scientific community. But some experimental facts are accepted. A synthesis of these similarities is given in [74,75]:

- **A high sensitivity to the age of concrete at loading**. The creep amplitude decreases with the age of concrete at loading (during and after the hydration process).
- **The influence of the W/C ratio**. The creep amplitude increases when the W/C ration increases.
- **The fundamental role played by the water in the basic creep mechanism**, [76–80].
- **The influence of the type of cement and the mineral addition** [81].
- **The localization of the creep strain in the C-S-H of the cement paste** [82,83].
- **The creep recovery is only partially reversible** [84]**.The increase of temperature leads to higher creep deformations** [85]**.**

Another commonly accepted point of the basic creep is the non-linear behaviour of basic creep for which the creep strain depnds on the level of loading. According to the level of loading, the creep strain can be divided in three parts (Figure 5):

- The primary phase (level of loading < 30-50 % of the compressive strength) during which the creep strain is proportional to the stress.
- The secondary phase, the relationship becomes nonlinear between creep strain and stress.
- The tertiary phase, during which if the stress level exceeds 85 % of the strength the failure can occur in a very short period. Before failure a high increase of cracking occurs.

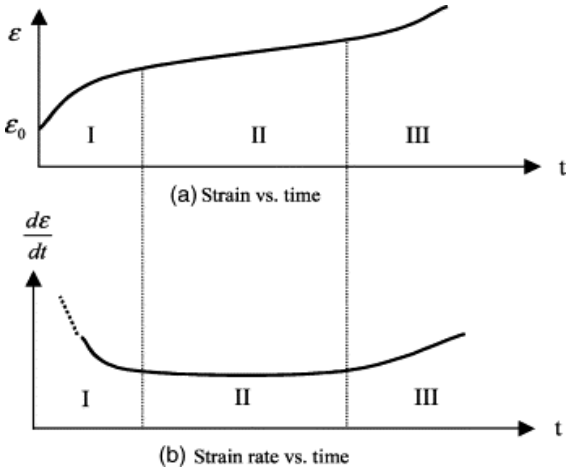

Figure 5 - Development of the complete creep strains [86]

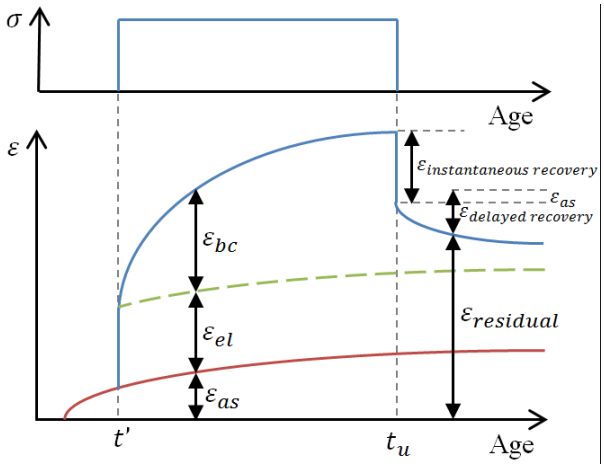

Figure 6 – Decomposition of the strain in autogenous condition during loading [87]

Among many previous studies like those reported in [62,88–95], several theories were developed to clarify mechanisms related to creep behaviour. However each theory alone does not allow explaining all experimental observations. Globally each theory can be linked to two mechanisms: direct mechanisms linked to the cement paste and responsible of the highest part of the creep amplitude and indirect mechanisms linked to the heterogeneity of the concrete. Direct mechanisms are related to the water mobility and to the solidification of the material and can be separated in short and long terms phenomena [80,96–98]. The short term phenomenon is reversible with a small characteristic time of about 10 days, is linked to a stress-induced water movement towards the largest diameter pores and to the solidification [98,99] of the material, and occurs under increasing volume for uniaxial compression. The long term phenomenon is irreversible with a high characteristic time and related to viscous flow in the hydrates and occurs under almost constant volume. The creep rate of this long term phenomenon evolves as a power function t^n [100–102] with an exponent n between -1 and -0.9 according to [103], between -0.72 and -0.69 according to results of [104] on concrete and an exponent n between -0.86 and -0.6 on cement paste according to results of [94]. Nanoindentation tests were carried out on C-S-H by Vandamme, *et al* [105]. It was shown that C-S-H exhibits a logarithmic creep which is in agreement with results obtained on concrete. Vandamme [106] compared also this logarithmic behaviour with other heterogeneous and porous materials with porosity including several orders of magnitude (soils and wood). For these non-ageing materials, a logarithmic long-term creep was also observed. It can then be assumed that this long term creep is not linked to a hydration process or any chemical specificity of the C-S-H.

The indirect mechanisms are due to micro-cracks which occur progressively in the cement paste and at the interface between cement paste and inclusions. Their presence can cause a redistribution of the stresses in the material. Rossi, *et al* [107–109] proposed an approach of the creep mechanisms by means of a micro-cracking process which occurs during loading and which is confirmed by acoustic emission. Over the time, an increase of the density of micro-cracks occurs. These micro-cracks are distributed through the volume of the specimen and allow water transfers inducing some additional self-desiccation shrinkage (but there is no experimental evidence of this additional self-desiccation).

The principal load-bearings function of concrete in structures is to carry compressive stresses. Reinforcement and prestressing tendons carry tensile stresses. For this purpose, most investigations were carried out for the determination of the mechanical properties of concrete in compression. Similarly, most explanations about mechanical properties concerned the compressive case. The creep

phenomenon was also mostly studied in compression for technical reasons. The study of tensile creep is more elaborated and complex than test in compression. It is yet more uncommon to have experimental results for the relaxation phenomenon. Indeed, the study of the relaxation is very complicated for a specific technological reason. The relaxation test needs to take into account in real time the subtraction between the total deformation and the free deformation. This subtraction has to be constant during the entire test, so that the jack of the machine must be controlled by this value. It is possible to avoid this technological problem thanks to the existing relation between the creep function and the relaxation function according to the superposition principle. Inversely it is also possible to find the creep function with the relaxation function. However, the direct use of the superposition principle implies making the assumption that creep is totally reversible.

Tanks and containments are not always prestressed. Tensile stresses occur in the structure and no cracking has to be ensured. To improve the prediction of the behaviour of the concrete structures and for economic reasons, designers need more information about tensile properties. In concrete structures, internal restraint causes a build up of tensile stresses within the material due to shrinkage whereas tensile creep counteracts the shrinkage as a stress relaxation mechanism. Importance of tensile creep is to be considered for the onset and the prediction of cracking propagation. The study of tensile creep has direct relevance for the design of concrete structures. Time that concrete takes to crack depends on the tensile strength and also the tensile creep. However, the current data about tensile creep at early age are very scarce. Data about restrained conditions are even less common.

A comparison between tensile and compressive creep were performed in [110]. The ratio between basic compressive creep strains and tensile ones according to several authors are plotted in Figure 7 and a very large dispersion can be observed. Much more investigations are thus required to understand the causes of this difference between tensile and compressive creep.

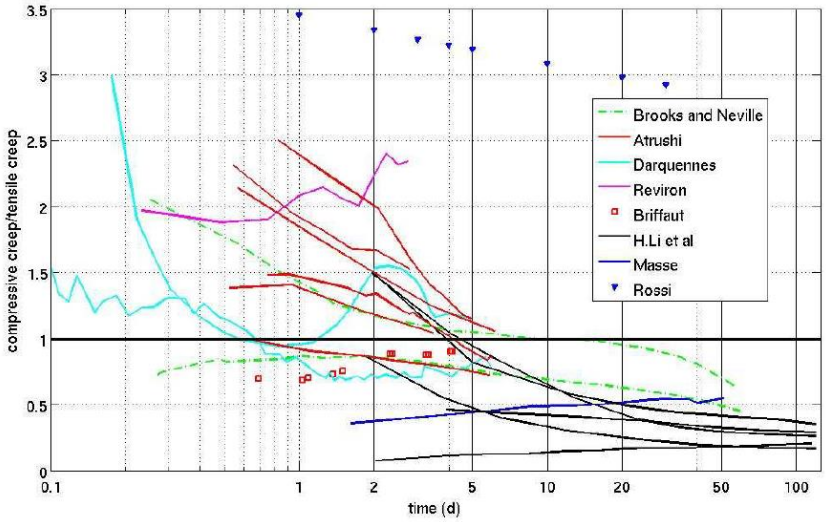

Figure 7 – ratio of compressive creep to tensile creep [110]

Tensile creep can be measured with different devices as uniaxial tensile test, ring test, restrained shrinkage test and bending test. Uniaxial tensile tests and bending tests are the most used for the study of the tensile creep. Differences from both tests were compared [107,111]. Carpinteri *et al.* [111] found that load level affect more the time of failure in bending tests than in tensile tests. Rossi *et al.* [107]with results of [112], highlight that during bending creep tests on notched sample, it exists at the notch tip very high tensile stresses and so a high *stress/tensile strength* ratio. However the compressive part is very weakly loaded and the *stress/compressive strength* ratio is very low in the

upper part of the beam. Consequently, several phenomena occur simultaneously during a creep bending test. The first point is the stress level. The stress level is far higher in tension than in compression and nonlinear creep can occur in tension. The second point comes from the dissymmetry of the creep behaviour in tension and in compression. Both points occur at the same time so that an important scale effect relating to creep in tension has to be considered.

On hardened high performance concrete, Ranaivomanana, *et al.* [84] compared tensile, compressive and flexural basic creep of specimens subjected to three different sustained stress levels (30, 40 and 50 % of the tensile or compressive strength), assumed to fall within the linear creep behaviour. Results of specific creep in compression, in tension and in flexure are presented in Figure 8. An increase in magnitude during the early days for each type of loading is observed, but differences in behaviour appear after about five days. During direct compression loading (Figure 8a), strains are increasing (very fast at the beginning and then slower). During direct tension loading (Figure 8b), strains are first increasing, but then are decreasing after about five days. During bending loading (Figure 8c), flexure-induce compression evolves similarly to direct compression, while flexure-induced tension are not decreasing as direct tension. The effect of the stress level is different for the different loading:

- For direct compression loading, Non-linearity occurs between 30 and 50%. Compressive specific creep is higher for higher stress level;
- For direct tensile loading, the results are quite scattered and no conclusion can be drawn about the stress level;
- For bending loading, a symmetrical trend is observed between flexure-induced compression and tension at 40 and 50% of the strength, but not at 30%. While specific creep for 30% is the lowest in tension, it is the highest in compression.

Results of specific recovery in compression, in tension and in flexure are plotted on Figure 9. Results are roughly similar for each type of loading. As creep recovery corresponds to the reversible part of creep, discrepancies should be due to the irreversible part of creep in which damage appears.

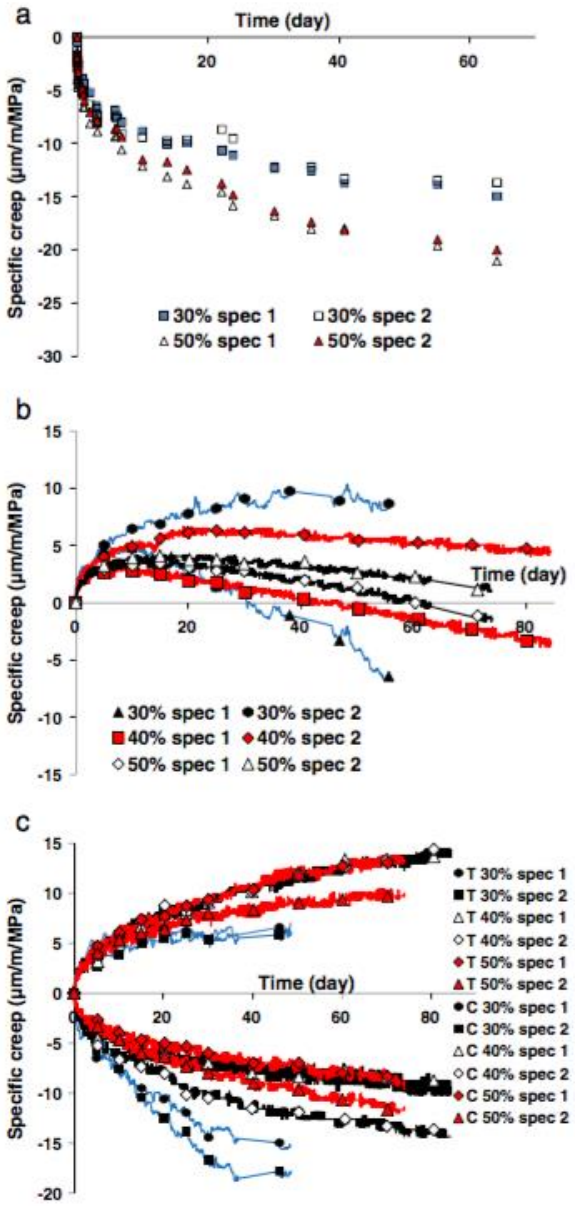

Figure 8 – Specific creep in compression (a), in tension (b) and in flexure (c) [84].

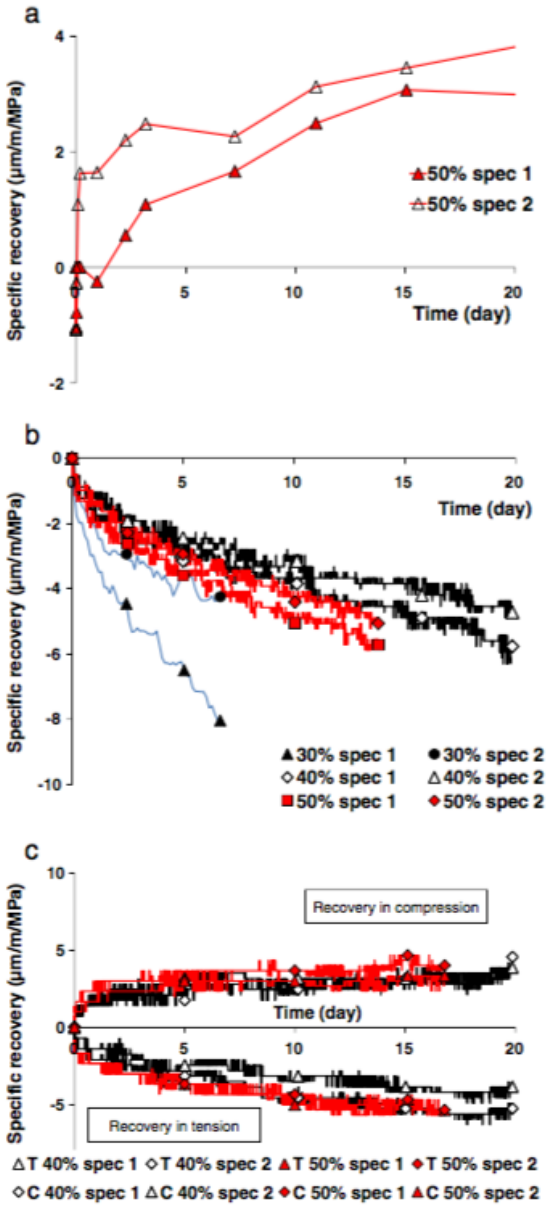

Figure 9 – Specific creep recovery in compression (a), in tension (b) and in flexure (c) [84].

A difference of behaviour in tension and in compression has already been noticed in the literature [62,107,113,114]. These **differences are relative to the amplitude and kinetic of the creep.** All they have in common is the importance of the *stress/strength* ratio [75] and of the *water/cement* ratio [81,114] on the creep strains. Rossi, *et al.* [107] suggested three arguments to explain on these contradictions found in the literature:

- Only few comparisons in tension and in compression on a same concrete were carried out. No real consensus exists concerning this comparison.
- Generally, literature does not give a lot of information of the sealed condition of the sample. In the past, sealed conditions were inadequate and are not reflective of the real basic creep situations.
- Tensile creep tests are technically very complex because of the low measurement of displacements and of the impact of the temperature on the displacement transducer.

An investigation of the physical mechanisms of the basic concrete behaviour in tension and in compression by using acoustic emission was carried out by [107]. The authors proposed explanations about the difference of results in tension and in compression. As presented above, Rossi *et al.* explained the creep mechanism with a microcracking process which allows the transfers of water through the concrete porosity. Generation of microcracks with loading creates vacuum in the concrete and generate local hygral shocks. Gradients of concentrations in water molecules as well as gradients of pressure appear and induce water vapor movements as well as liquid water movements. These movements lead to a drying of the capillaries surrounding the microcracks. This drying induced by cracking an additional shrinkage and increases the amplitude and the kinetics of the self-drying shrinkage. The origin of the difference between basic creeps in compression and in tension is explained by a difference of the density of microcracks which is higher in compression than in tension and a difference of the orientation of the microcracks in function of the loading direction.

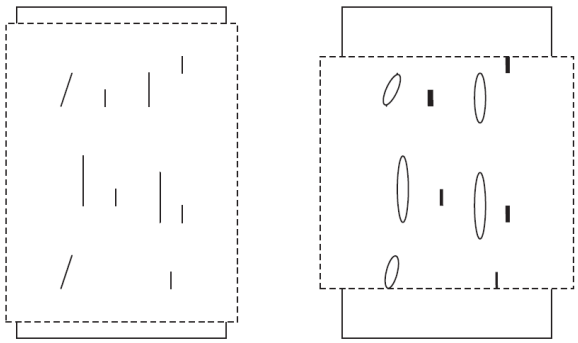

Figure 10 – Compressive creep: Strain and cracking before and after self-drying shrinkage [107]

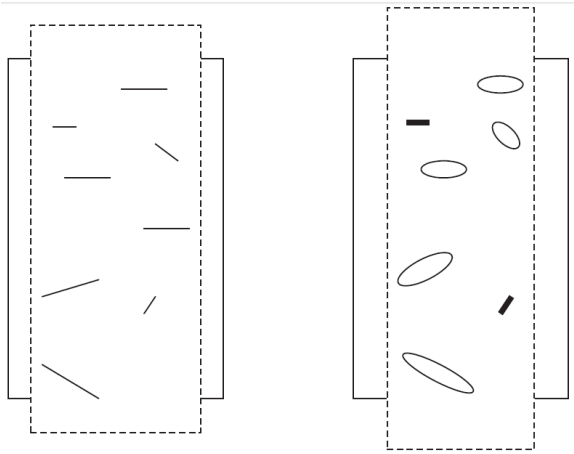

Figure 11 – Tensile creep: Strain and cracking before and after self-drying shrinkage [107]

As presented in Figure 10 and Figure 11, microcracks are oriented preferentially parallel in the loading direction in compression and perpendicular in the loading direction in tension. The self-drying shrinkage induced by microcracking is anisotropic and is important in the direction parallel to the microcracks and weak in the direction perpendicular to the microcracks. In the compressive case, the self-drying shrinkage is important in the direction of the loading and thus the apparent Poisson's of the concrete increases. In the tensile case, the self-drying shrinkage is important in the direction perpendicular to the loading. **The difference between the tensile and the compressive creep lies in the fact that for compressive case additional shrinkage increases the creep and for tensile creep the additional shrinkage reduces the creep**. The magnitude of this difference is therefore based on the development of the autogenous deformation before loading and thus is strongly dependent of the age of loading. The difference of tensile and compressive creep is shown in Figure 12.

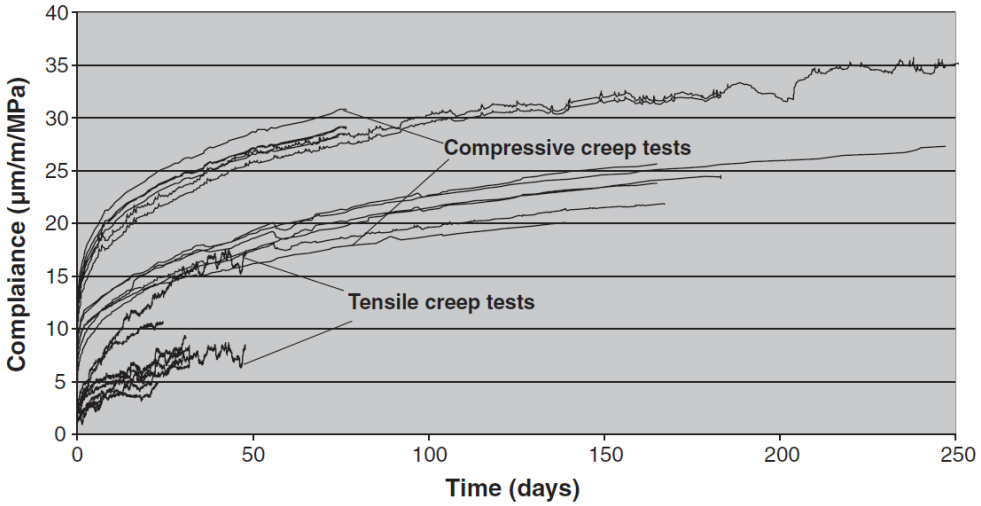

Figure 12 - Summary of the creep compliance curves related to the basic creep in compression and in tension [107].

Switek, *et al.* [66] have performed tensile creep tests on an UHPFRC at an age of 72 hours for four stress levels (13 – 30 – 60 and 90%). Non-linearity is observed in the tensile specific creep Figure 13 and Figure 14). The creep magnitude increases with the stress-level. For very low stress level of 13%, a decrease of the specific creep occurs after 10 hours of loading. This decrease is observed at an age after loading of 100 hours for a stress level of 30%. Therefore the stress level is a very significant parameter when studying tensile creep and when comparing it to the compressive creep.

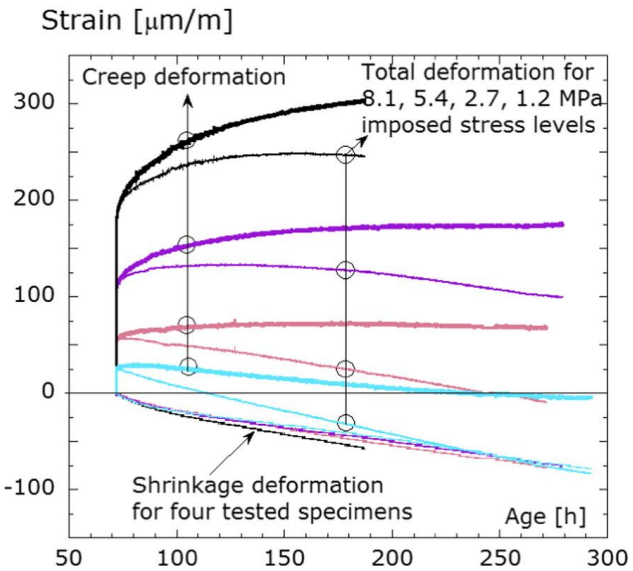

Figure 13 – Total shrinkage and creep strain for four stress levels (13 – 30 – 60 and 90%) at an age of 72 hours on an UHPFRC [66].

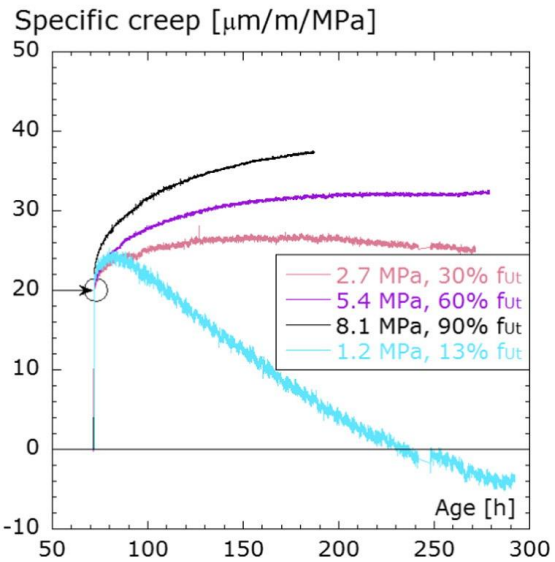

Figure 14 – Specific creep for three stress levels (13 – 30 – 60 and 90%) at an age of 72 hours on an UHPFRC [66].

Atrushi [62] studied the difference of behaviour in tension and in compression of the creep for a hardening concrete. Results of several tensile and compressive creep tests are shown in Figure 15. For both cases, the creep magnitude increases with the age of loading. The rate of creep is high during the first day and is then lower. Differences occurs for the kinetics, the short term creep in compression is consequent but is quickly stable. In tension, the short term creep is lower at the beginning but becomes linear along the time.

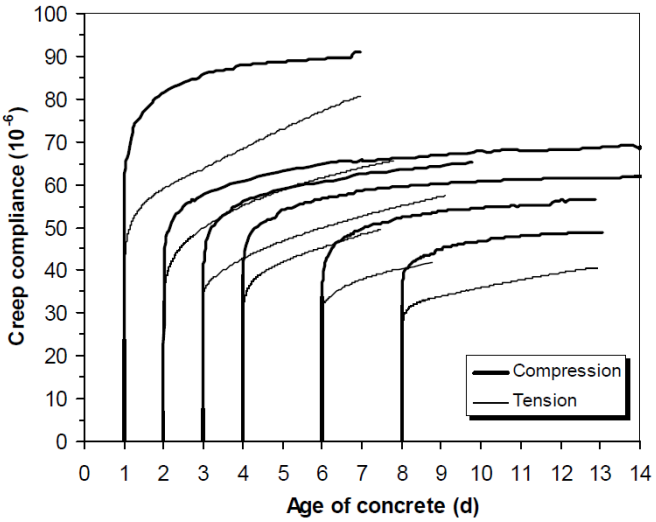

Figure 15 – Comparison between tensile and compressive creep (Atrushi, et al., 2005)

When concrete is loaded in unidirectional direction, creep occurs in the axial and the normal direction. Currently in the numerical code, creep equations are often extended in 3D with a constant Poisson's ratio and not with the creep dilatancy. Mazzotti, *et al.* [115] carried out different tests at different stress level to define how evolves the ratio between lateral and longitudinal strain during creep tests with one hour duration. For low stress level (20-30%), Poisson's ratio and creep dilatancy remained constant. For medium stress level (60-70%), only the Poisson's ratio increased due to microcracking. For high stress level (80-90%), both parameters increased. Ulm, *et al.* [96] carried out uniaxial compressive creep test at 20% of the strength and during 11 days at an age of 3 days. Lateral and longitudinal displacements were measured. Short term and long term behaviours of the creep dilatancy were identified. During short term creep, concrete was characterized by a viscous dilatant behaviour with a positive volume increase rate. The long term creep had a rather non-dilatant nature and occurred at constant volume. Zhaoxia [116] carried out several compressive creep tests at high stress level (83-85-90-95% of the compressive strength) at 28 days. He observed an increase of the ratio of the creep dilatancy and the Poisson's ratio. The ratio increased strongly (46.7 to 112.4%). This increase is strongly influenced by the microcracking development during the tertiary creep being perpendicular to the loading direction. Zhaoxia concludes that **the increase of the creep dilatancy is an important property of the failure of the concrete**. For high stress levels, the creep dilatancy has then to be considered.

Data about the temperature effect on the basic creep strain is not very common. **The effect of the temperature variation on the creep strain is not yet well known**. However at very early age, temperature increases strongly with the heat released during the hydration process. This effect is named load induced thermal strains (LITS). Some data exists for the creep in compression but no data are given for the tensile creep. Umehara, *et al.* [117] observed an increase of the basic creep strain for high constant temperature. Hauggard, *et al.* [69] observed an increase of the basic creep strain during variation of temperature. The increase of the creep strains with increase of temperature can be caused by a decrease of the water viscosity or the relaxation of the micro prestress [98]. More investigation has to be done on the influence of the temperature on the creep and the relaxation at early ages.

Some experimental facts are commonly accepted by the scientific community for the creep mechanisms (importance of age of loading, W/C ratio, type of mineral addition, the fundamental rule played by the water movement, the localization of the creep strain in the C-S-H of the cement paste).

Creep can be divided in two types of mechanisms : direct and indirect mechanisms.

Difference between creep in tension and in compression was noticed by different authors. Rossi, *et al.* [107] identify the difference between the tensile and the compressive creep lies that for compressive case additional shrinkage increases the creep and for tensile creep the additional shrinkage reduces the creep.

The tensile creep is strongly dependent on the stress level.

A difference of kinetic and amplitude was noticed at early age between the tensile and compressive creep.

The creep dilatancy is an important property of the failure of the concrete.

The effect of the temperature on the creep is not yet well known.

Through this state of art, different questions have to be answered:

- How does the difference between the basic creep in tension and in compression evolves with time?
- Is there really a difference between the elastic modulus in tension and in compression?
- Which physical mechanisms can explain the difference between the creep strain in tension and in compression for hardened and hardening concrete?
- Which protocol of loading can define correctly the basic creep strain at very early age in compression and in tension?
- How does the creep dilatancy evolve for low and high stress level at early age and for longer duration of loading than 1 hour?
- Which model can correctly predict the basic creep strain at very early age?
- How does the basic creep strain evolve in tension and in compression with temperature?

REFERENCES

[1] W. Hansen, Report on Early-Age Cracking, Concr. Int. 33 (2011) 2–5.

[2] Tailhan J.L., Dal Pont S., Rossi P., From local to global probalistic modeling of concrete cracking, Ann. Solid Struct. Mech. 1 (2010) 103–105.

[3] Dal Pont S., Meftah F., Schrefler B.A., Modeling concrete under severe conditions as a mutliphases material, Nucl. Eng. Des. 241 (2011) 562–572.

[4] C. Boulay, Développement d'un dispositif de mesure de retrait endogène d'un béton au jeune âge, in: Huit. Édition Des Journées Sci. Du Regroupement Francoph. Pour La Rech. La Form. Sur Le Bét. $(RF)^2B$, 2007.

[5] D. Lootens, P. Jousset, L. Martinie, N. Roussel, R.J. Flatt, Yield stress during setting of cement pastes from penetration tests, Cem. Concr. Res. 39 (2009) 401–408. doi:10.1016/j.cemconres.2009.01.012.

[6] A. Darquennes, S. Staquet, B. Espion, Determination of time-zero and its effect on autogenous deformation evolution, Eur. J. Environ. Civ. Eng. 15 (2011) 1017–1029. doi:10.1080/19648189.2011.9695290.

[7] M. Azenha, F. Magalhães, R. Faria, Á. Cunha, Measurement of concrete E-modulus evolution since casting: A novel method based on ambient vibration, Cem. Concr. Res. 40 (2010) 1096–1105. doi:10.1016/j.cemconres.2010.02.014.

[8] H.W. Reinhardt, C.U. Grosse, Continuous monitoring of setting and hardening of mortar and concrete, Constr. Build. Mater. 18 (2004) 145–154. doi:10.1016/j.conbuildmat.2003.10.002.

[9] C.U. Grosse, H.-W. Reinhardt, Ultrasound in through transmission, in: Adv. Test. Cem. Based Mater. Dur. Setting Hardening, RILEM Publications SARL, 2005: pp. 162–190.

[10] T. Voigt, Comparison of ultrasonic wave transmission and reflection measurements with P- and S-waves on early age mortar and concrete, Mater. Struct. 38 (2005) 729–738. doi:10.1617/14267.

[11] A. Boumiz, C. Vernet, F. Cohen Tenoudji, Mechanical properties of cement pastes and mortars at early ages, Adv. Cem. Based Mater. 3 (1996) 94–106. doi:10.1016/1065-7355(95)00072-0.

[12] L. Arnaud, C.U. Grosse, Wave propagation by transmission, The case of the setting phenomenon in heterogeneous materials, in: Adv. Test. Cem. Based Mater. Dur. Setting Hardening, RILEM Publications SARL, 2005: pp. 191–238.

[13] C. Dumoulin, G. Karaiskos, J. Carette, S. Staquet, A. Deraemaeker, Monitoring of the ultrasonic P-wave velocity in early-age concrete with embedded piezoelectric transducers, Smart Mater. Struct. 21 (2012) 47001. doi:doi:10.1088/0964-1726/21/4/047001.

[14] G. Sant, M. Dehadrai, D. Bentz, P. Lura, C.F. Ferraris, J.W. Bullard, et al., Detecting the fluid-to-solid transition in cement pastes, Concr. Int. 31 (2009) 53–58.

[15] N. Robeyst, E. Gruyaert, C.U. Grosse, N. De Belie, Monitoring the setting of concrete containing blast-furnace slag by measuring the ultrasonic p-wave velocity, Cem. Concr. Res. 38 (2008) 1169–1176. doi:10.1016/j.cemconres.2008.04.006.

[16] J. Carette, S. Staquet, Monitoring the setting process of mortars by ultrasonic P and S-wave transmission velocity measurement, Constr. Build. Mater. 94 (2015) 196–208. doi:10.1016/j.conbuildmat.2015.06.054.

[17] J. Carette, S. Staquet, Monitoring the setting process of eco-binders by ultrasonic P-wave and S-wave transmission velocity measurement: Mortar vs concrete, Constr. Build. Mater. 110 (2016) 32–41. doi:10.1016/j.conbuildmat.2016.02.019.

[18] M. Krüger, R. Bregar, G.A. David, J. Juhart, Non-destructive evaluation of eco-friendly cementituous materials by ultrasound, in: Proc. Int. RILEM Conf. Mater. Syst. Struct. Civ. Eng., 2016: pp. 503–512.

[19] L. Buffo-Lacarrière, A. Sellier, P. Souyris, Use of original percolation approach in homogenization methods for the prediction of concrete hydro-mechanical behavior at early age, in: Numer. Model. Strateg. Sustain. Concr. Struct., 2012: p. Aix-en-Provence, France.

[20] H.K. Lee, K.M. Lee, Y.H. Kim, H. Yim, D.B. Bae, Ultrasonic in-situ monitoring of setting process of high-performance concrete, Cem. Concr. Res. 34 (2004) 631–640. doi:10.1016/j.cemconres.2003.10.012.

[21] Japan Concrete Institute, Guidelines for Control of Cracking of Mass Concrete, 2008.

[22] V. Waller, Relations entre compositions des bétons, exothermie en cours de prise et résistance en compression, PhD thesis, Laboratoire Centrale des Ponts et Chaussées, 2000.

[23] M. Bouasker, P. Mounanga, P. Turcry, A. Loukili, A. Khelidj, Chemical shrinkage of cement pastes and mortars at very early age: Effect of limestone filler and granular inclusions, Cem. Concr. Compos. 30 (2008) 13–22. doi:10.1016/j.cemconcomp.2007.06.004.

[24] Ø. Bjøntegaard, T.. Hammer, E.J. Sellevold, On the measurement of free deformation of early age cement paste and concrete, Cem. Concr. Compos. 26 (2004) 427–435. doi:10.1016/S0958-9465(03)00065-9.

[25] R. Cortas, E. Rozière, S. Staquet, A. Hamami, A. Loukili, M.-P. Delplancke-Ogletree, Effect of the water saturation of aggregates on the shrinkage induced cracking risk of concrete at early age, Cem. Concr. Compos. 50 (2014) 1–9. doi:10.1016/j.cemconcomp.2014.02.006.

[26] V. Baroghel-Bouny, P. Mounanga, A. Khelidj, A. Loukili, N. Rafaï, Autogenous deformations of cement pastes, Cem. Concr. Res. 36 (2006) 123–136. doi:10.1016/j.cemconres.2004.10.020.

[27] G. Sant, B. Lothenbach, P. Juilland, G. Le Saout, J. Weiss, K. Scrivener, The origin of early age expansions induced in cementitious materials containing shrinkage reducing admixtures, Cem. Concr. Res. 41 (2011) 218–229. doi:10.1016/j.cemconres.2010.12.004.

[28] P.K. Mehta, Mechanism of expansion associated with ettringite formation, Cem. Concr. Res. 3 (1973) 1–6. doi:10.1016/0008-8846(73)90056-2.

[29] D. Min, T. Mingshu, Formation and expansion of ettringite crystals, Cem. Concr. Res. 24 (1994) 119–126. doi:10.1016/0008-8846(94)90092-2.

[30] I. Odler, J. Colán-Subauste, Investigations on cement expansion associated with ettringite formation, Cem. Concr. Res. 29 (1999) 731–735. doi:10.1016/S0008-8846(99)00048-4.

[31] P. Chaunsali, P. Mondal, Physico-chemical interaction between mineral admixtures and OPC–calcium sulfoaluminate (CSA) cements and its influence on early-age expansion, Cem. Concr. Res. 80 (2016) 10–20. doi:10.1016/j.cemconres.2015.11.003.

[32] E. Roziere, B. Delsaute, A. Loukili, S. Staquet, Experimental Assessment of Autogenous Shrinkage, in: CONCREEP 10 Mech. Phys. Creep, Shrinkage, Durab. Concr. Concr. Struct., 2015: pp. 983–992.

[33] L. Barcelo, M. Moranville, B. Clavaud, Autogenous shrinkage of concrete: a balance between

autogenous swelling and self-desiccation, Cem. Concr. Res. 35 (2005) 177–183. doi:10.1016/j.cemconres.2004.05.050.

[34] V. Baroghel-bouny, Caractérisation des pâtes de ciment et des bétons, Méthodes, Analyse, Interprétation, PhD thesis, Ecole Nationale des Ponts et Chaussées, 1994.

[35] B. Persson, Consequence of cement constituents, mix composition and curing conditions for self-desiccation in concrete, Mater. Struct. 33 (2000) 352–362. doi:10.1007/BF02479644.

[36] K. Van Breugel, Simulation of hydration and formation of structure in hardeningcement-basedmaterials, PhD Thesis, TU Delft, 1991.

[37] A. Darquennes, S. Staquet, M.-P. Delplancke-Ogletree, B. Espion, Effect of autogenous deformation on the cracking risk of slag cement concretes, Cem. Concr. Compos. 33 (2011) 368–379. doi:10.1016/j.cemconcomp.2010.12.003.

[38] T. Aly, J.G. Sanjayan, Shrinkage cracking properties of slag concretes with one-day curing, Mag. Concr. Res. 60 (2008) 41–48. doi:10.1680/macr.2007.00038.

[39] E. Holt, Contribution of mixture design to chemical and autogenous shrinkage of concrete at early ages, Cem. Concr. Res. 35 (2005) 464–472. doi:10.1016/j.cemconres.2004.05.009.

[40] A.N.M. Lopes, E.F. Silva Prof., D.C.C. Dal Molin Prof., R.D.T. Filho Prof., Shrinkage-reducing admixture: Effects on durability of high-strength concrete, ACI Mater. J. 110 (2013) 365–374.

[41] Y. Wei, W. Hansen, J.J. Biernacki, E. Schlangen, Unified shrinkage model for concrete from autogenous shrinkage test on paste with and without ground-granulated blast-furnace slag, ACI Mater. J. 108 (2011) 13–20.

[42] Z. Liu, W. Hansen, Aggregate and slag cement effects on autogenous shrinkage in cementitious materials, Constr. Build. Mater. 121 (2016) 429–436. doi:10.1016/j.conbuildmat.2016.06.012.

[43] Y. Zhuang, D. Zheng, Z. Ng, T. Ji, X. Chen, Effect of lightweight aggregate type on early-age autogenous shrinkage of concrete, Constr. Build. Mater. 120 (2016) 373–381. doi:10.1016/j.conbuildmat.2016.05.105.

[44] I. Maruyama, a. Teramoto, Impact of time-dependant thermal expansion coefficient on the early-age volume changes in cement pastes, Cem. Concr. Res. 41 (2011) 380–391. doi:10.1016/j.cemconres.2011.01.003.

[45] O.M. Jensen, P.F. Hansen, Influence of temperature on autogenous deformation and relative humidity change in hardening cement paste, Cem. Concr. Res. 29 (1999) 567–575. doi:10.1016/S0008-8846(99)00021-6.

[46] M. Briffaut, F. Benboudjema, J.-M. Torrenti, G. Nahas, Effects of early-age thermal behaviour on damage risks in massive concrete structures, Eur. J. Environ. Civ. Eng. 16 (2012) 589–605. doi:10.1080/19648189.2012.668016.

[47] G. De Schutter, Finite element simulation of thermal cracking in massive hardening concrete elements using degree of hydration based material laws, Comput. Struct. 80 (2002) 2035–2042. doi:10.1016/S0045-7949(02)00270-5.

[48] R. Faria, M. Azenha, J.A. Figueiras, Modelling of concrete at early ages: Application to an externally restrained slab, Cem. Concr. Compos. 28 (2006) 572–585. doi:10.1016/j.cemconcomp.2006.02.012.

[49] X. Liu, W. Jiang, G. De Schutter, Y. Yuan, Q. Su, Early-age behaviour of precast concrete immersed tunnel based on degree of hydration concept, Struct. Concr. 15 (2014) 66–80. doi:10.1002/suco.201300027.

[50] Y. Yuan, Z.. Wan, Prediction of cracking within early-age concrete due to thermal, drying and creep behavior, Cem. Concr. Res. 32 (2002) 1053–1059. doi:10.1016/S0008-8846(02)00743-3.

[51] J. Zreiki, F. Bouchelaghem, M. Chaouche, Early-age behaviour of concrete in massive structures, experimentation and modelling, Nucl. Eng. Des. 240 (2010) 2643–2654. doi:10.1016/j.nucengdes.2010.07.010.

[52] Code-type models for structural behaviour of concrete: Background of the constitutive relations and material models in the fib Model Code for Concrete Structures 2010, Fib Bull. 70. (2013) 196.

[53] M.S. Siddiqui, D.W. Fowler, Optimizing coefficient of thermal expansion of concrete and its importance on concrete structures, Constr. Mater. Struct. (2014) 47–56. doi:10.3233/978-1-61499-466-4-47.

[54] M.S. Siddiqui, D.W. Fowler, Effect of Internal Water Pressure on the Measured Coefficient of Thermal Expansion of Concrete, J. Mater. Civ. Eng. 27 (2015) 4014151. doi:10.1061/(ASCE)MT.1943-5533.0001095.

[55] E.J. Sellevold, · Ø Bjøntegaard, Coefficient of thermal expansion of cement paste and concrete: Mechanisms of moisture interaction, Mater. Struct. 39 (2006) 809–815. doi:10.1617/s11527-006-9086-z.

[56] P. Laplante, C. Boulay, Evolution du coefficient de dilatation thermique du béton en fonction de sa maturité aux tout premiers âges, Mater. Struct. 27 (1994) 596–605. doi:10.1007/BF02473129.

[57] P. Kumar Mehta, P.J.M. Monteiro, Concrete: Microstructure, Properties, and Materials, Fourth Edition, Third, The McGraw-Hill Companies, 2006.

[58] I. Yoshitake, Y. Ishikawa, H. Kawano, Y. Mimura, On the tensile Young's moduli of early age concrete, Doboku Gakkai Ronbunshuu E. 63 (2007) 677–688. doi:10.2208/jsceje.63.677.

[59] S. Swaddiwudhipong, H.R. Lu, T.H. Wee, Direct tension test and tensile strain capacity of concrete at early age, Cem. Concr. Res. 33 (2003) 2077–2084. doi:10.1016/S0008-8846(03)00231-X.

[60] Y. Aoki, K. Shimano, D. Iijima, Y. Hirano, Examination on simple uniaxial tensile test of concrete, in: Proc. Japan Concr. Inst., 2007: pp. 531–536.

[61] I. Yoshitake, F. Rajabipour, Y. Mimura, A. Scanlon, A Prediction Method of Tensile Young's Modulus of Concrete at Early Age, Adv. Civ. Eng. 2012 (2012) 1–10. doi:10.1155/2012/391214.

[62] D.S. Atrushi, Tensile and Compressive Creep of Early Age Concrete : Testing and Modelling, PhD thesis, The Norwegian University of Sciences and Technology, Trondheim,Norway, 2003.

[63] B. Bissonnette, M. Pigeon, A.M. Vaysburd, Tensile creep of concrete: Study of its sensitivity to basic parameters, ACI Mater. J. 104 (2007) 360–368.

[64] S. Hagihara, S. Nakamura, Y. Masuda, M. Kono, Experimental study on mechanical properties and creep behavior of high-strength concrete in early age, Concr. Res. Technol. 11 (2000) 39–

50.

[65] V.Y.G. Yanni, Multi-scale investigation of tensile creep of ultra- high performance concrete for bridge applications, PhD thesis, Georgia Institute of Technology, 2009.

[66] A.E. Switek, E. Denarié, E. Brühwiler, Early age creep and relaxation of UHPFRC under low to high tensile stresses, Cem. Concr. Res. 83 (2016) 57–69. doi:10.1016/j.cemconres.2016.01.005.

[67] M. Krauß, K. Hariri, Determination of initial degree of hydration for improvement of early-age properties of concrete using ultrasonic wave propagation, Cem. Concr. Compos. 28 (2006) 299–306. doi:10.1016/j.cemconcomp.2006.02.007.

[68] R. Goel, R. Kumar, D.K. Paul, Comparative Study of Various Creep and Shrinkage Prediction Models for Concrete, (2007) 249–260.

[69] A. Hauggaard, L. Damkilde, F. Hansen, Transitional Thermal Creep of Early Age Concrete, Engineering. 125 (1999) 458–465. doi:10.1061/(ASCE)0733-9399(1999)125:4(458).

[70] G. De Schutter, L. Taerwe, Degree of hydration-based description of mechanical properties of early age concrete, Mater. Struct. 29 (1996) 335–344. doi:10.1007/BF02486341.

[71] D.P. Bentz, P. Lura, J.W. Roberts, Mixture proportioning for internal curing, Concr. Int. 27 (2005) 35–40. http://concrete.nist.gov/~bentz/Mixpropfin/CI2702Bentz.pdf.

[72] F. Benboudjema, J.M. Torrenti, Early-age behaviour of concrete nuclear containments, Nucl. Eng. Des. 238 (2008) 2495–2506. doi:10.1016/j.nucengdes.2008.04.009.

[73] E.M.R. Fairbairn, M.M. Silvoso, R.D. Toledo Filho, J.L.D. Alves, N.F.F. Ebecken, Optimization of mass concrete construction using genetic algorithms, Comput. Struct. 82 (2004) 281–299. doi:10.1016/j.compstruc.2003.08.008.

[74] M. Briffaut, Étude de la fissuration au jeune âge des structures massives en béton : influence de la vitesse de refroidissement , des reprises de bétonnage et des armatures, PhD thesis, Ecole Normale Superieure de Cachan, 2010.

[75] A. Darquennes, Comportement au jeune âge de bétons formulés à base de ciment au laitier de haut fourneau en condition de déformations libre et restreinte, PhD thesis, Université Libre de Bruxelles, 2009.

[76] J. Glucklich, O. Ishai, Creep mechanism in cement mortar, ACI J. Proc. 59 (1962) 923–948. http://www.concrete.org/PUBS/JOURNALS/OLJDetails.asp?Home=JP&ID=7946.

[77] S.E. Pihlajavaara, A review of some of the main results of a research on the ageing phenomena of concrete: Effect of moisture conditions on strength, shrinkage and creep of mature concrete, Cem. Concr. Res. 4 (1974) 761–771. doi:10.1016/0008-8846(74)90048-9.

[78] P. Acker, Comportement mécanique des bétons : Apport de l'approche physicochimique, PhD thesis, Ecole Nationale des Ponts et Chaussées, 1988.

[79] M. Cheyrezy, M. Behloul, Creep and Shrinkage of Ultra-High Performance Concrete, in: Creep, Shrinkage Durab. Mech. Concr. Other Quasi-Brittle Mater. (Concreep 6), 2000: pp. 527–538.

[80] P. Acker, F.J. Ulm, Creep and shrinkage of concrete: Physical origins and practical measurements, Nucl. Eng. Des. 203 (2001) 143–158. doi:10.1016/S0029-5493(00)00304-6.

[81] B. Bissonnette, Pigeon M., Tensile creep at early ages of ordinary, silica fume and fiber

reinforced concretes, Cem. Concr. Compos. 25 (1995) 1075–1085.

[82] B.T. Tamtsia, J.J. Beaudoin, Basic creep of hardened cement paste. A re-examination of the role of water, Cem. Concr. Res. 30 (2000) 1465–1475. doi:10.1016/S0008-8846(00)00279-9.

[83] P. Acker, Sur les origines du retrait et du fluage du béton, Rev. Française Génie Civ. 7 (2003) 761–776. doi:10.1080/12795119.2003.9692521.

[84] N. Ranaivomanana, S. Multon, A. Turatsinze, Tensile, compressive and flexural basic creep of concrete at different stress levels, Cem. Concr. Res. 52 (2013) 1–10. doi:10.1016/j.cemconres.2013.05.001.

[85] A. Sellier, S. Multon, L. Buffo-Lacarrière, T. Vidal, X. Bourbon, G. Camps, Concrete creep modelling for structural applications: non-linearity, multi-axiality, hydration, temperature and drying effects, Cem. Concr. Res. 79 (2016) 301–315. doi:10.1016/j.cemconres.2015.10.001.

[86] J.L. Zeng, K.H. Tan, Z.F. Huang, Primary creep buckling of steel columns in fire, J. Constr. Steel Res. 59 (2003) 951–970. doi:10.1016/S0143-974X(03)00027-0.

[87] I. Guénot-Delahaie, Contribution à l'analyse physique et à la modélisation du fluage propre du béton, PhD thesis, Laboratoire Central des Ponts et Chaussées, Paris, France, 1997.

[88] P. Laplante, Propriétés mécaniques des bétons durcissants: analyse comparée des bétons classiques et à très hautes performances, Ecole Nationale des Ponts et Chaussées, 1993.

[89] R. Le Roy, Déformations instantanées et différées des bétons à hautes performances, PhD thesis, Ecole Nationale des Ponts et Chaussées, Paris, France, 1995.

[90] A.-W. Gutsch, Properties of early age concrete-Experiments and modelling, Mater. Struct. 35 (2002) 76–79. http://link.springer.com/article/10.1007/BF02482104 (accessed December 17, 2013).

[91] M. Briffaut, F. Benboudjema, J.-M. Torrenti, G. Nahas, Concrete early age basic creep: Experiments and test of rheological modelling approaches, Constr. Build. Mater. 36 (2012) 373–380. doi:10.1016/j.conbuildmat.2012.04.101.

[92] G. De Schutter, Applicability of degree of hydration concept and maturity method for thermo-visco-elastic behaviour of early age concrete, Cem. Concr. Compos. 26 (2004) 437–443. doi:10.1016/S0958-9465(03)00067-2.

[93] W. Jiang, G. De Schutter, Y. Yuan, Degree of hydration based prediction of early age basic creep and creep recovery of blended concrete, Cem. Concr. Compos. (2013). doi:10.1016/j.cemconcomp.2013.10.012.

[94] B.T. Tamtsia, J.J. Beaudoin, J. Marchand, The early age short-term creep of hardening cement paste: load-induced hydration effects, Cem. Concr. Compos. 26 (2004) 481–489. doi:10.1016/S0958-9465(03)00079-9.

[95] J.P. Forth, Predicting the tensile creep of concrete, Cem. Concr. Compos. 55 (2014) 70–80. doi:10.1016/j.cemconcomp.2014.07.010.

[96] F.-J. Ulm, F. Le Maou, C. Boulay, Creep and shrinkage coupling : New review of some evidence, in: ACI-RILEM Work. Creep Shrinkage Concr. Struct., 1999: pp. 21–37.

[97] O. Bernard, F.-J. Ulm, E. Lemarchand, A multiscale micromechanics-hydration model for the early-age elastic properties of cement-based materials, Cem. Concr. Res. 33 (2003) 1293–1309. doi:10.1016/S0008-8846(03)00039-5.

[98] Z.P. Bažant, A.B. Hauggaard, S. Baweja, F.-J. Ulm, Microprestress-Solidification Theory for Concrete Creep. I Aging and Drying Effects, J. Eng. Mech. 123 (1997) 1188–1194.

[99] Z.P. Bazant, S. Prasannan, Solidification theory for aging creep. I: Formulation, J. Eng. Mech. 115 (1989) 1691–1703. doi:10.1016/0008-8846(88)90028-2.

[100] Z.P. Bažant, Double-power logarithmic law for concrete creep, Cem. Concr. Res. 14 (1984) 793–806.

[101] F.H. Wittmann, Creep and Shrinkage Mechanisms, in: Z.P. Bažant, F.H. Wittmann (Eds.), Creep Shrinkage Concr., 1982: pp. 129–161.

[102] O. Bernard, F.-J. Ulm, J.T. Germaine, Volume and deviator creep of calcium-leached cement-based materials, Cem. Concr. Res. 33 (2003) 1127–1136.

[103] Z.P. Bažant, Creep and shrinkage prediction model for analysis and design of concrete structures - Model B-3, Mater. Struct. 28 (1995) 357–365.

[104] F.H. Wittmann, Useful Fundamentals of Shrinkage and Creep of Concrete, in: Concreep 10, 2015: pp. 84–93.

[105] M. Vandamme, F.-J. Ulm, Nanogranular origin of concrete creep., Proc. Natl. Acad. Sci. U. S. A. 106 (2009) 10552–7. doi:10.1073/pnas.0901033106.

[106] M. Vandamme, A Few Analogies Between the Creep of Cement and of Other Materials, in: Concreep 10, 2015: pp. 78–83.

[107] P. Rossi, J.-L. Tailhan, F. Le Maou, L. Gaillet, E. Martin, Basic creep behavior of concretes investigation of the physical mechanisms by using acoustic emission, Cem. Concr. Res. 42 (2012) 61–73. doi:10.1016/j.cemconres.2011.07.011.

[108] P. Rossi, J.-L. Tailhan, F. Le Maou, Comparison of concrete creep in tension and in compression: Influence of concrete age at loading and drying conditions, Cem. Concr. Res. 51 (2013) 78–84. doi:10.1016/j.cemconres.2013.04.001.

[109] P. Rossi, N. Godart, J.L. Robert, J.P. Gervais, D. Bruhat, acoustic emission, Mater. Struct. 27 (1994) 510–514.

[110] F. Benboudjema, M. Briffaut, A. Hilaire, J.M. Torrenti, G. Nahas, Early Age Behavior of Massive Concrete Structures: From Experiments To Numerical Simulations, in: CONCRACK 3-RILEM-JCI Int. Work. Crack Control Mass Concr. Relat. Issues Concern. Early-Age Concr. Struct., 2012: pp. 1–12.

[111] A. Carpinteri, S. Valente, F.P. Zhou, G. Ferrara, G. Melchiorri, Tensile and flexural creep rupture tests on partially-damaged concrete specimens, Mater. Struct. 30 (1997) 269–276. doi:10.1007/BF02486351.

[112] M. Omar, A. Loukili, G. Pijaudier-cabot, Y. Le Pape, Creep-damage coupled effects: experimental investigation on bending beams with various sizes, J. Mater. Civ. Eng. 21 (2009) 65–72.

[113] I. Pane, W. Hansen, Early age creep and stress relaxation of concrete containing blended cements, Mater. Struct. 35 (2002) 92–96. doi:10.1617/13800.

[114] P.L. Domone, Uniaxial tensile creep and failure of concrete, Mag. Concr. Res. 26 (1974) 144–152. doi:10.1680/macr.1974.26.88.144.

[115] C. Mazzotti, M. Savoia, Experimental study of non-linear creep of concrete at high stress

level, in: Creep, Shrinkage Durab. Mech. Concr. Other Quasi-Brittle Mater., 2001.

[116] L. Zhaoxia, Effective creep Poisson's ratio for damaged concrete, Int. J. Fract. 66 (1994) 189–196. doi:10.1007/BF00020083.

[117] H. Umehara, T. Iisaka, T. Uehara, A. Sugiyame, Effect of creep in concrete at early ages on thermal stress, Therm. Crack. Concr. Early Ages. 1 (1995) 79–86.

CHAPTER 3:
MATERIALS AND METHODS

The investigation of the physical mechanisms at the origin of the development of the properties of cement based materials since the earliest age is not an easy task. However, for the sake of predictions of structural behaviour, measurement of these parameters at early age is of great interest [1,2]. That is why several devices allow already monitoring properties of cement based materials since setting or even before. Such methods are generally non-destructive and are needed for the study of an evolving material as concrete. From the experimental data, the concrete behavior is defined. These data can also be used to validate numerical models. For a good understanding of the physical mechanisms occurring at early age, several compositions are tested and are presented in the first section of this chapter. The existing method which has been developed in the past for the characterization of cement based materials and which has been used in this work are presented in the second section of this chapter. Finally the main principles of the experimental program are stated in the third section.

SECTION 3.1 – COMPOSITIONS AND MIXING PROCEDURE

Over a six years period, five phases of testing were performed to observe the influence of the age at loading, the water-cement ratio, the substitution of cement by slag and limestone filler on the early development of the free deformation and the viscoelastic properties of cement based materials. This work was also extended to the study of a very-high performance self-compacting concrete ('Mikti'), to concrete used for nuclear powerplant ('Vercors'), to multi-scale analysis and to tensile creep.

3.1.1. Ordinary concrete (OC)

The development of a new approach for the monitoring and the modeling of the early age properties of cement based materials was performed on an ordinary concrete which has already widely been studied experimentally at Ifsttar. This composition is called OC. The mix proportions are given in Table 1. All materials come from the same batch of production. An ordinary Portland cement of type CEMI 52.5 N was used. Its chemical composition is given in Table 2. Siliceous sand and gravel coming from Sandrancourt (France) were used. Sand and gravel were oven-dried. The coefficient of absorption of sand and gravel were determined by [3]. The effective water-to-cement ratio is 0.45. The initial and final setting times are defined by the criteria developed by Carette, *et al*. in [4,5] and based on the monitoring of the ultrasound P- and S-waves transmission through concrete. The same mixing procedure is used at Ifsttar and ULB and is as followed: gravel, sand and cement are mixed during (60 s) and then water is added (150 s mixing). The same speed is always applied (300 rpm).

Table 1 – Mixture proportions in kg/m³ and materials properties of the ordinary concrete.

Components	OC
CEMI 52.5 N – SR 3 CE PM-CP2 NF	340
Sand (Sandrancourt 0/4)	739
Gravel (Sandrancourt 6.3/20)	1072
Added water	184
W_{added}/C	0.54
W_{eff}/C	0.45
Slump class	S1
Paste Volume (L/m³)	260
$f_{c,1d}$ (MPa)	12
$f_{c,2d}$ (MPa)	22
$f_{c,28d}$ (MPa)	40
Initial setting time t_i (h)	5.7
Final setting time t_f (h)	6.7

Table 2 - Chemical composition of the cement of the ordinary concrete.

Element	Clinker	C_3S	C_2S	C_3A	C_4AF	MgO	Gypsum	Loss on ignition
Content (%)	98.5	62	16	2.1	15.2	1.1	2.4	0.9

3.1.2. Influence of the water-cement ratio and multi-scale analysis

The influence of the water-cement ratio is studied on three concretes with different water-cement ratio for which mix proportions are given in Table 3. For each composition, the aggregate content is the

same. Only the water and cement content are not the same. All materials come from the same batch of production. An ordinary Portland cement of type CEMI 52.5 N was used. Its chemical composition is given in Table 4. Sand and gravel were oven-dried. The effective water-to-cement ratio are 0.33 – 0.44 and 0.53. These compositions are respectively called C0.4, C0.5 and C0.6. The mixing procedure is the same for each concrete mixture and is as followed: gravel and sand are mixed during (20 s), 20% of water is added (20 s mixing), cement is added (30 s mixing) and then the rest of the water is added (150 s mixing). The same speed is always applied (300 rpm).

Table 3 - Mixture proportions (kg/m³) and materials properties of the concretes, mortars and cement pastes

	P0.3	P0.4	P0.5	P SCM	M0.3	M0.4	M0.5	M0.6	M SCM	C0.4	C0.5	C0.6	C SCM
Sand 0/4	-	-	-	-	1339	1339	1339	1339	1339	853	853	853	853
Gravel 6/10	-	-	-	-	-	-	-	-	-	210	210	210	210
Gravel 10/14	-	-	-	-	-	-	-	-	-	873	873	873	873
CEMI 52.5 N CE CP2 NF	1620	1394	1223	333	789	679	596	531	162	432	379	338	103
BFS	-	-	-	528	-	-	-	-	257	-	-	-	164
LMF	-	-	-	400	-	-	-	-	195	-	-	-	124
Gypsum	-	-	-	71	-	-	-	-	35	-	-	-	22
Added water	486	558	612	533	237	271	298	318	260	173	190	203	165
Wabs/B [/]	0.30	0.40	0.50	0.40	0.30	0.40	0.50	0.60	0.40	0.40	0.50	0.60	0.40
Weff/B [/]	0.30	0.40	0.50	0.40	0.27	0.36	0.46	0.55	0.36	0.35	0.44	0.53	0.34
t_i (h)	4.7	6.3	6.6	3.8	3.2	4.1	5.0	5.7	5.9	3.5	4.3	3.8	4.6
t_f (h)	5.8	7.2	8.3	11.6	3.9	5.1	6.2	7.1	8.6	4.1	5.2	5.5	6.7

For multi-scale analysis, the study is extended to mortars and cement pastes. On mortars, four compositions with different water-cement ratio (Table 3) are tested. For each composition, the sand content is the same and the volume ratio between the sand and the binder is the kept constant. The determination of the mix proportions are done without the consideration of the absorption of water by the gravel 6/10 (0.63% as coefficient of absorption), the gravel 10/14 (0.57% as coefficient of absorption) and the sand (1.99% as coefficient of absorption). Per consequent, the effective water-cement ratios are slightly different from the concrete compositions: 0.27 – 0.36 – 0.46 and 0.55. The mixing procedure corresponds to the one of concrete compositions. These compositions are respectively called M0.3, M0.4, M0.5 and M0.6. For cement pastes, three compositions with different water-cement ratio (Table 3) are tested. For each composition, the water-cement ratios are: 0.3 – 0.4 and 0.5. These compositions are respectively called CP0.3, CP0.4 and CP0.5. The mixing procedure is the same for each cement paste mixture and has duration of 2 minutes. This study is also extended to an eco-concrete called CSCM which corresponds to the composition C0.4 for which the cement is replaced by blast furnace slag (BFS) at 50% and by limestone filler (LMF) at 25%. This concrete was partially characterized during the PhD thesis of Jérôme Carette [6]. An equivalent mortar and cement paste are also tested for multi-scale study. These compositions are respectively called MSCM and CPSCM. According to the scale of the composition, a same mixing procedure is used as the compositions with different water-cement ratio. The chemical composition of the slag and the limestone filler is given in Table 4.

Table 4 - Chemical composition of the cement, slag, limestone filler and gypsum [7]

		CEM I	BFS	LMF	Gypsum
C2S	[%]	12.6	–	–	–
C3S	[%]	63.49	–	–	–
C3A	[%]	8.09	–	–	–
C4AF	[%]	9.8	–	–	–
SiO2	[%]	20.12	33.3	–	–
Al2O3	[%]	5.03	12.5	–	–
CaO	[%]	64.53	41.5	–	–
MgO	[%]	0.98	7	–	–
CaCO3	[%]	–	–	98	–
CaSO4	[%]	4.5	–	–	100
SO3	[%]	3.36	0.16	0.00	-
Blaine	[cm2/g]	365	450	647	354
Density	[kg/m3]	3.15	2.89	2.71	2.3

3.1.3. Very High Performance self-compacting Concrete

In the frame of the French national project “Mikti”, a very-high performance self-compacting concrete was designed in 2005 [8] for pre-cambered beams. The Mikti composition has widely been studied experimentally at LCPC (now IFSTTAR). A compressive strength of 99 MPa is obtained at 28 days. The mix proportions are given in Table 5. All materials come from the same batch of production. An ordinary Portland cement of type CEMI 52.5 N was used. Siliceous-calcareous sand coming from Sandrancourt (France) and limestone sand and gravel coming from the quarry “Boulonnais” (France) were used. Sand and gravel were oven-dried.

Table 5 – Mixture proportions in kg/m³ and materials properties of the Mikti composition

Gravel Boulonnais limestone 4 to 12,5 mm 0.920	920
Sand 1 Boulonnais limestone 0 to 4 mm 0.379	379
Sand 2 Silico-calcareous sand from river Seine 0 to 4 mm 0.369	369
Cement CEM I 52,5N "Bussac" 0.500	500
Silica fume SEPR 0.050	50
Superplasticizer Optima 175 0.010	10
Water added 0.165	165
total mass	2393
Slump flow [cm]	70
Air content [%]	1.8
$f_{c,1d}$ (MPa)	50
$f_{c,2d}$ (MPa)	67
$f_{c,28d}$ (MPa)	99
t_i (h)	10.4
t_f (h)	11.4

3.1.4. Concrete of nuclear power plant

In the context of the 'Vercors' (French acronym of "Verification Réaliste du Confinement des RéacteurS") project of EDF [9], a concrete used for nuclear power plant is tested and is called V-OC. The mix proportions are given in Table 6. All materials come from the same batch of production. An ordinary Portland cement of type CEMI 52.5 N was used. Its chemical composition is given in

Table 7. Siliceous sand from Sandrancourt (France) and siliceous-calcareous gravels were used. Sand was oven-dried. The effective water-to-cement ratio is 0.52. The same mixing procedure is as followed [11]: gravel and sand are mixed during (30 s), cement is added (30 s mixing) and then the water and plasticizer are added (150 s mixing). The same speed is always applied (300 rpm).

Table 6 - Mixture proportions in kg/m³ and materials properties of the composition V-OC

	V-OC
Cement CEM I 52,5 N CE CP2 NF Gaurain	320
Sand 0/4 REC GSM LGP1 (13% of CaO and 72% of SiO2)	830
Gravel 1 : 4/11 R GSM LGP1 (rounded, containing silicate and limestone)	446
Gravel 2 : 8/16 R Balloy (rounded, containing silicate and limestone)	551
Sp (SIKAPLAST techno 80)	2.5
Added water*	171
W_{eff}/C	0.52
$f_{c,1d}$ (MPa)	12
$f_{c,2d}$ (MPa)	21
$f_{c,28d}$ (MPa)	42
t_i (h)	10.4
t_f (h)	11.5

*Added water = Effective water (obtained from Weff/C ratio) – 0.8*amount of P (80% of P mass is water) + water theoretically absorbed by the sand (0.77% as coefficient of absorption).

Table 7 - Chemical composition of the cement.

Element	Clinker	C_3S	C_2S	C_3A	C_4AF	MgO	Gypsum	Loss on ignition	Limestone
Content (%)	96	68	10	9	7	2.2	3.3	2.1	4

3.1.5. Concrete with high substitution of slag

Finally, for the study of the effect of the replacement of cement by slag a last composition is tested and is called CBFS. The mixture proportions were designed in [6] and are presented in Table 8. This composition corresponds to the composition C0.4 for which the cement is substituted by blast furnace slag (BFS) at 75%. The same mixing procedure as C0.4 is used

Table 8 - Mixture proportions in kg/m³ and materials properties of the composition CBFS [12]

Sand 0/4	853
Gravel 6/10	210
Gravel 10/14	873
CEMI 52.5 N CE CP2 NF	103
BFS	291
Gypsum	22
Added water	167
Wabs/B [/]	0.40
Weff/B [/]	0.34
t_i (h)	6.1
t_f (h)	8.5

SECTION 3.2 – TEST METHODS

3.2.1. Compressive strength

Compressive strength f_c was measured from the setting to the hardened state and up to 28 days of age or even more for some compositions. Compressive strength is measured on cylinders on cubes. However, cylinders are not efficient for very early age measurements since they require non-destructive rectification methods such as surfacing with a fast-setting mortar, which is time-consuming and induces significant delay before the first measurements can be performed. During the sample preparation, the concrete is exposed to the environment and drying occurs which could lead to a small artifact in the determination of the compressive strength at very early age. In addition, any rectification method can sometimes lead to non-parallel opposite facets, and therefore to a non-homogenous distribution of stresses in the cylinder and to invalid compressive strength values. An alternative consists in testing cubic samples. Given that the moulds are designed for this purpose, this method ensures that at least two facets are parallel to their opposite. No additional treatment is needed, making early age testing considered as soon as careful unmoulding is possible without damaging the sample, which generally occurs between the initial and the final setting. Due to the effect of boundary conditions (confinement induced by restrain to transversal contraction), that cannot be neglected when the slenderness ratio is equal to one, of cubic samples in comparison with cylinders, higher compressive strengths are generally obtained. Torenti & Royis [13] show that the difference is mainly due to the friction at the interface between the concrete and the steel plates of the testing machine. It was numerically shown that for such typical setups, the cylinder/cube compressive strength (for the same contact area) is 0.78 [14]. According to the EN 206-1 classification of hardened concrete, depending on the class of strength, this ratio is in average 0.82 [15].

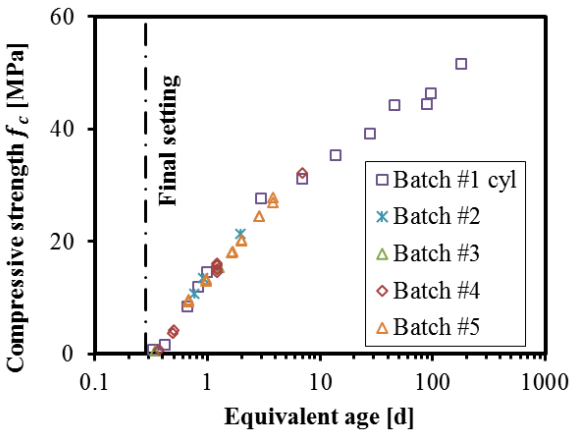

Figure 1 – Comparison between compressive strength results obtained on cylinders (110x220 mm) and cubes (100x100x100 mm) after applying a factor 0.79 on cubes results

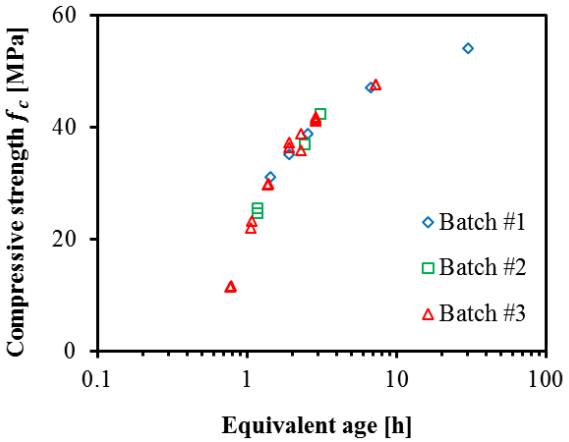

Figure 2 - Comparison between compressive strength results obtained on cubes 50x50x50 mm and cubes 100x100x100 mm after applying a factor 0.935 on cubes results 50x50x50 mm.

The dimension of the sample depends on the scale of the material. For concrete, the results are obtained on 110x220 mm cylinders and 100x100x100 mm cubes. For mortars, results are obtained on 100x100x100 mm and 50x50x50 mm cubes. And tests on cement pastes are performed with 50x50x50 mm cubes. For each compressive strength tests, a thermocouple is placed in the middle of the sample in order to consider temperature effect on the maturity of the sample. From measurements, the ratio cubes (100x100x100 mm)/cylinders is 0.79 and could be used independently of the concrete composition and of the hydration degree. The compressive strength results were obtained mainly on

cubes, but will be expressed as equivalent cylinder strength (Equation 1). For the ordinary concrete, Figure 1 shows the results of the compressive strength on cylinders and cubes after using the factor 0.79 on cubes results. A conversion factor of 0.935 is used between cubes 50x50x50 and 100x100x100. The Figure 2 presents results on the composition M0.4 and shows that this factor could be used independently of the age of the material.

$$f_c = f_{c,cyl} = 0.79 f_{c,cube10} = 0.79 * 0.935 * f_{c,cube5} \quad (1)$$

For each test, a hydraulic press Galdabini of 3000 kN is used. The sensitivity of the device is 1 kN. The same press is used for splitting tensile strength test.

3.2.2. Tensile strength

The determination of the tensile strength f_t parameter was made by splitting tensile tests. Such tests are more easily performed than uniaxial (or direct) tensile tests as they only require a cylinder sample with no need to use a specific anchorage system. However, such indirect measurements cannot be directly correlated with the direct tensile strength. It is often considered that f_t is 10% lower than f_{ts}. The splitting tensile strength f_{ts} can be obtained through the following formula which derives from the theory of elasticity, with F the measured peak load [kN], D the sample diameter [cm], and L the length of the specimen [cm]:

$$f_t = 0.9 f_{ts} = 0.9 \frac{20.F}{\pi.D.L} \quad (2)$$

For concrete, cylinders with a dimension of 110x110 mm are used (Figure 3).

Figure 3 – Splitting tensile test on the Vercors concrete.

3.2.3. Heat release

Isothermal calorimetry allows a continuous measurement of hydration heat. The device used for this purpose is the TAM Air micro-calorimeter. It contains eight measuring channels, allowing parallel measurement of eight different samples. Working in isothermal conditions annihilates the entrapment of heat and thus separates the combined effects of hydration and increased curing temperature. The data obtained from this type of experiment is the exothermal heat flow q [J/g/h] generated by the sample. The integration of the heat flow yields the cumulated heat Q [J/g].

$$Q(t) = \int_0^t q(t).dt \quad (3)$$

Based on this measurement, the advancement degree of reaction can be defined according to Equation 3. The duration of the isothermal calorimetric tests is limited in time since its accuracy becomes limited as the heat flow decreases. Isothermal calorimetry tests were performed on 20g mortar samples.

3.2.4. Monitoring of the setting

Three devices were used for the determination of the setting. According to the standards, the ASTM C403 standard [16] can be used on mortar and sieved concrete (Figure 4). The initial and final setting time are defined as the time when the penetration resistance reaches respectively 3.5 MPa and 27.6 MPa. These tests are performed in three 150 × 150 × 150 mm plastic sealed cubes for each concrete mix. A thermocouple was placed in the centre of one of the three samples to record the temperature evolution [5]. The European standard EN 196-3 [17] is used on cement pastes. The initial setting time is reached when the hint stops at a distance of 6mm from the bottom plate. The final setting is determined with a specific needle composed of a hint and a circle around it. The test is performed on the back of the sample (turned upside down for compaction matters) and is positive when the hint makes a mark but not the circle. Both approaches are qualitative and results depend of threshold values defined by the standard. In addition, for the Vicat test, the initial and final setting time depends on the weight of the needle.

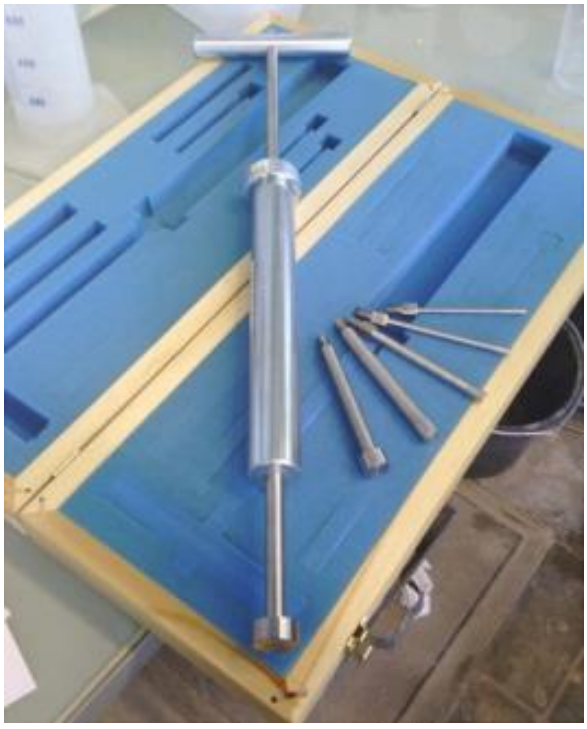

Figure 4 – Penetration resistance test [17]

Figure 5 – Vicat test needle

The P-wave and S-wave transmission was measured with a FreshCon system (Figure 6) developed at the University of Stuttgart [18]. For P-waves transmission velocity, this device has already been used in several studies. Each of the two wave types were simultaneously measured on separate moulds. Every minute, a 5 μs pulse is sent through the sample by a piezoelectric broadband transmitter (centre frequency of 0.5 MHz and 0.25 MHz fpr the P- and S-wave respectively). A similar sensor situated on the other side of the sample transmits the signal to a computer through a DAQ card. The sensors are semi-embedded inside the concrete and overstep the surface of the walls by approximately 1.5 mm

each. The optimal distance between sensors is the result of a compromise between the signal/noise ratio and the accuracy on the velocity.

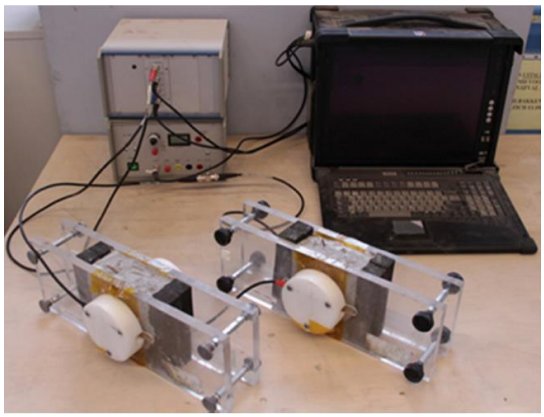


Figure 6 – FreshCon system and mould used for cement paste, mortar and concrete.

Depending on the mixture studied, an adequate mold is chosen in order to reduce the increase of temperature inside the mixture. Different types (see Figure 6) and dimensions (see Table 9) of the molds are depicted below.

Table 9 – Dimension of the FreshCon mould according to the scale of the material

		Cement Paste	Mortar	Concrete
Thickness	[cm]	2.5	5	5
Width	[cm]	10	11	10
Heigth	[cm]	11	11	10

3.2.5. Autogenous strain measurement

► BTJADE

The free deformation of concrete and mortar is measured from casting using the BTJADE (from the French acronym 'BéTon au Jeune Age, Déformation Endogène') device designed at IFSTTAR by Claude Boulay [19]. The test rig (Figure 7) is composed of a vertical flexible corrugated PVC mould to monitor the free deformation and fixed metallic parts. The whole frame is placed in a temperature controlled bath and is designed to accommodate 3 tests rigs simultaneously. The sensors for each channel are the central displacement, the temperature of the sample with a thermocouple, the temperature of the surrounding water in the tank with a platinum probe and the temperature in the air above the cover of the tank, near the displacement transducer, with a platinum probe also. For a good consideration of the heterogeneity of the concrete, the diameter of the cylinder has to be greater than the coarse aggregate (a factor 5 is a minimum). For that reason, a diameter of 125 mm is used. The base length of the sample is approximately 225 mm. More details about the BTJADE are given in [19].

When measurements are done, free deformation of the concrete is defined by removing the influence of the temperature variations itself inside the tank and the influence of the temperature of the room on the displacement transducer located above the cover of the tank. As the test is carried out in sealed condition, the free deformation corresponds to the sum of the autogenous deformation and the thermal deformation. Therefore the total deformation of the concrete ε_{tot} (m/m) is defined according to Equation 4.

$$\varepsilon_{tot} = \varepsilon_{au} + \alpha_c . \Delta T_c = \frac{\Delta L}{L_0} - \alpha_{wt} . \Delta T_{wt} - \alpha_{at} . \Delta T_{at} \quad 4$$

where ΔL is the displacement measured by the displacement sensor (mm), ε_{au} is the autogenous strain (m/m), α_c is the coefficient of thermal expansion of the concrete (m/m/°C), ΔT_c is the thermal variation of the concrete, the index wt is related to the thermal variation of the water in the tank and the index at is related to the thermal variation of the air above the cover of the tank.

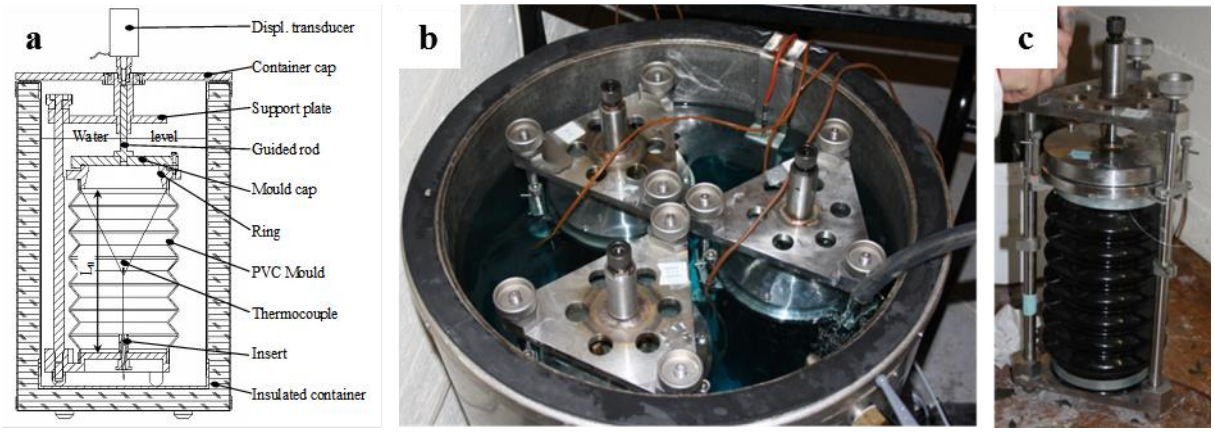

Figure 7 - BTJADE test set up – section of the whole test setup (a) – water tank with three tests rigs [19] (b) – test rig before introduction in the water tank (c).

► AUTOSHRINK

The free deformation of cement paste and mortar is measured from casting using the Autoshrink device [20]. The test rig is composed of a horizontal flexible corrugated PE mould to monitor the free deformation and fixed metallic parts. The device is designed to accommodate 3 samples simultaneously. For each sample, one sensor is used to monitor the total displacement of the sample. The diameter of the sample is 30 mm and the base length is 400 mm. More details about the autoshrink are given in [20].

► Comparison

BTJADE and AUTOSHRINK can be used to monitor the autogenous strain of a mortar. For multi-scale experimental analysis, preliminary tests were performed on a same mortar from the same batch in order to compare results from both devices. Autogenous strains are set to zeros at the final setting time. Results from this comparison are shown in Figure 8. During the first hours after setting, results evolve similarly. When swelling occurs, a high difference in term of magnitude is observed (around 40 µm/m). The peak of swelling appears at the same equivalent age for both devices. At an age of around 32 hours, results are again similar. Then the evolution of the autogenous strain evolves with a very similar trend. Therefore, the main difference between both devices occurs during the swelling period between an age of 10 and 32 hours. This difference can be explained by the position of the displacement sensor. With the BTJADE, a vertical displacement is measured whereas with AUTOSHRINK a horizontal displacement is measured. As explained in chapter 2, swelling can be linked to the excess of water coming from bleeding or the aggregate. If swelling is related to the bleeding of the cement paste, therefore this effect will be localized on the top of the sample and will be mostly measured in the vertical direction. After the peak of swelling, when self-desiccation starts significantly, the distribution of water is therefore not uniform inside the sample of the BTJADE. Consequently, it is possible that the self-desiccation will be higher on the bottom of the sample. While, for the AUTOSHRINK sample, the water distribution is quite uniform due to the low diameter and the horizontal position of the sample. This uniform distribution of water in the sample cans results

as a lower evolution of the self-desiccation than in the BTJADE. However this explanation is just an interpretation of the difference observed. Information about the distribution of the relative humidity inside the sample is needed in order to prove such affirmation.

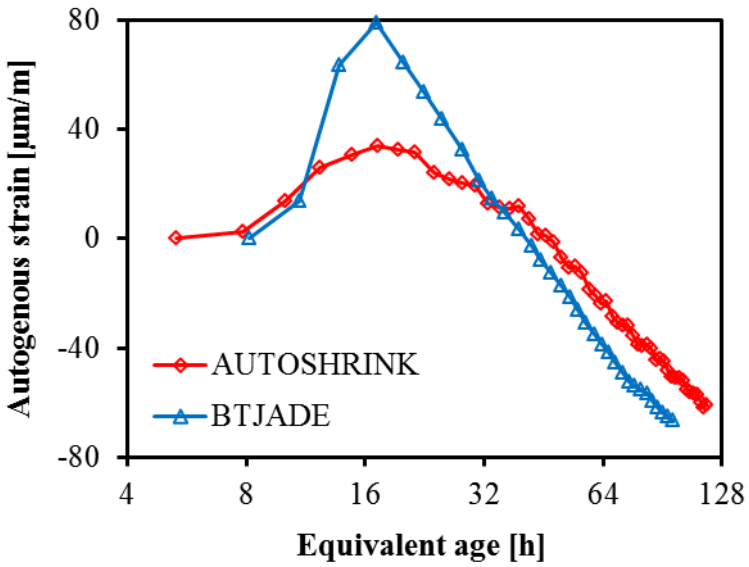

Figure 8 – Comparison between results from BTJADE and AUTOSHRINK on composition M0.4.

SECTION 3.3 – EXPERIMENTAL PROGRAM

Tests methods are presented, aiming at allowing a description of some concrete properties from the time of mixing to the hardened state (compressive strength, tensile strength, heat release, setting and autogenous strain). The chapter 4 presents devices and test protocols which are developed to monitor automatically the evolution of the free deformation and the viscoelastic behavior of cement based materials. All results become from the same concrete composition (OC).

The chapter 5 is an extension of the use of ultrasonic technics for the monitoring of the setting of cement pastes.

The test methodology defined in the chapter 4 is extended to:

- The effect of the water-cement ratio on the early age properties in the chapter 6 with the composition C0.4, C0.5 and C0.6.
- The effect of the substitution of cement by slag and limestone filler in the chapter 7 with the composition C0.4, CSCM and CBFS. In addition the method will be also extended to an Very High Performance self-consistant Concrete: Mikti.
- The study of the multi-scale behavior of concrete C0.4, C0.5, C0.6 and CSCM with their equivalent mortars and cement pastes in chapter 8.

The last chapter concerns the comparison between the tensile and compressive creep of several compositions: OC, OM, V-OC, V-MOC, V-MOM and Mikti.

REFERENCES

[1] Tailhan J.L., Dal Pont S., Rossi P., From local to global probalistic modeling of concrete cracking, Ann. Solid Struct. Mech. 1 (2010) 103–105.

[2] Dal Pont S., Meftah F., Schrefler B.A., Modeling concrete under severe conditions as a mutliphases material, Nucl. Eng. Des. 241 (2011) 562–572.

[3] NF EN 1097-6 : 2014, Essais pour déterminer les caractéristiques mécaniques et physiques des granulats ; Partie 6 : détermination de la masse volumique réelle et du coefficient d'absorption d'eau, (2014).

[4] J. Carette, S. Staquet, Monitoring the setting process of mortars by ultrasonic P and S-wave transmission velocity measurement, Constr. Build. Mater. 94 (2015) 196–208. doi:10.1016/j.conbuildmat.2015.06.054.

[5] J. Carette, S. Staquet, Monitoring the setting process of eco-binders by ultrasonic P-wave and S-wave transmission velocity measurement: Mortar vs concrete, Constr. Build. Mater. 110 (2016) 32–41. doi:10.1016/j.conbuildmat.2016.02.019.

[6] J. Carette, Towards Early Age Characterization of Eco-Concrete containing blast-furnace slag and limestone filler, PhD thesis, ULB-BATir, Brussel, Belgium, 2015.

[7] J. Carette, S. Staquet, Monitoring and modelling the early age and hardening behaviour of eco-concrete through continuous non-destructive measurements: Part I. Hydration and apparent activation energy, Cem. Concr. Compos. 73 (2016) 10–18. doi:10.1016/j.cemconcomp.2016.07.002.

[8] S. Staquet, L. Lauvin, J.-C. Renaud, S. Dubroca, F. Toutlemonde, Expérimentation sur poutres préfléchies à talon BTHP, Paris, 2005.

[9] EDF, http://researchers.edf.com/research-activities/generation/vercors-an-experimental-mock-up-of-a-reactor-containment-building-290900.html, (n.d.).

[10] COST Action TU 1404, TOWARDS THE NEXT GENERATION OF STANDARDS FOR SERVICE LIFE OF CEMENT-BASED MATERIALS AND STRUCTURES, (n.d.). http://www.tu1404.eu/ (accessed October 18, 2016).

[11] COST Action TU 1404, RRT+ Extended Round Robin Testing programme for TU1404, 2015.

[12] J. Carette, S. Staquet, Monitoring and modelling the early age and hardening behaviour of eco-concrete through continuous non-destructive measurements: Part II. Mechanical behaviour, Cem. Concr. Compos. 73 (2016) 1–9. doi:10.1016/j.cemconcomp.2016.07.003.

[13] J.-M. Torrenti, P. Royis, Etude numérique du dimensionnement d'un appui anti-frettage pour le béton, Mater. Struct. Constr. 22 (1989) 149–158.

[14] F. Indelicato, M. Paggi, Specimen shape and the problem of contact in the assessment of concrete compressive strength, Mater. Struct. 41 (2007) 431–441. doi:10.1617/s11527-007-9256-7.

[15] EN 206-1, Concrete - Part 1: Specification, performance, production and conformity, (2000) 1–72.

[16] ASTM C403, Standard test method for time of setting of concrete mixtures by penetration resistance, in: Am. Soc. Test. Mater., 2008. doi:10.1520/C0403_C0403M-08.

[17] EN 196-3:2005, Methods of testing cement. Determination of setting times and soundness,

2005.

[18] H.W. Reinhardt, C.U. Grosse, Continuous monitoring of setting and hardening of mortar and concrete, Constr. Build. Mater. 18 (2004) 145–154. doi:10.1016/j.conbuildmat.2003.10.002.

[19] C. Boulay, Test rig for early age measurements of the autogenous shrinkage of a concrete, in: Proc. RILEM-JCJ Int. Work. ConCrack 3, 2012: pp. 111–122.

[20] O. Mejlhede Jensen, P. Freiesleben Hansen, A dilatometer for measuring autogenous deformation in hardening portland cement paste, Mater. Struct. 28 (1995) 406–409. doi:10.1007/BF02473076.

CHAPTER 4:
DEVELOPMENT OF AN EXPERIMENTAL STRATEGY FOR THE MONITORING AND THE MODELLING OF CEMENT BASED MATERIALS.

In order to understand the evolution of the free deformation and the viscoelastic behaviour of cement based materials, several tests have been performed, and thus different tests procedure have been developed and described in the literature. The free deformations occurring in sealed condition are divided in two parts: the autogenous and the thermal deformation. These properties depend on several parameters as indicated in chapter 3. Moreover these properties are very sensitive to the conditions of preservation of the specimen and to many factors related to the test rig. For that reason several recommendations where developed in the past [1–4]. The main common requirements for all the apparatus for free deformation test in sealed condition are their ability to:

- perfectly seal the specimen in order to avoid any external drying or water uptake;
- keep the temperature constant, which requires external control because the hydration of cement paste releases heat;
- limit the friction with the specimen.

The viscoelastic behaviour of cement based materials in sealed condition is composed of two parameters: the elastic modulus and the basic creep coefficient. These properties depend on several parameters as indicated in chapter 3. Moreover the creep properties are very sensitive to the conditions of preservation of the specimen during the test and to many factors related to the test rig. For that reason several recommendations where developed in the past. For both properties, recommendations [5–7] were developed for hardened concrete. Currently no recommendation or standard test method exists for the determination of the elastic modulus and the basic creep for concrete at very early age. The main common requirements for all the apparatus for testing elastic modulus and basic creep in sealed condition are their ability to:

- ensure uniform stress distribution over the cross section of the specimen;
- apply a load very quickly;
- operate in a room with controlled temperature and humidity;
- maintain a constant known load during the whole testing period.

In addition, the measurement of the strain must be carried out in the central part of the specimen in order to eliminate the edge effects. As for the measurement of the free deformations, the specimen must be perfectly sealed to avoid any external drying or water uptake.

For the purpose of performing a monitoring of the free deformation and the viscoelastic properties of cement based materials since setting time, a new testing equipment and a new testing protocol were designed at ULB and at Ifsttar.

For the development of this new tests procedure, an ordinary concrete is used. The main advantages of this ordinary concrete are:

- The water-cement ratio of the ordinary concrete is high, which limits the shrinkage development during the creep tests and thus limits the error which occurs when the free deformation are subtracted from the total strain in order to obtain the mechanical strain composed by the elastic and creep strain.
- The heat release by the cement paste is quite low during the very early age which limits the development of the temperature in the specimen during the test.
- This composition uses only a classical Portland cement without any mineral addition, making easier the understanding of the physical mechanisms during the hydration process.
- No superplasticizer is used in this composition, making also easier the understanding of what happens at very early age.

The testing and modelling strategy developed in this chapter is then extended in the next chapters to several other compositions for which the water-cement ratio or the nature of the binder are significantly different from this ordinary concrete. The extension to such composition will allow validating the testing and modelling strategy developed in this chapter.

Therefore this chapter is organized in 6 sections. The development of a new methodology for the monitoring of the free deformation is presented in the first section.

The description of the new developed experimental equipment for the monitoring of the viscoelastic properties is given in sections 2 and 3. Section 2 is related to the new advances in the design of a TSTM device at ULB. Section 3 presents the existing tensile creep rigs and the choice carried out for the design of the new tensile creep rigs developed at ULB.

The section 4 presents the development of a new testing procedure for the monitoring of the static elastic modulus since casting (Ifsttar) or since setting time (ULB). Results obtained on the ordinary concrete are presented.

Results from section 4 are compared to new testing methodology based on the dynamic response of a system to ambient vibration (EMM-ARM) and to ultrasonic testing methods (FreshCon, BTPULSE and embedded piezoelectric transducers) in section 5. For this comparison, the effect of the magnitude of loading and the loading rate are tested and modelled.

The sections 6 and 7 present new advances of the monitoring and the modelling of the basic creep. In section 6 a new protocol of loading is developed. This protocol is based on a coupling between a repeated minute-long loading tests and basic creep tests of long duration. Based on the experimental results and the observations made in section 6, the section 7 presents a new approach for the modelling of the basic creep since setting time.

SECTION 4.1 – CHARACTERIZATION OF THE FREE DEFORMATIONS OF CEMENT BASED MATERIALS SINCE CASTING.

At early age, the autogenous deformation and the coefficient of thermal expansion (CTE) are two of the most important concrete properties that are responsible of volume changes of cement based materials and therefore to possible cracking in concrete structures (especially for massive structure). A new experimental approach is developed at ULB to define both properties with a single test.

This first part of this section presents the existing method for the monitoring of the autogenous strain and the CTE and the key points in the development of a test protocol for the characterization of both properties. The second part of this section presents the new protocol of the test developed. The results obtained on an ordinary concrete with the BTJADE [8] device are presented in the third part of the section. Finally, an extension of this methodology on cement paste and mortar is presented.

4.1.1. Existing methods

Several devices aimed at monitoring the thermal and autogenous deformations were developed in the past. The methods can be in general divided in two categories: linear [8–15] and volumetric [12,16–22]. Whereas volumetric methods are mainly used on cement pastes and mortars, the linear methods have been used on three scales including concrete. Horizontal and vertical setups have been designed. Both methods can be divided into two groups: rigid moulds and flexible moulds. Rigid moulds have been reported to underestimate the magnitude of autogenous shrinkage because of friction between the specimen and the mould. It is assumed that volumetric free deformations are isotropic. Thus volumetric free deformation corresponds to three times of the linear one. However, no clear evidence of this relation has been shown in the literature till now. This could be explained to the different artifact of measurement coming from volumetric and linear methods. In the linear method, elongation and shortening of the sample is monitored with either direct measurement of the sample length change or by displacement measurement with e.g. LVDT, strain gauges [23]. For correct consideration of the temperature variation, it is needed to have knowledge in depth of the thermal sensitivity of the test rig. The volume change of the cement paste or mortar is monitored by using hydrostatic weighing method. The sample is immersed in a bath containing liquid of known density and is supported to a balance. The volume change is measured through the apparent mass changes of the immersed sample. This method was significantly improved during the last decade in order to remove artifacts coming from the absorption of the water by the membrane [17], the liquid used for the thermal regulation [24], bleeding of the cement paste [25].

Several authors have developed different methodologies to assess the CTE and the autogenous deformations [23]. A first method consists in removing the autogenous deformation by differences between two samples subjected to two histories of temperature. For that it is needed to take into account the maturity of both samples when autogenous deformations are eliminated [26]. However, the temperature has an effect on the evolution of the autogenous deformation and the CTE. Thus it is needed to have very close temperature histories which lead to a lack of accuracy in the determination of the CTE [23]. The second method uses only one sample on which thermal variations are applied [27]. Several protocols and mathematical treatments were developed for the determination of the CTE. In Table 1, the parameter of several test protocols coming from the literature are presented. The main variations in the protocol come from:

- The amplitude of the thermal variation (ΔT)
- The duration of the isothermal phase (Δt)
- The nature of the material tested (cement paste (CP, mortar (M) or concrete (C))
- The evolution of the temperature between the different cycles (sinusoidal variation of the temperature, thermal variation around a constant temperature, thermal variation around a temperature history corresponding to the evolution of the temperature in a massive structure).

Table 1 – Parameters of test protocols for the determination of the CTE and the autogenous deformation by using only one sample.

References	ΔT, °C	Δt, min	Kind of device	Remark
[20–22]	6	90	Volumetric (CP & M)	-
[28,29]	5	240	Linear (C)	-
[30]	7	N.A.*	Linear (C)	Sinusoidal variation
[31]	5	N.A.	Linear (CP)	Isothermal and various temperature histories
[32]	6	120	Linear (C)	
*N.A. = not available				

The mathematical treatment used for the characterization of the autogenous deformation and the CTE is generally realized in two steps. First the autogenous strains are defined by consideration of the value of the total concrete strain obtained when the temperature is constant inside the sample. When considering all these values at the same temperature, autogenous strains correspond to the interpolate value obtained between each plateau in temperature. Then the CTE is defined by removing the autogenous strains from the total concrete strain. An example of such method is presented in Figure 1 for volumetric method [20]. This method has the disadvantage to not correctly consider the thermal variation of the sample due to the heat release during the hydration process. Indeed, it is assumed that autogenous strains correspond directly to the value obtained at each plateau of temperature without consideration of the thermal variation due to hydration process.

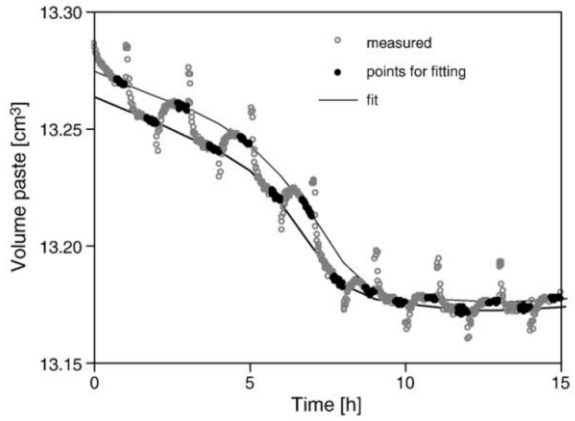

Figure 1 – Fitting of the autogenous strain by taking into account values of the volume of the cement paste obtained at the end of the plateau in temperature for volumetric method [15].

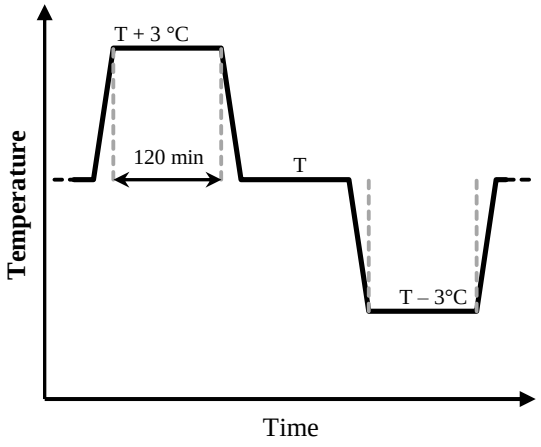

Figure 2 – Test protocol

Recently, Zhutovsky, *et al.* [33] have developed a new methodology based on ultrasonic pulse velocity measurement for the assessment of the coefficient of thermal expansion. The calculation of the CTE is based on poromechanics theory. However, this method does not consider the self-desiccation of the material and thus the increase of the coefficient of thermal expansion which leads to an underestimation of the CTE and therefore to an underestimation of the tensile stress when concrete displacements are restrained.

4.1.2. New protocol of test

During hydration process, both autogenous and thermal strains occur simultaneously and cannot be directly distinguished. A new experimental protocol and a new mathematical analysis strategy were defined to characterize the autogenous deformation and the coefficient of thermal expansion during the same single test. This new methodology considers correctly the evolution of the autogenous strain when the thermal variation due to hydration occurs.

The thermal variations must be designed by optimizing the three following parameters: the duration of the temperature increase, the thermal variation amplitude and the duration of the isothermal phase in the tank. The duration of the temperature increase in the tank must be as fast as possible in order to minimize concrete autogenous deformation amplitude between two sets of measurements. The thermal variations amplitude must be high enough to allow measuring significant displacement (digital displacement transducer with accuracy of 1 µm over the whole stroke). The duration of the isothermal phase in the tank must be high enough to avoid any thermal gradient inside the concrete sample at the end of the plateau of temperature.

Several preliminary tests were performed on hardened concrete with the BTJADE [8] device in order to optimize these parameters. The test protocol is presented in Figure 2. The recording of data provided by each thermal and displacement sensor is done every minute. The phase of temperature increase is limited to 10 min; the magnitude of the temperature variation is +/- 3°C and the duration of the isothermal phase is 120 min. Temperature stabilization in the concrete is well reached after 120 min. At this period, an identical temperature is measured in the tank and in the concrete sample for hardened concrete as shown in Figure 3.

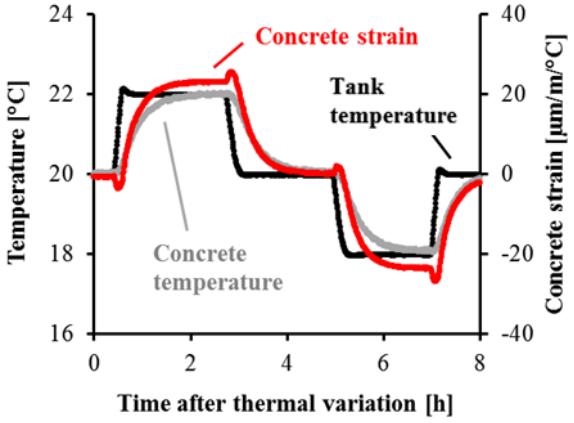

Figure 3 – Preliminary test on hardened concrete.

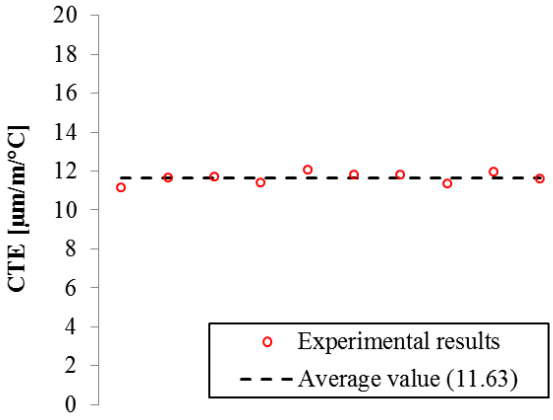

Figure 4 – Results of the CTE for a hardened concrete.

Therefore no thermal gradient occurs at the end of the plateau of temperature. 10 cycles were performed on this hardened concrete for which it is assumed that no significant autogenous strain

occurs (the age of the sample was higher than one month at the start of the test). Results of the CTE are presented inFigure 4. An average value of 11.6 µm/m/°C is obtained. The minimal value is 11.1 µm/m/°C and the maximal value is 12.0 µm/m/°C. The standard deviation is very low and is equal to 0.3 µm/m/°C which corresponds to 2.3% of the average value of the CTE Through these results, it is concluded that such protocol is enough accurate for the assessment of the CTE on hardened concrete. As the variation of the thermal conductivity with aging of concrete is limited [34,35], it is assumed that no thermal gradient occurs because of the temperature variation in the tank during the hardening process of the concrete. The thermal gradient due to the hydration is assumed to be unchanged.

This last assumption is checked with the realization of two tests for which the temperature histories are different. For the first test, a constant temperature of 20°C is imposed. The second test uses the protocol of temperature illustrated previously in Figure 2. For each test, two test rigs are used in order to assure the repeatability of the results. For a good comparison, both tests use a concrete coming from the same batch. The scheme of the experiment is presented in Figure 5.

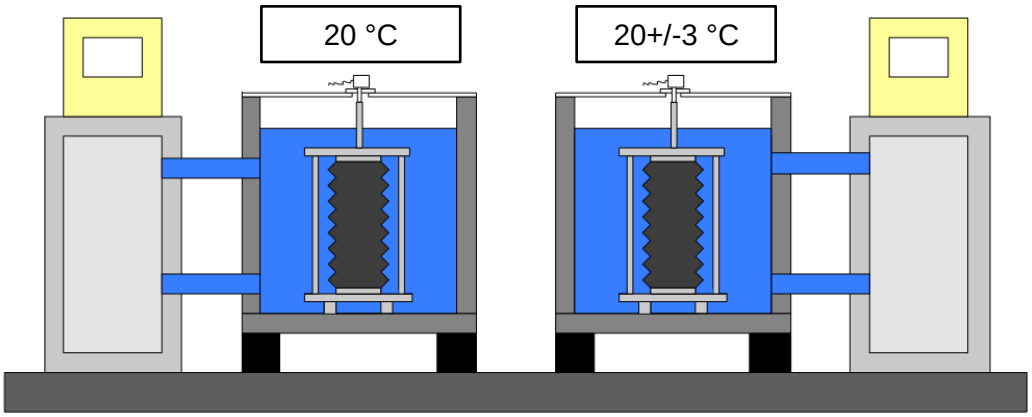

Figure 5 – Scheme of the experiment

The test starts approximately 1 hour after mixing. Results related to the evolution of the temperature at early age are presented in Figure 6 and Figure 7. Figure 6 shows the evolution of the temperature in the water tank and inside the sample. For each thermal variation, the temperature of the sample reaches the temperature imposed by the thermal regulation. At the end of the plateau of temperature, the temperature is stable in the sample. In Figure 7, the temperature inside samples from both tests is compared. Moreover the comparison is extended to two additional curves which correspond to the temperature of the sample with a constant thermal cure of 20°C on which an addition or a subtraction of 3°C is operated. For each end of plateau of temperature, a very good correspondence of the temperature is obtained between both tests. This very good correspondence is also observed during the peak of hydration occurring the first 24 hours. It is therefore concluded that the thermal variations cause no significant change in the thermal gradient due to hydration.

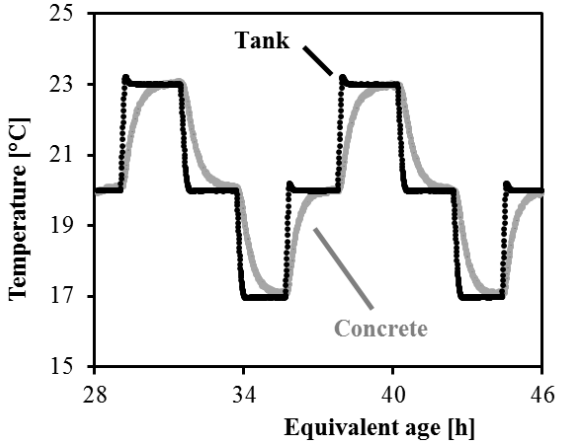

Figure 6 – Thermal variation in the water tank and inside the sample.

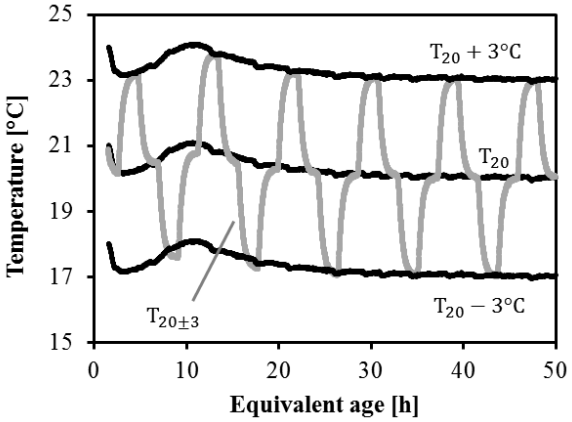

Figure 7 – Evolution of the temperature of the sample for both tests.

The total concrete strains from both tests are compared in Figure 8 since final setting time. Results obtained at the end of the plateau of temperature at 20°C are very close to the results obtained at a constant temperature of 20°C. It is therefore possible to fit results obtained at the end of the plateau at 20°C in order to define the total strain obtained for a cure at 20°C. The same methodology can be used to define the free strain at 17 and 23°C. In Figure 9, the temperature and the total strain in the sample with repeated thermal variation are compared. A good coherence between both evolutions is observed. At the beginning of each thermal variation, a discontinuity in the evolution of the total strain is observed. This discontinuity comes from the computation of the total concrete strains. When the displacement induced by the dilation/contraction of the test rig is removed from the total measurement, it is assumed that each component of the test rig has an instantaneous thermal response. The thermal inertia of each component is not considered. That is why such variations in the total concrete strains are observed. Therefore only results obtained at the end of the plateau of temperature have a physical meaning.

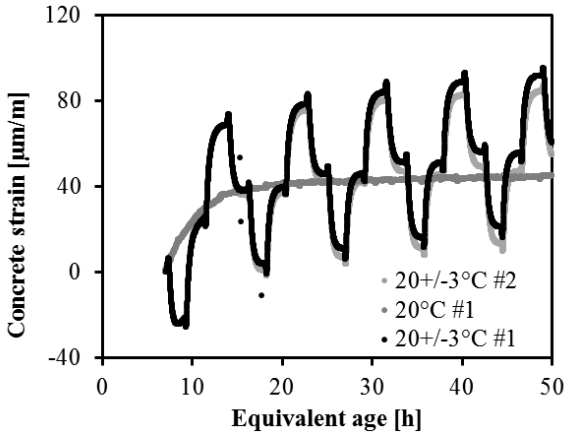

Figure 8 – Evolution of the total strain for both temperature histories

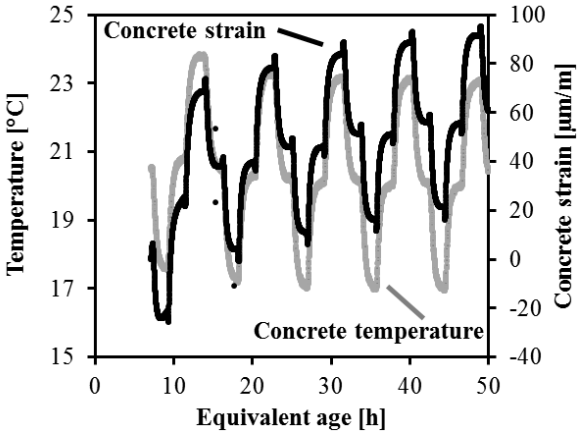

Figure 9 – Evolution of the total strain and the temperature for the test with repeated thermal variations.

The coefficient of thermal expansion (CTE) and the autogenous strain are computed in several steps. First the concrete strain is defined by removing thermal displacement of the test rig (see description of the BTJADE in chapter 3). Then only physical values of the total strain are considered. This physical

value corresponds to the moment when the test rig and the concrete have no thermal gradient and have a constant temperature. This moment corresponds to the end of the plateau of temperature. An average value of the last five data recorded during the plateau in temperature is considered in order to reduce the noise coming from the measurement of the temperature and the displacement sensors. To define the autogenous strain and the CTE, it is needed to have two temperature histories. For that purpose, a fictive temperature history is created by considering only the values obtained during the plateau of temperature at 20°C. With a cubic interpolation (function spline in Matlab©), it is possible to create new data (total strain and temperature) which correspond to a constant cure at 20°C. Therefore a predictive value of the total strain and temperature is obtained for a constant temperature of 20°C in the tank. For both temperature histories, the variation of the total strain, the autogenous strain and the thermal strain between two plateaus of temperature is given in Equation 1.

$$\Delta\varepsilon_{tot} = \Delta\varepsilon_{au} + \alpha_c.\Delta T \quad (1)$$

The effect of the temperature on the evolution of the autogenous deformation and the CTE [36] was previously demonstrated by several authors. However the difference of evolution was highlighted for a very large difference of temperature. For a very small difference of temperature, as here 3°C, the effect of the temperature on the evolution of the autogenous deformation and the CTE is very low. In consequence it could be considered that, for both temperature histories, the evolution of the autogenous strain during 130 minutes and the value of the CTE is the same. Therefore, with value of the thermal variation and total strain variation for both temperature histories, the CTE is defined as expressed in Equation 2. In this equation, the index 1 and 2 are relative to the two different temperature histories.

$$\alpha_c = \frac{\Delta\varepsilon_{tot,1} - \Delta\varepsilon_{tot,2}}{\Delta T_1 - \Delta T_2} \quad (2)$$

4.1.3. Results obtained with the BTJADE

Results of the CTE are given in Figure 10. The CTE changes strongly during the few first hours after casting till an age of 8 hours. Afterwards, the CTE follows a very constant value. The age when this change takes place corresponds to the setting of the concrete. This observation was already done by [20] for cement paste. For this composition, the CTE seems very constant after setting. This is in coherence with results obtained in the literature on ordinary concrete. Indeed, for concrete with a high water-cement ratio, no strong variation of the CTE occurs because the value of the relative humidity stays high during the whole hydration process. Figure 11 presents only results of the CTE obtained after setting. The scattering in the results is very low. However just after setting a higher scattering is observed. It is due to the strong increase of the autogenous strain during this period. An average value of 11.6 µm/m/°C is obtained for the CTE.

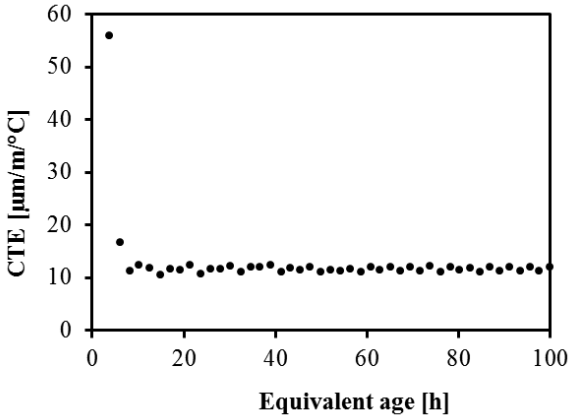

Figure 10 – Evolution of the coefficient of thermal expansion according to the equivalent age.

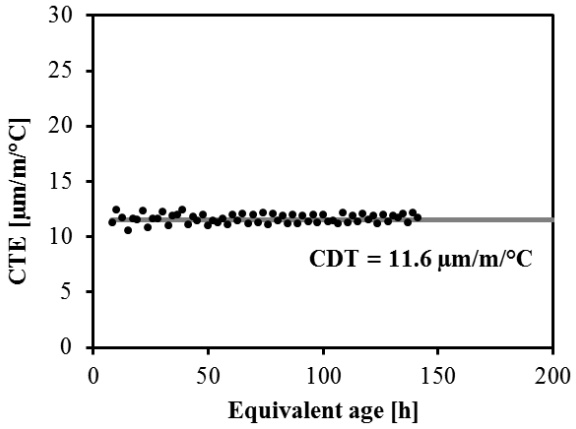

Figure 11 – Evolution of the coefficient of thermal expansion after setting.

When the CTE is defined, the evolution of the autogenous deformation is defined with the removal of the thermal strain on the total strain (Equation 1). Figure 12 presents the evolution of the autogenous strain by considering a constant value of the CTE of 11.6 µm/m/°C. Results are strongly dependent on the time when the autogenous strains are initialized. In order to correctly compare results, each curve is initialized at an equivalent age of 140 hours (Figure 13). Results from both tests give very equivalent results and show a very good repeatability.

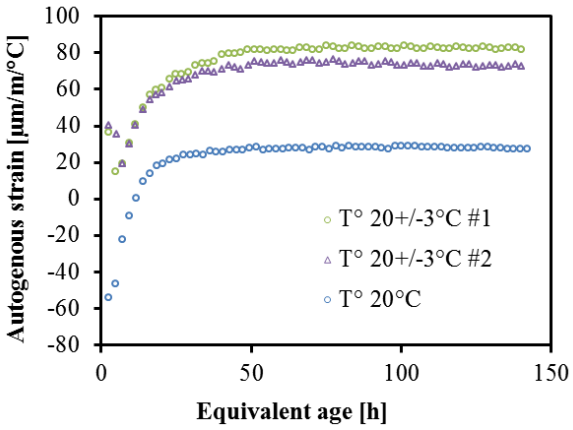

Figure 12 –autogenous strain evolution

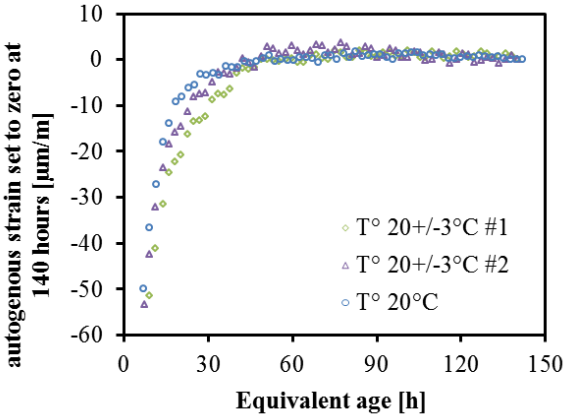

Figure 13 – Normalized autogenous strain at 140 hours

It is then concluded that the new methodology developed here is able to monitor the evolution of the CTE and the autogenous strain since setting in one single test.

For the next part of this thesis, a change in the protocol is carried out. For one mix, it was observed that the temperature is not fully stabilized at the end of the 120 minutes-long plateau of temperature. Therefore the duration of this plateau was extended to 150 minutes. The general scheme of this modified protocol is presented in Figure 14.

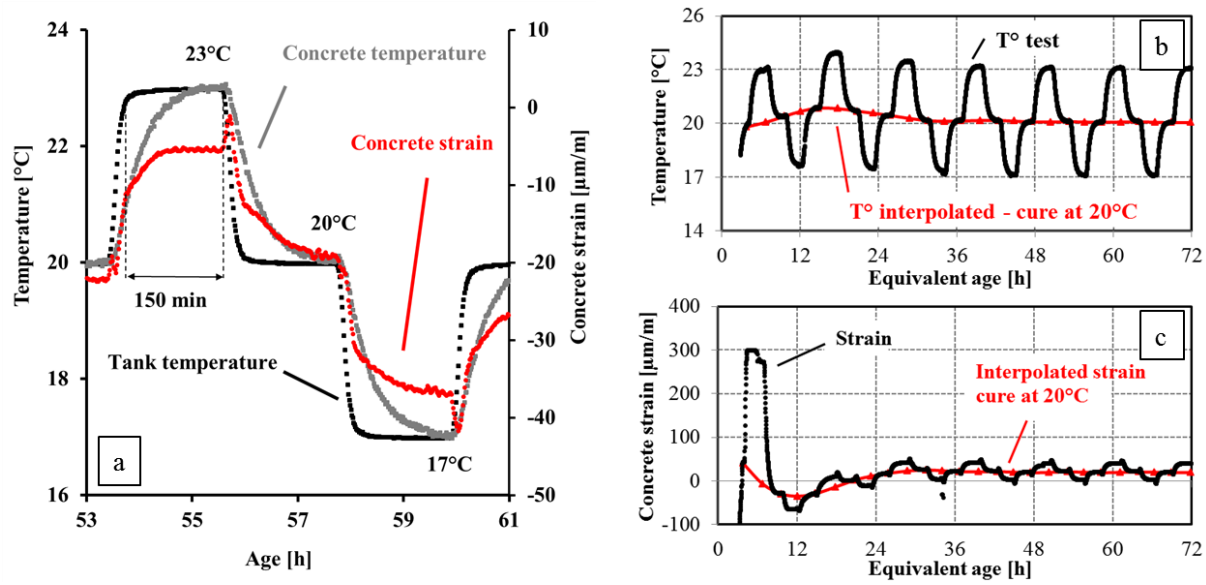

Figure 14 - Test protocol (a), evolution of the temperature during the test (b) and evolution of the concrete strain during the test (c).

4.1.4. Extension to cement paste and mortar

In order to study the multiscale aspect of the free deformation, a similar strategy is used for the monitoring of the CTE and the autogenous strain of cement paste and mortar. However the BTJADE device cannot be used for cement paste and mortar composition for which the size of the sample needs to be reduced in order to decrease the thermal gradient inside the sample during hydration. For that reason, tests on cement paste and mortar are carried out with the Autoshrink device [9]. Classical description of the Autoshrink device is presented in chapter3.

In order to apply thermal variations on the test rig, a thermal regulation was designed. The temperature of the sample is controlled by a flow of a specific liquid for thermal regulation circulating in a convolution system which surrounds the Autoshrink device. In order to improve the thermal regulation, the whole system is surrounded by a box with thermal insulation which limits exchanges with the ambient environment. The equipment is located in an air-conditioned room with a control system of the temperature and the humidity. The thermal regulation and the Autoshrink device are presented in Figure 15. The effects of the temperature changes on the test rig must be taken into account so a characterization of these effects must be carried out before using the rig. For that reason, a thermal calibration of the test rig has been carried out by using a stainless steel rod for which the CTE is known.

For the measurement of the displacement and the temperature, a Solartron network is used. It is composed by three displacement sensors Solartron LE2 and two temperature sensors. A thermocouple is used to monitor the temperature of one sample (embedded in the middle) and one PT100 is used to monitor the temperature of the air inside the convolution system.

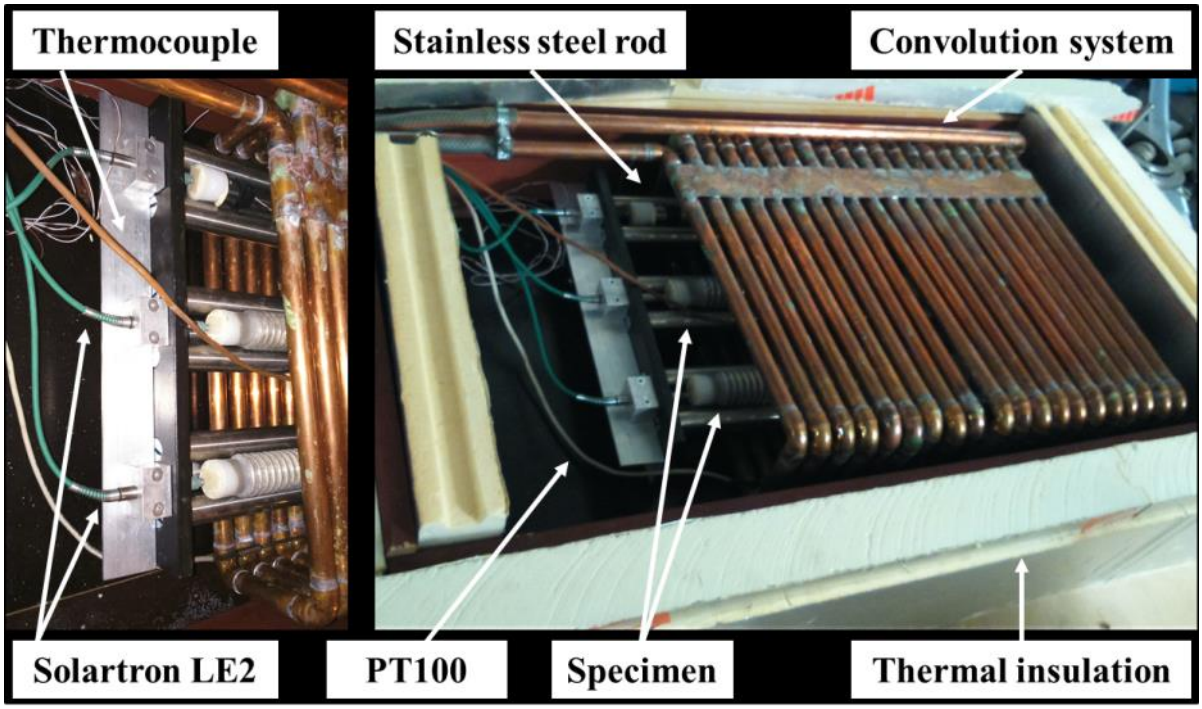

Figure 15 – Autoshrink device with thermal regulation developed at ULB.

The thermal regulation is not performing as the one in the BTJADE system. The main difference between both thermal regulations comes from the environment surrounding the sample. The BTJADE system uses a special fluid designed for thermostatic bath and mainly composed by water and the Autoshrink uses air. Therefore it is not possible to use exactly the same protocol of temperature. An adaptation of the protocol for the Autoshrink is presented in Figure 16.

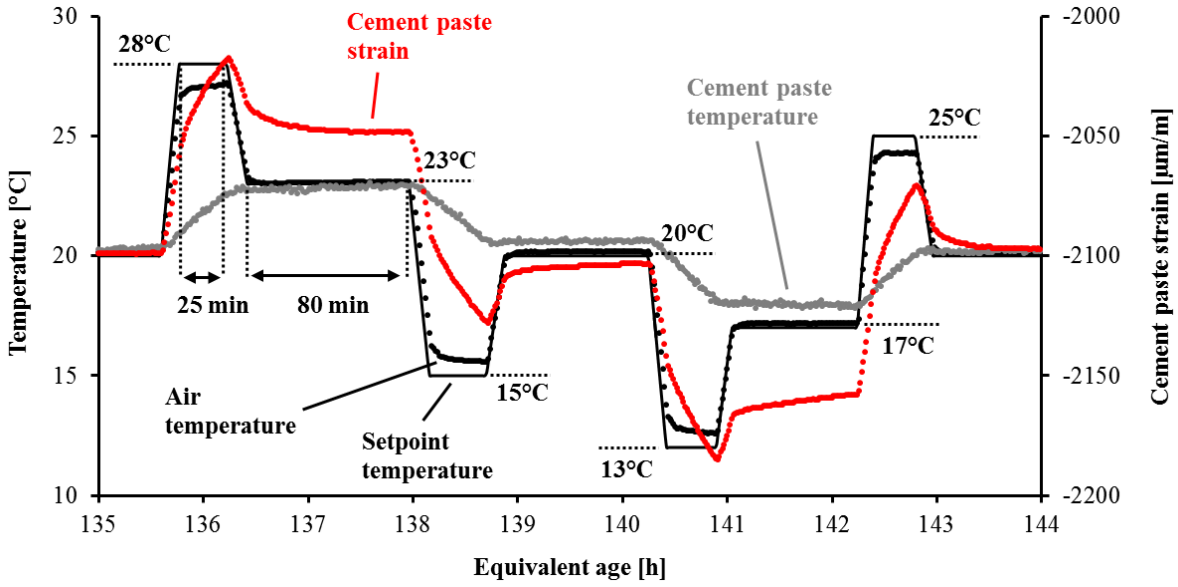

Figure 16 – Test protocol for cement paste and mortar with Autoshrink device

A first thermal variation of +/- 8°C is applied in 10 min. The temperature is kept constant during 25 minutes. Then a thermal variation of -/+ 5°C is applied in 10 minutes. Finally the temperature is kept constant during 80 minutes. The final magnitude of the temperature variation is +/- 3°C and the

duration of the isothermal phase is 80 min. Temperature stabilization in the cement paste or mortar is well reached after 80 min as shown in Figure 16.

Results from Autoshrink device with repeated thermal variations are presented in the chapter 7.

SECTION 4.2 – DESIGN OF A REVISITED TSTM SYSTEM FOR TESTING CONCRETE SINCE SETTING TIME UNDER FREE AND RESTRAINT CONDITIONS.

The first and second parts of this chapter are based on the joint publication of Stéphanie Staquet, Brice Delsaute, Aveline Darquennes and Bernard Espion entitled "Design of a revisited TSTM system for testing concrete since setting time under free and restraint conditions" published in: Concrack 3 - RILEM-JCI Int. Work. Crack Control Mass Concr. Relat. Issues Concern. Early-Age Concr. Struct., 2012: p. 12 and the third and final parts are an extension made in the framework of this PhD thesis manuscript.

Restraint deformations in concrete structures induce the development of tensile stresses and sometimes cracking. The durability and the functionality of the structure can then be affected. Some examples of restraint conditions are friction between the formworks and the concrete in case of casting by successive phases or the friction between concrete and rebars. The autogenous, thermal and drying deformations are at the origin of the restraint shrinkage. The knowledge of the mechanical properties (restriction degree of material, the relaxation of its stresses, the evolution of the tensile strength and the stiffness,…) and the free deformation are needed to quantify the risk of cracking. Several tests have been developed to estimate the cracking risk of cementitious materials, such as the ring tests, the plate tests and the passive longitudinal tests [37]. Generally, these experimental tests allow determining the number of cracks, their width and the stresses evolution inside the concrete sample. However, this evolution strongly depends on the geometry and the rigidity of the material used to obtain the restraint conditions. To eliminate these drawbacks, an active longitudinal test named Temperature Stress Testing Machine (TSTM) was developed from the beginning of the 1980's. With this device, a full degree of restriction of the concrete sample can be obtained by means of the application of a compressive/tensile stress on a dog-bone shaped concrete specimen to keep its length constant with a manual or an automatic system.

The paper will summarize our analysis of the development of the TSTM's. This analysis allowed us to develop our own testing system and experimental procedure to study the sensitivity to cracking of concretes. The first part of this section is related to principle of a TSTM. The history of the development TSTM in a dozen of other laboratories as well as a synthesis of the key elements in the design of a TSTM is presented in the second part of this section. Then the first development of the TSTM carried out during the PhD thesis of Aveline Darquennes is presented and is followed by the new technical advances performed on the TSTM for the study of the viscoelastic behaviour of cement based materials in the third and final part of this section.

4.2.1. Principle of TSTM's

The determination of the different parameters is based on the hypothesis of independence of the deformation components. The total deformation is assumed to be equal to the sum of the elastic ε_e, creep ε_{cr} and shrinkage ε_{sh} deformations. The degree of restriction of deformations is equal to zero if this sum is null. For the study of the evolution of the different parameters, compensation cycles are used with a threshold value of deformation ε_l equal to a few microns (or microstrains) for applying the restriction conditions during the experimental test (Figure 17). As soon as this value is exceeded, a load is applied on the concrete sample to cancel the deformation. Then, the concrete sample can shrink again and the load is kept constant but the stress/strength ratio increase with the time. Then

another compensation cycle begins (Figure 18). So the cycles succeed to themselves during the entire test until cracking of the sample occurs.

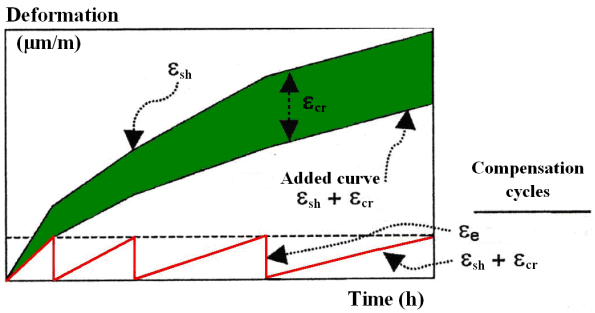

Figure 17 – schematic description of the compensating cycles to obtain the restriction conditions with the TSTM [13]

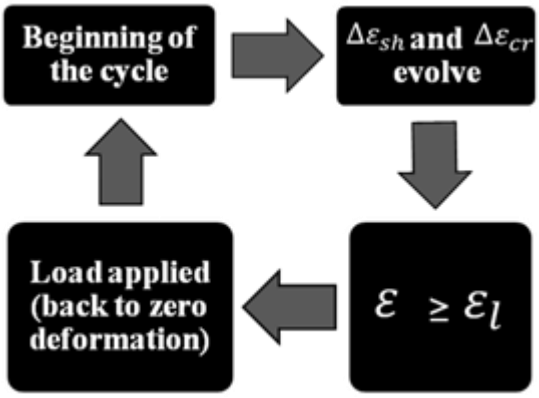

Figure 18 – steps inside each compensating cycle

Following these compensation cycles, the sum of all elastic deformations is equal to the sum of the restraint deformations, i.e. creep and shrinkage (Figure 17). From these experimental results, the creep deformation can be calculated as the difference between the curves of free shrinkage and restraint shrinkage. Another parameter can also be estimated from this test: the relaxation stresses.

4.2.2. History of the development of TSTM's

One of the oldest TSTM equipment was developed in the beginning of the 1980's by Springenschmid *et al.* [38] at the Technical University of Munich in Germany. In this equipment, the dog-bone sample is characterized by a square cross section 150 x 150 mm² and a length equal to 1500 mm [39]. The restriction conditions were obtained for a deformation threshold equal to 1 µm and were applied when the material is characterized by a significant stiffness. For example, this time is the moment when the stresses begin to develop inside the concrete sample. For the experimental tests realized with this TSTM, the displacement was measured by means of steel bars placed in the concrete sample in its central part at an interval equal to 500 mm. The same device was used for measuring the free shrinkage. This boundary condition was obtained by cancelling the force applied on the concrete sample when the stress inside the concrete reaches a value equal to 0.01 MPa. It appears that this first device is already characterized by two main parameters limiting the artifacts of restraint shrinkage measurements: a thermal regulation of the concrete sample and a system of deformation measurement directly placed on the concrete sample. At about the same time, Paillière *et al.* [40] also developed a TSTM equipment in which a dog-bone sample was tested in vertical position. However, this device cannot be used at early age because its specimen must be firstly casted in a horizontal mould before its placement in the TSTM. Moreover, this device is not equipped with a thermal regulation and the vertical position of the sample can lead to an early cracking localized in its upper part as a consequence of the non-uniform stress distribution arising from the hanging self-weight. These first TSTM devices allow underlining several major parameters which must be taken into account for their design: the position of the deformation measurement system, the presence of a thermal regulation on the concrete sample and the sample position.

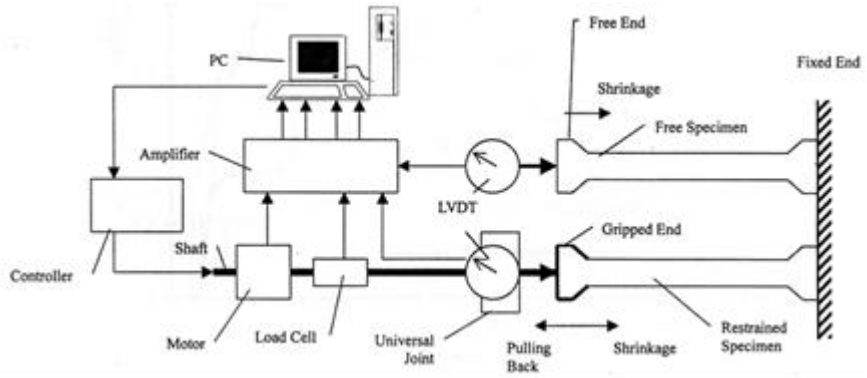

Figure 19. System for monitoring free and restraint shrinkages at the Israel Institute of Technology [41]

At the beginning of the 1990's, a TSTM was set up at the Israel Institute of Technology (Technion) at Haifa [41,42]. The free and restraint shrinkages were simultaneously measured on samples that differ only by one of their extremities, which is free for the sample used for measuring the free shrinkage and which is piloted in the other case. With this equipment, the deformation was measured by means of LVDT sensors placed on the moving head of the restraint sample. It has been demonstrated that this kind of method can generate some artifacts of displacement measurements [43]. Indeed, the interaction between the grip and the concrete sample can pollute the displacement measurements and induces a decrease in the restraint degree of sample. Moreover, a sliding between the sample and the grip is always possible. During these tests, the thermal regulation was provided by means of the room air conditioning only.

Several tests on TSTM's devices were carried out for several applications at the Norwegian University of Sciences and Technology (NTNU) at Trondheim in Norway [11] and at the Technical University of Delft (DTU) in the Netherlands [44,45]. Tests on high performance concrete were realized at NTNU. Bjøntegaard investigated the effect of different isothermal curing temperatures and realistic histories of temperature on high performance concretes. For this purpose, they equipped the TSTM mould with a thermal regulation system. This system consists of copper pipes disposed along the mould. It allows obtaining an isothermal temperature of 20°C after about 1-2 hours. Moreover, the temperature increase due to the hydration of a Portland cement concrete sample is limited to 1.5 °C. However, a thermal gradient in the longitudinal and transverse axis always exists because the temperature of the regulation liquid coolant varies from its initial temperature during its travel following its calorific losses. They also demonstrated that the value of the deformation threshold directly affects the value of Young's modulus calculated from each compensative cycle. From these first experimental results, it seems better to evaluate the value of the elastic modulus from complementary tests.

More recently, several university laboratories, namely at the University of Illinois at Urbana Champaign in the USA [46], the Swiss Federal Institute of Technology in Lausanne in Switzerland [47], the Monash University in Australia [48], the University of Tokyo in Japan [49] and the Polytechnical School of Sao Paulo in Brazil [50], equipped themselves with a TSTM equipment. Although these equipments bear some similarities (a dog-bone sample, a horizontal position for the specimen…), it appears that their design and their test method differ by several points. These differences are summarized below:

- Position (top or sides of the straight part of dog-bone specimen) and accuracy of the LVDT sensors, as well as the gauge length generally included between 500 and 750 mm.

- Size of the sample: length of the straight part (about 1000 mm), cross section (from 40 x 40 mm² to 150 x 150 mm²).
- Existence of a thermal regulation system around the specimen for stabilizing the temperature at the beginning of the test, keeping an isothermal temperature during the test and limiting the thermal gradient in the sample.
- System for controlling the displacement of concrete sample during the compensation cycles (manual or automatic).
- Kind of device for monitoring the free shrinkage (rectangular or dog-bone sample).
- Value of the deformation threshold used for obtaining the restriction conditions which varies from a value close to 0 (0.1 µm/m; 0.6 µm/m) to a value equal to a few microstrains (4 µm/m; 6 µm/m).
- Starting time of the restraint shrinkage test: setting of material, stress threshold, material age…

Table 2 - Differences between TSTM systems

	Springenschmid [38]	**Igarashi *et al.*** [41] **and Bloom *et al.*** [42]	**Bjøntegaard** [11]	**Toma** [51] **and Charron** [18]	**Lokhorst** [44] **and Lura** [45]
Test Start	0.01 MPa	24h	setting time	24h	8h
Deformation treshold	2 µm/m	5 µm/m	0.86 µm/m	6 µm/m	6 µm/m
Sample cross section	150x150 mm	40x40 mm	90x100 mm	50x50 mm	150x150 mm
Sample length	1500 mm	1000 mm	1000 mm	1000 mm	1000 mm
Gauge length	500 mm	-	700 mm	750 mm	750 mm
Deformation measurement	side	mobile head	side	top	side
Thermal regulation	yes	room conditionning	yes	yes	yes

However, these TSTM devices allowing the study of the visco-elastic behaviour of concrete at early age respect the recommendations of the technical committee Rilem 42-CEA [52] for uniaxial tensile testing of concrete at early age:

1. The experimental tests are realized horizontally to avoid the dead load effect of specimen.

2. The friction between the sample and the mould is minimized by using specific material like the combination of Teflon and plastic film.

3. The sample is prismatic and its extremities are larger than its central part.

4. The length of the longitudinal central part of the sample is at least four times higher than that of its cross section.

So, these different parameters have been taken into account in the design of the mould with a thermal regulation of the TSTM sample and the system monitoring the concrete displacement at the laboratory of the Université Libre de Bruxelles (ULB). Moreover, an appropriate test method for studying the

restraint shrinkage has been also chosen to limit the early cracking of the sample. The details of the revisited TSTM system are presented in the next part.

4.2.3. Design testing system and applications

► Part 1: Before the thesis [53]

A revisited TSTM system was developed (since 2006) in the laboratory of civil engineering at the ULB for testing concrete since setting time under free and restraint conditions. For this purpose, the testing machine is a Walter+Bay LFMZ 400 kN electromechanical testing setup. The machine is totally programmable and controlled (force and displacement of each sensor) by computer. The machine is composed by a fixed steel head, a central unidimensional part and a moving end. The moving end is controlled by a motor moving the steel head. The transition area between the ends and the central part is characterized by a rounded shape in order to minimize a possible stress concentration and the risk of premature cracking in this zone. In the central part where the measurements of the displacements are taken, the stress field is assumed to be homogenous. The shape of the mould is a dog-bone (Table 3). The dimensions of the cross section are 100x100 mm² in the central part and 150x100 mm² at the ends. The total length of the straight part equals to 1000 mm. With these dimensions, it is possible to realize tests for concrete with a maximal aggregate size of 20 mm. The shape of the mould induces stress concentration in the junction between the head and the straight part of the specimen. The failure of the sample takes often place in this part of the sample. The fresh concrete is cast inside the mould until a level of 100 mm. One T type thermocouple is placed in the middle of the sample during the casting, at each end and at mi-length of the central part of the mould. The temperature of the sample is controlled by a flow of a specific liquid for thermal regulation circulating on all the sides of the specimen.

Table 3 - Dimensions of the specimen in the TSTM device

Length of the span	1 m	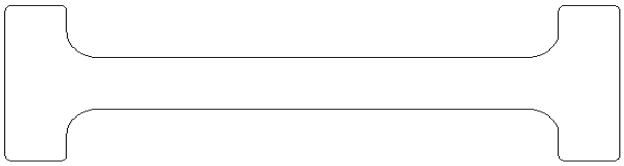
Width of the span	0.1 m	
Radius of curvature	0.5 m	
Width of head	0.3 m	
Length of head	0.1 m	

A plastic sheet is placed, before casting, in the mould to ensure sealed conditions. Moreover, the plastic sheet helps also to reduce, with the presence of Teflon, the friction between the sample and the mould. The walls of the mould are made of aluminum (Figure 20) which was chosen for its high thermal conductivity (237 W/m.K) and its low density (2700 kg/m³). The deflection of the mould is very limited (+/-2mm) and the isothermal conditions are ensured thanks to a fast heat transfer with the zinc boxes. A specific liquid for thermal regulation flows inside zinc boxes beams which are placed all around the central part and on the ends and under them. Each box is independent and has its own water input and output system. A thermal insulation limits exchanges with the ambient environment. The equipment is located in an air-conditioned room with a control system of the temperature and the humidity.

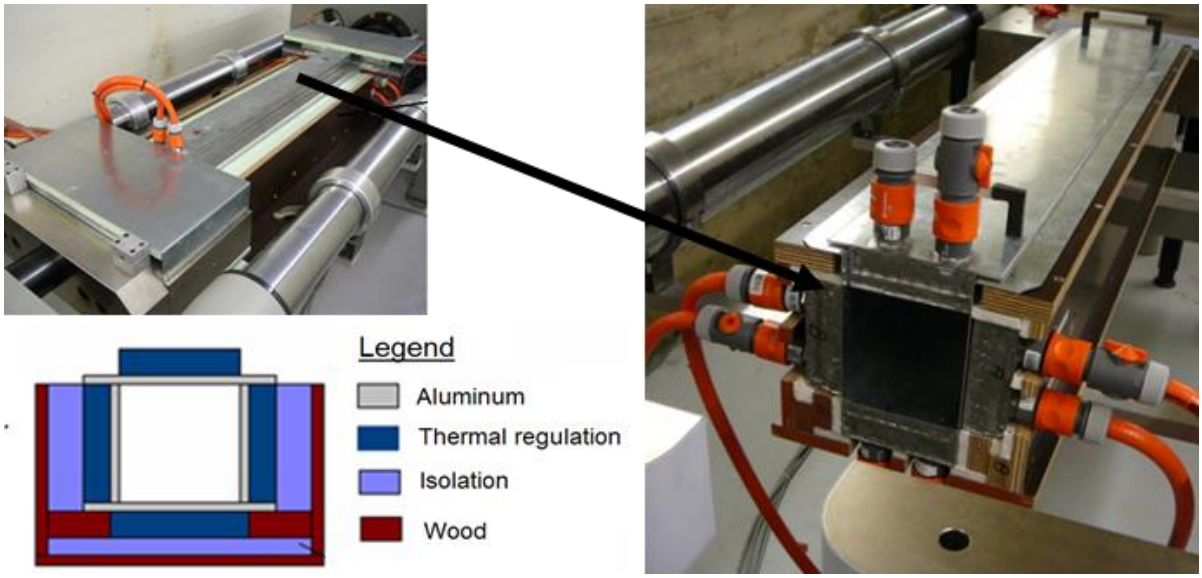

Figure 20 - Thermal insulation

In this equipment, the displacement is measured by means of two transducers (Solartron LE12). The sensors of displacement are placed on invar supports which are fixed on a rigid frame made of steel bars externally supported by the TSTM (Figure 21). The distance between both sensors is 750 mm (where the stress field is homogenous in the sample). These sensors are characterized by a measuring range of 12 mm and accuracy of about 0.4 µm.

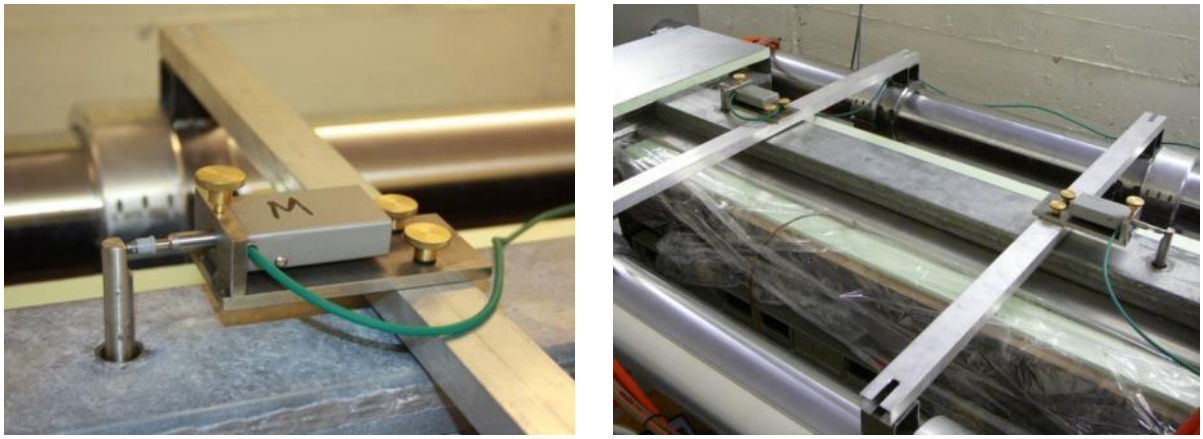

Figure 21 - displacement sensors in the central part of the specimen

Invar rods are anchored in the concrete at a depth of 50 mm. The link between the concrete displacement and the sensor is then assured. These invar rods are characterized by a low dilatation coefficient limiting the effect of ambient temperature on the deformations measurement. They are kept in their initial position thanks to a brass ring before the beginning of the test.

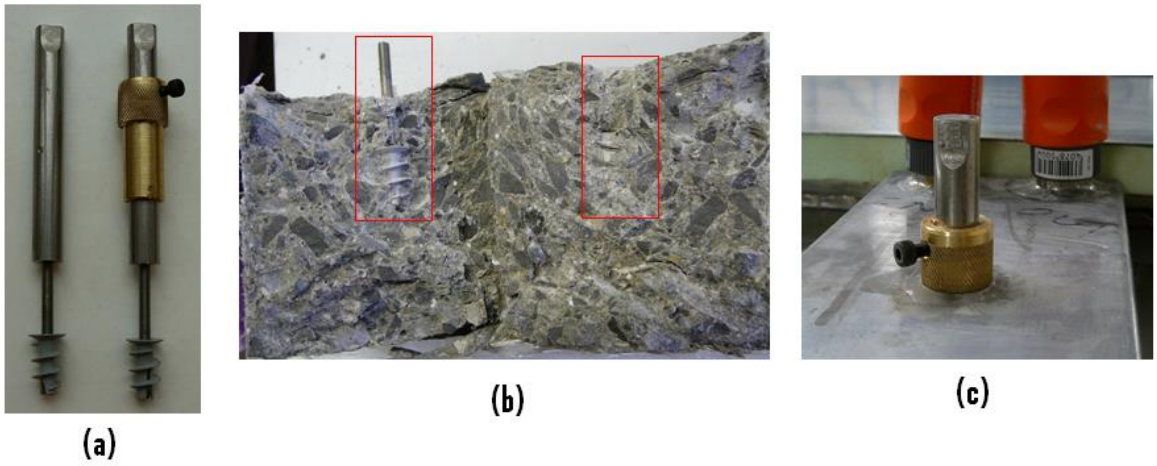

Figure 22 – Stem (Invar, threaded stem in steel) with plastic plug and brass ring (a) – incorporate stem in the concrete (b) – embedding system in steel of the Invar rod (c) [53]

The horizontality of the TSTM device is an advantage for the efficiency of the casting. Moreover, sensors are well anchored at mid-height and not in the superficial layer of the sample, what could have induced an error by a possible different behaviour between the core layer and the superficial layer (less aggregates presence).

Historically, the TSTM was developed for the study of the restrained shrinkage. A test method has been defined to measure the restraint shrinkage (Figure 23). At the beginning of the test, the sample placed in the TSTM is initially restraint by the stiffness of the frame with the motor being turned off until the stress inside the concrete reaches a threshold value of 0.01 MPa. At that moment, the displacement transducer readings are zeroed and the concrete sample can deform freely until the recorded deformation in the central part of the specimen reaches a deformation threshold equal to 6.7 µm/m. This moment coincides with the end of the first cycle. From this time on, the load is adjusted to pull the specimen back to its initial length. Then, the applied load at the end of the adjustment process is kept constant throughout the following cycles until the sample deformation reaches again the deformation threshold value. The test goes on until the specimen cracks. This kind of experimental process is quite similar to the one used by Charron [20] and allows avoiding an early cracking of the specimen. During this test, four parameters were continually monitored: the load applied on the sample, its deformation, its temperature and the displacement of the moving head.

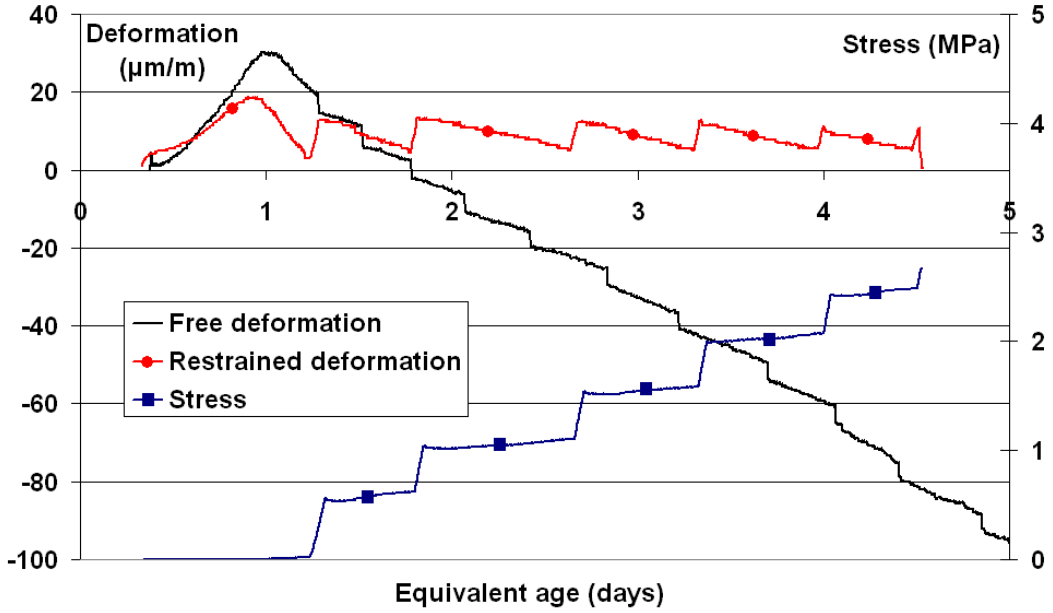

Figure 23 – Free and restraint shrinkage evolution of a Portland cement concrete and stress build-up in the concrete sample [53]

Other applications have been designed as the tensile and compressive creep. For this purpose, different changes were carried out on the TSTM device during this thesis.

► Part 2: Development of the TSTM during the thesis

In addition to the creep and elastic deformations, thermal and shrinkage deformation must also be known. For this purpose, a dummy mould was realized for the measurement of the thermal and free shrinkage deformations. This mould has exactly the same geometry as the first one. The only difference is the total free movement of one of the ends (Figure 24).

Figure 24 – Left to right: Mould (boundary conditions) – dummy mould (free moving end thanks to ball bearings).

For the study of the creep at high stress level, the stress concentration at the junction between the head and the straight part of the sample has to be decreased. A modification of the geometry of the head

would also make easier the demoulding of the concrete specimen. For these reasons, the geometry of the head was changed (Figure 25).

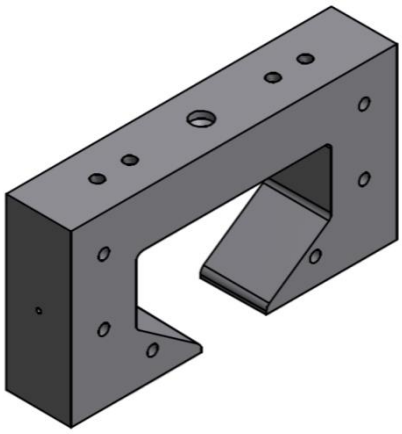

Figure 25 – New geometry of the head

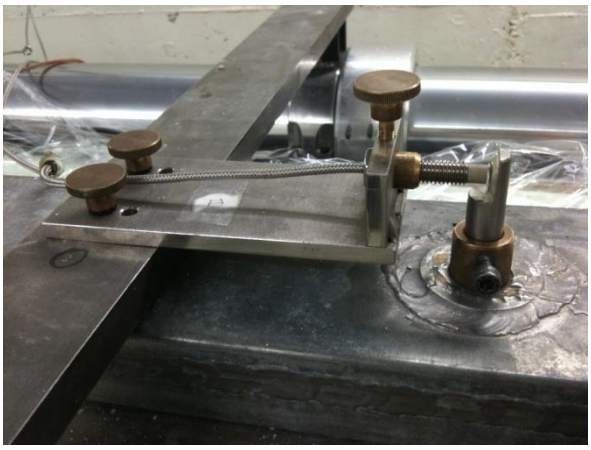

Figure 26 – Displacement sensor without contact

Displacement sensors in the central part of the specimen were replaced by Foucault current's sensors (without contact sensor) (Figure 26). Sensors have an accuracy of 0.014 µm. These sensors have two advantages. Firstly, the absence of contact between the sensors and the mould avoids measurement artifacts. Secondly, an instantaneous volt conversion in micrometer of the sensors allows piloting the TSTM system with the displacement directly measured in concrete.

For some tests, the failure occurs in the straight part of the specimen where the anchorage is placed. To decrease the risk of failure and to avoid a preliminary damage in this zone, the plastic plug was removed to limit the reduction of the concrete cross section. However different problems were observed for the measurement of the Young's modulus in tension and in compression. Damage by fatigue phenomenon is observed. A problem of adherence/deterioration was also observed for the anchorage of the stem as illustrated in Figure 27 for one cycle of loading. During the beginning of loading, when a compressive load is applied to the sample, the stress increases as expected but the strain increases as if a tensile load is applied. Then the strain develops in the good direction. This problem is assumed to be a wobble in the sample due to damage around the anchorage. This phenomenon was observed in different concrete when cyclic loading is applied. The higher the W/C ratio and sooner this phenomenon appears. For the ordinary concrete studied in this work, the problem appears after one week. For cyclic loading, internal anchorage has to be disallowed.

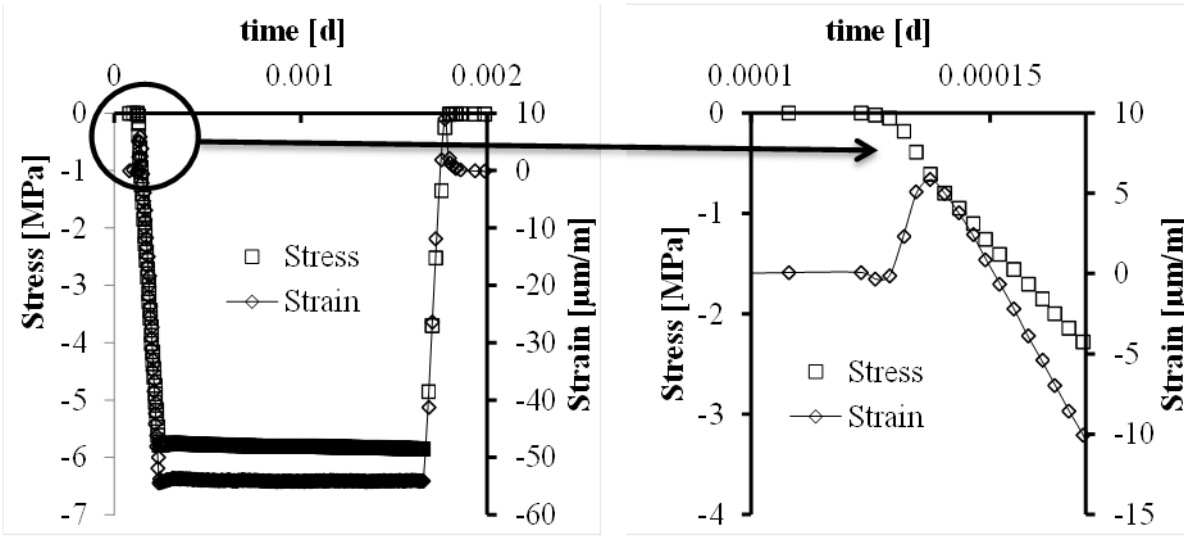

Figure 27 – Illustration of adherence/deterioration in the concrete around the stem anchorage in the sample.

Without contact sensors are very sensitive to the air conditioning. A good protection of the sensor is needed. Figure 28 shows the perturbation of the air conditioning on the sensor. The different "waves" are in direct relation with the air conditioning. The use of displacement sensor with contact as LVDT decreases the impact of the air conditioning. However this problem was solved by protecting the sensor from the air conditioning. A wood box was designed in order to protect completely the sensor from the ambient air.

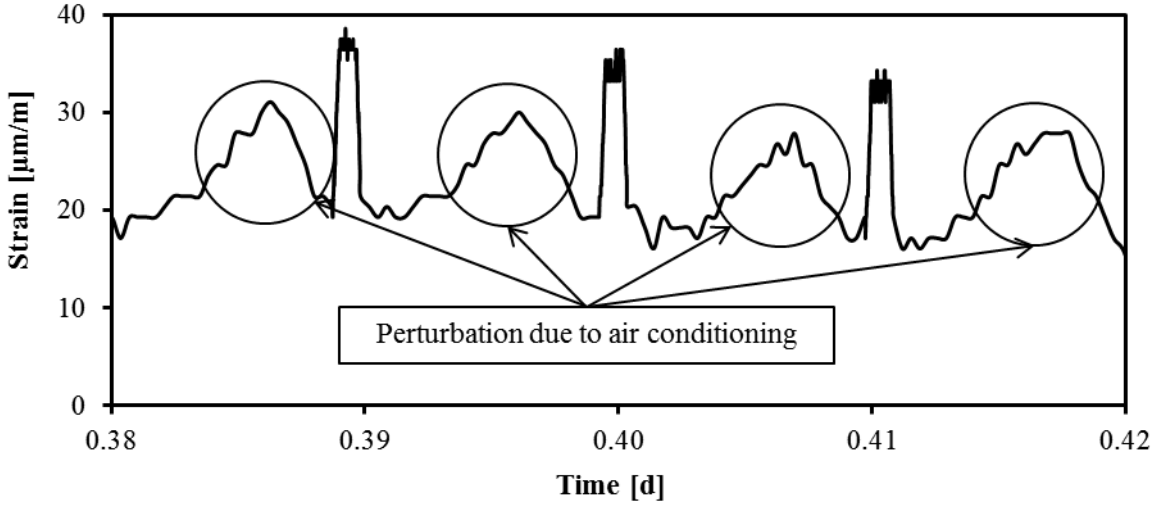

Figure 28 – Perturbation on the sensor of displacement

For these reasons, a new experimental measurement tool was designed for the measurement of the longitudinal strain. This tool is an extensometer which is adapted to the TSTM device. The transversal measurement is added for the study of the Poisson's ratio and the creep dilatancy. Here are the different criteria which are on the basis of the design of the extensometer:

- For the limitation of the thermal dilation of the extensometer, all structural elements of the extensometer are in INVAR©.
- All elements for the measurement of longitudinal and transversal displacement have to be protected from the air conditioning.
- Sensors with a high accuracy are needed for the measurement of the transversal displacement. For this purpose, Solartron LE12 sensors (numerical sensor) are used.
- External anchorages are used to avoid internal damage in the section of the concrete specimen. From these criteria, an extensometer composed of two parts with a U shape has been designed. The Figure 29 presents this new extensometer. Three elastic anchorages from the J2P company have been used (see section 3 of this chapter for more information) to assure a good contact between the extensometer and the sample.
- Measurement of the transversal displacement has to be done in the same section as the anchorage to follow the longitudinal displacement and avoid artifacts of measurements.
- A free lateral displacement of the specimen has to be allowed during the test to avoid confinement effect when a compressive load is applied.

From these criteria, an extensometer composed of two parts with a U shape has been designed. Figure 29 shows the new extensometer.

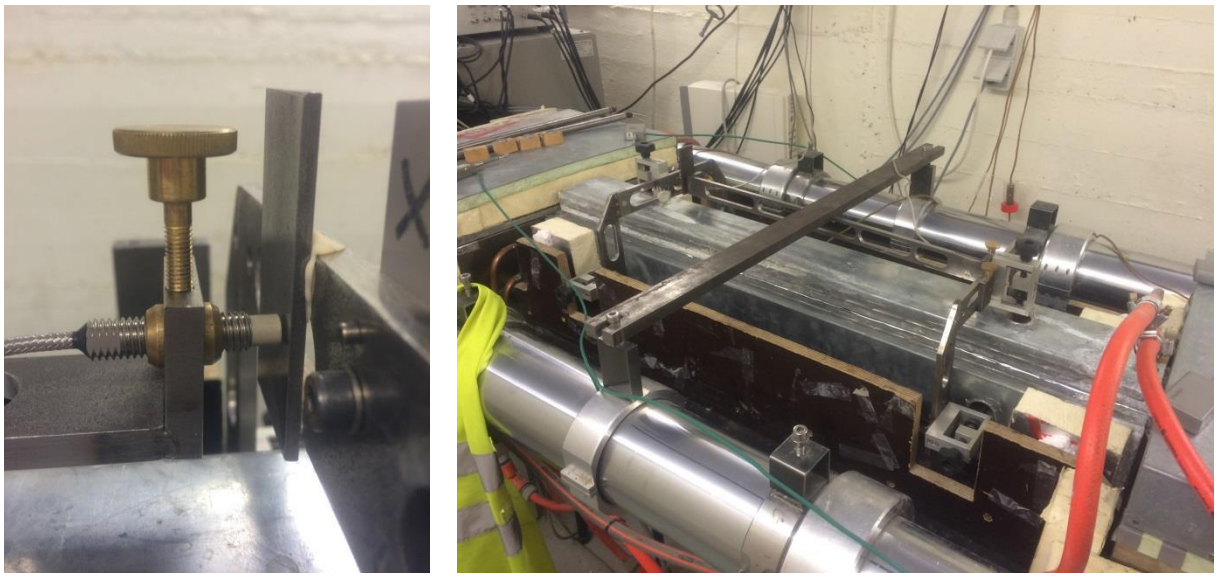

Figure 29 – New extensometer designed for the TSTM device

For the study of the restrained shrinkage since setting time, such instrumentation cannot be used. Indeed, in that case the test must start just after the setting. The implementation of the extensometer takes time and needs to remove the formwork. For this reason, all tests are performed with the new extensometer except test of restrained shrinkage. For restrained shrinkage, anchorage elements are used.

Other applications with the TSTM system have been designed. The system is controlled in displacement (measured in the straight part of the concrete sample or at the end of the moving steel head) and in force. The direct measurement of the evolution of the Young's modulus and the creep behaviour can be carried out. This TSTM has been also developed for the monitoring of the relaxation. A real time subtraction between the deformation of the specimen in the TSTM and the specimen in the companion (passive) mould allows piloting the TSTM system on basis of the mechanical parameters excluding the free deformations due to thermal variations ε_{th} and due to shrinkage ε_{sh}. So, the direct measurement of the elastic ε_e and creep ε_c deformations or the relaxation stresses is possible with the simultaneous use of the first and the second mould (Table 2).

Table 2 – Deformation measurements for each mould

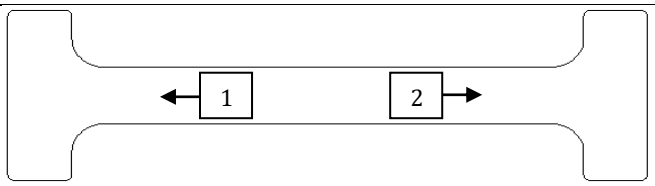	Mould 1 : $\frac{S1+S2}{750\,mm} = \varepsilon_e + \varepsilon_c + \varepsilon_{th} + \varepsilon_s$
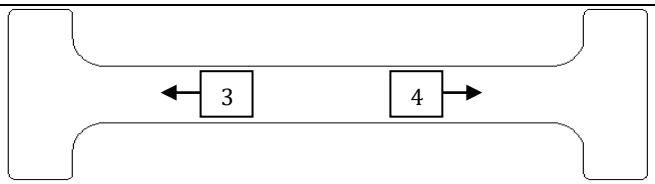	Mould 2: $\frac{S3+S4}{750\,mm} = \varepsilon_{th} + \varepsilon_s$
TSTM device is controlled by (S1+S2)-(S3+S4) which corresponds to creep and elastic deformations.	

SECTION 4.3 – DEVELOPMENT OF TENSILE CREEP RIGS

When the contraction of the concrete is restrained (internally or externally) tensile stresses develop. The determination of the tensile creep is essential for the computation of the stress in case of restrained shrinkage. Direct and indirect test rigs were developed in order to characterize the tensile creep of cement based material. For direct test rigs, a constant tensile load is applied to a sample. The stress state in the material is assumed constant. Therefore such tests allow defining directly the tensile creep. Indirect methods are related to tests for which the free shrinkage of the material is restrained. For such method, inverse analysis is needed in order to characterize the tensile creep. A complete review of such devices is presented in [53] and is not presented in this thesis.

For direct test rigs, several devices were developed. The main common point is the presence of a dummy mould for each kind of tensile creep test. The first part of this section presents the two main categories of tensile creep test: uniaxial tensile creep test and bending creep test. The instrumentation used for the measurement of the displacement is presented in the second part of this section. The third part of this section presents the different ways to connect the sample to the test rig. Some additional instrumentation for the study of the tensile creep is briefly introduced in the fourth part of this section. Through the observations carried out on the different tensile creep devices and the several instrumentations, new tensile creep rigs were designed at ULB for the determination of the tensile creep and relaxation function. This final development is presented in the fifth and last part of this section.

4.3.1. Existing devices

In the literature, two active methods are used to assess the tensile creep: uniaxial tensile creep rig and bending creep device. The uniaxial tensile creep rig is the most common way to monitor the tensile creep properties [54–61]. Three types of uniaxial tensile creep tests for cement based materials exist in the literature:

- test rig with lever arm
- Electromechanical testing device.
- Temperature Stress Testing Machine (see section 2 of this chapter)

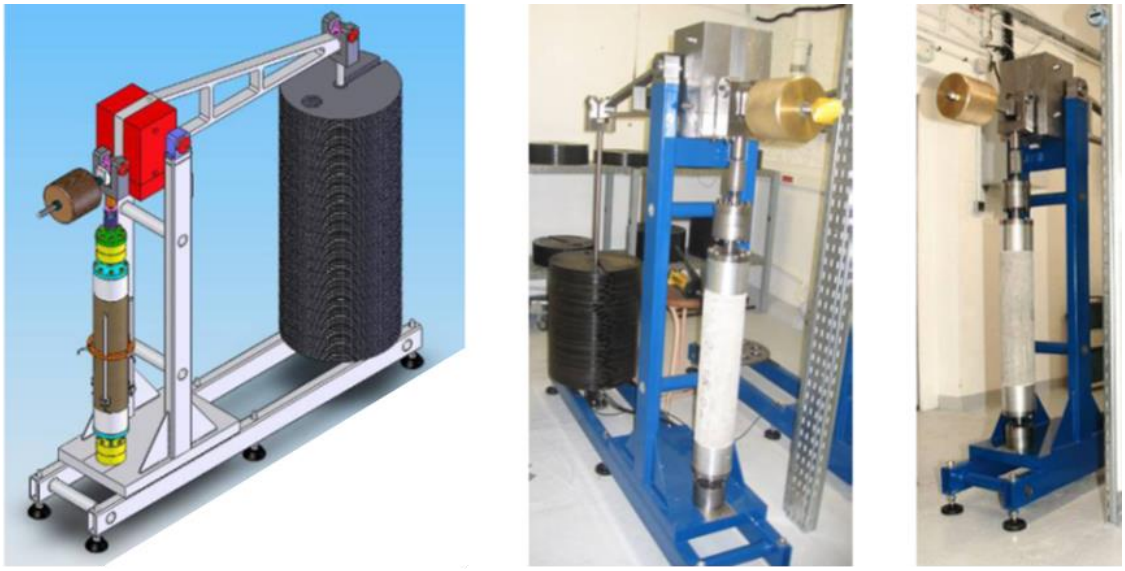

Figure 30 – Uniaxial tensile creep rig with lever arm at Ifsttar [61]

For the test rig with a lever arm, the loading of the sample is performed by a pile of metallic mass on a suspended tray at the extremity of the lever arm [55,62–66]. The sample stands in the opposite extremity of the device (Figure 30). This device has the advantage to maintain the load perfectly constant during the entire duration of the test. Moreover there is no need of supplementary device for controlling the load. However this device is quite limited in term of use. The test rig is not able to control the test in displacement, to work in compression and to apply automatically a history of loading on the sample. A variant of this sort of device exists with the addition of a hydraulic jack at the extremity of the lever arm instead of the pile of metallic mass. This allows controlling in force the device (Figure 31).

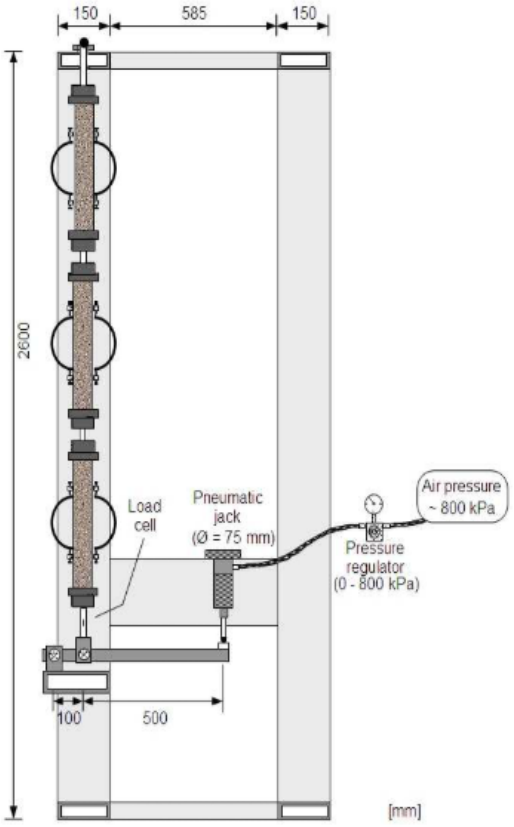

Figure 31 : Uniaxial tensile creep rig with lever arm with hydraulic jack [3]

In place of test rig with lever arm, electromechanical test rig can also be used to assess tensile creep. The main advantage of such test rig is the possibility to control the device in force and in displacement by computer. Moreover compressive load can also be applied which leads to higher possibilities of test. Therefore electromechanical test rig allows testing concrete in tension or in compression for creep or relaxation test. The main drawback for early age study of cement based material is the time when the test can start. Indeed, before testing several steps are needed for the preparation of the sample. These preparations can only start when the specimen has developed a suitable strength in order to not damage it. A solution to this issue is the use of a TSTM device which allows testing cement based materials since setting. However, the realization of a TSTM test represents a heavy experimental work and is high time consuming for the preparation of the test. Moreover when concrete is casted in the TSTM, no other test can be realized during this period. For that reason, TSTM test should be limited for very early age test. A synthetic comparison of the three tensile creep devices is presented in Table 4.

Table 4 – Comparison between existing tensile creep rig

Capacity of the device	**Test rig with lever arm**	**Electromechanical test rig**	**TSTM**
Tension	v	v	v
Compression	x	v	v
Start of the test	After 1 day	After 1 day	setting

Thermal regulation	x	x	v
Relaxation test	x	v	v
Control in			
Force	generally manual	v	v
Displacement	x	v	v

For the study of the coupling between tensile creep and damage, creep bending test has been used by several authors. Two configurations of bending test has been generally used: 3 points bending test [67,68] and 4 points bending test [62,63,69] (Figure 32). Creep strain can be defined by monitoring the evolution of the vertical displacement of the beam [67,68] or by monitoring the longitudinal displacement of the top and the bottom of the beam [62,63,69].

The monitoring of the tensile creep with bending creep test is currently questioned by several authors [62,69]. Through results of uniaxial tensile and compressive creep tests, Tailhan, *et al.* [69] showed that it is not possible to simulate numerically the bending creep behaviour of a "standard" concrete. They explain this observation by the scale effect related to the tensile and bending behaviour. Ranaivomanana, *et al.* [62,63] highlighted also a difference between the results obtained from bending creep test and those obtained from uniaxial tensile creep test. From this observation, it seems that the most appropriate test for the monitoring of the tensile creep is the use of an uniaxial tensile creep rig.

Figure 32 – 4 points bending creep device at Ifsttar [69]

4.3.2. Measurement instrumentation

Tensile creep strains of cement based materials are difficult to assess because of the following reasons:

- The tensile strength of cement based materials is very low. Consequently the applied force in the sample during the test is also very low as well as the displacement measured.
- The strains arising from the free deformations (autogenous and thermal strain) are in the same order of magnitude as the tensile creep strains.
- The thermal strains of the measurement instrumentation arising from the thermal variation of the ambient air are in the same order of magnitude as the tensile creep strains.

Therefore, the measurement instrumentation must be:

- an instrumentation with a very high accuracy;
- identical for the dummy specimen;
- composed of material with very low coefficient of thermal expansion;
- in an environment with a very stable temperature.

Several types of instrumentation are used in the literature for the determination of the tensile creep strain. The main instrumentations are based on:

- internal measurement;
- sensor fixed directly on the sample;
- element anchored in the sample during the casting;
- external extensometer.

An internal measurement (gauge with vibrating wire for example) of the displacement has two disadvantages. The presence of the sensor can cause artifact in the measurement [65]. Only one gauge is placed in the sample which leads to a lack of knowledge about the eccentricity of the load.

The fixation of sensors directly on the sample is the easiest way to measure the displacement of a sample. The instrumentation is generally composed of a square glued in one end of the sample and which supports a longitudinal rod. In the other end of the sample, the sensor is fixed on another square which is also glued to the sample (Figure 33). This method allows performing tests on several base length of the displacement measurement (between few centimeters till several dozen of centimeters). This instrumentation has the following disadvantages:

- The good implementation of the instrumentation on the sample is time consuming and requires good precision from the user;
- The different elements of the instrumentation can have different coefficient of thermal expansion which makes difficult the removal of the thermal strain of the instrumentation and introduces error in the measurement.
- The fixation of the square is difficult on hardening concrete.
- This instrumentation alone is not able to measure transversal displacement.

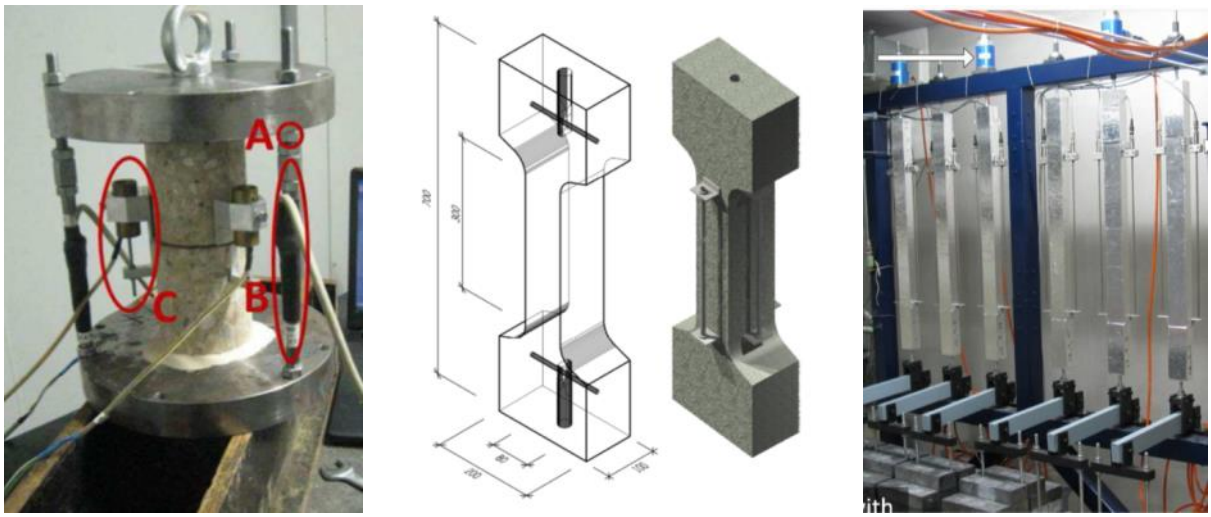

Figure 33 – Instrumentation based on the fixation of the sensor on the sample, left to right: [66,70,71].

For measurement at very early age, it is possible to anchor elements such as rod or metal insert. These pieces allow monitoring the relative displacement of the sample between two points or more. For that, a rod is fixed to a first anchored element and a sensor is fixed to a second anchored element for the measurement of the relative displacement between the two anchored elements (Figure 34). Another possibility uses an external support on which two displacement sensors are fixed to monitor the displacement of two anchored elements (Figure 35 and Figure 36). The main drawback of this instrumentation is the local damage which can occur around the anchored element when working at high stress level (Figure 34) [72] or when repeated loading are applied to the sample due to fatigue phenomenon at the interface between the element anchored and the cement based material.

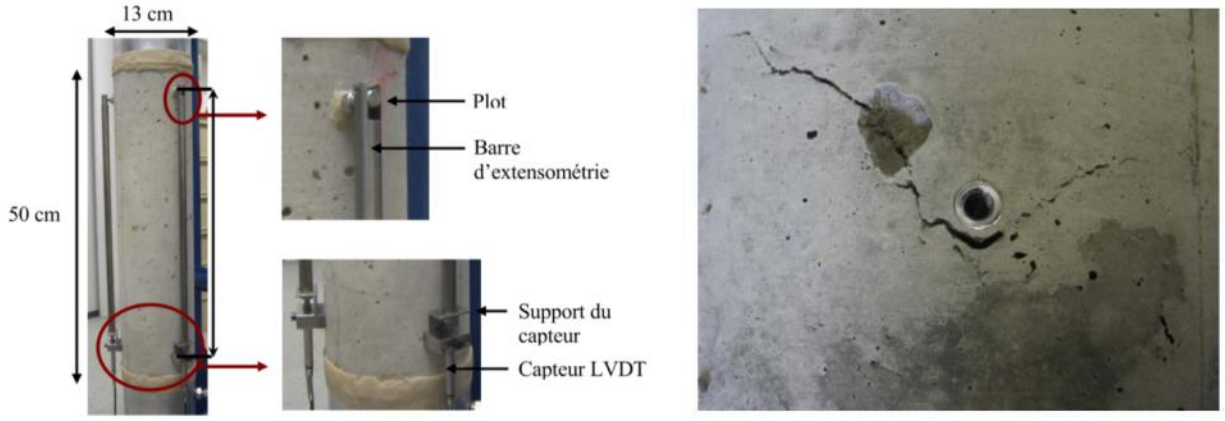

Figure 34 – Instrumentation with insert anchored in the sample and bearing a rod or a displacement sensor [72]

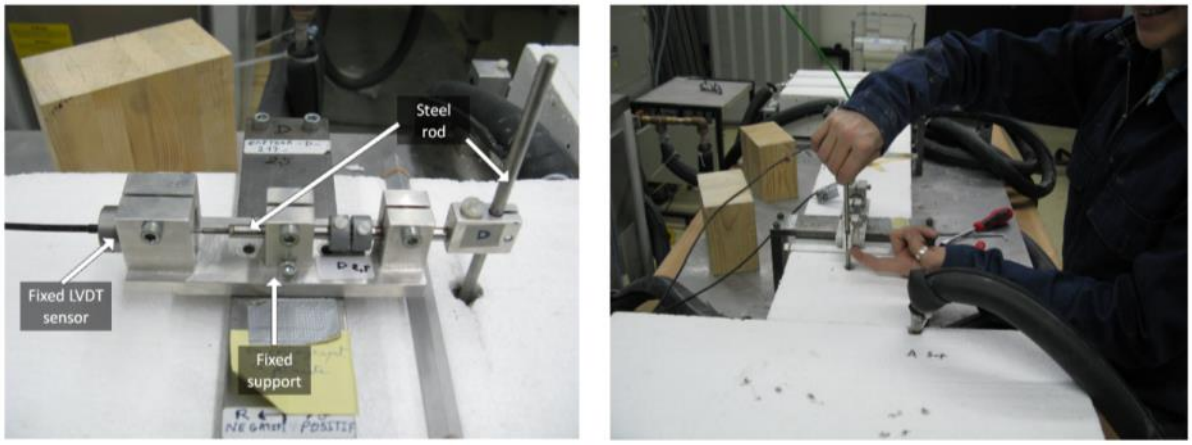

(a) LVDT sensor on a support (b) Attaching the LVDT sensor

Figure 35 – Instrumentation with rod anchored on the sample and external support bearing the displacement sensors [71]

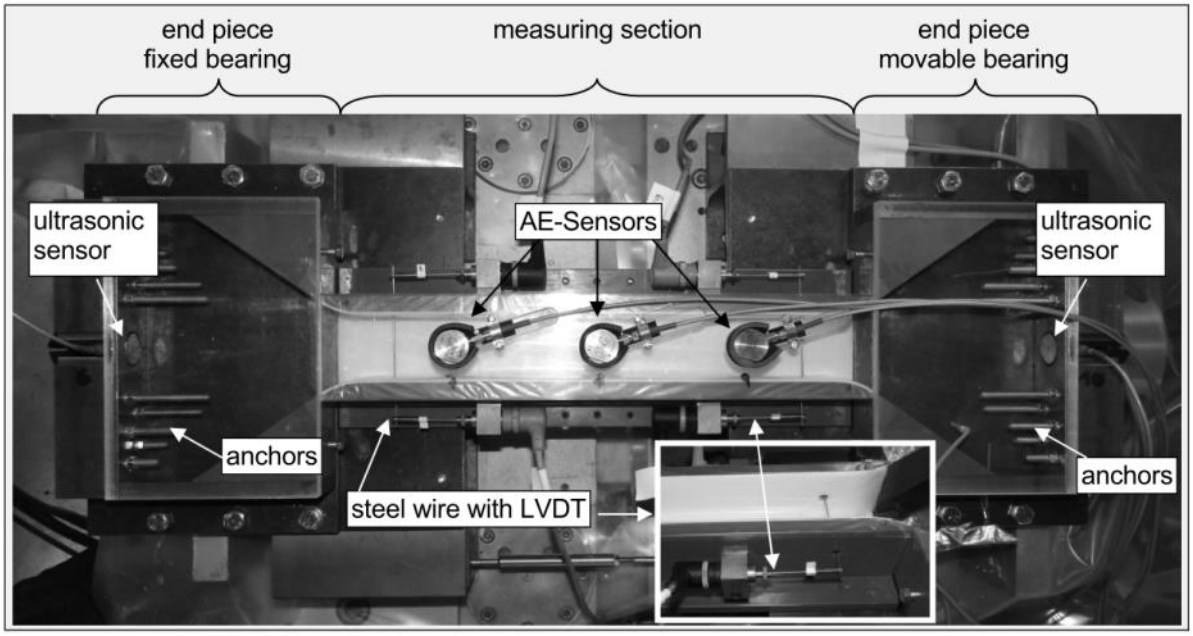

Figure 36 - Instrumentation with rod crossing the sample and external support bearing the displacement sensors [73]

Several extensometers exist in the literature. The most common extensometer for cylinder is composed of two rings fixed with screws placed at 120°. The space between both rings represents the base length for the displacement measurement. Generally, three displacement sensors are used to define the relative displacement. The main advantages of this instrumentation are:

- the easy implementation of the extensometer;
- test can start several hours after setting;
- the eccentricity of the load is measured.

And the main disadvantages of this instrumentation are [74]:

- the stiffness of the rings is very high and consequently that induces perturbation of the measurement due to interference fit for small deformation. This phenomenon occurs also for high deformation (close to the failure).
- When repeated loading are applied to the sample, the screws penetrate in the sample during the increase of the load. When the load is decreased, a backlash is created between the sample and the screw. Therefore the ring is not anymore correctly linked to the sample. This phenomenon increases when new loadings are applied.
- As the stiffness of the ring and the screw is very high, the lateral displacement of the sample is partially restrained and the screw sinks partially into the sample. Consequently, this kind of extensometer is not able to correctly measure the lateral displacement.

These problems can be resolved by using elastic anchorages [74]. This kind of anchorage can keep a nearly constant load between the anchorage and the sample when an external load is applied. This connection is carried out with elastic blade (Figure 37c, mark 1) which induces no backlash. The constant holding force on the sample is obtained with an additional spring (Figure 37c, mark 2). Moreover, displacement sensors can be added on one ring for the measurement of the lateral displacement. Here no artifact occurs in the measurement of the lateral displacement. The company J2P instrument built such anchorage. The extensometer built by this company has one main drawback coming from the material used. The extensometer is composed of aluminum. This material has a significant coefficient of thermal expansion of 24 µm/m/°C. For creep testing, such value of the CTE is unacceptable.

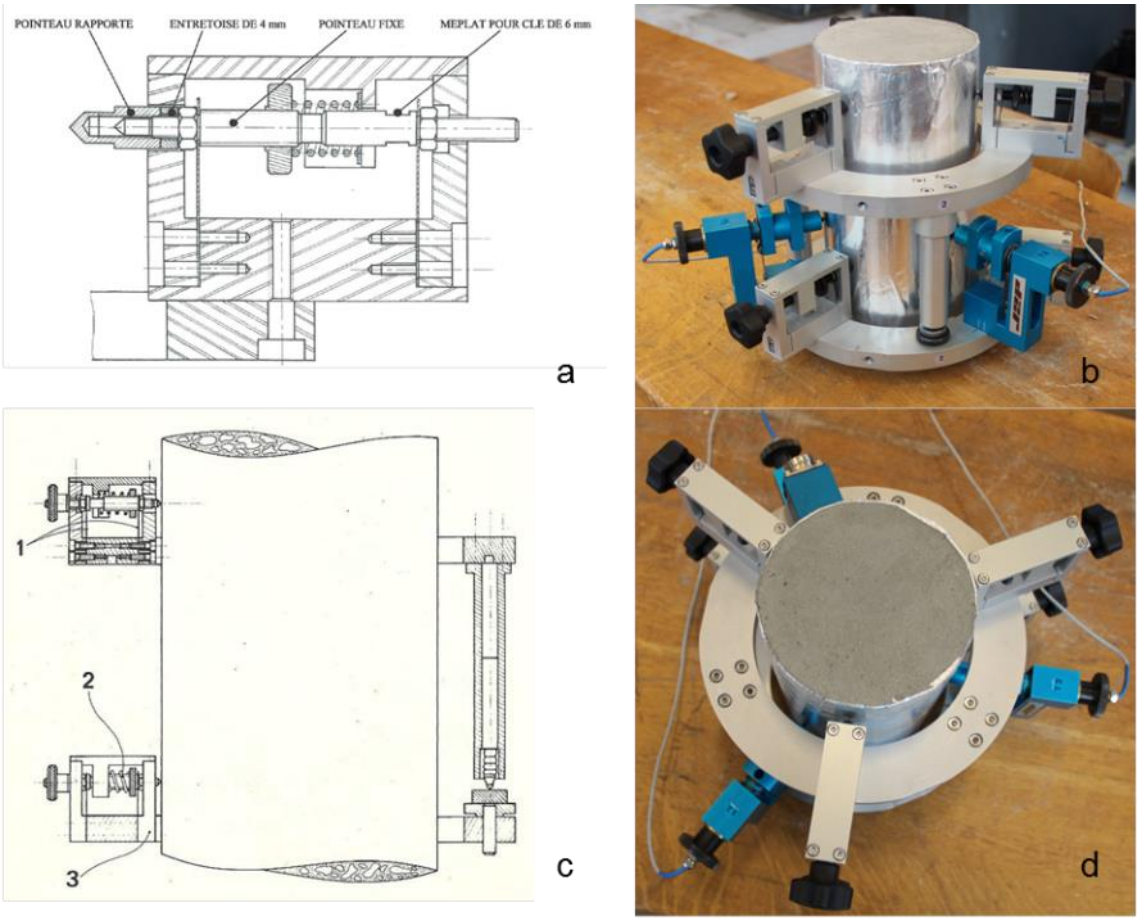

Figure 37 – Extensometer from J2P company allowing the measurement of the longitudinal and lateral displacement by using elastic anchorage

A synthetic comparison of the different sort of instrumentation for uniaxial tensile creep test is presented in Table 5.

Table 5 – Comparison between different sort of instrumentation for uniaxial tensile creep test.

	System with glued elements	**System with anchored elements**	**Extensometer with elastic anchorage**
Implementation	Difficult at early age	v	v
Base length	From few centimeters till +/- 40 cm	From 20 cm till 75 cm	From 10 à 20 cm
Start of the test	After an age of 24 hours	Setting of the concrete	Few hours after setting
Thermal dilation of the instrumentation	Several element with different CTE	OK if element in Invar	Element in aluminum with a strong CTE

Lateral measurement	x	x	v
High stress level	x	x	v
Repeated loading	x	x	v

Other kinds of instrumentation are under development such as the image correlation method. Currently the resolution of this method is too low for tensile creep test. However very interesting results [75] about stable crack propagation control shows very nice perspectives in the frame of the characterization of the coupling between tensile creep and damage.

3.3.3. Connection between the sample and the test rig

Several methods aimed at fixing a concrete sample to a test rig exists [76]:

- fixation with lateral friction;
- anchorage of metallic bar at the extremity of the sample placed during the casing;
- use of sample with a dog bone shape;
- bonding.

Figure 38 presents the three first sorts of connection. The mechanical difference associated to these fixations is related to the stress state in the material when a tension load is applied. Fixation with lateral friction leads to high stress concentration where the friction occurs. The use of anchorage bars placed during the casting of the sample decrease the stress concentration. In that case main stress concentration occurs where the anchorage bars are placed. The use of a dog bone shape allows a better distribution of the stress along the section. However three methods present significant perturbation of the stress state at the fixation zone. When working at high stress level this perturbation causes a faster failure of the sample.

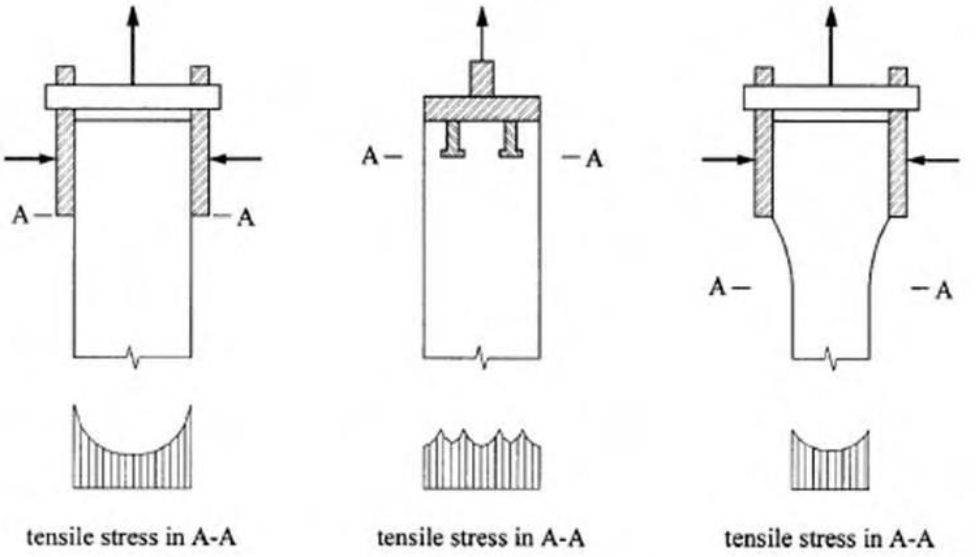

Figure 38 – fixation method between the sample and the test rig and associated stress state. Left to right: fixation with lateral friction, anchorage of metallic bar at the extremity of the sample placed during the casing and use of sample with a dog bone shape [76].

Figure 39 presents two types of fixation using bonding. Bonding has the advantage to reduce the stress concentration at the fixation zone. From finite element analysis, Zheng, *et al.*[76] recommend to use two dollies connected mechanically to reduce the stress perturbation at the bonding zone. Another parameter allowing a reduction of these stress perturbations is the height of the dolly on which the specimen is bonded and the stiffness of the dolly.

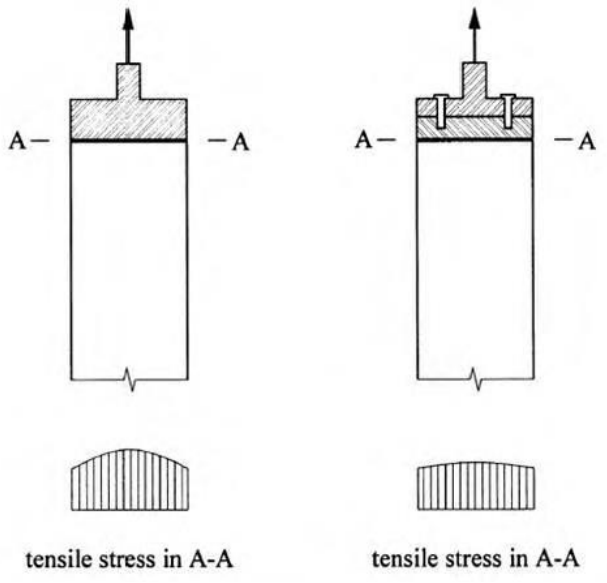

Figure 39 – fixation method between the sample and the test rig and associated stress state. Left to right: bonding using one dolly and bonding with two dollies mechanically connected [76].

4.3.4. Supplementary instrumentations

Tensile creep rigs can be composed of other instrumentations. For the study of the coupling between tensile creep and damage, acoustic emission [77,78] can be used to quantify and analysis the evolution

of damage when the load is applied and also when the load is kept constant. Another interesting method for the monitoring of damage during a tensile creep test is the ultrasound method. Sensor can be placed at the extremities of the sample [73] or can be embedded inside the sample [79].

4.3.5. Tensile creep rig developed at ULB

Through the different comparison carried out in this section, it was decided to use the TSTM device for test occurring at very early age (<24h00) and two electromechanical testing devices for testing tensile creep on early age concrete (>24h00) and hardened concrete. The TSTM device is already described in section 2 of this chapter.

For the electromechanical testing device, the following choices are done:

- Dimension of the sample: For good comparison with compressive creep test and practical reasons, cylindrical specimen with the same diameter of 97 mm is used. The height of the sample is defined according to two parameters: the base length for the measurement of the displacement and the preparation of the sample. The base length must be higher as possible in order to measure significant displacement. The preparation of the sample is done in several steps among which the grinding of the sample. Generally grinding machines are designed for sample with a maximal height of 400 mm. For this study, an extension of this maximal height was asked. Also during the several steps of preparation of the sample, the experimental testing worker needs to easily transport and work on the sample. Therefore, the weigth and height of the sample must be minimized. A good compromise is reached with a height of 550 mm.
- The dummy specimen: The dummy specimen must be placed exactly in the same environmental condition that the loaded specimen. For that reason, the dummy specimen is placed close to the loaded specimen. The dimensions of the dummy specimen are exactly the same as those of the loaded specimen. Exactly the same instrumentation is used for the loaded and the dummy specimen.
- Climatic room: In order to reduce as far as possible the thermal perturbation coming from the ambient air, the whole test rig is placed in a climatic room at 20 +/- 1°C.
- Testing rig: A Walter+Bay LFMZ 100 kN electromechanical testing setup is used for this study. The test rig can be used for tensile and compressive test.
- Instrumentation: A J2P extensometer in Invar© including three anchorages with elastic blades was specifically designed. The base length for the measurement of the longitudinal displacement is 350 mm. Longitudinal displacement sensors are placed at 120°. Lateral displacement are also measured with this extensometer and placed at 120° on the bottom ring. The extensometer is placed in the central part of the specimen where the stress field is assumed to be homogenous.
- Displacement sensor: Longitudinal Solartron© sensors have a stroke of 0.5 mm, an accuracy of +/- 0.5 µm and are analogical. A conditioning signal system is used for the longitudinal sensors. The lateral Solartron© sensors have a stroke of 0.5 mm, an accuracy of +/- 0.01 µm and are numerical.
- Temperature sensor: In order to correctly consider the impact of the thermal variation on the hydration process, a thermocouple type T is placed in the center of the dummy specimen. A PT100 sensor is used for the monitoring of the ambient air in the room. Both sensors are linked to the Solartron© network.

- Control: The electromechanical testing setup is totally programmable and controlled (force and displacement of each sensor) by computer with the software DionPro. The longitudinal sensor can directly control the device. For relaxation test, the testing setup was designed in order to be controlled by the subtraction of the longitudinal displacement of the loaded and dummy specimen.
- Fixation of the sample: In tension the sample is linked to the test rig by bonding the specimen to a dolly at both extremities. Each dolly is linked to the test rig with a hinge. For test in compression, two trays are connected to the test rig (on the bottom and the top). The tray in the top part of the test rig is composed of a hinge.

Such test rig, allow performing the following tests:

- direct tensile strength test;
- tensile and compressive creep test;
- tensile and compressive relaxation test;
- test with several variation of loading;
- repeated minute-long loading test (see section 5 of this chapter);
- restrained shrinkage test for concrete after an age of 24 hours.

The general scheme of operation of the new tensile creep rigs developed at ULB is presented in Figure 40. Illustrations of the test rig and it components are presented in Figure 41.

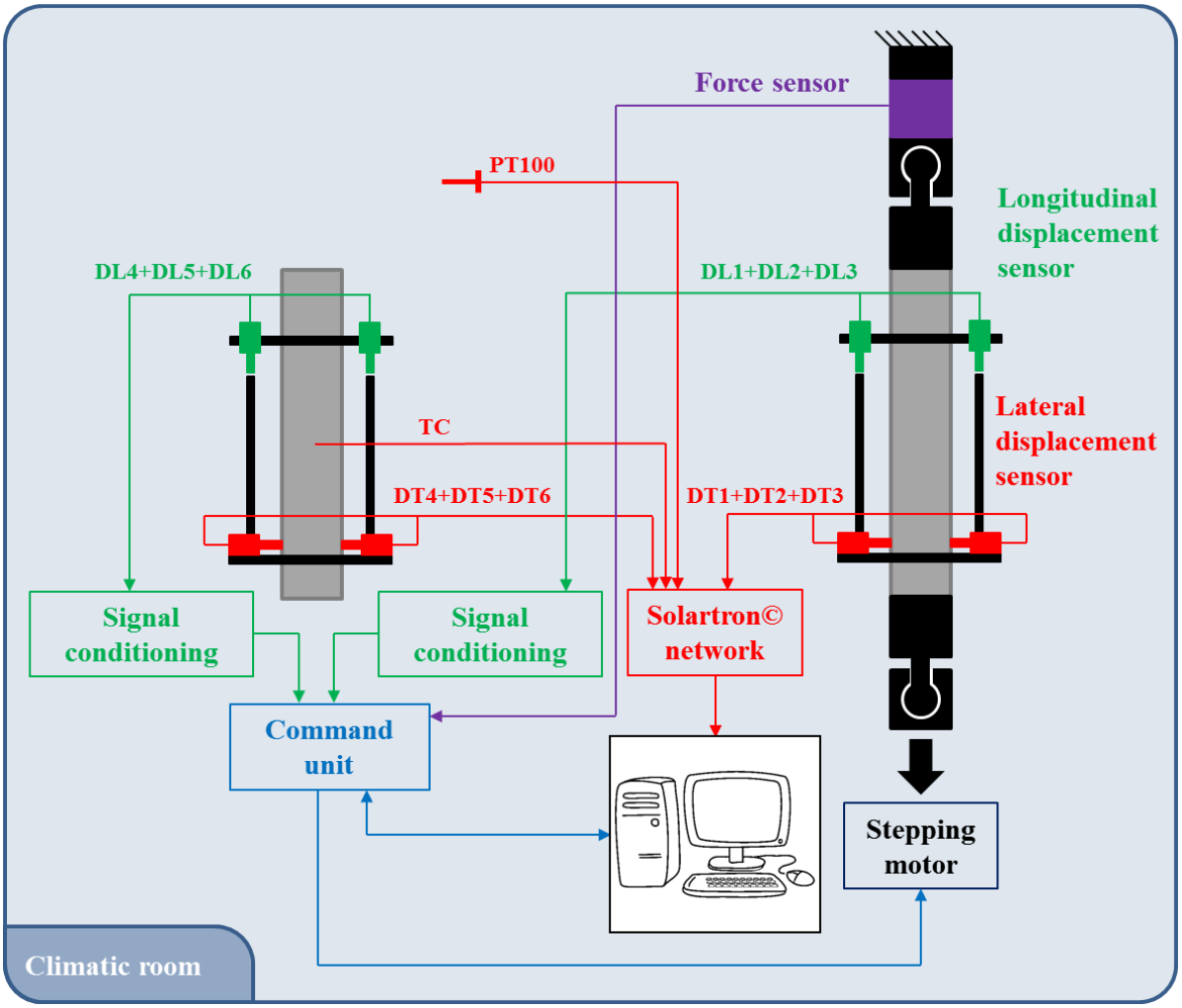

Figure 40 - General scheme of the new tensile creep rigs designed (laboratory of Civil Engineering, BATir, ULB).

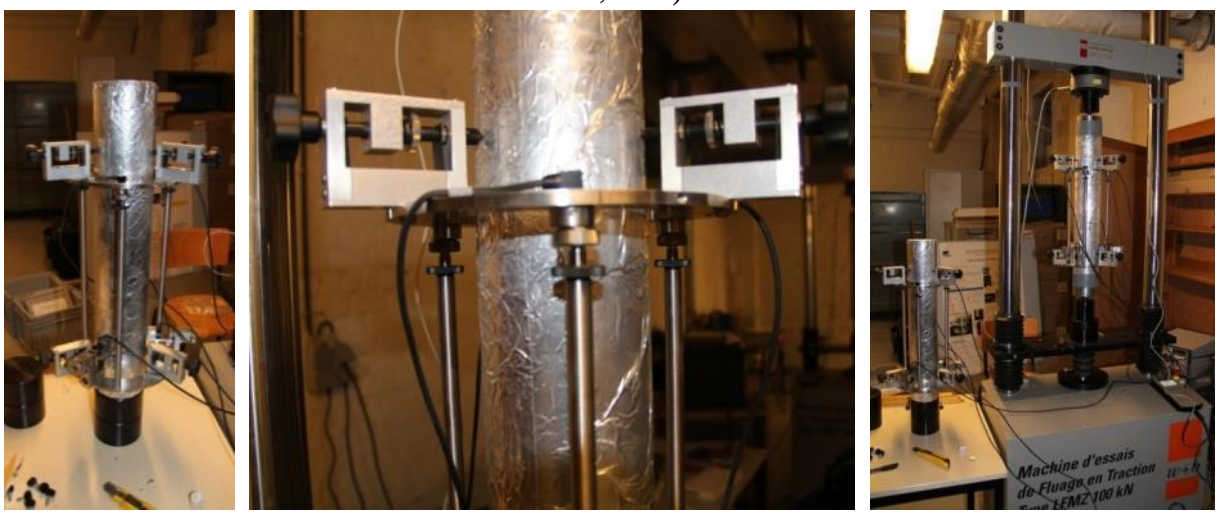

Figure 41 – Tensile creep test rig. Left to right: dummy specimen – top rig composed by 3 anchorages with elastic blade and 3 longitudinal sensors – general view.

The adaptation of the device for test in compression is presented in Figure 42.

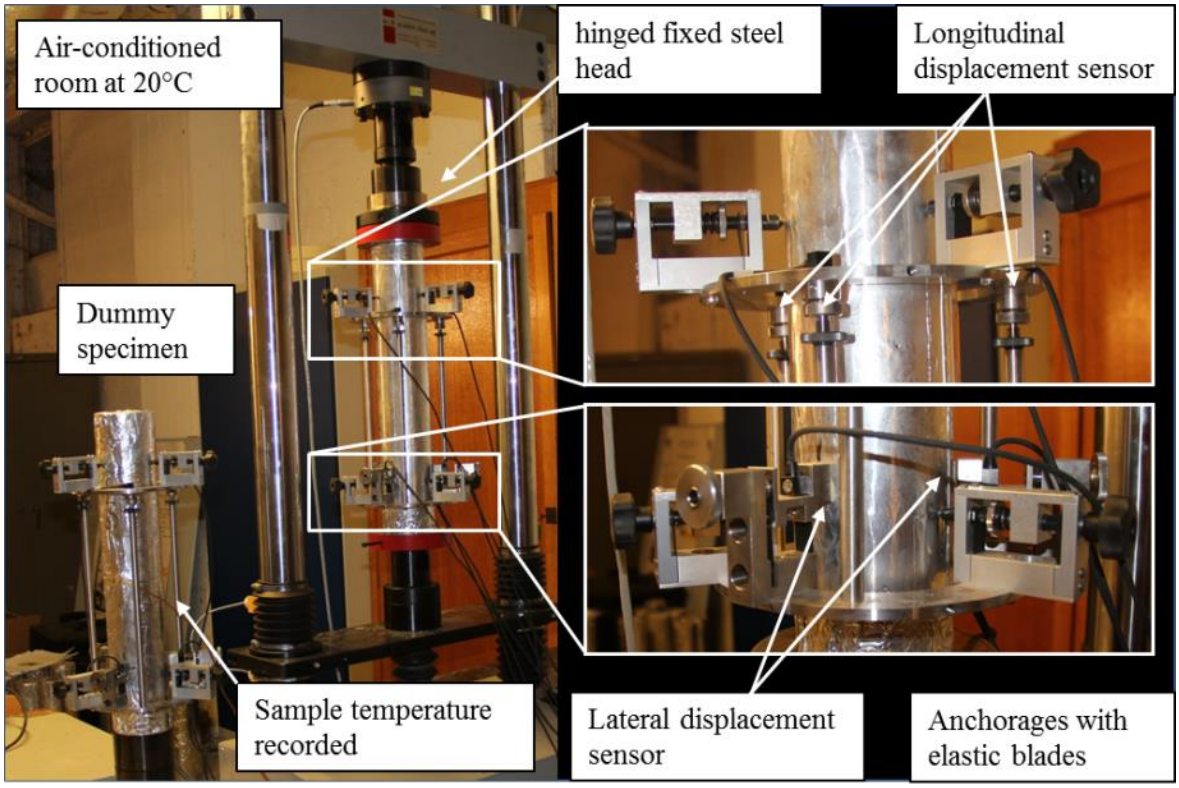

Figure 42 - Testing setup for the monitoring of the viscoelastic properties in compression (laboratory of Civil Engineering, BATir, ULB).

After casting, all specimens are placed in an air-conditioning chamber at 20°C and a relative humidity of 90%. Then samples are demolded, grinded on both circular end faces and surrounded by 2 self-adhesive aluminum sheets in order to keep the sample in sealed conditions. When test occurs at very early age in compression, a small layer of sieved concrete (+/- 1cm) is placed on the top of the sample in order to avoid any problem of pullout of the aggregate during the grinding. When test occurs in tension, the sample is bonded to two dollies after grinding with the 2-component fast curing adhesive X60 of HBM. The different steps of the sample preparation are presented in Figure 43.

(a) (b) (c) (d) (e) (f)

Figure 43 – Steps of the sample preparation. (a) Casting of the sample – (b) Glue is put at each extremity of the sample with the dollies and are placed in a rig which applied a small load on the glue during its hardening – (c) and (d) the extensometer is placed on the sample – (e) The hinges are connected to the dollies and the specimen is placed on the test rig – (f) An identical extensometer is placed on the dummy specimen.

SECTION 4.4 – HOW TO MONITOR THE MODULUS OF ELASTICITY OF CONCRETE, AUTOMATICALLY SINCE THE EARLIEST AGE?

This chapter is based on the joint publication of Claude Boulay, Stéphanie Staquet, Brice Delsaute, Jérôme Carette, Michela Crespini, Oumaya Yazoghli-Marzouk, Erick Merliot and Sandrine Ramanich entitled: "How to monitor the modulus of elasticity of concrete, automatically since the earliest age?" published in Materials and Structures, 47 (2014), 141–155. The contribution of Brice Delsaute was the development of the new test protocol used with the TSTM and the realization of the test performed with the TSTM and FreshCon.

It is generally accepted that, just after the casting of a concrete, a first period exists during which the material can be transported and cast into a mould where it can be vibrated and where it can flow to fill the mould (period of workability). Just after casting, the aggregates can move slowly under the effect of the gravity and, eventually, a bleeding can appear. Cracking is then possible under the effects of these movements, especially when reinforcement bars are present. A second period, or period of the setting, commonly defined after the results of penetration tests on cement pastes or mortars, corresponds to a progressive coalescence of a continuous path of hydrates. At the beginning of this period, the concrete stiffness is almost inexistent while, at the end of this period (t_0), the concrete starts to stiffen [80]. In a third period, after t_0, stiffness, thermal and autogenous deformations change rapidly so that risks of cracking become critical, especially when deformations are restrained. It is then considered that the material behaves like a solid. For the sake of predictions of structural behaviours, measurements of these parameters at early age are of a great interest [81,82].

This section presents new methodologies to monitor the hardening process of a concrete and more specifically the elastic modulus. Tests are performed on three different devices using a different test protocol are used and are compared. At ULB, the TSTM device is used. At Ifsttar, a new apparatus has been designed specifically the determination of t_0 and the monitoring of the sample stiffness for concrete. The device is called hereafter BTJASPE (French acronym for "BéTon au Jeune Age, Suivi de la Prise et du module d'Élasticité"). Both results are compared to classical tests which use unconfined samples removed from their cardboard moulds just after the final setting. These last experiments are considered as a reference to validate the new testing device. The Young's modulus can then be monitored during the first few hours and days with these two methods. Indeed, the reference tests could be performed without the need of a new testing device but they are really difficult to perform especially when samples are removed from their mould (brittleness of the sample) and when an extensometer has to be fixed on them. That's why the BTJASPE has been designed.

For each apparatus, the methodology consist in applying repeated loadings in compression, soon after the casting (BTJASPE) or the setting (TSTM and unconfined sample) of a concrete sample. The sample is kept at a constant temperature during the test.

Finally, complementary experiments gave i) the compressive and tensile strengths ($f_c(t)$ & $f_t(t)$) evolutions from the concrete setting until several weeks; ii) the heat released (q(t)) by the cement hydration and, iii) the ultrasonic pulse velocity (UPV) of compression waves (p-waves).

This section was realized in collaboration with Claude Boulay who has developed the BTJASPE and has performed the whole tests carried out at IFSTTAR (slump test, semi-adiabatic calorimetry, splitting tensile strength, compressive strength, BTPULS, BTJASPE and tests on unconfined sample).

4.4.1. Tests setups

► Material

The tests presented here were performed on the ordinary concrete for which the composition is presented in chapter 3. The slump is equal to 6.5 cm. An amount of 15 batches were made to cover the entire early age characterization (classical tests and automatic loadings) in both laboratories. Compressive test were performed on cylinders capped with sulphur mortar (Ø11 cm x 22 cm and Ø 16 cm x 32 cm). Ultrasonic pulse velocities were measured on cylinders (Ø11 cm x 19.5 cm for BTPULS) and U-shaped samples (concrete volume equal to 450 cm^3 for FreshCon).

For the sake of the maturity calculations, the heat released by the hydration of the cement has been measured in a semi adiabatic calorimeter for concretes [83,84]. Two tests were performed at two initial temperatures in order to obtain the activation energy (see below).

► Ultrasonic pulse velocity

The ultrasonic measurements were performed with BTPULS and FreshCon devices. Results obtained with these two equipments have already been compared [85] and they were in good agreement. BTPULS is a prototype designed in the 90's at IFSTTAR which provides three independent channels. Each channel is equipped with a pair of piezoelectric transmitter-receivers working with p-waves [86,87]. FreshCon has been developed more recently at the University of Stuttgart and allows p- or s-waves transmission time and frequency measurements through the sample [88].

► Strength measurements in compression and tension

Compressive and tensile tests were performed according to the European standards [89–93]. Specimens were cylinders, capped with a sulphur mortar. They were cured inside their mould for the early age determinations and cured at 20 °C in aluminium auto adhesive tapes for long term determinations.

► Stiffness monitoring with BTJASPE (confined specimens)

It is assumed that the results of the tests performed on unconfined samples are reference values for the Young's modulus. Such tests are reliable but at very early age, they are performed on very low strength samples and the operator has to be present when the concrete setting occurs. At this moment, the specimen must be handled very carefully just before starting the automatic loadings. A remaining problem for this type of sample is the fact that, due to the hydration process, the sample temperature does not remain constant during the test. It means that, comparisons between different concretes are not easy.

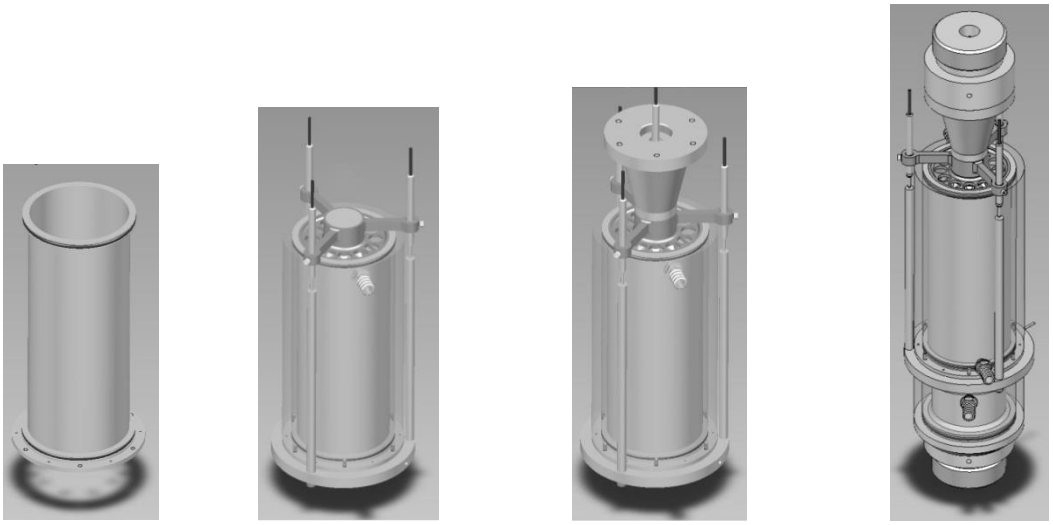

Figure 44 – BTJASPE. (a) Mould – (b) float, 3 LVDT's and double wall – (c) Upper bearing – (d) lower bearing and clamping devices.

A solution is provided by the equipment presented here. It has been designed in order to apply a testing procedure soon after the casting. Cyclic loadings in compression are applied every 10 to 60 minutes on a sample confined in a cylindrical stainless steel mould. The sample remains in the mould all along the testing and a circulation of water around the mould allows keeping the temperature constant. The mould (Figure 44a) is 100 mm in internal diameter, 102 mm in external diameter (1 mm in thickness) and 254 mm in height. It is fixed to a base (Figure 44b) together with three columns placed at 120 °. A thermocouple, passing through a hole centred at the base of the mould and sealed with a silicon elastomer, is embedded in the concrete after casting. The thermocouple measures the temperature at the centre of the sample. When the concrete has been poured inside the mould and levelled at about 200 mm from the base, an upper bearing plate (Figure 44c and Figure 45), called the "piston", is then placed on the solid phase of the fresh concrete. It is guided inside the remaining upper part of the mould. An application of grease inside the mould, before casting, is enough to avoid any movement of water and fine particles through the space between the inner walls of the mould and the piston. Holes, through the lower part of the piston (Figure 45), allow the bleed water to pass through so that the piston is always in contact with the solid phase of the concrete.

Through these holes, the amount of drying is negligible so that the autogenous conditions are preserved. The pressure exerted by the mass of the piston (1.92 kg) on the bearing surface ($7.8\ 10^{-3}$ m^2) leads to a negligible dry-out of the sample. Indeed, considering a hydrostatic pressure, the effect is similar to a depth of concrete equal to about 0.1 m. In order to avoid a sticking of the piston on the sample, a layer of oil, as thin as possible, is applied under its lower face. At mid height of the piston, a ring participates to the guidance. Three arms supporting three LVDTs are fixed at the upper part of the piston. The mean displacement measured by these LVDTs, between the piston and the three columns, is used as a control variable for the loading.

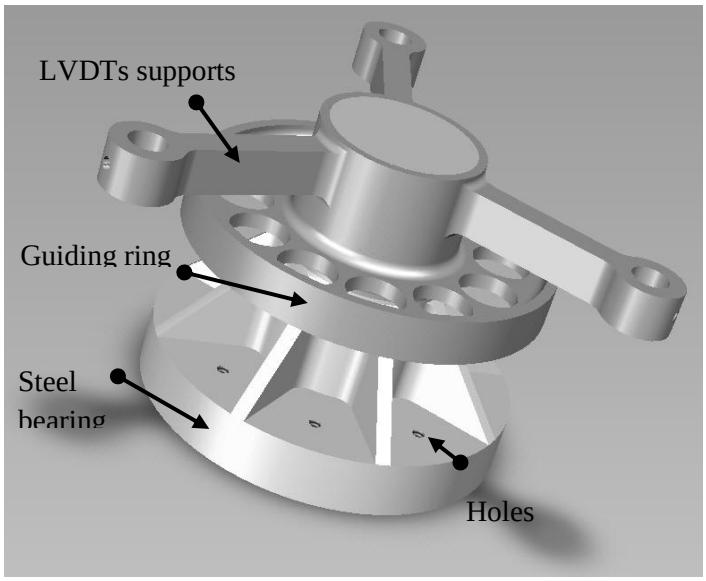

Figure 45 – Piston. It "floats" over the sample. A constant displacement is imposed at the level of the LVDTs support.

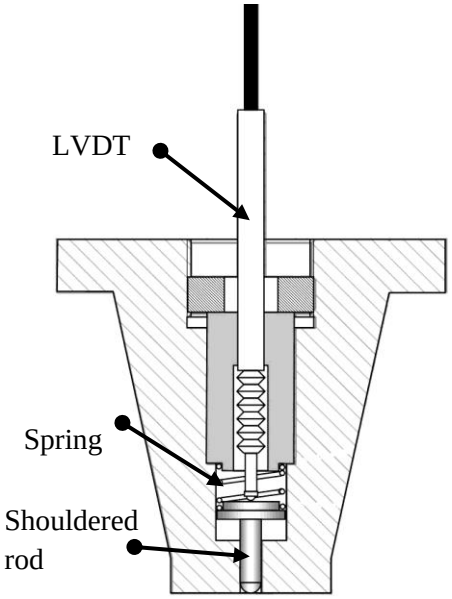

Figure 46 – Cut view of the upper bearing device. It is clamped under the load cell of the testing machine.

An upper bearing plate is fixed under the upper crosshead of the machine (Figure 44d and Figure 46). It is able to detect finely the contact with the sample, at the beginning of the loading cycles. Inside this conical bearing plate is located a small shouldered rod (spherical at the tip), acting like a piston, pushed downward by a spring. The position of this rod is measured by a displacement transducer. As a consequence, the contact with the sample can be detected, always at the same fixed position of this transducer, with a greater accuracy than with the testing machine load cell.

The hydraulic jack, located at the lower part of the machine, is actuated by oil under pressure. The heat flow coming from the oil (operating temperature: 50 °C) is evacuated by a circulation of water around the lower bearing plate (Figure 44d). The temperature of this bearing is controlled at 20 °C via the measurement of a platinum probe, embedded in the bearing, just under the sample.

Cyclic loadings are applied by a servo-controlled testing machine. Indeed, the process used with this equipment is as follow: for every cycle of loading, the piston of the jack moves up controlled with the piston displacement. The upper conical bearing detects the contact, and then the control is changed to the mean displacement measured by the 3 Linear Variable Differential Transformers (LVDTs) around the sample. A chosen displacement (the same for each cycle) is imposed, finally the sample is unloaded and the piston returns to its stand-by position (no contact with the sample). The load, the mean displacement of the 3 LVDTs and the temperature are recorded. This process can be manual but an automation of the cycles gives a real benefit.

The modulus of elasticity can be determined, for each loading cycle. The measurement of the mean value of the three displacements around the sample includes the deformations of the bearings and the effects of the mould reinforcement. In order to obtain the concrete modulus of elasticity, without bias, it is necessary to use complementary calculations to "extract" the sample deformation from the measurements. In this purpose, a finite element calculation has been performed, at the end of the design process (Figure 47). 3D elastic calculations were made for a series of increasing E-modulus values of the concrete sample. For each calculation, the stiffness of the sample is determined. This

stiffness is the slope of the curve *load / displacement*. An adjustment of a 2nd degree polynomial is applied to all pairs *stiffness / E-modulus* (Figure 48).

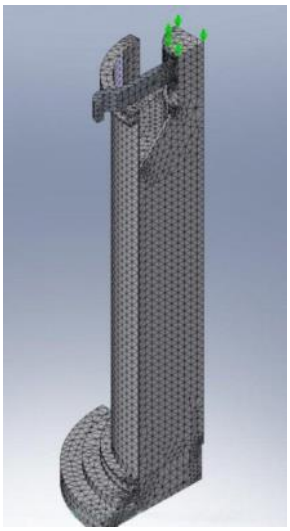

Figure 47 – Meshing used for the numeric computations

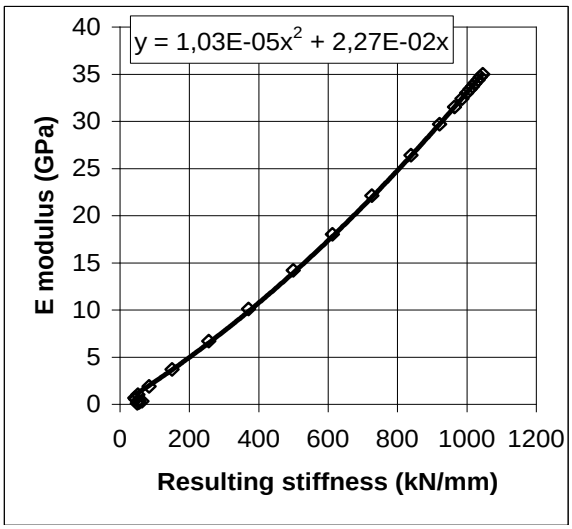

Figure 48 – Relation between the resulting stiffness and the E-modulus of concrete obtained by the numeric computation.

For each experimental cycle, the stiffness is the result of the measurements and the E-modulus can be determined with the function of the Figure 48. It was assumed, for finite elements calculations, a Poisson's ratio remaining constant (0.2) during the hardening process but this hypothesis has to be experimentally verified.

► Stiffness monitoring (unconfined specimens)

Results obtained with this last new procedure have been verified with measurements carried out on samples removed from their cardboard mould (Ø 112 mm x 220 mm in height) just after the setting time. The loading protocol is identical to that applied on confined samples.

For these reference tests, the mould is equipped with a thermocouple placed in the core. After the concrete is poured, the top of the mould is covered with cling film to prevent drying during the dormant period. Together with this sample, another sample is cast for UPV measurements. When the setting time is detected by the UPV measurements, the sample is removed from its mould and capped with a sulphur mortar according to EN 12390-3, after being wrapped in an aluminium self-adhesive film in order to avoid desiccation. It is then equipped with an extensometer (Figure 49) whose base length is 130 mm. This extensometer [74] is constituted by two rings made of aluminium alloy. Three cone-point rods are in contact with the sample on each ring. Each rod is guided by elastic blades and pushed toward the sample by a spring which exerts a constant load of about 0.2 kN. Three LVDTs at 120° from each other's measure the relative displacement between the rings. The mean displacement divided by the base length gives the deformation. Resolution and accuracy are equivalent to classical strain gauges. The same protocol of loading and the same upper and lower bearings than for the confined samples are used.

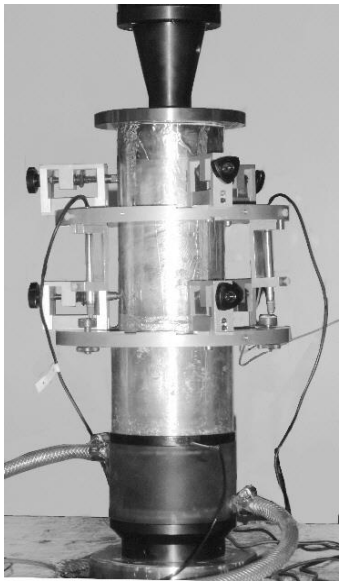

Figure 49 – The sample is between the bearing plates of the testing machine. An extensometer provides longitudinal and transversal deformations [74].

► Stiffness monitoring with the TSTM device

The process used with this equipment is as follow: for every cycle of loading, the piston of the jack moves, controlled with its displacement. The sample is then unloaded and the piston returns to a null force. Recordings are taken during the cycles. The Young's modulus is the result obtained for each loading cycle. In this test setup, the deformations in the span are not restrained (friction is supposed to be null with PTFE and plastic film). Results can be directly used to compute the Young's modulus.

4.4.2. Results and discussions

► Expression of the results in equivalent time

For all the tests performed during this experimental campaign, temperature histories can be different from each other. That is why it has been chosen expressing the results in an equivalent time scale (t_{eq}) [94–96].

For such an objective, the activation energy of the hydration reaction must be known. This determination was obtained with two calorimeters testing, performed at two different initial temperatures, thus providing two different temperature histories. The activation energy can then be adjusted in a calculation of the equivalent time of each sample in order to superimpose the two curves of heat release. For our concrete, a value of 32.2 kJ mol^{-1} allows superimposing the curves of the heat released over a period of 4 weeks.

All the tests performed at a constant temperature, different from the reference temperature, can be expressed in equivalent time at this reference temperature. Our tests performed on unconfined samples can also be expressed in equivalent time assuming that the temperature has been recorded. For the tests realised at the reference temperature, the equivalent time is equal to the real time.

► Relations between the Young's moduli, the strengths in compression and in tension

Knowledge of the elastic properties and strengths in compression and in tension was required in order to properly master the different protocols of loadings applied as well on BTJASPE as TSTM. That is why compression, splitting and E-modulus tests were performed at early age (0.36, 0.47, 0.79, 0.97, 1.16 and 3.23) on 11x22 cm² cylinders (3 samples at a time) capped with sulphur mortar whereas compression, splitting and E-modulus tests were performed on 16x32 cm² cylinders (3 samples at a time) at 7, 14, 28, 46 and 90 days. For each batch, a monitoring of a sample's temperature at early age was performed, in order to determine the equivalent time. Results are reported in the Table 6.

Table 6 – Mechanical properties (mean values of 3 samples).

Equivalent age (days)	Compressive strength (MPa)	Standard deviation (MPa)	Tensile strength (MPa)	Standard deviation (MPa)	E-modulus (GPa)	Standard deviation (GPa)
0.36	0.61	0.02	0.053	0.006	2,72	0.02
0.47	1.52	0.09	0.163	0.012	7,32	0.06
0.79	8.42	0.21	0.850	0.017	18,76	0.15
0.97	11.77	0.19	1.100	0.092	22,86	0.19
1.16	14.40	0.14	1.508	0.148	26,14	0.22
3.23	27.41	0.82	2.677	0.049	N/A	0.30
7.23	31.45	1.13	2.796	0.305	36,41	N/A
14.23	35.20	1.68	N/A	N/A	37,43	0.32
28.23	39.31	2.86	N/A	N/A	39,66	0.34
46.23	44.13	1.87	3.448	0.521	N/A	N/A
90.23	44.40	1.81	N/A	N/A	39,62	0.35

Time scale in equivalent age (T_{ref} = 20 °C)

In addition, it was also necessary to have models of the evolution of the mechanical properties in order to compute the loads applied to the samples at any age without risk of cracking. For our application, the Eurocode2 models (Part 1-1 - § 3.1) were not enough accurate between the setting time and one day. So, other models, proposed here, were applied taking the same notations than those used in Eurocode2.

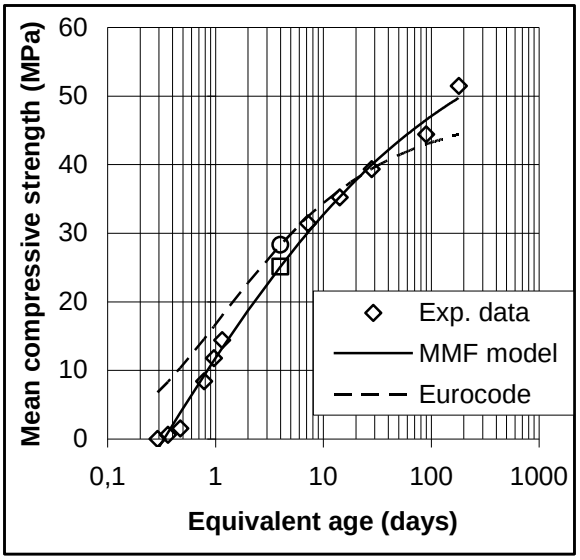

Figure 50 – Compressive strength function of the equivalent age.

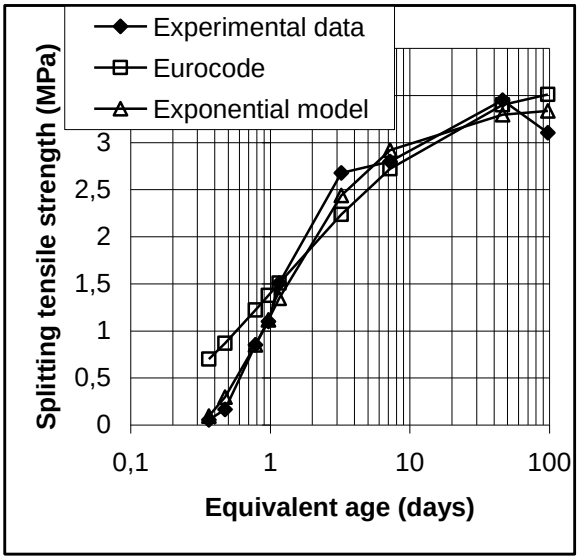

Figure 51 – Splitting tensile strength.

Concerning the evolution of the compressive strength, [97] proposed a model assuming a null strength before t_0. This model is accurate but does not describe very finely the period around the setting. That is why an S shape model [98], more accurate in this zone, has been chosen (Figure 50):

$$f_{cm}(t) = \frac{a\,b + c\,t_{eq}^{\,d}}{b + t_{eq}^{\,d}} \qquad 3$$

Where: $f_{cm}(t)$ is the compressive strength in MPa, t_{eq} is the equivalent time in days, a = -83.9 MPa, b = 0.56, c = 65.5 MPa and d = 0.3. In a similar way, the tensile strengths are well described by the following exponential model (Figure 51):

$$f_{ct,\,sp} = a\,\exp\left(-\frac{1}{t_{eq}}\right) - b \qquad 4$$

Where, for this concrete, $f_{ct,sp}$ is the tensile strength (splitting test) , t_{eq} is the equivalent time in days, a = 3.5 MPa, b = 0.13 MPa. Finally, two relations based on [98]: E / f_{cm} and f_{ct} / f_{cm} are proposed (Figure 52):

$$E = \frac{c'\,f_{cm}^{\,d'}}{b' + f_{cm}^{\,d'}} \qquad 5$$

$$f_{ct} = \frac{c''\,f_{cm}^{\,d''}}{b'' + f_{cm}^{\,d''}} \qquad 6$$

Where E is the Young's modulus, c' = 75000 MPa, d'= 0.75, b'=14.3 MPa, c'' = 5 MPa, d'' = 1.5 and b'' = 135 MPa.

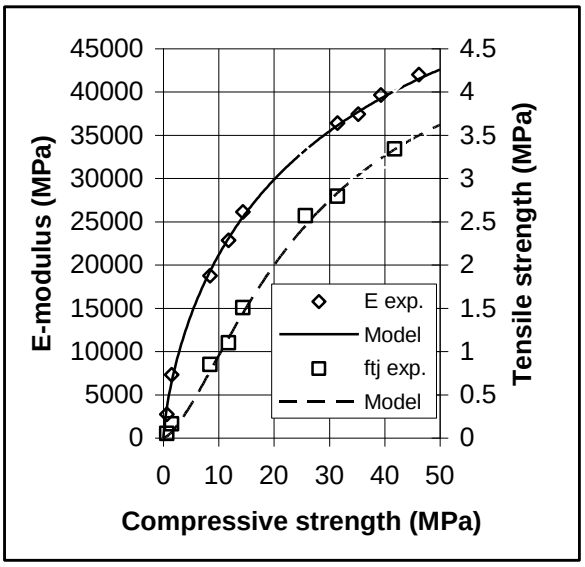

Figure 52 – Relations *fcj / E-modulus* and *fcj / ftj*.

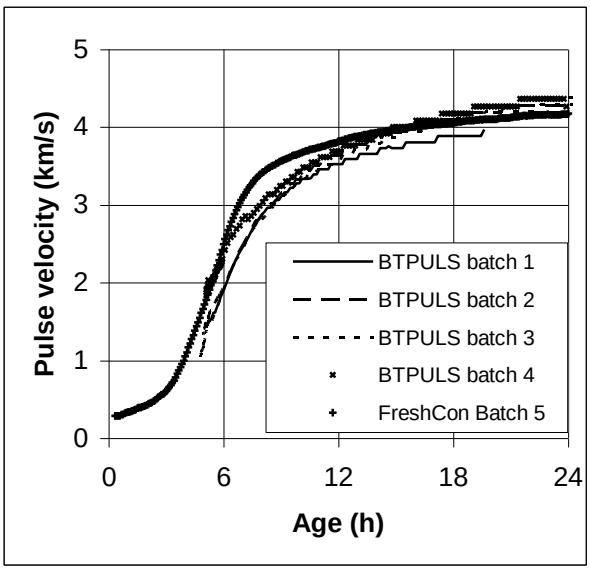

Figure 53 – UPV measurements with two types of apparatus.

► Monitoring of the UPV

The Figure 53 gives the 4 curves obtained with BTPULS and the recordings made by FreshCon. Results are in good agreement. FreshCon results indicate, according to [99], an initial and a final setting time respectively equal to 5.2 and 6.4 h. The initial setting time corresponds to the inflexion point of the curve *UPV / age*. This inflexion point can be found accurately on the derivative of the curve. A noise reduction process is adopted. In a first step, the *UPV / age* curve is fitted by a logistic function [100] having an "S" shape. The derivative doesn't present any noise. The peak of this derivative corresponds to the initial setting. The final setting corresponds to the time when the value of the derivative has decreased down to 80 % of the peak.

BTPULS results indicate, with less accuracy and with same criterions, an initial setting time, in function of the batch, ranging from 4.9 to 5.2 h and a final setting time included between 6.4 and 7.1 h.

► Monitoring the evolution of the E-modulus in compression with BTJASPE

Four samples of the same mix design were cast successively (at months of intervals), in the steel mould and four unconfined samples were cast and tested after their setting.

The loading protocols are similar. Measurements on confined samples start soon after the casting while they start after the setting for the others. The temperature of confined samples is set to 20 °C. The temperature recorded in the core of the specimen shows a flat response (Figure 54) indicating a perfect control due to the use of a metallic mould with good heat transfer properties. The temperature of the unconfined sample exhibits a peak due to the hydration reaction. As the temperature is not constant, results have to be expressed in equivalent age.

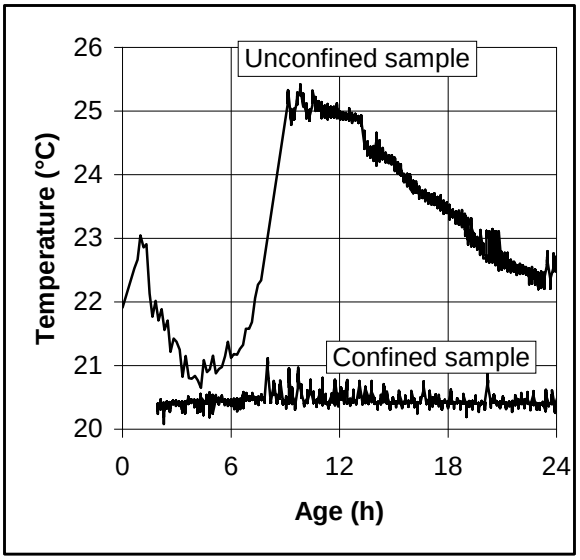

Figure 54 – Temperatures recorded in the core of the confined and unconfined samples.

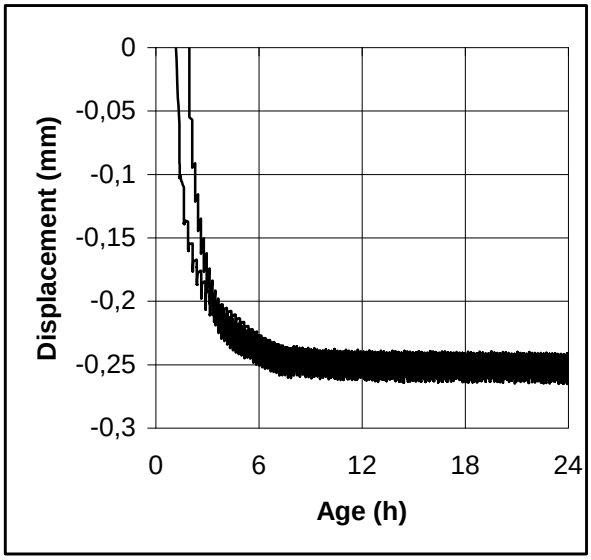

Figure 55 – Mean displacement around 2 samples tested in the steel mould. Cycles with 20 µm amplitude are visible.

In the dormant period, the base line of the displacements measured around the confined sample (Figure 55) shows clearly the effects of the gravity which compact the solid particles. This displacement corresponds to air bubbles and water going up. It can be observed that changes in the displacement rate of the base line occur between 3 and 8 hours. Before this period, displacements are counted in hundreds of µm while after they are counted in micrometers.

Applying a mean displacement around the sample (the same value for each cycle) induce an increasing of the load as the E-modulus of the concrete develops (Figure 56 and Figure 58) from one cycle to the other.

For each test in confined conditions, the stiffness (slope of the *Load / Displacement* curve) of the sample is computed for each cycle (Figure 57) from the set of recordings and entered in the functions of the Figure 48 in order to monitor the evolution of the Young's modulus.

For the unconfined samples, a *stress / strain* curve is directly obtained for each cycle (Figure 59). The E-modulus is the slope of this curve. It can be observed that, regardless of the cycle, the linearity of these graphs is always excellent. Thus, the question of the choice between a secant modulus of elasticity and a tangent modulus of elasticity does not appear.

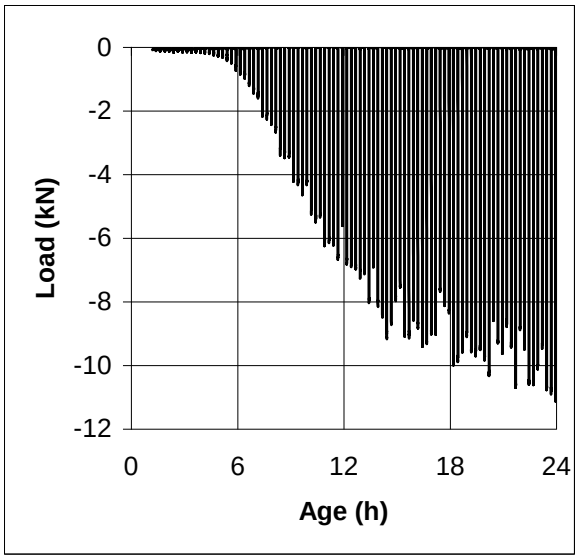

Figure 56 – As the stiffness of the sample increases, the maximum load increases under the effect of the imposed constant displacement. For confined samples, loadings start just after casting.

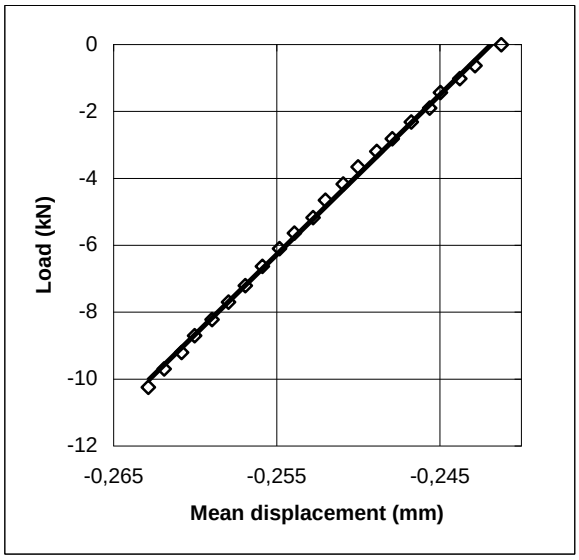

Figure 57 – During each cycle, the displacement is controlled. The rate is 1 µm / s. 16 µm are imposed for each cycle for the samples of the batches 1 to 3 and 70 µm for the others. On confined sample, an experimental stiffness is calculated for each cycle.

Results obtained with BTJASPE (at a constant temperature) are compared, at the Figure 63, to the results of the reference samples (whose temperature was not constant) after having expressed their data in equivalent time (Activation energy Ea = 32.2 kJ mol-1, T_{ref} = 20.3 °C).

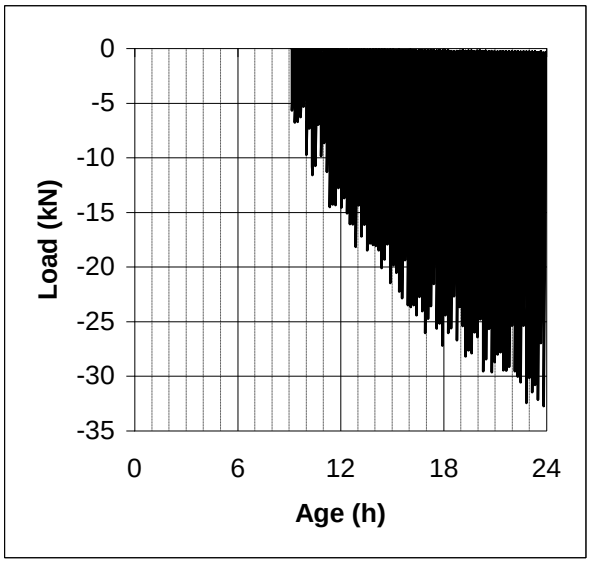

Figure 58 – For unconfined samples, the cycles start after the setting.

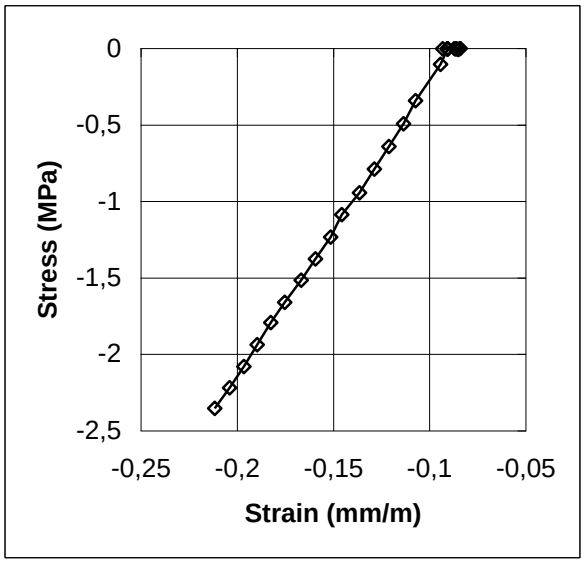

Figure 59 – For unconfined samples, a *stress / strain* curve is obtained for each cycle. The slope represents the E-modulus.

► Monitoring the evolution of the E-modulus, with the TSTM

One sample was cast in the TSTM device for the measurement of the evolution of the E-modulus. Measurements on the sample start soon after the setting. The temperature of the sample is controlled

at 20 °C. Except a little peak of 1 °C, the temperature recorded in the core of the specimen shows a flat response (Figure 60) which indicates a very good control due to the use of an aluminium mould with good heat transfer properties. Each loading is controlled based on force measurements. In order to avoid any damage on the sample, it was chosen to apply a constant *stress / strength* ratio equal to 20 %, assuming an elastic zone in the range 0 to 40 %. The resulting effect on the maximum strain for each cycle is given in Figure 61. The Figure 62 shows the evolution of the slope of the *strain / stress* curve of a typical cycle. A slight non linearity can be observed so it was chosen to remove the non linear part of the curve (slope calculated between 30% and 80% of the maximum load reached in the cycle).

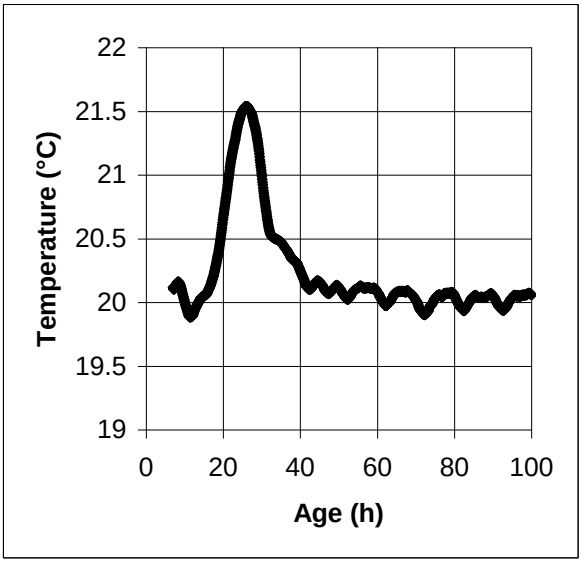

Figure 60 – Evolution of the temperature in the sample

► Comparison between the three methods

Figure 63 shows that the E-modulus evolutions of confined and unconfined samples are in good agreement. It means that the computations of confined samples give a realistic image (comparison with the reference unconfined samples) of the combination of the sample, the mould and the bearings. The differences observed here could be attributed to the concrete properties for the different batches that were mixed within a period of 12 months and different mixing techniques were used. The setting times gauged by UPV shows such discrepancies. It seems that the influence of the Poisson ratio used for the finite element calculations doesn't have a significant influence on the result. More investigations are needed.

Despite their slight discrepancies, the curves of the 8 tests performed on confined and unconfined specimens are grouped during the period of the setting (not represented). The E-modulus of all the tests starts to increase at about 5.6 h. This setting time is also detected at a similar time by UPV monitoring. According to the criterion indicated by [99] (decreasing at 80% of the peak of the derivative of the *UPV / time* curve), the final setting time is 6.4 h.

As expected, after the UPV results obtained by [85,88], recordings of the Figure 53, doesn't show a clear event indicating the end of the setting except the beginning of a linear part of the curve. For all the tests, this part starts when the value of the E-modulus crosses the 3 GPa line. It has been observed that such a value correspond to an UPV ranging from 2800 to 3000 m/s [101]. Such a value is also

reported by [102] as the value corresponding to the final setting given by penetration tests according to ASTM C403 procedure [103]. For the bunch of our samples, it leads to setting times ranging from 8.2 to 9.6 h. This setting process covers a period between 5.7 to 9.6 h for all the batches. For individual samples it covers about 2 hours. At 9.6 h the E-modulus for all the samples ranges from 3 to 6 GPa. Concerning the unconfined samples, they were handled quite safely after 7.5 h. It was then possible to remove the cardboard mould without breaking the sample but with infinite cares. The pin points of the extensometer entered the concrete easily. Nevertheless, the rings were correctly fixed.

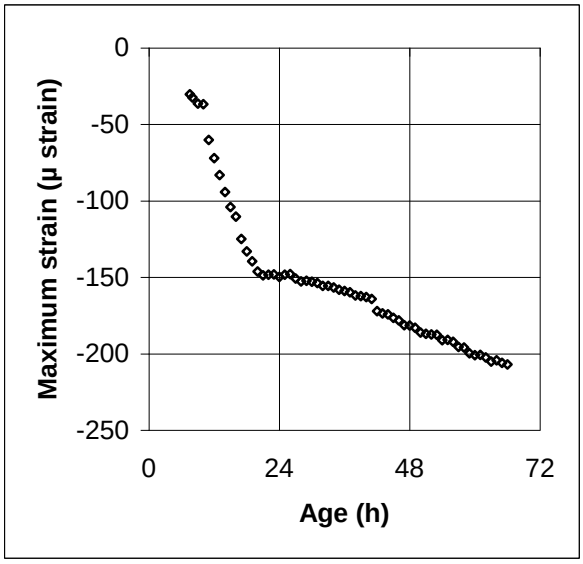

Figure 61 – Evolution of the maximum strain for each cycle

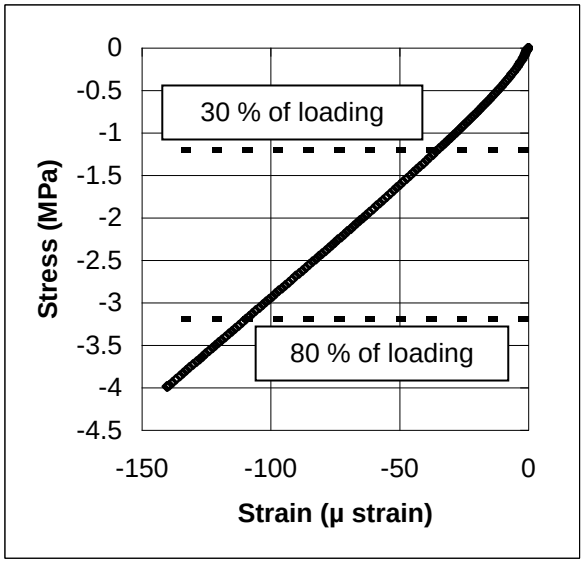

Figure 62 – Strain / stress curve during one cycle

The Figure 63 shows also the E-modulus evolution for one sample in the TSTM device. The general shape of the curve is similar to the other two despite a small gap at the beginning of the evolution of the stiffness. This point must be highlighted: indeed, the tests were performed by several operators, with different mixing techniques, three different testing setups, two different loading protocols and at different times. The components and the mix design of the concrete were the only similar things. Nevertheless, more testing are needed.

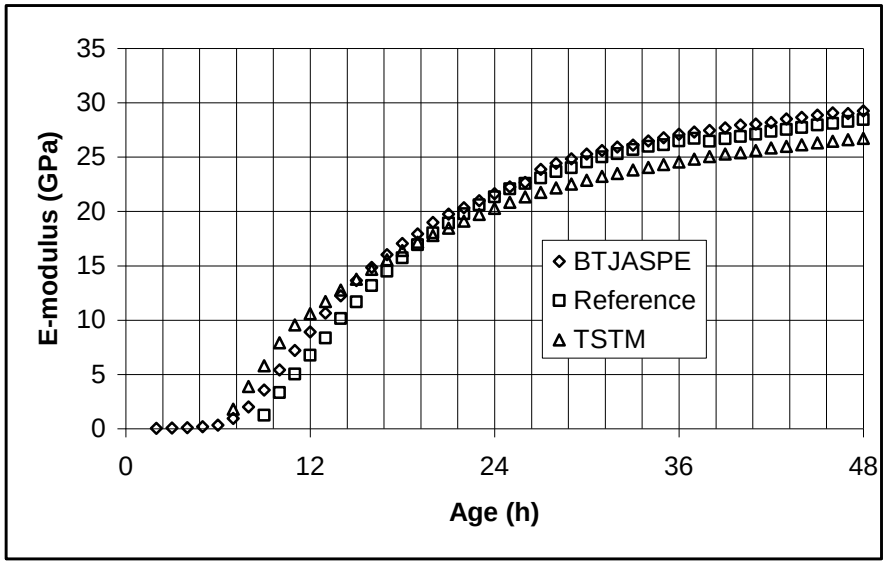

Figure 63 – Comparison of the evolutions of three techniques

SECTION 4.5 – TESTING CONCRETE E-MODULUS AT VERY EARLY AGES THROUGH SEVERAL TECHNIQUES: AN INTER-LABORATORY COMPARISON

This chapter is based on the joint publication of Brice Delsaute, Claude Boulay, José Granja, Jérôme Carette, Miguel Azenha, Cédric Dumoulin, Grégoris Karaiskos, Arnaud Deraemaeker and Stéphanie Staquet entitled "Testing concrete E-modulus at very early ages through several techniques: an inter-laboratory comparison" published in Strain Journal, volume 52, issue 2, April 2016, 91-109. Results from the BTJASPE and BTPULS were provided by Claude Boulay (Ifsttar), results from EMM-ARM were provided by José Granja and Miguel Azenha (UMinho) and results from the Smart Aggregate were provided by Cédric Dumoulin, Grégoris Karaiskos and Arnaud Deraemaeker at ULB.

The design of concrete structures is based on calculation rules, which often do not take into account the very early age behaviour of the material. However, during this period, structural concrete is subjected to strains due to the hydration process of cement. If these strains are restrained by concrete itself or surrounding boundaries, stresses start to build up that can lead to the formation of cracks. Among the parameters involved in the stress build up, the stiffness evolution is of major importance. This section reports the use of eight different techniques aimed at stiffness evolution assessment, applied on the same concrete mix, in a round robin experimental test within three laboratories.

Eight different techniques have been implemented in the three laboratories. They can, a priori, be sorted in three classes, according to their respective ranges of loading rates. There are four techniques of quasi-static loadings (**QS_0**: classical extensometry (all three labs); **QS_1**: automated loading with BTJASPE (IFSTTAR), **QS_2**: automated loading using QS_1 protocol (IFSTTAR), **QS_3**: automated loading with a TSTM (ULB)); one technique of resonant frequency loadings (**RF**: EMM-ARM testing technique (UMinho)) and three techniques of high frequency loadings (**HF_1**: classical UPV measurements with FreshCon (ULB), **HF_2**: classical UPV measurements with BTPULS (IFSTTAR) , **HF_3**: smart aggregates (ULB)). These different protocols were applied without necessarily controlling the temperature history of the specimens in the same way, often due to practical limitations associated to the test setups and the size of specimens themselves. That is why observations are compared after having expressed results at the same concrete maturity using the equivalent time method [104]. These techniques scan a wide variety of ways for monitoring the E-modulus of concrete since the earliest age. They are suitable for both industrial and research applications. In the following lines, device not yet presented will be described into details. It will be followed by the analysis of the results organized in three parts: firstly, a comparison between the results obtained with the low frequency testing methods (**QS_1, QS_2, QS_3, RF**) with a discussion on the effect of the stress amplitude and the stress-rate on the results obtained with the low frequency testing methods; secondly, a discussion on the results obtained with the high frequency testing methods only (**HF_1, HF_2, HF_3**) and thirdly, a discussion on the relation between the results obtained with the low frequency testing methods and the high frequency testing methods.

4.5.1. Specimen preparation and Material Characterization

The same material is used in the three laboratories. The mixture proportions are given in chapter 3. Fresh concrete was mixed mechanically or manually depending on the volume of the batch (from 2 liters to approx. 40 liters). Even though these differences can lead to scattered results, no significant effect was observed in the performed experiments on this concrete as presented in the newt part of this section.

The strength evolution was useful for quantifying the limits of the automatic loadings applied at early age in order to avoid any damage of the samples. The samples were cylinders (Ø 110 mm x 220 mm) or cubes (100 mm). They were cured inside adhesive aluminum tape at 20 ºC, and capped with sulphur mortar when necessary. Results are reported on Figure 64.

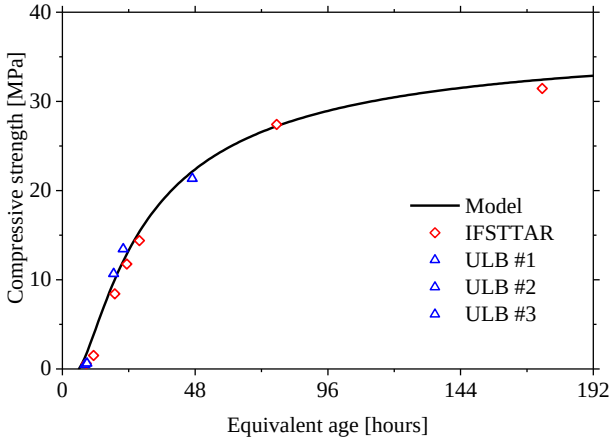

Figure 64 – Compressive strength results obtained by the teams of IFSTTAR and ULB.

For the sake of these calculations, the compressive strength is modelled by the following mathematical expression:

$$f_{cm} = a \cdot e^{-\frac{c}{t}} - b \qquad 7$$

With: $f_{cm}(t)$ expressed in MPa

a = 38.04 MPa, b = 1.67MPa, c = 24 hours

t: equivalent time since mixing (in hours)

The activation energy was determined through calorimetric testing. This parameter, associated to temperature recordings, allowed calculations, based on Arrhenius laws, of an equivalent age (t_{eq}) [8, 9,10] for each of our results. These calculations were performed at a fixed reference temperature equal to 20 °C.

Table 7: Classical test setup (QS_0) in the three laboratories.

	Extensometer	*Sample*		*Protocol of loading*	
	Spacing (cm)	*Heigth (cm)*	*Diameter (cm)*	*Loading (MPa)*	*Stress rate (MPa/s)*
IFSTTAR	12	22	11	5% to 30% of f_{cm}	0.5
ULB	12	22	11	20 % of f_{cm}	0.2 to 0.55
U Minho	10	30	15	0.8 to 33% of f_{cm}	0.3

The setting period corresponds to a period between the time when a needle penetrates completely a sample of mortar or cement grout and the time when it does not penetrate anymore the sample [103,105,106]. In field applications, the final setting time has also been identified, as mentioned by

Sant *et al.* [105], like the time when the bleeding water is reabsorbed which indicates the creation of vapour spaces in the matrix. As penetration tests do not apply specifically for concrete, the work of Robeyst *et al.* [99] compared ultrasonic testing to penetration tests performed on sieved concrete by removing the coarse aggregates. They used ultrasonic P-waves in transmission mode. The evolution of the ultrasonic pulse velocity shows an experimental S shape and the corresponding derivative function is calculated. The final setting was considered to occur when the value of this derivative function decreases down to 80 % of the peak value. This last technique was applied in the present research work. It is worth underlining that the final setting corresponds to a time when a sample can be manipulated, but gently to avoid any rupture. Before this time, any manipulation leads to a rupture. It is also the time when the stiffness of the material begins to increase significantly. This final setting is, here, called t_0 [107]. An estimation of this time is required for starting tests just after concrete setting.

Measurements of the modulus of elasticity were performed in the 3 laboratories and stress rates were ranging from 0.20 to 0.55 MPa/s for the three laboratories (see Table 7 and Table 8).

Table 9 shows the results of the mean values of the quasi-static loading E modulus obtained by the three laboratories according to the reference test set up (QS_0).

Table 8: Loading rates for each device.

Device	*Loading control (corresponding strain or stress rate)*	*Classification*
Classical tests (QS_0)	0.2 - 0.55 MPa/s	Low frequency
BTJASPE (QS_1)	5×10^{-6} /s (0.001 to 0.2 MPa/s)	
TSTM (QS_3)	10 s from 0 to 0.2 f_{cm} (0.002 to 0.5 MPa/s)	
EMM-ARM (RF)	9-45 Hz (0.1 to 1×10^{-6}/s*)	
BTPULS (HF_2)	10-100 kHz	High frequency
FreshCon (HF_1)	10-100 kHz	
Smart aggregates (HF_3)	10-100 kHz	

*Strain rate computed by double integration of recorded accelerations and use of analytical derivations [56] (beam theory).

As loading protocols are very similar, these results are mixed in order to obtain a single description of the evolution of the E-modulus by these classical means as it is shown in Figure 65.

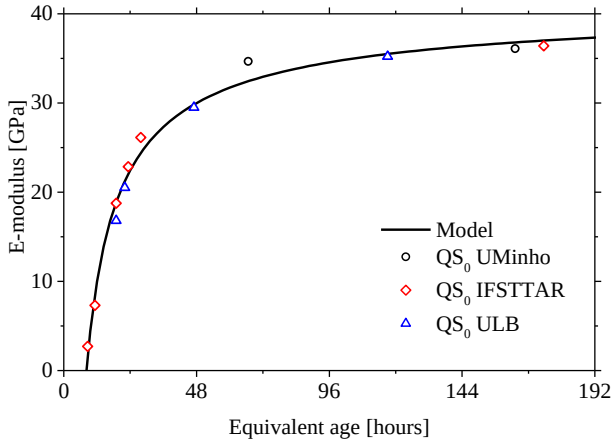

Figure 65 – Evolution of the quasi-static E-modulus obtained with classical methods (QS_0). A model for quasi-static E-modulus is calibrated on these data.

For the sake of the analysis of our results, the following mathematical expression is proposed (Figure 65):

$$E(t) = d - e.\left(\frac{\tau}{t}\right)^{f} \quad 8$$

Where *E(t)* is expressed in GPa,

t: equivalent time since mixing (in hours),

d = 41.57 GPa, *e* = 191.04 GPa, $\boldsymbol{\tau}$= 1 h and *f* = 0.72.

This mathematical expression has been calibrated to fit the quasi-static loading E-modulus results obtained with the reference set up (QS_0) and shown in Table 4. This model is used in Figure 65, Figure 73, Figure 74, Figure 76, Figure 77, Figure 85 and Figure 87 as a reference curve for comparison. This equation was already used in [98] to model the growth of bacteria populations but it has been chosen only for its mathematical properties for the determination of the early age properties of cement based material. This function is accepted as the reference for the comparisons between the different methods and will thus be used recurrently in the following sections.

This kind of test does not provide an accurate estimation of t_0; as the first measurement could only be made 1h and 40 minutes after a t_0 determined by other means (UPV, QS_1 or RF) presented in the next parts of this section.

4.5.2. Description of the methods

Methods using the BTJASPE (QS_1), unconfined specimen (QS_2) or the TSTM (QS_3) are not presented here. Full description of these devices and their associated tests protocol are given in section 2 and 4 of this chapter.

- Quasi-static loadings

REFERENCES TESTS (QS_0)

In the three laboratories, the reference tests (QS_0) were performed, after the concrete setting (t_0), on cylinders at different ages. For each test, strains were measured by extensometers. For the three laboratories, the extensometers are almost similar: i.e. three transducers (LVDTs) measuring the relative displacement between two rings fixed to the specimen, as presented on Figure 66. Prior to the test, specimens were kept in a curing chamber at 20ºC. However, the protocol of loading, size of the specimen and extensometers used for the E-modulus determination presented some differences among the three involved laboratories, as synthesized in Table 7 which follows the nomenclature of Figure 66. The selected testing ages associated to the results are given further in

Table 9.

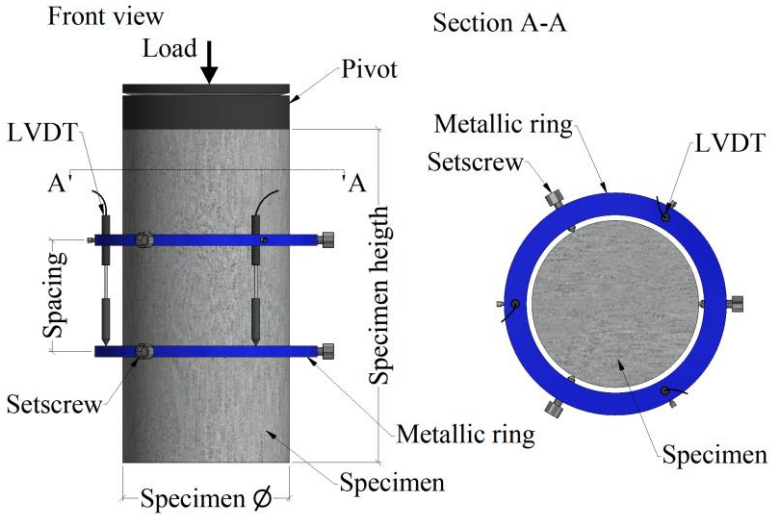

Figure 66 – Classical test setup (QS_0) with extensometers for quasi static loadings on concrete cylinder for quasi-static E-modulus monitoring.

At IFSTTAR, the testing specimens were cylinders with 110 mm in diameter and 220 mm in length. The first tests were performed as early as 7 hours after casting. Strains were measured by extensometers, with results comparable to those of strain gauges [74]. The protocol of loading consisted in applying four cycles between 5 and 30 % of the strength measured on other cylinders (with the same geometry) just before the test [108]. The quasi-static E-modulus is evaluated during the loading cycle. The loading rate was set to 0.50 MPa/s. The testing equipment included a hydraulic actuator with 500 kN of maximum load.

At ULB, similar cylinders and the same extensometer were used. 20% of the concrete strength at the time of the test was applied within 10 seconds, on four different samples. Corresponding stress rates were ranging from 0.20 to 0.55 MPa/s, depending on the age of the sample. The quasi-static E-modulus is evaluated during the loading cycle. The testing equipment included a hydraulic actuator with 1000 kN of maximum load.

At the University of Minho, cylinder specimens (150 mm in diameter and 300 mm in length), have been tested under cyclic compression according to LNEC E397 [109]. The protocol of loading consisted in applying five cycles between 0.80 MPa and 33 % of the ultimate strength at the age of testing. The quasi-static E-modulus is evaluated during the loading cycle. The loading rate was set to 0.30 MPa/s. The testing equipment included a hydraulic actuator with 2000 kN of maximum load.

Table 9: Classical extensometry tests (mean values) according to the reference set up QS_0.

IFSTTAR[(1)]		*ULB*[(2)]		*U Minho*[(3)]	
Time (hours)	*E-modulus (GPa)*	*Time (hours)*	*E-modulus (GPa)*	*Time (hours)*	*E-modulus (GPa)*
8.64	2.72	18.96	16.8	66.72	34.66
11.28	7.32	22.08	20.5	163.2	36.1
18.96	18.76	47.04	29.5		
23.28	22.86	117.12	35.2		
27.84	26.14				
173.52	36.41				

[(1)]Mean values of 3 specimens
[(2)]Value of 1 specimen
[(3)]Mean values of 3 specimens

RESONANT FREQUENCY METHOD (RF)

The EMM-ARM testing technique (Elasticity Modulus Measurement through Ambient Response Method) has been initially proposed by Azenha *et al.* [110] for the continuous measurement of concrete stiffness since the instant of casting. It is called here RF (Resonant frequency). Since its initial proposal for concrete testing, it has been extended towards application to cement paste [111], cement stabilized soil [112] and structural adhesives [113]. A more recent work has demonstrated the in situ applicability of the method and introduced changes that allow re-usability of parts [114]. The application of the RF method, in the context of this research, was fully made at the UMinho laboratory.

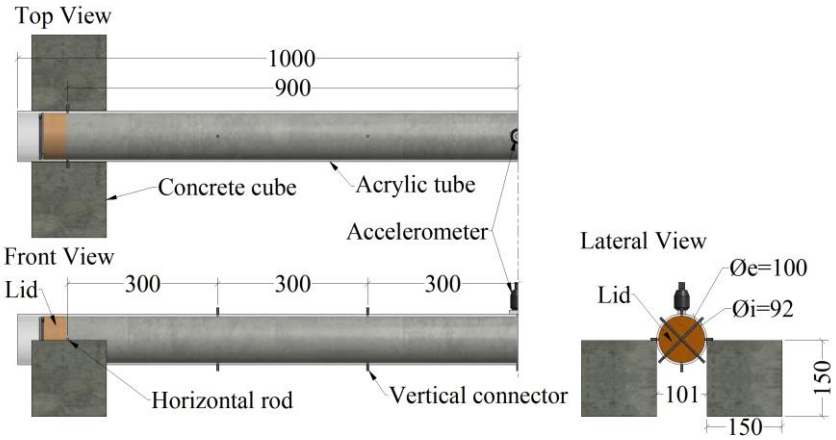

Figure 67 – EMM-ARM testing with acrylic mould (RF_A) for quasi-static E-modulus monitoring (units: mm).

The general principle of RF consists on continuously monitoring the first flexural resonant frequency of a composite beam with known geometry and support conditions, which contains the material to be tested since the fresh state. The evolution of resonant frequency can be directly and quantitatively correlated to the evolution of E-modulus of the tested material, without any kind of ambiguity of user dependency. The test procedure is fully automated and provides results in real time.

For the experiments envisaged in this research, three testing geometries have been adopted, both based on simply supported conditions for the test beam: (i) the cylinder shaped specimen inside an acrylic mould (RF_A) (Figure 67); (*ii*) a similar cylindrical shape beam similar to the one presented in Figure 67 but with internal/external diameters of 84/90 mm and 900 mm of span, and made of PVC (RF_P); (*iii*) the prismatic shaped specimen inside a reusable metallic mould (RF_M) (Figure 68). Even though the experimental setups, and interpretation techniques have been thoroughly explained and discussed in previous publications [110,112], some brief remarks are given here for the sake of self-sufficiency of this section.

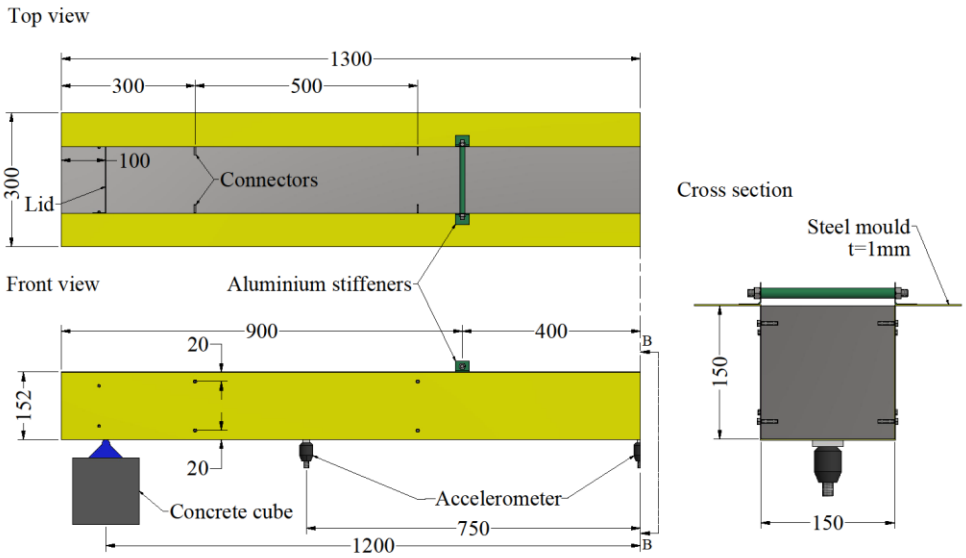

Figure 68 – EMM-ARM testing with metallic mould (RF_M) for quasi-static E-modulus monitoring (units: mm).

The acrylic mould (RF_A) is 2000 mm long, with internal/external diameter of 92/100 mm, density ρ = 1286.89 kg/m^3 and E-Modulus of $E_{acrylic}$ = 3.3 GPa. The PVC mould (RF_P) is 1000 mm long, with internal/external diameter of 84/90mm, density of 1463.49 kg/m^3 and Young's Modulus of 4.5 GPa. Both moulds are crossed by horizontal rods at their supporting points (longitudinally spaced by 1800 mm and 900 mm for the beams RF_A and RF_P, respectively) and vertical rods that act as connectors of mould/specimen. Lids are utilized at the extremities: one fixed lid, placed before casting and a removable lid, aimed to be placed after casting. Due to the nature of the moulds, they require inclined/vertical position for casting. As soon as the removable lid is placed in position and excess air is purged, the composite beams are placed under simply supported conditions on the rods which are in turn placed on concrete blocks. At this stage, an accelerometer is attached to the mid span section of each of the beams (see Figure 67), and the test starts.

The metallic beam was devised for reusability and increased robustness for in situ application [114]. It is made of a 'U-shaped' metallic alloy plate (ρ_{plate} = 7800 kg/m^3 and E_{plate} = 170 GPa), that has a total length of 2600 mm. The space for concrete placement spans through the central 2400 mm of the mould, with a cross section of 150 x 150 mm². The cross section shape of the mould was devised to assure that the centre of gravity of the metallic beam coincides with the centre of gravity of the tested concrete. Lids are placed near the extremity of the beam, right over the place where steel supports are placed to assure a free span of 2.4 m. Two aluminium stiffeners exist at 800 mm from the supports, in order to avoid significant transverse deformations of the metallic plates due to the weight of concrete. Connectors are also placed at 200 and 700 mm from the supports, according to the cross sectional scheme shown in Figure 8, in order to assure full bond conditions. Three accelerometers are placed on the bottom surface of the beam according to the positions shown in Figure 68. This variant geometry of EMM-ARM results in easier casting operations, as the mould is kept in its final testing position since the instant of casting, with the accelerometers placed in position even before casting, which was not possible with the acrylic/PVC moulds. Also, the reusability of the mould provides a more sustainable testing protocol, from both the economic and environmental points of view. The feasibility of the metallic mould for EMM-ARM has been tested and reported in a previous work [114] with satisfactory results. All mould beams are tested in the scope of this work to extend their mutual

validation and make a deeper analysis of the relative adequacy of these methods to test very early stiffness developments of concrete.

Accelerations of the monitored points have been measured for 28 days with sampling frequency of 200 Hz and PCB accelerometers with 10 V/g sensitivity, 0.15 to 1000 Hz frequency range and 225 grams of mass. Packets of 60 seconds of data have been taken every 15 minutes with a 24 bit data logger (NI 9234). Data processing to obtain the resonant frequency of the beams was made through the Welch procedure [115], involving windowing, averaging and Fourier transforms, according to a process that has been described in detail in [110]. Based on the resonant frequency of the composite beams, and the detailed knowledge of their geometries, mould stiffness and global masses, the stiffness of the tested concrete was obtained through analytical derivations based on the dynamic equations of motion of the corresponding composite beam (detailed explanations in [110]). This procedure was implemented in LabVIEW [116], thus allowing continuous automatic information about the calculated E- modulus in all tested beams. Temperature measurements took place in the central point of the cross section of each concrete specimen. The experiment was conducted in a climatic chamber with temperature of 19.2 ± 0.5 ºC.

A final remark is given in regard to the applicability of the analytical derivation of the equations of motion used for E modulus estimation: before the structural setting instant, such equations that rely on several assumptions related to concrete as a solid material may not hold, and therefore the EMM-ARM E-modulus estimations before setting time shown in Figure 66 are plotted as dashed lines. In fact, even though the reported evolutions seem quite feasible, they may not be rigorous at this period.

► Ultrasonic Pulse Velocity (UPV) measurements

CLASSICAL UPV MEASUREMENTS: HF_1 AND HF_2

On this concrete, two classical techniques of ultrasonic measurements were performed [88,117,118]. First, the FreshCon (HF_1) device (see Figure 69) developed at the University of Stuttgart was used due to its ability to detect very early age signals. Ultrasonic pulses of 5 μs at 800 V are sent through ultrasonic transducers (0.5 MHz resonant frequency). The ultrasonic pulse velocity (UPV) can therefore be computed before setting. In addition, the UPV was measured with a BTPULS (Béton Transmission Par Ultra Sons, HF_2) device developed at IFSTTAR [85,119]. This additional test, performed after the setting, was performed for comparative purposes between these two techniques.

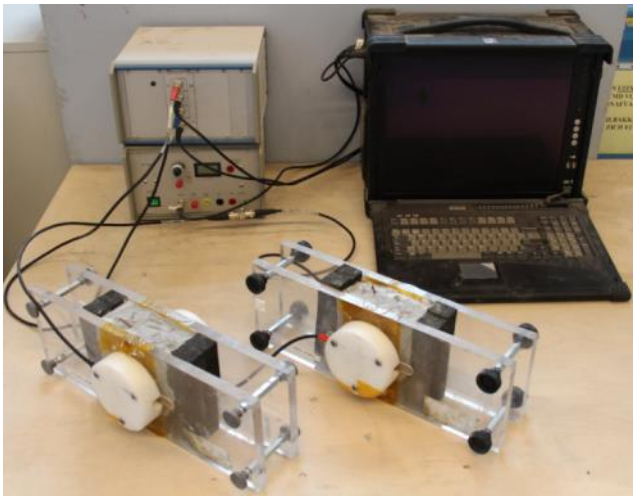

Figure 69 – FreshCon System (HF_1) for high frequency E-modulus monitoring.

For HF_1, the sample thickness is 47 mm, which is more than twice the size of the largest aggregate (44 mm). Two samples are cast inside two similar containers: one for P-waves measurements and one for S-waves measurements. Samples are placed in a thermally regulated chamber and their temperatures are measured continuously during the test. Detailed information about this method can be found in [118].

The P-waves (V_P) and S-waves (V_S) velocities can be used to compute the high frequency Poisson's ratio (ν_{HF}) and E modulus (E_{HF}) through equations 9 and 10, where ρ is the concrete density:

$$\nu_{HF} = \frac{1 - 2 \cdot \left(V_S^2 / V_P^2\right)}{2 - 2 \cdot \left(V_S^2 / V_P^2\right)} \quad 9$$

$$E_{HF} = V_P^2 \cdot \rho \cdot \frac{\left(1 + \nu_{HF}\right) \cdot \left(1 - 2 \cdot \nu_{HF}\right)}{\left(1 - \nu_{HF}\right)} \quad 10$$

These equations apply for a homogeneous and isotropic solid. When they are used during the hardening process of a concrete, it is assumed that these conditions are fulfilled as soon as the age is higher than t_0. Before this time, the UPV is highly affected by the presence of entrapped air inside the concrete [120]. Thus, even though very early age recordings are feasible, the relevance of the results remains controversial.

Figure 70 – BTPULS system (HF_2) for high frequency E-modulus monitoring.

For HF_2 [86], the P-waves are emitted at the bottom and received at the top of a 110 mm diameter and 220 mm height cylinder in its cardboard mould (Figure 70). Up to three samples can be tested simultaneously.

SMART AGGREGATES (HF_3)

The main drawback of the HF_1 and HF_2 systems is the use of a fixed sized mould which strongly limits the possible testing conditions of the sample. In particular, it does not allow applying specific hygral and/or mechanical boundary conditions on the concrete sample. An alternative is to perform ultrasonic testing directly inside a concrete specimen of an arbitrary shape and size using embedded piezoelectric transducers. The use of embedded transducers, also called "Smart Aggregates" (SMAGs) has been initially proposed by Gu *et al.* [121] to monitor the strength of concrete using harmonic excitation, and later to monitor the state of damage using chirp excitation [122,123]. Embedded transducers have also been used to monitor the elastic mechanical properties of concrete in

[124]. At ULB-BATir, transducers based on a similar design were recently developed. Each HF_3 consists in a flat piezoelectric patch which is wrapped in a waterproof coating and embedded in a small cube or cylinder made of mortar (Figure 71). One of the advantages of this technique is that no coupling agent is needed between the sensor and the concrete. The HF_3s made at ULB-BATir have been used for the monitoring of the P-wave velocity in early age concrete [79], and to monitor the crack growth in concrete and reinforced concrete in [125,126]. The results for early age testing are used in this paper and compared to the results obtained with the other techniques presented. We shortly recall the testing procedure which is detailed in [79].

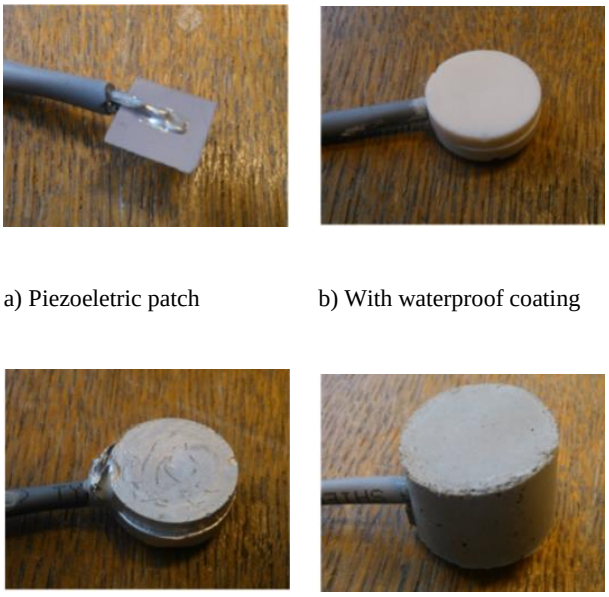

a) Piezoeletric patch b) With waterproof coating

c) With conductive paint d) Smart Aggregate

Figure 71 – SMAGs sensors (HF_3) for high frequency E-modulus monitoring.

A prismatic mould, containing a pair of HF_3s with a distance d = 56 mm is used (Figure 72). The HF_1 system is used to excite the emitter with a pulse of 800 V and 2.5 µs and record the wave at the receiver side. The testing procedure is therefore identical to the one described in Section 3.3.1, except for the fact that piezoelectric transducers of the mould are replaced by HF_3s directly embedded inside the concrete specimen.

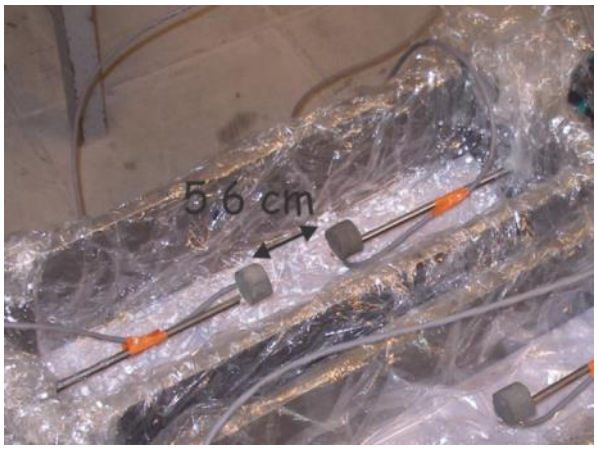

Figure 72 – Prismatic mould with SMAGs before casting the concrete.

4.5.3. Results and discussions

According to the results, this wide set of methods (quasi-static, resonant frequency and ultrasonic) can, finally, be divided in two groups: low frequency testing (QS_0, QS_1, QS_2, QS_3 and RF) and high frequency testing (HF_1, HF_2 and HF_3). The strain rates or loading rates, covered by these methods, are gathered in Table 3. It is worth underlining that stress amplitudes or strain amplitudes are also different from one technique to the other. Comparisons of the results obtained with these techniques are largely influenced by these parameters [127,128].

► Low frequency testing

AUTOMATED QUASI STATIC LOADING RESULTS (QS_1 AND QS_2)

Eight tests with cyclic loadings were performed: four with BTJASPE (QS_1) and four validation tests on samples removed from the mould after the setting called QS_2. All these results are plotted in Figure 73a. For each cycle, the behaviour was sufficiently linear so that the modulus of elasticity could be calculated with a simple linear regression [119].

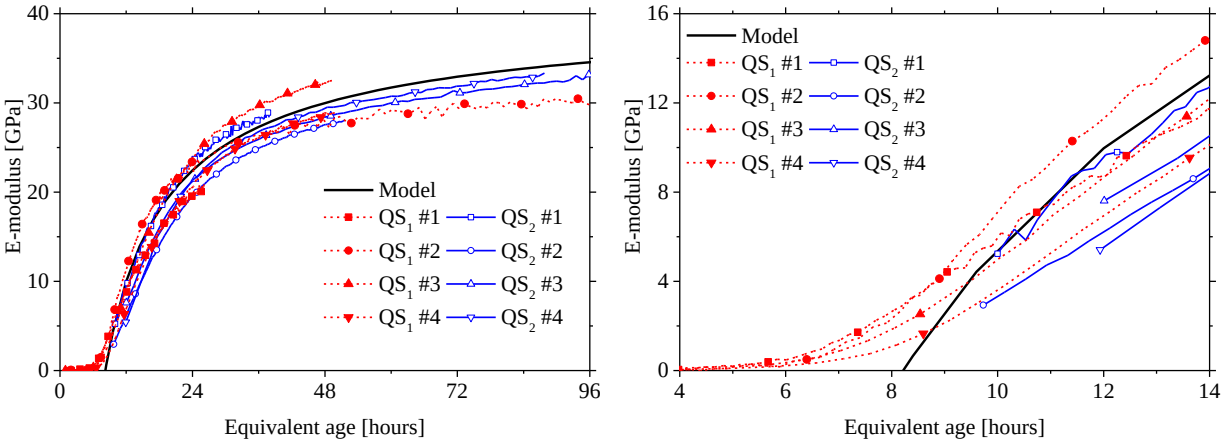

Figure 73 – (a) Determination of the quasi-static E-modulus with BTJASPE (QS_1) and cyclic loadings on unconfined specimens (QS_2) compared to calibrated model for quasi-static E-modulus; (b) Detail of the beginning of the recordings during the concrete setting.

It can be observed (Figure 73a) that these data are fairly in good agreement, both between themselves and also when compared to classical measurements (whose stress rate was 0.50 MPa/s).

Just after t_0, from the time when the E-modulus starts to become different from a null value (6 hours) to the time when its evolution reaches a quasi-straight line (8 hours), the 4 QS_1 recordings are in a range of variation of ± 1 GPa (Figure 73b). They become more scattered after 8 hours. Considering the validation tests (QS_2), as soon as the data are available, this range presents the same type of scattering. Despite this scattering, from one batch to the other, the global response of such a protocol is quite satisfying. Indeed, the series of eight tests led to a coefficient of variation of E-modulus not greater than 13 % over a period ranging from the setting of the concrete to 48 hours.

If a single concrete setting time has to be defined, from QS_1 results, a value between 6 and 8 hours can be adopted depending on a chosen definition. In our case, this definition could be the time when the data start to increase at 6 hours. In real time this point is ambiguous. Indeed, one cannot decide if

this value is included in the noise of the measurements. The beginning of the quasi linear part of the recordings, at 8 hours, is totally unambiguous but, may be, a little late. A definition of a point situated between the two times could suit our problem. Indeed, such a point is clearly outside the noise and it is very close to the intersection of the extrapolated linear part with the x axis. This extrapolation could be used even if no data are available before this point.

TSTM RESULTS (QS_3)

Three samples have been cyclically loaded according to the protocol described in Section 4.4. In this protocol, 20 % of the compressive strength is reached in 10 seconds. This means that a constant stress rate is applied at each cycle but, as the strength is evolving continuously, this stress rate is increasing with the age of the sample. The range covered goes from 0.002 to 0.50 MPa/s over the first four days. On this period, and based on the results reported in Figure 74, a very good agreement, between the E-modulus evolutions for one sample in the QS_3 device and the model of the classical tests, can be observed, despite the fact that stress rates are not strictly similar. As a consequence, it can be inferred that the influence of the stress rate on the evolution of the E-modulus is low as it was observed for QS_1 results.

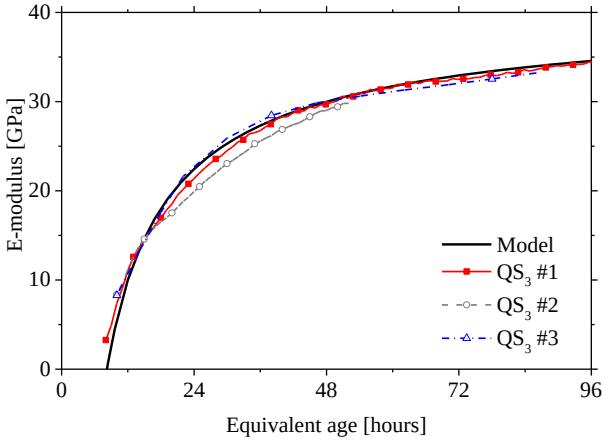

Figure 74 – Quasi-static E-modulus with TSTM (QS_3) compared to calibrated model for quasi-static E-modulus.

EMM-ARM RESULTS (RF)

The resonant frequency evolutions for the three composite beams (concrete-filled moulds), resulting from processing the recordings of the accelerometers are shown in Figure 15a. All the data of EMM-ARM (RF) is plotted according to the equivalent age, normalized to 20 ºC. By observation of Figure 75a, it is clear that all composite beams endured a significant frequency shift ranging between 27.49 Hz in the beam RF_M and 109.12 Hz in the beam RF_P. However, the differences in the resonant frequency shift in the beams reveal that the three experimental setups have quite different sensitivities. To better illustrate such added sensitivity, parametric analyses with the equations of motion of both composite beams were made, as to infer the changes in resonant frequency (dF) that occur per each GPa of increase in E-modulus of the tested concrete (dE), along the process of hardening of concrete. The results of such parametric analyses for all test setups is shown in Figure 75b, where three main conclusions can be drawn: (i) the sensitivity of all experimental setups decreases with the increase in concrete E-modulus; (ii) the frequency sensitivity of the PVC mould (RF_P) setup to changes in concrete E-modulus is markedly during the all hardening process; (*iii*) the metallic beam (RF_M) is the one that has the lower sensitivity to changes in the E-modulus of the material inside the mould despite

being almost constant. This point indicates that the results should be more accurate in the beam RF_P when compared to the other beams.

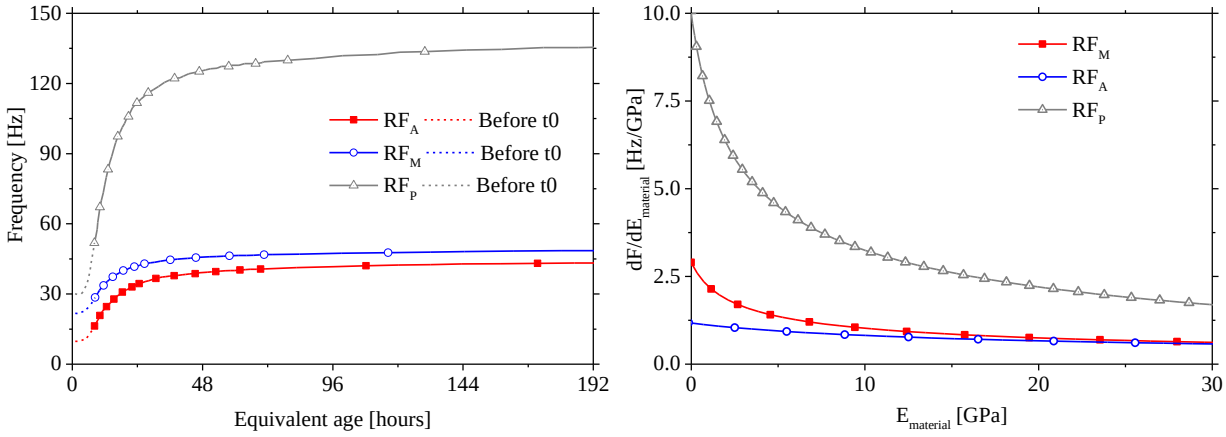

(a) (b)

Figure 75 – (a) Resonant frequency evolution for the acrylic, metallic and PVC EMM-ARM composite beams (RF_A, RF_M, RF_P); (b) Frequency variation per E-modulus variation of concrete according to the type of mould and the state of hardening.

The overall results of E-modulus measured by the three EMM-ARM composite beams and the reference curve of classical tests are shown in Figure 76. It is evident that the coherence of the four methods is very good at most ages of testing, once more confirming the feasibility and robustness of RF. It is however remarked that the E-modulus obtained from the metallic mould test is always slightly higher than the E-modulus obtained from the other beams (acrylic and PVC). This may be partially explained by some uncertainties in the geometry of the metallic beam due to its high local deformability (1 mm thick plates) that resulted in some local warping due to previous uses of the mould. A slight under-estimation of the final E-modulus value of RF methods in regard to the model can also be observed in Figure 76.

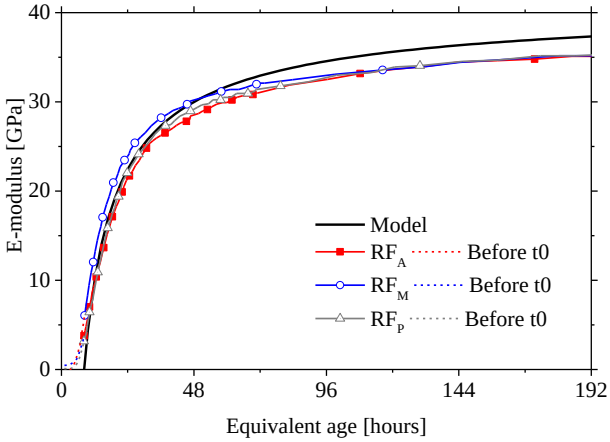

Figure 76 – Quasi-static E-modulus obtained through EMM-ARM (acrylic, metallic and PVC composite beams RF_A, RF_M, RF_P) compared to calibrated model for quasi-static E-modulus.

COMPARISON BETWEEN LOW FREQUENCY TESTING METHOD

All low frequency testing results are shown in Figure 77. For these testing methods, the standard deviations are plotted in dashed lines. The beginning of the increase of the E-modulus seems to well correspond to the final setting whatever the testing method. Between the setting and 48 hours, the

kinetic of the E-modulus looks very similar whatever the testing method whereas a limited scattering is observable between the results, especially at very early age. It appears that the difference of protocol of loading (strain rate, stress amplitude) and the type of testing method did not induce any strong effect on the kinetic and the amplitude of the E-modulus. All low frequency testing method have a very good correspondence with classical extensometry results.

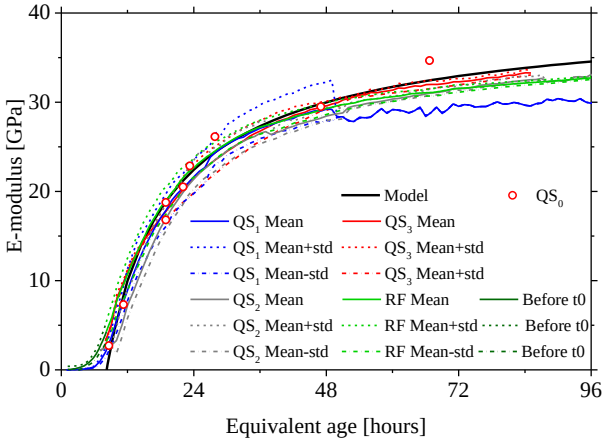

Figure 77 – Quasi-static E-modulus obtained with low frequency testing methods QS_0, QS_1, QS_2, QS_3, RF compared to calibrated model for quasi-static E-modulus.

EFFECT OF THE STRESS AMPLITUDE AND STRESS-RATE ON LOW FREQUENCY TESTING METHOD

The variation of E-modulus as measured by these different methods is attributed to their variable strain rates and amplitude of loading. In order to quantify these effects the study of these two parameters, two types of additional tests are performed with the TSTM device at ULB. First, the effect of loading amplitude is studied. A cyclic test started a few hours after the setting. Then, every hour, a load up to 5, 10, 20 or 40 % of the compressive strength is applied to the sample within 10 s. Secondly, a similar test was performed with constant load amplitude up to 20 % of the compressive strength. In this second test, the loads were applied within 5, 10, 30 or 300 s.

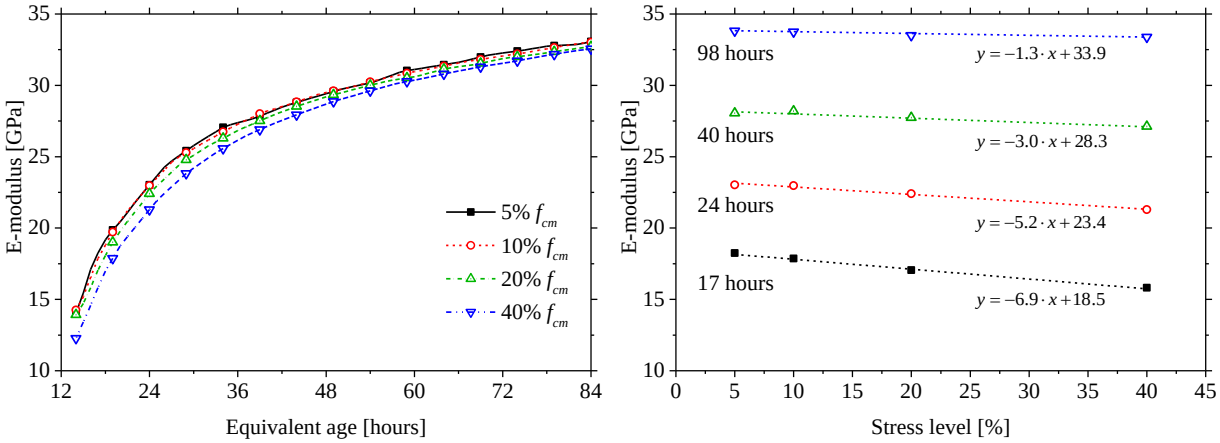

(a) (b)

Figure 78 – (a) Evolution of the E-Modulus for loading amplitudes of 5 – 10 – 20 – 40 % of the compressive strength; (b) Evolution of the E-modulus according to the stress level for several ages of loading.

The E-modulus values corresponding to the variable stress/strength ratio are displayed in Figure 78a. It is observed that with the increase of the applied stress, the estimated E-modulus decreases, and this effect progressively diminishes as the concrete hardens. On Figure 78b, this amplitude effect is quantified. Each point is obtained by linear interpolation of the experimental results. For any given loading age, a non-linear relationship is observed between the loading amplitude and the E-modulus. This confirms that the stress-strain relationship is in fact non-linear, and can be described by a quadratic equation [128] such as equation 11, where *m* is the non-linear parameter. This expression is not based on any mechanical concept but it is the result of a mathematical fitting on basis of the experimental results. As it was shown in [128], the non-linear parameter *m* in the stress-strain relationship is dependent on the concrete mix design and the degree of hydration. As concrete hardens and the E-modulus increases, the slope of this stress-strain relationship decreases.

$$\sigma = E \cdot \varepsilon - m \cdot \varepsilon^2 \qquad 11$$

The dependency of E to the stress/strength ratio is described in equation 12, where σ is the applied stress, f_{cm} is the compressive strength, E_{ref} is the elastic modulus corresponding to a reference stress/strength ratio of 20 % applied in 10 s, and A is a time-dependent amplitude parameter describing the effect of a variation of stress on the apparent measurement of E.

$$E\left(t, \frac{\sigma}{f_{cm}}\right) = E_{ref}(t) + A(t) \cdot \left(\frac{\sigma(t)}{f_{cm}(t)} - 0.2\right) \qquad 12$$

Where $E(t, \sigma/f_{cm})$, $E_{ref}(t)$ and $A(t)$ are expressed in GPa,
t: equivalent time since mixing (in hours),
$\sigma(t)$, $f_{cm}(t)$ are expressed in MPa.

The evolution of parameters E_{ref} and A are shown in Figure 80a. The evolution of A confirms that the decrease of E due to an increase of the loading amplitude is especially strong at very early age, and drops to low values during hardening. The expression of A is provided in equation 13.

$$A(t) = A_1 \cdot \left(\frac{t}{\tau}\right)^{A_2} \qquad 13$$

Where A_1= -128 GPa, A_2=-1.015 and $\boldsymbol{\tau}$=1 h.

A second test was performed at various loading durations ($t_{loading}$) of 5, 10, 30 and 300 seconds for a constant load corresponding to 20 % of the compressive strength. The results presented in Figure 79a suggest that for longer loading duration, the E-modulus decreases. For any loading age, it is observed that the E-modulus increases as a power law of $t_{loading}^{-1}$. The best-fit parameters indicate that as the E-modulus increases, the relative impact of the loading duration decreases. In other words, as hydration advances, the E-modulus is less affected by variations in the loading stress rate. This observation is due to the visco-elastic behaviour of concrete, which viscous properties decrease with hydration.

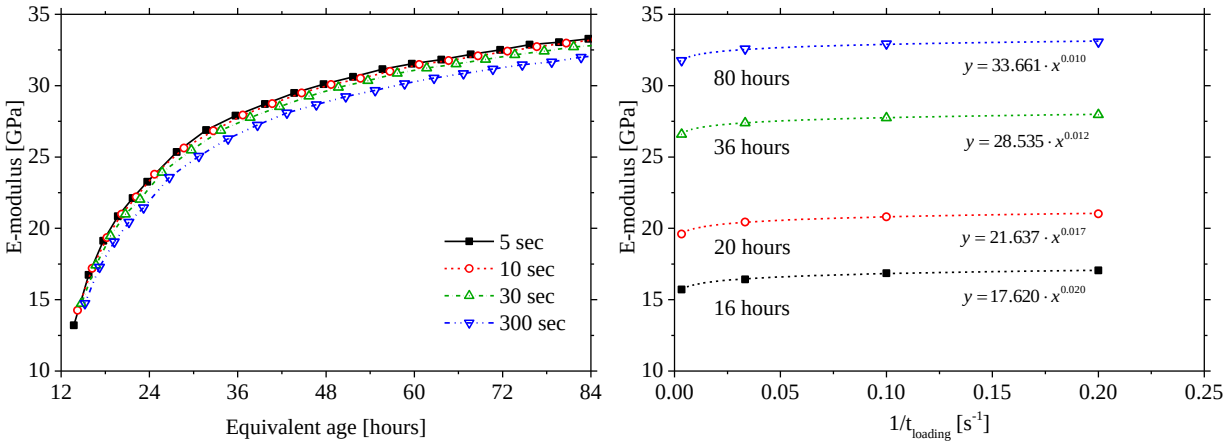

(a) (b)

Figure 79 – (a) Evolution of the E-Modulus for a stress applied in 5 – 10 – 30 or 300 seconds; (b) Evolution of the E-modulus according to the velocity of loading for several ages of loading.

This loading stress rate effect is taken into account in equation 14, where E_{ref} represents the E-modulus corresponding to a loading duration of 10 seconds up to a stress/strength ratio of 20 %, $t_{loading}$ is the loading duration, and V is a time-dependent velocity parameter describing the effect of a variation of the loading stress rate on the apparent measurement of E.

$$E\left(t,t_{loading}\right)=E_{ref}\left(t\right)\cdot\left(\frac{10.\ \tau}{3600.\ t_{loading}}\right)^{V(t)} \qquad 14$$

The evolution of parameters E_{ref} and V are shown in Figure 80b. The evolution of V confirms that the decrease of E due to an increase of loading stress rate is especially strong at very early age, and drops to low values during hardening. The expression of V is provided in equation 15.

$$V\left(t\right)=\frac{V_1}{\ln\left(\frac{t}{\tau}\right)+V_2} \qquad 15$$

Where $E(t, t_{loading})$ and $E_{ref}(t)$ are expressed in GPa,

V_1=0.03, V_2=-1.179 and $\boldsymbol{\tau}$= 1 h.

t is expressed in equivalent time since mixing (in hours) and $t_{loading}$ is expressed in hours

Ultimately, the combined effect of loading stress rate and amplitude can be taken into account by equation 16.

$$E\left(t,\frac{\sigma}{f_{cm}},t_{loading}\right)=\left(E_{ref}\left(t\right)+A(t)\cdot\left(\frac{\sigma(t)}{f_{cm}(t)}-0.2\right)\right)\cdot\left(\frac{10.\ \tau}{t_{loading}}\right)^{V(t)} \qquad 16$$

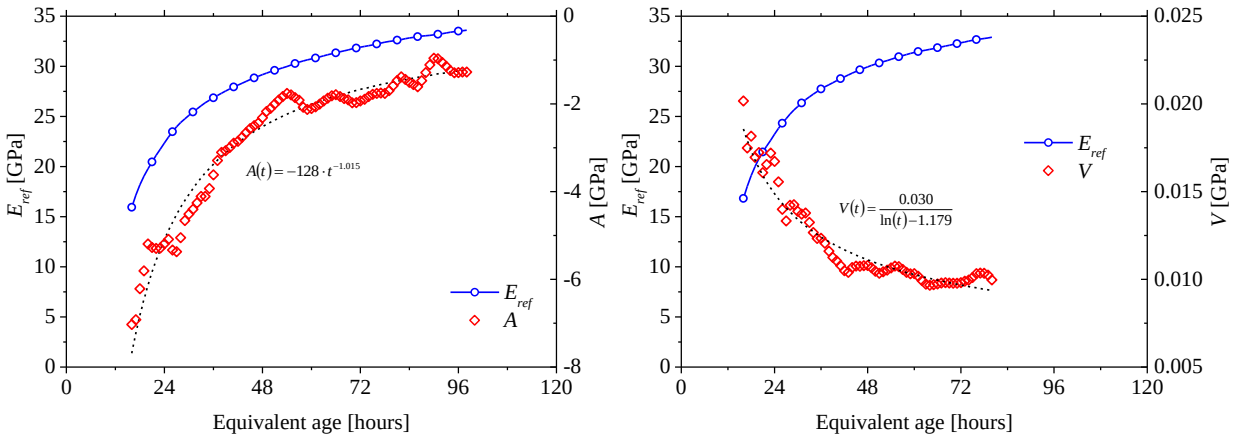

(a) (b)

Figure 80 – (a) Evolution of E_{ref} and amplitude parameter A determined with a single TSTM test (QS_3); (b) evolution of E_{ref} and velocity parameter V determined with a single TSTM test (QS_3).

Quasi-static testing for the determination of E-modulus is generally performed for loading durations between 1 and 300 seconds and that the loading amplitude is generally between 5 and 40 % of f_{cm}. Based on these parameters, two envelope curves can be computed, showing the upper and lower boundaries of the E-modulus based on the effect of loading stress rate and amplitude. The envelope curves are shown in Figure 81 and confronted to the experimental E-modulus results obtained by extensometry at ULB, IFSTTAR and U Minho (Figure 65). These experimental points, obtained for similar testing parameters, indicate that the error relative to the reproducibility of the test is of the same order of magnitude than the effect of loading stress rate or amplitude. As explained later on, by changing by several orders of magnitude the loading stress rate and/or amplitude (such as in the case of ultrasonic testing) these effects are much more visible.

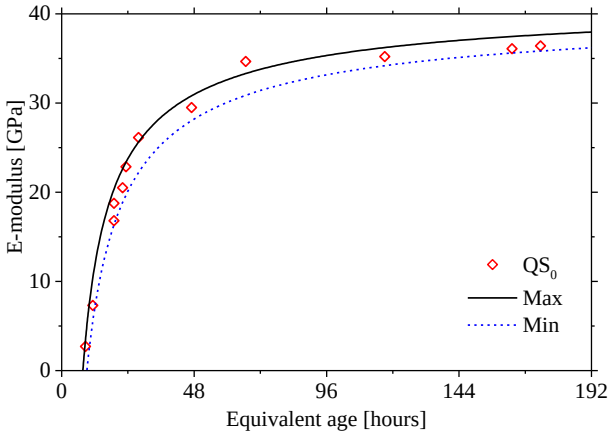

Figure 81 – Lower and upper boundaries for the effect of loading stress rate and amplitude on quasi-static determination of E-modulus.

► High frequency testing (HF_1, HF_2, HF_3)

The results obtained on three batches with the FreshCon (HF_1) for the transmitted P-waves and S-waves velocity are shown in Figure 82. The P-waves velocity increases rapidly during setting and stabilizes after the final setting time to a value slightly superior to 4000 m/s. However, the S-waves hardly propagate though fluids. It is only at the beginning of the hardening that the S-waves velocity increases. Then, it slowly reaches a value close to 2500 m/s. These observations are in good

agreement with the few results found in the literature [129,130]. The results obtained on three batches with the BTPULS (HF_2) for the P-waves velocity transmission are shown in Figure 83a.

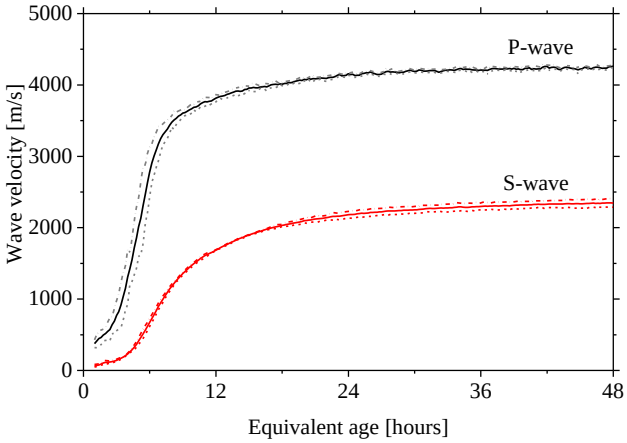

Figure 82 – P-waves and S-waves velocity evolution through the FreshCon system (HF_1).

The P-wave velocity results obtained, for the same concrete, with the SMAGs (HF_3) and the BTPULS (HF_2) systems are compared to the results obtained with the FreshCon (HF_1). Results are plotted on Figure 83b. In this figure, the average of three samples is shown for the HF_1 and the HF_2.

HF_1 seems to give slightly different results, in the first part of the curve. However, this difference mainly occurs before t_0. More explanations about this observation are given in [131]. From 12 hours onward, the overall tendency is the same for all techniques, with similar values of P-waves velocity. Discrepancies before t_0 can be due to different air content in the different moulds. Indeed, different techniques are used for placing the concrete in the moulds. HF_3s are placed in a large steel mould. Its high weight (concrete + steel) makes the vibrating table less effective. On the other hand, the HF_1 samples are efficiently vibrated until no more air bubbles are trapped between the concrete and the sensors. Vibrating needles are used for HF_2. Indeed, it is known that a strong dependency of the early age P-waves velocity to the air content of the mix exists. In aired mixes, the initial velocity is around 250 m/s, whereas for de-aired mixes, initial values close to 1500 m/s can be observed [99,120]. Ultimately, the coherence between the three experimental techniques and the good reproducibility of HF_1, the distance of 47 mm between sensors is enough in order to provide representative measurements.

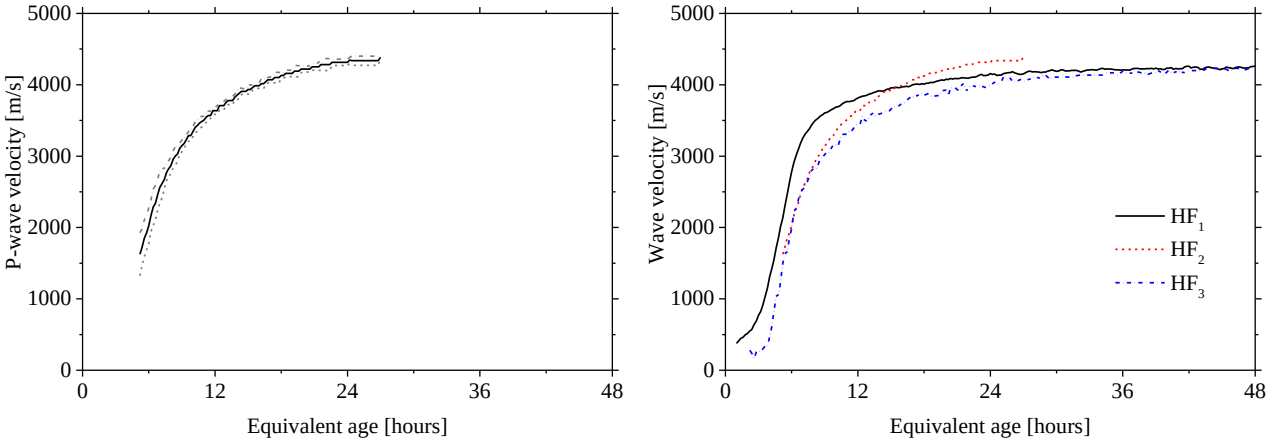

(a) (b)

Figure 83 – (a) Three sets of results obtained with BTPULS system (HF_2); (b) Comparison of the measured P-wave velocities using FreshCon (HF_1), BTPULS (HF_2), and SMAGs (HF_3).

With the HF_1 system, P-waves and S-waves were simultaneously measured on the same concrete with dedicated HF_1 containers, which allows an accurate computation of the high frequency E-modulus (E_{dyn}) and Poisson's ratio as shown on Figure 84.

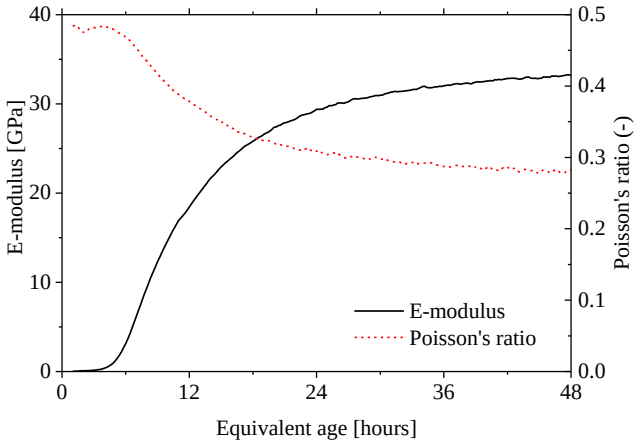

Figure 84 – Evolution of high frequency E modulus and Poisson ratio computed from the P-wave and S-wave velocity with the FreshCon system (HF_1).

In the case where no S-waves measurements is possible, taking a constant value of v_{dyn} in the equation for the computation of E_{dyn} (equation 10) leads to substantial errors, especially at early age. Indeed, the E_{dyn} value is governed by the S-waves velocity evolution. The approximation made by considering a constant v_{dyn} results in an overestimation of the early age high frequency modulus. However, in order to evaluate the relevance of HF_3 and HF_2 methods compared to usual UPV measurements, a constant v_{dyn} of 0.3 has been considered as no S-wave measurements have yet been performed with these techniques. In Figure 85 – Comparison of the high frequency E-modulus computed from the P-wave velocity only with v_{dyn} = 0.3 (FreshCon (HF_1), BTPULS (HF_2), SMAG (HF_3)) and from the P-wave and S-wave velocity (HF_1) with the quasi-static E-modulus calibrated model., the values for the HF_1 mean curve with a constant v_{dyn} equal to 0.3 and the HF_3 mean curve seem to stabilise after 30 hours, whereas the values of the HF_1 mean curve with consideration of the evolution of v_{dyn} follows the trend of the static E-modulus given by the model with increasing values after 30 hours.

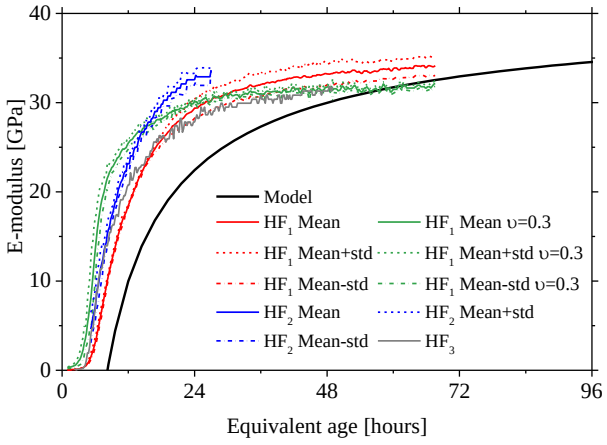

Figure 85 – Comparison of the high frequency E-modulus computed from the P-wave velocity only with v_{dyn} = 0.3 (FreshCon (HF_1), BTPULS (HF_2), SMAG (HF_3)) and from the P-wave and S-wave velocity (HF_1) with the quasi-static E-modulus calibrated model.

Before the setting time, a scattering is observable between all the high frequency testing methods (see Figure 85). However, the results computed from the P-wave and S-wave velocity (HF_1) exhibit the lowest amplitude because, before t_0, the values of v_{dyn} are much higher than 0.3. After t_0, the kinetic looks similar whatever the high frequency testing method is. On the contrary for this case, the results computed from the P-wave and S-wave velocity (HF_1) exhibit the highest amplitude because, after t_0, the values of v_{dyn} tend to lower values than 0.3 (see Figure 84). Therefore, as observed in [129], the computation of E_{dyn} only from P-wave velocity should be considered as a qualitative indicator of the E-modulus development.

► Relation between quasi-static or low-frequency and high frequency measurements

Since the 1970s, high frequency determination of the elastic modulus began to be performed on concrete due to obvious advantages of non-destructive and continuous aspects of this method [132–134]. Some authors found relationships linking the quasi-static or low-frequency elastic modulus to the high frequency elastic modulus (Table 10) of hardened concretes.

Table 10: Relations between high frequency modulus E_{HF} and quasi-static or low frequency modulus E_{LF}.

References	*Model*
Shkolnik [128]	$E_{LF} = 0.83 \cdot E_{HF}$
Van Den Abeele, *et al.* [129]	$E_{LF} = 1.25 \cdot E_{HF} - 19$
Benmeddour, *et al.* [130]	$E_{LF} = 1.033 \cdot E_{HF} - 7.245$

These empirical equations illustrate the fact that high frequency values are always higher than low-frequency values of elastic modulus, which is generally true for all viscoelastic materials. This observation was confirmed experimentally at early age by several authors as well as in this study [135–137]. However, in this research, these three relations do not seem to apply, especially at very early age. Two main drawbacks to these equations are advanced here. First, the lack of physical meaning to p and q in the general equation: $E_{LF} = p \cdot E_{HF} - q$ which does not allow to take into account different concrete compositions (w/c, paste volume, cement type). Secondly, as shown in this study, the "low-frequency" or "high frequency" value can be dependent on the measuring method. Depending on the strain rate or loading amplitude for the low-frequency and high frequency measurements, different values of E_{HF} and E_{LF} can be obtained [128]. Therefore, the relationship between both values is ambiguous and certainly not intrinsic for a given concrete. In summary, the p and q parameters are dependent on the concrete composition, on the measurement method of low-frequency and high frequency modulus and, certainly, on the hydration degree. However, based on the hypothesis that the main parameters affecting the difference between E_{HF} and E_{LF} are the loading stress rate and amplitude, such a linear relationship between both properties is consistent with the modelling approach of equation 16.

In the case of a given experimental protocol to determine E_{HF} and E_{LF} on a given concrete, an equation of the type $E_{LF} = p \cdot (E_{HF} - q)$ (with $p > 1$ and $q > 0$) seems appropriate to describe the behaviour of concrete throughout the hardening process. Indeed, at the initial setting time, the low-frequency modulus is close to 0. However, due to the initial increase of the ultrasonic pulse velocity

before that time, the high frequency modulus has already reached a significant value. The *q* parameter represents this initial gap. Then, as concrete hardens, E_{LF} tends to increase whereas E_{HF} stabilizes more rapidly. Therefore, the gap between low-frequency and high frequency values tends to decrease throughout hydration, thus explaining the *p* parameter, which is representative of the different kinetics of the low-frequency and high frequency modulus evolution.

Figure 86 shows this relationship in this case by comparison of the HF_1 results and the classical extensometry results between the setting time and 66 hours. No linearity between E_{HF} and E_{LF} is directly observable here. But if only results after 18 hours (E_{LF} = 16 GPa) are considered, a linear relationship is observable. Then, it appears that the relationship between E_{HF} and E_{LF} cannot be assumed as fully linear. Here, this assumption is only available between 18 and 66 hours. Further research should be carried out in order to be able to determine with precision the loading stress rate and amplitude of the high frequency measurements. Such measurement could improve the model presented in equation 16, and confirm the hypothesis that through the mechanism of very short term creep, the loading stress rate and amplitude are indeed the main parameters affecting the apparent value of the E-modulus.

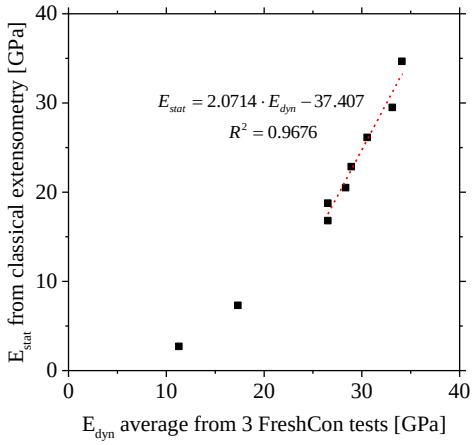

Figure 86 – Relationship between high frequency E-modulus through HF_1 (from the P-wave and S-wave velocity) and modelled quasi-static E-modulus through classical extensometry with the reference test set up QS_0.

Finally Figure 87 presents the synthesis of all results. Only mean values of each testing method are shown here. As expected, clear differences appear between low-frequency and high frequency results. High frequency modulus values with consideration of the evolution of v_{HF} are always higher than low-frequency results. A faster evolution of high frequency results is also observable.

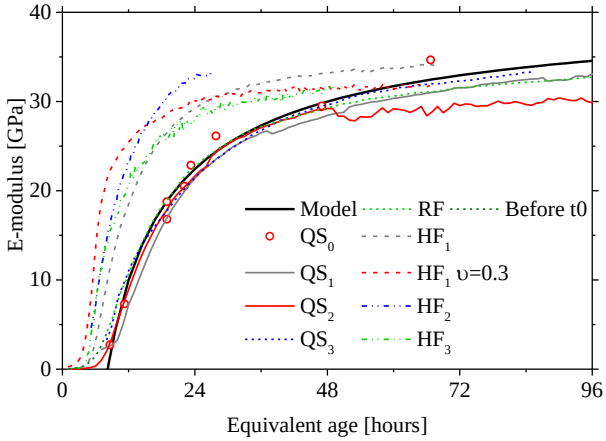

Figure 87 – Comparison of E-modulus obtained with quasi-static (QS_0, QS_1, QS_2, QS_3, RF) and high frequency (HF_1, HF_2, HF_3) testing methods and with calibrated model for quasi-static E-modulus.

SECTION 4.6 – CREEP TESTING OF CONCRETE SINCE SETTING TIME BY MEANS OF PERMANENT AND REPEATED-MINUTE LONG LOADINGS

This chapter is based on the joint publication of Brice Delsaute, Claude Boulay and Stéphanie Staquet entitled "Creep testing of concrete since setting time by means of permanent and repeated-minute long loadings" published in Cement and Concrete Composite, 73 (2016) 75–88. Results from the BTJASPE were provided by Claude Boulay at Ifsttar.

Nowadays, the construction phases of modern concrete structures (high-rise buildings, piers of a bridge…) become more and more challenging. Consequently, for the design of concrete structures it is important to have knowledge in depth of the early age behaviour of concrete, which influences the whole service life. Even though the mechanical behaviour of hardened concrete can usually be correctly predicted; it is not always the case for the early age behaviour of concrete, when the mechanical properties change rapidly in function of the advancement of the hydration reaction. Among all the usual parameters (strengths, E-modulus…) needed for the design of the concrete structures, creep and relaxation must also be taken into account. Stress induced by the restriction of the thermal and autogenous strain can be significantly reduced thanks to relaxation. For example, in the design of a concrete dam, Slowik, et al. [138] showed that at early age, the relaxation phenomenon is responsible for a decrease of 70% of the thermally induced stresses in the structure.

For field applications or research purposes, measuring early age deformations as input data for modelling is of a great interest and should be included in numerical codes [81,82]. For ordinary concrete (composed by Portland cement), existing models allow obtaining satisfied results for material properties like compressive strength and Young's modulus but not for early age creep [139]. For concrete with high substitution of cement by mineral additions like slag, fly ash, limestone filler, the early age properties of concrete are not necessarily well predicted by models coming from standards [140]. In fact, just after setting, deformations in concrete change very fast. According to the superposition principle, in sealed and isothermal conditions, the total strain ($\varepsilon(t)$) is the sum of three terms: the autogenous strain ($\varepsilon_{au}(t)$), the elastic strain ($\varepsilon_{el}(t)$) and the basic creep strain ($\varepsilon_{bc}(t)$) (Equation 17).

$$\varepsilon(t) = \varepsilon_{au}(t) + \varepsilon_{el}(t) + \varepsilon_{bc}(t) \quad (17)$$

For the monitoring of the autogenous strain, many tests rigs have already been developed in the past [8,141]. The elastic strain depends on the evolution of the Young's modulus. Several existing testing devices for the measurements of the Young's modulus are presented in [119,142]. The basic creep strain depends on the evolution of the creep function. Even if experimental tests consisting in applying a permanent loading at different ages were previously reported in [25,64,143–149], no specific testing methodology aimed at monitoring early age creep has already been developed for concrete.

Creep and relaxation of concrete have not been thoroughly investigated at early age. Some studies related to the compressive creep have been carried out and are reported in [25,64,143–149] for concrete with an age at loading of 1 day and more. For practical reasons, it is difficult to access creep before an age of 1 day (minimal concrete age required before mould release, grinding the sample, fixing the extensometer, very low magnitude of load applied and consequently very low displacement

measured). It is even more uncommon to find experimental results in the literature for the relaxation phenomenon of concrete at early age. The experimental testing of the relaxation is very complicated for technological reasons. The relaxation testing needs to take into account in real time the difference between the total deformation and the shrinkage added to the thermal deformation. This difference must be performed all along the test, so that the jack of the testing frame can be controlled by this value. All these reasons explain why the study of the creep and the relaxation in compression at very early age is not very developed. Only one kind of experimental methodology is used till now to monitor the evolution of the creep of concrete: static loading on a series of samples [25,64,143–149]. This experimental procedure requires the completion of a large number of tests which is time consuming and the earliest obtained results often correspond to an age of concrete of one day. The period situated between the setting and an age of one day is then often missing. However, in several structural cases, concrete elements are in compression during the first 24 hours as a result of the restrained thermal strain. An underestimation of the compressive creep and relaxation phenomenon during the heating period leads to an underestimation of the evolution of the tensile stresses which occur during the cooling period of the concrete [150,151]. Following these observations, the aim of this collaborative work between the BATir-ULB and IFSTTAR laboratories is to develop a new experimental testing methodology of creep and relaxation of concrete since setting by means of the lowest possible number of tests [152–154]. The present section reports on the experimental results obtained from a comprehensive test program on creep and relaxation of an ordinary concrete. Creep and relaxation tests have been investigated since the end of setting in isothermal conditions at 20°C and in sealed conditions.

4.6.1 Experimental Program

- Materials and Mixtures

The tests presented here were performed on an ordinary concrete for which the mix proportions is presented in chapter 3.

- Assessment of Creep and relaxation

The assessment of the creep and the relaxation is performed by using three devices. For the study of short duration of loading, the TSTM (see Section 2 of this chapter) or the BTJASPE (see Section 4 of this chapter) are used. The study of long duration of loading is performed with classical creep rigs adapted for early age. The compressive creep rigs are presented below.

Compressive creep tests were performed on a frame designed at ULB (Figure 88). The load is applied on the sample by increasing flat jack pressure with a pump till 40% of the compressive strength. Once the target pressure is obtained, the pump is disconnected. A cell force is placed on the top of the sample. According to the age at loading and the force applied the size of the flat jack is adapted. For loading at very early age, flat jacks with very small diameter are used with a transition piece to assure a good stability of the load and a very low eccentricity. The criteria used to choose the size of the flat jack is that the maximal applied force must be situated at the three quarters of the stroke of the jack. Displacements are measured with an extensometer composed by two rings in aluminum spaced of 200 mm and three rods in INVAR© which support the 3 displacement sensors (Solartron range 2 mm) placed at 120°. A dummy specimen is used for each series of test to monitor the thermal and autogenous strain. Thermocouples are placed inside the dummy mould and in the room in order to monitor the ambient and concrete temperature. The measurement of displacement, force and temperature are sent to a computer for data recording. The sample is a cylinder with a height of 320

mm and a diameter of 100 mm. After casting, the samples are placed in an air-conditioning room (20°C and RH 90%). The mould removal takes place just after setting (for the very early age loading) or later (for later age loading). Samples are then grinded on both circular end faces and surrounded by two self-adhesive aluminum sheets. For sample grinded at very early age, a small layer of sieved concrete (+/- 1cm) is placed on the top of the sample during the casting in order to avoid any problem of pullout of the aggregate during the grinding. Tests are carried out in a climatic room with a temperature of 20+/-1°C.

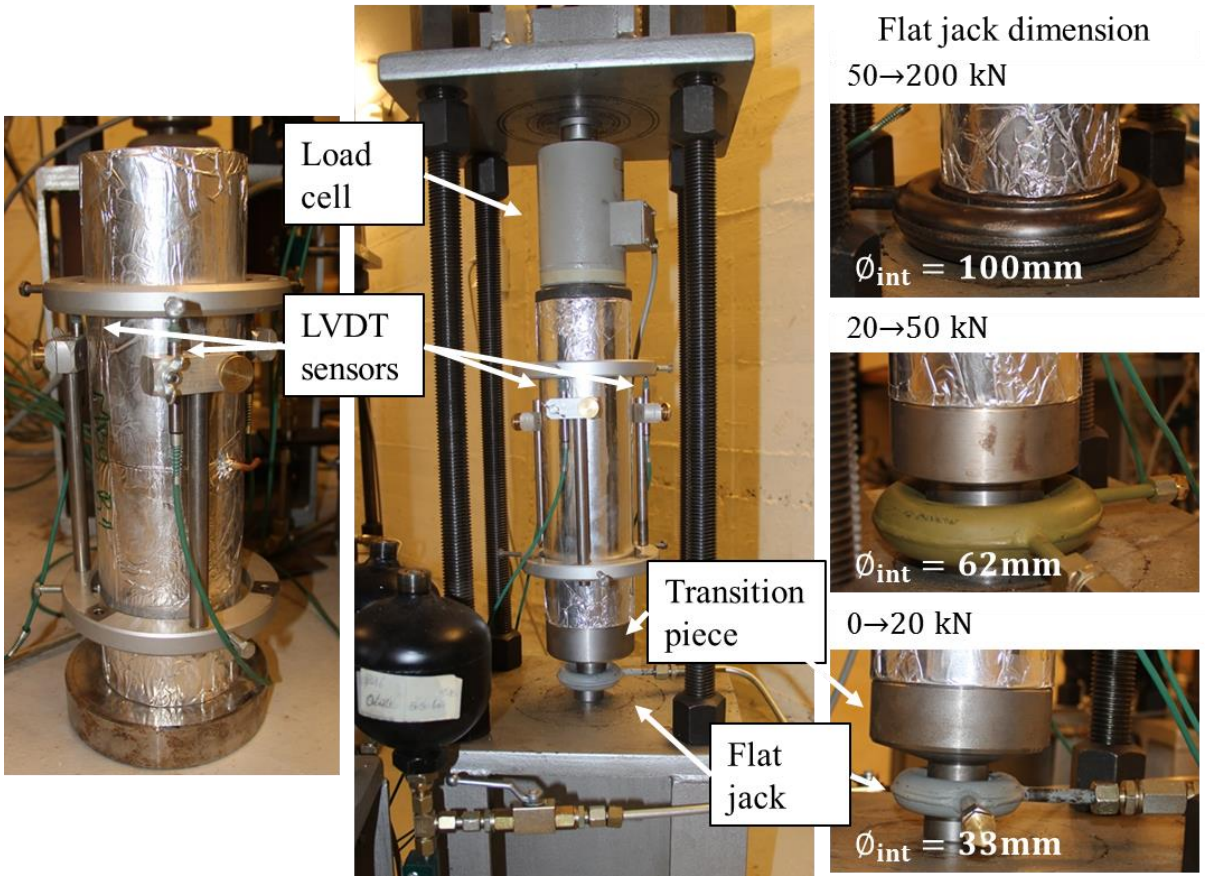

Figure 88 – left to right: shrinkage test setup, creep test setup and dimension of the flat jack according to the loading applied.

4.6.2. Experimental results

► Analysis of creep testing with permanent loadings

Several groups of concrete compressive creep tests are carried out at different ages of loading: 15h, 20h, 24h, 40h and 72h. The load is kept constant during at least 6 days and the stress/strength ratio at the age at loading is 40%. For each age, tests were carried out on 3 samples to assure a good repeatability of the result. The evolution of the creep strain for the different ages at loading is given in Figure 89a.

Here the basic creep behaviour is described through the coefficient $\varphi_c(t, t')$:

$$\varphi_c(t,t') = \frac{\varepsilon_{cr}(t,t')}{\varepsilon_{el}(t')} \quad (18)$$

where ε_{cr} is the creep strain, ε_{el} is the elastic strain at the age of loading t'.

The basic creep function φ_c is given at Figure 89b for each age at loading. Two main parameters change according to the age at loading: the amplitude and the kinetic. The increase of the amplitude is inversely proportional to the age at loading. When each curve is normalized by the value obtained at an age after loading of 145 hours (Figure 90), the fastest kinetic corresponds to the earliest age at loading. These two experimental observations are in agreement with results obtained in the literature [146,155,156].

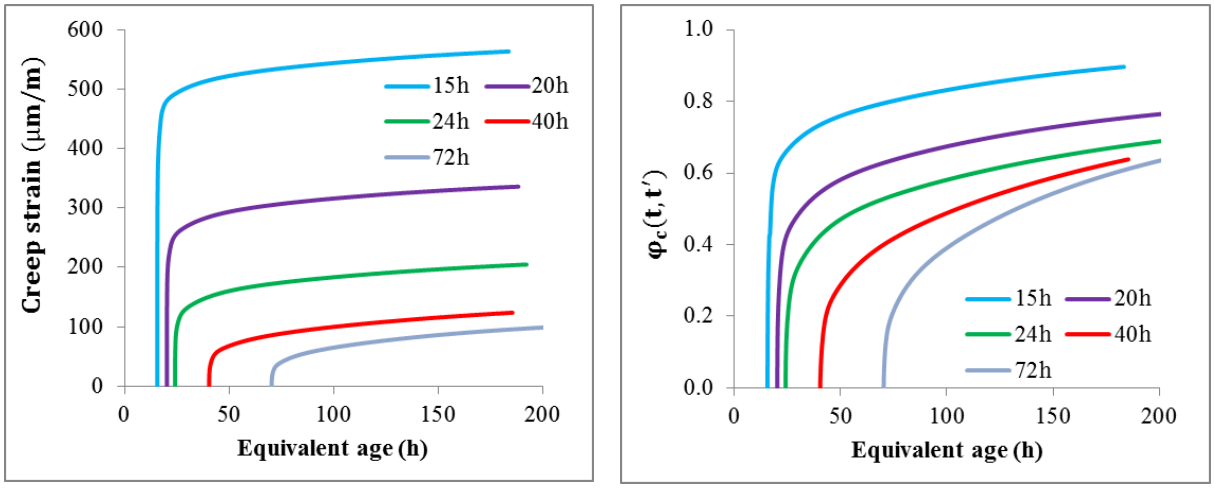

a b

Figure 89 – Creep strain (a) and creep coefficient (b) for several ages at loading.

However, if each creep curve is set to zero at an age corresponding to 145 hours after loading, two distinct stages can be observed in the evolution of the curves of the basic creep coefficient. During the first hours after loading, the age effect is strongly observable (Figure 91). After this period, the age effect is much less pronounced.

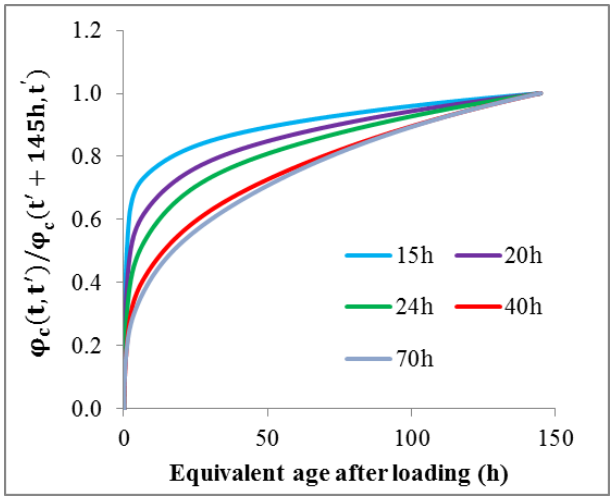

Figure 90 – Creep coefficient normalized by the value obtained at an age after loading of 145 hours.

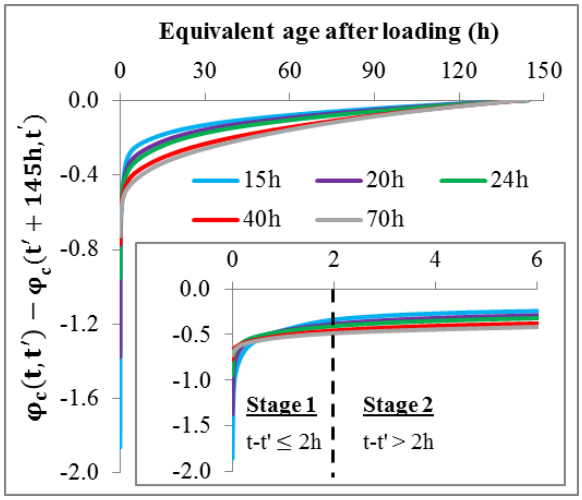

Figure 91 – Creep coefficient set to zero at an age after loading of 145 hours.

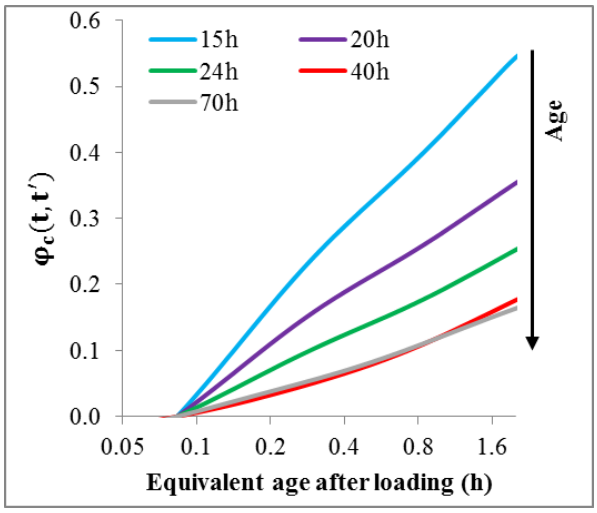

Figure 92 – First two hours after loading of the creep coefficient.

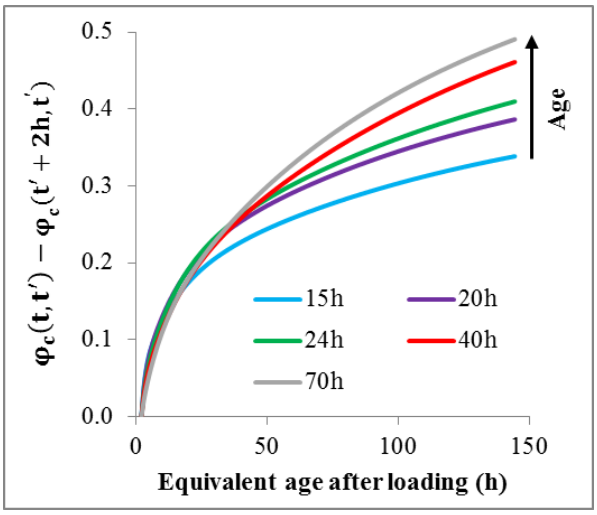

Figure 93 – Creep coefficient set to zero at an age after loading of 2 hours.

To highlight this observation each creep curve is separated in two parts, the first part corresponds to the first two hours after loading (Figure 92) and the second part, to the period after these first two hours of loading (Figure 93). The amplitude of the creep coefficient during the two first hours after loading is strongly depending on the age at loading. When the creep coefficient evolutions are normalized at the same age after loading (two hours), the kinetic is not significantly influenced by the age of loading. The results obtained after two hours of loading are superimposed and initialized at two hours after loading in Figure 93. No strong variation of the amplitude linked to the age of loading is observable in Figure 93. However, the kinetic changes according to the age at loading. The border, between both stages, is not clear but it is observed that a first mechanism occurs very fast during the first hours and a second mechanism develops continuously on longer duration. In synthesis, it could be considered here that the short term creep for permanent loading during one week can be divided in two terms. The first term occurs during the first hours after loading. It has a constant kinetic and an amplitude which is inversely proportional to the age at loading. The second term occurs after the first

hours of loading and has an amplitude and a kinetic which are not strongly influenced by the age at loading.

Similar observations have already been published in the literature. Early age creep can be divided in two terms corresponding together to the short term creep. Ageing impacts strongly the first term of the short term creep. The duration of each stage depends on the nature of the paste (binder, water cement ratio…). Some values found in the literature of the duration of the first term are given in Table 11. Of course for long duration of permanent loading (beyond 14 days), a long term creep should be considered [157].

	Atrushi [64]	Briffaut, *et al.* [145]	Jiang, *et al.* [147]
Time between stage	< 1 day	0.3 day	< 1.5 day
W/B	0.43	0.25	0.35
Binder	CEM 1 52.5 LA	Portland composite cement (6% of limestone)	Portlant cement (72%) Blast furnace slag (14%) Fly ash (14%)

Table 11 - Values of durations of the first term of the short term creep.

Through these observations, it is proposed that the basic creep can be characterized by two kinds of experimental test:

- **Long duration loading tests** (> one week) carried out at two different ages to define the duration of the first term of the short term creep and also to characterize the second term of the short term creep.
- **Repeated-minute long loading tests** carried out at several ages of loading to quantify the evolution of the amplitude of the first term of the short term creep.

This experimental methodology allows characterizing basic creep of a concrete but implies to carry out a huge number of test. To overcome this limitation, a new experimental strategy is proposed by means of a repeated-minute long loading test.

► Analysis of creep testing with repeated-minute long loadings

A new protocol of loading was developed for the determination of the first term of the short term creep. This methodology consists in applying repeated-minute long loading on a sample. The loading has to be applied as fast as possible and automatically to monitor the creep properties. For this purpose several parameters must be defined:

- Time of application of the first repeated-minute long loading;
- Protocol of loading ;
- Duration of loading.

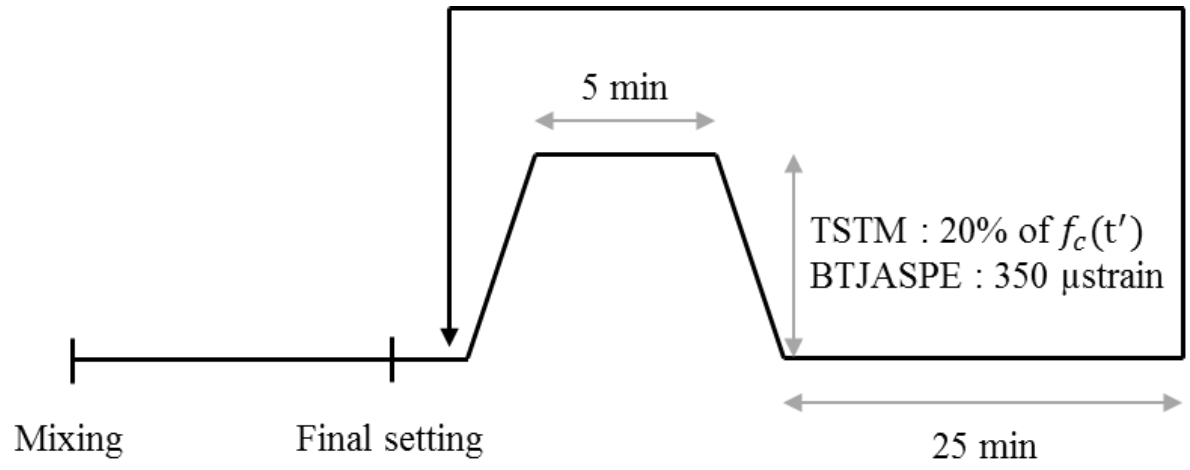

Figure 94 – Scheme of the protocol of loading.

After several tests, it was observed that the test can begin just after the final setting and the repeated-minute long loading can be repeated every 30 min (Figure 94). Two methodologies were used for the loading. At ULB, the loading was controlled in force and corresponds to 20 % of the compressive strength. For batch T1 (T for TSTM), a constant displacement velocity of 1.2 µm/s is applied. For batch T2, the load is applied in 10 seconds and in 1 second for batch T3. The load (for creep) or the strain (for relaxation) is kept constant during 5 min. An alternation between relaxation and creep is done at each repeated-minute long loading (batch T2). At IFSTTAR, the loading was controlled in displacement. The load and unload are applied in 7 min and correspond to a deformation of 350 µstrain (displacement velocity of 1 µstrain/s). The load (batch B1, B for BTJASPE) or the strain (batch B2) is kept constant during 5 min. The first protocol assures no damage inside the sample. The second protocol does not imply to wait for the setting time before starting the test and does not require knowing the evolution of the compressive strength. In compression, it is assumed that no damage is applied to the sample whatever the age is. However this assumption is checked in section below. All tests are carried out at 20°C and in sealed conditions.

Three creep tests and two relaxation tests are presented here (Table 12). One relaxation test and one creep test have started just after the casting and other tests have begun just after the setting.

Table 12 – Experimental program for repeated-minute long loading test.

Device	Batch	beginning of the test	kind of test	protocol pf loading	
				load/strain	velocity/duration of loading
TSTM	T1	8h00	Relaxation	20% of fc	1.2x10-6 m/s
	T2	8h00	Relaxation & creep	20% of fc	10 s
	T3	9h00	Creep	20% of fc	1 s
BTJASPE	B1	7h00	Relaxation	350x10-6 strain	10-6 strain/s
	B2	7h00	Creep	350x10-6 strain	10-6 strain/s

YOUNG'S MODULUS

For each repeated-minute long loading, the Young's modulus is defined with the record of the displacement and the force during the loading and the unloading. In [119], a complete and detailed description of the way to compute the Young's modulus with both devices is given.

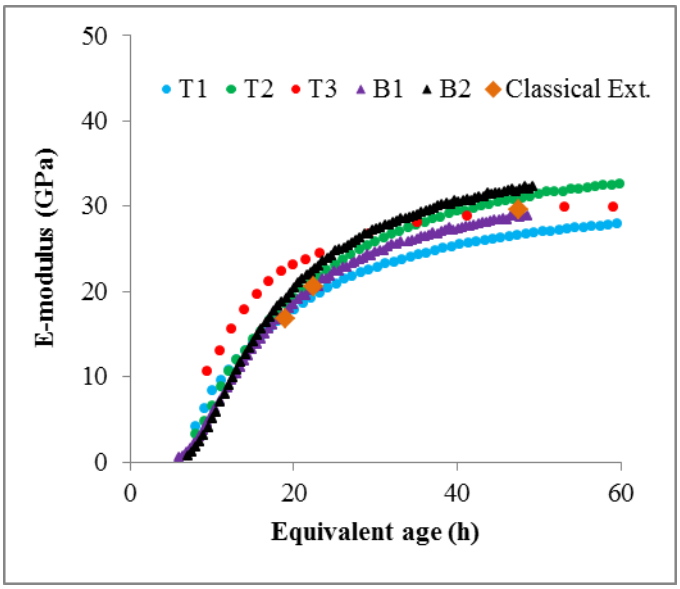

Figure 95 – Experimental E-modulus obtained with the TSTM (T), the BTJASPE (B) and classical extensometry.

Results shown in Figure 95 and obtained with the TSTM device, the BTJASPE device and the classical extensometry are in good agreement. Nonetheless some differences are observed and attributed to several reasons. First, samples were casted within a period of 18 months (with the same cement sample). Secondly, tests were performed by several operators and with different devices. Thirdly, the protocol of loading is also different. The influence of the type of device has already been studied in [119] and it was shown that it is very limited. The mixing procedure and the curing have also been studied and no major effect was observed in the evolution of the Young's modulus and the compressive strength. In the protocol of loading, two parameters can explain the slight difference visible in Figure 10: the amplitude of loading (constant stress/strength ratio with the TSTM and constant deformation with the BTJASPE) and the rate of loading. Between the setting and 20 hours, the effect of the loading rate is predominant. For batch "T3", the time to apply the load was 1 s whereas for the other samples the time was 10 s and even up to 7 min. It could then be observed that the loading rate has a predominant influence for loading just after the setting. Faster the load was applied, higher was the Young's modulus. This observation is directly linked to the viscoelastic behaviour of concrete.

In order to assure that no damage, irreversibility or effect of bleeding occurs during the test, classical extensometry was performed on cylinders with a J2P extensometer [74]. The load corresponds to 20% of the compressive strength and is applied in 10 s which corresponds to protocol of loading of batch T2. These results showed that with exactly the same protocol of loading, very similar results were obtained with the J2P and TSTM.

FREE DEFORMATION

Figure 97 shows the evolution of the autogenous free strain recorded in the dummy mould as well as the temperature in the straight part of the specimen. The strains were compared to the results obtained with a specific device so called BTJADE and designed for the monitoring of the autogenous shrinkage of concrete [8,141]. At the end of the test carried out with the BTJADE, when there is no significant evolution of the autogenous strain anymore, a variation of temperature of 3°C was applied to the sample in order to define the coefficient of thermal expansion. A value of 11 µm/m/°C was obtained and used to remove the thermal strain from the raw measurement and then define the autogenous strain in isothermal conditions. Figure 97 shows that the autogenous strains obtained with both devices are in very good agreement. Limited scattering occurs during the first hours after casting so that the time zero was set to 10 hours instead of 7 hours (end of setting) as in Figure 96. The free strains of the loaded specimen and the unloaded one are also compared (Figure 96). The free strains in the loaded specimen are taken into account up to the start of a new loading. Results are again very close.

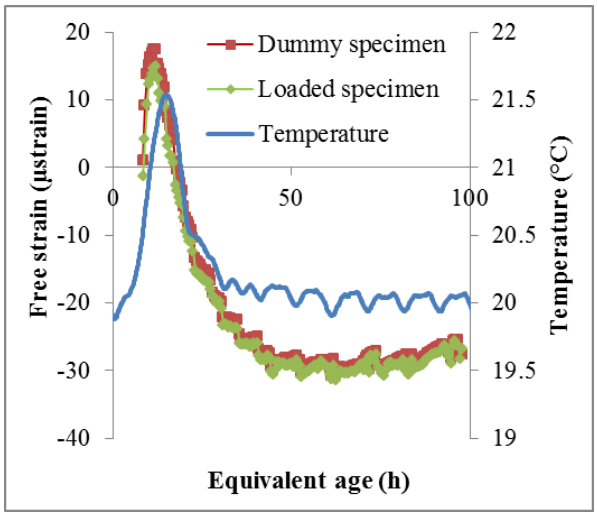

Figure 96 – Autogenous free strain with the dummy mould and the cumulated one at the end of each repeated minute long loading with the TSTM. Time zero is set to end of setting (7 hours).

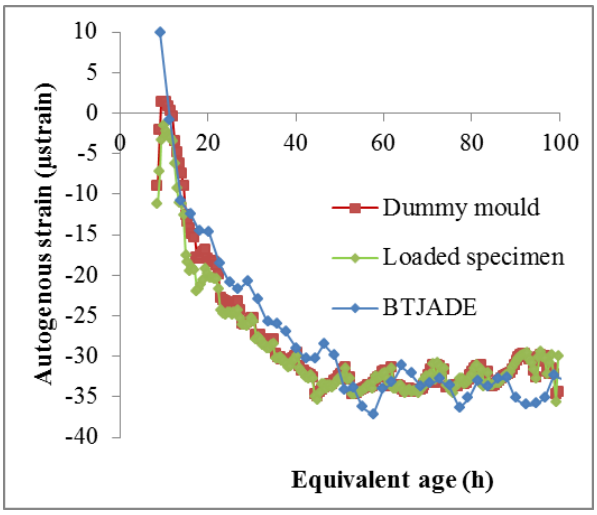

Figure 97 – Autogenous free strain with the BTJADE, the dummy mould and the cumulated one at the end of each repeated minute long loading with the TSTM. Time zero is set to 10 hours.

The Young's modulus and the autogenous shrinkage obtained with the TSTM device are in very good agreement with the other classical test devices. It could then be concluded that very short duration of loading (5 min) followed by a total unloading do not induce irreversible effect on the sample. Therefore, after the unloading, a full recovery is obtained.

CREEP AND RELAXATION RESULTS

In Figure 98, the force and the displacement recorded in the straight part of the specimen were very well controlled continuously during the plateau of strain or stress. At each repeated-minute long loading, the relaxation/creep is recorded as soon as the plateau is reached (t'). Creep and relaxation are defined through Equations **19** and **20** in which $C(t, t')$ is the specific creep function, $R(t, t')$ is the specific relaxation function and $\sigma(t, t')$ is the stress at an age t for a loading applied at an age t'.

$$C(t,t') = \frac{\varepsilon_{cr}(t,t')}{\sigma(t',t')} \quad (19)$$

$$R(t,t') = \frac{\sigma(t,t') - \sigma(t',t')}{\varepsilon_{el}(t')} \quad (20)$$

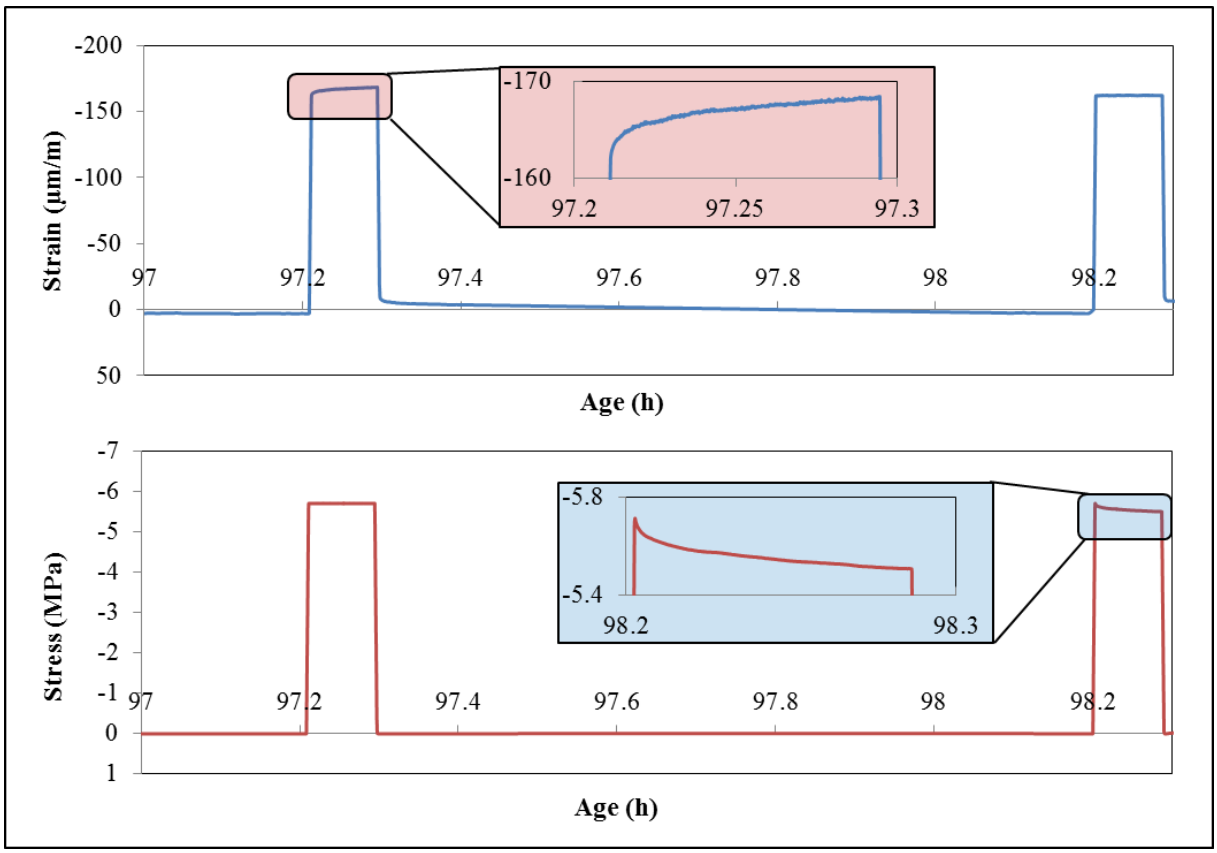

Figure 98 – Record of strain during a creep repeated minute long loading and stress during a relaxation repeated minute long loading.

First, all creep and relaxation curves have been superimposed on the same graph to investigate the effect of aging on the amplitude. It was done in Figure 99a for batch T2 and the amplitude of the specific creep depends strongly on the age of concrete at loading. For very early ages at loading, the amplitude is higher than for older ages. All specific creep curves of each repeated-minute long loading were normalized by the value reached at the end of the plateau (300 s in Figure 99b): 0 at the beginning of the ratio and 1 at the end. In that case, all repeated-minute long loadings are quasi superimposed (Figure 99b). The maximal value of the standard deviation is equal to 0.026 at 142.5 sec (+) and 0.032 at 94 sec (-).The standard deviation is very limited what raises the conclusion that the kinetics of the specific creep is independent of the age at loading at early age for duration of loadings limited to 5 min. The same data analysis has been made for the specific relaxation curves. A significant effect of the age at loading on the amplitude is also observed but not on the kinetic. Same observations have then been made for specific creep and relaxation. Mean values of normalized specific creep and normalized specific relaxation are shown in Figure 99c. A same kinetic is observed for creep and relaxation.

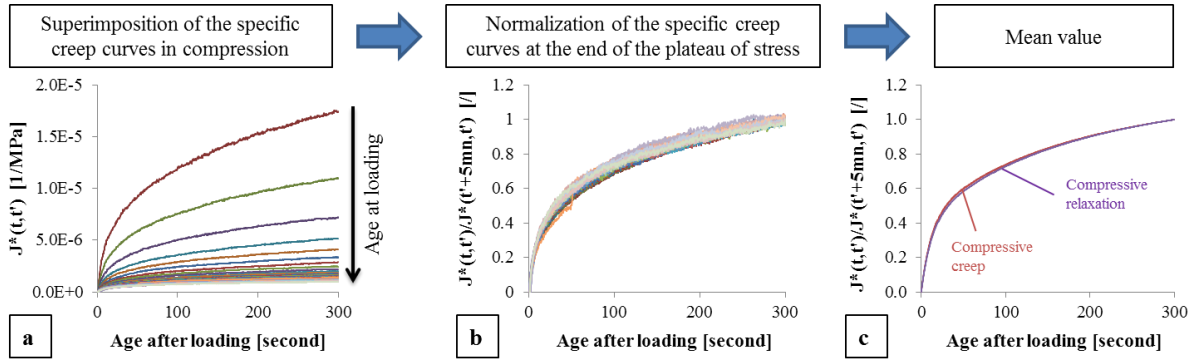

Figure 99 – Repeated minute long loadings. a: for each repeated minute long loading, creep curves are superimposed and set to zero when the load is kept constant. b: for each repeated minute long loading, creep curves are normalized by the value obtained after 5 minutes of loading. c: mean values of normalized curve for creep and relaxation repeated minute long loadings.

For the analysis of the amplitude, all relaxation and creep curves were fitted with least and square method by means of 3 Maxwell's chains in parallel (relaxation) or 3 Kelvin-Voigt chains in series (creep) [158,159]. The amplitude corresponds to the value of the creep coefficient φ_c or the relaxation coefficient Ψ_r (Equation 21) after a plateau of 5 min with constant stress or strain. This value is called here the amplitude factor.

$$\Psi_r(t,t') = \frac{\sigma(t,t') - \sigma(t',t')}{\sigma(t',t')} \qquad 21$$

Figure 100 shows the evolution of the amplitude factor of the creep and relaxation coefficient in function of the age at loading for several tests (C for creep, R for relaxation). The amplitude factor is inversely proportional to the age at loading. Slight differences can be seen between results obtained with the TSTM and the BTJASPE due to the protocol of loading (see Table 12). The time duration to apply the load is a key parameter to take into account the determination of the amplitude. For test with higher time duration to apply the load, the amplitude is lower due to the very fast creep/relaxation which already occurs when the load is applied. For short duration of loading, the kinetic is a constant parameter, then, it could be assumed that each amplitude factor curve is a multiple of another amplitude factor curve. To demonstrate that, each amplitude factor curve is normalized at an age at loading of 24 hours (Figure 101). Any age of loading could be chosen for the normalization. However, as some scattering occurs during first hours after setting, an age of 24 hours was used for the normalization. Normalized results of each test for both devices are very close and show that each protocol of loading can be used for the study of creep and relaxation for short duration of loading. Due to the remarkable agreement between results of both devices with the different protocol of loading, it is observed that no irreversible effect, damage or bleeding effect occurred during the test.

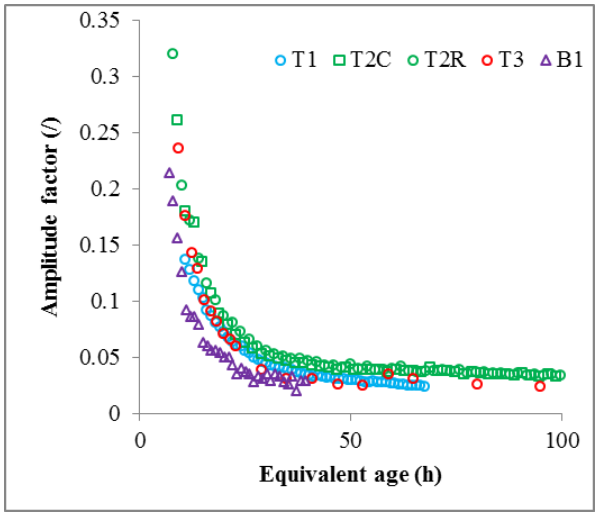

Figure 100 – Amplitude factor for all repeated minute long loading tests.

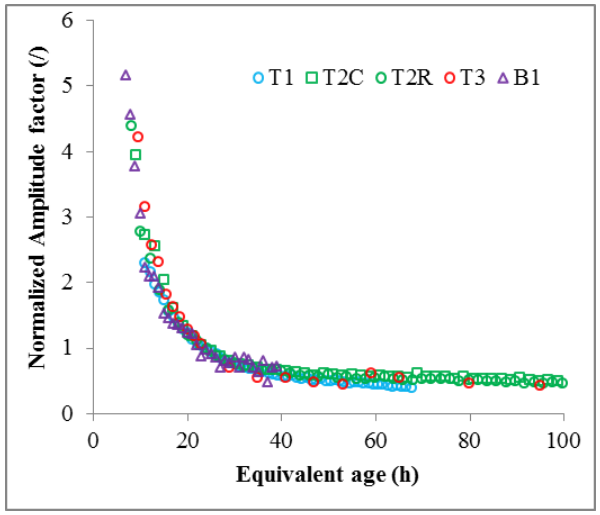

Figure 101 – Normalized amplitude factor.

At this point, it can be observed that all the specific creep and relaxation occurring over short periods of 5 minutes can be modeled by the product of these two terms:

- A dimensionless kinetic term which is constant
- An amplitude term, function of the age of concrete at loading.

4.6.3. Discussion

► Comparison between results of permanent and repeated-minute long loadings

As explained above, a repeated-minute long loading test was used for the determination of the aging of the amplitude of the very short term creep. The amplitude of the creep coefficient for duration of loading of 5 minutes (repeated-minute long loading) and two hours (classical creep test) are given in Figure 102. Both results have the same trend and the values of the creep coefficient obtained for duration of loading of 2 hours are about 5.5 times higher than those obtained for repeated-minute long loadings. Limited scattering can be observed for the results coming directly from classical creep tests. The amplitude of the creep coefficient after 2 hours of loading is modeled by Equation 22. This model allows well-fitting the evolution of the amplitude of the creep coefficient by using least and square method.

$$\varphi_c(t' + 2\text{hours}, t') = \frac{1}{a * \ln(t') + b} \qquad 22$$

Where $a = 2.87$ and $b = -5.56$

For this comparison, each curve is normalized by the value obtained at an age at loading of 24 hours (Figure 103). A very good agreement is obtained between normalized results of repeated-minute long loading and classical creep tests. Moreover the model proposed in Equation 22 is well adapted to the prediction of the value of the normalized amplitude factor for ages at loading situated between the setting and 15 hours. It can then be concluded that a repeated-minute long loading test allows determining the aging of the amplitude term.

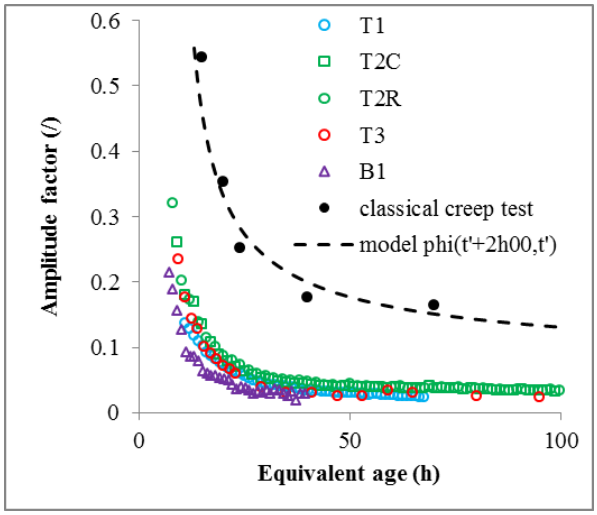

Figure 102 – evolution of the amplitude factor with repeated minute long loadings and classical creep tests.

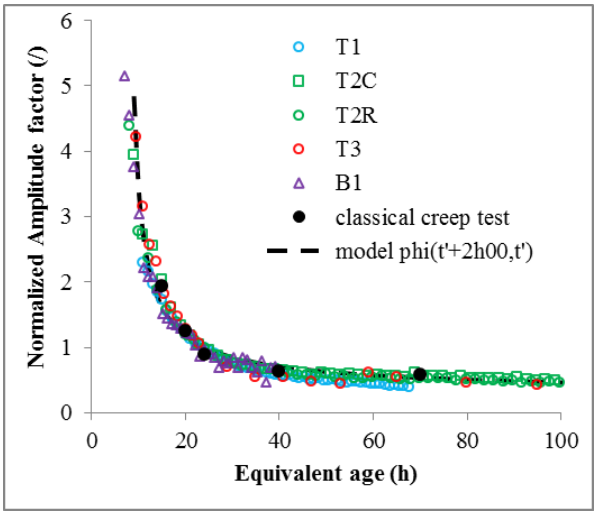

Figure 103 – evolution of the normalized amplitude factor with repeated minute long loadings and classical creep tests.

The amplitude factor can also be expressed in function of the advancement degree of hydration reaction α. Isothermal calorimetry with a Tam Air device [160] is used for the determination of α. In equation 23 it is shown that α is computed as the heat release Q at time t divided by the corresponding apparent ultimate value Q_∞. To define Q_∞, equation 24 is used [161] in which $\alpha_\infty = 1$, and τ and a are material parameters. Nonetheless this equation does not fit well experimental data. The equation 24 is then extended by considering two exponential terms (Equation 25). In this new equation, α_1+α_2=1; τ_1, τ_2, a_1 and a_2 are fitting parameters. Values of each parameter are summarized in Table 13. In Figure 104, the normalized amplitude factor of repeated-minute long loadings and classical creep tests is expressed in function of the advancement degree of reaction. The relation between both is quite linear for α higher than 0.3. This observation is in agreement with results obtained by De Schutter, *et al.* [146]. In fact, the model developed for the basic creep is based on two aging coefficients corresponding to the amplitude and the kinetic of the basic creep. This amplitude coefficient is linearly proportional to the advancement degree of reaction. Nevertheless, to model the amplitude factor since the setting a linear relation is not well adapted. For that purpose, a new model based on classical creep tests data was developed and is given in Equation 26. This model allows well-fitting the evolution of the amplitude of the creep coefficient by using least and square method.

$$\alpha(t) = \frac{Q(t)}{Q_\infty} \qquad 23$$

$$\alpha(t) = \alpha_\infty \exp\left[-\left(\frac{\tau}{t}\right)^a\right] \qquad 24$$

$$\alpha(t) = \alpha_1 \exp\left[-\left(\frac{\tau_1}{t}\right)^{a_1}\right] + \alpha_2 \exp\left[-\left(\frac{\tau_2}{t}\right)^{a_2}\right] \qquad 25$$

Table 13 – Isothermal calorimetry parameters of Equation 25

α_1	τ_1	a_1	α_2	τ_2	a_2
0.70	15.32	1.85	0.30	125.31	1.47

$$\varphi_c(t' + 2\text{hours}, t') = a.\exp(b.\alpha(t') + c) \quad (26)$$

Where a=1.20; b=-2.85;c=-0.1328

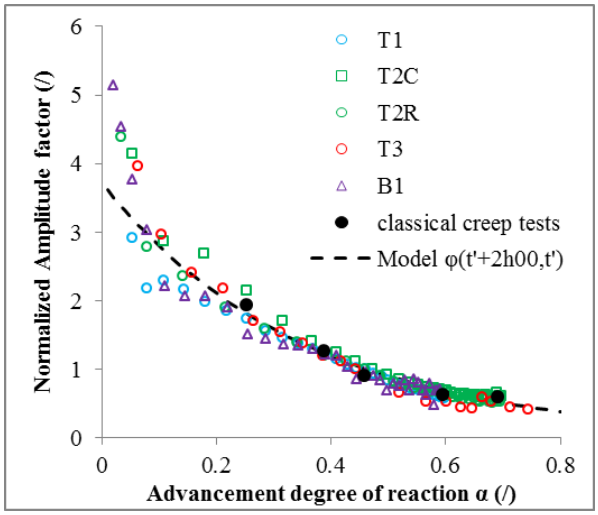

Figure 104 - evolution of the normalized amplitude factor with repeated minute long loadings and classical creep tests in function of the advancement degree of reaction.

► Microstructural interpretation

Two main observations are done through experimental results of classical creep tests:

- The amplitude of the basic creep coefficient is strongly influenced by aging during the first hours after loading. Earlier is the application of the loading and higher is the basic creep coefficient.
- After the first hours of loading, no significant effect of the aging is observed on the kinetic and the amplitude of the basic creep coefficient. However a general trend shows that after few hours of loading aging increases the amplitude of the basic creep coefficient.

For the physical understanding of these observations, the evolution of the microstructure of the cement paste corresponding to this ordinary concrete is computed with the NIST's software VCCTL (V9.5) [162]. Results of the heat release predict by VCCTL were compared to experimental results. A very good agreement is obtained between both. According to results from the literature, two main parameters are studied: the evolution of the volume fraction of the porosity and the one of the CSH. These both parameters are the main drives of the two mechanisms associated to the short term creep. Porosity governs the general behaviour of cement based materials but particularly here the porosity is linked to the water mobility inside the concrete. It is suggested that there is a stress-induced water movement towards the largest diameter pores [163]. The water diffusion between pores was suggested by several authors with observations of the effect of the temperature during the first days of loading [164] or during creep recovery [165]. The activation energy associated to this short term creep is close to a mechanism of free water migration [166] which explains the reversible behaviour of the short term creep. Powers [167] attributed the short term creep to the thermodynamic equilibrium which occurs when a load is applied. Water migrates by diffusion in the layer of absorbed water to the

capillarity pores where the pressure is lower which leads to a global progressive contraction of the cement paste. The evolution of the volume fraction of the CSH is linked to the progress of the mechanical properties of the cement paste. This evolution leads to stiffen the material during the loading [168,169].

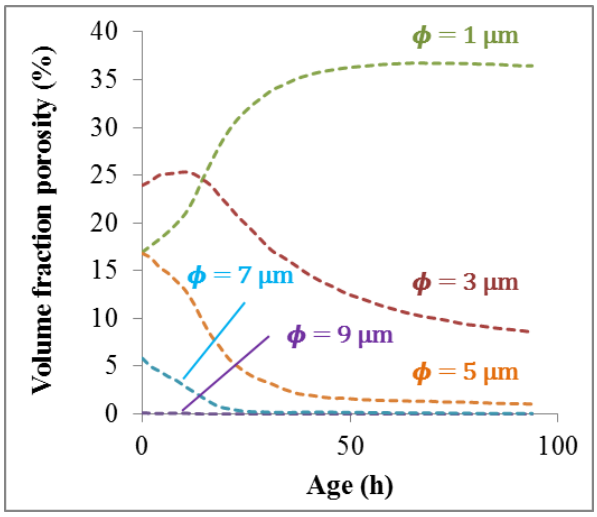

Figure 105 – Evolution of the porosity for different pores size.

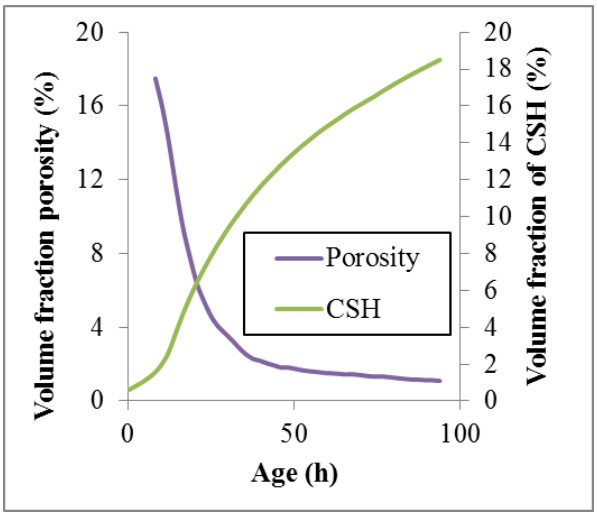

Figure 106 – Evolution of the porosity (pores diameter size from 5 to 9 µm) and CSH.

Different categories of porosity should be considered according to the pores size. The distribution of the volume fraction porosity for different pores diameter at early age is shown in Figure 105. Different tendencies are observed according to the pores size. For pores diameter lower than 1 µm, a significant increase of the volume fraction occurs till an age of 24 hours. The opposite trend is observed after an age of 65 hours, a slow decrease of the volume fraction porosity appears. For pores diameter between 5 and 9 µm, a major decrease of the volume fraction porosity occurs during the first 24 hours. After this period, a slower decrease of the volume fraction porosity is observed. Thus, the subsequent can be observed, for the highest capillarity pores in the cement paste [170], the evolution of the volume fraction porosity follows a same trend that the amplitude factor of creep. In Figure 106 and Figure 107, the volume fraction porosity of diameter between 5 and 9 µm is compared to the evolution of the CSH and the creep amplitude factor. In Figure 107, the evolution of the porosity has the same trend as the amplitude factor when each parameter is normalized by the value obtained at an age of 24 hours. The agreement between both curves is excellent especially during the first hours after setting. After an age of 24 hours, the agreement between them does not correspond so well anymore. In fact, the porosity decreases more than the amplitude factor after an age of 24 hours. It is then observed that the creep during the first hours after loading is well correlated to the evolution of the porosity of pores with diameters higher than 5 µm. A similar correlation exists between capillarity pores and the coefficient of permeability [171]. At very early age, the decrease in the total capillarity porosity is associated with segmentation of large capillarity pores. This segmentation decreases the size and the number of channel flow in the cement paste which leads to a strong decrease of the coefficient of permeability. Later in the hydration, when only smaller capillarity pores exist and disappear, the decrease of the coefficient of permeability is very low because the interconnection between capillarity pores is already strongly reduced. Thus the following interpretation is proposed: the large capillarity pores are the main drives of water migration in the cement paste and when they disappear, the cement paste become less permeable due to the decrease of interconnection between capillarity pores. Therefore the migration of the absorbed water to the capillarity pores decreases

strongly. In addition to the porosity, the production of the CSH and their viscoelastic behaviour should be also considered [157]. When the load is applied, it is considered that stress-induced water movement occurs towards the largest diameter capillarity pore and also creep strain occurs through the CSH. It is thus observed that the first mechanism is associated to the state of the material (capillarity pores, CSH…) when the load is applied and this mechanism is strongly correlated to the largest diameter pores for which the volume fraction decreases sharply during the very early age.

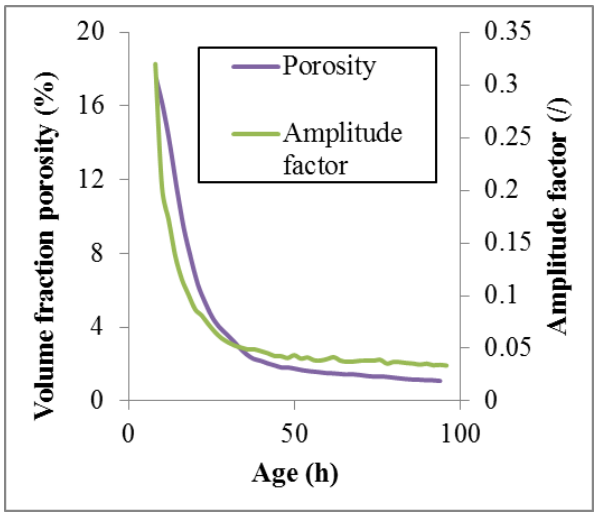

Figure 107 – Evolution of the porosity (pores diameter size from 5 to 9 µm) and the amplitude factor.

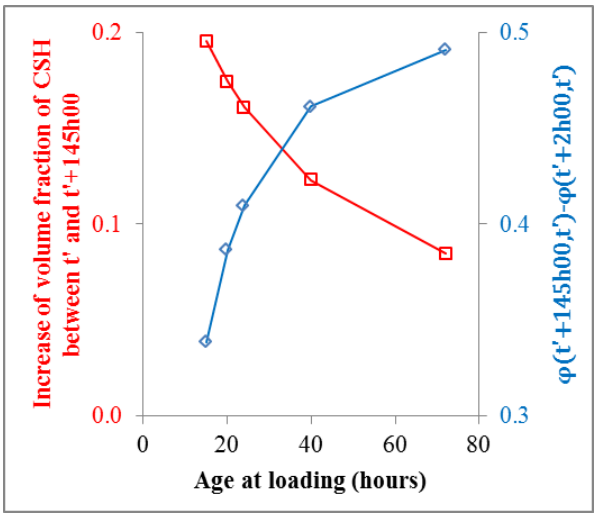

Figure 108 – Increase of volume fraction of CSH and creep coefficient for different age at loading.

The second observation can be directly correlated to the Microprestressed-Solidification theory of Bazant [168]. This theory describes the visco-elastic behaviour of cement based materials by considering the formation of new hydration products on the aging. When a load is applied, hydration products should be considered in the elastic response. If the load is kept constant, new hydration products will take place in the capillarity pores and will bear also the load and others hydration products will be partially unloading. The reduction of the load on the hydration products will decrease the amplitude of the creep. Here only CSH layer are considered as hydration products which bear the load (Figure 108). Between the setting and 72 hours, the volume fraction of CSH swelled from 0.01 to 0.16 which corresponds to 3.7% and 56% of the value obtained at an age of 28 days. Volume fraction of CSH is given in Table 14 for the different age at loading and for an age after loading of 145 hours. Difference of volume fraction of CSH between the age at loading and an age after loading of 145 hours is also given. The difference of volume fraction of CSH decreases strongly with the age at loading. A comparison between the increase of volume fraction of CSH after 145 hours of loading and the increase of the creep coefficient between 2 hours of loading and 145 hours of loading is given in Figure 108 for the different age at loading. Results are in good agreement with the theory of solidification. For very early age of loading, a high increase of CSH occurs while a low increase of the creep coefficient is observed after duration of loading of two hours. For loading applied at later ages, the increase of volume fraction of CSH develops in an inverse way than the creep coefficient. That explains why after few hours of loading, the evolution of the creep coefficient is higher for specimen loaded at higher age. It is thus observed that the second mechanism is associated to the solidification [169,172] of the cement paste during loading which is linked to the evolution of the CSH and ipso facto to the decrease of the capillarity pores.

Table 14 – Evolution of the volume fraction of CSH for the different age at loading.

Age (h)	Volume fraction of CSH (/)	Age + 145h00 (h)	Volume fraction of CSH (/)	Difference of volume fraction of CSH (/)
15	0.030	**160**	0.226	0.195
20	0.054	**165**	0.228	0.174
24	0.069	**169**	0.230	0.161
40	0.113	**185**	0.235	0.123
72	0.161	**217**	0.245	0.084

Through these observations performed with VCCTL software and experimental results, the short term creep is divided in two mechanisms:

- The first mechanism is associated to the state of the material (capillarity pores, CSH…) when the load is applied and this mechanism is strongly correlated to the largest diameter pores for which the volume fraction decreases sharply during the very early age.
- The second mechanism is associated to the solidification [169,172] of the cement paste during loading which is linked to the evolution of the CSH and ipso facto to the decrease of the capillarity pores.

All experimental observations were compared to the evolution of the microstructure of the cement paste. Good correlations are done between both approaches however one important parameter is not considered in this analysis: microcracking which occurs in the cement paste and at the interface between cement paste and rigid inclusions. For further investigation this parameter should also be studied.

SECTION 4.7 – MODELLING BASIC CREEP OF CONCRETE SINCE SETTING TIME

This chapter is based on the joint publication of Brice Delsaute, Jean-Michel Torrenti and Stéphanie Staquet entitled "Modelling basic creep of concrete since setting time" and has been submitted in June 2016 at Cement and Concrete Composites Journal. All experimental results from this section have been carried out at ULB whereas the modelling approach has been discussed between all the authors.

During this last decade, different creep models have been developed for early age concrete. These models are generally based on the decomposition of the total strain ε_{tot} of a loaded concrete sample in a sum of the elastic strain ε_{el}, the creep strain ε_{cr}, the autogenous strain ε_{au} and the thermal strain ε_{th} as expressed in Equation 27. Here drying effect is not considered. For a constant uniaxial stress σ, the uniaxial mechanical strain can be defined as in Equation 28 where t is the age of the concrete, t' the age of the concrete at loading, J(t,t') is the compliance function, E(t') is the elastic modulus and C(t,t') is the specific creep. Generally authors use the creep deformation, the creep compliance, the specific creep or the creep coefficient $\varphi(t,t')$ to model creep. The link between these three last parameters is given in Equation 29.

$$\varepsilon_{tot} = \varepsilon_{el} + \varepsilon_{cr} + \varepsilon_{au} + \varepsilon_{th} \quad (27)$$

$$\varepsilon_{el}(t') + \varepsilon_{cr}(t,t') = \sigma.J(t,t') = \sigma.\left(\frac{1}{E(t')} + C(t,t')\right) \quad (28)$$

$$J(t,t') = \frac{1}{E(t')} + C(t,t') = \frac{1+\varphi(t,t')}{E(t')} \quad (29)$$

As concrete creep at early age is still not well understood, mathematical expressions are used to fit experimental data. Several models developed for hardened concrete are given in [173]. Models are often composed of two terms: an amplitude term and a kinetic term. For consideration of ageing both parameters can be expressed in function of the age at loading [64,173–178], the advancement degree of reaction at loading [146,179] or the equivalent age at loading [144,180,181]. The advancement degree of reaction α is defined as the relative amount of hydrated cement and can be computed as a function of the heat release Q and the heat release at an infinite time Q_∞ (Equation 30). The equivalent time t_{eq} is based on the Arrhenius equation in order to take into account the main temperature effect on the hydration process. Equation 31 defines the equivalent time which is function of the age of the material t, the evolution of the temperature T (°C), a reference temperature T_r (generally 20°C), the universal gas constant R (=8.314 J/mol/K) and the apparent activation energy (material parameter in J/mol).

$$\alpha(t) = \frac{Q(t)}{Q_\infty} \quad (30)$$

$$t_{eq}(t,T) = \int_0^t \exp\left(\frac{E_a}{R}.\left(\frac{1}{273+T(s)} - \frac{1}{273+T_r}\right)\right).ds \quad 31$$

Ageing of the creep function can be linked to other parameters such as the mechanical strength [149,182] and the effect of the stress level could be included [149]. A set of these models are given in Table 15. Complete details about the different models shown in Table 15 can be found on the references given in the table itself. For these models no real physical mechanism is associated to the amplitude or kinetic terms. With only one amplitude term and one kinetic term, it is assumed in these models that only one mechanism is responsible of creep or that all mechanisms develop with same kinetics but different amplitudes.

Table 15 - Creep models existing in the literature

	Model	**References**
Hyperbolic law	$\varepsilon_{cr}(t,t') = \frac{t-t'}{k_2+k_1.(t-t')}$	[174] [175]
	$\varphi(t,t') = \left(\frac{\frac{t-t'}{t_1}}{\beta_H+\frac{t-t'}{t_1}}\right)^{0.3} . \frac{1}{\left(0.1+\left(\frac{t'}{t_1}\right)^{0.2}\right)} . \frac{5.3}{\sqrt{\frac{f_{cm}}{f_{cm0}}}}$	[176]
	$C\left(t_{\mathrm{eq}}, t'_{\mathrm{eq}}\right) = \mathrm{C_C}\left(t'_{\mathrm{eq}}\right).\frac{\left(t_{eq}-t'_{eq}\right)^{\mathrm{A}}}{B_C\left(t'_{eq}\right)+\left(t_{eq}-t'_{eq}\right)^{A}}$	[180,181]
Power law	$\varepsilon_{cr}(t,t') = k_1.(t-t')^{k_2}$	[177,178]
	$\varphi(\alpha,\alpha_0) = c_1(\alpha).\left(\frac{\alpha-\alpha_0}{1-\alpha_0}\right)^{c_2(\alpha)}$	[146,179]
	$\varphi\left(t_{eq}, t'_{eq}\right) = P_1(\alpha).\left(\frac{t_{eq}-t'_{eq}}{\mathrm{t_c}}\right)^{P_2(\alpha)}$	[144]
Double power law	$J(t,t') = \frac{1}{E(t')}.[1+\varphi_0.(k+t')^{-d}.(t-t')^{p}]$	[64,173]
Triple power law	$\frac{\partial J(t,t')}{\partial t} = \frac{\psi}{E(t')}.\frac{t'^{-d}}{\left(\frac{t}{t'}\right)^{p}}.\frac{1}{(t-t')^{1-p}}$	[64]
Logarithmic law	$C(t,t') = \frac{\beta_{bc}(f_{cm})}{E_{28}}.\ln[k.(t-t')+1]$	[182]

Among many previous studies like those reported in [25,64,144–146,148,149,179,180], several theories were developed to clarify mechanisms related to creep behaviour. However each theory alone does not allow explaining all experimental observations. Globally each theory can be linked to two mechanisms: direct mechanisms linked to the cement paste and responsible of the highest part of the creep amplitude and indirect mechanisms linked to the heterogeneity of the concrete. Direct mechanisms are related to the water mobility and to the solidification of the material and can be separated in short and long terms phenomena [163,168,183,184]. The short term phenomenon is reversible with a small characteristic time of about 10 days, is linked to a stress-induced water movement towards the largest diameter pores and to the solidification [168,169] of the material, and

occurs under increasing volume for uniaxial compression. The long term phenomenon is irreversible with a high characteristic time and related to viscous flow in the hydrates and occurs under almost constant volume. The creep rate of this long term phenomenon develops as a power function t^n [185–187] with an exponent n between -1 and -0.9 according to [188], between -0.72 and -0.69 according to results of [189] on concrete and an exponent n between -0.86 and -0.6 on cement paste according to results of [148]. Nanoindentation tests were carried out on C-S-H by Vandamme, *et al* [157]. It was shown that C-S-H exhibits a logarithmic creep which is in agreement with results obtained on concrete. Vandamme [190] compared also this logarithmic behaviour with other heterogeneous and porous materials with porosity including several orders of magnitude (soils and wood). For these non-ageing materials, a logarithmic long-term creep was also observed. It can then be assumed that this long term creep is not linked to a hydration process or any chemical specificity of the C-S-H.

The indirect mechanisms are due to micro-cracks which occur progressively in the cement paste and at the interface between cement paste and inclusions. Their presence can cause a redistribution of the stresses in the material. Rossi, *et al* [77,78,191] proposed an approach of the creep mechanisms by means of a micro-cracking process which occurs during loading and which is confirmed by acoustic emission. Over the time, an increase of the density of micro-cracks occurs. These micro-cracks are distributed through the volume of the specimen and allow water transfers which induce some additional self-desiccation shrinkage (but there is no experimental evidence of this additional self-dessication).

On basis of the results coming from the literature presented above, it could be considered that creep is separated in three functions which correspond to the short term creep, the long term creep and a term related to the formation of micro-cracks. In the model B3 of Bazant [188,192], both short and long term creep are considered separately as expressed in Equation 32 and 33. Complete details about the different parameters of the model can be found in the references [188,192]. The short term creep is linked to the solidification theory [169,193] and corresponds to the terms with parameter q_2 and q_3 in the equations. The long term creep is linked to the microprestress theory [168,172] and corresponds to the term with parameter q_4 in the equation.

$$\frac{\partial \mathrm{C}(\mathrm{t},\mathrm{t}')}{\partial \mathrm{t}} = \frac{\mathrm{n}.(\mathrm{q}_2.t^{-m} + q_3)}{(t-t') + (t-t')^{1-n}} + \frac{q_4}{t} \qquad 32$$

$$\mathrm{C}(\mathrm{t},\mathrm{t}') = \mathrm{q}_2.\int_{t'}^{t} \frac{\mathrm{n}.\tau^{-\mathrm{m}}.(\tau-t')^{n-1}}{1+(\tau-t')^n} d\tau + q_3.\ln[1+(t-t')^n] + q_4 \ln\left(\frac{t}{t'}\right) \qquad 33$$

The consideration of the formation of micro-cracks is not directly given in the model B3 but it could be considered by using a new function based on a fracture mechanics approach coupled to creep [194], a general damage factor d with effective stress concept [195] (Equation 34) or a damage factor related to the stiffness of the material coupled to a factor β which connects a part of the creep strain to damage (Equation 35) [196].

$$\sigma = (1-d).\breve{\sigma} = (1-d).E.\varepsilon_{el,d} \qquad 34$$

$$\tilde{\varepsilon} = \sqrt{\langle \varepsilon_{el,d} + \beta\varepsilon_{cr}\rangle_+ : \langle \varepsilon_{el,d} + \beta\varepsilon_{cr}\rangle_+} \qquad 35$$

Where $\tilde{\varepsilon}$ is the equivalent strain and $\langle . \rangle_+$ is the positive part operator.

Another way to model the viscoelastic behaviour of concrete is the use of rheological model where the creep behaviour is associated to spring and dashpot in series or in parallel. There is an infinite number of associations of springs and dashpots, several examples are given in [197]. Bazant advises to use Kelvin Voigt chains in series for creep [159] and Maxwell chains in parallel for relaxation [158]. To consider ageing creep, spring and dashpot parameters have to change according to the age of the concrete. De Schutter [146] linked the creep coefficient to a Kelvin-Voigt chain by considering that the spring and the dashpot develop according to the amplitude term of a model depending on the advancement degree of hydration. This model has the advantage of being very simple because it uses only two parameters. However this model is limited for early age study and for a limited duration of loading. To extend the use of the model of De Schutter, Benboudjema and Torrenti [198] generalized this model by means of several Kelvin-Voigt chains in series with different springs and dashpots. The ageing of each element of each Kelvin-Voigt chain depends on the evolution of one parameter which is function of the advancement degree of hydration. In case of complex loadings with partial or total unloadings, Briffaut [145] added a dashpot in series to the three Kelvin-Voigt chains where the creep strains predicted by the additional dashpot are totally irreversible. Then the Kelvin-Voigt chains are linked to the short term creep and the dashpot is linked to the long term creep. A more general rheological scheme of the concrete behaviour is given in Figure 109 [168,199] where elastic, creep (short term and long term), shrinkage and thermal strain are represented on a same rheological model. Another way to consider ageing by using rheological model is done by Hermerschmidt [200] who uses 4 Maxwell units and 1 single spring in parallel to model tensile creep test with several histories of loading. The influence of the hardening process on the viscoelastic behaviour is carried out by increasing the stiffness of the single spring and the viscosities of the dashpots according to the age of the concrete.

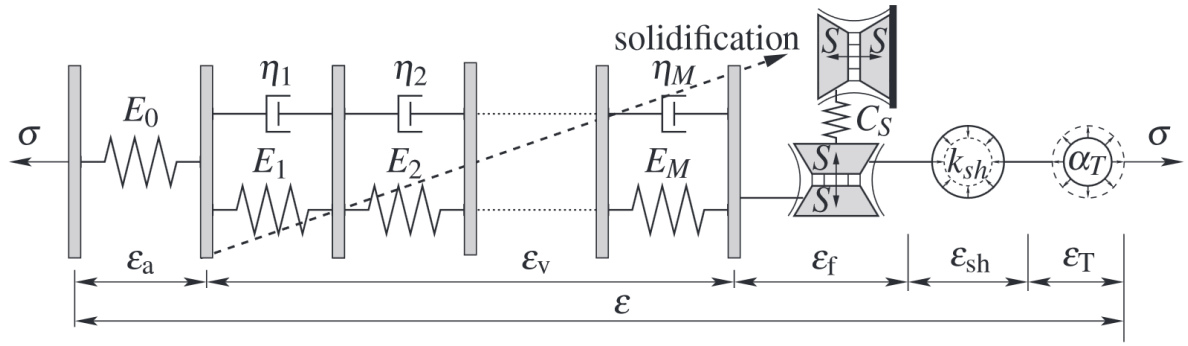

Figure 109 - Rheological scheme of the concrete behaviour [199]

Therefore several approaches were proposed in the literature and in the design codes to model creep behaviour for early age or for hardened concrete. The present section reports on a new strategy for the modelling of the basic creep since setting time. The model is based on physical mechanisms presented above and experimental results on an ordinary concrete studied in isothermal conditions at 20°C and in sealed conditions reported in [201]. A comparison between the experimental results and the Model Code 2010 is carried out in order to point out a certain deficiency in application to very early age and to suggest a modification which may eliminate this deficiency.

4.7.1. Experimental details

The results presented here were performed on an ordinary concrete for which mix proportions are presented in Chapter 3.

4.7.2. Results and observations

All results and observations used for the modelling of the basic creep are based on the Section 4.6.

4.7.3. Modelling

- Part1: Modelling of the repeated minute-long duration loadings test

Two models were developed to best fit the creep coefficient for each repeated minute-long duration loadings. A first model was introduced in [202]. The model is given in Equation 36. The model is a power law and is inspired from the work of Gutsch [144] and De Schutter [146]. The model has the advantage to consider only two parameters: a parameter A_1 linked to the amplitude of the creep coefficient after 5 minutes of loading and a parameter K_1 linked to the kinetic evolution of the creep coefficient.

$$\varphi_c(t,t') = A_1(t').\left(\frac{t-t'}{t_{A1}}\right)^{K_1(t')} \quad 36$$

where $t_{A1} = 0.083\text{h} = 300\text{s}$. The second model developed is a logarithmic law and is inspired from the Model Code 2010 (Equation 37). The model is also based on an amplitude parameter A_2 and linked to the amplitude of the creep coefficient after 5 minutes of loading and a parameter K_2 linked to the kinetic evolution of the creep coefficient.

$$\varphi_c(t,t') = A_2(t').\ln\left(1+(e-1).\left(\frac{(t-t')}{t_{A2}}\right)^{K_2(t')}\right) \quad 37$$

where $t_{A2} = 0.083h = 300s$. The calculation of both parameters was carried out in two steps. Firstly, each creep curve was fitted with three Kelvin-Voigt chains in order to remove noise from the measurement. The value of the fitted curve after 5 minutes of loading corresponds to the amplitude parameter for each age of loading. Secondly, the value of the kinetic coefficient is computed with least and square method (by using the fminsearch function in Matlab©). To compare the power and logarithmic expression in term of performance, the error is computed by considering the experimental and modelling value of the creep coefficient for each cycle at the same time according to Equation 38. N_c and N_p are respectively the number of cycles during the test and the number of measuring points for each cycle. The error is 0.0020 for the power law and 0.0014 for the logarithmic law. A reduction of error by a factor 1.5 is observed. This is coherent with results of long duration which show a logarithmic trend for each age of loading since setting time during the first hours of loading. Then, only results from the logarithmic law will be considered on the next parts of this paper.

$$error = \sqrt{\frac{1}{N_c . N_p} \sum_{i=1}^{N_c} \sum_{j=1}^{N_p} \left(\varphi_c(t_i + t_j, t_i) - \varphi_c^{mod}(t_i + t_j, t_i) \right)^2} \quad 38$$

Coefficient of the logarithmic model is given in Figure 110. The amplitude parameter decreases strongly with the age at loading and has an evolution inversely proportional to the age at loading as indicated in Equation 39. The kinetic parameter is relatively constant as expected with experimental results obtained. Then, for this concrete, a constant value of 0.35 is considered for the kinetic parameter K_2. The evolution of both parameters is given in function of the age at loading and not in function of the advancement degree of reaction as it has been done in [146] due to technical reasons. Calorimetry testing in isothermal, semi-adiabatic or adiabatic condition is generally used to define the evolution of the advancement degree of reaction. These methods are very accurate for the early age but not for long term. Indeed, after several weeks the heat flow of the hydration of the cement paste is very low and is very difficult to assess experimentally. Thus after few weeks, the advancement degree of hydration does not develop significantly whereas the mechanical properties such as the compressive strength and the elastic modulus continue to change significantly [119]. That is the reason why it has been chosen that the expression of all parameters is given according to the equivalent time. A value of 35 kJ/mol is used for the activation energy [203]. In Figure 111, modeled and experimental data are compared for several ages at loading. A very good agreement is obtained between both.

$$A_2(t') = \frac{1}{\mathrm{a}.\ln\left(\frac{\mathrm{t'_{eq}}}{t_A}\right) + \mathrm{b}} \quad 39$$

where a = 11.26, b = -19.62 and t_A = 1h.

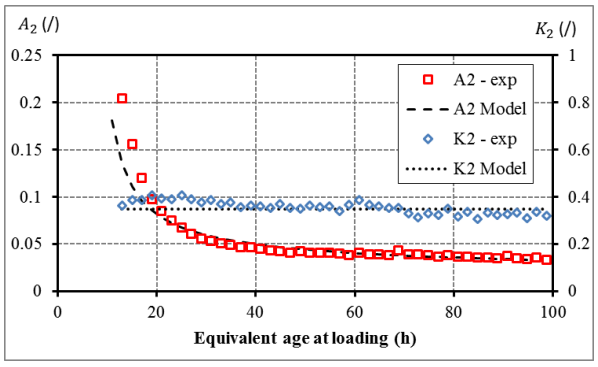

Figure 110 – Evolution of the amplitude and kinetic parameter of Equation 37 according to the age at loading.

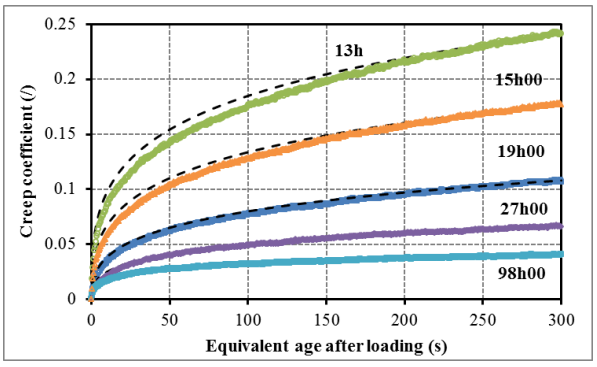

Figure 111 – Experimental data of the creep coefficient and modeled curves for several ages at loading from Equation 37.

► Part 2 : Modelling of the permanent loading

RHEOLOGICAL MODEL WITH AGEING FACTOR

Based on experimental observations explained in section “Results and observations”, a new approach is used for the modelling of the basic creep function at early age. Several Kelvin-Voigt units in series

were used. The stiffness E and the viscosity η of the chain with retardation time $\boldsymbol{\tau}$ lower than 2 hours depend on the evolution of the amplitude parameter A_2 which is determined by means of a minute-long duration loadings test. The Figure 112 illustrates the different models proposed before by De Schutter [146], Benboudjema & Torrenti [198] and the one developed in this study.

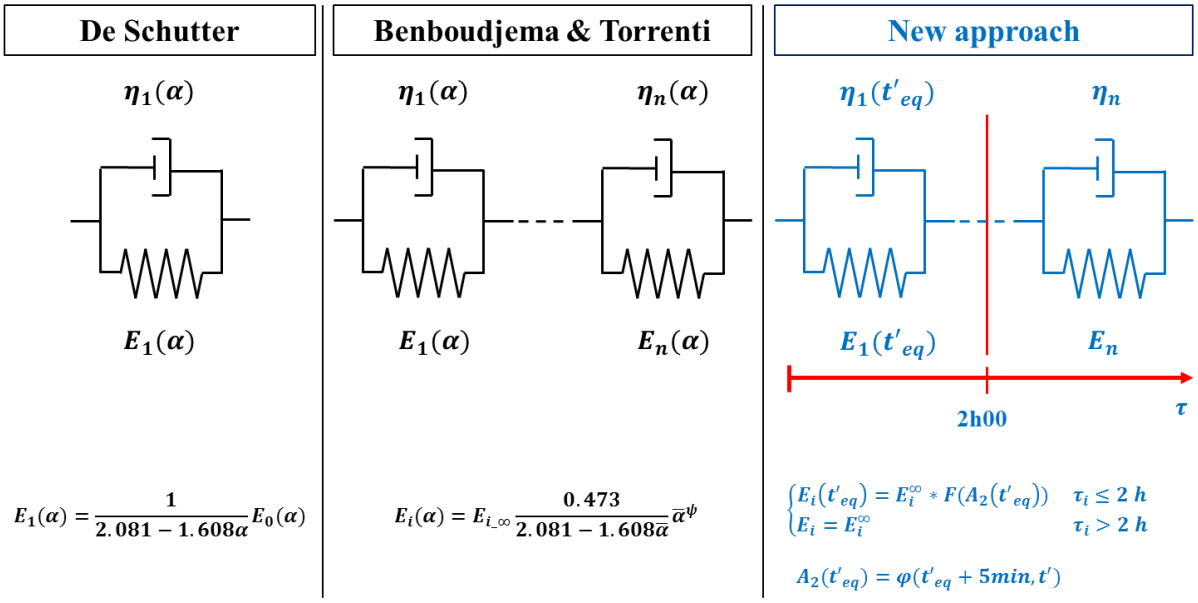

Figure 112 - Comparison between the approach of De Schutter [146], Benboudjema & Torrenti [198] and the new strategy developed

The stiffness of the spring of each unit (expressed in MPa) is imposed to be positive by using Equation 40 in which the parameter **d** is computed by using least and square method (with the fminsearch function of Matlab©) by considering each creep curve at the same time. Only 4 Kelvin-Voigt chains are necessary to model the ageing of each creep curve for a period of 145 hours.

$$\begin{cases} E_i(t'_{eq}) = 10^6.\exp\left(-A_2(t'_{eq}).d_i\right) & \tau_i \leq 2h \\ E_i = 10^6.\exp(-d_i) & \tau_i > 2h \end{cases} \quad 40$$

Values of the parameters of the 4 Kelvin-Voigt chains are given in Table 16 and the results of the modelling are compared to experimental results in Figure 113.

Table 16 - Basic creep coefficient for 4KV model.

τ_1 (h)	d_1	τ_2 (h)	d_2	τ_3 (h)	d_3	τ_4(h)	d_4
0.34	24.58	0.94	27.33	19.32	1.66	145	2.80

A good agreement is found between the experimental results and the modelling. This way to model creep curve has the advantage to be easily implemented in finite element software. For the study of loading of short duration, as the case of restrained shrinkage, this way to model creep can be very convenient. However it has also several disadvantages:

- The modelling is not able to predict creep for long duration of loading.
- The modelling needs several creep tests of long duration to be calibrated. If only two tests are used to fit the parameters, the model cannot predict with a very good accuracy results for other ages.

- The model does not highlight correctly the mechanisms which occur during the loading and does not distinguish between reversible and irreversible creep.

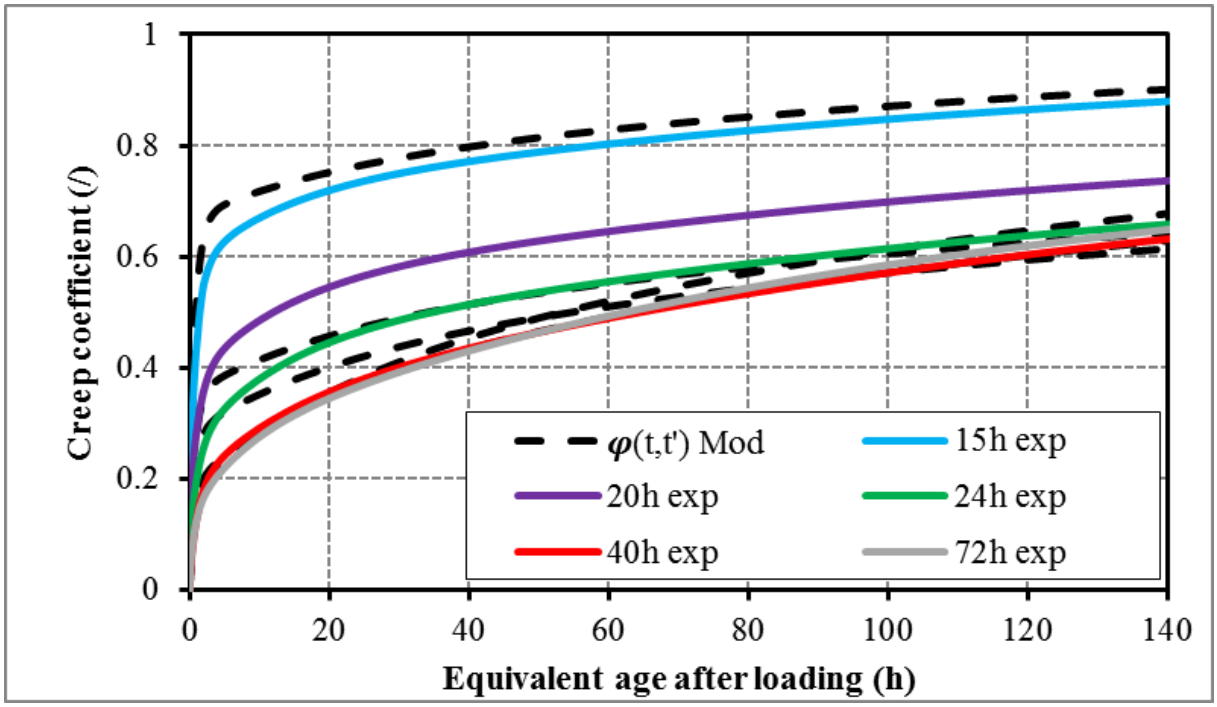

Figure 113 – Comparison between 3 KV chains model developed with minute-long duration loading testing for long duration and experimental results of long duration creep tests.

MODEL WITH SEPARATION BETWEEN SHORT TERM AND LONG TERM CREEP

To improve the model, several physical mechanisms must be taken into account. By considering the model B3 of Bazant [188] and also the observations carried out by Ulm, Acker [163] and Torrenti [204] with regards to the results of Leroy [25] and Laplante [180], it appears that the long term creep corresponds to a logarithm function. It is particularly highlighted by comparing the evolution of the derivative of the creep function of several creep curves according to the age of the concrete (Figure 114). The derivative of the creep function follows a power function trend after several days for early age loading or after several weeks for loading at later ages. The same observations can be done with the concrete studied in this article as shown in Figure 115. In a previous work [205], Rossi have carried out creep tests of long duration on the same concrete studied in this paper for a hardened state (age of 28 days). Results of Rossi are also shown in Figure 115 and are in very good agreement with all results obtained at early age and very early age. It appears that with very early age loading, the long term creep can be identified very easily, very accurately and with a short duration of loading (one week of loading is clearly enough for early age loading). The long term creep corresponds also to a power expression and is given by equations 41 and 42. As the exponent g of the equation is very close to a value of -1, the long term creep can be identified as a logarithm expression. Results from the literature shows that the exponent of the derivative of the creep function can vary between -1 and -0.69. For that reason, the long term creep is considered as a power expression as shown in Equation 42.

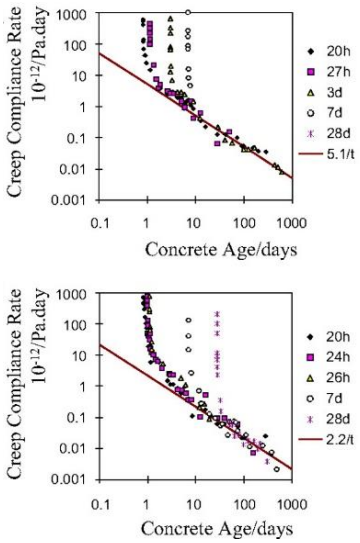

Figure 114 – Derivative of the creep function according to the age of the concrete from [157].

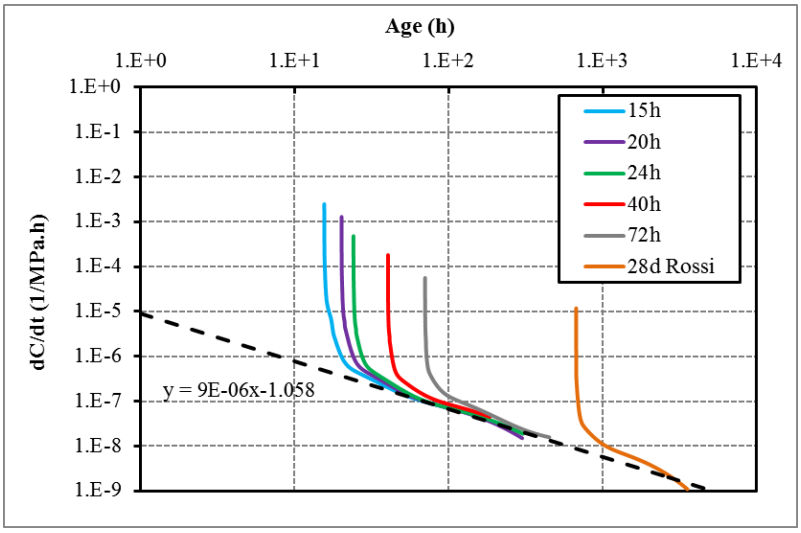

Figure 115 – Derivative of the creep function according to the age of the concrete for results obtained in this study and results obtained by Rossi [205].

$$\frac{dC_{LT}(t)}{dt} = f * t^{g} \quad (41)$$

$$\varphi_{LT}(t,t') = E(t').C_{LT}(t,t') = E(t').\frac{f}{g+1}.(t^{g+1} - t'^{g+1}) \quad (42)$$

Where f = 9E-6 MPa-1 and g =-1.048. In Figure 118, the long term creep is removed from the experimental results by using Equation 42 in order to isolate the short term creep. For early age loading, the short term creep changes strongly during the first hours after loading with a logarithmic trend and after approximately ten hours no short term creep occurs anymore. For later ages at loading, a logarithmic evolution is observed during the first week of loading. Short term creep can then be separated in two functions:

- A logarithmic function which is function of the actual state of the material (capillarity porosity, CSH) when the load is applied. The function is linked to the amplitude term of the minute-long duration loadings test which is strongly correlated to the evolution of the largest diameter pores (Figure 116). The function has two materials parameters. This part is called here the initial short term creep and is marked φ_{IST}.
- Another function which is linked to the solidification of the material and associated to the quantity of formed CSH during loading (Figure 117) and ipso facto to the decrease of the capillarity pores. This part is called here the solidification term creep and is marked φ_{ST}.

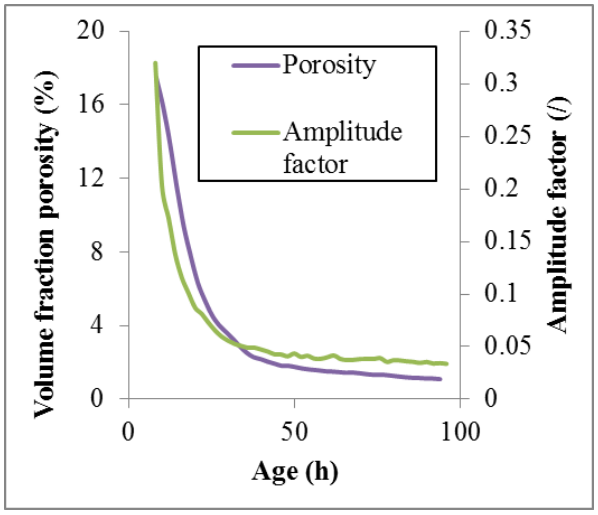

Figure 116 - Evolution of the porosity (pores diameter size from 5 to 9 µm) and the amplitude factor [201].

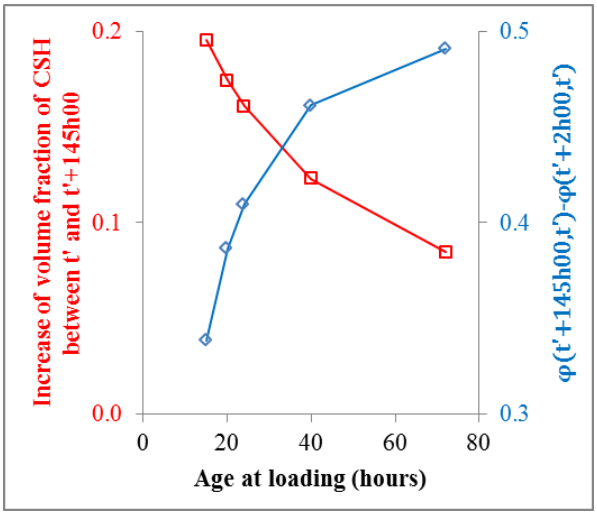

Figure 117 - Increase of volume fraction of CSH and creep coefficient for different age at loading [201].

Firstly the initial short term creep is modelled by a logarithmic expression as given in Equation 43. The equation used to model the initial short term creep is inspired from the second term of the model B3 [188] as for the modelling of the creep coefficient with the minute-long duration loadings test. The modelling of the initial short term creep is compared to experimental results for which the long term creep is removed in Figure 118. For early age loading, a very good agreement is observed during the first hours of loading. For later ages (here loadings at 2 or 3 days), the agreement is good till one week of loading. In Figure 118, it is also shown that the model developed for minute-long duration loadings test (Equation 37) is not able to predict alone the creep behaviour for long duration. This can easily be explained by the fact that only the initial state of the material is considered and not the mechanisms which develop during the hardening process as the solidification of the material and the viscous flow in the hydrates. The results presented here are in good agreement with the observation carried out by Irfan, *et al.* [206] who show that creep results from repeated minute-long duration loadings on cement paste are enough to predict the evolution of the creep function for several days.

$$\varphi_{IST}(t,t') = h.A_2(t').\ln\left(1+(t-t')^k\right) \quad 43$$

Where h = 20 and k = 0.08. Secondly, the initial short term creep is removed also from the experimental results in order to identify the solidification part of the creep for each age of loading. In Figure 119, results of this subtraction are given. For early age loading, the solidification term creep is very important and changes strongly during the first days of loading. For later ages of loading, the amplitude of this parameter seems very low. In order to compare only the kinetics aspect of the solidification term creep, each solidification creep curve is normalized at a time corresponding to an age after loading of 145 hours. In Figure 120, it is observed that the kinetics evolution of the solidification term creep does not depend on the age at loading of the concrete. Results from the loading applied at an age of 72 hours are not included in Figure 120 because for later ages corresponding to an high advancement degree of reaction (the advancement degree of reaction for an age of 72 hours has a value of 0.69), the solidification phenomenon is very low and therefore is very difficult to analyse. The kinetic of the solidification term creep is modelled by the use of Kelvin-Voigt chains in series which best fits the experimental data (Figure 119). Three Kelvin-Voigt chains in

series are used for the modelling of the solidification term. Values of the parameters of the Kelvin-Voigt chains are given in Table 17.

Table 17 - Solidification creep parameters for 3 KV model

τ_1 (h)	E_1 (MPa)	τ_2 (h)	E_2 (MPa)	τ_3 (h)	E_3 (MPa)
1	8344450	11.94	2788404	142.5	1153883

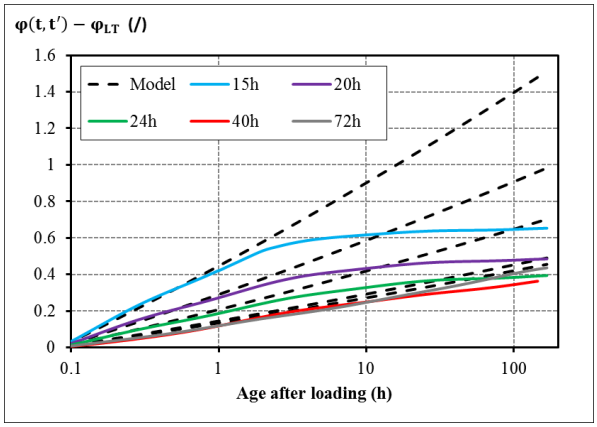

Figure 118 – Evolution of the creep coefficient with subtraction of the long term part and modelling of the very short term creep

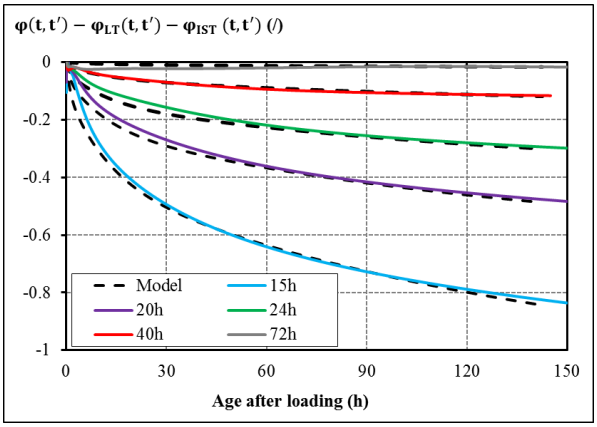

Figure 119 – Evolution of the creep function with subtraction of the long term and very short term part and modelling of the consolidation creep

Then, the evolution of the amplitude of the solidification term creep is given in Figure 121. The amplitude is defined as the value of the solidification term creep at an age after loading of 145 hours. The solidification mechanism is not directly dependent of the state of the material when the load is applied. This is dependent of how the material will harden during its hydration. That is why a macroscopic parameter such as the strength and the E-modulus or a microscopic parameter such as the porosity and the CSH cannot directly be used to characterize the amplitude of the solidification creep. As the amplitude of the solidification is linked to a mechanism which develops during the hydration, this parameter should be linked to the evolution rate of one parameter such as the CSH at microstructural scale (see Section 6 of the Chapter 4) or the elastic modulus at macroscopic scale. Parameters such as the compressive strength could not be considered because there are not relative to the general behaviour of the concrete but relative to the behaviour of the material at failure which is not what is studied here. In Figure 121, the amplitude of the solidification term creep is plotted according to the derivative of the elastic modulus. A linear relation is observed between both parameters. Therefore it could be concluded that both parameters develop with a same kinetics and that the solidification term creep and the derivative of the elastic modulus are directly proportional.

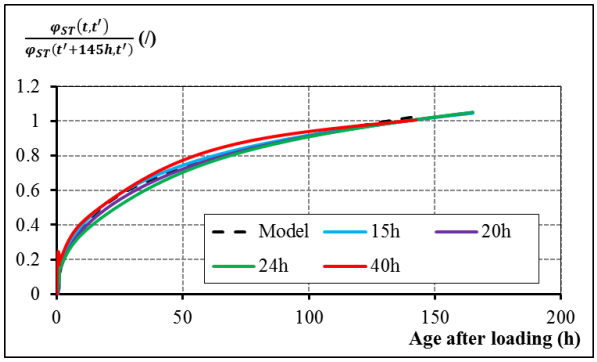

Figure 120 – Normalization at 145 hours of the creep function after subtraction of the long term creep and the very short term creep. Modelling of the kinetics of the solidification term creep.

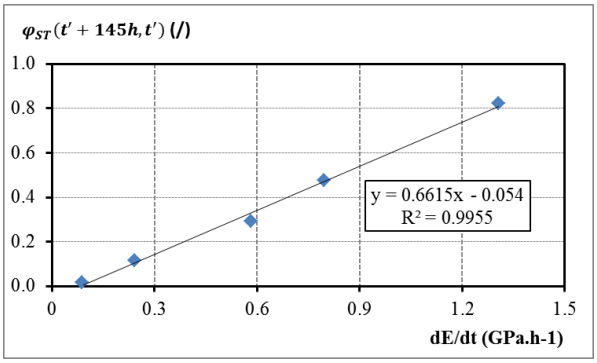

Figure 121 – Comparison between the amplitude of the solidification term creep after 145 hours of loading and the derivative of the elastic modulus according to the age at loading.

Finally the solidification term creep can be defined by the multiplication of two functions:

- One function which is linked to the kinetics evolution of the solidification and is independent of the age at loading. Three Kelvin-Voigt chains are used to model it.
- One function which is linked to the amplitude of the solidification, dependent of the age at loading and directly proportional to the evolution of the derivative of the elastic modulus. This amplitude term is noticed A_{ST} and is given in Equation 44.

$$A_{ST}(t') = l.\frac{dE(t')}{dt'} + m \qquad 44$$

Where l = 0.6615 and m = -0.054. In Figure 122, the contribution of the very short term, the solidification term and the long term are summed and compared to the experimental results. A very good agreement for each age at loading is observed. It is then concluded that the creep function is divided in three terms and can be defined since the setting with one early age loading test of long duration and one minute-long duration loadings test which begins just after setting. The methodology used to identify each term has three steps:

1. The long term creep is defined with one creep test for which the load is applied at early age during one week or more. After one day or more, the creep compliance rate follows a power law which corresponds to the long term creep.
2. The initial short term creep is obtained after having removed the long term creep and corresponds to a logarithmic law. The kinetic is constant and the amplitude depends on the amplitude parameter defined with the minute-long duration loadings test. This term fits well the results obtained during the first hours of loading or more. This term is function of the actual state of the material (capillarity porosity, CSH) when the load is applied. The function is linked to the amplitude term of the minute-long duration loadings test which is strongly correlated to the evolution of the largest diameter pores (Figure 116).
3. The solidification creep is obtained after having removed the long term and the initial short term creep. The kinetic is constant and the amplitude depends on the derivative of the elastic modulus at the age of loading.

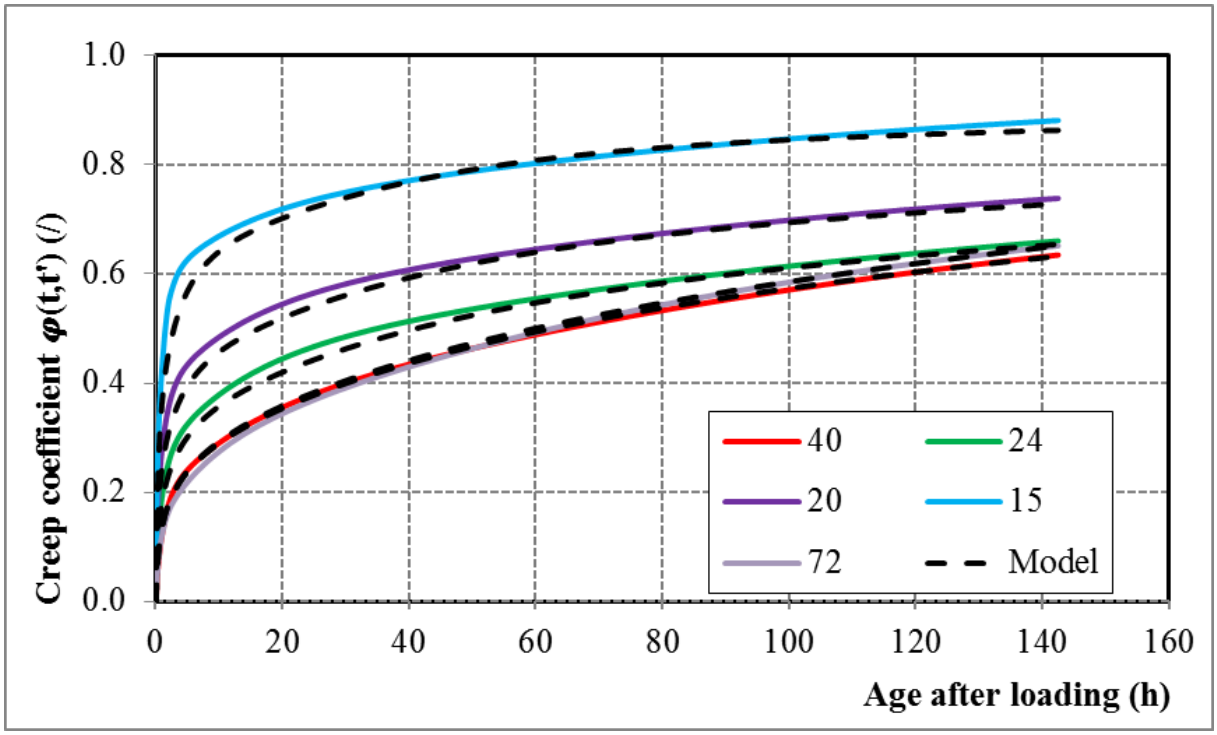

Figure 122 – Modelling of the creep coefficient by identification of the long term creep, the short term creep and the solidification creep.

MODEL CODE 2010

In the recent Model Code 2010 (MC2010) [182], basic creep is expressed as the multiplication of an amplitude term $\varphi_{0,bc}$ which is linked to the mean compressive strength at an age of 28 days and a kinetic term $\beta_{bc}(t,t')$ which is function of the age at loading, the age after loading and the type of cement (Equation 45 and 46). For one composition defined, all parameters are constant except the age at loading which is the only parameter which considers the ageing. When the time approaches infinity, the creep compliance rate approaches a value corresponding to the inverse of the time. Then MC2010 considers the long term creep,

$$\varphi_c(t,t') = \varphi_{0,bc}(f_{cm}).\beta_{bc}(t,t') = \frac{1.8}{(f_{cm})^{0.7}}.\ln\left(\left(\frac{30}{t_{0,adj}} + 0.035\right)^2 (t-t') + 1\right) \quad 45$$

$$t_{0,adj} = t'.\left(1 + \frac{9}{2 + t'^{1.2}}\right)^{\alpha_{cem}} \quad 46$$

where α_{cem} depends on the type of cement and is equal to 1 for CEM 52.5 N, f_{cm} is the mean compressive strength at an age of 28 days (here f_{cm} = 48 MPa). In Figure 123, results from MC2010 are compared to the experimental results. For age at loading of 40 and 72 hours, the predicted values of MC2010 are quite close to the experimental results. However for earlier loadings, a significant difference is observed. To understand this difference, results of the elastic modulus and its derivative are compared to the predictive value of MC2010 (Equation 47 and 48) in Figure 124. Several

significant differences are highlighted. The elastic modulus is highly overestimated till an age of 20 hours. The derivative of the elastic modulus is always underestimated and particularly during the two first days. This underestimation is also noted on the amplitude of the creep compliance (Figure 123). As mechanical properties are not well predicted for the very early age, it is normal that MC2010 is not able to predict correctly a parameter such as creep compliance at very early age. In order to improve the prediction of the creep compliance it is necessary to adapt the model by changing the effect of the age at loading.

$$E_{ci}(t') = \beta_E(t').E_{ci} \quad (47)$$

$$\beta_E(t') = \left(\exp\left(s.\left(1-\left(\frac{28}{t'}\right)^{0.5}\right)\right)\right)^{0.5} \quad (48)$$

Where $E_{ci}(t')$ is the elastic modulus in MPa at an age t' in days, E_{ci}=36300 MPa is the elastic modulus at an age of 28 days and depends on the concrete grade, s=0.2 depends on the strength class of cement.

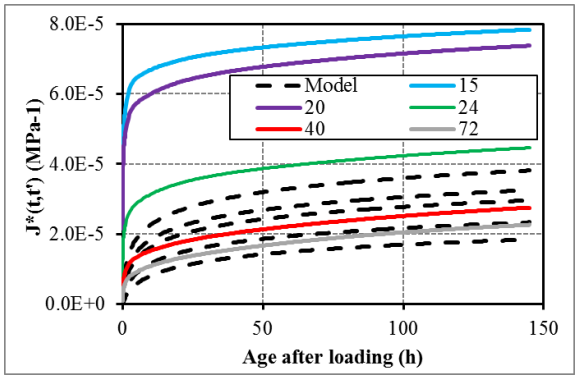

Figure 123 – Comparison between predicted value of the creep compliance obtained with MC2010 and experimental results

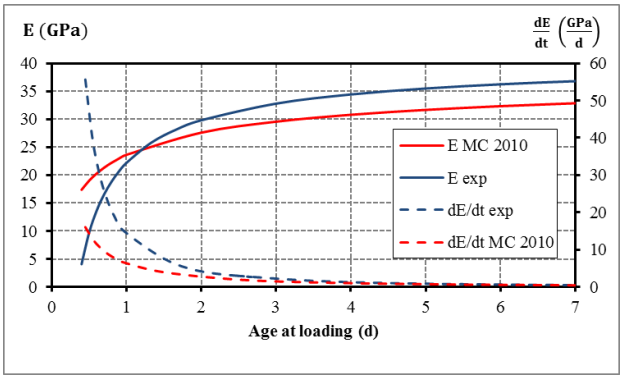

Figure 124 – Comparison between predicted value of the elastic modulus and the derivative of the elastic modulus obtained with MC2010 and experimental results.

ADAPTED MODEL CODE 2010

Torrenti [204] puts forward that MC2010 can be expressed as in Equation 49. The parameter C is constant for one concrete composition and τ is the only parameter which changes according to the age at loading. By adjusting both parameters for different set of results coming from tests carried out on ordinary and high performance concrete, Torrenti shows that MC2010 could be able to predict the basic creep coefficient. The same methodology is used on the concrete studied in this paper and results of the fitting of the creep curve are given in Figure 125. The model is able to fit very well the experimental results. A value of C=217.8 GPa is found. The value of the parameter τ for the different age of loading is given in Table 18.

$$\varphi_c(t,t') = \frac{E(t')}{C}.\ln\left(1+\frac{t-t'}{\tau}\right) \quad (49)$$

Table 18 - Value of parameter τ from Equation 49

t′ (h)	15	20	24	40	72
τ (d)	2.49E-07	8.20E-07	3.90E-04	1.62E-02	4.76E-02

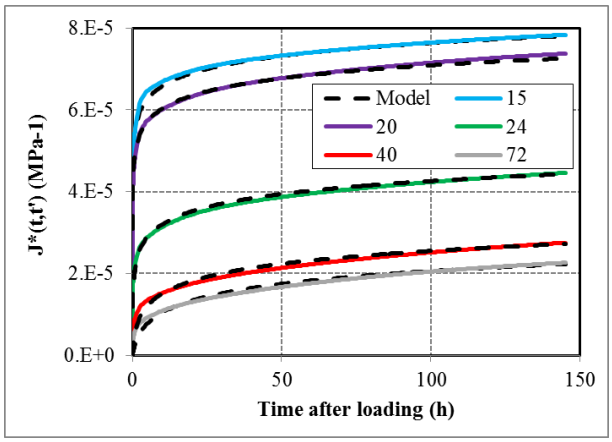

Figure 125 – Comparison between experimental creep curves, creep curves coming from a model inspired by the model code 2010.

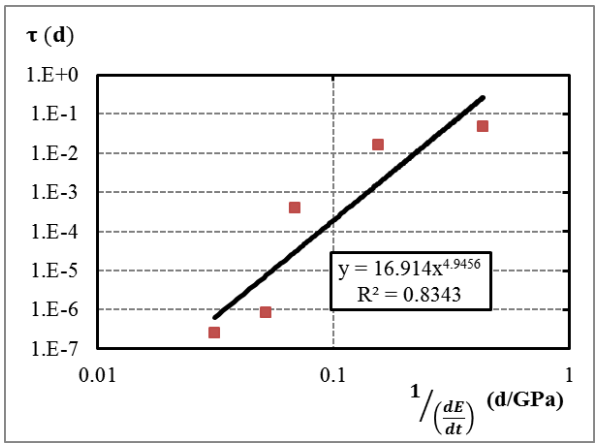

Figure 126 – Comparison between the derivative of the elastic modulus and the parameter τ of the adapted model code 2010

Results of the parameter τ are compared to the inverse of the derivative of the elastic modulus in Figure 126. A power law linking the parameter τ and the derivative of the elastic modulus is highlighted. Therefore the derivative of the elastic modulus seems to be a very good indicator of the ageing of the creep function. As for the second model presented, this observation can be explained by the link between the rate of the elastic modulus and the velocity of the hardening of the cement paste and thus to the solidification of the material. In comparison, the predictive values of τ are plotted according to the inverse of the derivative of the elastic modulus predicted by MC2010 in Figure 127. An excellent linear correlation is done between both parameters. In Figure 128, data from experimental results and MC2010 are superimposed. Two kinds of trend are observed. For very early age (between setting up to 40 hours), the relation between the parameter τ and the inverse of the derivative of the elastic modulus follows a power trend. Values by MC2010 are not able to predict this trend. For higher ages (after 40 hours), experimental results and predicted values of MC2010 are very close and follow a same linear trend. Through results presented in the previous models, this change of trend at an age at loading of 40 hours can be interpreted as an effect of the solidification of the material. Indeed, before an age of 40 hours, the amplitude of the solidification of the material is significant on the evolution of the creep coefficient. For later ages at loading, the solidification of the material has a low impact on the value of the evolution of the creep coefficient. The mathematical expression linking the parameter τ and the derivative of the E-modulus is given in Equation 50 and 51 where n=0.0884 GPa, q=22542 d, p=-7.41 and t_E=1 d.GPa-1.

$$\begin{cases} \tau = q.\left(\frac{dE}{dt}.t_E\right)^p & if\ t \le 40h \\ \tau = n.\left(\frac{dE}{dt}\right)^{-1} & if\ t > 40h \end{cases} \quad 50 \quad 51$$

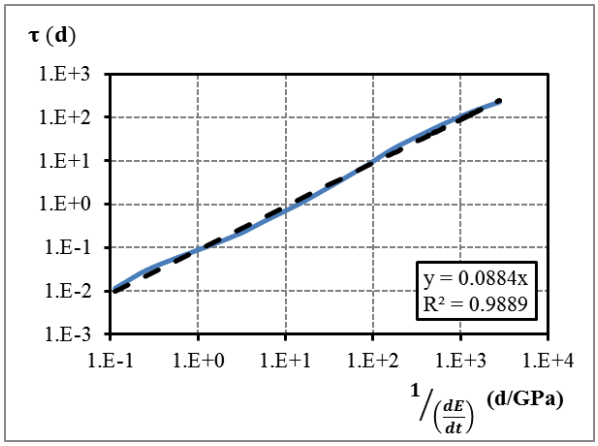

Figure 127 – Evolution of the parameter τ from Model code 2010 according to the derivative of the elastic modulus.

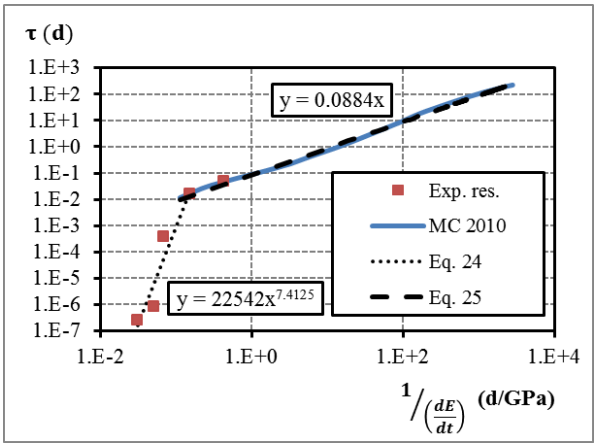

Figure 128 - Comparison of the relation between the inverse of the derivative of the elastic modulus and τ from experimental results and Model Code 2010.

CONCLUSIONS

The conclusion of this chapter is divided according to the different sections.

Section 1

A new test protocol is defined for the monitoring of the autogenous strain and the coefficient of thermal expansion. Every 130 minutes, thermal variations of 3°C are applied on a concrete sample with the device so-called BTJADE. Thermal and autogenous strains are distinguished by creating a fictive thermal cure at 20°C from the experimental results. A similar strategy is developed for the monitoring of the autogenous deformation and the coefficient of thermal expansion for cement paste and mortar by usin the Autoshrink device.

Section 2

The Temperature Stress Testing Machine (TSTM) allows monitoring the mechanical behaviour of concrete since setting time under restraint conditions. Actually, the restraint shrinkage test set up designed with a TSTM system takes into account all the parameters affecting the stresses development inside the concrete sample: the degree of restriction, the relaxation of stresses, the evolution of the strength and the stiffness… On basis of this kind of test, several parameters can be quantified such as the elastic deformation, free and restraint shrinkages and also, creep and relaxation. The design of this system must include a thermal regulation in contact with all sides of the concrete sample and, especially, for the very early age, displacement sensors without contact to limit the measurement artefacts on the concrete. A dummy mould was added to the revisited TSTM system for monitoring the free shrinkage and the thermal deformation. So, the direct measurement of the creep deformation and the relaxation stresses is possible with the simultaneous use of the first and the dummy mould. The test method for measuring the early age properties of concrete must also avoid an early cracking of the concrete sample. To do so, the test method starts after the end of setting time of concrete when the stiffness of the studied material is sufficient. A revisited testing design for monitoring the mechanical properties of concrete in tension and in compression since setting time (Young's modulus, creep and relaxation) was introduced.

Section 3

Section 3 presents a literature review of the existing tensile creep rigs. The different criteria needed for the design of a tensile creep rig are highlighted and explained in details. From these criteria, it was chosen to use two types of tensile creep rig. For very early age tests, the TSTM device is used. For early age or hardened concrete, two electromechanical testing devices are used. For the measurement of the longitudinal and lateral displacement, these two tests rigs are equipped of extensometer in Invar with elastic anchorage from the J2P company. The connection between the test rig and the sample is done with two dollies which are bonded on the ends of the sample and connected to the test rig with a hinge. In addition, the same instrumentation is used for the dummy specimen

Section 4

A new tool, specifically designed at IFSTTAR and aimed at stiffness monitoring of concrete at early age, has been designed and applied to an ordinary concrete. Samples are cast and tested inside a double walled mould. In the double wall, a flow of water ensures the control of the temperature of the sample and thus its maturity. This test rig must be used in conjunction with testing machines able to be controlled in load and in displacement.

Results obtained with this new tool were compared to results obtained at ULB with a modified Temperature Stress Testing Machine (TSTM). The agreement was good. This modified TSTM has been specifically designed to control the maturity. A dummy sample has also been added in order to take into account autogenous strains measurements in the case of creep or relaxation tests at early age. It allows compressive and tensile testing starting just after the setting time.

Two protocols of loading were applied on the concrete samples. For the first protocol, the same deformation (100 to 250 10^{-6} depending on the tests) is applied on the sample, at regular intervals, at a constant strain rate (5 10^{-6} / s). For the second protocol, 20 % of the compressive strength is applied at each cycle. This second protocol implies that the evolution of the compressive strength is known. In the limits of the loading protocols, it seems that no damage affected the samples.

The E modulus monitoring is useful for research applications but it can be used also for field applications when the early age characteristics of concrete are of the first importance. Tests are in progress in order to explore the possibility using the devices of IFSTTAR and ULB for other properties such as creep or relaxation of concrete at early age. In these cases, the loading protocols must be adapted. It is also possible to use the systems of temperature control to apply any temperature histories to perform measurements of coefficient of thermal expansion.

Other characterizations were performed on the concrete: heat released by the hydration process, monitoring of the compressive and the tensile strength and monitoring of the ultrasonic pulse velocity. These tests were performed to obtain a set of characteristics of the concrete allowing choosing the right settings for automatic loadings.

Section 5

Different automatic techniques aimed at measuring changes in the stiffness of a concrete at early age were used in three different laboratories. They were grouped in low-frequency and high frequency methods.

The low-frequency methods gave responses similar to classical measurements. These classical measurements consist in performing the test after having removed the samples from their mould just after the setting time. Despite the fact that the samples are very brittle, the concrete begins to harden at the end of the working day thus, automatic methods are almost obligatory to study this initial phase of concrete behaviour. Two of the low-frequency methods are based on the use of laboratory testing machine (TSTM or QS_3, BTJASPE or QS_1) whereas the third method (EMM-ARM or RF) is well adapted for laboratory testing and in field. Their mutual performances are in good agreement. For such inter-laboratories tests, the protocols of mixing and loading should be improved, though.

Both the loading stress rate and amplitude are observed to have an effect on the determination of the low-frequency elastic modulus. This observation, which might be explained by very short term creep, is of limited importance when quasi-static measurements are performed, regarding the reproducibility of such tests. However, similar mechanisms could explain the difference between the low-frequency and high frequency elastic modulus, since both are measured at very different loading rate and amplitudes.

The ultrasonic measurements are also automatic methods and they are good candidates for the monitoring of the stiffness of the concrete at very early age. Two classical techniques (FreshCon or HF_1, BTPULS or HF_2) are compared to a newly developed technique (SMAGs or HF_3). Ultrasonic measurements provide values of E-modulus that are higher than the values provided by the quasi

static or low frequency tests at the time of the concrete setting. This difference decreases as the concrete hardens. Their results show a clear effect of the loading rate on the E-modulus calculation compared to values obtained with quasi static tests. A correlation between the results of high frequency techniques and low frequency ones is not yet clearly accessible and models should be found to promote the use of ultrasonic techniques applied to the monitoring of the concrete stiffness at very early age.

Further experimentations are needed to quantify accurately the effect of the strain or stress rates on the evolution of the elastic modulus in the low frequency and high frequency ranges.

Section 6

Compressive creep frame were used for classical basic creep tests at different age of loading (15 – 20 – 24 – 40 – 72 hours) with duration of loading of one week and a stress level of 40%. It is observed that the short term of basic creep can be divided in two terms. The first term occurs just after the loading and has duration of few hours (for the concrete studied). During this period, basic creep coefficient has constant kinetic and variable amplitude which is inversely proportional to the age at loading. The second term occurs on longer duration of loading and has amplitude and a kinetic which are not strongly influenced by the age at loading.

A new test is developed for the monitoring of the first term of the short term creep. The test is based on repeated-minute long loadings which are applied each 30 minutes for duration of 5 minutes. For that purpose, a TSTM and a device called BTJASPE were used. It is showed that the autogenous deformation, the Young's modulus and the amplitude of the very short term creep can be determined since setting in only one test. An excellent agreement between the experimental data has been obtained with the BTJASPE and the TSTM device. What is validated the credibility of the results and the protocols of loadings with both devices.

A comparison between the experimental observations and the evolution of the microstructure was done. The short term creep is divided in two mechanisms:

- The first mechanism is associated to the state of the material (capillarity pores, CSH…) when the load is applied and this mechanism is strongly correlated to the largest diameter pores for which the volume fraction decreases sharply during the very early age.
- The second mechanism is associated to the solidification [169,172] of the cement paste during loading which is linked to the evolution of the CSH and ipso facto to the decrease of the capillarity pores.

This conclusion is however limited to early age concrete, for short durations of loading (one week of loading) and limited stress levels (40 %). A next step of this research is the study of creep in tension, higher stress level and the coupling between damage and creep at early age. More sophisticated tests with more complex histories of loadings (various plateau durations) are still needed for computational purposes. The measurement of transversal displacement is also needed for future studies.

Section 7

The section 7 presents a new methodology to model basic creep in compression since setting by means of minute-long duration loadings test with low duration of loading (5 minutes) and classical creep tests with duration of loading of 6 days or more. Results from the minute-long duration loadings test allow defining the elastic modulus and an ageing creep factor corresponding to the

value of the creep coefficient after 5 minutes of loadings. Based on experimental observations, a new approach is developed for the modelling of the creep function.

For short duration of loading (5 minutes), basic creep is modeled since setting time with a logarithmic expression inspired of the Model Code 2010. Only one parameter varied according to the age of loading. This parameter corresponds to the value of the creep coefficient after 5 minutes of loading.

For long duration of loading (6 days or more), several approaches are used to model creep:

1. Four Kelvin-Voigt units in series are used. Only units with a characteristic time lower than 2 hours have an ageing factor which corresponds to the value of the creep coefficient after 5 minutes of loading. This way to model creep curve has the advantage to be easily implemented in finite element software. For the study of loading of short duration, as the case of restrained shrinkage, this way to model creep can be very convenient. However it has also several disadvantages:
    a. The modelling is not able to predict creep for long duration of loading.
    b. The modelling needs several creep tests of long duration to be calibrated. If only two tests are used to fit the parameters, the model cannot predict with a very good accuracy results for other ages.
    c. The model does not highlight correctly the mechanisms which occur during the loading and does not distinguish between reversible and irreversible creep.
2. In previous studies it was highlighted that creep is divided in two terms: the short and long term creep. Here, it is proposed to divide also the short term creep in two terms: the initial short term creep and the solidification creep. Thus the creep function is divided in three terms. Each term is identified since the setting in three steps:
    a. The long term creep is defined with one creep test for which the load is applied at early age during one week or more. After one day or more, the creep compliance rate follows a power law which corresponds to the long term creep.
    b. The initial short term creep is obtained after having removed the long term creep and corresponds to a logarithmic law. The kinetic is constant and the amplitude depends on the amplitude parameter defined with the minute-long duration loadings test. This term fits well the results obtained during the first hours of loading or more. This term is function of the actual state of the material (capillarity porosity, CSH) when the load is applied. The function is linked to the amplitude term of the minute-long duration loadings test which is strongly correlated to the evolution of the largest diameter pores.
    c. The solidification creep is obtained after having removed the long term and the initial short term creep. The kinetic is constant and the amplitude depends on the derivative of the elastic modulus at the age of loading.
3. The Model Code 2010 is used and compared to experimental results. For ages at loading of 40 and 72 hours, the predicted values of MC2010 are quite close to the experimental results. However for earlier loadings, a significant difference is observed.
   An adapted version of the Model Code 2010 is proposed. In this version, the effect of the age at loading is considered by using the inverse of the derivative of the elastic modulus.

The concrete studied is an ordinary concrete with water-cement ratio of 0.54 and was kept in isothermal condition at 20°C.

This conclusion is however limited to medium stress levels (40 %). A next step of this research is the study of creep in tension, higher stress levels and the coupling between damage and creep at early age. More sophisticated tests with more complex histories of loadings or temperatures are still needed for computational purposes. The measurement of transversal displacement is also interesting for future studies.

REFERENCES

[1] Ø. Bjøntegaard, T.A. Martius-Hammer, M. Krauss, H. Budelmann, RILEM Technical Committee 195-DTD Recommendation for Test Methods for AD and TD of Early Age Concrete, Springer Netherlands, Dordrecht, 2015. doi:10.1007/978-94-017-9266-0.

[2] T.A. Hammer, Testing of autogenous deformation (AD) and thermal dilation (TD) of early age mortar and concrete - Recommended test procedure, in: Int. RILEM Conf. Vol. Chang. Hardening Concr. Test. Mitig., RILEM Publications, 2006: pp. 341–346. doi:10.1617/2351580052.036.

[3] ASTM Standard C1698, Test Method for Autogenous Strain of Cement Paste and Mortar, i (2014) 1–8. doi:10.1520/C1698-09R14.

[4] O.M. Jensen, P.F. Hansen, Autogenous deformation and RH-change in perspective, Cem. Concr. Res. 31 (2001) 1859–1865. doi:10.1016/S0008-8846(01)00501-4.

[5] ASTM C469 / C469M-14, Standard Test Method for Static Modulus of Elasticity and Poisson's Ratio of Concrete in Compression, ASTM Int. (2014). doi:10.1520/C0469_C0469M.

[6] ASTM C512 / C512M-15, Standard Test Method for Creep of Concrete in Compression, ASTM Int. (2015) 3–7. doi:10.1520/C0512_C0512M-15.

[7] ISO 1920-9:2009, TESTING OF CONCRETE -- PART 9: DETERMINATION OF CREEP OF CONCRETE CYLINDERS IN COMPRESSION, (2009) 1–13.

[8] C. Boulay, Test rig for early age measurements of the autogenous shrinkage of a concrete, in: Proc. RILEM-JCJ Int. Work. ConCrack 3, 2012: pp. 111–122.

[9] O. Mejlhede Jensen, P. Freiesleben Hansen, A dilatometer for measuring autogenous deformation in hardening portland cement paste, Mater. Struct. 28 (1995) 406–409. doi:10.1007/BF02473076.

[10] V. Baroghel-bouny, Caractérisation des pâtes de ciment et des bétons, Méthodes, Analyse, Interprétation, PhD thesis, Ecole Nationale des Ponts et Chaussées, 1994.

[11] O. Bjontegaard, Thermal dilation and autogenous deformation as driving forces to self-induced stresses in high-performance concrete, 1999.

[12] M. Bouasker, Etude Numerique Et Experimentale Du Retrait Endogene Au Tres Jeune Age Des Pates De Ciment Avec Et Sans Inclusions, PhD thesis, Université de Nantes, 2007.

[13] K. Kovler, Testing system for determining the mechanical behaviour of early age concrete under restrained and free uniaxial shrinkage, Mater. Struct. 27 (1994) 324–330. doi:10.1007/BF02473424.

[14] A. Kronlöf, M. Leivo, P. Sipari, Experimental study on the basic phenomena of shrinkage and cracking of fresh mortar, Cem. Concr. Res. 25 (1995) 1747–1754. doi:10.1016/0008-8846(95)00170-0.

[15] A.M. Paillere, J.J. Serrano, Appareil d'étude de la fissuration du béton, Bull. Liaison Du Lab. Cent. Des Ponts Chaussées. 83 (1976) 29–38.

[16] A. Loukili, D. Chopin, A. Khelidj, J.-Y. Le Touzo, A new approach to determine autogenous shrinkage of mortar at an early age considering temperature history, Cem. Concr. Res. 30 (2000) 915–922. doi:10.1016/S0008-8846(00)00241-6.

[17] H. Mitani, Variations volumiques des matrices cimentaires aux très jeunes âges : approche expérimentale des aspects physiques et microstructuraux, PhD thesis, Ecole Nationale des Ponts et Chaussées, 2003.

[18] J.P. Charron, Contribution à l'étude du comportement au jeune âge des matériaux cimentaires en conditions des déformations libre et restreinte, PhD thesis, Université Laval, 2003.

[19] L. Stefan, Étude Expérimentale Et Modélisation De L'Évolution Des Propriétés Mécaniques Au Jeune Âge Dans Les Matériaux Cimentaires, Ecole normale supérieure de Cachan, 2009. http://tel.archives-ouvertes.fr/tel-00624989/.

[20] R. Loser, B. Münch, P. Lura, A volumetric technique for measuring the coefficient of thermal expansion of hardening cement paste and mortar, Cem. Concr. Res. 40 (2010) 1138–1147. doi:10.1016/j.cemconres.2010.03.021.

[21] M. Wyrzykowski, P. Lura, Controlling the coefficient of thermal expansion of cementitious materials - A new application for superabsorbent polymers, Cem. Concr. Compos. 35 (2013) 49–58. doi:10.1016/j.cemconcomp.2012.08.010.

[22] M. Wyrzykowski, P. Lura, Moisture dependence of thermal expansion in cement-based materials at early ages, Cem. Concr. Res. 53 (2013) 25–35. doi:10.1016/j.cemconres.2013.05.016.

[23] C. Boulay, Determination of the coefficient of thermal expansion, in: A. Bentur (Ed.), Early Age Crack. Cem. Syst. - Rep. RILEM Tech. Comm. 181-EAS - Early Age Shrinkage Induc. Stress. Crack. Cem. Syst., RILEM Publications SARL, 2003: pp. 217–224.

[24] P. Lura, F. Durand, Volume Changes of Hardening Concrete : Testing and Mitigation, in: O.M. Jensen, P. Lura, K. Kovler (Eds.), Concrete, Lyngby, 2006: pp. 57–65.

[25] R. Le Roy, Déformations instantanées et différées des bétons à hautes performances, PhD thesis, Ecole Nationale des Ponts et Chaussées, Paris, France, 1995.

[26] P. Laplante, C. Boulay, Evolution du coefficient de dilatation thermique du béton en fonction de sa maturité aux tout premiers âges, Mater. Struct. 27 (1994) 596–605. doi:10.1007/BF02473129.

[27] Ø. Bjøntegaard, T.. Hammer, E.J. Sellevold, On the measurement of free deformation of early age cement paste and concrete, Cem. Concr. Compos. 26 (2004) 427–435. doi:10.1016/S0958-9465(03)00065-9.

[28] D. Cusson, T. Hoogeveen, Measuring early-age coefficient of thermal expansion in high-performance concrete, in: Int. Rilem Conf., 2006: pp. 321–330. doi:10.1617/2351580052.034.

[29] D. Cusson, T. Hoogeveen, An experimental approach for the analysis of early-age behaviour of high-performance concrete structures under restrained shrinkage, Cem. Concr. Res. 37 (2007) 200–209. doi:10.1016/j.cemconres.2006.11.005.

[30] M. Ozawa, H. Morimoto, Estimation method for thermal expansion coefficient of concrete at early ages, in: Int. RILEM Conf. Vol. Chang. Hardening Concr. Test. Mitig., 2006: pp. 331–339. doi:10.1617/2351580052.035.

[31] I. Maruyama, A. Teramoto, G. Igarashi, Strain and thermal expansion coefficients of various cement pastes during hydration at early ages, Mater. Struct. 47 (2014) 27–37. doi:10.1617/s11527-013-0042-4.

[32] Ø. Bjøntegård, E.J. Sellevold, Interaction between thermal dilation and autogenous deformation in high performance concrete, Mater. Struct. 34 (2001) 266–272.

doi:10.1617/13731.

[33] S. Zhutovsky, K. Kovler, Application of ultrasonic pulse velocity for assessment of thermal expansion coefficient of concrete at early age, Mater. Struct. 50 (2017) 5. doi:10.1617/s11527-016-0866-9.

[34] G. De Schutter, L. Taerwe, Specific heat and thermal diffusivity of hardening concrete, Mag. Concr. Res. 47 (1995) 203–208. doi:10.1680/macr.1995.47.172.203.

[35] M. Briffaut, F. Benboudjema, J.-M. Torrenti, G. Nahas, Effects of early-age thermal behaviour on damage risks in massive concrete structures, Eur. J. Environ. Civ. Eng. 16 (2012) 589–605. doi:10.1080/19648189.2012.668016.

[36] Ø. Bjøntegaard, Basis for and practical approaches to stress calculations and crack risk estimation in hardening concrete structures – State of the art, 2011.

[37] A. Bentur, Evaluation of early age cracking characteristics in cementitious systems, Mater. Struct. 36 (2003) 183–190. doi:10.1617/14014.

[38] R. Springenschmid, R. Breitenbücher, M. Mangold, Development of the Cracking Frame and the Temperature-Stress Testing Machine, RILEM Proc. 25, Therm. Crack. Concr. Early Ages. (1994) 137–144.

[39] K. Schöppel, M. Plannerer, R. Springenschmid, Determination of Restraint Stresses and of Material Properties During the Hydration of Concrete with Temperature-Stress Testing Machine, RILEM Proc. 25, Therm. Crack. Concr. Early Ages. (1994).

[40] A.M. Paillere, M. Buil, J.J. Serrano, Effect of fiber addition on the autogenous shrinkage of silica fume concrete, ACI Mater. J. 86 (1989) 139–144. doi:10.14359/2295.

[41] S.I. Igarashi, A. Bentur, K. Kovler, Autogenous shrinkage and induced restraining stresses in high-strength concretes, Cem. Concr. Res. 30 (2000) 1701–1707. doi:10.1016/S0008-8846(00)00399-9.

[42] R. Bloom, A. Bentur, Free and restrained shrinkage of normal and high-strength concretes, ACI Mater. J. 92 (1995) 211–217. doi:10.14359/9771.

[43] S.A. Altoubat, D.A. Lange, Grip-Specimen Interaction in Uniaxial restrained tests, in: ACI (Ed.), Concr. Mater. Sci. to Appl., 2002: pp. 189–204. doi:10.14359/12253.

[44] S.J. Lokhorst, Deformational behaviour of concrete influenced by hydration related changes of the microstructure, 1998.

[45] P. Lura, Autogenous Deformation and Internal Curing of Concrete, PhD thesis, Delft University of Technology, 2003.

[46] S.A. Altoubat, D.A. Lange, Creep, shrinkage, and cracking of restrained concrete at early age, ACI Mater. J. 98 (2001) 323–331. doi:10.14359/10401.

[47] A. Kamen, E. Denarié, H. Sadouki, E. Brühwiler, Thermo-mechanical response of UHPFRC at early age - Experimental study and numerical simulation, Cem. Concr. Res. 38 (2008) 822–831. doi:10.1016/j.cemconres.2008.01.009.

[48] T. Aly, J.G. Sanjayan, Shrinkage cracking properties of slag concretes with one-day curing, Mag. Concr. Res. 60 (2008) 41–48. doi:10.1680/macr.2007.00038.

[49] T. Kishi, Z. Lin, A tentative experimental evaluation on early-age creep, in: Creep, Shrinkage Durab. Mech. Concr. Concr. Struct., 2008: pp. 285–291. doi:10.1201/9780203882955.pt3.

[50] A.A. Melo Neto, M.A. Cincotto, W.L. Repette, Desenvolvimento de metodologia e equipamento para a medida da retração restringida, Brazil, 2007.

[51] T. Grazia, Comportement des bétons au jeune âge, PhD thesis, Université Laval, 1999.

[52] Rilem 42-CEA, Properties of set concrete at early ages state-of-the-art-report, Matériaux Constr. 14 (1981) 399–450. doi:10.1007/BF02476348.

[53] A. Darquennes, Comportement au jeune âge de bétons formulés à base de ciment au laitier de haut fourneau en condition de déformations libre et restreinte, PhD thesis, Université Libre de Bruxelles, 2009.

[54] P.L. Domone, Uniaxial tensile creep and failure of concrete, Mag. Concr. Res. 26 (1974) 144–152. doi:10.1680/macr.1974.26.88.144.

[55] B. Bissonnette, Pigeon M., Tensile creep at early ages of ordinary, silica fume and fiber reinforced concretes, Cem. Concr. Compos. 25 (1995) 1075–1085.

[56] K. Kovler, A new look at the problem of drying creep of concrete under tension, J. Mater. Civ. Eng. 11 (1999) 84–87. doi:10.1061/(ASCE)0899-1561(1999)11:1(84).

[57] L. Østergaard, D. a. Lange, S. a. Altoubat, H. Stang, Tensile basic creep of early-age concrete under constant load, Cem. Concr. Res. 31 (2001) 1895–1899. doi:10.1016/S0008-8846(01)00691-3.

[58] H.-W. Reinhardt, T. Rinder, Tensile Creep of High-Strength Concrete, J. Adv. Concr. Technol. 4 (2006) 277–283. doi:10.3151/jact.4.277.

[59] A. Kamen, E. Denarié, H. Sadouki, E. Brühwiler, UHPFRC tensile creep at early age, Mater. Struct. 42 (2008) 113–122. doi:10.1617/s11527-008-9371-0.

[60] A.E. Switek, E. Denarié, E. Brühwiler, Early age creep and relaxation of UHPFRC under low to high tensile stresses, Cem. Concr. Res. 83 (2016) 57–69. doi:10.1016/j.cemconres.2016.01.005.

[61] J.-L. Tailhan, P. Rossi, F. Le Maou, C. Boulay, E. Martin, É. Merliot, Essais de fluage en compression, en traction et en flexion pour l'étude du comportement différé des bétons à hauts niveaux de contrainte, 2011.

[62] N. Ranaivomanana, S. Multon, A. Turatsinze, Basic creep of concrete under compression, tension and bending, Constr. Build. Mater. 38 (2013) 173–180. doi:10.1016/j.conbuildmat.2012.08.024.

[63] N. Ranaivomanana, S. Multon, A. Turatsinze, Tensile, compressive and flexural basic creep of concrete at different stress levels, Cem. Concr. Res. 52 (2013) 1–10. doi:10.1016/j.cemconres.2013.05.001.

[64] D.S. Atrushi, Tensile and Compressive Creep of Early Age Concrete : Testing and Modelling, PhD thesis, The Norwegian University of Sciences and Technology, Trondheim,Norway, 2003.

[65] J.J. Brooks, A.M. Neville, A comparison of creep, elasticity and strength of concrete in tension and in compression, Mag. Concr. Res. 29 (1977) 131–141.

[66] H.-W. Reinhardt, T. Rinder, Tensile creep of high-strength concrete, J. Adv. Concr. Technol. 4 (2006) 277–283.

[67] M. Omar, A. Loukili, G. Pijaudier-cabot, Y. Le Pape, Creep-damage coupled effects:

experimental investigation on bending beams with various sizes, J. Mater. Civ. Eng. 21 (2009) 65–72.

[68] J. Saliba, a. Loukili, F. Grondin, J.-P. Regoin, Experimental study of creep-damage coupling in concrete by acoustic emission technique, Mater. Struct. 45 (2012) 1389–1401. doi:10.1617/s11527-012-9840-3.

[69] J.-L. Tailhan, C. Boulay, P. Rossi, F. Le Maou, E. Martin, Compressive, tensile and bending basic creep behaviours related to the same concrete, Struct. Concr. 14 (2013) 124–130. doi:10.1002/suco.201200025.

[70] G. Zhao, M. di Prisco, L. Vandewalle, Experimental investigation on uniaxial tensile creep behavior of cracked steel fiber reinforced concrete Experimental investigation on uniaxial tensile creep behavior of cracked steel fiber reinforced concrete, Mater. Struct. (2014) 0–11. doi:10.1617/s11527-014-0389-1.

[71] A.E. Switek, Time-Dependent Response of Ultra High Performance Fibre Reinforced Concrete (UHPFRC) under Low to High Tensile Stresses, 4899 (2011).

[72] N. Reviron, Etude du fluage des bétons en traction . Application aux enceintes de confinement des centrales nucléaires à eau sous pression., PhD thesis, Ecole Normale Supérieure de Cachan, 2009.

[73] S. Pirskawetz, F. Weise, P. Fontana, Analysis of early-age cracking of cementitious materials by combination of various non destructive testing methods, in: 2nd Int. Conf. Microstruct. Durab. Cem. Compos., 2012: pp. 350–359.

[74] C. Boulay, A. Colson, Un extensomètre à béton éliminant l'influence des déformations transversales sur la mesure des déformations longitudinales, Mater. Struct. 14 (1981) 35–38.

[75] A. Carpuic-Prisacari, Stable crack propagation control for mixed-mode concrete fracture, in: TINCE 2016, 2016.

[76] W. Zheng, A.K.H. Kwan, P.K.K. Lee, Direct Tension Test of Concrete, ACI Mater. J. 98 (2001) 63–71. doi:10.14359/10162.

[77] P. Rossi, N. Godart, J.L. Robert, J.P. Gervais, D. Bruhat, acoustic emission, Mater. Struct. 27 (1994) 510–514.

[78] P. Rossi, J.-L. Tailhan, F. Le Maou, L. Gaillet, E. Martin, Basic creep behavior of concretes investigation of the physical mechanisms by using acoustic emission, Cem. Concr. Res. 42 (2012) 61–73. doi:10.1016/j.cemconres.2011.07.011.

[79] C. Dumoulin, G. Karaiskos, J. Carette, S. Staquet, A. Deraemaeker, Monitoring of the ultrasonic P-wave velocity in early-age concrete with embedded piezoelectric transducers, Smart Mater. Struct. 21 (2012) 47001. doi:10.1088/0964-1726/21/4/047001.

[80] W. Hansen, Report on Early-Age Cracking, Concr. Int. 33 (2011) 2–5.

[81] Tailhan J.L., Dal Pont S., Rossi P., From local to global probalistic modeling of concrete cracking, Ann. Solid Struct. Mech. 1 (2010) 103–105.

[82] Dal Pont S., Meftah F., Schrefler B.A., Modeling concrete under severe conditions as a mutliphases material, Nucl. Eng. Des. 241 (2011) 562–572.

[83] P. Acker, J.J. Chauvin, Essais calorimétriques sur béton : banque de données, Paris, 1990.

[84] C. Boulay, J.M. Torrenti, J. Andre, R. Saintilan, Quasi-adiabatic calorimetry for concretes :

Influential factors, Bull. Des Lab. Des Ponts Chauss Ees. (2010) 19–36. https://hal.archives-ouvertes.fr/hal-00562100%5Cn.

[85] S. Staquet, C. Boulay, N. Robeyst, N. De Belie, Ultrasonic monitoring of setting and autogenous shrinkage development of high performance concrete, in: 8th Int. Conf. Creep, Shrinkage Durab. Concr. Concr. Struct. (CONCREEP 8), Ise-Shima, Japan, 2008: pp. 321–327. doi:10.1201/9780203882955.ch41.

[86] G. Cannard, G. Orcel, J. Prost, Le suivi de la prise des ciments par ultrasons, BLPC. 168 (1990) 89–95.

[87] H. Krautkramer, J. Krautkramer, Ultrasonic Testing of Materials, Springer Berlin Heidelberg, 1983.

[88] H.W. Reinhardt, C.U. Grosse, Continuous monitoring of setting and hardening of mortar and concrete, Constr. Build. Mater. 18 (2004) 145–154. doi:10.1016/j.conbuildmat.2003.10.002.

[89] EN12390:2004, Shape, dimensions and other requirements for specimens and moulds, 2003.

[90] BS EN 12390-2-2009, Making and curing specimens for strength test, 2009.

[91] EN 12390-3, Testing hardened concrete. Compressive strength of test specimens, (2009).

[92] EN 12390-4, Compressive strength. Specification for testing machines, (2009).

[93] EN 12390-6, Concrete-determination of tensile splitting strength of test specimens, (1980) 3.

[94] E. Rastrup, Heat of hydration in concrete, Mag. Concr. Res. 6 (1954) 79–92.

[95] J.D. McIntosh, The Effects of Low Temperature Curing on Compressive Strenght of Concrete, RILEM Symp. Winter Concreting. (1956) Session BII.

[96] L. D'Aloia, Activation energy, maturity and equivalent age, in: Early Age Crack. Cem. Syst. - Rep. RILEM Tech. Comm. 181-EAS - Early Age Shrinkage Induc. Stress. Crack. Cem. Syst. Syst. Rep. RILEM Tech. Comm. TC 181-EAS, 2003: pp. 127–148.

[97] G. De Schutter, L. Taerwe, Degree of hydration-based description of mechanical properties of early age concrete, Mater. Struct. 29 (1996) 335–344. doi:10.1007/BF02486341.

[98] P.H. Morgan, L.P. Mercer, N.W. Flodin, General model for nutritional responses of higher organisms., Proc. Natl. Acad. Sci. U. S. A. 72 (1975) 4327–4331. doi:10.1073/pnas.72.11.4327.

[99] N. Robeyst, E. Gruyaert, C.U. Grosse, N. De Belie, Monitoring the setting of concrete containing blast-furnace slag by measuring the ultrasonic p-wave velocity, Cem. Concr. Res. 38 (2008) 1169–1176. doi:10.1016/j.cemconres.2008.04.006.

[100] A. Darquennes, S. Staquet, B. Espion, Determination of time-zero and its effect on autogenous deformation evolution, Eur. J. Environ. Civ. Eng. 15 (2011) 1017–1029. doi:10.1080/19648189.2011.9695290.

[101] C. Boulay, E. Merliot, S. Staquet, O. Marzouk, Monitoring of the concrete setting with an automatic method, Struct. Faults Repair - 2010. (2010) 11.

[102] P.R.C.A. Pinto, M.A.P. Irrigaray, R.T. Cerqueira, the Development of Ultrasound Pulse Velocity in Early Ages for Concrete , Mortar and Cement Pastes, Civ. Eng. (n.d.).

[103] ASTM C403, Standard test method for time of setting of concrete mixtures by penetration

resistance, in: Am. Soc. Test. Mater., 2008. doi:10.1520/C0403_C0403M-08.

[104] N.J. Carino, H.S. Lew, The maturity method: from theory to application, in: 2001 Struct. Congr. Expo., 2001: pp. 1–19.

[105] G. Sant, M. Dehadrai, D. Bentz, P. Lura, C.F. Ferraris, J.W. Bullard, et al., Detecting the fluid-to-solid transition in cement pastes, Concr. Int. 31 (2009) 53–58.

[106] EN 480-2:2006, Admixtures for concrete , mortar and grout. Determination of setting time, (n.d.).

[107] A. Bentur, Terminology and definitions, in: A. Bentur (Ed.), Early Age Crack. Cem. Syst. - Rep. RILEM Tech. Comm. 181-EAS - Early Age Shrinkage Induc. Stress. Crack. Cem. Syst., RILEM Publications SARL, 2003: pp. 13–15. doi:10.1617/2912143632.002.

[108] J.-M. Torrenti, P. Dantec, C. Boulay, J.F. Semblat, Projet de processus d'essai pour la détermination du module de déformation longitudinale du béton.pdf, BLPC. 220 (1999) 79–81.

[109] LNEC, E397 - Determinação do módulo de elasticidade em compressão, (1993) 2.

[110] M. Azenha, F. Magalhães, R. Faria, Á. Cunha, Measurement of concrete E-modulus evolution since casting: A novel method based on ambient vibration, Cem. Concr. Res. 40 (2010) 1096–1105. doi:10.1016/j.cemconres.2010.02.014.

[111] M. Azenha, R. Faria, F. Magalhães, L. Ramos, Á. Cunha, Measurement of the E-modulus of cement pastes and mortars since casting, using a vibration based technique, Mater. Struct. 45 (2012) 81–92. doi:10.1617/s11527-011-9750-9.

[112] M. Azenha, C. Ferreira, J. Silva, A.G. Correia, R. Aguilar, L.F. Ramos, Continuous stiffness monitoring of cemented sand through resonant frequency, Geotech. Spec. Publ. (2011) 174–183. doi:10.1061/47629(408)22.

[113] J.L. Granja, P. Fernandes, A. Benedetti, M. Azenha, J. Sena-Cruz, Monitoring the early stiffness development in epoxy adhesives for structural strengthening, Int. J. Adhes. Adhes. 59 (2015) 77–85. doi:10.1016/j.ijadhadh.2015.02.005.

[114] M. Azenha, L.F. Ramos, R. Aguilar, J.L. Granja, Continuous monitoring of concrete E-modulus since casting based on modal identification: A case study for in situ application, Cem. Concr. Compos. 34 (2012) 881–890. doi:10.1016/j.cemconcomp.2012.04.004.

[115] P.D. Welch, The Use of Fast Fourier Transform for the Estimation of Power Spectra: A Method Based on Time Aver. aging Over Short, Modified Periodograms, IEEE Trans. Audio Electroacoust. 15 (1967) 70–73.

[116] NI, LabVIEW, 2010.

[117] G. Karaiskos, A. Deraemaeker, D.G. Aggelis, D. Van Hemelrijck, Monitoring of concrete structures using the ultrasonic pulse velocity method, Smart Mater. Struct. 24 (2015) 113001. doi:10.1088/0964-1726/24/11/113001.

[118] M. Krüger, C.U. Grosse, F. Lehmann, Automated shear-wave techniques to investigate the setting and hardening of concrete in through-transmission, RILEM Bookseries. 6 (2012) 431–436. doi:10.1007/978-94-007-0723-8_61.

[119] C. Boulay, S. Staquet, B. Delsaute, J. Carette, M. Crespini, O. Yazoghli-Marzouk, et al., How to monitor the modulus of elasticity of concrete, automatically since the earliest age?, Mater. Struct. 47 (2014) 141–155. doi:10.1617/s11527-013-0051-3.

[120] J. Zhu, S.-H. Kee, D. Han, Y.-T. Tsai, Effects of air voids on ultrasonic wave propagation in early age cement pastes, Cem. Concr. Res. 41 (2011) 872–881. doi:10.1016/j.cemconres.2011.04.005.

[121] H. Gu, G. Song, H. Dhonde, Y.L. Mo, S. Yan, Concrete early-age strength monitoring using embedded piezoelectric transducers, Smart Mater. Struct. 15 (2006) 1837–1845. doi:10.1088/0964-1726/15/6/038.

[122] G. Song, H. Gu, Y.-L. Mo, Smart aggregates: multi-functional sensors for concrete structures—a tutorial and a review, Smart Mater. Struct. 17 (2008) 33001. doi:10.1088/0964-1726/17/3/033001.

[123] G. Song, H. Gu, Y. Mo, Concrete structural health monitoring using embedded piezoceramic transducers, Smart Mater. Struct. Mater. Struct. 16 (2007) 959–968. doi:10.1088/0964-1726/16/4/003.

[124] Z. Li, L. Qin, S. Huang, Embedded Piezo-Transducer in Concrete for Property Diagnosis, J. Mater. Civ. Eng. 21 (2009) 643–647.

[125] C. Dumoulin, G. Karaiskos, J.-Y. Sener, A. Deraemaeker, Online monitoring of cracking in concrete structures using embedded piezoelectric transducers, Smart Mater. Struct. 23 (2014) 115016. doi:10.1088/0964-1726/23/11/115016.

[126] G. Karaiskos, S. Flawinne, Design and Validation of Embedded Piezoelectric Transducers for Damage Detection Applications in Concrete Structures, 570 (2013) 805–811. doi:10.4028/www.scientific.net/KEM.569-570.805.

[127] S.H. Han, J.K. Kim, Effect of temperature and age on the relationship between dynamic and static elastic modulus of concrete, Cem. Concr. Res. 34 (2004) 1219–1227. doi:10.1016/j.cemconres.2003.12.011.

[128] I.E. Shkolnik, Effect of nonlinear response of concrete on its elastic modulus and strength, Cem. Concr. Compos. 27 (2005) 747–757. doi:10.1016/j.cemconcomp.2004.12.006.

[129] K. Van Den Abeele, W. Desadeleer, G. De Schutter, M. Wevers, Active and passive monitoring of the early hydration process in concrete using linear and nonlinear acoustics, Cem. Concr. Res. 39 (2009) 426–432. doi:10.1016/j.cemconres.2009.01.016.

[130] F. Benmeddour, G. Villain, O. Abraham, M. Choinska, Development of an ultrasonic experimental device to characterise concrete for structural repair, Constr. Build. Mater. 37 (2012) 934–942. doi:10.1016/j.conbuildmat.2012.09.038.

[131] J. Carette, C. Dumoulin, G. Karaiskos, S. Staquet, A. Deraemaeker, Monitoring of the E-modulus in early age concrete since setting time with embedded piezoelectric transducers, in: Proc. Struct. Faults + Repair, 14th Int. Conf. Exhib., 2012: p. 10.

[132] F.D. Lydon, R. V. Balendran, Some observations on elastic properties of plain concrete, Cem. Concr. Res. 16 (1986) 314–324. doi:10.1016/0008-8846(86)90106-7.

[133] A.M. Neville, J.J. Brooks, Concrete technology, 1987.

[134] D. Yuan, S. Nazarian, D. Zhang, Use of stress wave techniques to monitor and predict concrete strength development, in: Proc. Int. Symp. Non-Destructive Test. Civ. Eng., 2003: pp. 409–423.

[135] M. Krauß, K. Hariri, Determination of initial degree of hydration for improvement of early-age properties of concrete using ultrasonic wave propagation, Cem. Concr. Compos. 28 (2006) 299–306. doi:10.1016/j.cemconcomp.2006.02.007.

[136] H. Yildirim, O. Sengul, Modulus of elasticity of substandard and normal concretes, Constr. Build. Mater. 25 (2011) 1645–1652. doi:10.1016/j.conbuildmat.2010.10.009.

[137] S. Wen-bin, W. Cheng-qing, Analytical Solutions to Strain Rates of Reinforced Concrete Simply Supported Slabs under Blast Loads, J. Southwest Jiaotong Univ. 17 (2009) 212–217.

[138] V. Slowik, Schmidt D., Nietner L., Effect of stress relaxation on thermal stresses, in: Concreep 7, 2005: pp. 411–416.

[139] Charron J.-P., Marchand J., Bissonnette B., Pigeon M., Gérard B., Empirical models describing the behavior of concrete at early age, in: Early Age Crack. Cem. Syst. - Rep. RILEM Tech. Comm. 181-EAS - Early Age Shrinkage Induc. Stress. Crack. Cem. Syst., 2003: pp. 179–192.

[140] J. Carette, Towards Early Age Characterization of Eco-Concrete containing blast-furnace slag and limestone filler, PhD thesis, ULB-BATir, Brussel, Belgium, 2015.

[141] C. Boulay, Développement d'un dispositif de mesure de retrait endogène d'un béton au jeune âge, in: Huit. Édition Des Journées Sci. Du Regroupement Francoph. Pour La Rech. La Form. Sur Le Bét. $(RF)^2B$, 2007.

[142] C. Boulay, S. Staquet, M. Azenha, A. Deraemaeker, M. Crespini, J. Carette, et al., Monitoring elastic properties of concrete since very early age by means of cyclic loadings, ultrasonic easurements, natural resonant frequency of composite beam (emm-arm) and with smart aggregates, in: Fram. 8, 2013.

[143] P. Laplante, Propriétés mécaniques des bétons durcissants : analyse comparée des bétons classiques et à très hautes performances, PhD thesis, Ecole Nationale des Ponts et Chaussées, Paris, France, 1993.

[144] A.-W. Gutsch, Properties of early age concrete-Experiments and modelling, Mater. Struct. 35 (2002) 76–79. http://link.springer.com/article/10.1007/BF02482104 (accessed December 17, 2013).

[145] M. Briffaut, F. Benboudjema, J.-M. Torrenti, G. Nahas, Concrete early age basic creep: Experiments and test of rheological modelling approaches, Constr. Build. Mater. 36 (2012) 373–380. doi:10.1016/j.conbuildmat.2012.04.101.

[146] G. De Schutter, Applicability of degree of hydration concept and maturity method for thermo-visco-elastic behaviour of early age concrete, Cem. Concr. Compos. 26 (2004) 437–443. doi:10.1016/S0958-9465(03)00067-2.

[147] W. Jiang, G. De Schutter, Y. Yuan, Degree of hydration based prediction of early age basic creep and creep recovery of blended concrete, Cem. Concr. Compos. 48 (2014) 83–90. doi:10.1016/j.cemconcomp.2013.10.012.

[148] B.T. Tamtsia, J.J. Beaudoin, J. Marchand, The early age short-term creep of hardening cement paste: load-induced hydration effects, Cem. Concr. Compos. 26 (2004) 481–489. doi:10.1016/S0958-9465(03)00079-9.

[149] J.P. Forth, Predicting the tensile creep of concrete, Cem. Concr. Compos. 55 (2014) 70–80. doi:10.1016/j.cemconcomp.2014.07.010.

[150] P.J. Heinrich, D. Schlicke, N.V. Tue, Serviceability and Stability of Unreinforced Mass Concrete Structures – EC 2 Compatible Design Concept Derived from Comprehensive FE-Studies on Real Structural Behaviour, in: Concreep 10, 2015: pp. 1299–1307.

[151] D. Schlicke, N.V. Tue, Consideration of Viscoelasticity in Time Step FEM-Based Restraint

Analyses of Hardening Concrete, J. Mod. Phys. 4 (2013) 9–14.

[152] B. Delsaute, S. Staquet, C. Boulay, Monitoring of the creep and the relaxation behaviour of concrete since setting time, part 2 : traction, in: Strateg. Sustain. Concr. Struct., Aix-en-Provence, 2012: p. 10.

[153] C. Boulay, M. Crespini, B. Delsaute, S. Staquet, Monitoring of the creep and the relaxation behaviour of concrete since setting time, part 1 : compression, in: Strateg. Sustain. Concr. Struct., Aix-en-Provence, 2012: p. 10.

[154] B. Delsaute, S. Staquet, C. Boulay, Early age creep and relaxation behavior of concrete under tension and compression, in: Concr. Innov. Cinference CIC 2014, Oslo, 2014: p. 10.

[155] D. Atrushi, Ø. Bjøntegaard, D. Bosnjak, T. Kanstad, E.J. Sellevold, Creep deformations due to self-stresses in hardening concrete, effect of temperature, in: Concreep 6, 2001: pp. 613–618.

[156] F.S. Rostasy, A.-W. Gutsch, M. Laube, Creep and relaxation of concrete at early ages, in: Creep Shrinkage Concr., 1993: pp. 453–458.

[157] M. Vandamme, F.-J. Ulm, Nanogranular origin of concrete creep., Proc. Natl. Acad. Sci. U. S. A. 106 (2009) 10552–7. doi:10.1073/pnas.0901033106.

[158] Z.P. Bažant, A. Asghari, Computation of Age-Dependent Relaxation spectra, Cem. Concr. Res. 4 (1974) 567–579.

[159] Z.P. Bažant, A. Asghari, Computation of Kelvin chain retardation spectra of aging concrete, Cem. Concr. Res. 4 (1974) 797–806.

[160] T. Instruments, http://www.tainstruments.com/pdf/brochure/TAM%20AIR%20brochure.pdf, (2013) 23.

[161] I. Pane, W. Hansen, Investigation of blended cement hydration by isothermal calorimetry and thermal analysis, Cem. Concr. Res. 35 (2005) 1155–1164.

[162] NIST, http://www.nist.gov/el/building_materials/evcctl.cfm, (n.d.).

[163] P. Acker, F.J. Ulm, Creep and shrinkage of concrete: Physical origins and practical measurements, Nucl. Eng. Des. 203 (2001) 143–158. doi:10.1016/S0029-5493(00)00304-6.

[164] J.M. Illston, The componants of strain in concrete under sustained compressive stress, Mag. Concr. Res. 17 (1965) 21–28.

[165] E.J. Sellevold, C.W. Richards, Short-time creep transition for hardened cement paste, J. Am. Ceram. Soc. 55 (1972) 284–289.

[166] W.P.S. Dias, G.A. Khoury, P.J.E. Sullivan, An activation energy approach for the temperature dependance of the of basic creep of hardened cement paste, Mag. Concr. Res. 39 (1987) 141–147.

[167] T.C. Powers, Mechanisms of shrinkage and reversible creep of hardened cement paste, in: Struct. Concr. Its Behav. under Load, London, 1965: pp. 319–344.

[168] Z.P. Bažant, A.B. Hauggaard, S. Baweja, F.-J. Ulm, Microprestress-Solidification Theory for Concrete Creep. I Aging and Drying Effects, J. Eng. Mech. 123 (1997) 1188–1194.

[169] Z.P. Bazant, S. Prasannan, Solidification theory for aging creep. I: Formulation, J. Eng. Mech. 115 (1989) 1691–1703. doi:10.1016/0008-8846(88)90028-2.

[170] K. Mehta, P.R. Kumar, Concrete: Structure, Properties, and Materials, Prentice-Hall, 1986.

[171] P. Kumar Mehta, P.J.M. Monteiro, Concrete: Microstructure, Properties, and Materials, Fourth Edition, Third, The McGraw-Hill Companies, 2006.

[172] Z. Bazant, A.B. Hauggaard, S. Baweja, Microprestress-Solidification Theory for Concrete Creep. II: Algorithm and Verification, J. Eng. Mech. 123 (1997) 1195–1201.

[173] Z.P. Bazant, E. Osman, Double power law for basic creep of concrete, Matériaux Constr. 9 (1976) 3–11. doi:10.1007/BF02478522.

[174] A.D. Ross, Concrete creep data, Struct. Eng. 15 (1937).

[175] W.R. Lorman, The theory of concrete creep, Proc. ASTM. 40 (1940) 1082–1102.

[176] Thomas Thelford, Comité Eurointernational du Béton CEB/FIB Model Code 90, Design Code, 1993.

[177] H. Straub, Plastic flow in concrete arches, Proc. Am. Soc. Civ. Eng. 56 (1930) 49–114.

[178] J.R. Shank, Plastic flow of Portland Cement Concrete, Ind. Eng. Chem. 27 (1935) 1011–1014.

[179] W. Jiang, G. De Schutter, Y. Yuan, Degree of hydration based prediction of early age basic creep and creep recovery of blended concrete, Cem. Concr. Compos. (2013). doi:10.1016/j.cemconcomp.2013.10.012.

[180] P. Laplante, Propriétés mécaniques des bétons durcissants: analyse comparée des bétons classiques et à très hautes performances, PhD thesis, Ecole Nationale des Ponts et Chaussées, 1993.

[181] I. Guenot, J.-M. Torrenti, P. Laplante, Stresses in Early-Age Concrete: Comparison of Different Creep Models, ACI Mater. J. 93 (1996) 254–259.

[182] H. Muller, I. Anders, B. R., Concrete: treatment of types and properties in fib Model Code 2010, Struct. Concr. 14 (2013) 320–334. doi:10.1002/suco.201200048.

[183] F.-J. Ulm, F. Le Maou, C. Boulay, Creep and shrinkage coupling : New review of some evidence, in: ACI-RILEM Work. Creep Shrinkage Concr. Struct., 1999: pp. 21–37.

[184] O. Bernard, F.-J. Ulm, E. Lemarchand, A multiscale micromechanics-hydration model for the early-age elastic properties of cement-based materials, Cem. Concr. Res. 33 (2003) 1293–1309. doi:10.1016/S0008-8846(03)00039-5.

[185] Z.P. Bažant, Double-power logarithmic law for concrete creep, Cem. Concr. Res. 14 (1984) 793–806.

[186] F.H. Wittmann, Creep and Shrinkage Mechanisms, in: Z.P. Bažant, F.H. Wittmann (Eds.), Creep Shrinkage Concr., 1982: pp. 129–161.

[187] O. Bernard, F.-J. Ulm, J.T. Germaine, Volume and deviator creep of calcium-leached cement-based materials, Cem. Concr. Res. 33 (2003) 1127–1136.

[188] Z.P. Bažant, Creep and shrinkage prediction model for analysis and design of concrete structures - Model B-3, Mater. Struct. 28 (1995) 357–365.

[189] F.H. Wittmann, Useful Fundamentals of Shrinkage and Creep of Concrete, in: Concreep 10, 2015: pp. 84–93.

[190] M. Vandamme, A Few Analogies Between the Creep of Cement and of Other Materials, in:

Concreep 10, 2015: pp. 78–83.

[191] P. Rossi, J.-L. Tailhan, F. Le Maou, Comparison of concrete creep in tension and in compression: Influence of concrete age at loading and drying conditions, Cem. Concr. Res. 51 (2013) 78–84. doi:10.1016/j.cemconres.2013.04.001.

[192] Z.P. Bazant, S. Baweja, Creep and Shrinkage Prediction Model for Analysis and Design of Concrete Structures : Model B3, ACI Concr. Int. 83 (2001) 38–39.

[193] Z.P. Bažant, S. Prasannan, Solidification Theory for Concrete Creep. II: Verification and Application, J. Eng. Mech. 115 (1989) 1704–1725. doi:10.1061/(ASCE)0733-9399(1989)115:8(1691).

[194] Z.P. Bažant, Y. Xiang, Crack Growth and Lifetime of Concrete under Long Time Loading, J. Eng. Mech. 123 (1997) 350–358. doi:10.1061/(ASCE)0733-9399(1997)123:4(350).

[195] J.M. Torrenti, V.H. Nguyen, H. Colina, F. Le Maou, F. Benboudjema, F. Deleruyelle, Coupling between leaching and creep of concrete, Cem. Concr. Res. 38 (2008) 816–821. doi:10.1016/j.cemconres.2008.01.012.

[196] C. Mazzotti, M. Savoia, Nonlinear Creep Damage Model for Concrete under Uniaxial Compression, 129 (2004) 1065–1076.

[197] Y.-S. Yoon, S.-K. Lee, M.-S. Lee, J.-K. Kim, K.-Y. Kwon, Rheological concrete creep prediction model for prestressed concrete bridges constructed by the free cantilever method, Mag. Concr. Res. 63 (2011) 645–653. doi:10.1680/macr.2011.63.9.645.

[198] F. Benboudjema, J.M. Torrenti, Early-age behaviour of concrete nuclear containments, Nucl. Eng. Des. 238 (2008) 2495–2506. doi:10.1016/j.nucengdes.2008.04.009.

[199] M. Jirásek, P. Havlásek, Microprestress-solidification theory of concrete creep: Reformulation and improvement, Cem. Concr. Res. 60 (2014) 51–62. doi:10.1016/j.cemconres.2014.03.008.

[200] W. Hermerschmidt, H. Budelmann, Creep of Early Age Concrete under Variable Stress, in: CONCREEP 10, American Society of Civil Engineers, Reston, VA, 2015: pp. 929–937. doi:10.1061/9780784479346.111.

[201] B. Delsaute, C. Boulay, S. Staquet, Creep testing of concrete since setting time by means of permanent and repeated minute-long loadings, Cem. Concr. Compos. 73 (2016) 75–88. doi:10.1016/j.cemconcomp.2016.07.005.

[202] B. Delsaute, J. Carette, S. Staquet, Monitoring of the creep and the relaxation at very early age: complementary results on the CEOS concrete, in: VIII Int. Conf. Fract. Mech. Concr. Concr. Struct., 2013: pp. 453–458.

[203] S. Staquet, M. Azenha, C. Boulay, B. Delsaute, J. Carette, J. Granja, et al., Maturity testing through continuous measurement of e-modulus: an inter-laboratory and inter-technique study, in: Proc. ECO-CRETE Int. Symp. Sustain., 2014: p. 8.

[204] J.M. Torrenti, R. Le Roy, Analysis and Modelling of Basic Creep, in: S. Dray (Ed.), CONCREEP 10, American Society of Civil Engineers, Reston, VA, 2015: pp. 1400–1409. doi:10.1061/9780784479346.165.

[205] P. Rossi, J.L. Tailhan, F. Le Maou, Creep strain versus residual strain of a concrete loaded under various levels of compressive stress, Cem. Concr. Res. 51 (2013) 32–37. doi:10.1016/j.cemconres.2013.04.005.

[206] M. Irfan-ul-Hassan, B. Pichler, R. Reihsner, C. Hellmich, Elastic and creep properties of

young cement paste, as determined from hourly repeated minute-long quasi-static tests, Cem. Concr. Res. 82 (2016) 36–49. doi:10.1016/j.cemconres.2015.11.007.

CHAPTER 5:
APPLICABILITY OF ULTRASONIC MEASUREMENT ON THE MONITORING OF THE SETTING OF CEMENT PASTES: EFFECT OF WATER CONTENT AND MINERAL ADDITIONS

This chapter is based on the joint publication under review (September 2016 at ASTM International) of Mohamed Saleh, Jérôme Carette, Brice Delsaute and Stéphanie Staquet entitled "Applicability of ultrasonic measurement on the monitoring of the setting of cement pastes: effect of water content and mineral additions."

The knowledge of the setting process of cement-based materials is essential in the construction sector. There are two important parameters that can be defined during the setting process [1] mainly, the initial setting time t_i which is reached when any further mixing has an impact on the further properties development whereas, the final setting times t_f corresponds to the time when the material begins to develop mechanical properties. The initial and final setting can be interpreted as shown in Figure 1 with two quantifiable properties as the slump and the E-modulus. For instance, in the concrete industry, it needs to be ensured that the material is poured before t_i has been reached on the other hand, the knowledge of t_f may optimize the formwork removal process for quick construction phases. In addition, for modeling purposes, the knowledge of t_f is essential for the early age behaviour of the material since it characterizes the beginning of the stress development inside the material which has to be evaluated accurately in order to assess the early age cracking risk.

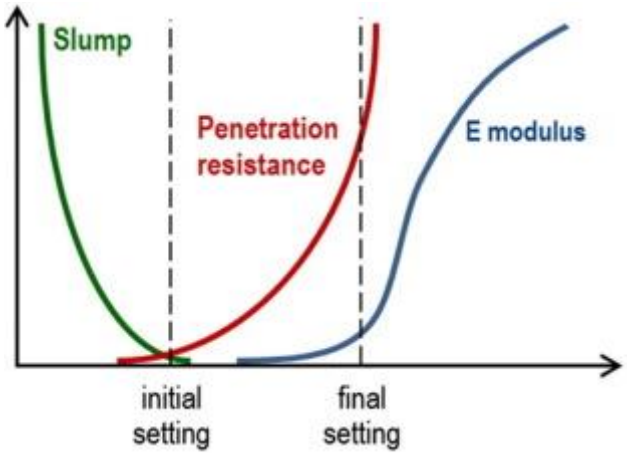

Figure 1 – Three stages interpretation of the setting process [1]

Furthermore, ultrasonic pulse velocity (UPV) measurements have been widely investigated and correlated with the early age evolution of cementitious materials properties such as the static elastic properties [1, 2, 3], compressive [4, 5] and tensile strengths [3, 6, 7, 8], the coefficient of thermal expansion [9] and the basic creep [10]. For instance, the concrete strength measured on cylinder or cube in a laboratory is different than the one of an in-situ concrete structure due to the fact that in a

laboratory, the curing and testing conditions are controlled while, in-situ, the curing (inducing thermal gradients inside the structure) and compaction conditions are variable. Thereby, in-situ strength is not directly comparable to the measured strength in the laboratory. Hence, there is a need for new techniques to measure the in-situ properties of concrete for quality assurance. These new techniques have to be non-destructive and continuous in order to monitor and evaluate changes in the properties during the overall hardening process.

The setting process can be described in a chemo-physical perspective as follow. At the beginning, the kinetics of hydration is slow. This corresponds to the dormant period where the workability decreases slowly until it is lost completely. At this stage, the initial setting time t_i has been reached and the hydration products start to develop significant continuous path. Afterwards, the stiffening process begins with an increasing rate which corresponds to the acceleration period where, the material solidifies and starts to resist shear or tensile load, which corresponds to the final setting time t_f.

Henceforth, several criteria based on continuous non-destructive measurements of UPV have been developed for the setting time detection for mortar and concrete specimens. In previous studies, only P-wave velocity was used to detect setting of the material. The initial setting time was computed as the time of occurrence of the inflection point of the P-wave velocity curve multiplied by 1.45 [11] whereas, the final setting time occurs when P-wave velocity curve had decreased to 20 % of its maximum [12].

A new methodology was introduced by Carette and Staquet to determine the initial and final setting time for mortar in [13] and concrete in [14] based on the combined monitoring of P-wave and S-wave velocity. They compared heat release, penetration resistance (for mortar) and static Young's modulus and compressive strength (for concrete), as well as ultrasonic transmission of P-wave and S-wave velocities. It was concluded that the ultrasonic method characterizes well the setting process and the following criteria have been developed to detect setting times. The initial setting time corresponds to the time of occurrence of the inflection point of the S-wave velocity curve while, the final setting time is computed as the time of occurrence of the inflection point of the dynamic Young's modulus curve.

In this study, UPV measurements are used to monitor the setting process and the subsequent development of the elastic properties of cement paste materials. In particular, the criteria mentioned above, developed for mortar and concrete, are evaluated and extended to cement paste mixtures. So far, there are two types of techniques that have been standardized in order to determine the setting times of cement paste materials, the VICAT test [15] and the Gillmore needles test [16].

However, these techniques have in common the feature of being destructive which can be considered as a major drawback. While these tests allow to determine setting times only of cement paste and mortar mixtures, UPV measurements have the advantage to monitor the evolution P-wave and S-wave velocities, which in return allow to compute setting times and dynamic properties such as, the dynamic Young's modulus E_{dyn}, the dynamic shear modulus G_{dyn} and the dynamic Poisson's ratio ν_{dyn} for cement paste, mortar and concrete.

SECTION 5.1 – MATERIALS AND METHODS

5.1.1. Materials

The materials used for this study are cement CEM I 52.5 N, limestone micro-filler (LMF), blast-furnace slag (BFS) and gypsum. There are three compositions with 100 % of ordinary Portland cement for which the water-cement ratio is 0.3 – 0.4 – 0.5. Whereas, for the last composition denoted as SCM composition, cement is substituted by limestone filler, blast-furnace slag and gypsum. The SCM composition has a water/binder ratio of 0.4 and it is studied in order to observe the effect of mineral additions on the setting process. These compositions are called CP0.3, CP0.4, CP0.5 and CPSCM and complete details about their composition and mixing procedure are given in chapter 3. After casting, all samples are placed in a climatic chamber at 20°C and are sealed in order to avoid any exchange between mixtures and the surrounding air.

5.1.2. Standard setting times

The initial and final setting times are determined with the Vicat normalized test (see Figure 2). Cement pastes are poured inside a mold of a conical shape where a needle is released at different times and the penetration is recorded. The setting times are determined when the needle penetration has reached a certain height. The initial setting time corresponds to the time when the needle stops at a distance of 6 ± 3 mm from the bottom plate whereas, the final setting time corresponds to the time when the needle has penetrated only 0.5 mm on the inverted filled mold. There is a specific needle for each setting time. Complete details about Vicat test are given in [15].

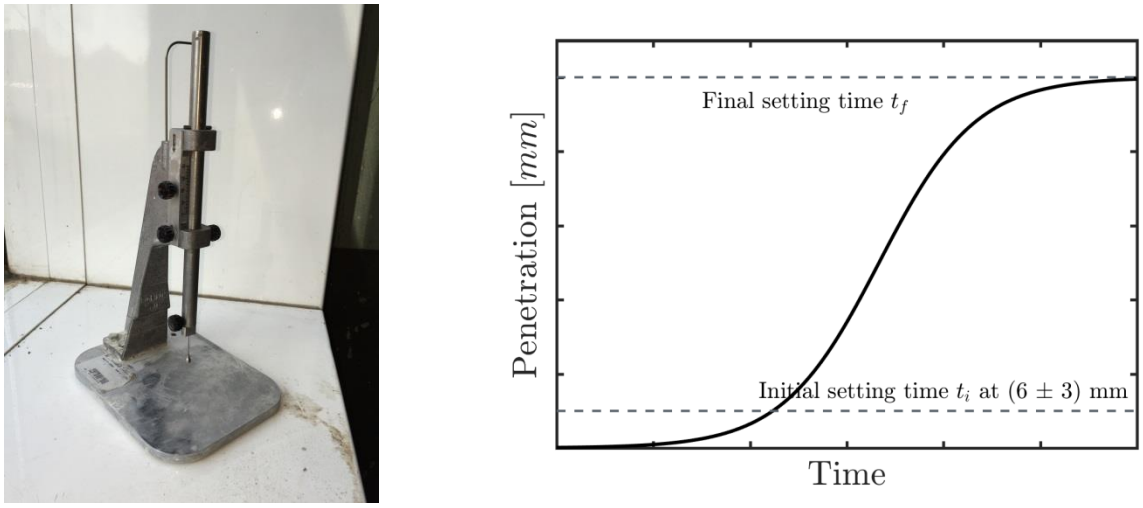

Figure 2 – The Vicat apparatus (left). Evolution of the needle penetration (right)

5.1.3. UPV measurements

The P-wave and S-wave transmission information was measured with a modified FreshCon system initially developed at the University of Stuttgart. A mathematical formula will be used to fit experimental results. The advantage of this model is the identification of specific points of the velocity curves. This model consists in 4 superimposed logistic functions (see Equation 1) as the P-wave and S-wave velocity behavior may have various curvatures. The values of parameters of both waves are given in Table 1 for each composition.

$$V(t) = c + \sum_{i=1}^{4} \frac{V_n}{1 + \exp((t - t_n)/g_n)} \quad (1)$$

where:

t is the age of the material, in h
$V(t)$ is the velocity, in m/s
V_n is the asymptotic value ($V(t \to \infty) = V_n$), in m/s,
t_n is the inflection point, in h
g_n is the slope, in h

P- and S-wave are simultaneously measured on separate molds. Every minute, a 5 µs pulse is sent through a 2.5 cm wide cement paste sample by a piezoelectric broadband transmitter (center frequency of 0.5 MHz for the P-wave sensor, 0.25 MHz for the S-wave sensor). A similar sensor situated on the other side of the sample transmits the signal to a computer through a DAQ card.

With V_P and V_S values, the dynamic properties of the cementitious materials can be computed with the following equations which are valid for isotropic homogeneous media:

$$\upsilon_{dyn} = \frac{V_P^2 - 2V_S^2}{2V_P^2 - 2V_S^2} \quad (2)$$

$$E_{dyn} = \rho V_P^2 \frac{(1+\nu_{dyn})(1-2\nu_{dyn})}{(1-\nu_{dyn})} = \rho V_S^2 (2 + 2\nu_{dyn}^2) \quad (3)$$

$$G_{dyn} = \frac{E_{dyn}}{(2+2\nu_{dyn}^2)} = \rho V_S^2 \quad (4)$$

where:

ν_{dyn} is dynamic Poisson's ratio [-],
E_{dyn} is the dynamic Young's modulus [Pa],
G_{dyn} is the dynamic shear modulus [Pa],
ρ is the density of the mixture [kg/m³].

Table 1 – Values of all parameters of P-waves and S-waves

		P-wave				S-wave			
		CP-0.3	**CP-0.4**	**CP-0.5**	**CP-SCM**	**CP-0.3**	**CP-0.4**	**CP-0.5**	**CP-SCM**
V_1	[**m/s**]	1018.8	767.9	954.0	1681.7	1005.7	364.4	667.1	454.1
g_1	[**h**]	-186.1	-0.3	-3.7	-20.5	-252.7	-21.1	-3.0	-7.0
t_1		45.1	2.7	12.0	36.4	1.0	25.3	13.6	33.6
V_2	[**m/s**]	953.1	865.3	384.6	1632.4	637.8	223.4	229.5	124.5
g_2	[**h**]	-0.8	-73.9	-4.8	-3066.6	-0.8	-0.4	-10.4	-5.1
t_2		7.5	90.4	19.2	74.7	7.4	11.5	36.2	65.9
V_3	[**m/s**]	2539.1	767.9	1056.3	1778.7	732.9	521.0	529.5	394.6
g_3	[**h**]	-6.0	-8.9	-40.8	-400.1	-0.9	-1.1	-500250.1	-83.0
t_3		1.0	17.6	40.5	126.8	4.4	6.2	30.9	39.7
V_4	[**m/s**]	1430.0	1568.9	1642.6	1286.2	637.8	1279.2	558.7	1375.9
g_4	[**h**]	-0.8	-3.3	-2.2	-3.0	-3.8	-7.3	-1.5	-6.1
t_4		2.6	9.3	2.5	3.7	7.8	2.3	6.7	3.7
c	[**m/s**]	-1738.7	163.7	-401.3	-1360.3	-585.3	-683.6	-277.0	-769.3

5.1.4. Apparent activation energy

The temperature evolution in cementitious materials depends on their massiveness. A continuous monitoring of the sample temperature was done during the measurements in order to take into account the effect of temperature on the setting process [17, 18, 19]. An equivalent time t_{eq} is computed with the Eq (5) proposed by Freiesleben Hansen and Pedersen in [20].

$$t_{eq}(t,T) = \sum_{0}^{t} \exp\left(-\frac{E_a}{R}.\left(\frac{1}{273+T} - \frac{1}{273+T_{ref}}\right)\right).\Delta t \qquad (5)$$

where:

- T is the temperature, in $°C$
- T_{ref} is the reference temperature, generally $20\ °C$
- R is the universal gas constant, $8.314\ J/mol/K$
- E_a is the apparent activation energy, in J/mol

This equation shows the accelerating effect of a given temperature history T in comparison with a reference temperature T_{ref}. The apparent activation energy E_a was determined from isothermal calorimetry measurements in another study on mortar with the same binder content [21]. The value of E_a of ordinary Portland cement and SCM composition equals to 38 kJ/mol and 48 kJ/mol respectively.

SECTION 5.2 – RESULTS AND DISCUSSIONS

5.2.1. Ultrasonic measurements

Figure 3 represents V_P and V_S values of three batches of the CP-0.4 mixture. V_P increases from roughly $500\ m/s$ for the fresh state to approximately $3500\ m/s$ in the hardened state whereas, V_S increases from $20\ m/s$ for the fresh state to roughly $1500\ m/s$ in the hardened state.

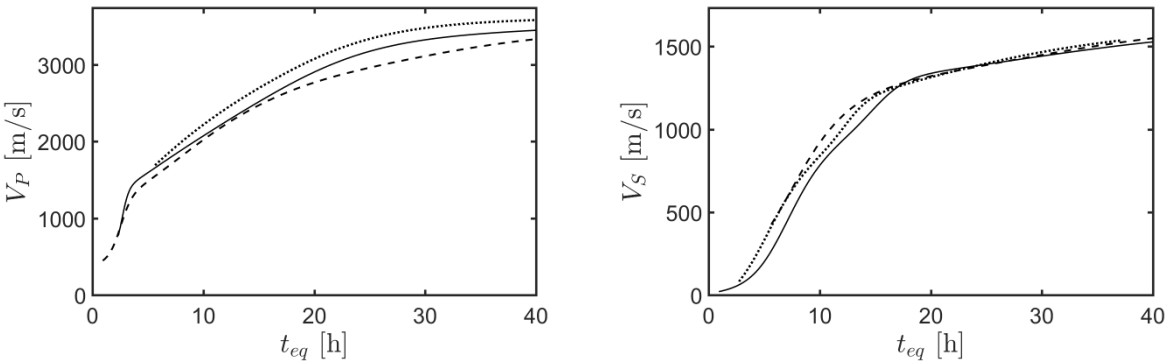

Figure 3 – Reproducibility of the FreshCon device - P-wave (left) & S-wave (right)

Prior to 2-3 hours of age, the signal detection of the waves is difficult due to the liquid state of the sample and the low signal/noise ratio [13]. This can be seen with one of the three CP-0.4 mixtures. On the other hand, in the long term, the V_P/V_S ratio is roughly equal to 2, which corresponds to observations made on previous studies on ultrasonic measurements in mortar and concrete [13, 14].

Nonetheless, the deviation is much higher between the V_P curves than the V_S curves. Therefore, a better reproducibility is obtained for the S-waves. It is worth mentioning that the same observation has been made for mortar and concrete [13, 14]. According to [22], S-wave velocity is less dependent on the air content compared to P-wave velocity in the very early age (before the final setting time). On the other hand, comparing cement paste, mortar and concrete for the same quantity of mixture and the same binder content, it can be noticed that the latter two will have small quantity of binder therefore, the influence of the air will be limited compared to cement paste mixture.

Figure 4 represents a qualitative evolution of V_P and V_S. On one hand, a three-stages trend can be identified in V_P. First, V_P reaches high values in the early age (Stage I). According to [23], the ongoing hydration reactions and the internal setting of the sample due to gravity forces may be responsible of the sharp rise of V_P. Therefore, the material microstructure consolidates while its stiffness does not change. Later on, V_P rises untils it reaches the inflection point where the velocity starts to rise slowly (Stage II). In the last stage, V_P reaches a plateau which represents the stiffening of the material.

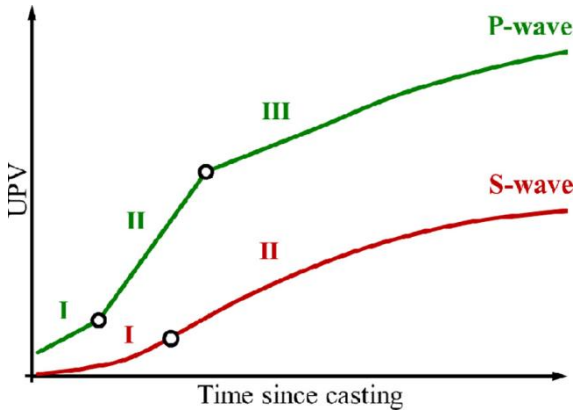

Figure 4 – Early age evolution of P-wave and S-wave [13]

On the other hand, S-wave curves can be divided in two stages. In the first stage, it can be observed that V_S has low values compared to V_P. According to [13], this stage corresponds to the initiation of the hydration reactions which will lead to the onset of the solid percolation. V_S will increase until it reaches its inflection point. At this point, the second stage begins and V_S will increase slowly until it reaches a plateau.

Figure 5 shows V_P, V_S, E_{dyn} and ν_{dyn} results of all cement paste mixtures studied in this experimental campaign. A detailed interpretation of the effect of w/c ratio and the determination of the setting times and the effect of mineral additions will be discussed hereafter.

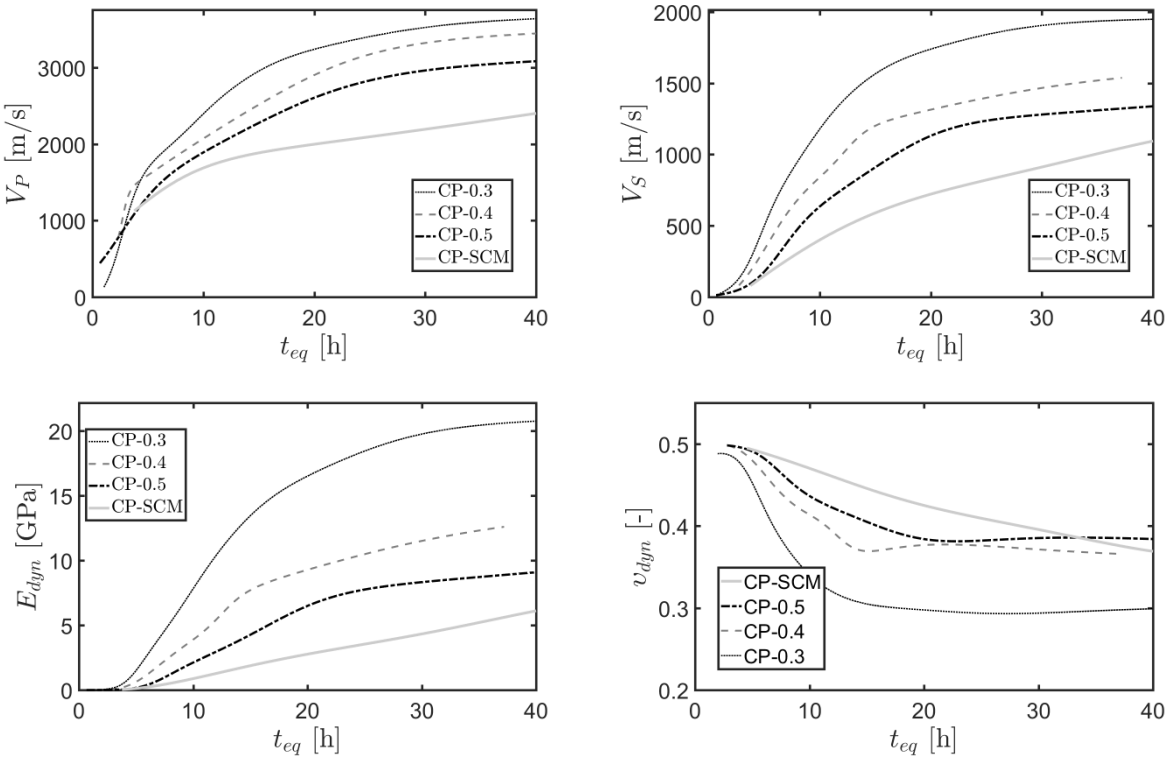

Figure 5 – VP, VS, Edyn, νdyn of all cement pastes

5.2.2. Effect of the water-cement ratio and the mineral additions

In Figure 5, it can be observed that an increase of the w/c ratio implies a decrease of P-wave and S-wave velocities and thus, the dynamic Young's modulus while, the initial and final setting times given

by the Vicat test increase (see Table 2). It is concluded that the setting process is affected by the water content in particular, a high water content slows the process due to the fact that the inter-particles spacing [24, 25] as well as the porosity [26] have increased.

A delay of roughly 2.7 h is observed for the initial setting time while, 4.5 h is observed for the final setting time when comparing mixes CP-0.3 and CP-0.5. According to [27], solid percolation needs a higher hydration degree in order to occur and thus explaining the delay observed. Furthermore, a delay of roughly 1.7 h is observed between setting times of CP-0.4 and CP-SCM mixtures while they have the same water/binder ratio of 0.4.

As reported by [14, 28, 29, 30], the limestone filler consists mainly in a physical contribution to the early age hydration of cement, as it acts as nucleation sites for the C_3A. From a chemical perspective, it only reacts up to 5% in mass to form hydration products, therefore it can be considered as an inert material. As a portion of the reactive cement is replaced with an inert material, the water content inside the mixture is increased and as mentioned earlier, this will increase the inter-particle spacing of the hydration products which in turn, will delay the setting process [14]. The same explanation can be made regarding the slag content inside the mixture. As stated in [14], the hydration kinetics of slag is slow compared to that of cement. In addition, during the first hours, slag is unreactive which will cause an increase of the water content inside the mixture. As a result, there will be a delay of the setting process and its duration will be increased likewise.

Table 2 – Criteria for initial and final setting determination: Vicat test & UPV measurements

				CP-0.3	**CP-0.4**	**CP-0.5**	**CP-SCM**
Criteria	Standard	Vicat initial setting time t_i	[**h**]	2.4	4.0	5.1	5.7
		Vicat final setting time t_f		3.1	7.0	7.6	8.6
		E_{dyn} at t_i	[**MPa**]	59	165	193	192
		$\Delta t_{(160\rightarrow200MPa)}$ [a]	[**min**]	5	7	7	11
		G_{dyn} at t_i	[**MPa**]	20	55	65	65
		$\Delta t_{(50\rightarrow70MPa)}$ [a]	[**min**]	7	11	11	16
	Initial	1.45*t(δV_P^{max}) [11]	[**h**]	4.0	4.0	3.6	N/A
		t(δV_S^{max}) [13, 14]		4.7	6.3	6.6	3.8
	Final	0.2*t(δV_P^{max}) [11, 12]	[**h**]	12.5	3.8	22.7	16.3
		t(δE_{dyn}^{max}) [13, 14]		5.8	7.2	8.3	11.6

[a] Δt represents the delay between the occurrence of the two values

5.2.3. Ultrasonic criteria for the setting time determination

Setting process can be divided in four stages as depicted in the following section (see Figure 6). During the first stage, P-wave velocity increases slowly until the end of the dormant period, which corresponds to the time of occurrence of the minimum of the heat release (gray curve). Afterwards, the derivative of P-wave velocity increases gradually up to its maximum, which represents the inflection point of the V_P curve and the end of the first stage. At this point, the mechanical properties start to develop as illustrated with the penetration resistance P_r. Stage 2 is ranged between the maximum rate of V_P and V_S. The solid percolation starts to develop owing to an increasing rate of the volume of hydrates. Thereafter, a continuous solid path starts to develop in the saturated medium. This corresponds to the initial setting time t_i, where any further mixing will break bonds and

deteriorate dramatically its mechanical properties. In stage 3, the dynamic Poisson's ratio and the Young's modulus E_{dyn} evolve gradually as well as the penetration resistance P_r. The rate of E_{dyn} increases up to its maximum which corresponds to the inflection point of E_{dyn} curve. At this point, the formation of the hydration products slows down whereas the mechanical properties increases with a decreasing rate. This point corresponds to the final setting time t_f. Finally, the last stage corresponds to the hardening process of the material where, the maximum of the heat release q_{max} occurs.

The setting process of cement paste material can be summarized as depicted in Figure 7. The latter represents the setting process of the CP-0.4 mixture which is a representative qualitative evolution of the setting process of all cement paste mixtures. The initial setting time occurs after the occurrence of the inflection point of the V_P curve while, the final setting corresponds to the time of occurrence of the maximum of the derivative of E_{dyn} curve.

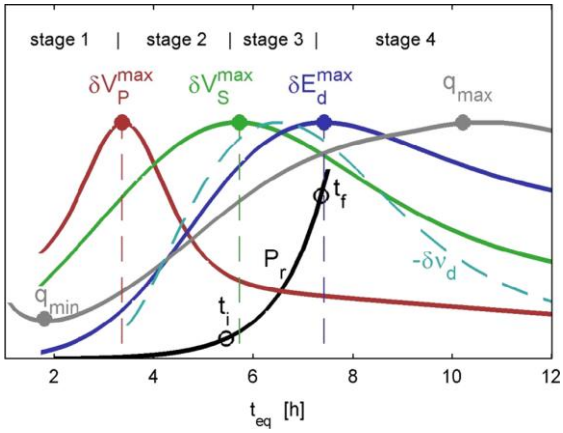

Figure 6 – From [13]. Four stage description of the setting behaviour based on the qualitative evolution of heat flow (grey), penetration resistance (black), and VP (red), VS (green), vdyn (cyan) and Edyn (blue) gradient on mortar

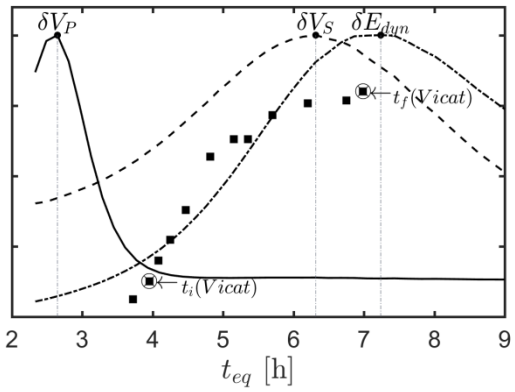

Figure 7 – Qualitative evolution of VP, VS and Edyn derivatives and the Vicat penetration test (Vi). CP-0.4 mixture.

► Initial Setting Time $\boldsymbol{t_i}$

In previous studies, two criteria have been developed in order to determine the initial setting time of cementitious materials based on the ultrasonic quantities V_P and V_S. Figure 8 represents the obtained results which are compared with the reference initial setting time t_i given by the Vicat test. t_i can be considered as the time:

- When the V_S curve has reached its inflection point. This criterion has been developed by [14, 13] for various mortar and concrete mixtures.

$$t_i = t(\delta V_S^{\max})$$

- When the V_P curve has reached its inflection point multiplied by 1.45. The latter has been developed by [11] for different concrete mixtures.

$$t_i = 1.45 * t(\delta V_P^{\max})$$

It is observed that the criteria based on V_P gives scattered results in comparison with the Vicat test. For CP-0.4 and CP-SCM mixtures, the difference between the time based on V_P criterion and the one of the Vicat test is roughly 0.2 h. On the other hand, for CP-0.5 mixture, a difference of roughly 1.5 h is observed between results from Vicat test and from the two ultrasonic criteria. However, both criteria give scattered results for the CP-0.3 mixture. This can be explained by the fact that a w/c ratio of 0.3 implies a bad workability of the mixture in which the reproducibility of the experiment is not guaranteed as well as the follow-up of the procedures of the Vicat test. Indeed, the mixture was vibrated a bit longer than the standard recommends [15] in order to pour it inside the mold as a consequence, a settlement of the mixture is induced before the setting process begins. On the other hand, with a w/c ratio of 0.3, the bad workability induces lump formation inside the mixture as a consequence, lumps will act as aggregates and can result in a decrease of the setting time.

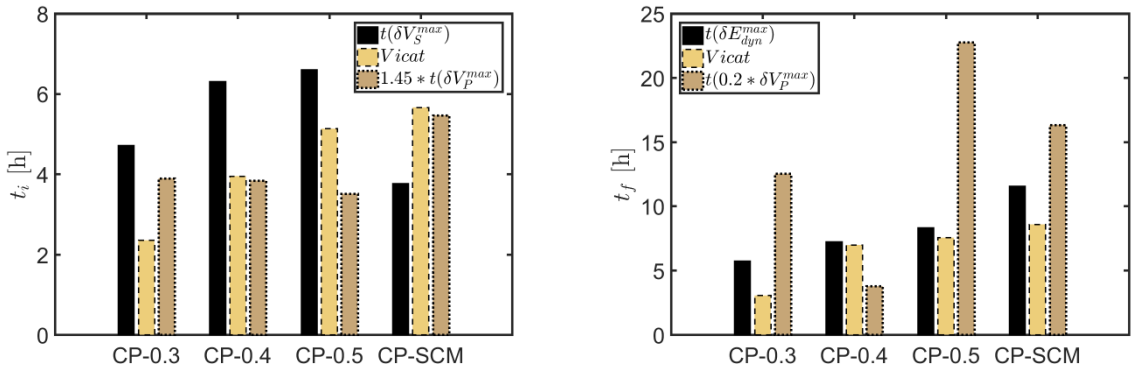

Figure 8 – Initial (left) and Final (right) Setting Times of all cement pastes mixtures. Comparison of UPV criteria and the Vicat test

Figure 9 represents the early age evolution of the dynamic shear modulus G_{dyn} and the dynamic Young's modulus E_{dyn}. The black diamonds represent the value of the quantity at the initial Vicat setting time (see Table 2). The average and the standard deviation of CP-0.4, 0.5 & SCM mixtures are also depicted. The mixture CP-0.3 has not been considered for the calculation because of the reason mentioned above. It is noticed that the standard deviation equals roughly 9 % of the average value, 60 MPa. For all mixes, if CP-0.3 is not taken into account, it is noticed that the quantity G_{dyn} varies between 50 and 70 MPa. Nonetheless, the average time Δt required to pass from 50 MPa to 70 MPa is roughly 10 min for CP-0.4 and CP-0.5 mixtures, and 16 min for CP-SCM mixture.

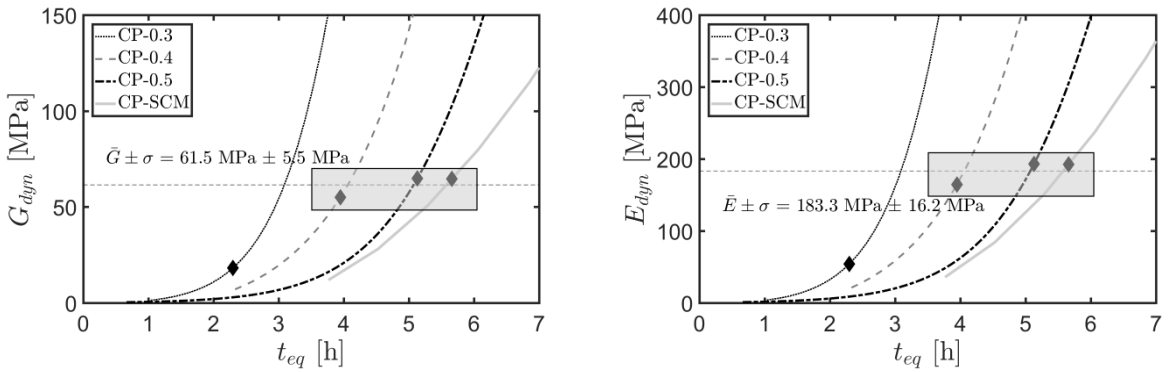

Figure 9 – Early age evolution of the dynamic shear modulus (left) & dynamic Young's modulus (right) of all cement pastes mixtures. Black diamonds represent the value at the initial time

Likewise, for the dynamic Young's modulus E_{dyn}, the standard deviation equals to roughly 9 % of the average value (183 MPa). Furthermore, the quantity E_{dyn} for all mixes, expect the mixture CP-0.3, varies between 160 and 200 MPa. In this case, the average time Δt for all mixes is roughly 10 min.

With the quantities G_{dyn} and E_{dyn}, a new criterion based on threshold value can be developed in order to assess the initial setting time t_i. The new indicator of t_i can be considered as:

- the time at which the dynamic shear modulus has reached a value situated between 50 and 70 MPa
- or, also expressed as the time at which the dynamic Young's modulus has reached a value situated between 160 and 200 MPa.

Nevertheless, as previously stated, S-wave velocity is less dependent on the air-content at early age compared to the P-wave velocity. Thereby, the criterion based on the dynamic shear modulus G_{dyn} can be considered as more reliable to determine the initial setting time [31] as it is a function of S-wave velocity only (see Eq 4), while E_{dyn} is a function of V_S and V_P (see Eq 3).

► Final Setting Time $\boldsymbol{t_f}$

The final setting times is determined by the following two criteria based on ultrasonic measurements:

- Time of occurrence of the inflection point of the E_{dyn}curve [14, 13]: $t_f = t\left(\delta E_{dyn}^{\max}\right)$
- The time at which the derivative of V_P curve has decreased by 20% [11, 12]: $t_f = t(0.2 * \delta V_P^{\max})$

Figure 8 compared both criteria with the final Vicat setting time. It can be noticed that the criterion based on V_P provides scattered results, while the criterion based on E_{dyn} gives results in agreement with the Vicat test. For instance, the difference between the time based on E_{dyn} criterion and the Vicat test is roughly 0.7 h for the CP-0.4 and CP-0.5 mixtures, while for the CP-SCM, the difference is 3 h. The mixture CP-0.3 has not to be considered for the reason that has been discussed earlier. It can be concluded that the criterion based on E_{dyn} is appropriate to determine the final setting time of cement pastes. The same conclusion has been made for mortar [13] and concrete [14].

5.2.4. Influence of the air content on the dynamic properties

Air content of all cement pastes mixtures was measured with an air meter device. Furthermore, additional data derived from a recent study made by Krüger et al. [31] has been analyzed. In [31], ultrasonic techniques have been used to compute elastic properties of cement pastes with the same device as used in this study: The FreshCon system. Two different compositions have been studied with three different consistencies each: compositions with 100 % ordinary Portland cement or, with mineral additions. Nonetheless, additional calculations have been performed in order to derive the air content of the investigated cement paste mixtures from the data provided. The fresh density was given for all compositions while, the theoretical density was calculated from the true density of the binder (cement and limestone) used in the paper. Air content was calculated with the following formula.

$$A\,[\%] = 100 \times \left(1 - \frac{\rho}{\rho_0}\right) \qquad 6$$

Where:

A is the air content, in %
ρ is the fresh density, in kg/m³ (given data)
ρ_0 is the theoretical density (without consideration of air), in kg/m³ (calculated values)

Figure 10 represents the effect the air content on the shear modulus G_{dyn} and the dynamic Young's modulus E_{dyn} at the initial setting time t_i. Mixtures based on ordinary Portland cement are denoted "Krüger et al. (OPC)" while, for the other composition denoted "Krüger et al. (ECO)", 60% of the Portland cement is replaced by mineral additions (ECO Filler). Compositions, based on ordinary Portland cement, investigated in this study are denoted "This paper (OPC)". The corresponding w/c ratio is also depicted in the figure. A linear relationship is observed between the dynamic properties G_{dyn} and E_{dyn} and the air content. Those dynamic properties decrease when the air content increases. Furthermore, air content is dependent on the w/c ratio as it can be noticed in Figure 11. When w/c increases, the air content decreases accordingly. Same observation can be made for the data provided by Krüger et al. [31].

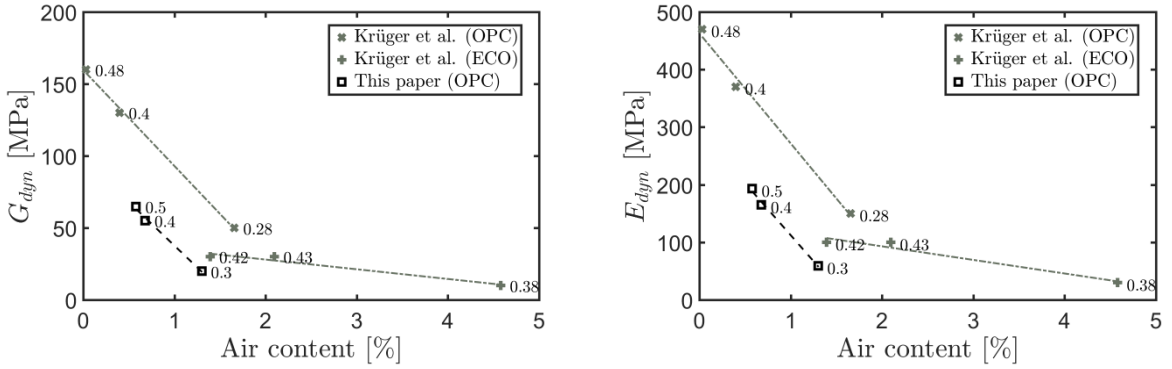

Figure 10 – Influence of the air content on the dynamic shear modulus (left) & dynamic Young's modulus (right)

The air content of the mixtures CP-0.4 & CP-0.5 equals to 0.68 % & 0.58 % respectively whereas, E_{dyn} equals to roughly 165 MPa & 193 MPa on the other hand (and G_{dyn} equals to 55 MPa & 65 MPa).

The air content can be considered as the same for these two mixtures (CP-0.4 and CP-0.5) since the difference equals to only 0.1 %. However, for the CP-0.3 mixture, the air content equals 1.3 % which is roughly the double than that of the CP-0.4 mixture. Accordingly, the dynamic properties E_{dyn} and G_{dyn} of the CP-0.3 mixture (20 MPa and 60 MPa respectively) decrease dramatically as it can be seen on the Figure 10. When the w/c ratio is very small, the workability becomes bad to such an extent that lumps are formed inside the mixture. Therefore, voids correspond not only to the theoretical voids between particles of cement and water, but also, to the voids between lumps. The latter acts as solid particles. Hence, the hardening occur much faster compared to other mixtures with higher w/c.

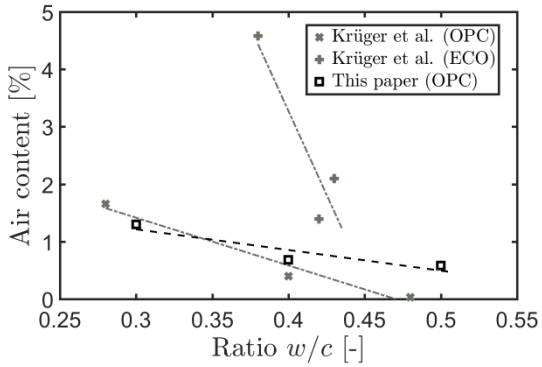

Figure 11 – Air content [%] vs. w/c ratio [-]

Another observation is the effect of the binder nature on the relationship between the dynamics properties E_{dyn} and G_{dyn} and the air content. Cement paste mixtures investigated in this paper are based on Portland cement as well as the ones of Krüger et al. [31]. From the Figure 10 showing the effect of the air content on E_{dyn} and G_{dyn} and, from the Figure 11 showing the effect of the water/cement ratio on the air content, it can be noticed that a similar slope appears in the case of ordinary Portland cement mixes (both investigated in this paper and the ones by Krüger et al. [31]) whereas, for the ECO-composition investigated by Krüger et al. [31], a different slope appears.

CONCLUSIONS

In conclusion, the following observations are drawn:

- Setting times of cement paste mixtures can be correlated with UPV measurements. The final setting time occurs when the dynamic Young's modulus has reached its inflection point. On the other hand, the initial setting times computed with previous criteria, based on P-waves and developed on mortar and concrete, gives scattered results compared to the initial setting time of the Vicat test. Nonetheless, these criteria can give an overall idea of the occurrence of the initial setting time. This can be explained by the fact P-waves are dependent on the air content compared to S-waves. In addition, for a same amount of mixture, mortar and concrete have small quantity of cement paste and thus, are less sensitive to the air content. For this reason, these criteria show a better compatibility for mortar and concrete than for cement paste mixtures.
- Nonetheless, threshold values of the elastic properties were observed when the initial setting time occurred. The initial setting time can be defined as the time at which the dynamic shear modulus has reached a value between 50 and 70 MPa or, when the dynamic Young's modulus has reached a value between 160 and 200 MPa. However, for very low water/cement ratio, this threshold value is no longer valid.
- For all different water/cement ratios, a linear relationship is observed between the air content at the fresh state and the values of the dynamic shear modulus and the dynamic Young's modulus at the initial setting time given by the Vicat test. This explains the influence of the air content on the early age evolution of the elastic properties.
- Finally, the relationship between the water/cement ratio and the air content is linear and is influenced by the binder nature (ordinary Portland cement or binder with mineral additions)

REFERENCES

[1] M. Krauß and K. Hariri, "Determination of initial degree of hydration for improvement of early-age properties of concrete using ultrasonic wave propagation," *Cement and Concrete Composites,* vol. 28, no. 4, pp. 299-306, 2006.

[2] D.-Y. Yoo, J.-J. Park, S.-W. Kim and Y.-S. Yoon, "Early age setting, shrinkage and tensile characteristics of ultra high performance fiber reinforced concrete," *Construction and Building Materials,* vol. 41, pp. 427-438, 2013.

[3] M. Shariq, J. Prasad and A. Masood, "Studies in ultrasonic pulse velocity of concrete containing GGBFS," *Construction and Building Materials,* vol. 40, pp. 944-950, 2013.

[4] R. Madandoust, R. Ghavidel and N. Nariman-zadeh, "Evolutionary design of generalized GMDH-type neural network for prediction of concrete compressive strength using UPV," *Computational Materials Science,* vol. 49, no. 3, pp. 556-567, 2010.

[5] R. Khan, J. Noorzaei, M. Kadir, A. Waleed and M. S. Jaafar, "UPV method for strength detection of high performance concrete," *Structural Survey,* vol. 25, no. 1, pp. 61-73, 2007.

[6] G. Trtnik, F. Kavčič and G. Turk, "Prediction of concrete strength using ultrasonic pulse velocity and artificial neural networks," *Ultrasonics,* vol. 49, no. 1, pp. 53-60, 2009.

[7] J. Keating, D. Hannant and A. Hibbert, "Correlation between cube strength, ultrasonic pulse velocity and volume change for oil well cement slurries," *Cement and Concrete Research,* vol. 19, no. 5, pp. 715-726, 1989.

[8] J. A. Bogas, M. G. Gomes and A. Gomes, "Compressive strength evaluation of structural lightweight concrete by non-destructive ultrasonic pulse velocity method," *Ultrasonics,* vol. 53, no. 5, pp. 962-972, 2013.

[9] S. Zhutovsky and K. Kovler, "Application of ultrasonic pulse velocity for assessment of thermal expansion coefficient of concrete at early age," *Materials and Structures,* vol. 50, no. 1, pp. 1-8, 2017.

[10] R. L. Al-Mufti and A. Fried, "Pulse velocity assessment of early age creep of concrete," *Construction and Building Materials,* vol. 121, pp. 622-628, 2016.

[11] B. Desmet, K. C. Atitung, M. A. A. Sanchez, J. Vantomme, D. Feys, N. Robeyst, K. Audenaert, G. D. Schutter, V. Boel, G. Heirman, O. Cizer, L. Vandewalle and D. V. Gemert, "Monitoring the early-age hydration of self-compacting concrete using ultrasonic p-wave transmission and isothermal calorimetry," *Materials and Structures,* vol. 44, p. 1537–1558, 2011.

[12] N. Robeyst, E. Gruyaert, C. U. Grosse and N. D. Belie, "Monitoring the setting of concrete containing blast-furnace slag by measuring the ultrasonic p-wave velocity," *Cement and Concrete Research,* vol. 38, no. 10, pp. 1169-1176, 2008.

[13] J. Carette and S. Staquet, "Monitoring the setting process of mortars by ultrasonic P and S-wave transmission velocity measurement," *Construction and Building Materials,* vol.94, p.196-208, 2015.

[14] J. Carette and S. Staquet, "Monitoring the setting process of eco-binders by ultrasonic P-wave and S-wave transmission velocity measurement: Mortar vs concrete," *Constuction and Building Materials,* vol.110, p.32-41, 2016.

[15] ASTM C191-13, "Standard Test Methods for Time of Setting of Hydraulic Cement by Vicat Needle," ASTM International, West Conshohocken, PA, 2013.

[16] ASTM C266-15, "Standard Test Method for Time of Setting of Hydraulic-Cement Paste by Gillmore Needles," ASTM International, West Conshohocken, PA, 2015.

[17] R. Pinto and K. Hover, "Application of maturity approach to setting times," *ACI Materials Journal,* vol. 96, no. 6, pp. 686-691, 1999.

[18] Á. García, D. Castro-Fresno and J. Polanco, "Maturity approach applied to concrete by means of vicat tests," *ACI Materials Journal,* vol. 105, no. 5, pp. 445-450, 2008.

[19] A. Schindler, "Prediction of concrete setting," *Proceedings of the RILEM International Symposium on Advances in Concrete through Science and Engineering,,* 2004.

[20] P. Freiesleben Hansen and E. J. Pedersen, "Maturity Analysis by Computer for Controlled Curing and Hardening of Concrete," *Nord Betong,* no. 1, pp. 21-25, 1977.

[21] J. Carette and S. Staquet, "Monitoring and modelling the early age and hardening behaviour of eco-concrete through continuous non-destructive measurements: Part I. Hydration and apparent activation energy," *Cement and Concrete Composites,* vol. 73, pp. 10-18, 2016.

[22] J. Zhu, S.-H. Kee, D. Han and Y.-T. Tsai, "Effects of air voids on ultrasonic wave propagation in early age cement pastes," *Cement and Concrete Research,* vol. 41, no. 8, pp. 872-881, 2011.

[23] T. Voigt, C. U. Grosse, Z. Sun, S. P. Shah and H. -W. Reinhardt, "Comparison of ultrasonic wave transmission and reflection measurements with P- and S-waves on early age mortar and concrete," *Materials and Structures,* vol. 38, pp. 729-738, 2005.

[24] D. P. Bentz, M. A. Peltz and J. Winpigler, "Early-Age Properties of Cement-Based Materials. II: Influence of Water-to-Cement Ratio," *Journal of Materials in Civil Engineering,* vol. 21, no. 9, pp. 512-517, 2009.

[25] J. Hu, Z. Ge and K. Wang, "Influence of cement fineness and water-to-cement ratio on mortar early-age heat of hydration and set times," *Construction and Building Materials,* vol. 50, pp. 657-663, 2014.

[26] V. Baroghel-Bouny, P. Mounanga, A. Khelidj, A. Loukili and N. Rafaï, "Autogenous deformations of cement pastes: Part II. W/C effects, micro–macro correlations, and threshold values," *Cement and Concrete Research,* vol. 36, no. 1, pp. 123-136, 2006.

[27] A. Boumiz, C. Vernet and F. Tenoudji, "Mechanical properties of cement pastes and mortars at early ages," *Advanced Cement Based Materials,* vol. 3, no. 3, pp. 94-106, 1996.

[28] C. Boulay, J. M. Torrenti, J. L. Andre and R. Saintilan, "Quasi-adiabatic calorimetry for concretes : Influential factors," *Bulletin des Laboratoires des Ponts et Chaussées,* pp. 19-36, 2010.

[29] D. Bentz, "Modeling the influence of limestone filler on cement hydration using CEMHYD3D," *Cement and Concrete Composites,* vol. 28, no. 2, pp. 124-129, 2006.

[30] T. Matschei, B. Lothenbach and F. Glasser, "The role of calcium carbonate in cement hydration, Cement and Concrete Research," vol. 37, no. 4, pp. 551-558, 2005.

[31] M. Krüger, R. Bregar, G. A. David and J. Juhart, "Non-Destructive Evaluation Of Eco-Friendly Cementituous Materials By Ultrasound," *International RILEM Conference on Materials, Systems and Structures in Civil Engineering,* Segment on Service Life of Cement-Based Materials and Structures, vol.2, edited by M.Azenhan I.Gabrijel, D.Schlicke, T.Kandstad and O.Mejlhede Jensen, Lyngby, Denmark, August 22-24, 2016, pp.503-512, 2016.

CHAPTER 6:
INFLUENCE OF THE WATER/CEMENT RATIO ON THE EARLY AGE PROPERTIES OF CEMENT BASED MATERIALS

During the design stage of concrete structures, the concrete mix design plays a prominent role. The control of the properties of concrete in a hardened state is not enough to insure no cracking risk at early age and consequently a good durability of the concrete structure. For the construction of prestressed, tight or massive structures the consideration of the early age properties is an asset. For example, if autogenous and thermal deformations (which evolve significantly at early age) are restrained, it will lead to the development of stress and might possibly yield to the development of prejudicial cracking, especially in concrete with low water-cement ratio. Among all material parameters, water-cement ratio (W/C) plays an important role in the development of the viscoelastic behaviour of cement based materials. Several studies have already shown that a decrease of the w/c ratio will lead to an increase of the amplitude of the strength and of elastic modulus whereas a decrease of the creep function [1].

SECTION 6.1 – INFLUENCE OF THE WATER/CEMENT RATIO ON THE EARLY AGE FREE DEFORMATION OF CEMENT BASED MATERIALS

This section is based on the publication under review (September 2016 at ASTM International) entitled "Influence Of The Water/Cement Ratio On The Early Age Free Deformation Of Cement Based Materials.".

The purpose of this section is to improve the understanding of the mechanisms and the modelling related to the effect of the water-cement ratio on the free deformation of concrete in sealed condition. Within this framework, a new experimental strategy was developed for the monitoring and the modelling of the free deformation since setting.

6.1.1. Materials And Methods

► MATERIALS AND MIXTURE COMPOSITION

The tests presented here were performed on the four concretes C0.4, C0.5, C0.6 and CSCM for which the compositions are given in chapter 3. For each composition, the aggregate content is the same. Only the water and cement content varies or the nature of the binder. The effective water-to-cement ratio are 0.35 – 0.44 and 0.53. 75% of the cement is substituted by ground granulated blast-furnace slag (GGBFS) and limestone filler (LMF) (25%) for the composition CSCM.

► TIME-SCALE

For consideration of the ageing and the main temperature effect, concrete properties are expressed in function of the equivalent time t_{eq} or the advancement degree of reaction α. The apparent activation energy was determined in [2] with the compressive strength results obtained at 3 different temperatures (38 kJ/mol for compositions with CEM I and 48 kJ/mol for CSCM composition).

► SETTING TIME

Setting time of the concretes was determined by monitoring of the transmission of the ultrasound P- and S-wave through concrete according to the method developed by Carette, *et al.*[3,4]. Values of the initial and final setting time are given in Chapter 3. The value obtained was compared to ASTM C403 [5] and very equivalent results were obtained for several compositions including composition C0.4 and CSCM [3].

► ASSESSMENT OF THE AUTOGENOUS STRAIN AND THE CTE

The free deformation of the studied concrete is measured from casting using the BTJADE [6] and the test protocole presented in the Chapter 4, section 1.

6.1.2. Results

► COEFFICIENT OF THERMAL EXPANSION

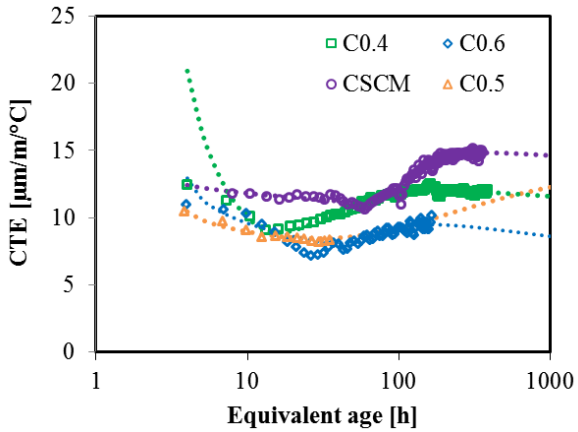

Figure 1 - Evolution of the coefficient of thermal expansion according to the equivalent age. Dashlines correspond to model presented in Equation 2.

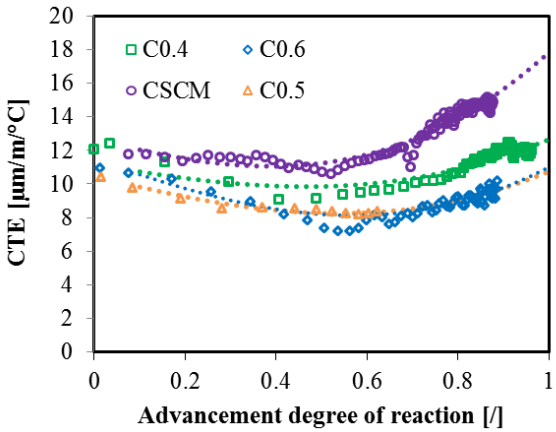

Figure 2 - Evolution of the coefficient of thermal expansion according to the advancement degree of hydration. Dashlines correspond to model presented in Equation 3.

Results of the CTE are given in Figure 1 according to the equivalent time and in Figure 2 according to the advancement degree of reaction. Three successive stages are observed in the results. Before the inital setting time, the value of the CTE is very high and is associated to the CTE of a liquid. General value obtained are around 100-200 µm/m/°C. However this results are not shown because measurements before setting are not purely related to the free deformation of the concrete (artifact coming from the settling and the sedimentation of the material occurs before setting). During setting, a strong and quasi instantaneous decrease of the CTE takes place. Then a low decrease of the CTE is observed for each composition till a minimum value varying between 7 and 10 µm/m/°C. After this minimum, an increase of the CTE is observed till a threshold value varying between 10 and 14 µm/m/°C. For composition with high water-cement ratio, the value of the CTE is globally higher except during the first hours after setting. The general substitution of cement by slag and limestone filler increases significantly the value of the CTE. The age of concrete when the minimum of the CTE occurs depends on the concrete composition. For composition with low water-cement ratio, the minimum value takes place just after setting and for high water-cement ratio the minimum value of the CTE occurs later. For CSCM mixture, the minimum of the CTE occurs at an equivalent age of 60 hours. This is explained by the very low rate of the hydration process during this period. However, when regarding the results according to the advancement degree of reaction, the minimum value of the CTE as well the start of the final threshold value of the CTE occurs during a very close interval (between 0.45 and 0.6) for each composition.

► AUTOGENOUS DEFORMATION

Results of the autogenous strain are given in Figure 3 according to the equivalent time and in Figure 4 according to the advancement degree of reaction. Autogenous strains are set to zero at the final setting time. Values obtained before the final setting are not associated to the autogenous strain. Two stages are observed in the results. Just after the final setting time, the swelling of the concrete takes place till a maximum value. Swelling can be induced by re-absorption of water (no bleeding was observed here during the casting and at the end of the test) or crystallization pressures generated due to solid phase

formation [7,8]. Then a shrinkage period (due to self-desiccation of the cement paste) occurs. As expected, for composition with high water-cement ratio the swelling is significant (40 µm/m for the composition C0.6) and close to zero for low water-cement ratio. Effect of substitution of cement by slag and limestone filler is strongly highlighted on the swelling. The age of concrete when the maximum of the autogenous strain occurs depends on the concrete composition. For composition with low water-cement ratio, the maximum value takes place just after setting and for high water-cement ratio the maximum value of the autogenous deformation occurs later. For CSCM mixture, the maximum of the autogenous strain occurs at an equivalent age of 60 hours. This is explained by the very low rate of the hydration process during this period. When regarding the results according to the advancement degree of reaction, the maximum value of the autogenous strain occurs during a very close interval (between 0.4 and 0.5) for each composition. Also the evolution of the autogenous strain is very similar for the different water-cement ratio between an advancement degree of reaction between 0.4 and 0.65.

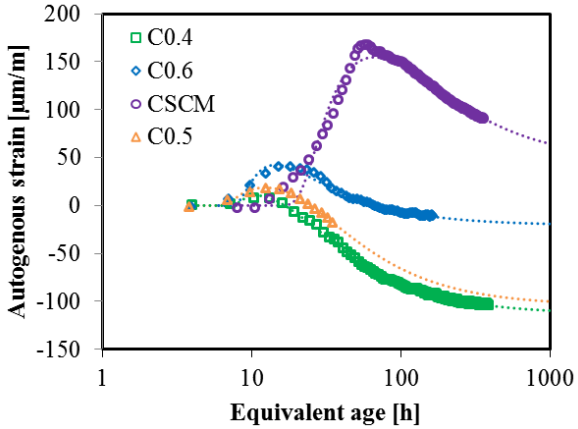

Figure 3 - Autogenous strain according to the equivalent age. Dashlines correspond to model presented in Equation 10.

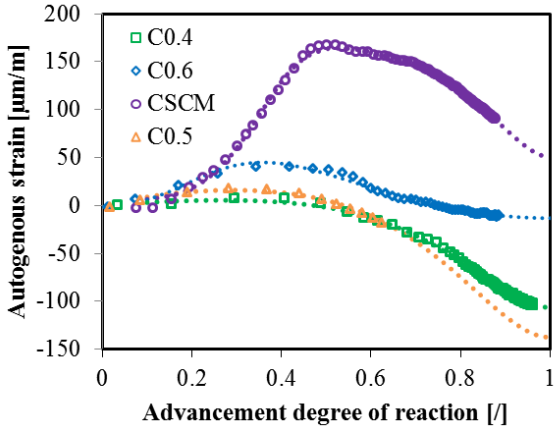

Figure 4 - Autogenous strain according to the advancement degree of reaction. Dashlines correspond to model presented in Equation 11.

6.1.3. Modelling

► COEFFICIENT OF THERMAL EXPANSION

As the evolution of the coefficient of thermal expansion is still not fully understood during early age, no general expression is able to predict the evolution of the CTE. Model using multi-layer theory and considering concrete as a three phases material (cement paste, aggregate and water) before final setting and two phases material (cement paste and aggregate) after the final setting time was developed by Mitsuo & Hiroaki [9]. This model is able to consider the decrease of the CTE during the setting period. However this model assumes that no change of the CTE occurs after the final setting. Mathematical expressions are used to fit experimental data. Such as the expression developed by Maruyama, *et al.* [10] presented in Equation 1.

$$\begin{cases} t < t_1 & \alpha(t) = a.\exp(b.t) + c.\ln(t) + d \\ t \geq t_1 & \alpha(t) = e.\ln(t - f) + g.t + h \end{cases} \quad (1)$$

Where t is expressed in hour, α is expressed in µm/m/°C and t_1 is a temporal parameter. However no direct physical mechanism is highlighted and there is no continuity in the expression which leads to the assumption that the mechanisms occurring at the beginning have no impact in the final value of

the CTE. The existing models found in the literature are therefore not able to correctly consider the physical mechanisms which occur during the hydration process in the evolution of the CTE. From this observation, a new model is developed. The model uses two terms which are related to the decrease of the CTE and a second term related to the increase of the CTE due to the internal decrease of relative humidity in the material. In equivalent time (Equation 2), the first term is an exponential law and the second term is inversely proportional to the equivalent age. With the advancement degree of reaction (Equation 3), the model developed by De Schutter for the Poisson's ratio [11] is used and adapted (sum of a sinusoid law and an exponential law). All parameters are defined by least square method using the function "fminsearch" in Matlab©. A very good agreement is obtained between experimental results and the modelling for each composition and both timescales.

$$\alpha_c(t_{eq}) = \alpha_{t1}\left(\frac{\tau_\alpha}{\tau_\alpha + t_{eq} - t_i}\right)^{r_1} + \alpha_{t2}.\exp\left(-\left(\frac{p_\alpha}{t_{eq}}\right)^{r_2}\right) \quad 2$$

$$\alpha_c(\alpha) = \alpha_{\alpha1}.\sin\left(\frac{\pi.\alpha}{2}\right) + \alpha_{\alpha2}.\exp(-c_\alpha.\alpha) \quad 3$$

Where t_{eq} and t_i are expressed in hour, τ_α=1 h, r_1, r_2 and p_α are kinetic parameters, α_{t1} and α_{t2} are amplitude parameters. For Equation 3, $\alpha_{\alpha1}$ and $\alpha_{\alpha2}$ are amplitude parameters and c_α is a kinetic parameter. The values of parameters of both models are given in Table 1 for each composition.

Table 1 - CTE parameters from Equation 2 and 3

	C0.4	**C0.5**	**C0.6**	**CSCM**
α_{t1}, µm/m/°C	25.68	10.23	11.92	12.59
r_1, /	0.48	0.07	0.12	0.03
α_{t2}, µm/m/°C	10.78	8.79	3.29	4.49
p_α, h	26.14	208.20	63.95	106.78
r_2, /	1.29	0.61	2.15	2.81
$\alpha_{\alpha1}$, µm/m/°C	-7.07	-8.27	-10.79	-11.32
$\alpha_{\alpha2}$, µm/m/°C	11.18	10.47	11.49	12.70
c_α, /	-0.57	-0.60	-0.64	-0.83

► AUTOGENOUS DEFORMATION

The modelling of the autogenous strain was studied by several authors in the past. Models are generally based on one global term and are expressed according to the age of the material [12,13] (Equation 4 and 5) or the degree of hydration [14] (Equation 6). These models are not able to consider swelling and shrinkage simultaneously. For the modelling of the autogenous strain of concrete composed of CEM III/A, Darquennes, *et al.* [15] have developed a model able to consider swelling and self-desiccation by using a single equation (Equations 7) where one sinusoid expression is used for the self-desiccation (Equation 8) and another expression is used for the swelling (Equation 9). However this model has the disadvantage to use several fitting parameters. Therefore it becomes difficult to use for comparison between several models. Complete details about the different models can be found on the references [12–14]

$$\varepsilon_{au}(t) = \varepsilon_0 . \exp\left(-\left(\frac{\tau}{t}\right)^m\right) \quad (4)$$

$$\varepsilon_{au}(t) = \varepsilon_{au0} . \left(\frac{a/c}{6}\right)^{-r_5} . \left(\frac{w/c}{0.38}\right)^{-r_4} . \left[1 + \left(\frac{\tau_{au}}{t}\right)^{\theta}\right]^{-r_2} \quad (5)$$

$$\varepsilon_{au}(\xi) = -\kappa(\xi - \xi_0) \quad \text{for } \xi > \xi_0 \quad (6)$$

$$\varepsilon(\xi) = \left[\varepsilon_{swelling} - \varepsilon_\infty\right] . \left[\left(\frac{\varepsilon_\infty}{\varepsilon_{swelling} - \varepsilon_\infty}\right) + T_{shrinkage}\right] . T_{swelling} - \left[\frac{\varepsilon_\infty + \left(\varepsilon_{swelling} - \varepsilon_\infty\right)}{1 + \alpha}\right] . (1 - \xi) \quad (7)$$

$$T_{shrinkage} = \left(\sin\left(\frac{\left(\left(1 - \xi_{swelling}\right) + (1 - \xi) - \left|\left(1 - \xi_{swelling}\right) - (1 - \xi)\right|\right)}{1 - \xi_{swelling}} . \frac{\pi}{4}\right)\right)^{\beta} \quad (8)$$

$$T_{swelling} = \left[1 + \alpha . \left(\frac{\left(1 - \xi - \left(1 - \xi_{swelling}\right) + \left|1 - \xi - \left(1 - \xi_{swelling}\right)\right|\right)}{2\left(1 - \left(1 - \xi_{swelling}\right)\right)}\right)^4\right]^{-1} \quad (9)$$

For this study, a new methodology is used for the modelling of the autogenous deformation. To model the autogenous strain, it is necessary to divide the modelling in two terms. The first term is relative to the swelling (index sw) and the second term is relative to the self-dessication (index sd). In equivalent time (Equation 10), both terms are associated to an exponential law. With the advancement degree of reaction (Equation 11), the term related to the swelling is the inverse of an exponential law and the self-desiccation is a sinusoid law. For both timescales, first the term related to the self-desiccation is defined with consideration of data only after the swelling peak. Least square method is used in order to optimize each parameter. Then, all data are considered to define the term related to the swelling. This methodology has the advantage to keep physical value in the model. If all parameters are defined simultaneously, then a best fit is obtained and parameters of the model have no physical meaning. Results of the modelling are presented in Figure 3 according to the equivalent time and Figure 4 according to the advancement degree of reaction. A very good agreement is obtained between experimental results and the modelling for each composition and both timescales.

$$\varepsilon_{au}(t_{eq}) = A_{sw} . exp\left(-\left(\frac{p_{sw}}{t_{eq} - t_f}\right)^{r_{sw}}\right) + A_{sd} . exp\left(-\left(\frac{p_{sd}}{t_{eq} - t_f}\right)\right) \quad (10)$$

$$\varepsilon_{au}(\alpha) = B_{sw} . \left(\frac{1}{1 + exp(-(\beta . \alpha)^{a_{sw}})} - \gamma\right) + B_{sd} . sin\left(\frac{\pi}{2} . \alpha^{a_{sd}}\right) \quad (11)$$

Where t_{eq} and t_{fs} are expressed in hour, p_{sw}, p_{sd} and r_{sw} are kinetic parameters, A_{sw} and A_{sd} are amplitude parameters. For Equation 11, B_{sw} and B_{sd} are amplitude parameters and β, a_{sw}, a_{sd} and γ are kinetic parameters. The values of parameters of both models are given in Table 1 for each composition. The parameters of both models are given in Table 2 for the different compositions. The final difference between the amplitude of the swelling and the shrinkage deformation defined by the models ($A_{sd} - A_{sw}$ for equivalent time model and $B_{sd} - B_{sw}(\alpha = 1)$ for advancement degree of hydration model) is also given in Table 2. It is observed that from results of both models this difference is higher for concrete with high water-cement ratio and the substitution of cement by slag and limestone filler increases this difference.

Table 2 - Autogenous strain coefficient for Equation 10 and 11.

	C0.4	**C0.5**	**C0.6**	**CSCM**
A_{sw}, µm/m	14.53	22.08	70.55	176.55
p_{sw}, h	4.37	2.68	4.34	20.77
r_{sw}, /	4.69	2.23	2.09	2.62
A_{sd}, µm/m	-127.60	-126.53	-91.20	-130.22
p_{sd}, h	27.41	34.54	16.70	147.71
B_{sw}, µm/m	1583	51325	307	330
β, /	0.15	3017.24	5.08	3.01
a_{sw}, /	0.0105	0.0009	1.5633	3.6756
γ, /	0.72	0.73	0.48	0.48
B_{sd}, µm/m	-116.96	-166.53	-173.86	-119.94
a_{sd}, /	4.16	3.90	0.99	5.73
$A_{sd} - A_{sw}$, µm/m	-142.13	-148.61	-161.75	-306.77
$B_{sd} - B_{sw}(\alpha = 1)$, µm/m	-127.52	-195.52	-334.60	-290.51

6.1.4. Discussion

► RELATION BETWEEN AUTOGENOUS STRAIN AND CTE

For both autogenous deformation and CTE, an extremum value is obtained for each composition. In Figure 5 and Figure 6, results of autogenous strain and CTE from composition C0.6 and CSCM are compared. For each composition, the extremum occurs around a value of 0.5 in advancement degree of reaction. For the CTE, the change of trend is very clear and occurs during a very small time window. With the autogenous strain, the change of trend occurs on a longer period. However, a clear decrease of the autogenous strain starts at an advancement degree of reaction of 0.5. For both compositions, the CTE and the autogenous strain evolve in an opposite direction during the whole hydration. The same observations are done with composition C.04 and C0.5. It is however more difficult to define the time when the extremum of the autogenous strain occurs for composition with low water-cement ratio because of the low amplitude of the swelling.

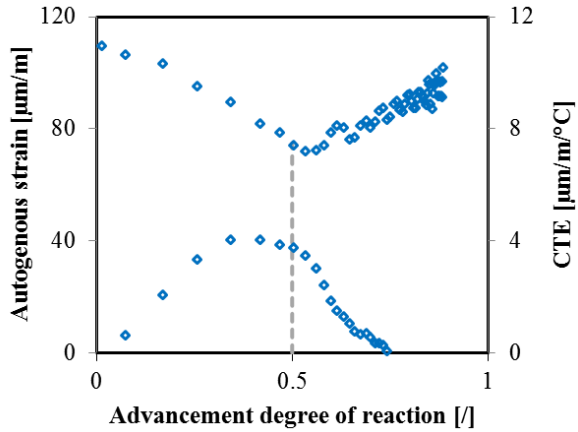

Figure 5 – Evolution of the CTE and the autogenous deformation for composition C0.6

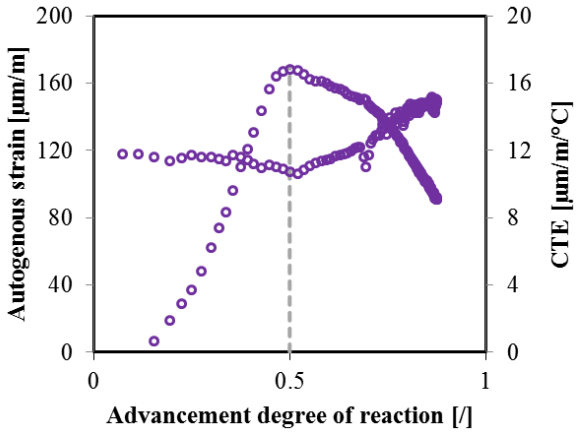

Figure 6 – Evolution of the CTE and the autogenous deformation for composition CSCM.

From these observations, value of the CTE and the autogenous deformation are compared in Figure 7 and Figue 8. For this comparison, autogenous deformations are set to zero when the extremum occurs. In Figure 7, results from the swelling period are presented. A general linear relation is observed between the autogenous deformation and the CTE. This relation is function of the water-cement ratio. The increase of the autogenous swelling will lead to a higher variation in the CTE for concrete mixture with lower water-cement ratio. For the SCM composition, the variation of the swelling deformation has a very low impact on the CTE. In Figue 8, results from the shrinkage period are presented. A general linear relation is also observed between the autogenous deformation and the CTE. The effect of the water-cement ratio is not clear but the general tendency shows that the increase of the autogenous shrinkage will lead to a higher variation in the CTE for concrete mixture with higher water-cement ratio. For the SCM composition, the variation of the shrinkage deformation has a significant impact on the CTE. Therefore it is observed that swelling and decrease of the CTE after the initial setting time are linked to a same mechanism as for the increase of the CTE and the self-desiccation. The relation between the CTE and the autogenous deformation is linear but the effect of the mixture content is not the same during the swelling and the shrinkage period.

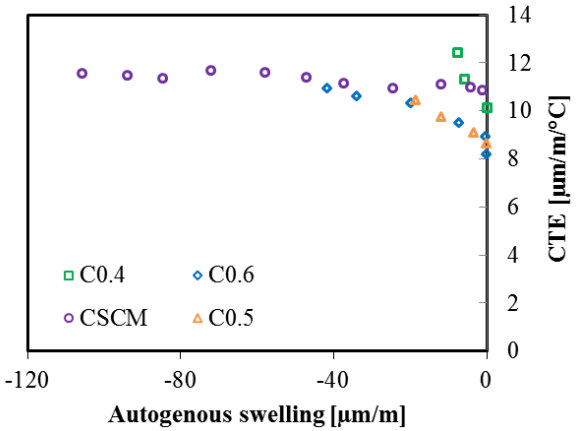

Figure 7 – Evolution of the CTE according to the autogenous swelling.

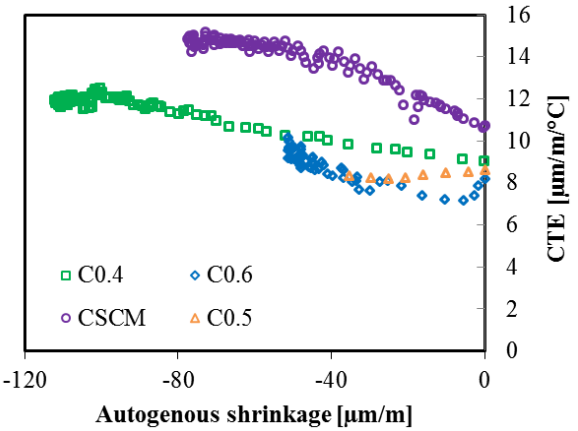

Figue 8 - Evolution of the CTE according to the autogenous shrinkage.

► SETTING TIME

Several methods were developed in the past for the determination of the initial and final setting time. In [16], it is shown that final setting time can be defined using the rate of autogenous strain development in a cement paste. The final setting time corresponds to the minimum of the derivative of the autogenous strain. In [17–19], final setting time is associated with the start of the decrease of the CTE from the liquid to the solid phase in cement paste. For this study, two criteria were used to define setting time. First, ultrasonic measurement using P-wave and S-wave for which the initial setting time corresponds to the maximum of the derivative of the S-wave. The final setting time corresponds to the maximum of the derivative of the dynamic E-modulus [3]. Secondly, for composition C0.4 and CSCM, resistance penetration tests were carried out in [3] using the ASTM C304 standard [5] on sieved concrete. In Figure 9, the evolution of the CTE during the setting process is compared to the initial setting time defined with both criteria. Results from ultrasonic measurement and penetration resistance tests are in very good agreement. It is observed that the initial setting time is associated to the moment when the value of the CTE does not correspond anymore to a liquid. No strong effect of the water-cement ratio (between 0.35 and 0.53) is observed on the detection of the initial setting time. Due to technical issue, no thermal variation were applied to the composition CSCM before an age of 7 hours, it is therefore not possible to define the initial setting for this composition with the CTE. This observation is in contradiction with results of [17–19] on cement pastes. In Figure 10, the evolution of the autogenous strain during the setting process is compared to the final setting time defined with both criteria. Some differences are obtained between ultrasonic measurement and penetration resistance tests. Results of final setting time from ultrasonic measurement occur earlier than results from resistance penetration tests. It is observed that the final setting time, defined according to the ASTM C403, takes place when the swelling strain starts. It is thus observed that the final setting time is associated, for the autogenous strain, to a minimum which corresponds to a zero value of the derivative on concrete. No strong effect of the water-cement ratio (between 0.35 and 0.53) is observed on the detection of the final setting time. For CSCM composition, a strong delay of the final setting time is observed. This is due to the slow hydration kinetics of the blast furnace slag. This observation is in agreement with results of [16] on cement pastes.

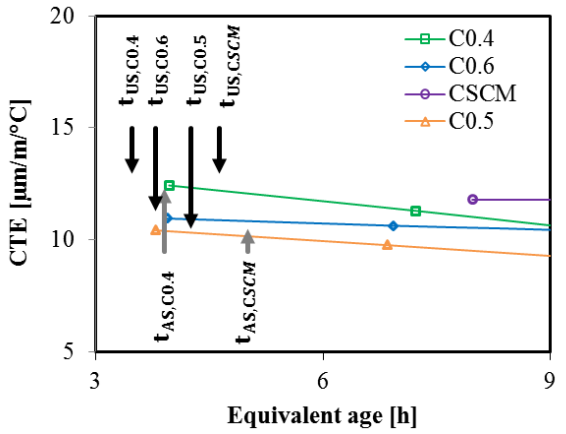

Figure 9 - Comparison between the initial setting time determined with ultrasonic criterion (index US) and ASTM C304 (index AS) and the evolution of the CTE during the setting process.

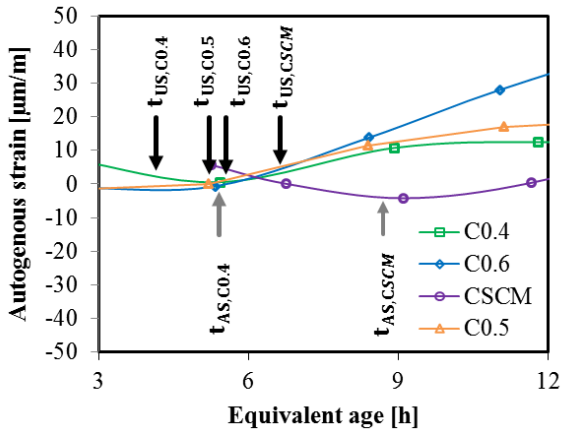

Figure 10 - Comparison between the final setting times determined with ultrasonic criterion (index US) and ASTM C304 (index AS) and the evolution of the autogenous strain during the setting process.

Only every 160 minutes a thermal variation is applied to the sample which corresponds to an accuracy of 80 minutes to define the initial and final setting time. By using spline interpolation method, it is possible to improve the determination of the zero value of the derivative of the autogenous strain. However for a better assessment of the initial setting time, it is needed to reduce the period of thermal variation. An easy way to override this is to impose smaller thermal variation during the very early age in order to get a faster stabilization of the temperature in the sample.

SECTION 6.2 – EFFECT OF WATER-CEMENT RATIO ON THE VISCOELASTIC BEHAVIOUR OF CEMENT BASED MATERIAL SINCE SETTING TIME

During these last decades, several predictive models for creep have been developed for the consideration of basic creep since early age for the design of concrete structures. Three well-known models, currently used, are the ACI models [20] (Equation 12), the Model Code 2010 [21] (Equation 13 and 14) and the model B3 of Bazant [22] (Equation 15).

$$\varphi(t,t') = \frac{(t-t')^{\Psi}}{d+(t-t')^{\Psi}}\phi_u \quad (12)$$

$$\varphi(t,t') = \varphi_{0,bc}(f_{cm}).\beta_{bc}(t,t') = \frac{1.8}{(f_{cm})^{0.7}}.\ln\left(\left(\frac{30}{t_{0,adj}(t')}+0.035\right)^2(t-t')+1\right) \quad (13)$$

$$t_{0,adj}(t') = t'.\left(1+\frac{9}{2+t'^{1.2}}\right) \quad (14)$$

$$C(t,t') = q_2.\int_{t'}^{t}\frac{n.\tau^{-m}.(\tau-t')^{n-1}}{1+(\tau-t')^n}d\tau + q_3.\ln[1+(t-t')^n] + q_4\ln\left(\frac{t}{t'}\right) \quad (15)$$

A comparison between these three models is carried out in Table 3. The ACI model contains a hyperbolic law which does not separate creep in basic and drying creep. Aging have an impact only on the ultimate creep coefficient ϕ_u. That means that aging has only an effect on the amplitude of the creep and not on the kinetics in this model. Effect of the water-cement ratio is considered indirectly in the ultimate creep coefficient via the slump and the air content. In the recent Model Code 2010 (MC2010) [21], the basic creep is expressed as the multiplication of an amplitude term $\varphi_{0,bc}$ which is linked to the mean compressive strength at an age of 28 days and a kinetic term $\beta_{bc}(t,t')$ which is function of the age at loading, the age after loading and the type of cement. For one composition defined, all parameters are constant except the age at loading which is the only parameter which considers the ageing. Water-cement ratio has indirectly an effect on the amplitude of the creep with the mean compressive strength. In the model B3 of Bazant [22,23], the basic creep is separated in three terms. The terms with parameter q_2 and q_3 correspond to the short term creep [24] which is linked to the solidification theory [25]. The last term with parameter q_4 corresponds to the long term creep [24] which is linked to the microprestress theory [26]. Aging is considered in the model B3 with parameters q_2 and q_4. The water-cement ratio is considered indirectly in the term q_2 which is linked to the mean compressive strength and is considered directly in the parameter q_3. In summary, it is observed that aging could have an impact in amplitude and kinetic and water cement ratio has only an impact on the amplitude of the creep but not on the kinetic. When creep is divided in short and long term creep, water-cement ratio has no effect on the long term creep. Complete details about the different models shown in Equations 12-15 can be found on the references given in the Table 3.

Table 3 - Consideration of aging and water-cement ratio in ACI model [20], B3 model [22] and Model code 2010 [21].

	ACI 209R-92 [20]	Model Code 2010 [21]	B3 [22]
Division between basic creep and drying creep	No	Yes	Yes
Consideration of aging?	Yes, on the final amplitude of the creep	Directly considered with $t_{0,adj}$	Directly considered for the short and long term creep
Effect of water-cement ratio?	Indirectly with the values of the slump and the air content which influences the final amplitude of the creep	Indirectly considered with f_{cm} which influences the final amplitude of the creep	Directly considered for the short term creep but not for the long term creep

For consideration of the aging and the main temperature effect, concrete properties are expressed in function of the equivalent time t_{eq}, the advancement degree of reaction α or the hydration degree ξ. The hydration degree ξ corresponds to the advancement degree of reaction multiplied by the final hydration degree ξ_∞. Waller [27] proposed a relation between ξ_∞ and the effective water-cement ratio (Equation 16).

$$\xi_\infty = 1 - \exp(-3.3.W_{eff}/C) \quad 16$$

The purpose of this research is to improve the understanding of the mechanisms and to propose a modelling related to the viscoelastic behaviour of concrete in sealed condition. Within this framework, a new strategy was developed recently at ULB and IFSTTAR for the monitoring [28] and the modelling [29] of the viscoelastic properties of cement based material since setting. The methodology is based on a repeated minute-long loading test for which each hour a load representing 20% of the compressive strength is applied during 5 minutes and a classical compressive creep test for which a load representing 40% of the compressive strength is applied during more than one week. It was highlighted that short term creep is divided in two mechanisms. The first mechanism is linked to the state of the material (capillarity porosity, CSH…) at the age of loading and has a logarithmic behaviour. The second mechanism is linked to the solidification theory of Bazant [25] which considers the evolution of the mechanical properties of the cement paste during the loading.

The effect of the water-cement within the range 0.28-0.60 will be investigated on several properties (compressive strength, heat release, E-modulus, Poisson's ratio, short and long term creep) since setting in relation to the development of the microstructure. Comparison with several results coming from the literature will be done. This study is carried out at 20°C and in sealed conditions.

6.2.1.Materials and mixtures

The tests presented here were fully performed in the laboratory of civil Engineering at ULB on three concretes with different water-cement ratio C0.4, C05 and C06 for which mix proportions are given in Chapter 3. For each composition, the aggregate content is the same. Only the water and cement content are not the same.

► Preliminary results

A certain number of fundamentals properties were determined before the study of the viscoelastic behaviour of the three concrete mixes. The setting is determined on basis of the monitoring of the transmission of the ultrasound p- and s-wave through concrete according to the method developed by Carette, *et al.* [3,4]. Values of the initial and final setting time are given in Table 1.

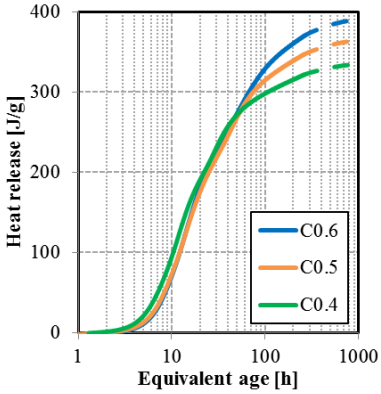

Figure 11 - Heat release for several water-cement ratio. Continuous lines correspond to the experimental results and dashlines correspond to interpolated value used to define the ultime heat release.

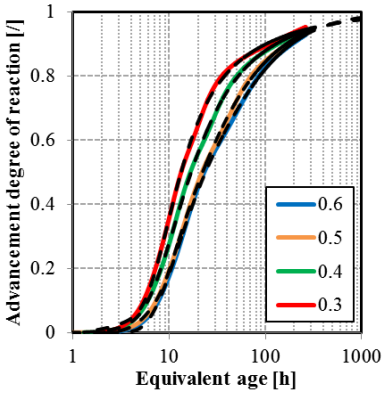

Figure 12 - Advancement degree of reaction according to the equivalent time for several water-cement ratios.

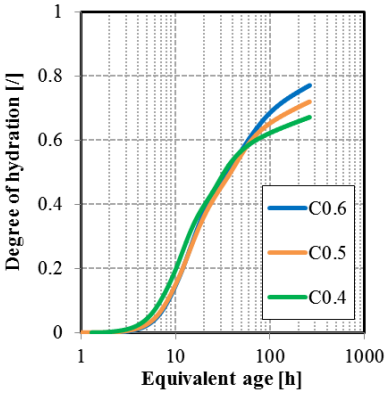

Figure 13 - Degree of hydration according to the equivalent time for different water-cement ratio

For the determination of the equivalent time, the apparent activation energy was determined in previous studies [2] with the compressive strength results obtained at 3 different temperatures (36 kJ/mol for each composition). Isothermal calorimetry testing with a Tam Air device [30] available at BATir, ULB is used for the determination of the advancement degree of reaction. The heat release for an infinite time is defined by linear extrapolation between the heat release and the inverse of the equivalent time and with only consideration of data with equivalent age higher than one week. The Equation 17 [28] is used to fit experimental data and to predict value of the advancement degree of reaction for equivalent age higher than two weeks. The Equation 17 is composed of two exponential terms with $\alpha_1 + \alpha_2 = 1$; τ_1, τ_2, a_1, a_2 are fitting parameters. Values of each parameter needed to model the advancement degree of reaction are given in Table 4 for the three water-cement ratios.

$$\alpha(t) = \alpha_1 \exp\left(-\left(\frac{\tau_1}{t_{eq}}\right)^{a_1}\right) + \alpha_2 \exp\left(-\left(\frac{\tau_2}{t_{eq}}\right)^{a_2}\right) \quad 17$$

Table 4 - Isothermal calorimetry parameters of Equation 17

	q_∞ [J/g]	α_1 [/]	τ_1 [h]	a_1 [/]	α_2 [/]	τ_2 [h]	a_2 [/]
C0.4	340.11	0.63	11.21	1.47	0.37	17.08	0.68
C0.5	371.29	0.08	11.08	4.10	0.92	16.96	0.95
C0.6	398.62	0.68	11.92	1.55	0.32	68.65	1.08

All experimental parameters obtained for this study will be presented in the next section according to three timescales. Equivalent time and advancement degree of reaction are classical timescales for which it is possible to impose in the model a value which corresponds to the final hydration of the cement paste ($\alpha = 1$ or $t_{eq} = \infty$). The degree of hydration allows comparing various compositions

according to a proportional quantity of cement hydrated. The modelling of the mechanical properties of the different composition with these three timescales will highlight:

- The predicted final value of a property (t_{eq} and α),
- The kinetic evolution of a property according to the evolution of three parameters,
- The value of a property when the cement paste is fully hydrated.

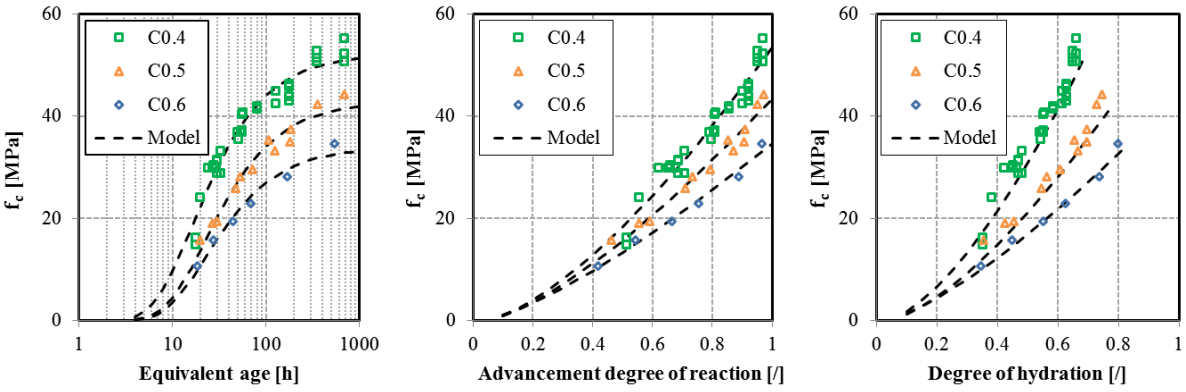

(a) (b) (c)

Figure 14 - Evolution of the compressive strength according to the equivalent time (a), the advancement degree of reaction (b) and the degree of hydration (c).

The compressive strength is defined since few hours after the final setting till 28 days. Results of the compressive strength f_c are given according to the equivalent time t_{eq} in Figure 14a, according to the advancement degree of reaction in Figure 14b and according to the degree of hydration in Figure 14c. Equation 18, 19 [2]and 20 are used to model the evolution of the compressive strength.

$$f_c(t_{eq}) = f_c(t_{eq} = \infty).\exp\left(-\frac{p_f}{t_{eq}}\right) \quad 18$$

$$f_c(\alpha) = f_{c,\alpha}.(\alpha - \alpha_0)^{a_{f,\alpha}} \quad 19$$

$$f_c(\xi) = f_{c,\xi}.(\xi - \xi_0)^{a_{f,\xi}} \quad 20$$

Where t_{eq} is expressed in hour, p_f and a_f are material parameters which are related to the kinetic evolution of the compressive strength, $f_c(t_{eq} = \infty)$ is expressed in MPa and corresponds to the value of the compressive strength at an infinite time, $f_{c,\alpha}$ is expressed in MPa, $f_{c,\xi}$ is expressed in MPa. Values of each parameter are given in Table 5. Each model well represents the evolution of the compressive strength.

Table 5 - Compressive strength parameters for different water-cement ratio

	$f_c(t_{eq} = \infty)$ [MPa]	p_f [h]	$f_{c,\alpha}$ [MPa]	$a_{f,\alpha}$ [/]	$f_{c,\xi}$ [MPa]	$a_{f,\xi}$ [/]	α_0 [/]	ξ_0 [/]
C0.4	52	16.87	56	1.47	97	1.54	0.035	0.024
C0.5	43	22.62	46	1.38	65	1.47	0.043	0.033
C0.6	34	22.88	36	1.31	46	1.35	0.035	0.021

In Figure 15, parameters of three models are plotted according to the effective water-cement ratio. A linear relation between material parameters and the effective w/c ratio is highlighted. Equations linking parameters and the effective w/c ratio are given in Equations 21, 22, 23 and 24. As expected, the final amplitude of the compressive strength decreases with the increase of the effective water-cement ratio. The kinetic is faster for concrete with a lower effective water-cement ratio.

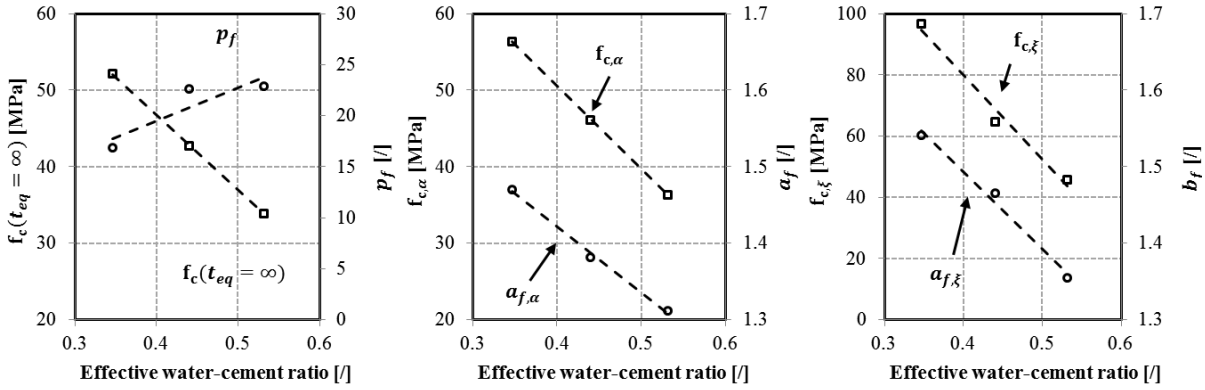

(a) (b) (c)

Figure 15 - Compressive strength parameter of Equation 18, 19 and 20 according to the effective water-cement ratio.

$$f_c(t_{eq}=\infty) = -98.\left(W_{eff}/_C\right) + 86 \quad (21)$$

$$p_f = 32.\left(W_{eff}/_C\right) + 6.5 \quad (22)$$

$$f_c(\alpha = 1) = -108.\left(W_{eff}/_C\right) + 94 \quad (23)$$

$$a_{f,\alpha} = -0.86.\left(W_{eff}/_C\right) + 177 \quad (24)$$

$$f_c(\xi = 1) = -276.\left(W_{eff}/_C\right) + 190 \quad (25)$$

$$a_{f,\xi} = -1.\left(W_{eff}/_C\right) + 1.89 \quad (26)$$

Several laws were already developed in the past to characterize the effect of the water-cement ratio on the compressive strength. Among the models developed during more than one century, four of the most popular empirical equations are used in order to compare the linear relation obtained: Bolomey [31], Feret [32], Powers and Brownyard [33] and Abrams [34]. The models are presented in Table 6. The main difference between each model comes from the nature of the law (linear, quadratic, power or exponential). The effect of the water-cement is based on the mass or volume proportion of the cement and the water. The other components are considered with one or two material parameters. All models are able to correctly consider the variation of W/C ratio on an interval of variation between

0.4 and 0.6 with a very good accuracy (R^2 is higher than 0.98 for each equations). For lower water-cement ratio, these relations are not necessarily true.

Table 6 - Models for compressive strength considering the W/C ratio.

Models	Equation	R^2	References
Feret (quadratic law)	$f_c = K.\left(\frac{v_c}{v_c+v_e}\right)^2$	0.9917	[32]
Bolomey (linear law)	$f_c = \left(\frac{C}{E} - 0.5\right).K''$	0.9899	[31]
Powers (power law)	$f_c = A.\left(\frac{W}{C}\right)^B$	0.9889	[33]
Abrams (exponential law)	$f_c = \frac{A}{(B)^{\frac{W}{C}}}$	0.9977	[34]
Linear law	$f_c = A.\frac{W}{C} + B$	0.9999	/

6.2.2 Repeated minute-long loading test

► Assessment of E-modulus, Poisson ratio and the short term creep

Cylindrical specimen with a diameter of 97 mm and a height of 550 mm are produced. For each test, a dummy specimen with exactly the same dimension is also produced. One T type thermocouple is placed in the center of the dummy specimen. After casting, all specimens are placed in an air-conditioning chamber at 20°C and a relative humidity of 90%. Then samples are demolded, grinded on both circular end faces and surrounded by 2 self-adhesive aluminum sheets in order to keep the sample in sealed conditions. The sealing has been checked by weighting the sample before and after the test with an high precision balance. As samples are grinded few hours after setting, a small layer of sieved concrete (+/- 1cm) is placed on the top of the sample in order to avoid any problem of pullout of the aggregate during the grinding.

A Walter+Bay LFMZ 100 kN electromechanical testing setup with an extensometer in Invar© designed and available at the laboratory of Civil Engineering at ULB is used for the monitoring of the E-modulus, the Poisson ratio and the creep by means of repeated minute-long duration loadings [28]. More information about the test rig and the instrumentation is given in chapter 4, section 3.

► Protocol of loading

Measurements on the sample have started a few hours after setting (between 4 and 9 hours). The whole test duration is 28 days. The temperature of the sample is set to 20°C and is recorded since the casting. Two strategies were used for the monitoring of the E-modulus. For the composition C04, repeated minute-long loadings were applied each hour during the first weeks and then the specimen was again loaded two times at an age of two weeks and four weeks. For the composition C05 and C06, specimens were loaded at an age of 15, 24, 40, 168 and 672 hours. These ages were chosen according to the evolution of the advancement degree of reaction in order to follow accurately the hardening process on the viscoelastic properties. Both methodologies give equivalent results [35] but the second one allows carrying out several tests on various mixtures during the same period.

► E-modulus

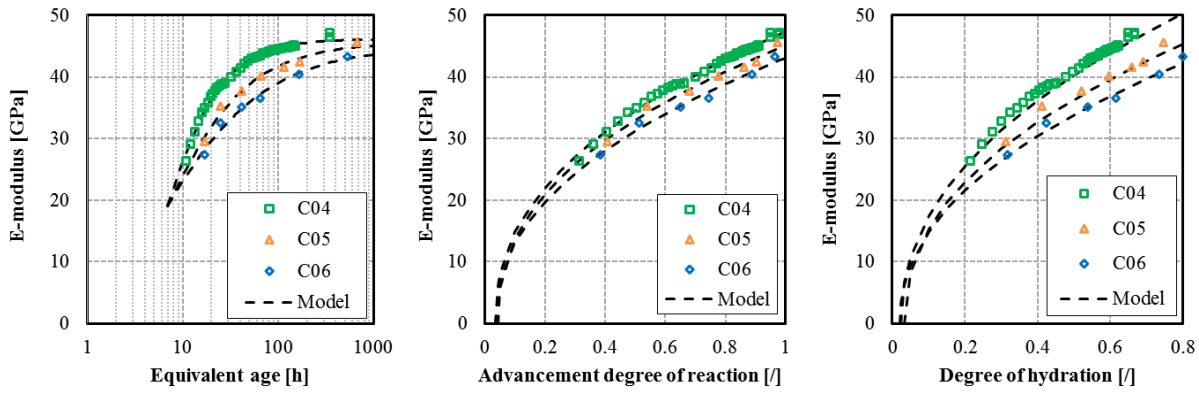

(a) (b) (c)

Figure 16 - Evolution of the E-modulus according to the equivalent time (a), the advancement degree of reaction (b) and the degree of hydration (c).

For each repeated minute-long loading, the E-modulus is calculated from the set of recordings (load and displacement in the central section) between 30% and 80% of loading [35]. In each case, the tangent elastic modulus E is computed by least square method. Results are given according to the equivalent time in Figure 16a, according to the advancement degree of reaction in Figure 16b and according to the degree of hydration in Figure 16c. Equation 27, 28 and 29 [36] are used to model the evolution of the E-modulus.

$$E(t_{eq}) = E(t_{eq} = \infty).\exp\left(-\left(\frac{p_E}{t_{eq}}\right)^{r_E}\right) \quad 27$$

$$E(\alpha) = E_{\alpha}.(\alpha - \alpha_0)^{a_{E,\alpha}} \quad 28$$

$$E(\alpha) = E_{\xi}.(\xi - \xi_0)^{a_{E,\xi}} \quad 29$$

Where t_{eq} is expressed in hour, p_E, r_E, $a_{E,\alpha}$ and $a_{E,\xi}$ are material parameters which are related to the kinetic evolution of the E-modulus, $E(t_{eq} = \infty)$ is expressed in GPa and corresponds to the value of the elastic modulus at an infinite time, E_{α} is expressed in GPa and $E(\xi = 1)$ is expressed in GPa. Value of each parameter is given in Table 7. Both models well represent the evolution of the elastic modulus.

Table 7 - E-modulus parameters for the three water-cement ratios

	$E(t_{eq} = \infty)$ [GPa]	p_E [h]	r_E [/]	$E(\alpha = 1)$ [GPa]	$a_{E,\alpha}$ [/]	$E(\xi = 1)$ [GPa]	$a_{E,\xi}$ [/]
C0.4	46.2	6.33	1.25	48.0	0.43	56.5	0.46
C0.5	45.7	5.99	0.85	45.9	0.42	51.1	0.45
C0.6	44.9	5.52	0.68	43.7	0.44	47.3	0.46

In Figure 17, parameters of each model are plotted according to the effective water-cement ratio. A linear relation between material parameters and the effective w/c ratio is highlighted. The kinetic parameters $a_{E,\alpha}$ and $a_{E,\xi}$ are not impacted by a variation of the effective w/c ratio and has an average value of 0.43 and 0.46 respectively. Equations linking E-modulus parameters and effective w/c ratio are given in Equations 30, 32 and 33. A very good agreement is obtained. The final values of the E-modulus predicted by Equations 27 and 28 are close. This parameter is not strongly influenced by the

w/c ratio in contrast with the compressive strength as previously observed by Byfors [37]. This is explained by the different factor related to both. The compressive strength is strongly related to the cracking occurring in the cement paste at the interface with the aggregate. While the E-modulus is highly dependent on the content and stiffness of the aggregates. More developments are realized in the chapter 7 about the multi-scale aspect of this observation.

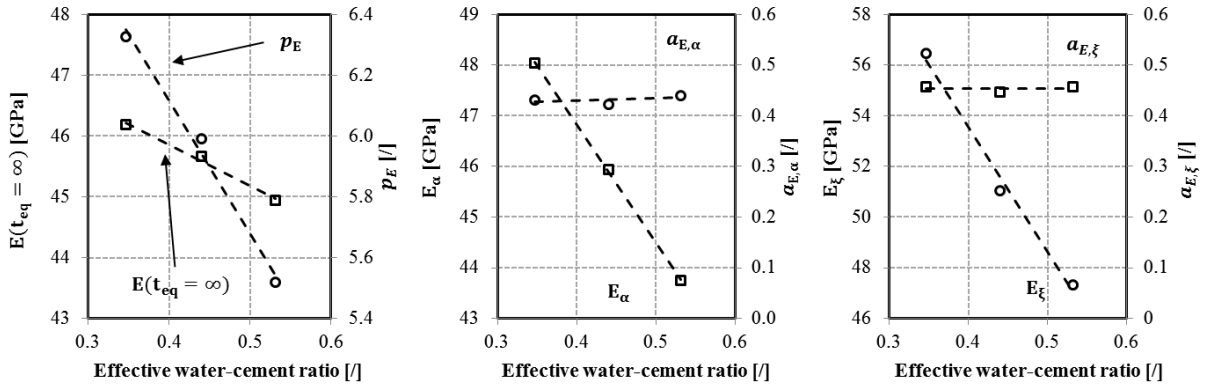

(a) (b) (c)

Figure 17 – E-modulus parameter of Equation 27, 28 and 29 according to the effective water-cement ratio.

$$E(t_{eq}=\infty) = -6.74.\left(W_{eff}/_{C}\right) + 48.55 \text{ [GPa]} \quad (30)$$

$$p_E = -4.36.\left(W_{eff}/_{C}\right) + 7.86 \text{ [h]} \quad (31)$$

$$r_E = -3.07.\left(W_{eff}/_{C}\right) + 2.28 \quad (32)$$

$$E_\alpha = -23.21.\left(W_{eff}/_{C}\right) + 56.11 \text{ [GPa]} \quad (33)$$

$$E_\xi = -49.47.\left(W_{eff}/_{C}\right) + 73.34 \text{ [GPa]} \quad (34)$$

► Poisson ratio

For each repeated minute-long loading, the Poisson's ratio is calculated from the set of recordings (longitudinal and lateral displacement in the central section) on the whole loading. Results are given according to the equivalent time in Figure 18a, according to the advancement degree of reaction in Figure 18b and according to the degree of hydration in Figure 18c. For mixture C0.4 and C0.5, the Poisson's ratio increases during the hardening process (from 0.12 to 0.15). For the composition C0.6, first the Poisson's ratio decreases till a value of 0.16 and then increases till a value of 0.18. From results of the literature [11,37,38], the static Poisson ratio starts at an approximative value of 0.5 (as

an incompressible liquid) and decreases till a minimal value, followed by an increase. But no clear effect of the water-cement ratio has been highlighted in the literature. According to Bernard, *et al.* [39], the decrease of the Poisson's ratio occurs as long as the water phase is continuous and is due to the consumption of water during the hydration process. When the cement begins to set, the water phase becomes discontinuous and the evolution of the Poisson's ratio is then governed by the solid stiffness evolution which will increase the Poisson's ratio.

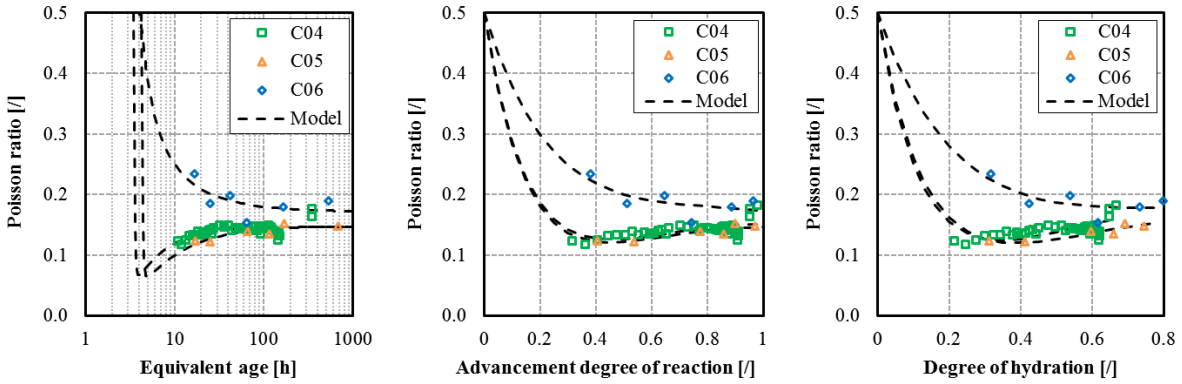

(a) (b) (c)

Figure 18 - Evolution of the Poisson ratio according to the equivalent time (a), the advancement degree of reaction (b) and the degree of hydration (c).

To model the Poisson's ratio, it is therefore necessary to divide the modelling in two terms. A first term associated to the water consumption and a second term associates to the solid stiffness evolution. In Equation 35, the first term is expressed as an inverse function of the equivalent time and the second term, as an exponential law. The initial setting time t_{is} is associated to both mechanisms. Both amplitude and kinetic parameters are used to consider the evolution of both mechanisms. For an equivalent time lower than t_{is}, the value of the Poisson's ratio must be imposed to a value of 0.5. In function of the advancement degree of reaction (Equation 36) and the degree of hydration (Equation 37), the model developed by De Schutter [11] is used with adaptation of the parameters. The first term is associated to an exponential law for which the amplitude is imposed to 0.50 when alpha is zero and the kinetic is governed by one material parameter. The second term is associated to a sinusoid law for which the amplitude is a material parameter. A good agreement is observed between model and experimental results for three time-scales.

$$\nu(t_{eq}) = \nu_{t,f}\left(\frac{\tau_\nu}{1+t_{eq}-t_i}\right)^{r_{\nu,f}} + \nu_{t,s}.\exp\left(-\left(\frac{t_{is}}{t_{eq}}\right)^{r_{\nu,s}}\right) \quad 35$$

$$\nu(\alpha) = 0.5.\exp(-c_\alpha.\alpha) + \nu_\alpha.\sin\left(\frac{\pi.\alpha}{2}\right) \quad 36$$

$$\nu(\xi) = 0.5.\exp(-c_\xi.\xi) + \nu_\xi.\sin\left(\frac{\pi.\xi}{2}\right) \quad 37$$

Where t_{eq} and t_{is} are expressed in hour, $\nu_{t,f}$ corresponds to the Poisson's ratio when the material is considered as a fluid, $\nu_{t,s}$ corresponds to the Poisson's ratio when the material is considered as fully hydrated, $r_{\nu,f}$ is a kinetic parameter which represents the velocity of the consumption of the free water by cement and $r_{\nu,s}$ is a kinetic parameter which is linked to the rate of the solid stiffness evolution. ν_α corresponds to the Poisson's ratio when the advancement degree of reaction is equal to 1, c_α is a kinetic parameter which is linked to the rate transition between the liquid and solid phase. ν_ξ

corresponds to the Poisson's ratio when the whole cement is fully hydrated and c_ξ is a kinetic parameter which is linked to the rate transition between the liquid and solid phase. Value of each parameter is given in Table 8.

Table 8 - Poisson's ratio parameters for the three water-cement ratios

	$\nu_{t,s}$ [/]	$r_{\nu,s}$ [/]	$\nu_{t,f}$ [/]	$r_{\nu,f}$ [/]	ν_α [/]	c_α [/]	ν_ξ [/]	c_ξ [/]
C0.4	0.15	1.50	0.45	13.01	0.15	6.36	0.18	8.07
C0.5	0.15	1.06	0.45	10.63	0.15	6.50	0.16	7.48
C0.6	0.17	25.18	0.44	0.86	0.16	3.44	0.16	3.87

In Figure 19, main parameters of the three models are plotted according to the effective water-cement ratio. The correlation between parameters and the effective water-cement ratio is not direct. However the following observations can be done:

- Both kinetic parameters of Equation 35 are shown in Figure 19a. The evolution of these parameters is in coherence with their linked mechanisms. For low water-cement ratio, the kinetic parameter $r_{\nu,f}$ is higher which means a faster consumption of the free water. The kinetic parameter $r_{\nu,s}$ is lower for low water-cement ratio which means a faster evolution of the solid stiffness.
- Both parameters of Equation 36 are shown in Figure 19b. Value of the final Poisson's ratio ν_α are very close (between 0.15 and 0.16). The kinetic parameter c_α is higher for low water-cement ratio which means a faster decrease of the free water in the cement paste.
- Both parameters of Equation 37 are shown in Figure 19c. Value of the Poisson's ratio corresponding to a full hydration of the cement ν_ξ depends on the water-cement ratio. For low water-cement ratio ν_ξ is higher which means that the value of the final Poisson's ratio depends on the quantity of cement hydrated. The kinetic parameter c_ξ is higher for low water-cement ratio which means a faster decrease of the free water in the cement paste.

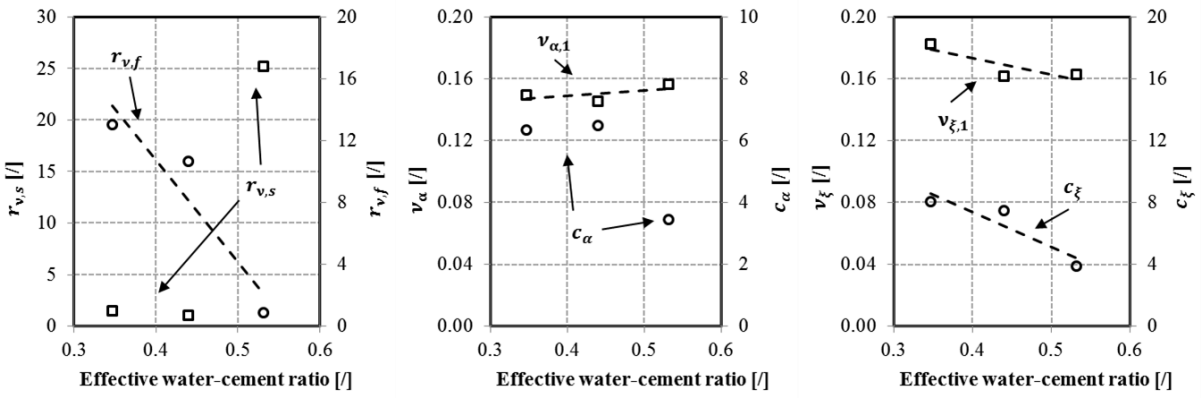

(a) (b) (c)

Figure 19 - Effect of water-cement ratio on the Poisson ratio parameter in Equations 35, 36 and 37.

► Creep for short duration of loading

For each repeated minute-long loading test, a load corresponding to 20% of the compressive strength is applied during 5 minutes. During these 5 minutes-long plateau of stress, the creep coefficient is computed from raw displacement measurements after having removed the free strain from the dummy

specimen (thermal and autogenous strain). In [29], basic creep for short duration of loading is modeled with a logarithmic expression inspired from the Model Code 2010 (Equation 38).

$$\varphi_c(t,t') = A(t').\ln\left(1+(e-1).\left(\frac{(t-t')}{t_A}\right)^{K(t')}\right) \quad 38$$

Where $t_A = 0.083h = 300s$, A is the amplitude creep factor which varies according to the age of loading and which corresponds to the value of the creep coefficient after 5 minutes of loading, K is a kinetic parameter and was previously observed as independent of the age at loading for an ordinary concrete [28,29].

The calculation of the amplitude creep factor was carried out by fitting experimental results with three Kelvin-Voigt chains in series in order to remove noise from the measurement. The value of the fitted curve after 5 minutes of loading corresponds to the amplitude creep factor for each age of loading. This parameter is modeled with the inverse of a logarithmic law in equivalent time (Equation 39) and with a power law with the advancement degree of reaction (Equation 40) and the degree of hydration (Equation 41).

$$A(t') = \frac{1}{A_{t,1}.\ln\left(\frac{t'_{eq}}{t_A}\right)+A_{t,2}} \quad 39$$

$$A(\alpha) = A_\alpha.(\alpha-\alpha_0)^{a_{A,\alpha}} \quad 40$$

$$A(\xi) = A_\xi.(\xi-\xi_0)^{a_{A,\xi}} \quad 41$$

Where $t_A = 1h$, $A_{t,1}$ and $A_{t,2}$ are material parameters, $a_{A,\alpha}$ and $a_{A,\alpha}$ are material parameters, A_α and A_ξ are material parameters related to the magnitude of the amplitude creep factor. Results of the amplitude creep factor according to the equivalent time, the advancement degree of reaction and the degree of hydration is given in Figure 20. Value of each parameter is given in Table 9. A good agreement is observed between model and experimental results for the three time-scales.

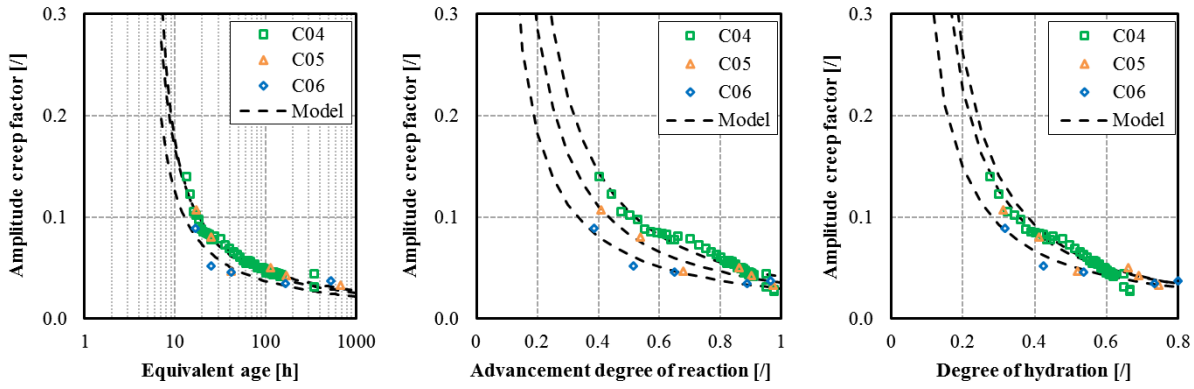

(a) (b) (c)

Figure 20 - Evolution of the amplitude of the creep factor according to the equivalent time (a), the advancement degree of reaction (b) and the degree of hydration (c)

For each composition, the amplitude creep factor decreases during the hardening process and is lower for concrete with higher water-cement ratio. However results of composition C04 and C05 are very close especially when regarding results according to the equivalent age and the degree of hydration.

For both time-scales the final value of the amplitude creep factor seems to converge to a same value. However, when regarding results according to the advancement degree of reaction, a clear difference is observed in the evolution of the creep factor for each water-cement ratio.

Table 9 – Amplitude creep factor parameters for different water-cement ratio

	$A_{t,1}$ [/]	$A_{t,2}$ [/]	A_α [/]	$a_{A,\alpha}$ [/]	A_ξ [/]	$a_{A,\xi}$ [/]
C0.4	6.58	-9.14	0.039	-1.38	0.024	-1.38
C0.5	7.32	-11.12	0.033	-1.26	0.025	-1.23
C0.6	8.28	-11.03	0.028	-1.10	0.024	-1.07

In Figure 21, main parameters of the three models are shown according to the effective water-cement ratio. A general linear relation is highlighted between parameters and effective w/c ratio. The kinetic parameters $a_{A,\alpha}$ and $a_{A,\xi}$ increase with the effective water-cement ratio meaning that a faster kinetic of the amplitude creep factor is observed for mixture with a higher water-cement ratio. Inversely, with the advancement degree of reaction, the amplitude creep factor decreases when the effective w/c ratio decreases. When regarding results according to the degree of hydration, the value A_ξ appears to be independent of the effective water-cement ratio with an average value of 0.024. This value is very close to the value of the amplitude creep factor at a degree of hydration equal to 1 and thus to the amplitude creep factor obtained with a complete hydration of the whole cement. Therefore, that means that the final value of the amplitude creep factor is dependent on the quantity of cement hydrated.

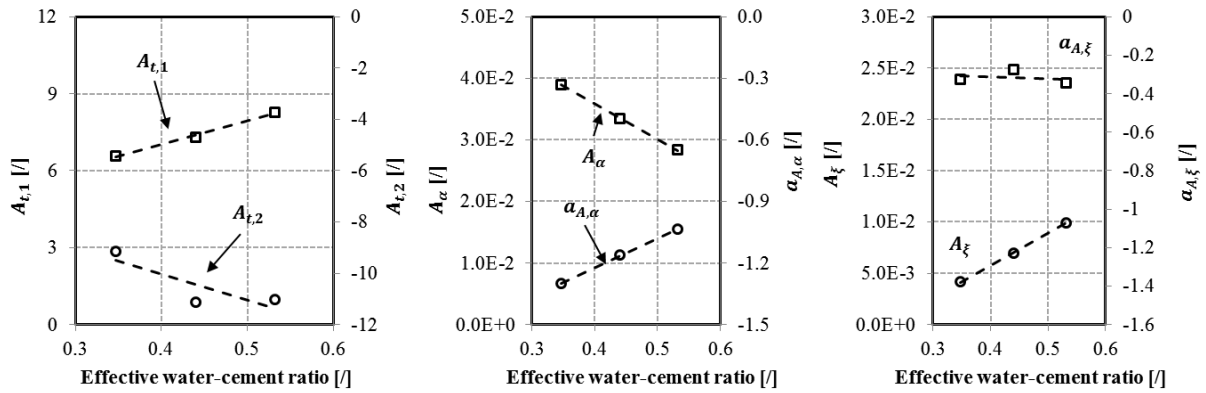

(a) (b) (c)

Figure 21 - Effect of water-cement ratio on the amplitude creep factor parameters of Equations 39, 40 and 41.

Equations linking parameters and effective water-cement ratio are given in Equations 42-45.

$$A_{t,1} = 9.19.\left(W_{eff}/C\right) + 3.35 \quad (42)$$

$$A_{t,2} = -10.25.\left(W_{eff}/C\right) - 5.93 \quad (43)$$

$$A_\alpha = -0.057.\left(W_{eff}/_C\right) + 0.059 \quad (44)$$

$$a_{A,\alpha} = 1.43.\left(W_{eff}/_C\right) - 1.79 \quad (45)$$

$$a_{A,\xi} = 1.66.\left(W_{eff}/_C\right) - 1.96 \quad (46)$$

The value of the kinetic coefficient is computed with least square method (by using the fminsearch function in Matlab©). Results of K are given in Figure 22 according to the equivalent time (a), the advancement degree of reaction (b) and the degree of hydration (c).

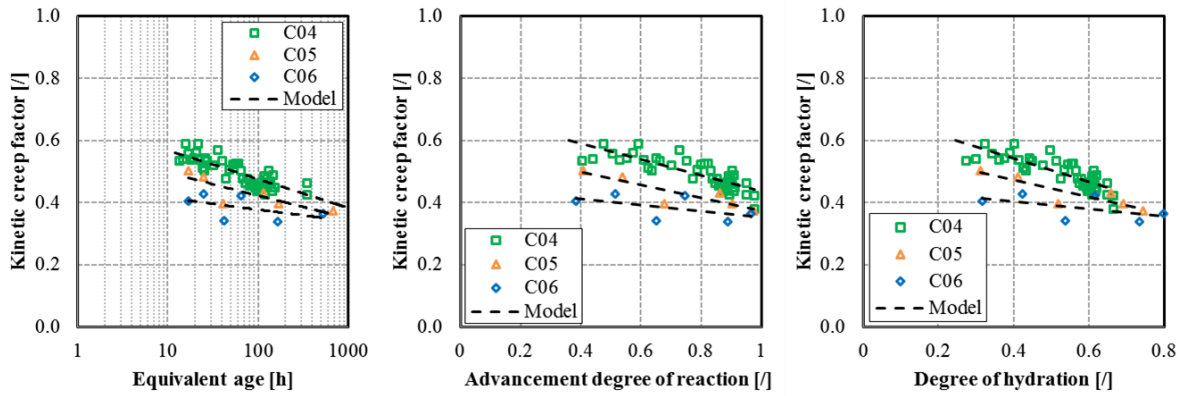

(a) (b) (c)

Figure 22 - Evolution of the kinetic creep factor according to the equivalent time (a), the advancement degree of reaction (b) and the degree of hydration (c)

For each composition, K decreases during the hydration process. For high water-cement ratio, the decrease of the kinetic parameter is very low and is nearly constant which is in coherence with results obtained in [28,29]. For lower water-cement ratio, the kinetic parameter varies significantly. In equivalent age, the kinetic parameter follows a logarithmic trend. With the advancement degree of reaction and the degree of hydration a linear trend is observed. Based on these observations, Equations 47, 48, and 49 are used to fit K (Figure 22).

$$K(t_{eq}) = K_{t,1}.\ln\left(\frac{t_{eq}}{t_K}\right) + K_{t,2} \quad (47)$$

$$K(\alpha) = K_\alpha.\alpha + P \quad (48)$$

$$K(\xi) = K_\xi.\xi + P \quad (49)$$

Where $t_K = 1h$, $K_{t,1}$, $K_{t,2}$, K_α, K and K_ξ are material parameters. Value of each parameter is given in Table 10 and is compared to the effective water-cement ratio in Figure 23. A linear relation is observed for all parameters. In addition, when regarding the value of K obtained for a degree of hydration equal to 1 ($K_\xi + P$), a same value of K is obtained for the three water-cement ratio (Table

10). Therefore, that means that the final value of the kinetic creep factor is dependent on the quantity of cement hydrated as the amplitude creep factor

Table 10 - Kinetic factor parameters for the three water-cement ratios

	$K_{t,1}$ (/)	$K_{t,2}$ (/)	K_α (/)	P (/)	K_ξ (/)	$K_\xi + P$ [/]
C0.4	-0.041	0.66	-0.26	0.69	-0.38	0.32
C0.5	-0.032	0.57	-0.21	0.58	-0.27	0.31
C0.6	-0.016	0.45	-0.10	0.45	-0.12	0.33

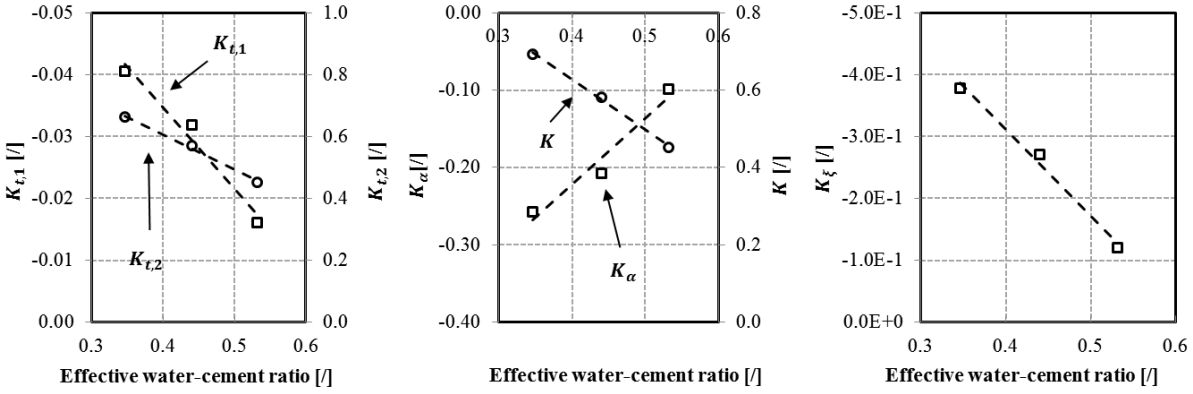

(a) (b) (c)

Figure 23 - Effect of water-cement ratio on the kinetic creep factor parameter of Equations 47, 48 and 49

Equations linking parameters and effective water-cement ratio are given in Equations 50-54.

$$K_{t,1} = 0.13.\left(W_{eff}/C\right) - 0.087 \quad (50)$$

$$K_{t,2} = -1.14.\left(W_{eff}/C\right) + 1.06 \quad (51)$$

$$K_\alpha = 0.86.\left(W_{eff}/C\right) - 0.56 \quad (52)$$

$$P = -1.30.\left(W_{eff}/C\right) + 1.15 \quad (53)$$

$$K_\xi = 1.40.\left(W_{eff}/C\right) - 0.87 \quad (54)$$

► Comparison with results of the literature

Repeated minute-long loading tests on cement paste with different water cement ratio (0.42, 0.45 and 0.5) were recently carried out [40]. A power law (Equation 55) was used to model the creep behaviour for short duration of loading.

$$\varepsilon_{cr}(t,t') = \sum_{i=1}^{n} \frac{F(t_i) - F(t_{i-1})}{A} \cdot \frac{1}{E_c(t')} \cdot \left(\frac{t-t'}{t_{ref}}\right)^{\beta} \qquad t_n \le t \le t_{n+1} \qquad 55$$

Where $t_{ref} = 1d$, E_c is the creep modulus which is related to the creep amplitude after 1 day of loading without change of the microstructure during loading, β is a material parameter which is related to the kinetic evolution of the basic creep. In this approach, the creep is also considered during the loading period. Creep strains develop already during the short loading process preceding the plateau of a creep test. In order to compare results obtained by Irfan, *et al.* [40] with the results obtained in this study, the creep strains are divided by the elastic strain which defines the creep coefficient (Equation 56). The ratio between the elastic modulus and the creep modulus corresponds to the creep coefficient after 1 day of loading with no evolution of the microstructure during the loading. This ratio is very close of the amplitude creep factor presented before in term of evolution. As the approach of Irfan, *et al.* [40] considered creep before the plateau of stress, the dimensionless ratio between the elastic modulus and the creep modulus is not exactly the same between both approaches

$$\varphi_c(t,t') = \frac{\varepsilon_{cr}(t,t')}{\varepsilon_{el}(t')} = \frac{E(t')}{E_c(t')} \cdot \left(\frac{(t-t')}{t_{ref}}\right)^{\beta} \qquad 56$$

In Figure 24, the evolution of the ratio E/E_c is shown for the different water-cement ratio. All results are very close and no impact of the water-cement ratio appears in the amplitude of the creep coefficient for short duration of loading. Thus the same observations are done here for water-cement ratio with a range 0.42 - 0.5. In contrast to the specific creep function, for short duration of loading the creep coefficient is not influenced by the water-cement ratio (till a value of 0.5).

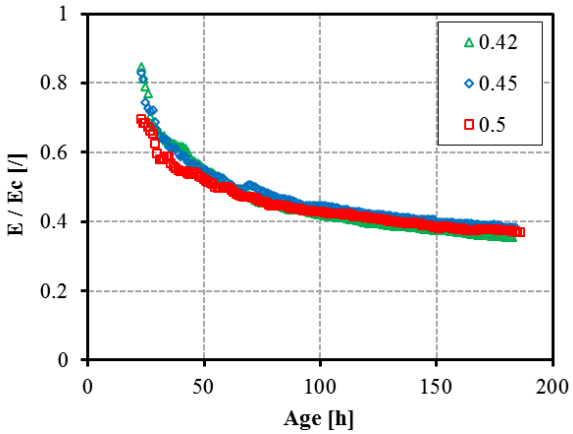

Figure 24 – Evolution of the ratio between the elastic modulus and the creep modulus for three cement pastes with different water-cement ratio (based on results of [40])

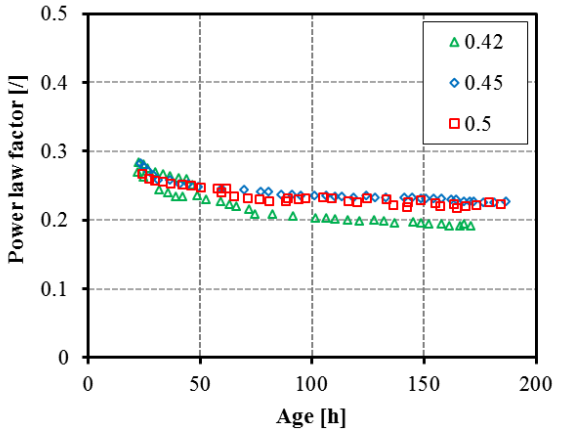

Figure 25 - Evolution of the power law factor of Equation 55 for three cement pastes with different water-cement ratio (based on results of [40])

In Figure 25, results of the power law factor β are presented for the three water-cement ratio. For a range of water-cement ratio between 0.4 and 0.5, no significant difference is observed for results obtained after an age of one day till an age of 2 days. After an age of 2 days, a smaller value of the power law factor is observed for the composition with a lower water-cement ratio (0.42). This observation is in discrepancy with results obtained on concrete.

6.2.3. Long duration creep test

► Modelling with separation of the short and long term creep

A new methodology is proposed in [29] to model basic creep for long duration of loading since very early age. The basic creep is divided in a short and long term creep. The short term creep is also divided in two terms: the initial short term creep and the solidification creep. Thus the specific creep function is divided in three terms (Equation 57):

- The initial short term creep C_{IST} is a logarithmic function (Equation 58) which depends on the actual state of the material (capillarity porosity, CSH…) when the load is applied. The initial short term creep is function of the E-modulus, two material parameters (k and h) and an amplitude creep factor A_{IST} which corresponds to the value of the creep coefficient after 2 hours of loading.
- The solidification term creep C_{ST} (Equation 59) is related to the development of the mechanical properties during loading [25]. This term is function of the E-modulus, a kinetic function K_{ST} (Equation 61) which is not dependent of the age at loading and an amplitude solidification factor A_{ST} (Equation 62) which depends on the age at loading.
- The long term creep C_{LT} is a power function (Equation 60) which is related to the viscous flow in the hydrates [24]. This term is function of two material parameters (f and g).

$$C(t,t') = C_{IST}(t,t') + C_{ST}(t,t') + C_{LT}(t,t') \quad (57)$$

$$C_{IST}(t,t') = \frac{h.A_{IST}(t')}{E(t')}.\ln\left(1+(t-t')^{k}\right) \quad (58)$$

$$C_{ST}(t,t') = \frac{A_{ST}(t')}{E(t')}.K_{ST}(t-t') \quad (59)$$

$$C_{LT}(t,t') = \frac{f}{g+1}.(t^{g+1}-t'^{g+1}) \quad (60)$$

$$K_{ST}(t-t') = \sum_{i=1}^{2}\frac{1}{E_i}.\left(1-\exp\left(-\frac{t-t'}{\tau_i}\right)\right) \quad (61)$$

$$A_{IST}(t') = \frac{1}{n.\ln\left(\frac{t}{1d}\right)+p}$$

$$A_{ST}(t') = l.\frac{dE}{dt}+m \quad (62)$$

Several creep tests of long duration on hardening and hardened concrete were carried out by Le Roy [41]. Through the several parameters studied during his PhD thesis, it included the effect of the water-cement ratio. Tests were carried out at an age of 1, 3, 7 and 28 days for mixture with an effective water-cement ratio range 0.28 – 0.42. The load applied to the sample corresponds to 30% of the compressive strength at the loading time. The description of the mixture proportions and value of the compressive strength and E-modulus are given in Complete details about the test procedure are presented in [41,42].

Table 11. Complete details about the test procedure are presented in [41,42].

Table 11 – Mixture proportions and materials properties of the concretes [41]

Composition	B1	B5	B6	B7
Gravel (Seine 5/20) (kg/m³)	1216	1204	1200	1202
Sand (Seine 0/5) (kg/m³)	669	660	658	659
CPA CEM I 52,5 (kg/m³)	398	355	429	373
Silica fume (kg/m³)	39.8	35.5	42.9	37.3
Superplasticizer (kg/m³)	19.3	17.2	20.1	18.1
Added water (kg/m³)	118	137	106	129
W_{tot}/C	0.33	0.419	0.279	0.379
$f_{c,1d}$ (MPa)	25.4	20.6	34.2	14.3
$f_{c,3d}$ (MPa)	51.5	35.6	53.7	37.8
$f_{c,7d}$ (MPa)	70.7	56.6	75.6	57.8
$f_{c,28d}$ (MPa)	92.1	74.6	97.3	79.5
E_{1d} (GPa)	30.8	29.2	38.6	23.1
E_{3d} (GPa)	43.1	41.1	47	40.7
E_{7d} (GPa)	46.4	44.6	51	43.7
E_{28d} (GPa)	50.4	46.9	53.4	45.3

A preliminary treatment of the Le Roy data is carried out in order to fit experimental data and remove noise from the measurement. This assures a better understanding of the physical mechanism which occurs at early age and in a hardened state for the study of the short and long term creep. The specific creep C(t,t') is fitted with 7 KV chains in series. The fitting carried out for each test is given in Figure 26 for each composition. Derivative of the E-modulus appears to be an important parameter which is related to the amplitude of the creep solidification (Equation 62). For that purpose, E-modulus is fitted with Equation 27. Results of the fitting are given in Figure 27. A very good agreement is observed between the fitting and the experimental results. Results of Le Roy are generally in coherence with results obtained in this paper. However, in term of water-cement ratio effect, the composition B7 does not follow the global tendency.

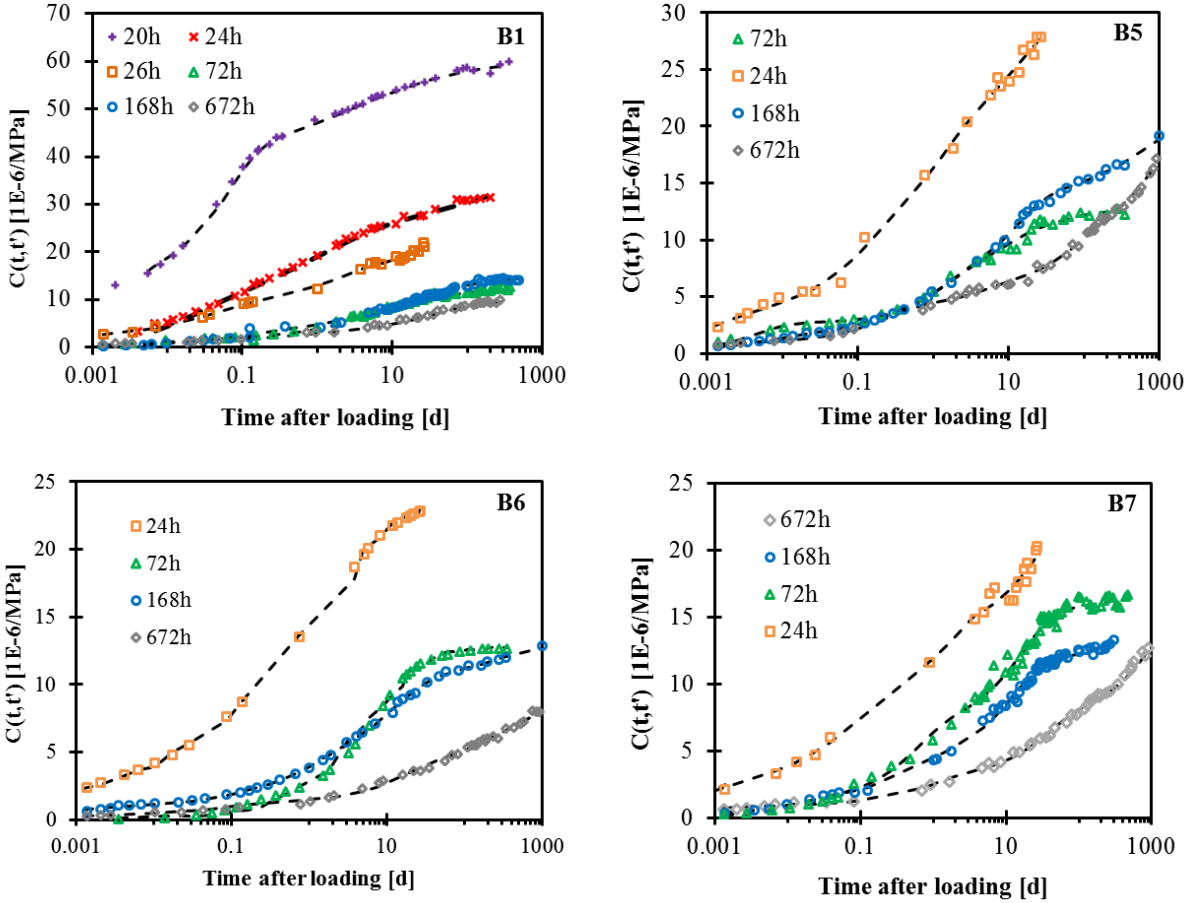

Figure 26 – Specific creep functions for several age at loading for the compositions B1, B5, B6 and B7

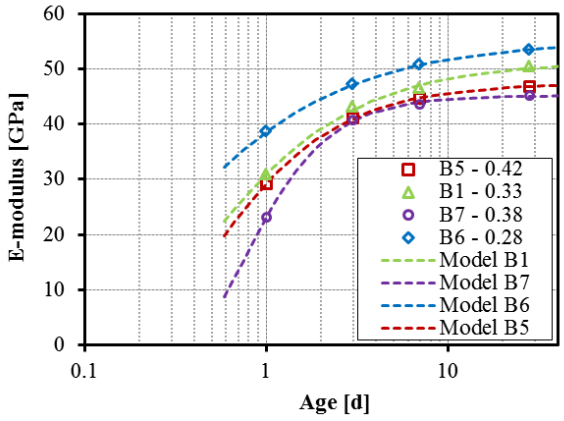

Figure 27 – E-modulus evolution for the different concrete composition of Le Roy [41] and modelling with Equation 27.

The first parameter studied is the long term creep. Acker, et al. [24] have highlighted that the basic creep rate follows a power trend after several days of loading (for early age loading) or several weeks (for loading at later age). Delsaute, et al. [29] highlights that for very early age loading (< 1d on an ordinary concrete), the power trend is already observable after one day of loading. The long term

creep of each composition is shown in Figure 28. All curves seem to follow the same trend especially at early age. However some dispersion is observable after an age of 10 days. This difference is in coherence with the variation of water-cement ratio. The amplitude of the creep rate decreases when the water-cement ratio decreases. Long term creep parameters f and g in Equation 60 are given according to the effective water-cement ratio in Figure 29. A linear relation with the water-cement ratio is observed for both parameters. The parameter f corresponds to the creep rate at an age of 1 day. This parameter appears to be lower for concrete with a higher water-cement ratio. The power parameter g decreases for concrete with lower water-cement ratio. The variation of amplitude of the long term creep is mainly governed by the parameter g. Several values of the parameter g were identified in the literature. For concrete a value between -1 and -0.9 is observed by [22] and between -0.72 and -0.69 is observed by [43]. Here values of g varying between -1.35 and -1.1 are obtained. For high water-cement ratio, the exponent parameter g is closer to value observed in the literature. This is in coherence with results obtained in [29] where for an effective water-cement ratio of 0.45, an exponent of -1 was obtained. This leads to the conclusion that the long term creep develops faster for concrete with a higher water-cement ratio. In the model B3 of Bazant [23], the water-cement ratio has no influence in the long term creep.

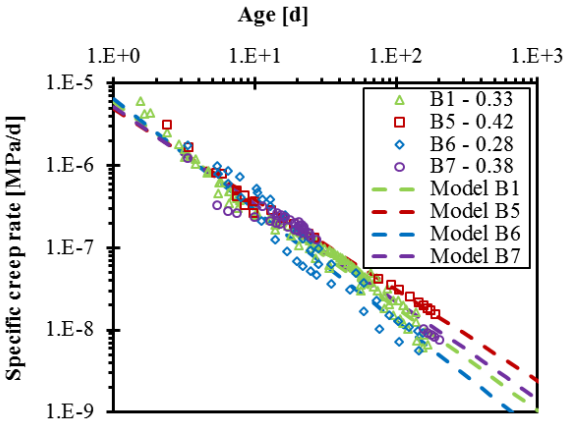

Figure 28 - Long term creep for different effective water-cement ratio

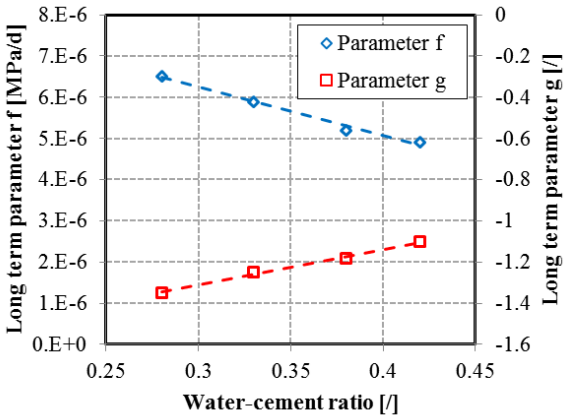

Figure 29 - Long term creep parameters according to the effective water-cement ratio

The second parameter studied is the initial short term creep. The amplitude of this parameter is linked to the value of the amplitude creep factor obtained with the repeated minute-long loading test (see Chapter 4, Section 6). It was shown in [28] that a direct linear relation exists between the creep coefficient obtained after 2 hours of loading and 5 minutes of loading. In order to define it, two operations are carried out on the results. First the long term creep is removed from the results. Secondly, each creep function, with the long term creep removed, is normalized by its value obtained after 2 hours of loading. In Figure 30, both operations are carried out for the different ages at loading of composition B1. All curves follow a same master curve during the first hours or days. As expected with results obtained with repeated minute-long loading test, the master curve follows a logarithmic trend (Equation 58). In Figure 31, results of the normalized initial short term creep coming from the 4 compositions are presented. Only results following the logarithmic trend are plotted. When this logarithmic trend is not followed anymore, it is assumed that it represents the effect of the solidification of the material. For specimen loaded at early age, the solidification phenomenon is already marked after few hours of loading (see Figure 30). For concrete loaded at later ages, solidification phenomenon appears after several days. During the first days after loading, no difference is observed in the kinetic of the initial short term creep for the different ages at loading and

the different compositions. Therefore it is observed that there is no effect of the age at loading (for age at loading higher than 1 day) and no effect of the water-cement ratio (for a range between 0.28 and 0.42) on the kinetic of the initial short term creep.

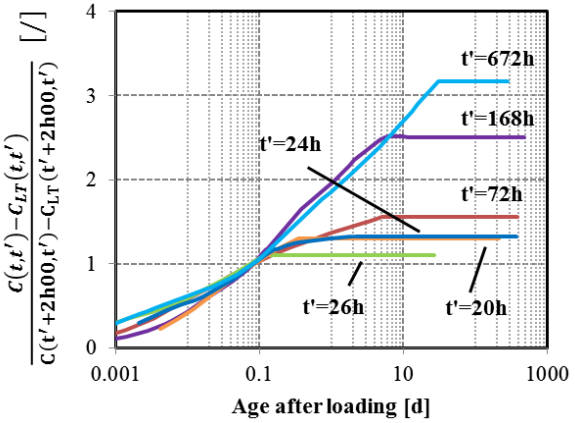

Figure 30 - Evolution of the specific creep after removing the long term creep and normalized each creep curves by their own values obtained at an age after loading of 2 hours for the composition B1.

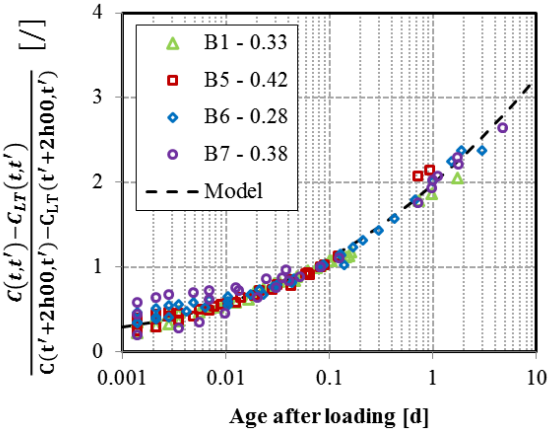

Figure 31 – Evolution of the normalized initial short term creep for each composition.

For each composition, the value of the initial short term creep coefficient obtained after 2 hours of loading is defined and is plotted according to the age at loading in Figure 32. All results seem generally to follow a same master curve. No effect of the water-cement ratio is detected. This is in coherence with results of repeated minute-long loading test obtained in this study and by [40]. For water-cement ratio lower than 0.42 no difference is observed in the evolution of the amplitude creep factor.

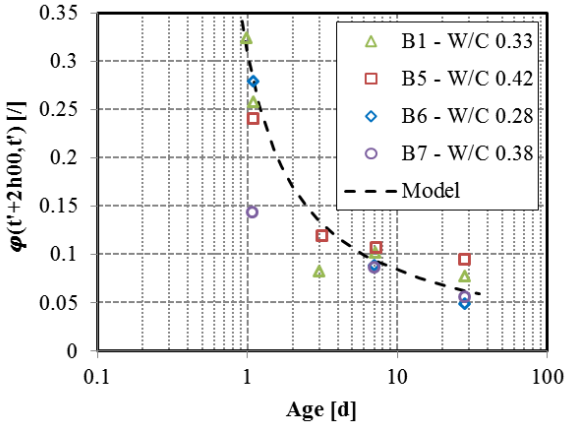

Figure 32 - Evolution of the creep coefficient after 2 hours of loading according to the age at loading.

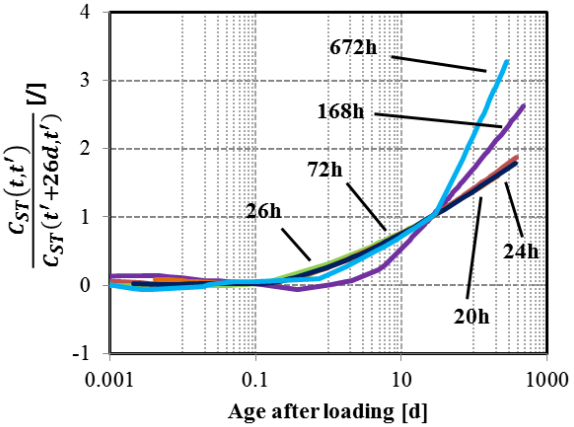

Figure 33 - Evolution of the normalized (26 days) solidification creep for the composition B1.

The third and last parameter studied is the solidification term creep. The amplitude of this parameter is linked to the derivative of the E-modulus [29]. As for the initial short term creep, two operations are needed in order to characterize the solidification term creep. First the solidification term creep is obtained after removing the long term creep and the initial short term creep from the results. Secondly, each solidification creep functions are normalized by their value obtained after 26 days of

loading. In Figure 33, both operations are carried out for composition B1. For early age loading ($\leq$ 3 days), the solidification term creep evolves strongly during the first days after loading and has high amplitude. When normalized, the solidification creep follows a same master curve. For later ages at loading, the amplitude of the solidification phenomenon is very low and therefore is very difficult to assess especially when already two subtractions were already applied to the results. That's certainly why, in Figure 33, results for an age at loading of 7 and 28 days do not follow the same tendency. The average results obtained from early age loading is presented for the different composition in Figure 34. No effect of the water-cement ratio is observed on the kinetic of the solidification term creep.

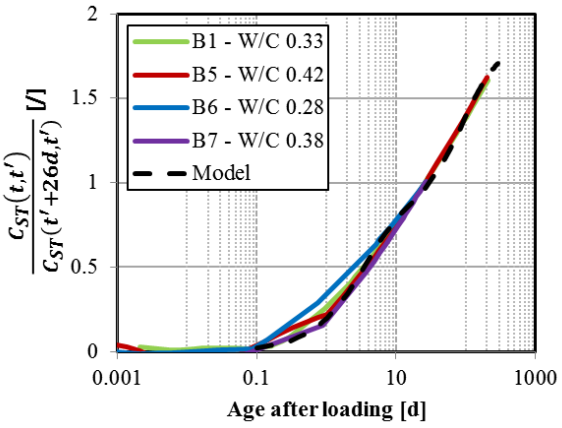

Figure 34 - Evolution of the normalized solidification creep for each composition.

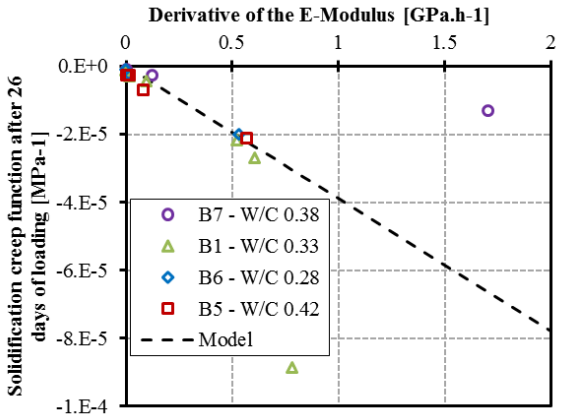

Figure 35 - Amplitude of the solidification creep obtained after an age after loading of 26 days versus the derivative of the E-modulus obtained at the age of loading

In Figure 35, the amplitude of the solidification term creep (corresponding to the value of the solidification creep function obtained after an age after loading of 26 days) is compared to the derivative of the E-modulus for each age at loading of each composition. A general same linear relation is obtained. However some dispersion occurs for age at loading of 1 day or less for composition B1 and B7. This dispersion can come from the computation of the derivative of the E-modulus or the experimental results. Indeed, for the composition B1, no data for age lower than 1 day exists and then the value of the E-modulus before this age could not be modeled with very good accuracy. For the composition B7, it was already noticed that the results of the E-modulus does not follow the general trend in term of amplitude and kinetic especially the result obtained for an age at loading of 1 day (Figure 27). For all other results, no effect of the water-cement ratio is detected. It could then be concluded that the relation between the amplitude of the solidification creep and the derivative of the E-modulus is independent on the water-cement ratio.

Values of each parameter of the model are given in Table 12 or are plotted in Figure 29.

Table 12 - creep factor parameters which are independent on the effective W/C ratio

h [/]	k [/]	l [h.GPa-1]	m [/]	n [/]	p [/]	E_1 [/]	τ_1 [d]	E_2 [/]	τ_2 [d]
2.9	0.325	-3.9E-5	0	3.8	3.2	1.39	3.4	0.97	94.6

It is thus concluded that the new methodology presented in [29] can be used for concrete for different low water-cement ratio (range 0.28-0.42). The main observations are:

- Long term creep is higher for composition with high water-cement ratio
- The kinetic and the amplitude of the initial short term creep is not influenced by the water-cement ratio.
- The kinetic of the solidification term creep is not influenced by the water-cement ratio. The linear relation between the derivative of the E-modulus and the amplitude of the solidification term creep is independent on the water-cement ratio.

It was also proposed in [29] to model long duration creep by using an adapted version of the Model Code 2010 (MC2010). As presented in [42,44], MC2010 can be simplified in Equation 63, where the parameter C is related to the general amplitude of the creep, is independent of the age at loading and is expressed in MPa. The parameter τ is only function of the age at loading and is expressed in [d].

$$C(t,t') = \frac{1}{C}.\ln\left(1+\frac{t-t'}{\tau}\right) \qquad 63$$

Results of the modelling with the adapted MC2010 are presented in Figure 36 for the four compositions. In order to improve the modelling, only creep results obtained after several days of loading were considered for concrete loaded at very early age (less than 26 hours). A general very good correspondence is obtained between experimental results and the modelling particularly for hardened concrete. For loading applied at an age of 26 hours or less, the model is not able to correctly fit in the same time creep occurring during the first days after loading and for long duration. That leads, at very early age, to an overestimation of the creep phenomenon during the first days after loading. In case of restrained deformation in massive structure, this conducts to a decrease of the compressive stresses and then to an increase of the tensile stresses. Therefore, for massive structure, the adapted version of MC2010 yields safe-side predictions (expected tensile stresses are overestimated). Whereas the inverse situation is obtained for thin concrete element such as a wall for which the displacements are restrained by its foundation. In that case, the tensile stresses are underestimated during very early age with the adapted MC2010. For long duration creep, the correspondence is very good whatever the age at loading. This is in coherence with results obtained with the previous model considering that creep is divided in three terms. Indeed, the variation of the exponent g of the long term creep was observed but this variation is small and in addition the value of the exponent was close to a value of -1 for each composition, therefore it is normal that a logarithmic law for which the compliance rate tends to 1/Ct can correctly fitted these creep results.

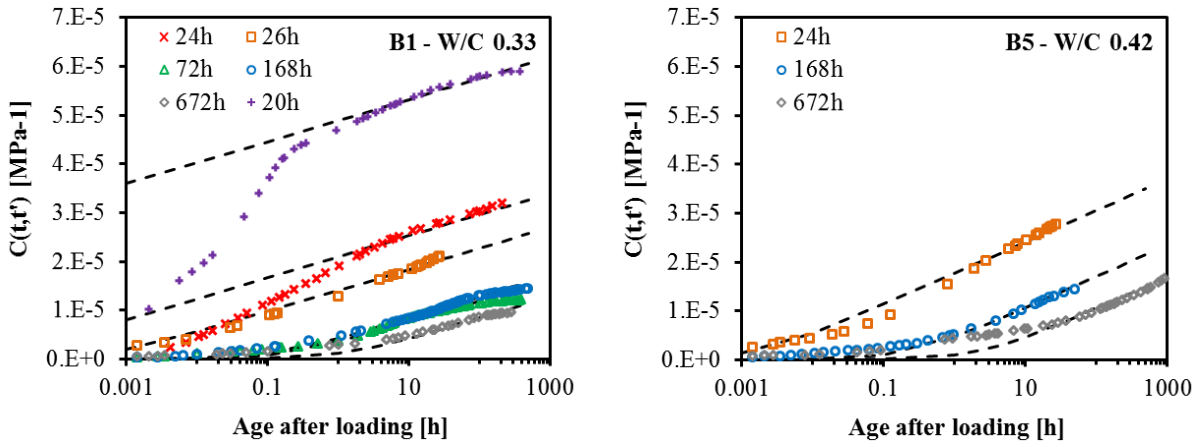

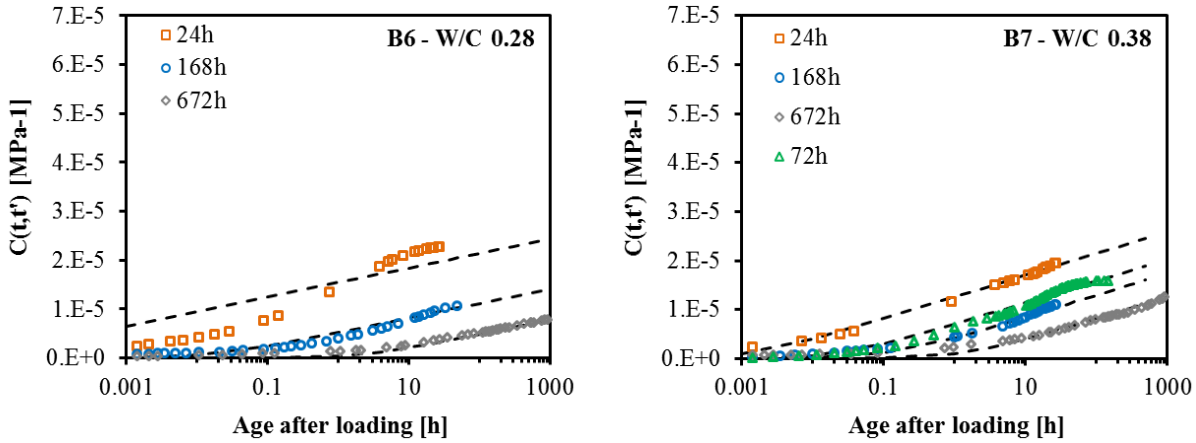

Figure 36 – Specific creep and adapted MC2010 (dashed lines) for composition B1, B5, B6 and B7

The amplitude parameter C of the adapted MC2010 is shown in Figure 37 according to the water-cement ratio. It is observed, as in [42], that this parameter is linearly dependent of the water/cement ratio for compositions with a same aggregate content. Higher is the water/cement ratio lower is the parameter. This means that creep on long duration is higher for concrete with a high water-cement ratio. These values obtained from experimental results are also compared in this figure to the value predicted by the Model Code 2010. Results are in very good agreement with the predicted value of MC2010.

The value of the parameter τ is plotted according to the inverse of the derivative of the E-modulus in Figure 38. Predictive values obtained with MC2010 are also presented. For hardened concrete, a very good correspondence is obtained. No effect of the water-cement ratio is observed whatever the age at loading for experimental results and predictive values of MC2010. For concrete loaded at an age around 24 hours, a difference occurs between the predictive values of MC2010 and the experimental results. This confirms the observations realized with the ordinary concrete in the chapter 4, section 7. MC2010, in its actual state, is not able to predict accurately the effect of the age at loading during the very early creep of high performance concrete and classical concrete. An adaptation is needed (as proposed in the chapter 4, section 7) for the parameter τ to correctly consider creep at early age and the parameter C needs to be changed for high performance concrete with low water-cement ratio.

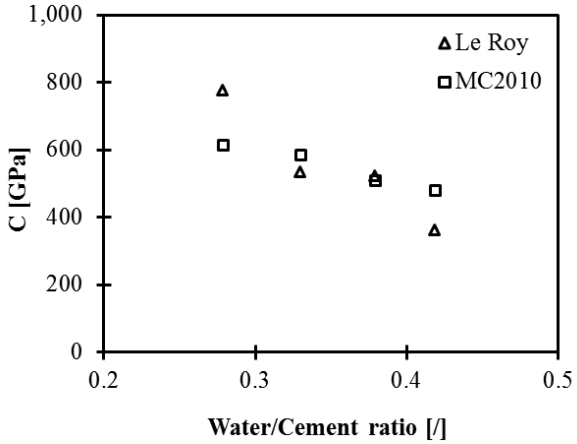

Figure 37 – Relation between the parameter C of the adapted MC2010 and the water/cement ratio.

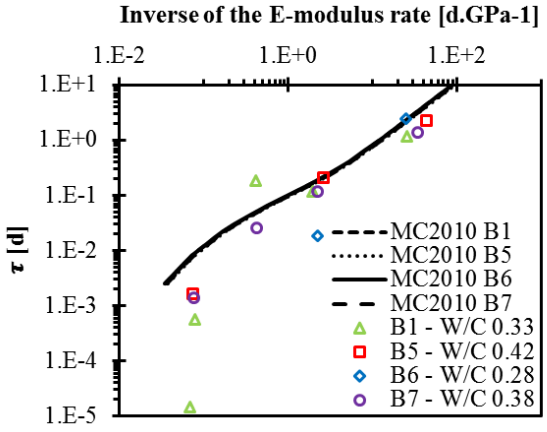

Figure 38 – Relation between the parameter τ of the adapted MC2010 and the inverse of the E-modulus rate.

6.2.4. Discussion

For the physical understanding of the different observations achieved, the evolution of the microstructure of the cement paste corresponding to the concretes called C0.4, C0.5 and C0.6 has been computed with the software VCCTL (V9.5) [45]. According to the literature, two main microstructural parameters govern the viscoelastic behaviour of cement based material: the capillarity pores and the CSH [28]. The E-modulus increases when the volume fraction of capillarity pore decreases and when the volume fraction of CSH increases. The creep has an opposite correlation with the capillarity pores and the CSH [28]. Several models, aimed at predicting the value of the E-modulus [39,45–48] and creep [49,50] on the basis of the knowledge of the microstructure, were developed in the past. However, the volume fraction of each constituent itself is not enough. Knowledge of the density [51] and the shape of the CSH are needed as also the size distribution [52], the number and the shape of capillarity pores [53]. In spite of all variables needed, the gel-space ratio GS alone is a good indicator which considers together capillarity pores and CSH [40,54]. The gel-space ratio is defined as the volume of gel divided by the sum of the volumes of gel and capillarity pores [54].

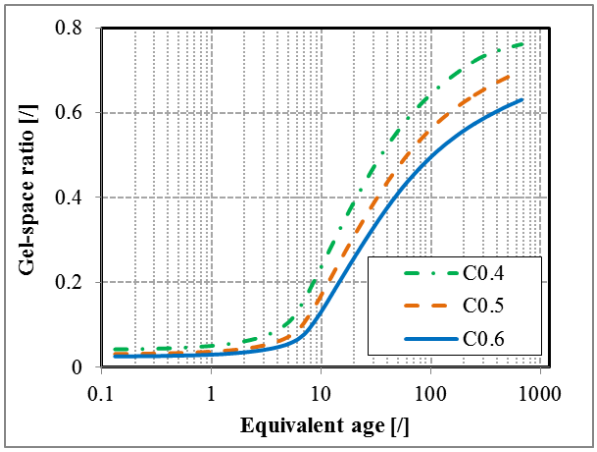

Figure 39 - Evolution of the gel-space ratio for different water-cement ratios (VCCTL V9.5).

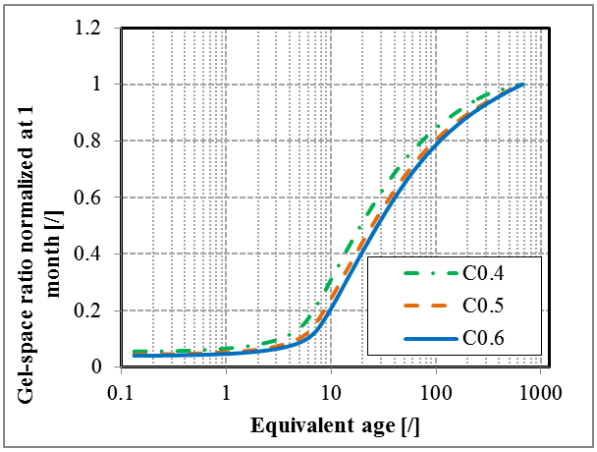

Figure 40 - Evolution of the gel-space ratio normalized at an equivalent age of 1 month for three water-cement ratios (VCCTL V9.5).

The evolution of the gel-space ratio is presented in Figure 39 for the three water-cement ratio. As expected, for low water-cement ratio a higher value of the gel-space ratio is obtained. A similar kinetic is observed for the different water-cement ratio. In order to highlight it, each evolution of the gel-space ratio is normalized by their own value obtained at an age of one month in Figure 40. Each evolution follows a nearly identical evolution especially for composition C0.5 and C0.6. However a slight variation in kinetic is observed for composition C0.4. Thus, the subsequent is observed, for the different water-cement ratio studied, the kinetic evolution of the gel-space ratio is very similar and only the amplitude of the gel-space ratio changes significantly. A similar observation is also done with the evolution of the mechanical properties such as the compressive strength and the E-modulus. Powers [54] has shown that the compressive strength of concrete is proportional to the gel-space ratio. The relationship between the gel-space ratio and the compressive strength is independent on the age of the concrete and its mix proportions. In Figure 41a, the compressive strength is plotted according to the gel-space ratio. A linear relation is observed for the different water-cement ratios for a range of compressive strength between 15 and 50 MPa. Therefore compressive strength is modelled according to the gel-space ratio with a linear relation. In comparison, results obtained since setting time till three months [28,55] of an ordinary concrete (OC) using a cement of a same class and a different

granulometry are shown. The linear relation obtained for the compositions C0.4 corresponds very well to the value of the compressive strength of the ordinary concrete since setting. Since setting time till several months, the relation between the gel-space ratio and the compressive strength is thus linear. From results of the literature, a less linear relation is observed. Powers [54] uses a cubic function and Pichler, *et al.* [56] use a power law for which the exponent varies between 2.11 and 3.42.

In Figure 41b, the E-modulus is presented according to the gel-space ratio for the three water-cement ratios and the ordinary concrete. No effect of the water-cement ratio is observed in the relation linking the gel-space ratio and the E-modulus. For a same gel-space ratio, a lower value of the E-modulus is observed for the ordinary concrete. This difference is explained by the difference of granulometry. The ordinary concrete has a lower quantity of aggregate. Whereas an increase of the aggregate content leads to a global increase of the evolution of the E-modulus of concrete and has no effect on the evolution of the gel-space ratio of the cement paste. It is then concluded that the relation between the E-modulus and the gel-space ratio is not affected by the water-cement content but by the aggregate content. The evolution of the E-modulus is modelled according to the gel-space ratio by Equation 64. This model allows well-fitting the evolution of the E-modulus by using least square method. More investigations about the effect of the aggregate on the evolution of the E-modulus are presented in chapter 7.

$$E = 60.74\text{GPa} * \exp\left(-\frac{0.201}{GS}\right) \qquad 64$$

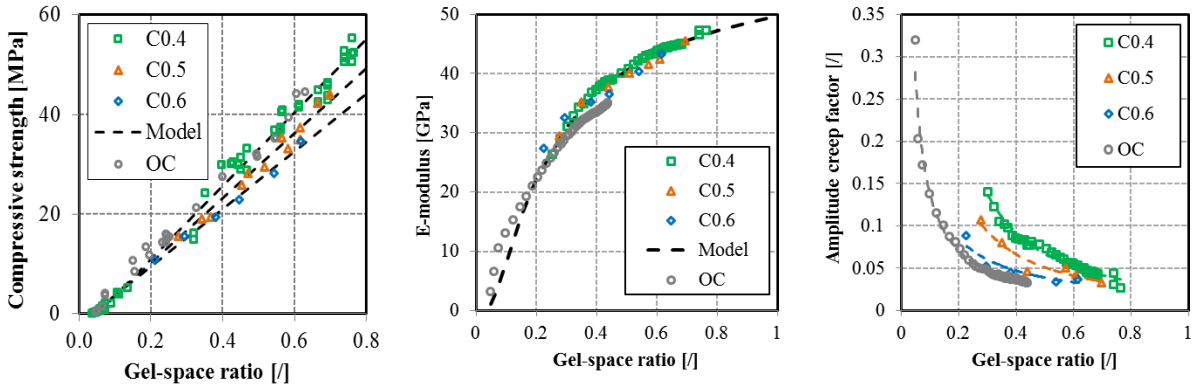

(a) (b) (c)

Figure 41 – Evolution of the compressive strength (a), the E-modulus (b) and the amplitude creep factor according to the gel space ratio.

In Figure 41c, the evolution of the aging creep factor is presented according to the gel-space ratio for the three water-cement ratio and the ordinary concrete. As with the advancement degree of reaction and the degree of hydration, an effect of the water-cement ratio is clearly visible. The amplitude creep factor corresponds to the creep coefficient obtained after duration of loading of 5 minutes. For a same gel-space ratio, the E-modulus is the same for each composition. Thus, the difference observed comes only from the creep strain. For a same E-modulus, the composition with a high water-cement ratio creeps less. This observation is strongly visible when concrete has a gel-space ratio lower than 0.5. For the understanding of this observation, the volume fraction of the capillarity pore and the CSH is plotted according to the gel-space ratio in Figure 42. The volume fraction of the CSH does not vary significantly between each composition. The volume fraction of capillarity pores differs relevantly between each composition for low gel-space ratio. For high water-cement ratio, the volume fraction of capillarity pore is higher. However it should be expected, according to the physical mechanism linked to the short term creep, that creep will be higher for composition with a high volume fraction of

capillarity pores. But here several aspects are not considered as the thickness of the adsorbed water layer and the internal surface area of empty pore. The thickness of the adsorption layer will change during the hydration process. Variation of the thickness will lead to a change of the surface energy of the gel particles. This change will be accompanied by external volume changes [57]. These parameters could explain this difference. Indeed, for a same E-modulus, the age of the material is not the same for the different composition. Therefore the state of the microstructure is not the same. Other parameter such as the pore size distribution could also give explanation on these observations. However, for a complete understanding of the mechanisms, experimental and modelling results are needed at the microstructural level.

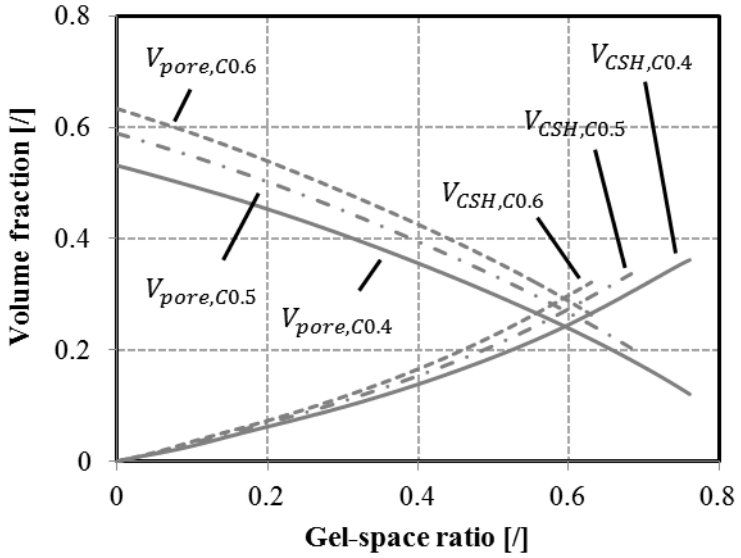

Figure 42 – Evolution of the volume fraction of CSH and capillarity pores according to the gel space ratio.

The evolution of the amplitude creep factor is modelled according to the gel-space ratio with a power function (Equation 65) for which two parameters (Equations 66 and 67) depend on the water-cement ratio. This model allows well-fitting the evolution of the amplitude creep factor since setting time (ordinary concrete) till one month by using least and square method. As shown in Figure 43, the amplitude (Equation 66) and the kinetic (Equation 36) factors depend linearly on the effective water-cement ratio.

$$A = A_{GS,1}.GS^{A_{GS,2}} \quad 65$$

$$A_{GS,1} = -0.021.\left(W_{eff}/_{C}\right) + 0.032 \quad 66$$

$$A_{GS,2} = 2.98.\left(W_{eff}/_{C}\right) - 2.46 \quad 67$$

From results of Irfan, *et al.* [40], the same comparison is done in Figure 44. A same power trend is observed between the ratio E/E_c and the gel-space ratio. Also a same linear relation is also observed between the water-cement ratio and the parameters $A_{GS,1}$ and $A_{GS,2}$.

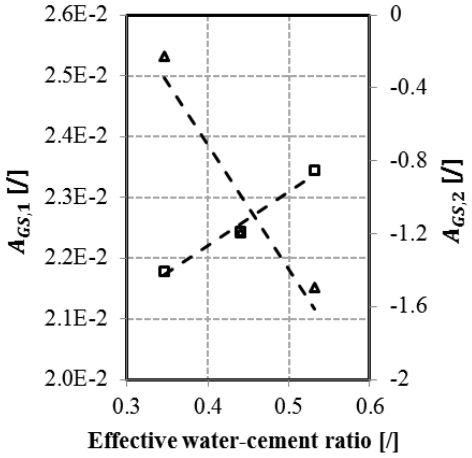

Figure 43 - Effect of water-cement ratio on the amplitude creep factor parameter of Equations 65, 66 and 67.

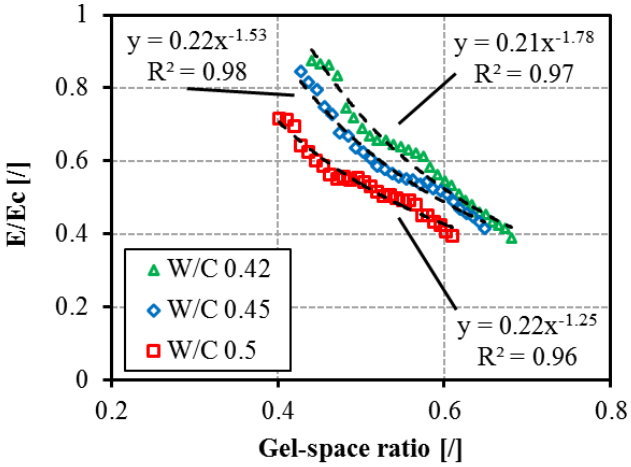

Figure 44 - E/Ec versus the gel-space ratio for cement pastes with three different W/C studied since an age of 24h00 [40].

CONCLUSIONS

Section 6.1

Every 160 minutes, thermal variations of 3°C are applied on a concrete sample with the device so-called BTJADE. Thermal and autogenous strains are distinguished by creating a fictive thermal cure at 20°C from the experimental results.

New models are proposed for the characterization of the autogenous strain and the coefficient of thermal expansion since setting. For both properties, models were developed according to the equivalent and the advancement degree of reaction for computational purpose. Physical mechanisms are highlighted and considered in the modelling.

Through results of the modelling of the autogenous strain, it is observed that the difference between the final amplitude of the swelling and the shrinkage is higher for concrete composition with a higher water-cement ratio.

It is observed that swelling and decrease of the CTE after the initial setting time are linked to a same mechanism as for the increase of the CTE and the self-desiccation. The relation between the CTE and the autogenous deformation is linear but the effect of the mixture content is not the same during the swelling and the shrinkage period.

Through comparison between the experimental results and the setting time obtained with ultrasonic measurement and penetration resistance test, it is observed that:

- the initial setting time is associated to the moment when the value of the CTE does not correspond anymore to a liquid.
- the final setting time is associated to a minimum of the autogenous strain obtained before the swelling of the concrete. This value corresponds to a zero value of the derivative of the autogenous strain.

For further study, the evolution of the relative humidity should be measured during the test and considered in the modelling.

Section 6.2

Repeated minute-long loading tests were applied on three concrete compositions with three different effective water-cement ratios (0.35, 0.44 and 0.53) since very early age. The Poisson's ratio, the E-modulus and an amplitude creep factor correspond to the creep coefficient obtained after 5 minutes of loading are defined. For all the investigated properties, new or existing models are used. Models are expressed in function of the equivalent time, the advancement degree of reaction and the degree of hydration for the understanding of the physical mechanisms associated to the water-cement ratio and also for computational modelling purpose. Results were compared with results of the literature on cement paste and show a very good agreement.

For the study of the long term creep, data from Le Roy [41] were used. A new modelling methodology is used for concrete with different low water-cement ratio (range 0.28-0.42). The main observations are:

- Long term creep is higher for composition with high water-cement ratio

- The kinetic and the amplitude of the initial short term creep is not influenced by the water-cement ratio.
- The kinetic of the solidification term creep is not influenced by the water-cement ratio. The linear relation between the derivative of the E-modulus and the amplitude of the solidification term creep is independent on the water-cement ratio.

An adapted version of the Model Code 2010 (MC2010) is also used to model basic creep. It is possible to model accurately the specific creep especially for hardened concrete. For very early age, creep is overestimated during few days after loading. Results predict by MC2010 are compared. The general amplitude of the creep is underestimated for law water-cement ratio. For hardened concrete, the effect of the age at loading is well considered and corresponds very well to the experimental results. For very early age, an adaptation of the aging factor is needed as proposed in chapter 4, section 7.

Short term creep is compared to the E-modulus for the different concrete compositions. It is observed that for a same E-modulus, concrete with low water-cement ratio creeps more.

REFERENCES

[1] W.R. Lorman, The theory of concrete creep, Proc. ASTM. 40 (1940) 1082–1102.

[2] J. Carette, S. Staquet, Monitoring and modelling the early age and hardening behaviour of eco-concrete through continuous non-destructive measurements: Part I. Hydration and apparent activation energy, Cem. Concr. Compos. 73 (2016) 10–18. doi:10.1016/j.cemconcomp.2016.07.002.

[3] J. Carette, S. Staquet, Monitoring the setting process of eco-binders by ultrasonic P-wave and S-wave transmission velocity measurement: Mortar vs concrete, Constr. Build. Mater. 110 (2016) 32–41. doi:10.1016/j.conbuildmat.2016.02.019.

[4] J. Carette, S. Staquet, Monitoring the setting process of mortars by ultrasonic P and S-wave transmission velocity measurement, Constr. Build. Mater. 94 (2015) 196–208. doi:10.1016/j.conbuildmat.2015.06.054.

[5] ASTM C403, Standard test method for time of setting of concrete mixtures by penetration resistance, in: Am. Soc. Test. Mater., 2008. doi:10.1520/C0403_C0403M-08.

[6] C. Boulay, Test rig for early age measurements of the autogenous shrinkage of a concrete, in: Proc. RILEM-JCJ Int. Work. ConCrack 3, 2012: pp. 111–122.

[7] G. Sant, B. Lothenbach, P. Juilland, G. Le Saout, J. Weiss, K. Scrivener, The origin of early age expansions induced in cementitious materials containing shrinkage reducing admixtures, Cem. Concr. Res. 41 (2011) 218–229. doi:10.1016/j.cemconres.2010.12.004.

[8] V. Baroghel-Bouny, P. Mounanga, A. Khelidj, A. Loukili, N. Rafaï, Autogenous deformations of cement pastes, Cem. Concr. Res. 36 (2006) 123–136. doi:10.1016/j.cemconres.2004.10.020.

[9] M. Ozawa, H. Morimoto, Estimation method for thermal expansion coefficient of concrete at early ages, in: Int. RILEM Conf. Vol. Chang. Hardening Concr. Test. Mitig., 2006: pp. 331–339. doi:10.1617/2351580052.035.

[10] I. Maruyama, A. Teramoto, G. Igarashi, Strain and thermal expansion coefficients of various cement pastes during hydration at early ages, Mater. Struct. 47 (2014) 27–37. doi:10.1617/s11527-013-0042-4.

[11] G. De Schutter, L. Taerwe, Degree of hydration-based description of mechanical properties of early age concrete, Mater. Struct. 29 (1996) 335–344. doi:10.1007/BF02486341.

[12] Z. Liu, W. Hansen, Aggregate and slag cement effects on autogenous shrinkage in cementitious materials, Constr. Build. Mater. 121 (2016) 429–436. doi:10.1016/j.conbuildmat.2016.06.012.

[13] R. Wendner, M.H. Hubler, Z.P. Bažant, The B4 Model for Multi-decade Creep and Shrinkage Prediction, in: Mech. Phys. Creep, Shrinkage, Durab. Concr., American Society of Civil Engineers, Reston, VA, 2013: pp. 429–436. doi:10.1061/9780784413111.051.

[14] F. Benboudjema, J.M. Torrenti, Early-age behaviour of concrete nuclear containments, Nucl. Eng. Des. 238 (2008) 2495–2506. doi:10.1016/j.nucengdes.2008.04.009.

[15] A. Darquennes, F. Benboudjema, Analyse de la sensibilité à la fissuration au jeune âge en conditions endogènes des matériaux cimentaires avec laitier de haut-fourneau, in: Regroupement Francoph. Pour La Rech. La Form. Sur Le Bét., Lyon, 2012.

[16] G. Sant, P. Lura, J. Weiss, A discussion of analysis approaches for determining “time-zero” from chemical shrinkage and autogenous strain measurements in cement paste, in: Int. RILEM

Conf. Vol. Chang. Hardening Concr. Test. Mitig., Lyngby, 2006: pp. 375–383. http://www.rilem.net/gene/main.php?base=500218&id_publication=57&id_papier=2271.

[17] R. Loser, B. Münch, P. Lura, A volumetric technique for measuring the coefficient of thermal expansion of hardening cement paste and mortar, Cem. Concr. Res. 40 (2010) 1138–1147. doi:10.1016/j.cemconres.2010.03.021.

[18] M. Wyrzykowski, P. Lura, Moisture dependence of thermal expansion in cement-based materials at early ages, Cem. Concr. Res. 53 (2013) 25–35. doi:10.1016/j.cemconres.2013.05.016.

[19] M. Wyrzykowski, P. Lura, Controlling the coefficient of thermal expansion of cementitious materials - A new application for superabsorbent polymers, Cem. Concr. Compos. 35 (2013) 49–58. doi:10.1016/j.cemconcomp.2012.08.010.

[20] ACI Committee 209, Guide for Modeling and Calculating Shrinkage and Creep in Hardened Concrete, 2008.

[21] H. Muller, I. Anders, B. R., Concrete: treatment of types and properties in fib Model Code 2010, Struct. Concr. 14 (2013) 320–334. doi:10.1002/suco.201200048.

[22] Z.P. Bažant, Creep and shrinkage prediction model for analysis and design of concrete structures - Model B-3, Mater. Struct. 28 (1995) 357–365.

[23] Z.P. Bazant, S. Baweja, Creep and Shrinkage Prediction Model for Analysis and Design of Concrete Structures : Model B3, ACI Concr. Int. 83 (2001) 38–39.

[24] P. Acker, F.J. Ulm, Creep and shrinkage of concrete: Physical origins and practical measurements, Nucl. Eng. Des. 203 (2001) 143–158. doi:10.1016/S0029-5493(00)00304-6.

[25] Z.P. Bazant, S. Prasannan, Solidification theory for aging creep. I: Formulation, J. Eng. Mech. 115 (1989) 1691–1703. doi:10.1016/0008-8846(88)90028-2.

[26] Z.P. Bažant, A.B. Hauggaard, S. Baweja, F.-J. Ulm, Microprestress-Solidification Theory for Concrete Creep. I Aging and Drying Effects, J. Eng. Mech. 123 (1997) 1188–1194.

[27] V. Waller, Relations entre compositions des bétons, exothermie en cours de prise et résistance en compression, PhD thesis, Laboratoire Centrale des Ponts et Chaussées, 2000.

[28] B. Delsaute, C. Boulay, S. Staquet, Creep testing of concrete since setting time by means of permanent and repeated minute-long loadings, Cem. Concr. Compos. 73 (2016) 75–88. doi:10.1016/j.cemconcomp.2016.07.005.

[29] B. Delsaute, J.-M. Torrenti, S. Staquet, Modeling basic creep of concrete since setting time, Cem. Concr. Compos. (2016) under review.

[30] T. Instruments, http://www.tainstruments.com/pdf/brochure/TAM%20AIR%20brochure.pdf, (2013) 23.

[31] J. Bolomey, Détermination de la résistance probable d'un béton connaissant son dosage et sa densité au moment du gâchage, Bull. Tech. La Suisse Rom. (1929). doi:http://dx.doi.org/10.5169/seals-42676 Nutzungsbedingungen.

[32] M. Féret, Sur la compacité des mortiers hydrauliques, Ann. Des Ponts Chaussées. 4 (1892) 427. http://gallicalabs.bnf.fr/ark:/12148/bpt6k4084622/f335.item.r=1844 Dupuit.zoom.

[33] T. C. Powers, T. L. Brownyard, Studies of the Physical Properties of Hardened Portland Cement Paste, 43 (1948).

[34] D.A. Abrams, Design of Concrete Mixtures, Struct. Mater. Res. Lab. Lewis Institute, Chicago. Bulletin 1 (1918).

[35] B. Delsaute, C. Boulay, J. Granja, J. Carette, M. Azenha, C. Dumoulin, et al., Testing Concrete E-modulus at Very Early Ages Through Several Techniques: An Inter-laboratory Comparison, Strain. 52 (2016) 91–109. doi:10.1111/str.12172.

[36] J. Carette, S. Staquet, Monitoring and modelling the early age and hardening behaviour of eco-concrete through continuous non-destructive measurements: Part II. Mechanical behaviour, Cem. Concr. Compos. 73 (2016) 1–9. doi:10.1016/j.cemconcomp.2016.07.003.

[37] J. Byfors, Plain concrete at early ages, PhD thesis, Swedish Cement and Concrete Res. Inst., 1980.

[38] H.A. Mesbah, M. Lachemi, P.-C. Aitcin, Determination of Elastic Properties of High-Performance Concrete at Early Ages, ACI Mater. J. 99 (2002) 37–41.

[39] O. Bernard, F.-J. Ulm, E. Lemarchand, A multiscale micromechanics-hydration model for the early-age elastic properties of cement-based materials, Cem. Concr. Res. 33 (2003) 1293–1309. doi:10.1016/S0008-8846(03)00039-5.

[40] M. Irfan-ul-Hassan, B. Pichler, R. Reihsner, C. Hellmich, Elastic and creep properties of young cement paste, as determined from hourly repeated minute-long quasi-static tests, Cem. Concr. Res. 82 (2016) 36–49. doi:10.1016/j.cemconres.2015.11.007.

[41] R. Le Roy, Déformations instantanées et différées des bétons à hautes performances, PhD thesis, Ecole Nationale des Ponts et Chaussées, Paris, France, 1995.

[42] R. Le Roy, F. Le Maou, J.M. Torrenti, Long term basic creep behavior of high performance concrete: data and modelling, Mater. Struct. 50 (2017) 11. doi:10.1617/s11527-016-0948-8.

[43] F.H. Wittmann, Useful Fundamentals of Shrinkage and Creep of Concrete, in: Concreep 10, 2015: pp. 84–93.

[44] J.M. Torrenti, R. Le Roy, Analysis and Modelling of Basic Creep, in: S. Dray (Ed.), CONCREEP 10, American Society of Civil Engineers, Reston, VA, 2015: pp. 1400–1409. doi:10.1061/9780784479346.165.

[45] NIST, http://www.nist.gov/el/building_materials/evcctl.cfm, (n.d.).

[46] L. Stefan, F. Benboudjema, J.-M. Torrenti, B. Bissonnette, Prediction of elastic properties of cement pastes at early ages, Comput. Mater. Sci. 47 (2010) 775–784. doi:10.1016/j.commatsci.2009.11.003.

[47] S. Bishnoi, K.L. Scrivener, μic: A new platform for modelling the hydration of cements, Cem. Concr. Res. 39 (2009) 266–274. doi:10.1016/j.cemconres.2008.12.002.

[48] K. van Breugel, Numerical simulation of hydration and microstructural development in hardening cement-based materials (I) theory, Cem. Concr. Res. 25 (1995) 319–331. doi:10.1016/0008-8846(95)00017-8.

[49] T. Honorio, B. Bary, F. Benboudjema, Multiscale estimation of ageing viscoelastic properties of cement-based materials: A combined analytical and numerical approach to estimate the behaviour at early age, Cem. Concr. Res. 85 (2016) 137–155. doi:10.1016/j.cemconres.2016.03.010.

[50] Q.H. Do, S. Bishnoi, K.L. Scrivener, Microstructural Modeling of Early-Age Creep in Hydrating Cement Paste, J. Eng. Mech. (2016) 4016086. doi:10.1061/(ASCE)EM.1943-

7889.0001144.

[51] M. Vandamme, F.-J. Ulm, Nanogranular origin of concrete creep., Proc. Natl. Acad. Sci. U. S. A. 106 (2009) 10552–7. doi:10.1073/pnas.0901033106.

[52] D.P. Bentz, E.J. Garboczi, C.J. Haecker, O.M. Jensen, Effects of cement particle size distribution on performance properties of Portland cement-based materials, Cem. Concr. Res. 29 (1999) 1663–1671. doi:10.1016/S0008-8846(99)00163-5.

[53] J.A. Choren, S.M. Heinrich, M.B. Silver-Thorn, Young's modulus and volume porosity relationships for additive manufacturing applications, J. Mater. Sci. 48 (2013) 5103–5112. doi:10.1007/s10853-013-7237-5.

[54] T.C. Powers, Structure and physical properties of hardened portland cement paste, J. Am. Ceram. Soc. 41 (1958) 1–6.

[55] C. Boulay, S. Staquet, B. Delsaute, J. Carette, M. Crespini, O. Yazoghli-Marzouk, et al., How to monitor the modulus of elasticity of concrete, automatically since the earliest age?, Mater. Struct. 47 (2014) 141–155. doi:10.1617/s11527-013-0051-3.

[56] B. Pichler, C. Hellmich, J. Eberhardsteiner, J. Wasserbauer, P. Termkhajornkit, R. Barbarulo, et al., Effect of gel–space ratio and microstructure on strength of hydrating cementitious materials: An engineering micromechanics approach, Cem. Concr. Res. 45 (2013) 55–68. doi:10.1016/j.cemconres.2012.10.019.

[57] G. Ye, E. Koenders, K. Van Breugel, Prediction of mechanical properties and durability of civil engineering structures, in: C. Miao, G. Ye, H. Chen (Eds.), 50-Year Teach. Res. Anniv. Prof. Sun Wei Adv. Civ. Eng. Mater., 2010: pp. 33–48.

CHAPTER 7:
INFLUENCE OF THE WATER-CEMENT RATIO AND THE NATURE OF THE BINDER ON THE EARLY AGE PROPERTIES OF CEMENT BASED MATERIALS BY MEANS OF MULTI-SCALE MONITORING

The testing and modelling strategy developed in the Chapter 4 is extended in this chapter to mortar and cement paste with different water-cement ratios. Water-cement ratio is known as a key parameter influencing strongly the development of all the properties of cement based materials, especially at early age. The aim of this chapter is to analyze and model the effect of the effective water-cement ratio on the development of the early age properties of cement based materials at different scales. Several tests are performed on cement paste, mortar and concrete with different water-cement ratio. In addition, this study is extended to an eco-concrete for which the cement is substituted by slag (50%) and limestone filler (25%).

This chapter is divided in two sections. In the first section, repeated minute-long loading tests are performed in order to characterize the short term mechanical properties of cement pastes, mortars and concretes since very early age. Several homogenization methods are used and compared in order to see the ability of these models to predict the E-modulus of concrete materials from cement paste data. Data from short term creep results are used in order to quantify the degree of restriction of the basic creep of cement paste by the sand and aggregate. The autogenous deformation and the coefficient of thermal expansion of cement pastes, mortars and concretes are defined in the second section of this chapter. Homogenization method is used in order to see the ability of the model to predict the coefficient of thermal expansion of concrete materials from cement paste data. Data from autogenous deformation results are used in order to quantify the degree of restriction of the autogenous deformation of the cement paste by the sand and aggregate.

SECTION 7.1 – MULTISCALE MONITORING AND MODELLING OF THE MECHANICAL PROPERTIES AND THE SHORT TERM CREEP

7.1.1. Materials and methods

The tests presented here were fully performed in the laboratory of civil Engineering at ULB on three concretes (C0.4, C0.5 and C0.6), four mortars (M0.3, M0.4, M0.5 and M0.6) and three cement pastes (CP0.3, CP0.4 and CP0.5) with different water-cement ratios. Additionally, tests were also performed on three compositions corresponding to the compositions C0.4, M0.4 and CP0.4 for which 75% of the cement is substituted by slag (50%) and limestone filler (25%). For each scale, the aggregate content is the same. The effective water-cement ratios of the concrete compositions are 0.35, 0.46 and 0.55. The effective water-cement ratios of the mortars compositions are 0.27, 0.36, 0.46 and 0.55. The effective water-cement ratios of the cement pastes are 0.3, 0.4 and 0.5. The calculation of the effective water-cement ratio is done by removing the water absorbed by the aggregate and the sand.

► Preliminary results

A certain number of fundamental properties were determined before the study of the viscoelastic behaviour of the thirteen mixtures. The setting is determined on basis of the monitoring of the transmission of the ultrasound p- and s-waves through concrete according to the method developed by Carette & Staquet [1,2]. Values of the initial and final setting time are given in Chapter 3.

For the determination of the equivalent time, the apparent activation energy was determined in previous studies [3] with the compressive strength results obtained at 3 different temperatures (36 kJ/mol for composition with cement only and 48kJ/mol for the compositions with substitution of cement by slag and limestone filler). The advancement degree of reaction is defined by means of isothermal calorimetry testing on the mortars M0.3, M0.4, M0.5 and M0.6. For the cement pastes and concretes compositions, linear interpolation is used in order to define the advancement degree of reaction according to the effective water-cement ratio. All experimental parameters obtained for this study will be presented according to the equivalent time and the advancement degree of reaction.

The compressive strength is defined since few hours after the final setting till 28 days. Results of the compressive strength f_c are given in Figure 1 according to the equivalent time and the advancement degree of reaction for cement pastes, mortars and concretes.

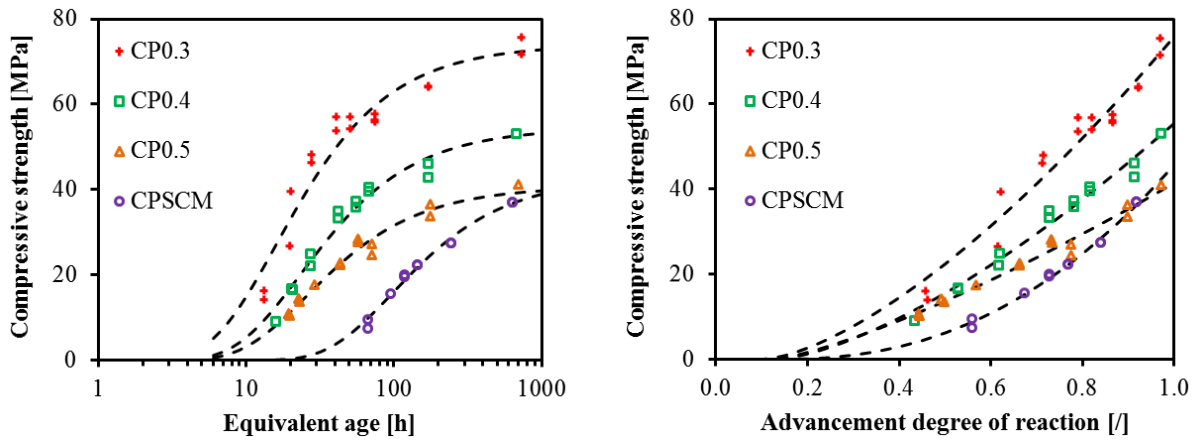

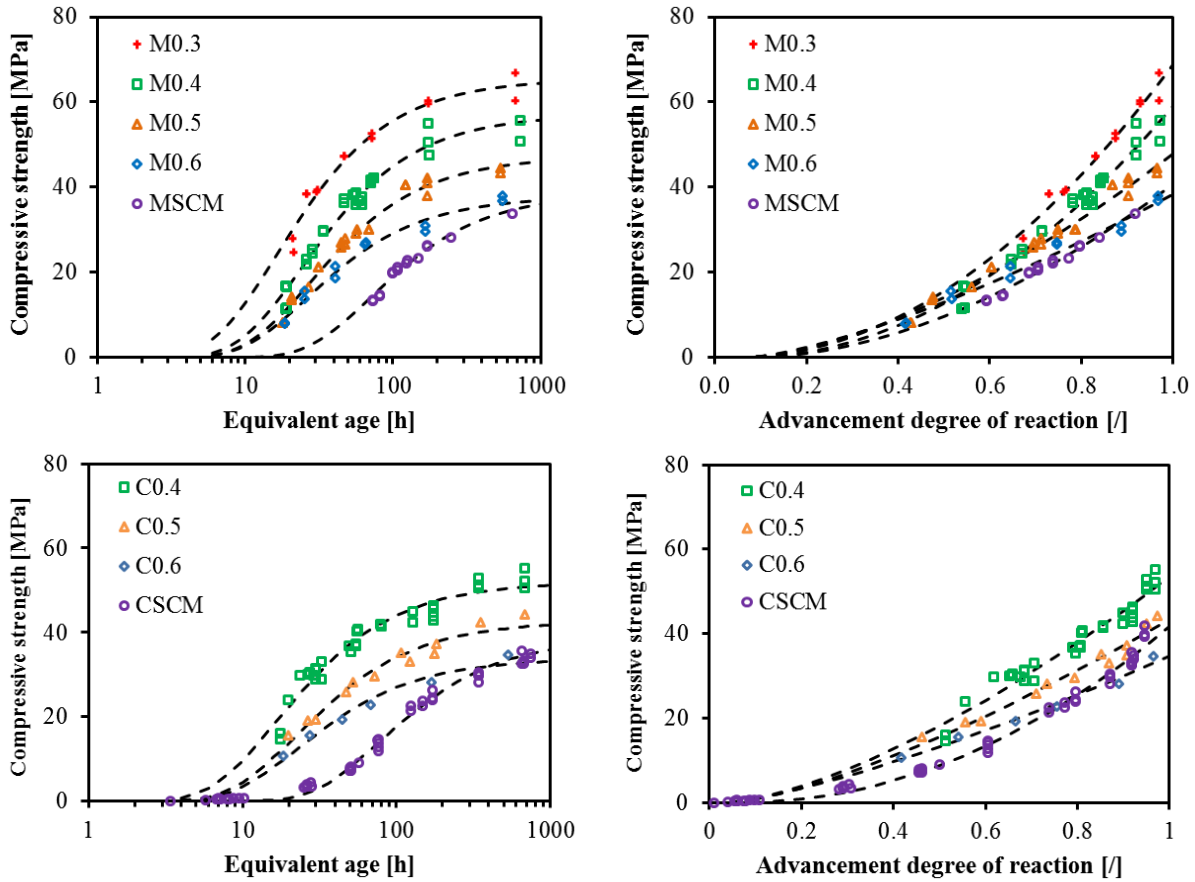

Figure 1 – Evolution of the compressive strength according to equivalent time and the advancement degree of reaction for cement pastes, mortars and concretes (dashed lines correspond to the model).

The exponential and power models used to fit the experimental results are the same as those in Chapter 6 (Equations 18 and 19). Each model well represents the evolution of the compressive strength whatever the scale of the material. Values of each material parameter are given in Table 1. The final value of the compressive strength is directly obtained in the model using the equivalent time but not the one using the advancement degree of reaction. The final value of the compressive strength obtained with the model using the advancement degree of reaction $f_c(\alpha = 1)$ is also given in the Table 1.

Table 1 – Compressive strength parameters for the three scales of the material

	$f_c(t_{eq} = \infty)$ [MPa]	p_f [/]	$f_{c,\alpha}$ [MPa]	a_f [/]	α_0 [/]	$f_c(\alpha = 1)$ [MPa]
CP0.3	74	16	89	1.49	0.10	76
CP0.4	54	23	68	1.49	0.13	56
CP0.5	41	26	49	1.30	0.13	41
CPSCM	43	98	63	2.33	0.13	46
M0.3	65	16	75	2.01	0.04	69
M0.4	57	24	68	2.01	0.06	59
M0.5	47	27	54	1.59	0.07	48
M0.6	38	26	43	1.40	0.07	38
MSCM	39	72	48	1.82	0.08	41
C0.4	52	17	45	1.47	0.03	53
C0.5	43	23	36	1.38	0.04	43
C0.6	34	23	29	1.31	0.03	35

CSCM	39	79	37	2.05	0.05	42

In Figure 2, parameters of the two models are plotted according to the effective water-cement ratio. A linear relation between the final value of the compressive strength and the effective w/c ratio is highlighted for both timescales and for each scale of the material. For effective water-cement ratio of 0.5 or higher, the final compressive strength of each material scale is very close. On the contrary, when the effective water-cement ratio decreases, changes occur between the different scales. Higher compressive strength values are obtained for cement pastes than for mortars and concretes. This can be explained by the stress concentration caused by the presence of aggregate and by the porosity existing at the interface transition zone (ITZ) between the aggregate and the cement paste. In the ITZ, the porosity is known to be much higher than the one in the hydrated cement paste being further away from the coarse aggregate [4]. This creates a weak point in the concrete. From the results obtained, it is observed that the difference of porosity between the cement paste situated at the ITZ and the cement paste being further away from the coarse aggregate is higher for low water-cement ratio. The kinetic parameters p_f and a_f are also presented in the Figure 2. In equivalent time, the kinetic parameter p_f increases with the effective water-cement ratio till an effective water-cement ratio of about 0.45. Then p_f does not evolve anymore. In advancement degree of reaction, the kinetic parameter a_f decreases linearly with the effective water-cement ratio for the three scales of the material. Very close values are obtained for cement pastes and concretes whereas a higher kinetic is obtained for mortars.

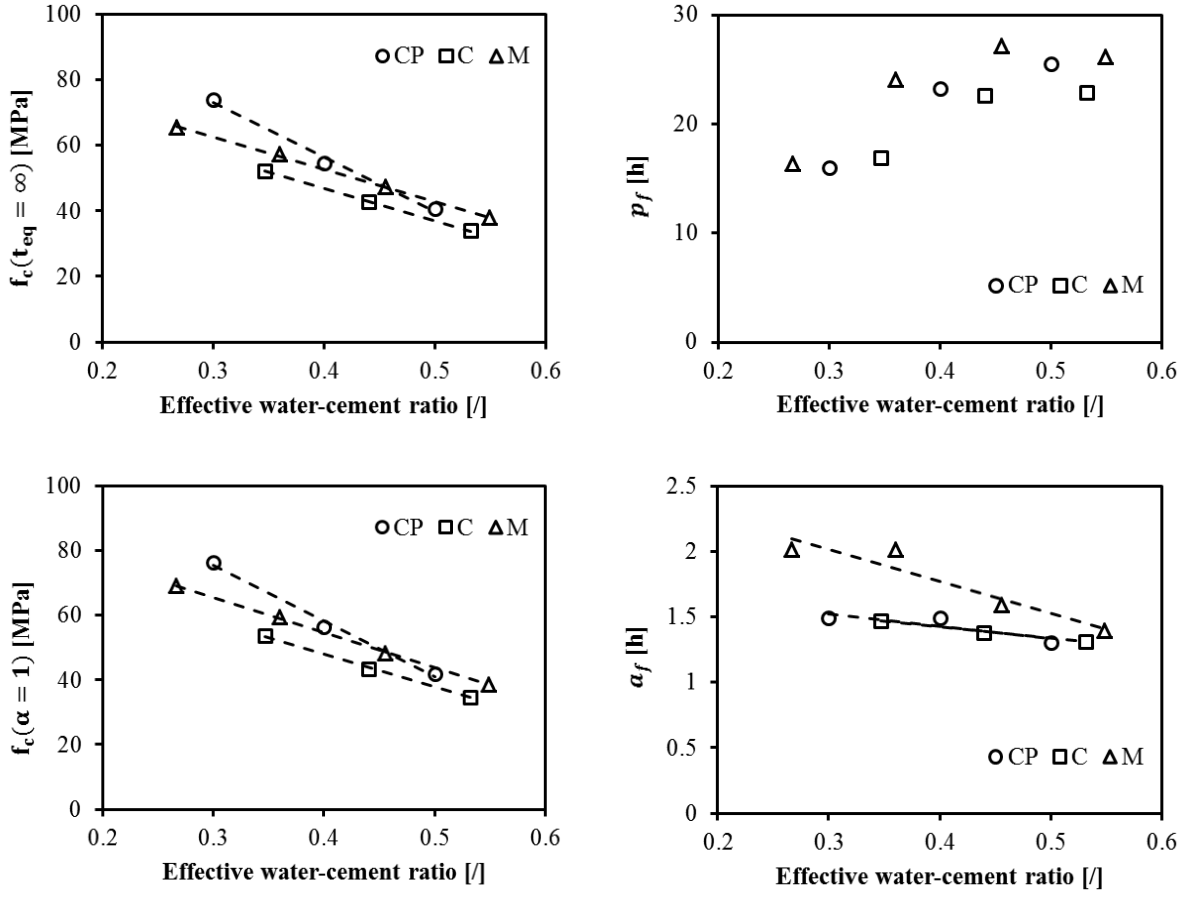

Figure 2 – Compressive strength parameters according to the effective water-cement ratio.

As it has been presented in chapter 4 and 6, the evolution of the microstructure of the cement paste corresponding to the composition without mineral addition[1] has been computed with the software VCCTL (V9.5) [5]. With this simulation, the gel-space ratio is defined. In Figure 3, the compressive strength is function of the gel-space ratio. As for concrete, a linear relation is obtained for each cement paste and mortar. For concrete and mortar, this relation is slightly influenced by the water-cement ratio whereas for cement paste the effect of the water-cement ratio is clearly more pronounced.

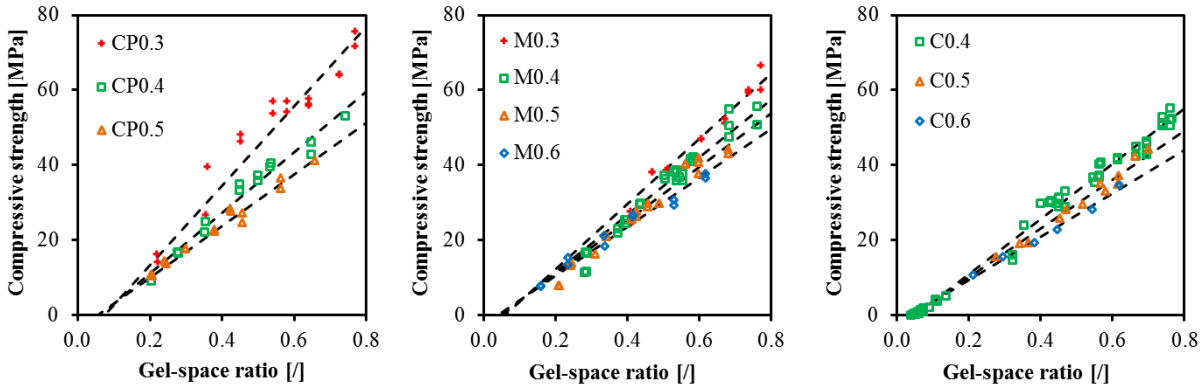

Figure 3 – Evolution of the compressive strength according to the gel-space ratio for cement pastes, mortars and concretes (dashed lines correspond to the model).

An adaptation of the equation presented in the Chapter 6 (Equation 64) is done with the consideration of the gel-space ratio at the final setting time GS_0 in Equation 1. Therefore only the parameter $f_{c,GS}$ related to the amplitude of the compressive strength (expressed in MPa) is needed to define the evolution of the compressive strength with the gel-space ratio since setting time.

$$f_c(GS) = f_{c,GS}.(GS - GS_0) \quad 1$$

The value of each parameter is given in Table 2. A good agreement is observed between the model and the experimental results.

Table 2 – Compressive strength parameters of Equation 1 for the three scales of the material

	CP0.3	CP0.4	CP0.5	M0.3	M0.4	M0.5	M0.6	C0.4	C0.5	C0.6
$f_{c,GS}$ [MPa]	106	81	69	87	77	71	65	74	65	58
GS_0 [/]	0.074	0.063	0.055	0.059	0.051	0.047	0.039	0.051	0.045	0.038

In Figure 4, the amplitude parameter $f_{c,GS}$ of the model is shown according to the effective water-cement ratio. A general linear relation is highlighted between this parameter and the effective w/c ratio. These results are in coherence with the results presented in Figure 2. In Figure 5, the gel-space ratio at the final setting GS_0 is presented according to the effective water-cement ratio. A linear trend is observed between both parameters. GS_0 decreases when the effective water-cement ratio increases. This is explained by the increase of porosity occurring when water-cement ratio increases. For a same quantity of hydrated cement, the gel-space ratio is lower for high water-cement ratio.

[1] For mixture with high substitution of cement by mineral addition, it has been observed that VCCTL (V9.5) is unable to define correctly the development of the microstructure

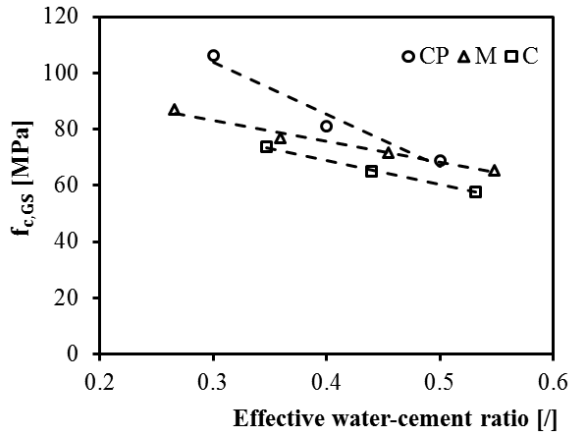

Figure 4 – Relation between $f_{c,GS}$ and the effective water-cement ratio

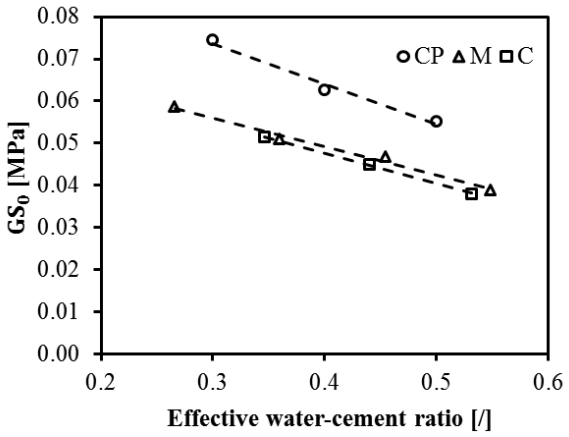

Figure 5 – Relation between GS_0 and the effective water-cement ratio

7.1.2. Repeated minute-long loading tests

► Assessment of E-modulus, Poisson ratio and the short term creep

Results on concrete correspond to the results presented in Chapter 6. For mortars, exactly the same methodology is used. The size of the specimen is changed for cement pastes. The dimension of the sample must be smallest as possible in order to decrease the thermal gradients inside the sample. The section was kept constant in order to avoid any problem of eccentricity of the load during the test. Therefore only the height of the cylinder was changed. On cement paste, the height of the sample is 200 mm instead of 550 mm on mortar and concrete. This difference of height changes the slenderness of the sample from a value of 5.5 to 2. Therefore it is possible that the friction between the sample and the testing machine affects the results. Tests were performed on concrete with both sizes of the sample in order to determine the effect of the friction on the measurement of the E-modulus [6]. No difference was observed in the determination of the E-modulus of an ordinary concrete. Despite the reduction of the height of the sample, thermal gradient stays consequent for such dimension with cement pastes. Per consequent, the thermal regulation of the sample was improved. After casting the cement paste sample was placed in a water tank thermo-regulated. A high decrease of the temperature in the core of the sample was observed thanks to this methodology as shown in Figure 6.

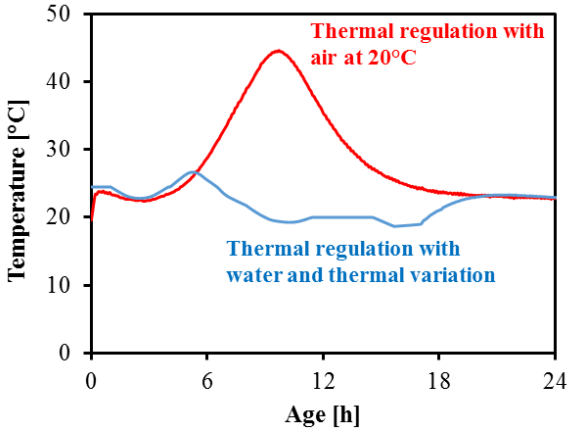

Figure 6 – Evolution of the temperature in the core of the cement paste sample for two different thermal regulation (in red, regulation by air – in blue, regulation by water)

► Protocol of loading

Measurements on the sample have started a few hours after setting (between 4 and 9 hours for composition without mineral addition). The whole test duration is 28 days. The temperature of the sample is set to 20°C and is recorded since the casting. Three strategies were used for the monitoring of the E-modulus. For the concrete compositions C0.4, CSCM and the mortar one M0.4, repeated minute-long loadings were applied each hour during the first weeks and then the specimen was again loaded two times at an age of two weeks and four weeks. For the cement paste compositions repeated minute-long loadings were applied till an age of 24 hours and then the specimen was again loaded four times at an age of 48, 168, 336 and 672 hours. For the compositions C0.5, C0.6 and mortars (except the M0.4 one), specimens were loaded at an age of 15, 24, 40, 168 and 672 hours. These ages were chosen according to the evolution of the advancement degree of reaction in order to follow accurately the hardening process on the viscoelastic properties.

► E-modulus

For each repeated minute-long loading, the E-modulus is calculated from the set of recordings (load and displacement in the central section) between 30% and 80% of loading [6]. The same procedure is used for cement paste, mortar and concrete. In each case, the tangent elastic modulus E is computed by least square method. Results are given in Figure 7 according to the equivalent time and the advancement degree of reaction.

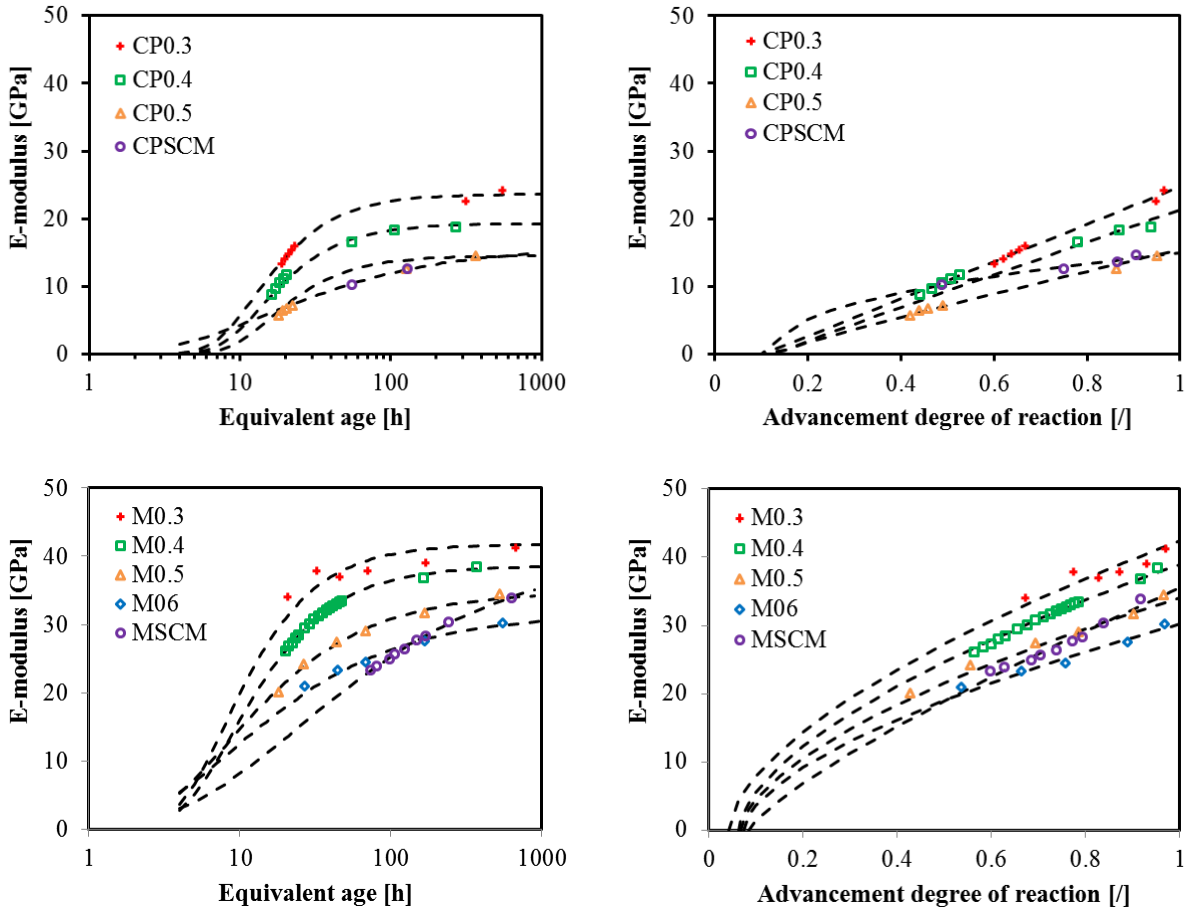

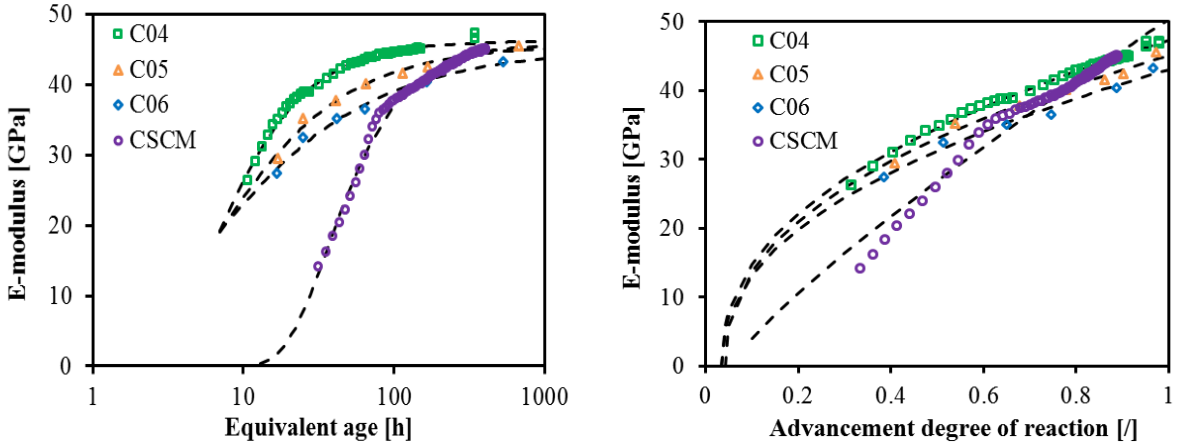

Figure 7 – Evolution of the E-modulus according to the equivalent time and the advancement degree of reaction for cement pastes, mortars and concrete (dashed lines correspond to the model).

The exponential and power equations presented in the Chapter 6 (Equations 27 and 28) are used to model the evolution of the E-modulus. Value of each parameter is given in Table 3. Both models well represent the evolution of the elastic modulus.

Table 3 – E-modulus parameters for the three scales of the material

	$E(t_{eq}=\infty)$ [GPa]	p_E [/]	r_E [/]	E_α [GPa]	a_E [/]	$E(\alpha=1)$ [GPa]
CP0.3	23.6	12.7	1.51	27.6	1.00	24.7
CP0.4	19.3	14.0	1.51	24.4	0.97	21.3
CP0.5	14.5	16.0	1.51	17.4	0.91	15.4
CPSCM	15.9	15.3	0.66	15.8	0.43	14.9
M0.3	41.8	8.0	1.30	43.5	0.60	42.4
M0.4	38.6	9.0	1.19	40.5	0.60	39.0
M0.5	34.8	8.5	0.85	35.6	0.60	34.1
M0.6	31.6	9.0	0.70	31.7	0.60	30.2
MSCM	40.7	24.8	0.53	38.1	0.8	35.5
C0.4	46.2	6.3	1.25	48.0	0.43	47.3
C0.5	45.7	6.0	0.85	45.9	0.42	45.1
C0.6	44.9	5.5	0.68	43.7	0.44	43.1
CSCM	45.8	36.5	1.52	52.8	0.83	50.4

In Figure 8, parameters of each model are plotted according to the effective water-cement ratio. A linear relation between material parameters and the effective w/c ratio is highlighted. The kinetic parameter $a_{E,\alpha}$ is not impacted by a variation of the effective w/c ratio for each material scale. In equivalent time, the value of the kinetic parameter p_E varies linearly with the effective water-cement ratio. According to the scale, this parameter increases (cement paste and mortar) or decreases (concrete) with an increase of the water-cement ratio. The final values of the E-modulus predicted by each model are close. This parameter is not strongly influenced by the w/c ratio for concrete whereas a significant change is observed for cement pastes and mortars. For concrete, the E-modulus is highly dependent on the content and stiffness of the aggregates. Therefore aggregate has a dilution effect on the amplitude of the E-modulus.

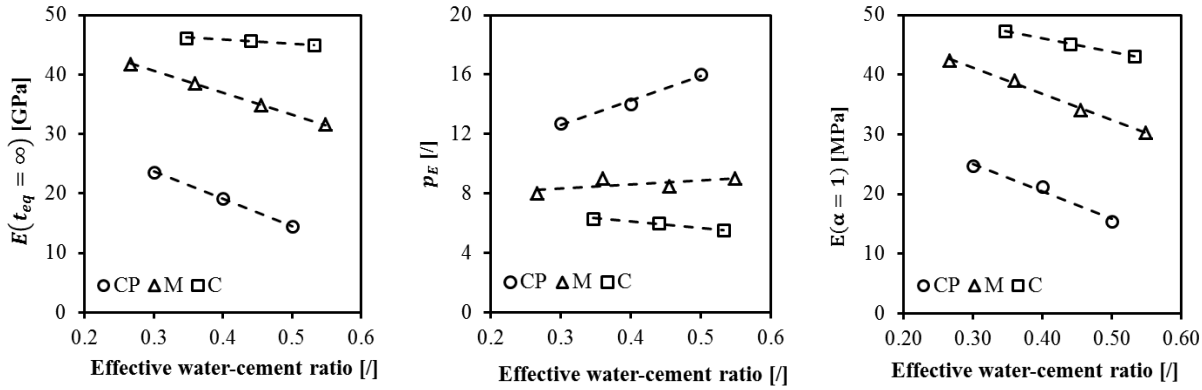

Figure 8 – E-modulus parameters according to the effective water-cement ratio.

In Figure 9, the E-modulus is function of the gel-space ratio. For each scale, a power relation is observed between both parameters. For concrete, this relation is very slightly influenced by the water-cement ratio whereas for mortars and cement pastes the effect of the water-cement ratio is clearly more pronounced.

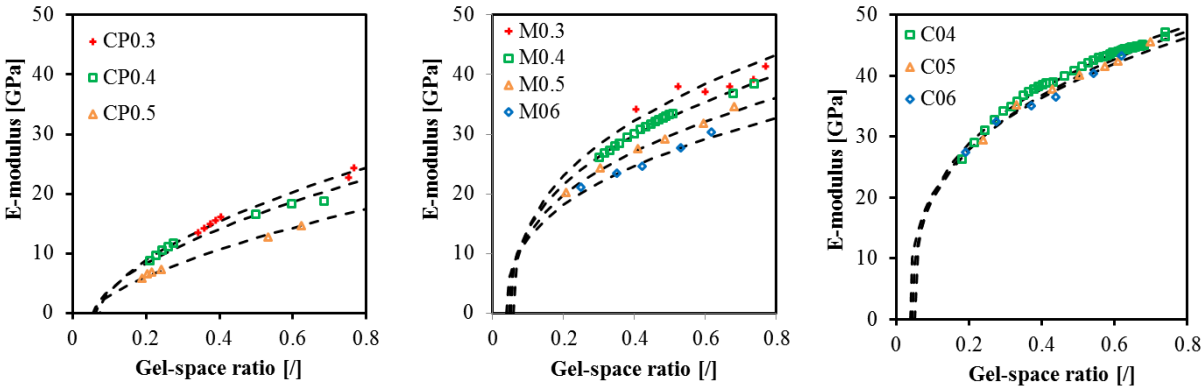

Figure 9 – Evolution of the E-modulus according to the gel-space ratio for cement pastes, mortars and concrete (dashed lines correspond to the model).

An adaptation of the equation presented in the Chapter 6 is done with the use of a power expression and the consideration of the gel-space ratio at the final setting time GS_0 (Equation 2).

$$E(GS) = E_{GS}.(GS - GS_0)^{s_E} \quad 2$$

Where E_{GS} is a material parameter related to the amplitude of the E-modulus (expressed in GPa) and s_E is a material parameter associated to the kinetic evolution of the E-modulus. Values of both parameters are given in Table 4 for each composition. The model well represents the evolution of the elastic modulus.

Table 4 - E-modulus parameters of Equation 2 for the three scales of the material

	CP0.3	CP0.4	CP0.5	M0.3	M0.4	M0.5	M0.6	C0.4	C0.5	C0.6
E_{GS} [GPa]	29.4	26.8	21.1	48.5	44.5	40.269	36.3	52.9	52.0	50.6
s_E [/]	0.58	0.59	0.65	0.38	0.38	0.38	0.38	0.32	0.33	0.32

A linear relation between the material parameter E_{GS} and the effective w/c ratio is obtained. On the contrary, the kinetic parameter s_E is not impacted by a variation of the effective w/c ratio for each material scale.

► Poisson's ratio

For each repeated minute-long loading, the Poisson's ratio is calculated from the set of recordings (longitudinal and lateral displacement in the central section) on the whole loading. Results are given according to the equivalent time and the advancement degree of reaction in Figure 10 for each scale of the material. For each water-cement ratio and each scale of the material, an increase of the Poisson's ratio is observed since an advancement degree of reaction of around 0.4 except for the composition C0.6 and CSCM for which the increase begins at an advancement degree of reaction of 0.5. As explained in Chapter 6, this increase is related to the solid stiffness evolution [7]. The amplitude of the Poisson's ratio is different for the three scales of the material. For cement pastes, the final value of the Poisson's ratio varies between 0.25 and 0.3. A range of Poisson's ratio between 0.18 and 0.2 is obtained on mortars whereas the final value of the Poisson's ratio varies between 0.15 and 0.18 on concrete. These final values are in agreement with the results found in the literature [8,9].

According to the scale of the material, the effect of the effective water-cement ratio on the amplitude of the Poisson's ratio is different. For concrete compositions, a decrease of the Poisson's ratio is observed for composition with low water-cement ratio. For mortar, no significant difference occurs in the development of the Poisson's ratio between the different compositions. Whereas for cement pastes, a general increase of the Poisson's ratio is observed when the water-cement ratio becomes lower. For the compositions CSCM, the value of the Poisson's ratio evolves more significantly than the other composition. This can be explained by the higher rate of evolution of the E-modulus during this period (Figure 7).

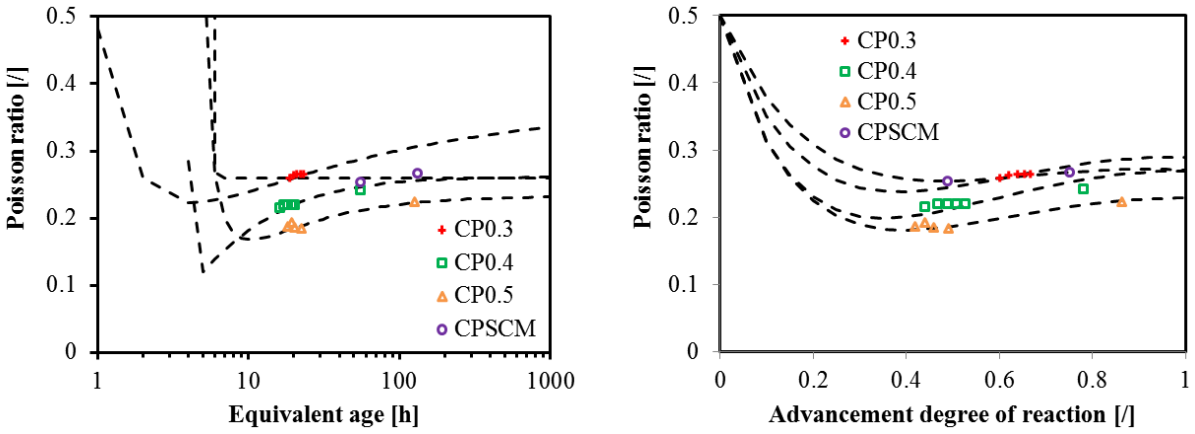

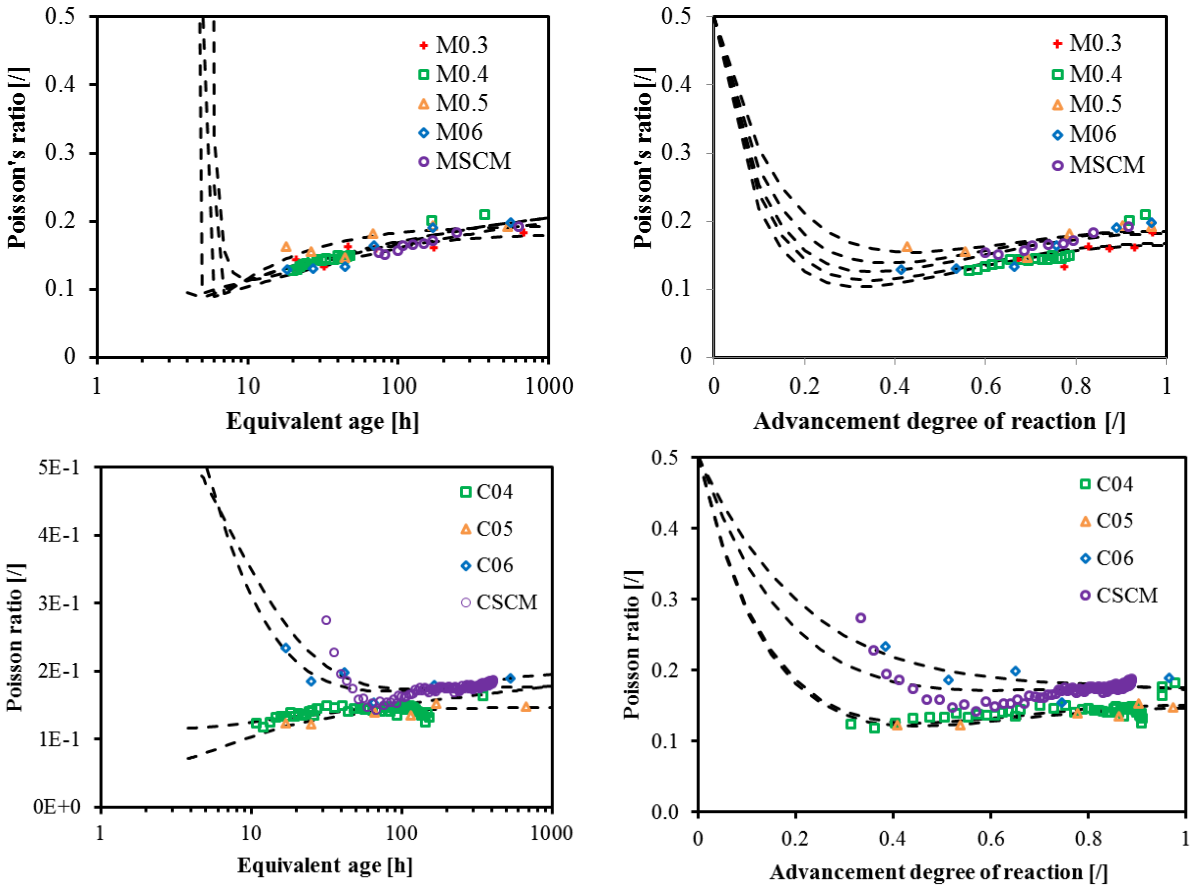

Figure 10 – Evolution of the Poisson's ratio according to the equivalent time and the advancement degree of reaction for cement pastes, mortars and concrete (dashed lines correspond to the model).

Equations 35 and 36 presented in the Chapter 6 are used to model the evolution of the Poisson's ratio. In order to assure that the model correspond physically to the evolution of the Poisson's ratio, it is imposed that the Poisson's ratio is equal to 0.5 at an advancement degree of reaction of 0 and at an equivalent age corresponding to the initial setting time. However, the validity domain of this model is limited to an advancement degree of reaction higher than 0.4. Before this value, the validity of the model is not checked due to missing experimental data. The values of each parameter are given in Table 5. Both models are able to represent the evolution of the Poisson's ratio for each scale of the material.

Table 5 – Poisson's ratio parameters for the three scales of the material

	$\nu_{t,f}$ [/]	$r_{\nu,f}$ [/]	$\nu_{t,s}$ [/]	$r_{\nu,s}$ [/]	ν_{α} [/]	c_{α} [/]
CP0.3	0.37	2.0	0.37	0.35	0.29	4.9
CP0.4	0.40	15.8	0.26	1.08	0.27	6.1
CP0.5	0.41	1.5	0.23	0.97	0.23	5.9
CPSCM	0.40	9.5	0.26	46.96	0.26	3.9
M0.3	0.43	5.6	0.18	0.63	0.16	9.5
M0.4	0.41	13.0	0.24	0.34	0.17	8.5
M0.5	0.43	6.3	0.19	0.97	0.18	5.9
M0.6	0.41	2.3	0.24	0.38	0.18	8.0
MSCM	0.41	8.8	0.24	0.32	0.18	7.0
C0.4	0.45	13.01	0.15	1.50	0.15	6.4

C0.5	0.45	10.63	0.15	1.06	0.15	6.5
C0.6	0.44	0.86	0.17	25.18	0.16	3.4
CSCM	0.16	-0.01	0.90	-0.60	0.17	4.4

In Figure 11, the amplitude parameters $\nu_{t,f}$, $\nu_{t,s}$ and ν_{α} are plotted according to the effective water-cement ratio. A linear relation between material parameters and the effective w/c ratio is highlighted. The parameter $\nu_{t,f}$ is related to the amplitude of the Poisson's ratio when the material is considered as a fluid. For concrete and mortar, this parameter is constant and has a mean value of 0.45 and 0.42 respectively. For cement paste, this parameter increases slightly and linearly with the effective water-cement ratio. An average value of 0.39 is obtained for cement pastes without mineral addition. The parameters $\nu_{t,s}$ and ν_{α} are related to the Poisson's ratio when the material has obtained its final stage. According to the scale, these parameters increase (concrete and mortar) or decrease (cement paste) with an increase of the water-cement ratio. The kinetic parameters $r_{\nu,f}$ and $r_{\nu,s}$ do not follow a specific trend and are strongly dependent on the way to fit the results. Whereas the kinetic parameter c_{α}, which is linked to the rate transition between the liquid and solid phase, does not vary so much.

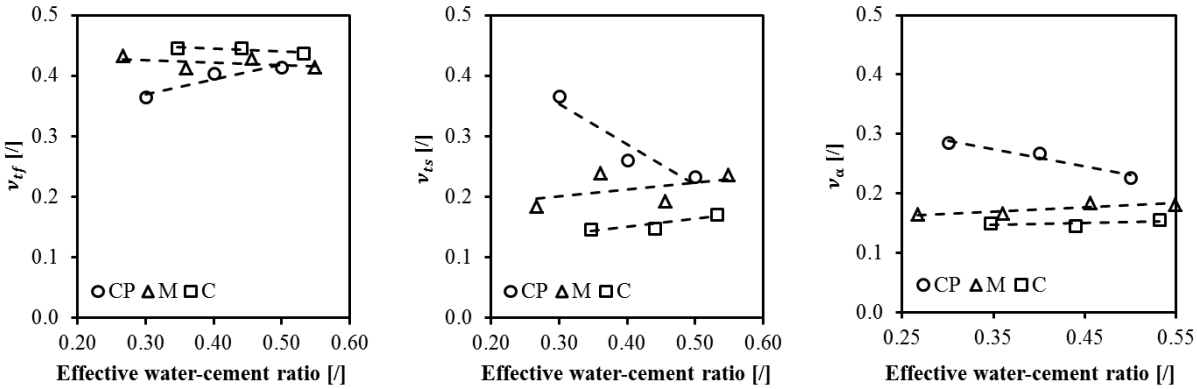

Figure 11 – Poisson's ratio parameters according to the effective water-cement ratio for the three scales of the material.

► Amplitude creep factor

For each repeated minute-long loading test, a load corresponding to 20% of the compressive strength is applied during 5 minutes. During these 5 minutes-long plateau of stress, the creep coefficient is computed from raw displacement measurements after having removed the free strain from the dummy specimen (thermal and autogenous strain). The creep coefficient is modeled with a logarithmic law as presented in Chapters 4 and 6 (Equation 38 in the Chapter 6). This equation is composed of two parameters in order to model the creep coefficient during the 5 minutes of loading: the amplitude creep factor and the kinetic creep factor.

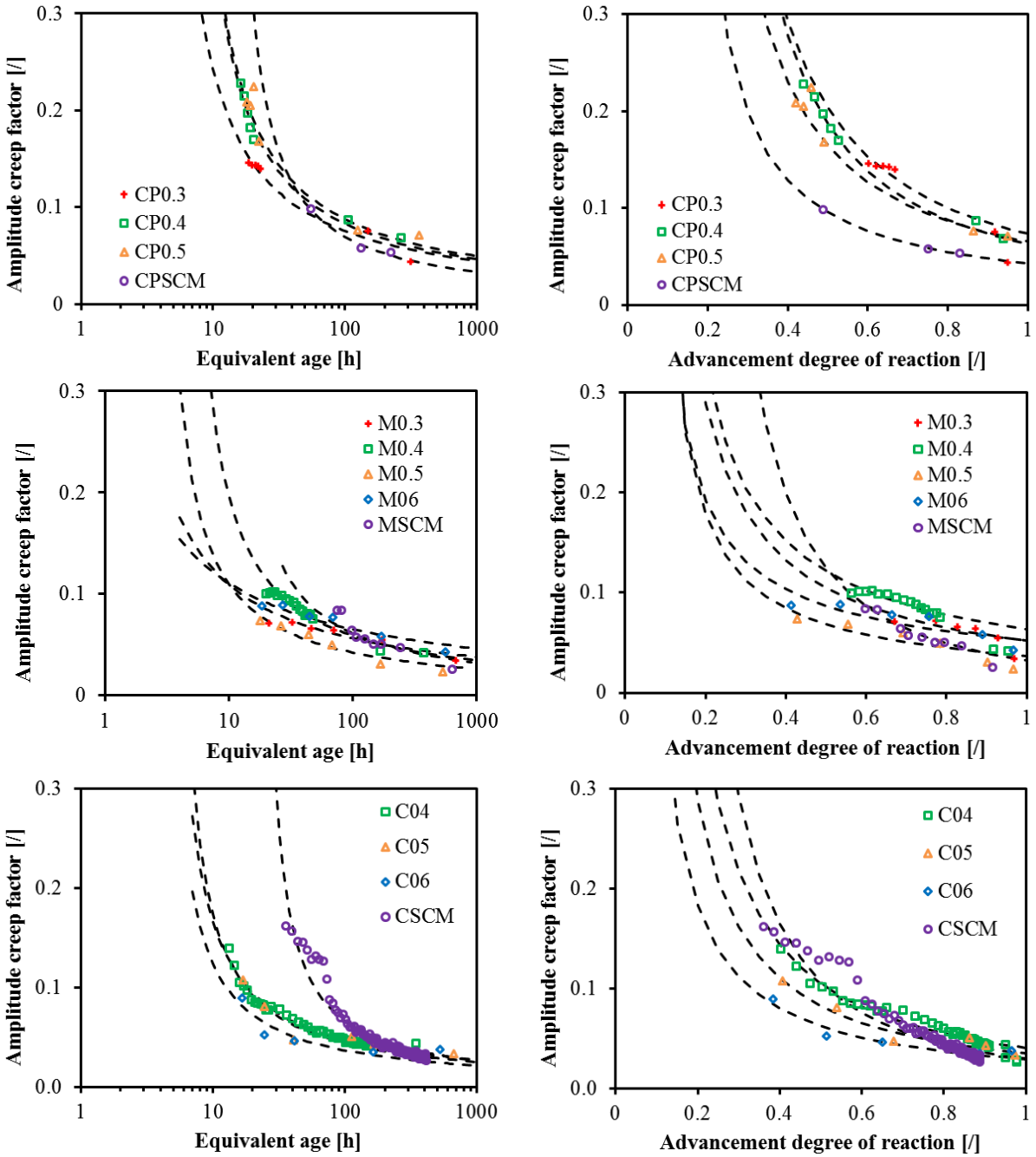

Figure 12 – Evolution of the Amplitude creep factor according to the equivalent time and the advancement degree of reaction for cement pastes, mortars and concrete (dashed lines correspond to the model).

Results of the amplitude creep factor are given according to the equivalent time and the advancement degree of reaction in Figure 12. For each scale and each water-cement ratio, the amplitude creep factor decreases during the hardening process and is lower for composition with higher water-cement ratio. For composition without mineral addition, results are very close especially when looking at the results according to the equivalent age. For both time-scales, the final value of the amplitude creep factor seems to converge to close values. For concrete, mortar and cement paste, the final amplitude

creep factor is respectively about 0.03, 0.04 and 0.06. This means that the creep strain represents 3, 4 and 6% of the elastic strain after only 5 minutes of loading for respectively concrete, mortar and cement paste with an advancement degree of reaction of 1.

Equations presented in the Chapter 6 are used to model the evolution of the amplitude creep factor for both time-scales (Equations 39 and 40 in Chapter 6). Value of each parameter is given in Table 6. A good agreement is observed between model and experimental data for the two time-scales and for each scale of the material (Figure 12).

Table 6 – Amplitude creep factor parameters for the three scales of the material

	A_{t1} [/]	A_{t2} [/]	A_{α} [/]	a_A [/]	$A(\alpha = 1)$ [/]
CP0.3	4.0	-5.0	0.064	-1.24	0.073
CP0.4	4.1	-6.9	0.053	-1.27	0.063
CP0.5	3.8	-6.3	0.057	-1.09	0.065
CPSCM	6.9	-17.6	0.038	-0.94	0.043
M0.3	3.8	0.5	0.050	-0.95	0.052
M0.4	5.2	-6.9	0.060	-0.85	0.063
M0.5	6.4	-5.5	0.035	-0.80	0.037
M0.6	2.8	2.7	0.050	-0.65	0.053
MSCM	6.5	-13.6	0.028	-1.70	0.033
C0.4	6.6	-9.1	0.039	-1.30	0.041
C0.5	7.3	-11.1	0.033	-1.16	0.035
C0.6	8.3	-11.0	0.028	-1.03	0.029
CSCM	9.8	-29.9	0.027	-1.693	0.030

In Figure 13, the parameters A_{t1}, A_{α} and a_A are plotted according to the effective water-cement ratio. The equation using equivalent time is able to fit correctly the data but its associated parameters cannot be correlated to any physical meaning. Even if the parameter A_{t1} seems to generally follow a linear trend with the effective water-cement ratio, it is not the case for the parameter A_{t2}. On the contrary, the equation using the advancement degree of reaction allows a better understanding of the physical mechanisms occurring during the hydration process. A systematic linear relation between material parameters and the effective w/c ratio is highlighted for both parameters of the equation. Results on concrete and cement paste follow a same trend for both parameters. Results on mortar are more scattered. It is generally observed that a decrease of the water-cement ratio induces an increase of the amplitude creep factor and a decrease of the parameter a_A which is related to the kinetic evolution of the amplitude creep factor.

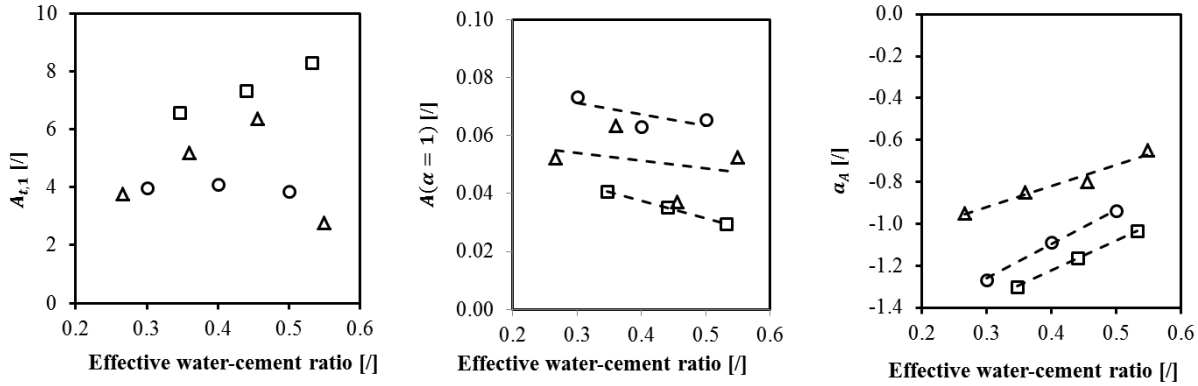

Figure 13 – Evolution of the amplitude creep factor according to the equivalent time

In Figure 14, the amplitude creep factor is function of the gel-space ratio. For each scale, a power relation is observed between both parameters. The influence of the water-cement is clearly observed for each scale for cement paste and concrete. An increase of the effective water-cement ratio leads to a decrease of the amplitude creep factor. For mortars, results are scattered and are difficult to interpret.

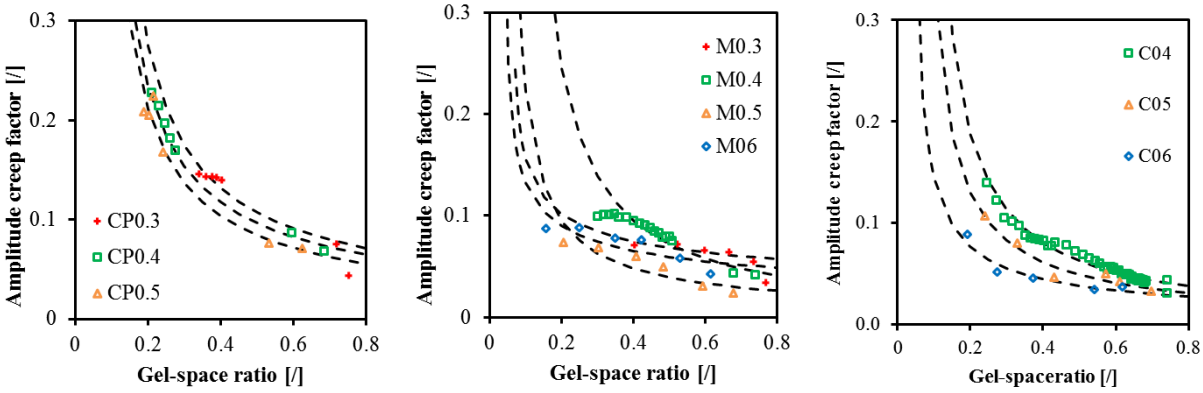

Figure 14 – Evolution of the amplitude creep factor according to the gel-space ratio (dashed lines correspond to the model).

An adaptation of the equation presented in the Chapter 6 is done with the use of a power expression and the consideration of the gel-space ratio at the final setting time GS_0 (Equation 2).

$$A(GS) = A_{GS}.(GS - GS_0)^{s_{GS}} \quad 3$$

Where A_{GS} is a material parameter related to the amplitude of the amplitude creep factor and s_{GS} is a material parameter associated to the kinetic evolution of the amplitude creep factor. Values of both parameters are given in Table 7 for each composition. The model well represents the evolution of the amplitude creep factor.

Table 7 – Amplitude creep factor parameters of Equation 3 for the three scales of the material

	CP0.3	CP0.4	CP0.5	M0.3	M0.4	M0.5	M0.6	C0.4	C0.5	C0.6
A_{GS} [/]	0.056	0.051	0.044	0.052	0.030	0.021	0.044	0.028	0.024	0.023
s_A [/]	-0.77	-0.76	-0.82	-0.34	-1.11	-0.80	-0.40	-1.00	-0.91	-0.66

A linear relation between the material parameter A_{GS} and the effective w/c ratio is obtained for cement pastes and concretes. Whereas the kinetic parameter s_{GS} is nearly constant for cement paste and increases with the effective water-cement ratio for concrete.

► Kinetic creep factor

In Figure 15, results of the kinetic creep factor K are presented. For each composition, K decreases during the hydration process. For high water-cement ratio, the decrease of the kinetic parameter is very low and is nearly constant especially for concrete and mortar. For lower water-cement ratio, the kinetic parameter varies significantly especially for cement paste. In equivalent age, the kinetic parameter follows a logarithmic trend. With the advancement degree of reaction and the degree of hydration a linear trend is observed for each scale of the material.

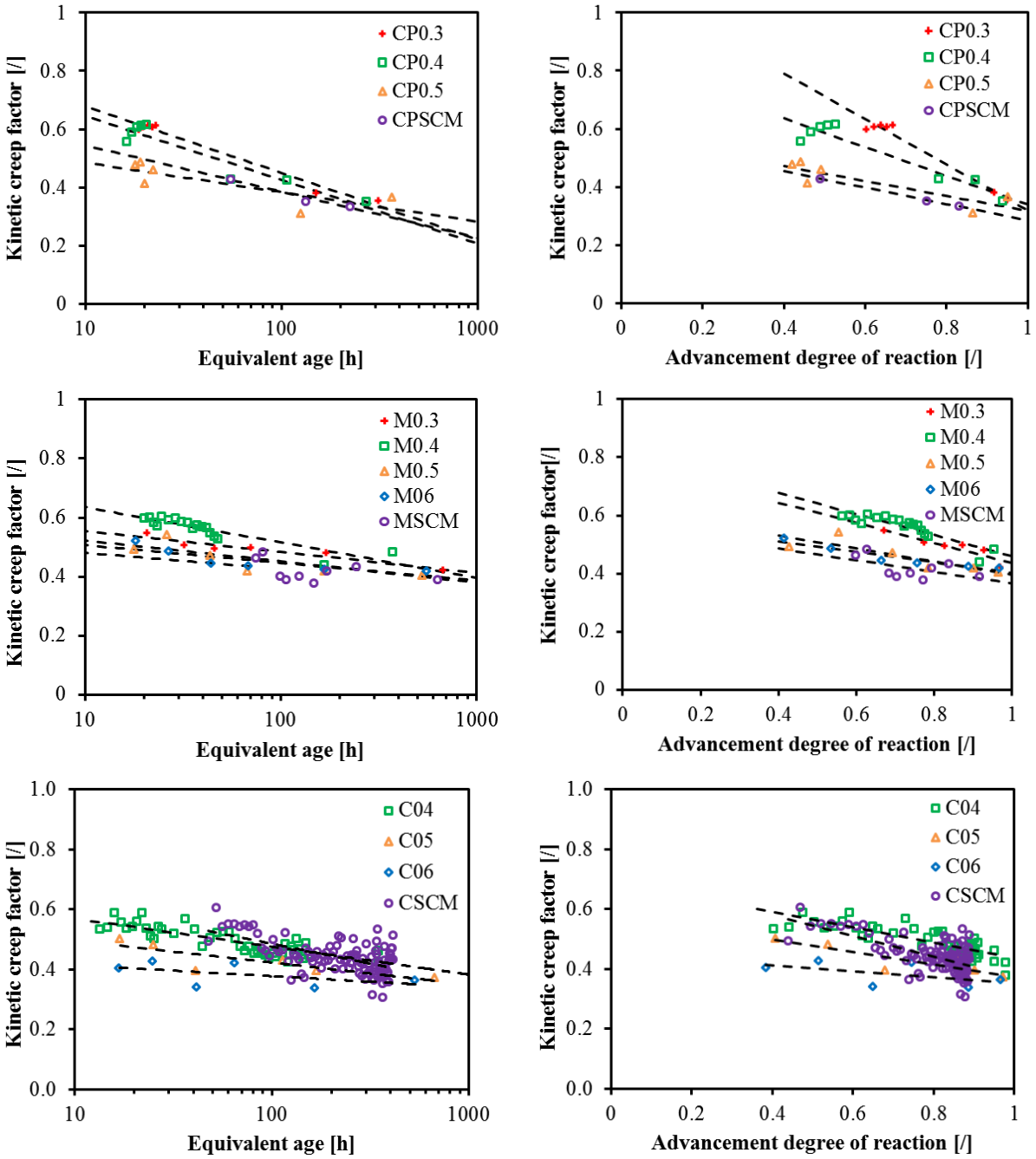

Figure 15 – Evolution of the kinetic creep factor according to the equivalent time and the advancement degree of reaction for cement pastes, mortars and concrete (dashed lines correspond to the model).

Equations presented in the Chapter 6 are used to model the evolution of the kinetic creep factor for both time-scales (Equations 47 and 48 in Chapter 6). Value of each parameter is given in Table 6. A good agreement is observed between model and experimental results for the two time-scales and for each scale of the material.

Table 8 - Kinetic creep factor parameters for the three scales of the material

	K_{t1} [/]	K_{t2} [/]	K_{α} [/]	P [/]
CP0.3	-0.100	0.91	-0.79	1.11
CP0.4	-0.095	0.86	-0.49	0.83
CP0.5	-0.44	0.59	-0.26	0.57
CPSCM	-0.069	0.70	-0.28	0.57
M0.3	-0.031	-0.63	-0.35	0.78
M0.4	-0.052	0.76	-0.36	0.82
M0.5	-0.031	0.59	-0.22	0.62
M0.6	-0.026	0.57	-0.18	0.58
MSCM	-0.024	0.54	-0.2	0.57
C0.4	-0.041	0.66	-0.26	0.69
C0.5	-0.032	0.57	-0.21	0.58
C0.6	-0.016	0.45	-0.1	0.45
CSCM	-0.057	0.75	-0.34	0.72

In Figure 13, the parameters K_{t1}, K_{α} and P are plotted according to the effective water-cement ratio. The equation using equivalent time is able to fit correctly the data but no link is observed between the parameters K_{t1} and K_{t2} and the effective water-cement ratio. Whereas the equation using advancement degree of reaction allows a better understanding of the physical mechanisms occurring during the hydration process. A systematic linear relation between material parameters and the effective w/c ratio is highlighted for both parameters of the equation.

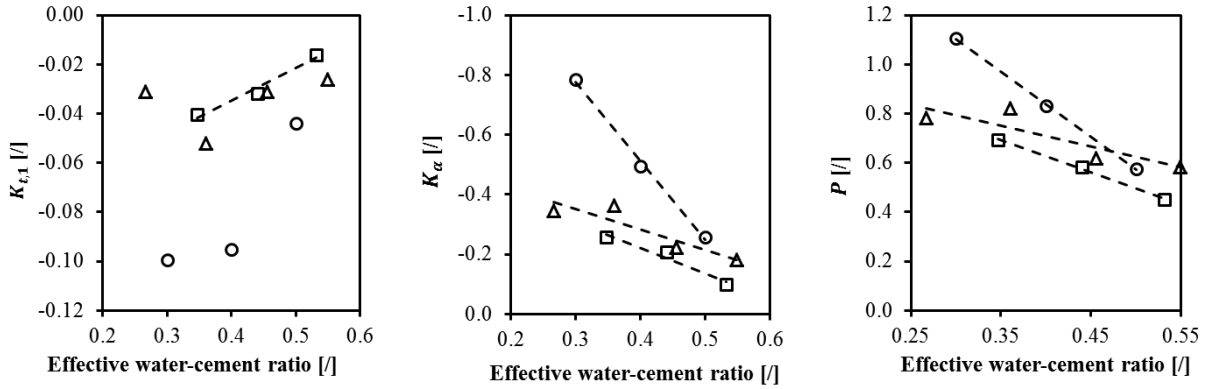

Figure 16 – Evolution of the kinetic creep factor according to the effective water-cement ratio

7.1.3. Multiscale Modelling

Concrete is a complex heterogeneous composite material for which the behaviour is studied on several scales ranging from the nanometer scale [10–15] to the macroscopic scale. Several approaches were developed in order to upscale the behaviour of concrete from very fine scales to larger scale with advanced homogenization methods. This part of the chapter focuses on the ability of some known models to perform the transition between cement paste, mortar and concrete in term of elastic and creep behaviour.

► E-modulus

Several analytical predictive models for two phases composite materials have been developed for the determination of the E-modulus in the past [16,17]. A synthesis of basic and more elaborated models is given in Table 9.

Table 9 – Two phases composite materials models for predicting the E-modulus of concrete.

Model	Equations	
Voigt	$E_{C,Voigt} = E_m V_m + E_a V_a$	4
Reuss	$\frac{1}{E_{C,Reuss}} = \frac{V_m}{E_m} + \frac{V_a}{Ea}$	5
Hirsch-Dougill	$\frac{1}{E_{C,Hirsch}} = 0.5\left(\frac{1}{E_{C,Voigt}} + \frac{1}{E_{C,Reuss}}\right)$	6
Popovics	$E_{C,Popovics} = 0.5\left(E_{C,Voigt} + E_{C,Reuss}\right)$	7
Counto	$\frac{1}{E_{C,Counto}} = \frac{1-\sqrt{V_a}}{E_m} + \left(\frac{1-\sqrt{V_a}}{\sqrt{V_a}}E_m + E_a\right)^{-1}$	8
Hashin	$E_{C,Hashin} = \left[\frac{(E_m + E_a) + (E_a - E_m)V_a}{(E_m + E_a) - (E_a - E_m)V_a}\right]E_m$	9
Bache and Nepper-Christensen	$E_{C,Bache} = (E_m)^{V_m} x (E_a)^{V_a}$	10
Mehmel-Kern	$E_{C,Mehmel-Kern} = \frac{\sqrt[3]{V_a^2}}{\frac{\sqrt[3]{V_a}}{E_a} + \frac{1-\sqrt[3]{V_a}}{E_m}} + E_m\left(1 - \sqrt[3]{V_a^2}\right)$	11
Illston	$E_{C,Illston} = \left[\frac{1-\sqrt[3]{V_a}}{E_m} + \frac{\sqrt[3]{V_a}}{E_a\sqrt[3]{V_a^2} + E_m\left(1-\sqrt[3]{V_a^2}\right)}\right]^{-1}$	12
Maxwell	$E_{C,Maxwell} = \frac{2E_m + E_a - 2V_a(E_m - E_a)}{2E_m + E_a + V_a(E_m - E_a)}E_m$	13
Hobbs	$E_{c,Hobbs} = E_m.\left[1 + \frac{2V_a(E_a - E_m)}{E_a + E_m - V_a(E_a - E_m)}\right]$	14

Where E_c is the E-modulus of the concrete, E_m is the E-modulus of the cement matrix, E_a is the E-modulus of the aggregate, V_m is the volume fraction of the cement matrix and V_a is the volume fraction of aggregate. In the next part of this chapter, the index a and m are related to respectively the aggregate and the cement matrix.

The physical representation of some of these models is given in Figure 17. The Reuss's and Voigt's models are respectively the lower and upper bounds of the predicted elastic modulus.

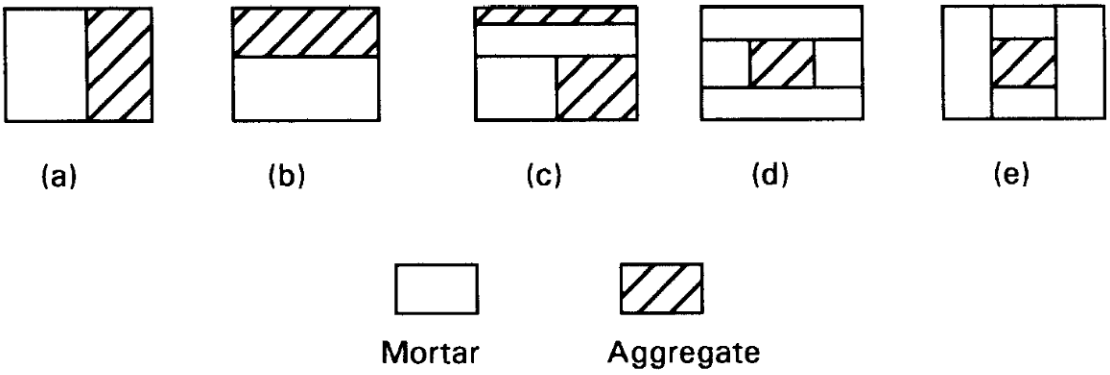

Figure 17 – Illustration of composite models [17], (a) Voigt – (b) Reuss – (c) Hirsch – (d and e) Counto.

These models assume that the Poisson's ratio of the cement matrix and the aggregate is constant and equal (generally it is considered that the Poisson's ratio of each component is equal to 0.2). It is possible to consider the real value of the Poisson's ratio of each component individually by using the bulk modulus K and the shear modulus G. The relations between the bulk and shear modulus with the elastic modulus and the Poisson's ratio are given in Equation 15 and 16.

$$K = \frac{E}{3.(1-2\nu)} \quad 15$$

$$G = \frac{E}{2.(1+\nu)} \quad 16$$

The Model of Mori-Tanaka [18] uses both parameters (Equations 17 and 18). As reported by [7], this model is appropriate for materials that exhibit a strong matrix-inclusion morphology and mechanical interactions between particles. This corresponds to the situation of concrete.

$$K_c = K_m + \frac{V_a.K_m.\left(\frac{K_a}{K_m}-1\right)}{1+\frac{3K_m}{3K_m+4G_m}(1-V_a)\left(\frac{K_a}{K_m}-1\right)} \quad 17$$

$$G_c = G_m + \frac{V_a.G_m.(G_a-G_m)}{1+\frac{6(4K_m+2G_m)}{5(3K_m+4G_m)}(1-V_a)\left(\frac{G_a}{G_m}-1\right)} \quad 18$$

Another assumption concerns the grain size distribution of the sand and aggregate and the associated compactness of the granular skeleton. This parameter is not considered in the models already presented. De Larrard and Le Roy [19,20] have developed the trisphere model (Equation 19) for which the compactness of the granular skeleton is considered with the parameter g^*.

$$E_C = \left(1 + 2V_a.\frac{E_a^2 - E_m^2}{(g^*-V_a).E_a^2 + 2.(2-g^*).E_a.E_m + (g^*+V_a).E_m^2}\right)E_m \quad 19$$

The parameter g^* depends on the type of aggregate. The Equation 20 is used for crushed aggregate, and the Equation 21 is used for rounded aggregate [21].

$$g^* = 1 - 0.45.\left(\frac{d}{D}\right)^{0.19} \quad 20$$

$$g^* = 1 - 0.39.\left(\frac{d}{D}\right)^{0.22} \quad 21$$

Where d is the equivalent diameter of the smallest aggregate and D the diameter of the biggest.

From E-modulus results obtained on cement paste, the predictive value of the mortar and concrete E-modulus is compared to the experimental results. For the homogenization, four data are missing: the E-modulus and the Poisson's ratio of the sand and aggregate. A Poisson's ratio of 0.2 and 0.15 are respectively considered for the sand and the aggregate. In the literature, no accurate data of the E-modulus was obtained and a wide range of data exists. The E-modulus of the sand (alluvial siliceous sand) varies between 60-120 GPa and the one of the aggregate (amphibolite crushed aggregate) varies in a range between 75-100 GPa [23–25]. Therefore these values will be optimized for each model separately and then compared to existing data from the literature. The experimental results were obtained for different effective water-cement ratio for the three scales. Per consequent, it is not possible to directly compare results. For that reason, the linear relations obtained between the parameters of the model and the effective water-cement ratio are used in order to define the evolution of the E-modulus in function of the advancement degree of reaction for the three scales of the material. Four effective water-cement ratios are used: 0.3, 0.4, 0.5 and 0.6. For the compositions with mineral additions, no correction is carried out on the effective water-cement ratio. For each model presented above, the homogenization is done in three steps. First, the results from the cement paste are used to define the E-modulus of the mortars. During this step, the E-modulus of the sand is defined by optimizing the correspondence between the results of the E-modulus of mortars obtained by homogenization and coming from the experimental results. This optimization is only done for results of the E-modulus obtained at an advancement degree of reaction of 1 in order to highlight the robustness of the model to correctly predict the evolution of the E-modulus at very early age. This optimization is based only on results obtained from compositions without mineral addition. Secondly, the same operation is performed in order to define the E-modulus of the aggregate by using data from mortar and concrete. Finally, from cement paste data, the E-modulus of concrete is directly defined. In Table 10, a synthesis of the data optimized for each model (E-modulus of the sand E_s and aggregate E_a) and the root-mean-square deviation obtained between predicted values by the model and the experimental results is presented. The root-mean-square deviation is computed according to the Equation 22. In this equation the index m is related to the model and the index h is related to the homogenization.

Table 10 – Synthesis of the data optimized for each model and the root-mean-square deviation obtained between predicted values of the E-modulus by the model and the experimental results.

Model	E_s	E_a	RMSD [GPa]		
	[GPa]	[GPa]	CP→M	M→C	CP→C
Voigt	48	56	30.5	12.1	27.0
Reuss	190	93	23.4	15.4	44.3
Hirsch-Dougill	67	68	6.4	6.5	12.5
Popovics	61	69	14.2	8.3	17.7
Counto	77	69	11.6	7.1	19.0
Hashin	72	72	11.6	8.7	21.9
Bache and Nepper-Christensen	70	70	2.9	6.8	8.1
Mehmel-Kern	66	73	8.2	8.3	17.2
Illston	66	66	5.3	7.3	10.6
Maxwell	63	68	5.8	6.8	12.4
Hobbs	92	73	14.8	8.7	25.5
Mori-Tanaka	45	57	10.6	7.0	24.2

Trisphere	64	69	4.7	6.7	9.8

$$RMSD = \sqrt{\frac{\sum_{i=1}^{n}\left(\left(E_{m03,i}-E_{h03,i}\right)^2+\left(E_{m04,i}-E_{h04,i}\right)^2+\left(E_{m05,i}-E_{h05,i}\right)^2+\left(E_{m06,i}-E_{h06,i}\right)^2\right)}{4.n}} \quad 22$$

Among the factors which influence the amplitude of the E-modulus of concrete, the E-modulus of the sand and aggregate plays an important role. From this synthesis, it is observed that the optimized value of the E-modulus of the sand varies between 45 GPa (Mori-Tanaka model) and 190 GPa (Reuss Model). But mainly the values of E_s are in a range between 61 and 77 GPa corresponding to the wide interval found in the literature (60-120 GPa). Lower variations are obtained in the optimized value of the E-modulus of the aggregate E_a. The extreme values are 56 GPa (Voigt's model) and 93 GPa (Reuss model) but the main part of the optimized values of E_a are in a very close range between 68 and 73 GPa. Therefore the optimized values of E_a are under the lower bound of results obtained in the literature (75-100 GPa). Nevertheless, this result is close to the lower bound. Therefore optimized values of the E-modulus of the inclusion can be considered as acceptable. For each transition between two scales, the root-mean-square deviation is computed from results between an advancement degree of reaction between 0.15 and 1. Even if the Bache and Nepper-Christensen's model is not associated to any physical meaning, it is the model providing the minimal error. The trisphere's and Illston's models give also a very low error which proves their ability to predict the E-modulus of mortars and concretes with knowledge of the cement paste E-modulus. It is generally observed that the transition between mortar and concrete is better predicted than the transition between cement paste and mortar. In order to highlight the main difference obtained in the homogenization, two models are tested: the model of Mori-Tanaka and the trisphere model. The Model of Mori-Tanaka has the advantage to predict the evolution of the E-modulus and at the same time the evolution of the Poisson's ratio whereas the trisphere model is the best physically-based model. Results from other homogenization models are given in Annexe I.

In Figure 18, the model of Mori-Tanaka is used. An optimized value of 44.5 and 57 GPa is obtained for respectively the E-modulus of the sand and aggregate. The transition between cement paste and mortar is globally well predicted for compositions without mineral addition. However the beginning of the development of the E-modulus is not well predicted till an advancement degree of reaction of 0.4. This is mainly due to the fact that the final setting occurs earlier for mortars. In contrast, the start of the evolution of the E-modulus is well predicted for the SCM composition whereas the evolution is underestimated for an advancement degree of reaction higher than 0.3. The transition between mortar and concrete is also well predicted globally for the composition without mineral addition. For an effective water-cement ratio of 0.6, the model underestimates the value of the E-modulus. For the composition SCM, the general evolution of the E-modulus is not well predicted by the model. No experimental data are available for the CPSCM composition before an advancement degree of reaction of 0.6. Results from the model and the homogenization of the CPSCM before an advancement degree of reaction of 0.6 are therefore strongly questionable and will be not discussed hereafter. When upscaling directly from the cement paste to the concrete, the differences observed just before are largely more marked. For a low effective water-cement ratio, a strong overestimation is done whereas the opposite phenomenon occurs for high effective water-cement ratio. The delay in the beginning of the development of the E-modulus is also significant. Therefore when predicting the E-modulus on concrete composition with Mori-Tanaka model, a clear underestimation of the E-modulus is done at very early age.

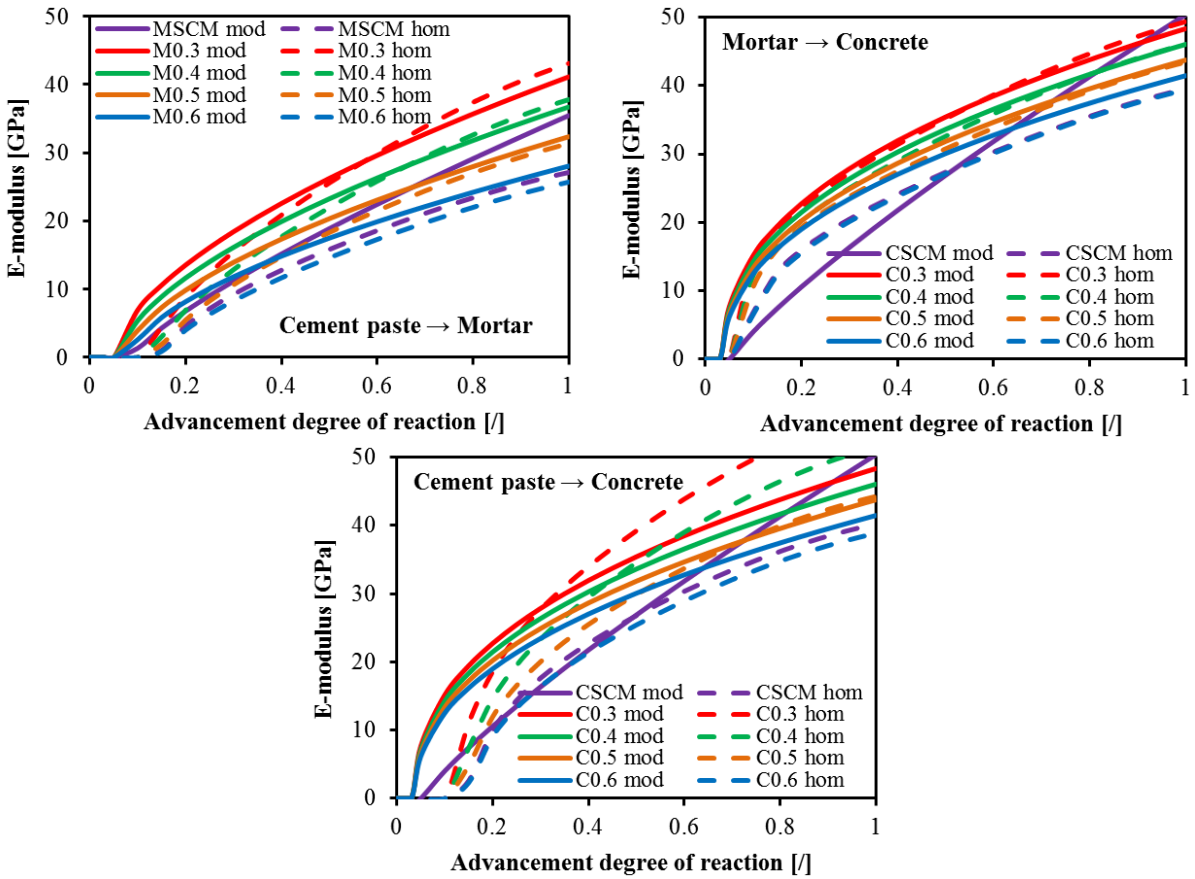

Figure 18 – Evolution of the E-modulus, comparison between values modeled from experimental data and values predicted by homogenization with the model of Mori-Tanaka [18].

The Mori-Tanaka model allows also predicting the Poisson's ratio. In Figure 19, the values predicted by the model are compared to the model calibrated with the experimental data. It is generally observed that:

- The transition between cement paste and mortar is not well predicted by the model. A clear overestimation of the Poisson's ratio is done whatever the age of the material and the composition.
- The model is able to accurately predict the Poisson's ratio of concrete by using data from mortar especially for composition with low water-cement ratio.
- The direct upscale between cement paste and concrete is not well predicted and leads to a global overestimation of the Poisson's ratio.
- The effect of the water-cement ratio on the final amplitude of the Poisson's ratio does not change according to Mori-Tanaka model. Therefore the difference of trend according to the scale of the material observed previously in this chapter cannot be explained by the simultaneous consideration of the bulk and shear modulus.

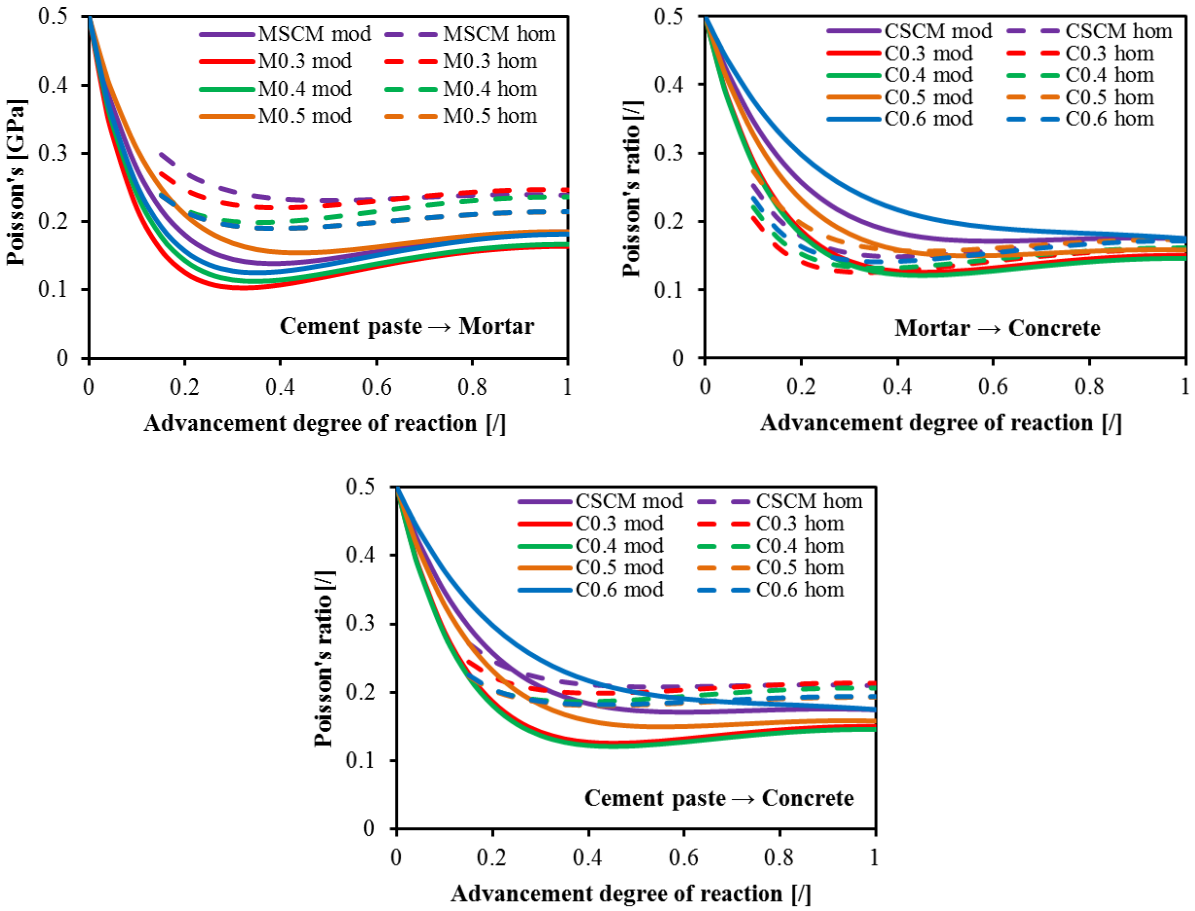

Figure 19 – Evolution of the Poisson's ratio, comparison between values modeled from experimental data and values predicted by homogenization with the model of Mori-Tanaka [18].

In Figure 20, the trisphere model is used. An optimized value of 64 and 69 GPa is obtained for respectively the E-modulus of the sand and the aggregate. The transition between cement paste and mortar is globally well predicted for compositions without mineral addition. As with Mori-Tanaka model, a slight difference is observed just after the setting period. The transition between mortars and concrete is also well predicted for the composition without mineral addition. A slight overestimation is observed for composition with low water-cement ratio and inversely an underestimation of the E-modulus occurs for composition with high water-cement ratio. When passing directly from the cement paste to the concrete, the difference observed just before are slightly more marked. For low effective water-cement ratio, an overestimation of the E-modulus is done whereas the opposite phenomenon occurs for high effective water-cement ratio. The delay in the beginning of the development of the E-modulus is marked till an advancement degree of reaction of 0.2. As with Mori-Tanaka model, the results of the composition SCM are not well predicted for each upscaling. But globally, this model is able to correctly define the evolution of the E-modulus in term of kinetic. Per consequent, the trisphere model is a robust tools when working on multi-scale analysis of cement based materials. The only drawback of this method comes from the assumption related to the value of the Poisson's ratio of the cement paste and aggregate which is considered as equal to 0.2.

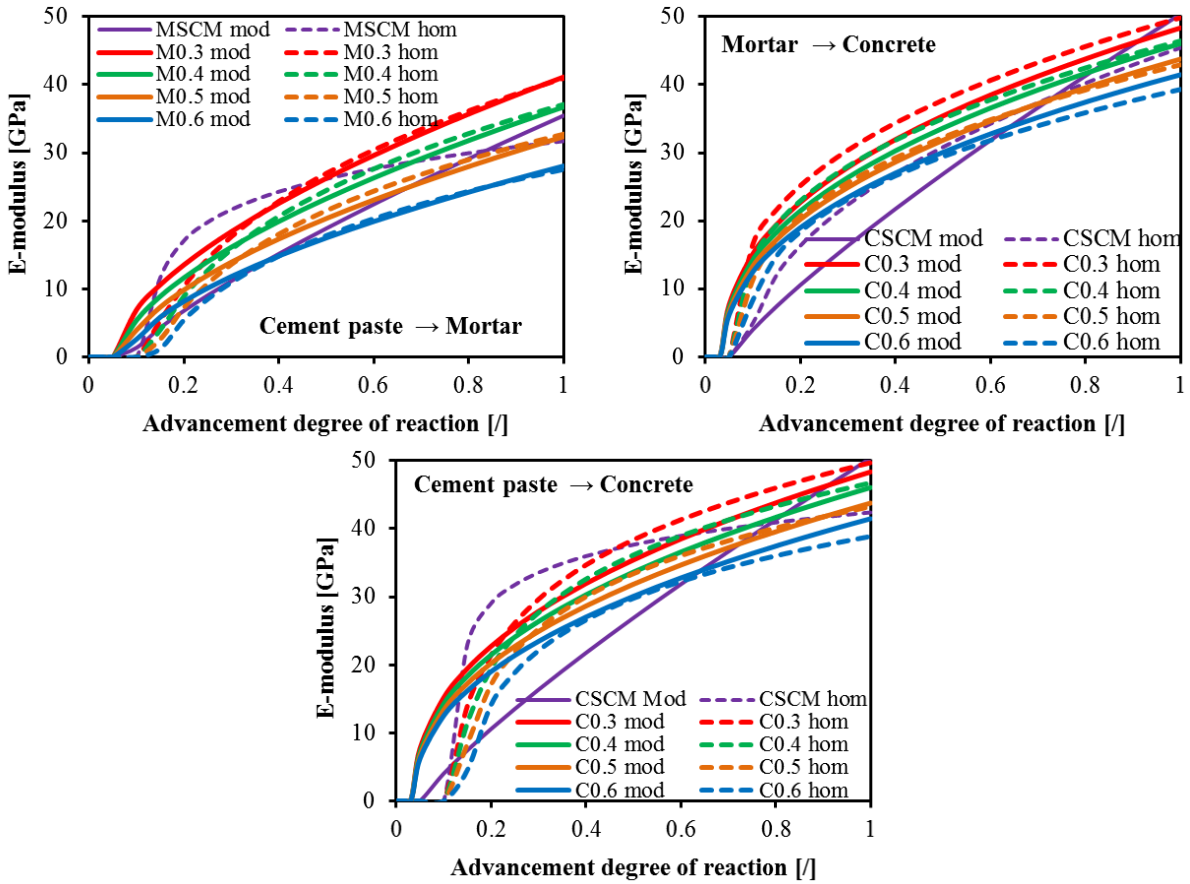

Figure 20 – Evolution of the E-modulus, comparison between values modeled from experimental data and values predicted by homogenization with the trisphere model [19,20].

The prediction of the E-modulus could be improved by considering directly the ITZ in the calculation. The cement paste would then be considered a two component material. The first component of the cement paste is close and around of the aggregates and corresponds to the ITZ and the second component corresponds to the cement paste farther from the aggregates. However, it is still necessary to know the thickness of this ITZ and its mechanical properties.

► Amplitude creep factor

From experimental results, it was observed that the presence of aggregate increases the difference in the development of the amplitude creep factor between different water-cement ratios. This is in contrast with other properties as the E-modulus for which aggregate has a dilution effect on the variations observed on the cement paste. To understand the influence of the aggregate on the development of the short term creep, concrete is simplified into a single spherical non-creeping aggregate particle coated by a homogeneous spherical creeping body. The relative creep ratio between two phases is governed by the aggregate content V_a and a restraining factor n_A (Equations 23, 24 and 25). A similar methodology was used in [26] to define the restriction of the shrinkage by the aggregate.

$$A = \frac{\varepsilon_{cr}(t' + 5min, t')}{\varepsilon_{el}(t')} \leftrightarrow \varepsilon_{cr}(t' + 5min, t') = A(t').\varepsilon_{el}(t') = A(t').\frac{\sigma}{E(t')} \quad 23$$

$$\frac{\varepsilon_{cr,C}(t'+5min,t')}{\varepsilon_{cr,M}(t'+5min,t')} = \frac{\left(A_C.\frac{\sigma}{E_C}\right)}{A_M.\frac{\sigma}{E_M}} = \frac{A_C}{A_M}.\frac{E_M}{E_C} = (1-V_a)^{n_A} \quad 24$$

$$\mathrm{n_A} = \frac{\ln\left(\frac{A_C}{A_M}.\frac{E_M}{E_C}\right)}{\ln(1-V_a)} \quad 25$$

In Figure 21, the creep ratio between cement paste, mortar and concrete is presented according to the advancement degree of reaction of the material. It is generally observed that:

- When upscaling from cement paste to mortar, the creep ratio increases during the hydration process for each composition without mineral addition. The creep ratio is very low at very early age and corresponds to a value of 0.1 for an advancement degree of reaction of 0.3 whereas the creep ratio varies between 0.3 and 0.45 for an advancement degree of reaction equal to 1. The kinetic of evolution of this creep ratio is similar between each composition. For composition with high water-cement ratio, the creep ratio is lower and this difference increases during the hydration process. Therefore it is observed that when upscaling from cement paste to mortar, the influence of the aggregate is not the same on creep for different water-cement ratios. For the SCM composition, the trend of the creep ratio is completely different. At very early age, the creep ratio is high and decreases during the hydration process. For an advancement degree of reaction of 1, the creep ratio is equivalent to the one of the other composition without mineral addition.
- Similar observations on the influence of the aggregate are done for the upscaling between mortar and concrete. However the kinetic of evolution of the creep ratio is different. For high water-cement ratios, the effect of the age of the material on the creep ratio is very small whereas a decrease of the creep ratio is observed for low water-cement ratios. At very early age, the creep strain of concrete are nearly equivalent to the corresponding mortar for an effective water-cement ratio of 0.3. For the SCM composition, a similar evolution of the ratio is observed except at very early age when the creep ratio increases.
- When upscaling directly from cement paste to concrete, the evolution of the creep ratio is very similar to the creep ratio corresponding to the upscaling between cement paste and mortar. The difference of magnitude of the creep ratio is higher for the different water-cement ratios.

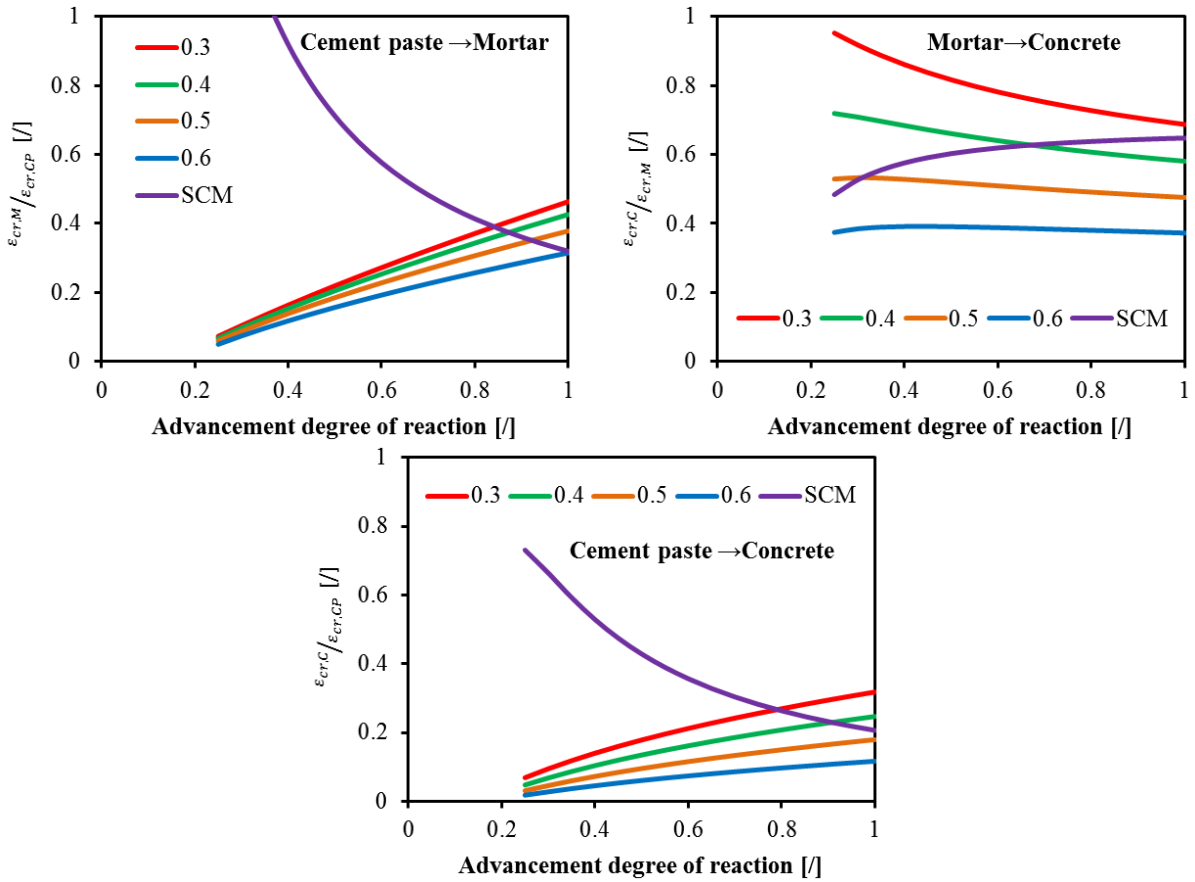

Figure 21 – ratio of the creep deformation of two different scales of the material according to the advancement degree of reaction.

The evolution of the restraining factor n_A is presented in Figure 22 according to the advancement degree of reaction. A value of 1 of the restraining factor means that a mix law could be directly used to upscale. When this factor is higher than one, this means that the creep deformations are restrained by the presence of aggregate. A clear effect of the age of the material is observed on the value of the restraining factor. When upscaling, the restraining factor is always higher for composition with higher water-cement ratios. The restriction of the creep deformation of the cement paste by sand is higher during early age which corresponds to the period when the cement paste has a low E-modulus. When upscaling from mortar to concrete, the restriction does not change strongly with the age at loading. A value of n_A lower than 1 is obtained for composition with an effective water-cement ratio of 0.3 and 0.4. This means that the presence of aggregate increases the creep deformation of the cement paste for low water-cement ratio. The direct upscale from cement paste to concrete is very similar in term of kinetic for the different water-cement ratios. Only the amplitude of the restriction seems to change. A general decrease of the restraining factor is observed. For an effective water-cement ratio of 0.3, the factor n_A is very close to a value of one. The general trend of evolution of the restraining factor is linked to the upscale from cement paste to mortar and therefore by the restriction of the creep deformation by the sand. While the aggregate seems to have an impact more on the general amplitude of the restraining factor. For the SCM composition, the evolution of the restraining factor is different. n_A has a very low value lower than 1 at very early age and then increases during the hydration process. This means that, at very early age, the presence of sand increases the creep strain of the cement paste. However for higher advancement degree of reaction (when slag has reacted), the restraining factor corresponds to the one of the other composition without mineral addition.

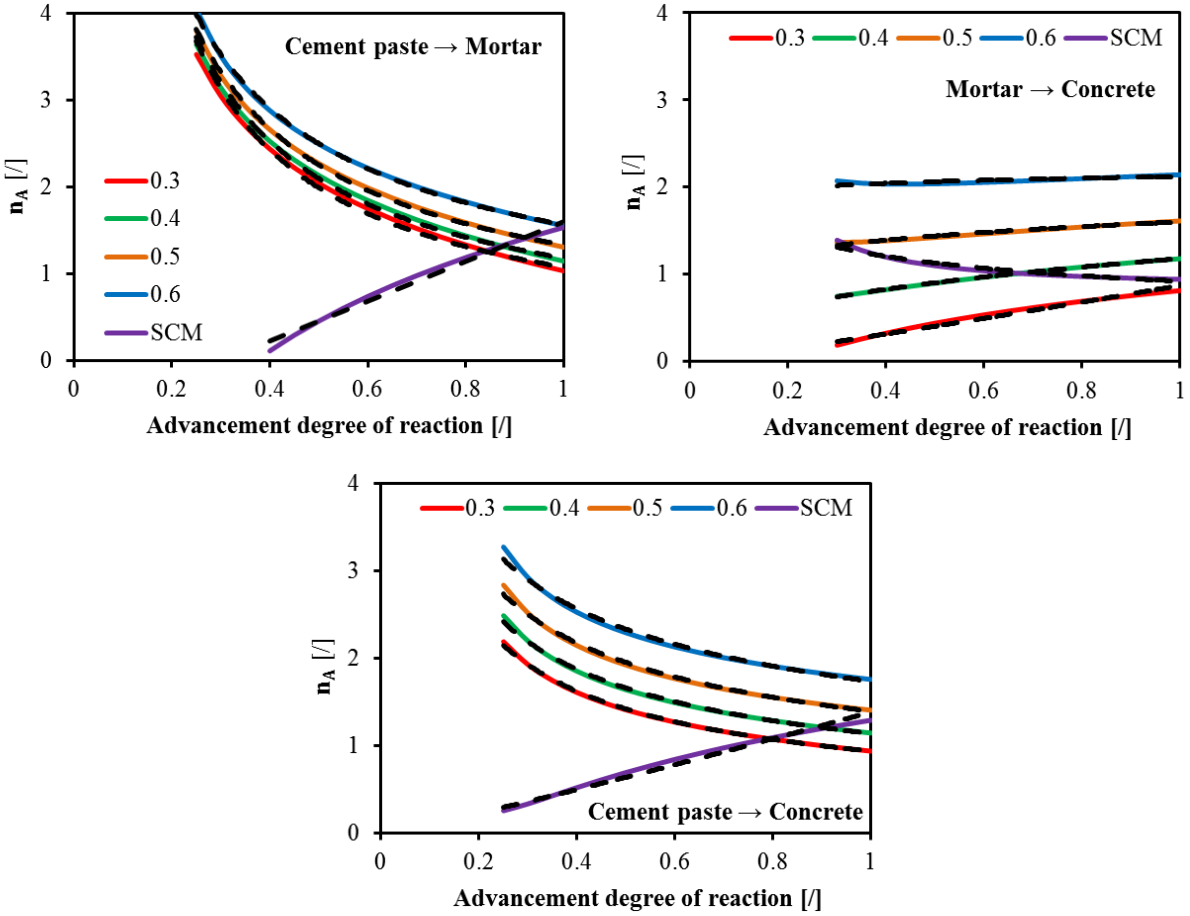

Figure 22 – Evolution of the restraining factor n_A according to the advancement degree of reaction.

In contrast to the results obtained with the E-modulus, the influence of the water-cement ratio is low for cement paste whereas more significant change is observed for concrete. Therefore, the presence of the aggregate increases the influence of the water-cement ratio on the development of the creep strain. Two mechanisms can be associated to this difference:

- The change of porosity at the ITZ,
- The development of microcracking during the hydration.

Based on the results obtained on the compressive strength, it was observed that the change of porosity at the ITZ is more marked for concrete composition with low water-cement ratio. Therefore, it is possible that a higher quantity of water movement occurs in this area and leads to an increase of the creep strain. During hydration, autogenous and thermal deformations of the cement paste are partially restrained by the aggregate. If the amplitude of the restriction is too significant, microcracking inside the cement paste can take place. This can provoke an increase of the creep strain especially for low water-cement ratio for which the amplitude of the free deformation of the cement paste is very significant. However these explanations are just an interpretation of the difference observed. More information about the distribution of the porosity and the development of microcracking at the ITZ are needed in order to prove such affirmation.

The restraining factor is modeled with a power law as expressed in Equation 26.

$$n_A = \omega_A . \alpha^{\chi_A}$$

where ω_A and χ_A are material parameters. Value of each parameter is given in Table 11. A good agreement is observed between results of Equation 26 and experimental results.

Table 11 – Parameters of Equation 26 for the different effective water-cement ratio and the different transitions in the scales of the material.

	W_{eff}/C	0.3	0.4	0.5	0.6	SCM
CP→M	ω_A	1.08	1.18	1.33	1.57	2.28
	χ_A	-0.89	-0.83	-0.76	-0.68	-0.68
M→C	ω_A	0.87	1.18	1.60	2.12	0.92
	χ_A	1.11	0.39	0.15	0.04	-0.30
CP→C	ω_A	0.94	1.14	1.40	1.74	0.92
	χ_A	-0.60	-0.54	-0.49	-0.42	-0.30

In Figure 23 and Figure 24, the parameters ω_A and χ_A are plotted according to the effective water-cement ratio. The parameter ω_A is linked to the effective water-cement ratio by a logarithmic expression. Whereas the parameter χ_A is linked to the effective water-cement ratio by a linear law, except for the transition between mortar and concrete where this relation follows an exponential law.

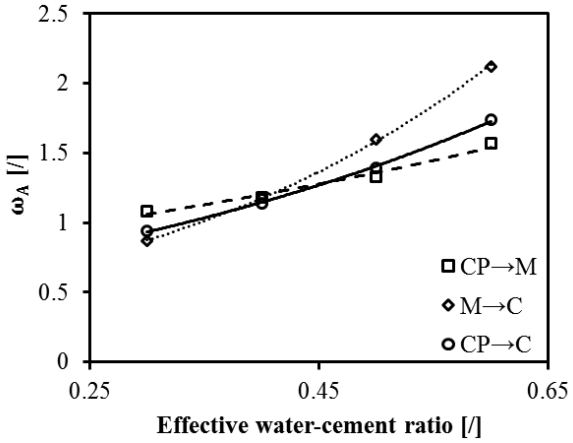

Figure 23 – Evolution of ω_A according to the effective water-cement ratio

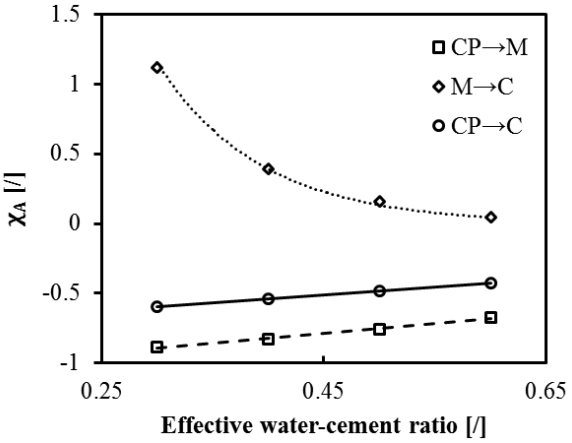

Figure 24 – Evolution of χ_A according to the effective water-cement ratio

SECTION 7.2 – MULTISCALE MONITORING AND MODELLING OF AUTOGENOUS DEFORMATION AND COEFFICIENT OF THERMAL EXPANSION

7.2.1. Materials and methods

► Materials and mixture compositions

The tests presented here were fully performed in the laboratory of civil Engineering at ULB on three concretes (C0.4, C0.5 and C0.6), four mortars (M0.3, M0.4, M0.5 and M0.6) and two cement pastes (CP0.3 and CP0.5) with several water-cement ratios. Additionally, tests were also performed on three

compositions corresponding to the compositions C0.4, M0.4 and CP0.4 for which 75% of the cement is substituted by slag (50%) and limestone filler (25%). For each scale, the aggregate content is identical. The effective water-cement ratios of the concrete compositions are 0.35, 0.46 and 0.55. The effective water-cement ratios of the mortar compositions are 0.27, 0.36, 0.46 and 0.55. The effective water-cement ratios of the cement paste are 0.3, 0.4 and 0.5. The calculation of the effective water-cement ratio is done by removing the water absorbed by the aggregate and the sand. It is assumed that the sand and the aggregate are fully saturated when samples are tested.

► Time-scale

For consideration of the ageing and the main temperature effect, concrete properties are expressed in function of the equivalent time t_{eq} or the advancement degree of reaction α. The apparent activation energy was determined in [3] with the compressive strength results obtained at 3 different temperatures (38 kJ/mol for compositions with CEM I and 48 kJ/mol for SCM composition).

► Setting time

Setting time of the concretes was determined by monitoring of the transmission of the ultrasound P- and S-waves through concrete according to the method developed by Carette & Staquet [1,2]. Values of the initial and final setting time are given in Chapter 3.

► Assessment of the autogenous strain and the coefficient of thermal expansion CTE

The free deformation is measured from casting by using the BTJADE [27] for concrete and the AUTOSHRINK [28] for cement paste and mortar. The tests protocol used with each device is presented in the Chapter 4, section 1.

7.2.2. Results

► Coefficient of thermal expansion CTE

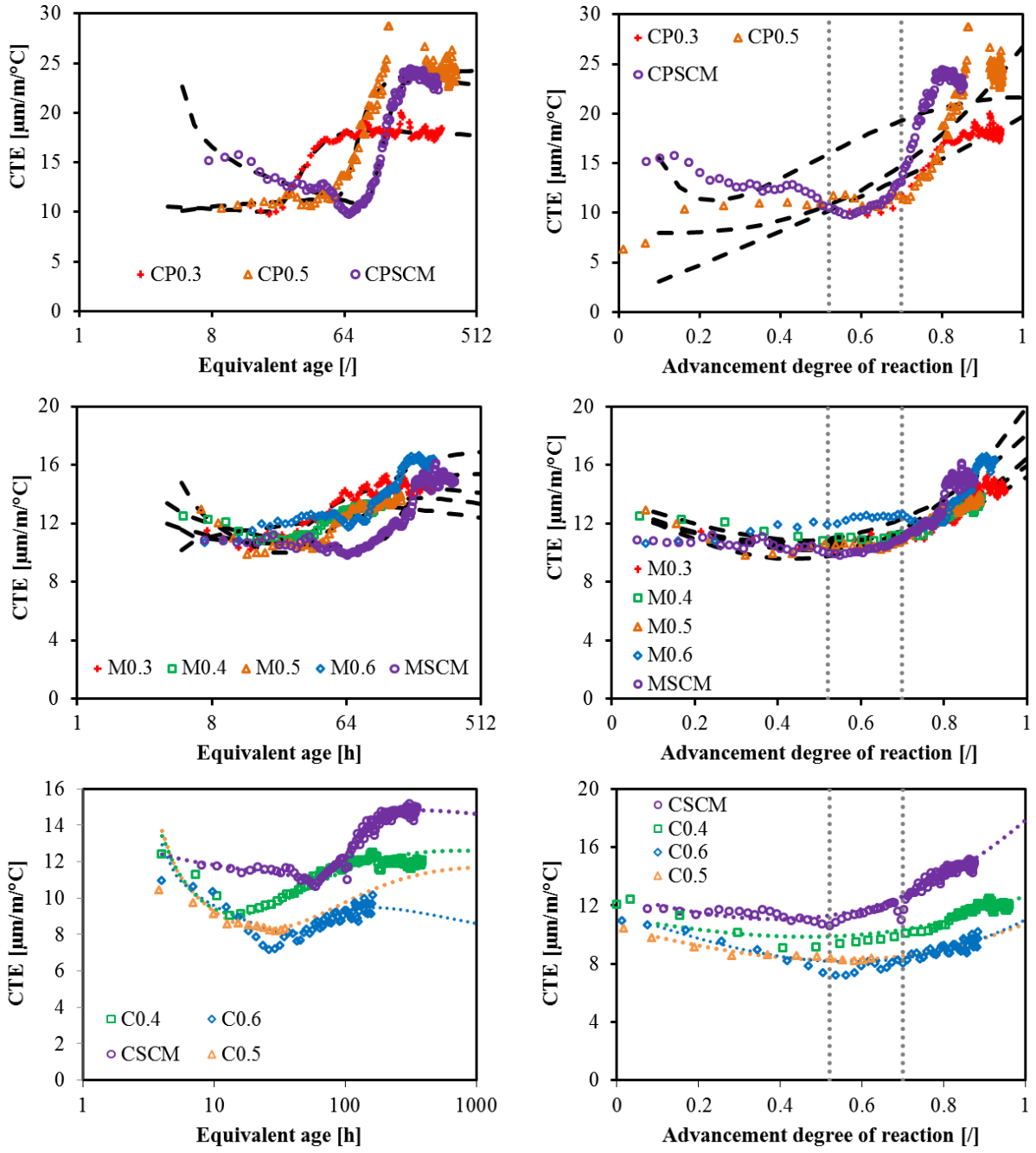

Figure 25 – Evolution of the coefficient of thermal expansion according to the equivalent age and the advancement degree of reaction. Dash lines correspond to the model.

Results of the CTE are given in Figure 25 according to the equivalent time and the advancement degree of reaction. Three successive stages are observed in the results. Before the initial setting time, the value of the CTE is very high and is associated to the CTE of a liquid. The main values obtained before the initial setting time are around 100-200 µm/m/°C. However these results are not shown because these measurements before setting are not purely related to the free deformation of the concrete but also to the artifact coming from the settling and the sedimentation of the material which occurs before setting. During setting, a strong and quasi instantaneous decrease of the CTE takes

place. Then a low decrease of the CTE is observed for each composition till a minimum value varying between 7 and 10 µm/m/°C for concrete, 9 and 12 µm/m/°C for mortar and 10 and 12 µm/m/°C for cement paste. After this minimum, an increase of the CTE is observed till a threshold value varying between 10 and 14 µm/m/°C for concrete, 13 and 16 µm/m/°C for mortar and 17 and 26 µm/m/°C for cement paste. The effect of the water-cement ratio is different according to the scale of the material. For concrete, the value of the CTE is globally higher for composition with low water-cement ratio except during the first hours after setting. The partial substitution of cement by slag and limestone filler increases significantly the value of the CTE. The age of concrete when the minimum of the CTE occurs depends on the concrete composition. For composition with low water-cement ratio, the minimum value takes place just after setting but for high water-cement ratio the minimum value of the CTE occurs later. For CSCM mixture, the minimum of the CTE occurs at an equivalent age of 60 hours. This is explained by the very low rate of the hydration process during this period. When looking at the results obtained with mortar according to the advancement degree of reaction, no significant difference is observed in the evolution of the CTE. The final amplitude of the CTE is slightly higher for the composition with high water-cement ratio and for the mixture with mineral additions. At the cement paste scale, the results of the CTE are quite close till an advancement degree of reaction of 0.7. Then a high increase of the CTE occurs. In term of advancement degree of reaction, this increase takes place in a very short period for the CPSCM composition. This increase for the compositions CP0.3 and CP0.5 has a same kinetic but a different amplitude. For higher water-cement ratio, the final amplitude of the CTE is higher. Therefore the effect of the water-cement ratio is different according to the scale of the material. For concrete, the final amplitude of the CTE is higher for low water-cement ratio while for cement paste, the inverse trend is observed. For each scale, when regarding the results according to the advancement degree of reaction, the minimum value of the CTE as well as the start of the final threshold value of the CTE occurs during a very close interval (between 0.52 and 0.7) for each composition.

► Autogenous deformation

Results of the autogenous strain are given in Figure 26 according to the equivalent time and the advancement degree of reaction. Autogenous strains are set to zero at the final setting time. Values obtained before the final setting are not directly associated to the autogenous strain. Values of the final setting time are given in chapter 3. Two stages are observed in the results. Just after the final setting time, the swelling of the concrete takes place till a maximum value. Then a shrinkage period (due to self-desiccation of the cement paste) occurs. As expected, for composition with high water-cement ratio, the swelling is significant (40 µm/m for the composition C0.6, 70 µm/m for the composition M0.6 and 220 µm/m for the composition CP0.5) and close to zero for low water-cement ratio. The effect of the partial substitution of cement by slag and limestone filler is strongly highlighted on the swelling. The age of the material when the maximum of the autogenous strain occurs depends on the composition. For composition with low water-cement ratio, the maximum value takes place just after setting but for low water-cement ratio, the maximum value of the autogenous deformation occurs later. For SCM mixture, the maximum of the autogenous strain occurs at an equivalent age of 60 hours. This is explained by the very low rate of the hydration process during this period. When looking at the results according to the advancement degree of reaction, the maximum value of the autogenous strain occurs during a very close interval (between 0.45 and 0.55) for each composition. Also the evolution of the autogenous strain is very similar for the different water-cement ratios between an advancement degree of reaction between 0.52 and 0.7 for each scale of the material.

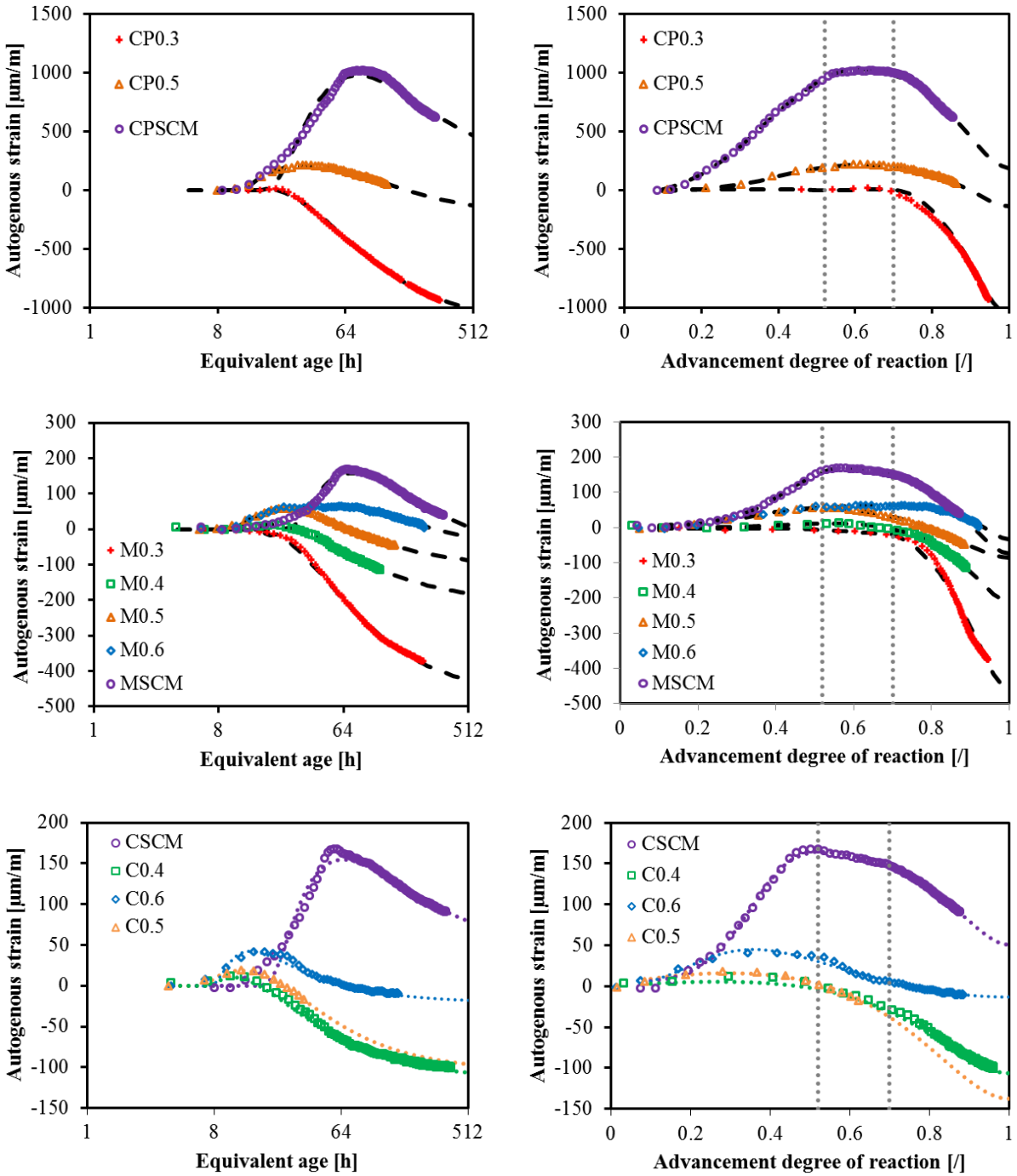

Figure 26 – Autogenous strain according to the equivalent time and the advancement degree of reaction. Dash lines correspond to the model.

7.2.3. Modelling

► Coefficient of thermal expansion

Equations presented in the Chapter 6 are used to model the evolution of the coefficient of thermal expansion. Values of each parameter are given in Table 12. Both models well represent the evolution of the CTE of mortar and concrete as shown in Figure 25. For cement paste, the model using the equivalent time is also able to correctly fit the results while the model using the advancement degree of reaction cannot represent correctly the evolution of the CTE because of the high increase of the CTE occurring during a short period (between an advancement degree of reaction between 0.6 and 0.8).

Table 12 – CTE parameters

	α_{t1} [µm/m/°C]	r_1 [/]	α_{t2} [µm/m/°C]	p_α [h]	r_2 [/]	$\alpha_{\alpha1}$ [µm/m/°C]	$\alpha_{\alpha2}$ [µm/m/°C]	c_α [/]
CP0.3	11.1	0.03	8.8	30.0	3.8	8.2	1.5	-2.1
CP0.5	10.1	-0.03	12.1	75.0	5.7	-9.4	8.1	-1.5
CPSCM	19.6	0.14	14.4	112.3	6.5	21.6	31.2	9.4
M0.3	12.4	0.06	5.4	37.1	2.1	-11.9	12.9	-0.77
M0.4	13.2	0.06	3.5	42.2	3.1	-12.0	13.7	-0.69
M0.5	14.7	0.14	7.4	46.6	1.7	-14.2	13.4	-0.83
M0.6	10.7	-0.04	3.6	114.4	4.6	-13.0	13.0	-0.88
MSCM	11.2	0.02	5.4	141.4	3.9	-18.6	13.5	-1.05
C0.4	15.0	0.27	11	35.0	0.8	-7.1	11.2	-0.57
C0.5	16.0	0.29	10	50	0.9	-8.3	10.5	-0.6
C0.6	17.0	0.3	9	65	1.0	-10.8	11.5	-0.64
CSCM	12.6	0.03	4.5	106.8	2.81	-11.3	12.7	-0.83

In Figure 27, the parameters p_α, $\alpha_{\alpha1}$ and $\alpha_{\alpha2}$ are plotted according to the effective water-cement ratio. The parameter p_α follows a same exponential trend for each scale of the material. This parameter is related to the time when the CTE starts to increase because of the self-desiccation phenomenon. The other parameters of the equivalent time model vary strongly with the parameter p_α and it is thus difficult to correlate these parameters to the effective water-cement ratio. For the parameters $\alpha_{\alpha1}$ and $\alpha_{\alpha2}$ coming from the model using the advancement degree of reaction, a good correlation is obtained with the advancement degree of reaction. The parameter $\alpha_{\alpha1}$ decreases linearly when the effective water-cement ratio increases while the parameter $\alpha_{\alpha2}$ seems constant for mortar and concrete with a value of respectively 13.3 µm/m/°C and 11.1 µm/m/°C.

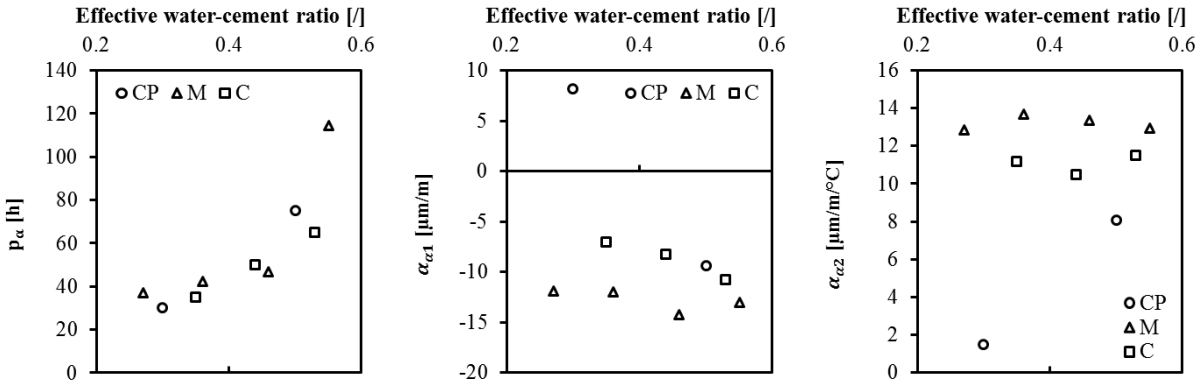

Figure 27 – Evolution of the CTE parameters according to the effective water-cement ratio.

► Autogenous strain

Equations presented in the Chapter 6 are used to model the evolution of the autogenous strain. Values of each parameter are given in Table 3. Both models well represent the evolution of the autogenous deformation for each scale of the material.

Table 13 – Autogenous strain parameters

	A_{sd} [µm/m]	p_{sd} [h]	A_{sw} [µm/m]	p_{sw} [h]	r_{sw} [/]	B_{sd} [µm/m]	a_{sd} [µm/m]	B_{sw} [µm/m]	β [/]	a_{sw} [/]	γ [/]
CP0.3	-1175	-58	33	11.3	11.8	-1244	7.7	336	1.5	10.0	0.48
CP0.5	-443	-115	224	7.3	2.3	-368	7.8	472	2.6	3.1	0.51
CPSCM	-1023	-164	1211	21.3	1.8	-968	6.3	2361	2.9	2.3	0.51
M0.3	-486	-49	16	15.8	17.8	-493	7.8	72	1.5	15.0	0.54
M0.4	-224	-59	19	8.54	3.6	-226	8.1	31	2.4	5.1	0.50
M0.5	-174	-59	67	6.8	2.4	-151	5.4	127	3.0	2.9	0.49
M0.6	-131	-193	67	5.8	1.6	-104	11.5	174	3.8	1.4	0.60
MSCM	-266	-188	189	28.3	2.9	-257	7.0	354	2.5	4.0	0.48
C0.4	-128	-27	15	4.4	4.7	-117	4.2	1583	0.2	0.0	0.7
C0.5	-127	-35	22	2.7	2.2	-166	3.9	51325	3017.0	0.0	0.7
C0.6	-91	-17	71	4.3	2.1	-174	1.0	307	5.1	1.6	0.5
CSCM	-130	-148	177	20.8	2.6	-120	5.7	330	3.0	3.7	0.5

In Figure 28, the parameters A_{SD} and r_{sw} coming from the equivalent time model are plotted according to the effective water-cement ratio. The parameter A_{SD} represents the final amplitude of the self-desiccation deformation. A strong increase of this parameter is observed for effective water-cement ratio lower than 0.4. The parameter r_{sw} is related to the kinetic of the swelling. This parameter follows a same trend for each scale of the material. In Figure 28, the final value of the autogenous strain obtained from the model using the advancement degree of reaction $\varepsilon_{au}(\alpha = 1)$ is also presented. An exponential trend is observed for each scale of the material.

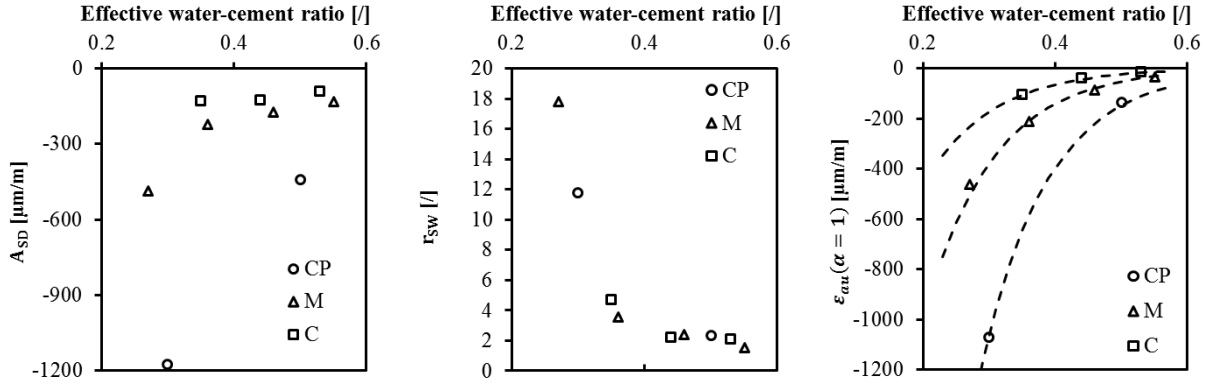

Figure 28 – Evolution of the autogenous deformation parameters according to the effective water-cement ratio. Dash lines correspond to model of Equation 27.

The final value of the autogenous deformation $\varepsilon_{au}(\alpha = 1)$ is modeled according to the effective water-cement ratio with the Equation 27.

$$\varepsilon_{au}(\alpha = 1) = A_{au}.\exp\left(\frac{W_{eff}}{C}.B_{au}\right) \quad 27$$

where B_{au} is equal to -9.8 and A_{au} depends on the scale of the material. A_{au} is equal to 20000, 7150 and 3300 µm/m for respectively cement paste, mortar and concrete.

7.2.4. Multiscale modelling

The methodology used for the multi-scale modelling of the E-modulus and the amplitude creep factor is extended here for the CTE and the autogenous deformation.

► Coefficient of thermal expansion

From experimental results, a difference of the influence of the water-cement ratio has been observed on the evolution of the CTE according to the scale of the material. The presence of aggregate has generally a dilution effect on the phenomenon occurring at the level of the cement paste. However properties of the cement paste such as the E-modulus and the Poisson's ratio are also important to consider when upscaling the CTE. Indeed, if a thermal variation is applied, the deformation of the cement paste is partially restrained by the aggregate. The degree of restriction of the cement paste depends on the difference of stiffness and CTE between the aggregate and the cement paste.

M. Wyrzykowski and P. Lura [29] have shown that the CTE of a mortar can be well predicted on the basis of the behaviour of the cement paste and the aggregate by using the Hobb's model [30] and the Rosen-Hashin bounds [31]. The same strategy is used here to predict the CTE of mortar and concrete with experimental data obtained on cement pastes. For the homogenization, six data are missing: the E-modulus, the Poisson's ratio and the CTE of the sand and aggregate. Values for Poisson's ratio of 0.2 and 0.15 are respectively be taken for the sand and the aggregate. According to the results obtained in the previous section, the E-modulus of the sand varies between 61 and 77 GPa and the E-modulus of the aggregate varies between 68 and 73 GPa. Therefore, an average value of 69 and 70.5 GPa is considered for respectively the E-modulus of the sand and aggregate. The linear CTE of the sand can be estimated within a range of 6-12 µm/m/°C and the one of the aggregate (amphibolite crushed aggregate) varies in a range between 3 and 10 µm/m/°C [32,33]. However, as no very accurate data of the CTE of the aggregate used is available, these values will be optimized separately and then compared to existing data from the literature. The homogenization is performed in two steps during which the CTE of the sand and aggregate are optimized.

The Hobb's model and the Rosen-Hashin bounds are given respectively in Equations 28 and 29-30.

$$\alpha_C = \alpha_m - \frac{(\alpha_m - \alpha_a).V_a.2.K_a}{K_m + K_a + V_a.(K_a - K_m)} \quad (28)$$

$$\alpha_C \leq (V_m.\alpha_m + V_a.\alpha_a) + \frac{4.V_m.V_a.G_a.(K_m - K_a)(\alpha_m - \alpha_a)}{3.K_m.K_a + 4.G_a.(V_m.K_m + V_a.K_a)} \quad (29)$$

$$\alpha_C \geq (V_m.\alpha_m + V_a.\alpha_a) + \frac{4.V_m.V_a.G_m.(K_m - K_a)(\alpha_m - \alpha_a)}{3.K_m.K_a + 4.G_m.(V_m.K_m + V_a.K_a)} \quad (30)$$

The results of the multi-scale modelling of the CTE are given in Figure 29. As the value obtained on mortar does not correspond in term of effective water-cement ratio to the cement paste, linear interpolation is used in order to define the value of the CTE on mortar for an effective water-cement ratio of 0.3 and 0.5. For concrete, a same methodology is used for an effective water-cement ratio of 0.5. However, for an effective water-cement ratio of 0.3, this methodology cannot be used. Therefore the evolution of the CTE obtained from the composition C0.4 (effective water-cement ratio of 0.35) is directly used for comparison with the predicted value on concrete at advancement degree of reaction

of 0.3. When upscaling from cement paste to mortar, an optimized value of 10.6 µm/m/°C is obtained for the CTE of the sand. This value is in agreement with results obtained in the literature.

In Figure 29, the results from the Hobb's model (dotted lines) are very close to the upper bound of the Rosen-Hashin's model (broken lines). For the SCM composition, the model well predicts the final value of the CTE and the evolution of the CTE till an advancement degree of reaction of 0.7. During the increase of the CTE (between an advancement degree of reaction of 0.7 and 0.8), the value of the CTE is overestimated. For an effective water-cement ratio of 0.3 and 0.5, the evolution of the CTE is globally very well predicted. When upscaling from experimental results of mortar to concrete, a strong dilution effect of the aggregate is observed. All results from the homogenization are very close and no significant difference is observed between the different compositions. An optimized value of 8.9 µm/m/°C of the CTE of aggregate is found. This is in coherence with range found in the literature (3 – 10 µm/m/°C). Finally, the upscaling to concrete is directly performed on the basis of the cement paste data. The evolution of the CTE is well predicted in term of kinetic of evolution. However, some differences in the general amplitude of the CTE are observed. For the composition CSCM and for a concrete with an effective water-cement ratio of 0.5, a general gap of 1.5 µm/m/°C is obtained. It is also observed that the difference of influence of the water-cement ratio on the scale of the material cannot be explained by this homogenization. The consideration of the bulk and shear modulus is not enough. Only a dilution effect of the aggregate on the evolution of the CTE is observed.

Per consequent, the experimental results confirm the ability of the Hobb's model to upscale from cement paste to mortar for classical compositions with effective water-cement ratio of 0.3 and 0.5 and compositions with 75% of cement substituted by mineral additions. The upscale from mortar to concrete is not so well predicted by the Hobb's model and the Rosen-Hashin bounds. The aggregate has a global dilution effect on the amplitude of the CTE.

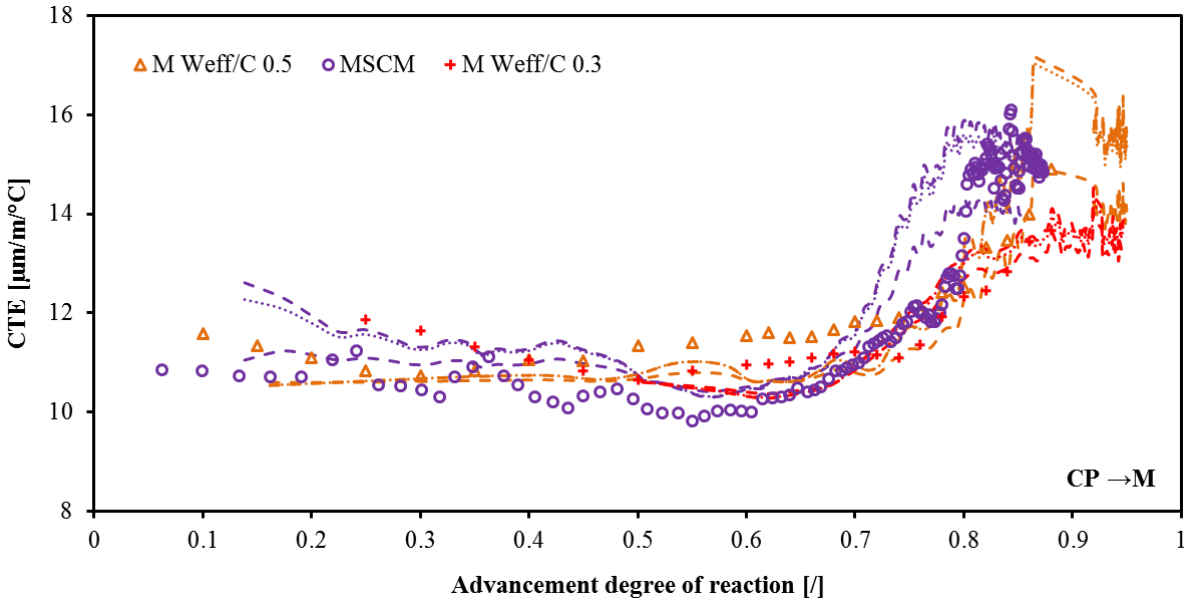

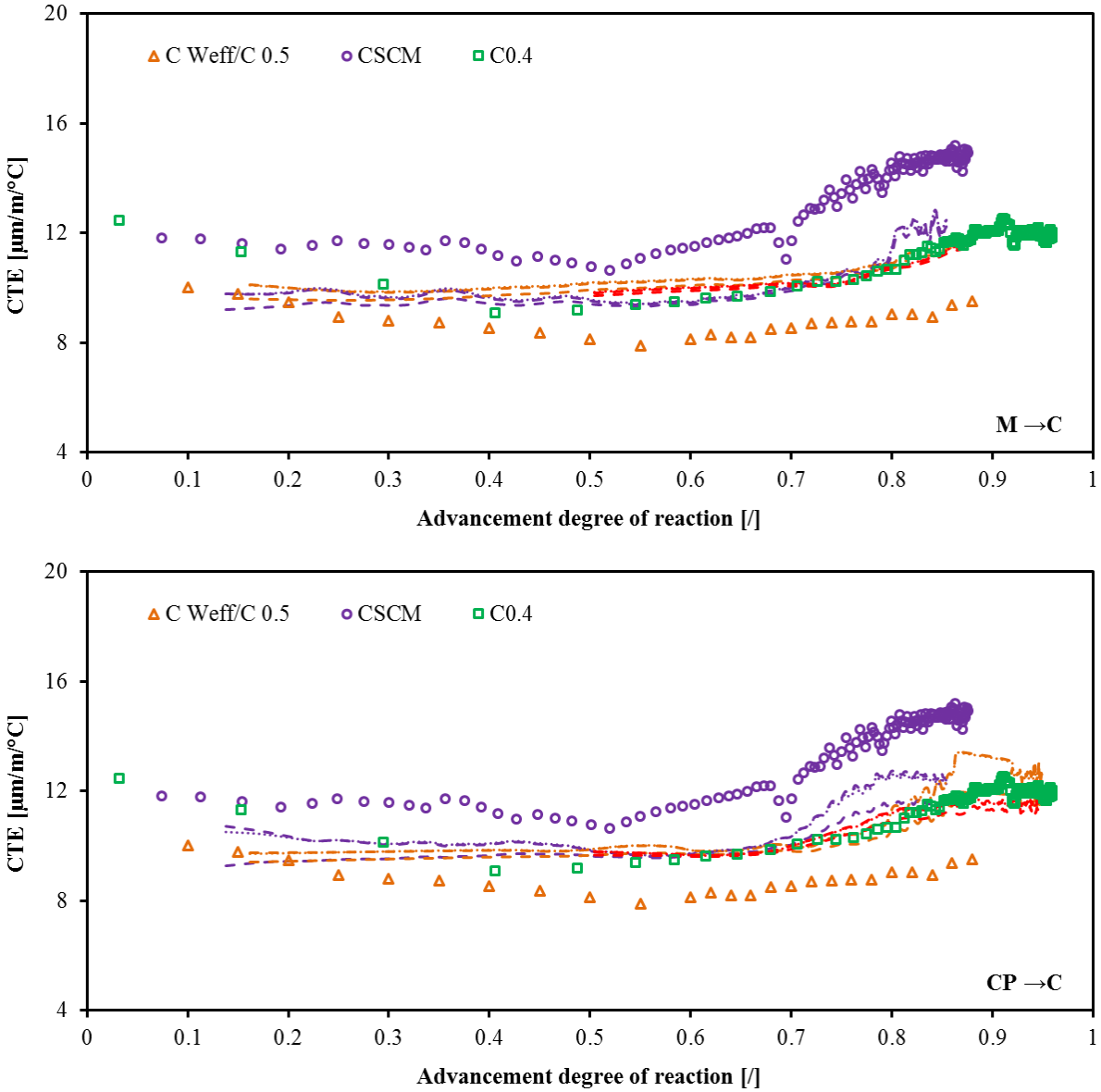

Figure 29 - Evolution of the coefficient of thermal expansion, comparison between interpolated values from experimental data and values predicted by homogenization. Broken lines correspond to the Rosen-Hashin bounds [31] and dotted lines correspond to Hobb's model [30].

► Autogenous strain

As described in [26], the restriction of the autogenous deformation of the cement paste by the sand and the aggregate can be modeled by a single spherical non-shrinking aggregate particle coated by a homogeneous spherical shrinking body. The relative shrinkage ratio between the two phases is governed by the aggregate content V_a and a restraining factor n_{au} as presented in Equation 31. For this modelling, it is assumed that aggregate stays saturated during the whole test. Therefore no transfert of water between cement paste and aggregate is considered here.

$$\frac{\varepsilon_M}{\varepsilon_{CP}} = (1 - V_a)^{n_{au}} \quad 31$$

In Chapter 3, some differences were observed in the evolution of the autogenous strain between results coming from the AUTOSHRINK and the BTJADE device. Therefore only results obtained on cement paste and mortar with AUTOSHRINK device are compared.

The analysis of the results is divided in two parts: the swelling and the shrinkage. As the value obtained on mortar does not correspond in term of effective water-cement ratio to the cement paste, linear interpolation is used in order to define the value of the CTE on mortar for an effective water-cement ratio of 0.3 and 0.5. For the SCM composition, data are directly compared. In Figure 30, the ratio of the autogenous swelling strain of mortar and equivalent cement paste is presented according to the advancement degree of reaction. Results obtained for an effective water-cement ratio of 0.3 are not presented because of the very low amplitude of the swelling. The autogenous swelling starts significantly at an advancement degree of reaction of 0.2. For an effective water-cement ratio of 0.5, the evolution of the swelling strain of the cement paste and mortar is nearly equivalent at very early age with a ratio close to 1. Then a strong decrease of this ratio occurs. This means that the presence of sand decreases strongly the evolution rate of the autogenous strain of the cement paste when the mortar hardens. Whereas the opposite observation is done for the SCM composition. The swelling of the mortar is almost zero in comparison of the mortar for very low advancement degree of reaction. Then the ratio increase but stays lower than the composition with an effective water-cement ratio of 0.5.

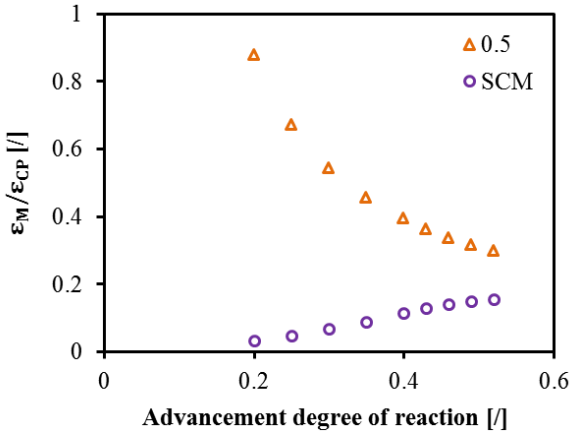

Figure 30 – Ratio of the autogenous swelling strain of mortar and equivalent cement paste according to the advancement degree of reaction.

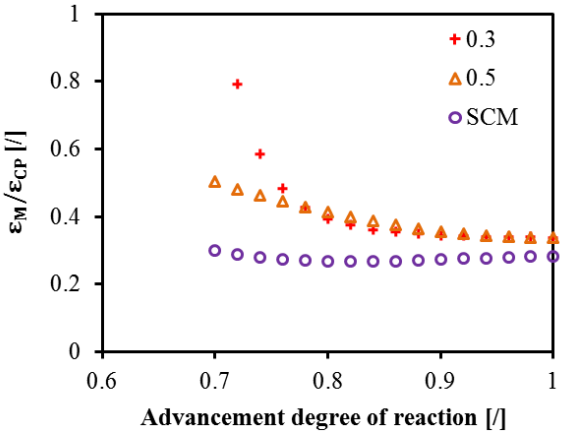

Figure 31 - Ratio of the autogenous shrinkage strain of mortar and equivalent cement paste according to the advancement degree of reaction.

In Figure 31, the ratio of the autogenous shrinkage strain of mortar and equivalent cement paste is presented according to the advancement degree of reaction. For each composition, the autogenous shrinkage starts significantly at an advancement degree of reaction of 0.7. In order to compare correctly the evolution of the autogenous shrinkage strain, the autogenous shrinkage strain are set to zero at an advancement degree of reaction of 0.7. The evolution of the ratio seems to be dependent on the nature of the binder but not on the effective water-cement contain. For the compositions with an effective water-cement ratio of 0.3 and 0.5, a same evolution is obtained. Small differences are observed at the start of the autogenous strain but these difference are not significant. For the SCM composition, this ratio is nearly constant and seems therefore independent on the age of the material.

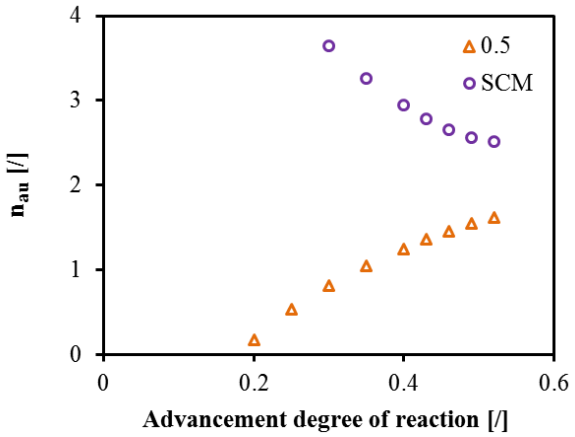

Figure 32 – Evolution of the restraining factor n_{au} according to the advancement degree of reaction during the swelling period.

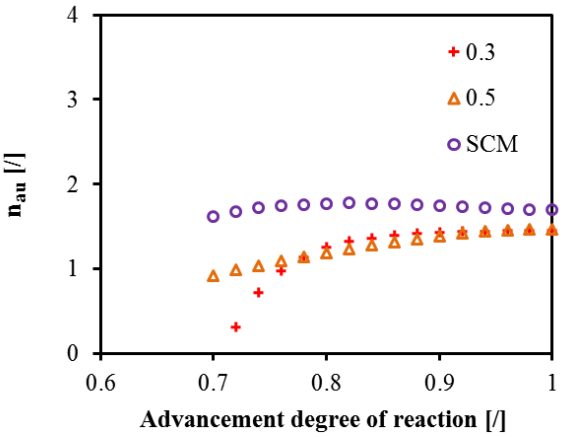

Figure 33 – Evolution of the restraining factor n_{au} according to the advancement degree of reaction during the shrinkage period.

In Figure 32, the restraining factor of the autogenous swelling strain is presented according to the advancement degree of reaction. It is observed that the restriction of the autogenous swelling strain of the cement paste is very consequent for the SCM composition at very early age. This restriction decreases with the advancement of the hydration but is still strong at the end of the swelling period. For an effective water-cement ratio of 0.5, the restraining of the cement paste is lower than 1 till an advancement degree of restriction of 0.3. Then this ratio increases till a value of 1.5 which represents a small restriction of the cement paste. This difference of evolution of the restraining factor can be explained by two parameters which are related to the viscoelastic behaviour of the material:

- When looking at the results expressed in equivalent time, the evolution of the autogenous swelling strain takes place in a very small time window of few hours for classical composition. This is in contrast with the SCM composition for which the development of the autogenous swelling occurs on a duration of few days. Therefore the creep/relaxation phenomenon is more limited in time for the composition without mineral addition.
- The E-modulus of the composition SCM is very low during the swelling period in comparison to the aggregate. Therefore the displacement of the cement paste is more restrained by the sand with the composition SCM than with the compositions without mineral addition.

Even if the degree of restriction is higher for the SCM composition, the development of the stress can be lower. Therefore, the restrain of the autogenous deformation of the cement paste can lead to the development of a largely higher quantity of microcrack in the cement paste CP0.5 than in CPSCM. These microcracks can explained the low degree of restriction of the cement paste.

In Figure 33, the restraining factor of the autogenous shrinkage strain is presented according to the advancement degree of reaction. As for the swelling period, the restraining factor is higher for the SCM composition. However, this difference is lower than the one occurring during the swelling period when the advancement degree of reaction decreases. For the SCM composition, the restraining factor is nearly constant during the whole shrinkage period whereas for the composition without mineral addition, n_{au} increases during the period. A very similar evolution is observed for an effective water-cement ratio of 0.3 and 0.5.

7.2.5. Relation between autogenous strain and CTE

It was observed in Chapter 6 that a linear relation exists between the CTE and the autogenous strain during the swelling and the self-desiccation period. This observation is extended here to cement paste and mortar. Since an advancement degree of reaction corresponding to the final setting till a value of 0.52, the autogenous strain increases (swelling) and the CTE decreases or stays constant. An increase of the water-cement ratio increases the magnitude of the swelling of the autogenous strain. For low water-cement ratio, this period is thus not well highlighted because of the very low amplitude of the swelling. After an advancement degree of reaction of 0.7, a clear decrease of the autogenous strain is observed for each scale of the material. For the CTE, an increase is observed till an advancement degree of reaction of 0.8 (SCM composition) or 0.9 (composition without mineral addition). Between an advancement degree of reaction of 0.52 and 0.7, both autogenous strain and CTE do not evolve significantly. During this period it can be assumed that mechanisms linked to the swelling and the self-desiccation occur simultaneously and cancel each other. From these observations, the values of the CTE and the autogenous deformation are compared in Figure 34. The autogenous swelling is compared to the decrease of the CTE between an advancement degree of reaction corresponding to the final setting and a value of 0.52. The autogenous shrinkage is compared to the evolution of the CTE between an advancement degree of reaction of 0.7 and 1. Autogenous shrinkage is set to zero at the maximum of the autogenous strain for this comparison.

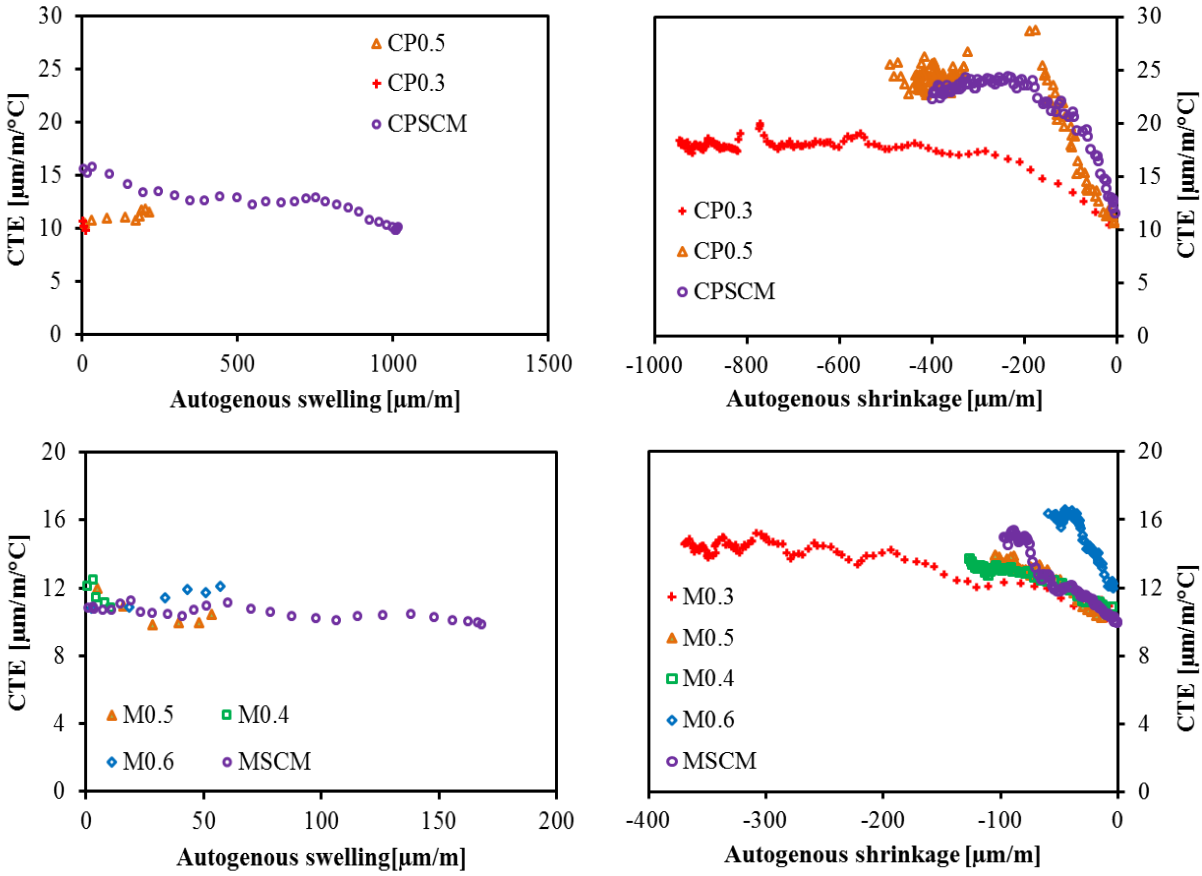

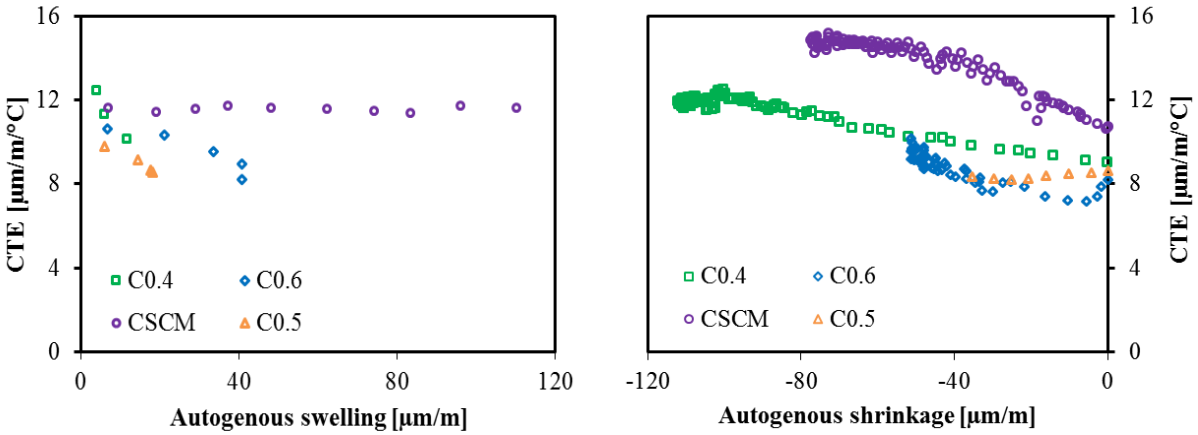

Figure 34 - Evolution of the CTE according to the autogenous swelling or the autogenous shrinkage.

The swelling period takes place during a very short period counted in hours. Per consequent only few data are available for the compositions without mineral addition during this period. The results obtained on the three scales of the material show a global decrease of the CTE during this period except on cement paste for which the CTE stays constant for the composition CP0.5. The influence of the water-cement ratio depends on the scale of the material. On concrete, the decrease of the CTE is higher for composition with a low water-cement ratio. Whereas no effect of the water-cement ratio is observed on cement paste and mortar. For the SCM composition, more data are available during the swelling period. For this composition, the scale of the material seems also to play an important role. On concrete, no evolution of the CTE is observed during the swelling period while a small decrease of the CTE is observed on mortar and a significant decrease is observed on cement paste. During the shrinkage period, a clear link between the evolution of the CTE and the autogenous shrinkage is observed. The influence of the water-cement ratio is also strongly marked on the results. For high water-cement ratio and for a same increase of the autogenous shrinkage, a higher increase of the CTE is observed on cement paste and mortar. This increase occurs till an advancement degree of reaction of 0.8 (SCM composition) or 0.9 (composition without mineral addition). Then the autogenous shrinkage continues to evolve significantly but not the CTE. However, the evolution of both parameters is governed by the evolution of the relative humidity. In Figure 35, the evolution of the relative humidity of several cement pastes with different water-cement ratios is shown. It is observed that the relative humidity stays very high for compositions with a water-cement ratio higher than 0.59 while a maximum decrease of 25% of the relative humidity is observed for cement paste with a water-cement ratio of 0.27. The most part of the decrease of the relative humidity occurs during the first ten days of the material.

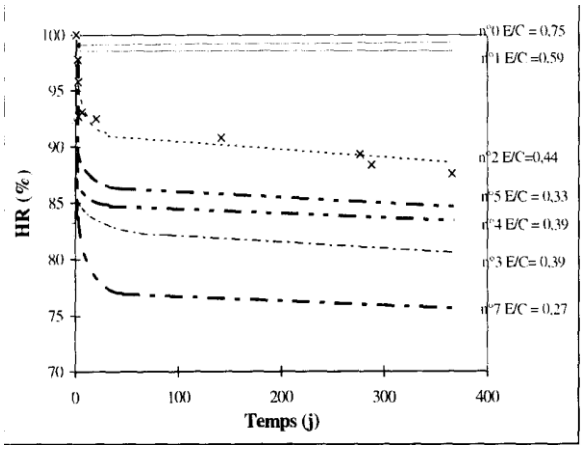

Figure 35 – Evolution of the relative humidity according to the age of cement pastes for different water-cement ratios.

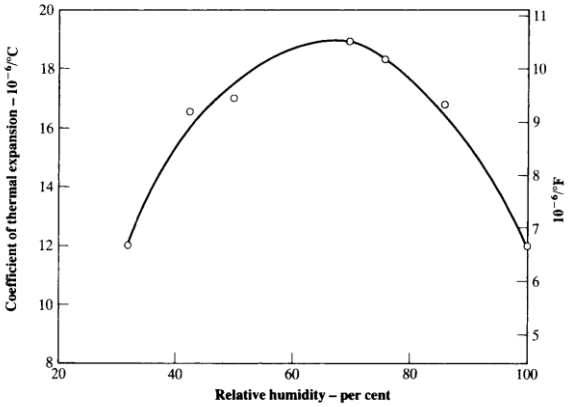

Figure 36 – Evolution of the CTE in function of the effective water-cement ratio [34]

The autogenous shrinkage is related to the self-desiccation of the cement paste during the hydration process. This results in a decrease of the relative humidity till a value of around 75% [35–38]. In this range, the main mechanisms involved in self-desiccation shrinkage would be capillary tension[2] and disjoining pressure[3] [39]. The coefficient of thermal expansion is related to the degree of water saturation in the pore system excluding the air/macro pores [40]. In Figure 36, the relation between the coefficient of thermal expansion and the relative humidity is presented [ref]. It is observed that the CTE increases till a threshold value of the relative humidity of 75% as for the self-desiccation shrinkage. Therefore, experimental results can be interpreted as follows: the CTE is not linked to all mechanisms responsible of the self-desiccation but only to a part of them. However more works are needed in order to interpret correctly these mechanisms and their link with the evolution of the CTE.

Therefore it is observed that the autogenous strain and the CTE are linked in term of mechanism. When the swelling of the cement paste occurs, a decrease of the CTE is observed. The influence of the water-cement ratio on the amplitude of the variation of the CTE depends on the scale of the material and also on the nature of the binder. On the contrary, the autogenous strain associated to the self-desiccation of the material are linearly linked to the increase of the CTE till a threshold value of the advancement degree of reaction. After this threshold, the self-desiccation phenomenon goes on to develop while the CTE keeps constant.

[2] Capillary pores are initially filled with water. As water is consumed by the hydration of cement, voids appear and liquid-vapour menisci are created in the pores. Thus capillary tension develops in the pore water and compressive stresses are generated.

[3] The disjoining pressure develops in the microstructure of cement paste in the areas of hindered adsorption. The formulation of this approach of hindered adsorption was first developed by Powers, then by Feldman and Sereda [41] and Bazant [42]. At a given temperature, the thickness of the adsorbed water layer depends on the local relative humidity. If the distance between two solid surfaces is lower than two times the thickness of the free adsorbed layer, adsorption is hindered and disjoining pressure develops. It tends to separate the adjacent surfaces. A decrease of the relative humidity results in a decrease of this pressure thus it causes shrinkage.

CONCLUSIONS

Section 7.1.

Repeated minute-long loading tests were applied since very early age on thirteen cement based materials including four concretes, fives mortars and four cement pastes. For each scale of the material, three or four different water-cement ratios are studied. In addition, ECO-composition is also studied at each scale. The Poisson's ratio, the E-modulus and an amplitude creep factor corresponding to the creep coefficient obtained after 5 minutes of loading are defined. For all the investigated properties, models developed in chapter 6 are used. Models are expressed in function of the equivalent time, the advancement degree of reaction and the gel-space ratio for the understanding of the physical mechanisms associated to the water-cement ratio and also for computational modelling purpose.

Based on the experimental results obtained on cement paste (E-modulus and Poisson's ratio), 13 existing predictive models for two phases composite material are used to predict the evolution of the E-modulus at concrete scale. Values of the E-modulus of the sand and aggregate are optimized in order to have a good agreement with experimental data on concrete for an advancement degree of reaction equal to 1. It is observed that the model of Bache and Nepper-Christensen, the trisphere model and the Illston model are able to accurately predict the evolution of the E-modulus of concrete since very early age and by using cement paste data. In contrast, the model of Mori-Tanaka, which considers the development of the Poisson's ratio, is not able to accurately predict the evolution of the E-modulus and Poisson's ratio since very early age on concrete. In addition, the use of these models cannot correctly define the properties of concrete around setting because of the non-consideration of the offset of the final setting between the different scales of the material.

In contrast with other mechanical properties, the presence of aggregate increases the influence of the water-cement ratio on the development of the amplitude creep factor. To understand the influence of the aggregate, concrete is simplified into a single spherical non-creeping aggregate particle coated by a homogeneous spherical creeping body. It is observed that the presence of sand restrained strongly the development of the cement paste during the very early age whereas the aggregate has a similar restraining effect on the creep strain whatever the age of the material especially for high water-cement ratio.

The linear trends observed between the effective water-cement ratio and the material parameters of several models are valid for effective water-cement ratio between 0.25 and 0.55. For lower or higher effective water-cement ratio, more tests are needed to prove if this linear relation is still valid.

Section 7.2.

Every 160 minutes, thermal variations of 3°C are applied on a cement paste, mortar and concrete with the devices so-called BTJADE and AUTOSHRINK. Thermal and autogenous strains are distinguished by creating a fictive thermal cure at 20°C directly derived from the experimental results. Models developed in the Chapter 6 are used for the modelling of the autogenous deformation and the coefficient of thermal expansion (CTE). Physical mechanisms are highlighted and considered in the modelling.

From the experimental results, a difference of the influence of the water-cement ratio has been observed on the evolution of the CTE according to the scale of the material. For concrete, the final amplitude of the CTE is higher for low water-cement ratio while for cement paste the inverse trend is

observed. Properties of the cement paste and inclusions (E-modulus, Poisson's ratio, CTE) are important to consider when upscaling the CTE. The Hobb's model and the Rosen-Hashin bounds consider these properties. This methodology allows predicting very accurately the CTE of mortar but not the one of concrete.

The restriction of the autogenous deformation of the cement paste by the sand and the aggregate is modeled by a single spherical non-shrinking aggregate particle coated by a homogeneous spherical shrinking body. This modelling is divided in two parts: the swelling and the shrinkage. During the swelling period, the restriction of the autogenous strain of the eco-cement paste caused by the sand decreases with the advancement of the hydration but stays strong. For an effective water-cement ratio of 0.5, the restraining of the cement paste is lower than 1 till an advancement degree of restriction of 0.3. A lower restrain occurs during the shrinkage period.

For the SCM composition, the restraining factor is nearly constant during the whole shrinkage period. Whereas for the composition without mineral addition, the restraining factor increases during the hydration process. A very similar evolution is observed for an effective water-cement ratio of 0.3 and 0.5.

Finally, it is observed that the autogenous strain and the CTE are linked in term of mechanism. When the swelling of the cement paste occurs, a decrease of the CTE is observed. The influence of the water-cement ratio on the amplitude of the variation of the CTE depends on the scale of the material and also on the nature of the binder. On the contrary, the autogenous strain associated to the self-desiccation of the material are linearly linked to the increase of the CTE till a threshold value of the advancement degree of reaction. After this threshold, self-desiccation phenomenon goes on to develop while the CTE keeps constant.

For further study, the evolution of the relative humidity should be measured during the test and considered in the modelling. 3D modelling with the consideration of the creep could also help to interpret the restriction of the cement paste due to aggregate.

REFERENCES

[1] J. Carette, S. Staquet, Monitoring the setting process of eco-binders by ultrasonic P-wave and S-wave transmission velocity measurement: Mortar vs concrete, Constr. Build. Mater. 110 (2016) 32–41. doi:10.1016/j.conbuildmat.2016.02.019.

[2] J. Carette, S. Staquet, Monitoring the setting process of mortars by ultrasonic P and S-wave transmission velocity measurement, Constr. Build. Mater. 94 (2015) 196–208. doi:10.1016/j.conbuildmat.2015.06.054.

[3] J. Carette, S. Staquet, Monitoring and modelling the early age and hardening behaviour of eco-concrete through continuous non-destructive measurements: Part I. Hydration and apparent activation energy, Cem. Concr. Compos. 73 (2016) 10–18. doi:10.1016/j.cemconcomp.2016.07.002.

[4] K.L. Scrivener, E.M. Gartner, Microstructural gradients in cement paste around aggregate particles, Mater. Res. Soc. Symp. Proc. 114 (1988) 77–86.

[5] NIST, http://www.nist.gov/el/building_materials/evcctl.cfm, (n.d.).

[6] B. Delsaute, C. Boulay, J. Granja, J. Carette, M. Azenha, C. Dumoulin, et al., Testing Concrete E-modulus at Very Early Ages Through Several Techniques: An Inter-laboratory Comparison, Strain. 52 (2016) 91–109. doi:10.1111/str.12172.

[7] O. Bernard, F.-J. Ulm, E. Lemarchand, A multiscale micromechanics-hydration model for the early-age elastic properties of cement-based materials, Cem. Concr. Res. 33 (2003) 1293–1309. doi:10.1016/S0008-8846(03)00039-5.

[8] A.M. Neville, J.J. Brooks, Concrete technology, 1987.

[9] S. Harsh, Z. Shen, D. Darwin, Strain-rate sensitive behavior of cement paste and mortar in compression, ACI Mater. J. 87 (1990) 508–516. doi:10.14359/1931.

[10] M. Vandamme, F.-J. Ulm, Nanogranular origin of concrete creep., Proc. Natl. Acad. Sci. U. S. A. 106 (2009) 10552–7. doi:10.1073/pnas.0901033106.

[11] W.R.L. da Silva, J. Němeček, P. Štemberk, Application of multiscale elastic homogenization based on nanoindentation for high performance concrete, Adv. Eng. Softw. 62–63 (2013) 109–118. doi:10.1016/j.advengsoft.2013.04.007.

[12] J. Xiao, W. Li, Z. Sun, D.A. Lange, S.P. Shah, Properties of interfacial transition zones in recycled aggregate concrete tested by nanoindentation, Cem. Concr. Compos. 37 (2013) 276–292. doi:10.1016/j.cemconcomp.2013.01.006.

[13] J. Frech-Baronet, L. Sorelli, J.-P. Charron, New evidences on the effect of the internal relative humidity on the creep and relaxation behaviour of a cement paste by micro-indentation techniques, Cem. Concr. Res. (2016). doi:10.1016/j.cemconres.2016.10.005.

[14] M. Vandamme, F.-J. Ulm, Nanoindentation investigation of creep properties of calcium silicate hydrates, Cem. Concr. Res. 52 (2013) 38–52. doi:10.1016/j.cemconres.2013.05.006.

[15] C.A. Jones, Z.C. Grasley, Short-term creep of cement paste during nanoindentation, Cem. Concr. Compos. 33 (2011) 12–18. doi:10.1016/j.cemconcomp.2010.09.016.

[16] T. Bilir, Investigation of performances of some empirical and composite models for predicting the modulus of elasticity of high strength concretes incorporating ground pumice and silica fume, Constr. Build. Mater. 127 (2016) 850–860. doi:10.1016/j.conbuildmat.2016.10.054.

[17] F.P. Zhou, F.D. Lydon, B.I.G. Barr, Effect of coarse aggregate on elastic modulus and compressive strength of high performance concrete, Cem. Concr. Res. 25 (1995) 177–186. doi:10.1016/0008-8846(94)00125-I.

[18] T. Mori, K. Tanaka, Average stress in matrix and average elastic energy of materials with misfitting inclusions, Acta Metall. 21 (1973) 571–574. doi:10.1016/0001-6160(73)90064-3.

[19] F. de Larrard, R. Le Roy, Relation entre formulation et quelques propriétés mécaniques des bétons à hautes performances, Mater. Struct. 25 (1992) 464–475. doi:10.1007/BF02472636.

[20] R. Le Roy, Déformations instantanées et différées des bétons à hautes performances, PhD thesis, Ecole Nationale des Ponts et Chaussées, Paris, France, 1995.

[21] F. de Larrard, P. Tondat, Sur la contribution de la topologie du squelette granulaire à la résistance en compression du béton, Mater. Struct. 26 (1993) 505–516. doi:10.1007/BF02472861.

[22] No Title, (n.d.). http://community.dur.ac.uk/~des0www4/cal/dams/geol/mod.htm (accessed February 11, 2016).

[23] W. Zhou, D. Fan, Y. Liu, H. Xie, Measurements of wave velocity and electrical conductivity of an amphibolite from southwestern margin of the Tarim Basin at pressures to 1.0 GPa and temperatures to 700 °C: Comparison with field observations, Geophys. J. Int. 187 (2011) 1393–1404. doi:10.1111/j.1365-246X.2011.05220.x.

[24] J. Trckova, Physical, Mechanical and Deformational Properties of Meta-Basalts, Amphibolites and Gneisses From Ksdb-3 Compared With Surface Analogues, Acta Geodyn. Geomater. 2 (2005) 39. http://irsm.cas.cz/materialy/acta_content/2005_04/4_Trckova.pdf.

[25] S. Ji, T. Shao, K. Michibayashi, C. Long, Q. Wang, Y. Kondo, et al., A new calibration of seismic velocities, anisotropy, fabrics, and elastic moduli of amphibole-rich rocks, J. Geophys. Res. E Planets. 118 (2013) 4699–4728. doi:10.1002/jgrb.50352.

[26] Z. Liu, W. Hansen, Aggregate and slag cement effects on autogenous shrinkage in cementitious materials, Constr. Build. Mater. 121 (2016) 429–436. doi:10.1016/j.conbuildmat.2016.06.012.

[27] C. Boulay, Test rig for early age measurements of the autogenous shrinkage of a concrete, in: Proc. RILEM-JCJ Int. Work. ConCrack 3, 2012: pp. 111–122.

[28] O. Mejlhede Jensen, P. Freiesleben Hansen, A dilatometer for measuring autogenous deformation in hardening portland cement paste, Mater. Struct. 28 (1995) 406–409. doi:10.1007/BF02473076.

[29] M. Wyrzykowski, P. Lura, Controlling the coefficient of thermal expansion of cementitious materials - A new application for superabsorbent polymers, Cem. Concr. Compos. 35 (2013) 49–58. doi:10.1016/j.cemconcomp.2012.08.010.

[30] D.W. Hobbs, The dependence of the bulk modulus, Young's modulus, creep, shrinkage and thermal expansion of concrete upon aggregate volume concentration, Matériaux Constr. Constr. 4 (1971) 107–114. doi:10.1007/BF02473965.

[31] B.W. Rosen, Z. Hashin, Effective thermal expansion coefficients and specific heats of composite materials, Int. J. Eng. Sci. 8 (1970) 157–173. doi:10.1016/0020-7225(70)90066-2.

[32] T. Marciniszyn, A. Sieradzki, SELECTED PROPERTIES OF AMPHIBOLITES AND MIGMATITES FROM THE G.A.M. KLUCZOWA MINE, AGH J. Min. Geoengin. 36 (2012) 75–81.

[33] E.C. Robertson, Thermal properties of rocks, Reston,Virginia, 1988.

[34] S.L. Meyers, How temperature and moisture changes may affect the durability of concrete, Rock Prod. Devoted to Prod. Sale Rock Clay Prod. 54 (1951) 153–158.

[35] O.M. Jensen, Thermodynamic limitation of self-desiccation, Cem. Concr. Res. 25 (1995) 157–164. doi:10.1016/0008-8846(94)00123-G.

[36] A. Loukili, A. Khelidj, P. Richard, Hydration kinetics, change of relative humidity, and autogenous shrinkage of ultra-high-strength concrete, Cem. Concr. Res. 29 (1999) 577–584. doi:10.1016/S0008-8846(99)00022-8.

[37] O.M. Jensen, P.F. Hansen, Influence of temperature on autogenous deformation and relative humidity change in hardening cement paste, Cem. Concr. Res. 29 (1999) 567–575. doi:10.1016/S0008-8846(99)00021-6.

[38] F.. Wittmann, Surface tension, shrinkage, and strength of hardened cement paste, Mater. Constr. 1 (1968) 547–552. doi:10.1007/BF02473643.

[39] F. Beltzung, F.H. Wittmann, Role of disjoining pressure in cement based materials, Cem. Concr. Res. 35 (2005) 2364–2370. doi:10.1016/j.cemconres.2005.04.004.

[40] E.J. Sellevold, · Ø Bjøntegaard, Coefficient of thermal expansion of cement paste and concrete: Mechanisms of moisture interaction, Mater. Struct. 39 (2006) 809–815. doi:10.1617/s11527-006-9086-z.

[41] R.F. Feldman, P.J. Sereda, A model for hydrated Portland cement paste as deduced from sorption-length change and mechanical properties, Matériaux Constr. 1 (1968) 509–520. doi:10.1007/BF02473639.

[42] Z.P. Bažant, Thermodynamics of hindered adsorption and its implications for hardened cement paste and concrete, Cem. Concr. Res. 2 (1972) 1–16. doi:10.1016/0008-8846(72)90019-1.

CHAPTER 8:
MONITORING AND MODELLING OF THE VISCOELASTIC PROPERTIES OF UHPSCC AND CONCRETES WITH HIGH SUBSTITUTION OF PORTLAND CEMENT

The testing and modelling methodology developed in chapter 4 is extended in this chapter to "non-classical" compositions. The first "non-classical" class of concrete is related to 2 concrete mixtures for which 75% of the Portland cement is substituted by blast furnace slag or limestone filler. Both compositions are compared to a reference composition C0.4 for which no substitution of the cement is carried out and for which the aggregate and water content is exactly the same (paragraph 3.1.2.). The second "non-classical" class of concrete is an ultra-high performance self-compacting concrete (UHPSCC) corresponding to the Mikti composition described in details in paragraph 3.1.3. Tests are performed on this composition in order to validate once more the observations carried out with the data of Le Roy [1,2] for long duration creep tests (chapter 6 section 2). These tests are also achieved in order to extend the previous observations to very early age. The first part of the chapter presents the experimental program and the preliminary results needed for this study. The second part of the chapter focuses on the short term viscoelastic behaviour of the 4 compositions. The third part of the chapter is related to the monitoring and the modelling of the long duration creep.

SECTION 8.1 – EXPERIMENTAL PROGRAM

For each composition, a repeated minute-long loading test and 4 compressive creep tests of long duration are performed. The program of the long duration creep tests is presented in Table 1.

Table 1 – Experimental program for long duration creep tests. The age at loading is defined according to the advancement degree of reaction (α).

α	C0.4		CBFS		CSCM		α	Mikti	
/	t_{eq} [h]	f_c [MPa]	t_{eq} [h]	f_c [MPa]	t_{eq} [h]	f_c [MPa]	/	t_{eq} [h]	f_c [MPa]
0.38	12	22.8	41	7.3	39	5.4	0.29	17	10.8
0.45	15	26.9	49	9.9	48	7.7	0.45	23	23.8
0.6	23	36.8	66	14.5	70	12.3	0.6	33	60.9
0.7	32	42.0	120	26.3	118	21.3	0.83	88	74.3

For concrete compositions related to the study of the substitution of cement by mineral addition, concrete specimens were tested according to 4 advancement degree of reaction (0.38 – 0.45 – 0.6 and 0.7). The choice of the advancement degree of reaction is based on the development of the heat release of the CBFS and CSCM compositions. Complete details about the four compositions are given in Chapter 3. The heat release of each composition is presented in Figure 1. Results were obtained from [3]. For the composition C0.4, as expected [3–5], a strong increase of the heat release occurs during the setting period and the few hours which follow. For composition CBFS and CSCM, the amplitude of the peak is much lower. Moreover, a significant peak occurs between an equivalent age of 40 and 60 hours. From this observation, it was decided to test the CBFS and SCSM compositions during this period and after in order to track the effect of the slag on the evolution of the creep properties. For a good comparison with the reference composition C0.4, each composition is tested at a same advancement degree of reaction. Values of the compressive strength at loading age are given in Table 1. Equivalent data are also presented for the Mikti composition. The cumulated heat release of the four compositions is presented in Figure 2. A significant decrease of the cumulated heat release is observed when substituting cement by slag and limestone filler. The evolution of the cumulated heat release is very similar for the compositions CBFS and CSCM. The substitution of 25% of slag by limestone filler in the CSCM composition slightly affect the heat release. The first peak of heat release start sooner and has a higher amplitude. The second peak is less pronounced and occurs on a longer duration.

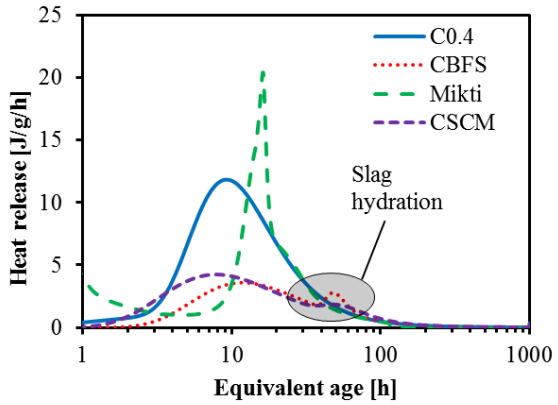

Figure 1 - Heat release evolution from isothermal calorimetry.

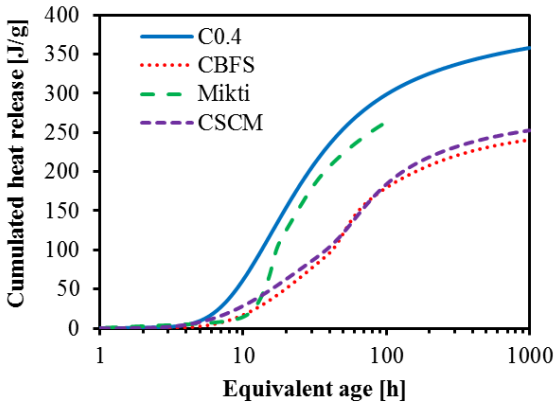

Figure 2 – Cumulated heat release from isothermal calorimetry.

8.1.1. Compressive strength

For the achievement of the repeated minute-long loading test, the evolution of the compressive strength must be known since very early age. For that purpose, compressive strength tests were performed since setting time. For the compositions, C0.4, CSCM and CBFS the determination of the evolution of the compressive strength was already performed during the PhD thesis of Jérôme Carette [6]. The most important point of these results is the very similar evolution of the compressive strength for the composition CBFS and CSCM. The replacement of 25% of slag by limestone filler has a very small impact and leads to a general small decrease of the compressive strength. No difference is observed in term of the kinetic evolution of the compressive strength.

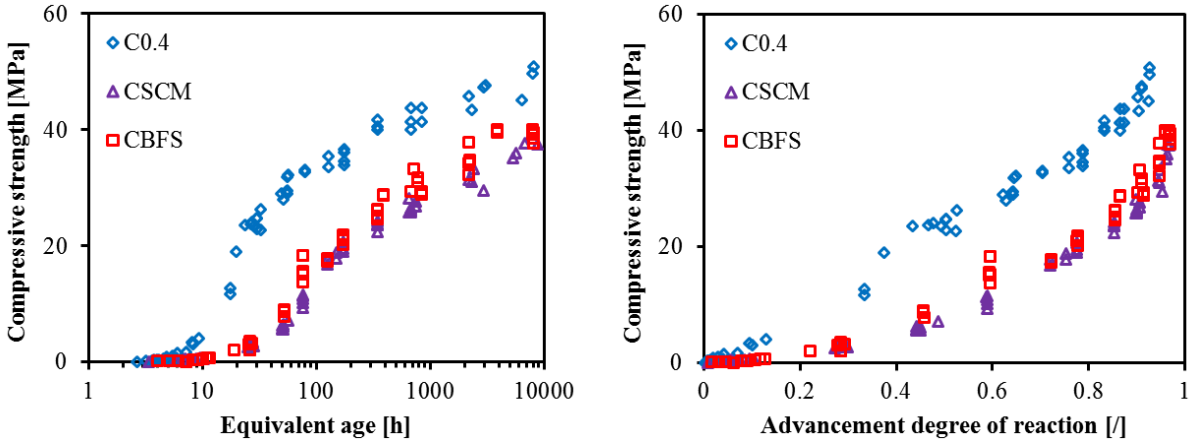

Figure 3 – Concrete compressive strength from initial setting to one year (left) and relative compressive strength as a function of advancement degree of reaction (right) [6].

For the Mikti composition, tests were performed since the final setting time. Results are presented according to the equivalent time in Figure 4 and according to the advancement degree of reaction in Figure 5. Results from [7] are also reported in these figures and are in very good agreement with the results obtained during this study.

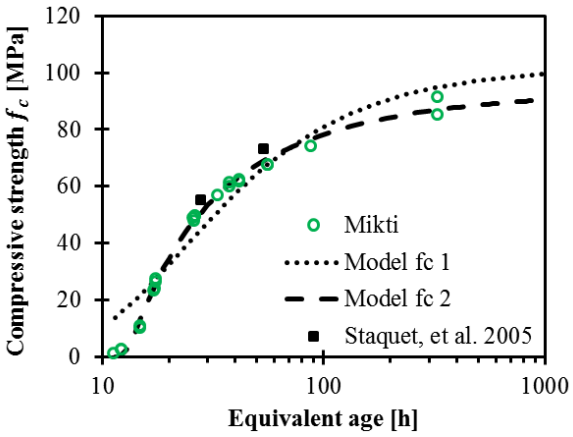

Figure 4 – Compressive strength of the Mikti composition according to the equivalent age

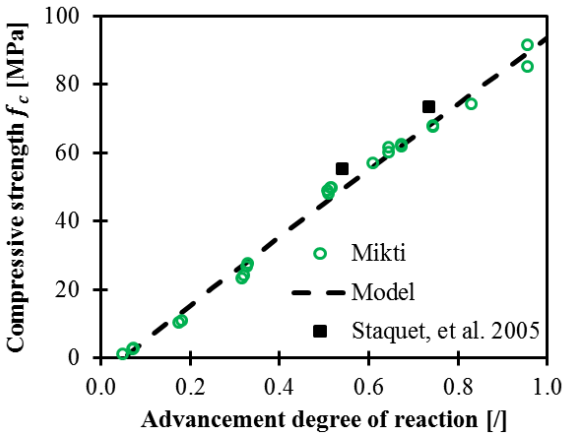

Figure 5 – Compressive strength of the Mikti composition according to the advancement degree of reaction

As in chapter 6, the Equation 1 is used to model the evolution of the compressive strength according to the equivalent time. However, for the Mikti composition, this equation is not able to correctly fit the experimental results as shown in Figure 4 where this equation is called "Model fc 1". The Mikti composition has the particularity to be composed of a relatively high quantity of superplasticizer to assure a good fluidity of the concrete during the casting. Because of the presence of the superplasticizer at high dosage, a delayed of the setting occurs. In addition, the increase of the compressive strength is very fast. Equation 1 is not able to fit results correctly when a high increase of the compressive strength occurs during a very small time window. Therefore a new equation has been developed to correctly correspond to the experimental results and is called "Model fc 2". The Equation 2 is composed of three material parameters and considers the final setting time $t_{eq,f}$. As shown in Figure 4, this equation is able to correctly fit the experimental data. As in the Chapter 6, the Equation 3 is used to model the evolution of the compressive strength according to the advancement degree of reaction (Figure 5).

$$f_c(t_{eq}) = f_c(t_{eq} = \infty).\exp\left(-\frac{p_f}{t_{eq}}\right) \quad (1)$$

$$f_c(t_{eq}, t_{eq,f}) = f_c(t_{eq} = \infty).\exp\left(-\left(\frac{p_f}{t_{eq}-t_{eq,f}}\right)^{r_f}\right) \quad (2)$$

$$f_c(\alpha, \alpha_0) = f_{c,\alpha}.(\alpha - \alpha_0)^{a_f} \quad (3)$$

Where t_{eq} is expressed in hour, p_f, r_f and a_f are material parameters which are related to the kinetic evolution of the compressive strength, $f_c(t_{eq} = \infty)$ is expressed in MPa and corresponds to the value of the compressive strength at an infinite time, $f_{c,\alpha}$ is expressed in MPa. Values of each parameter are given in Table 2. Equations 2 and 3 well represent the evolution of the compressive strength of the Mikti composition.

Table 2 - Compressive strength parameters for the Mikti composition of Equations 2 and 3.

$t_{eq,f}$ [h]	$f_c(t_{eq} = \infty)$ [MPa]	p_f [/]	r_f [/]	α_f [/]	$f_{c,\alpha}$ [MPa]	a_f [/]
11.4	93	8.4	.075	0.05	98	0.97

SECTION 8.2 – REPEATED MINUTE-LONG LOADING TESTS

The test protocol developed in the sixth section of the Chapter 4 is used for the monitoring of the elastic properties (E-modulus and Poisson's ratio) and the short term creep. For the concretes C0.4, CBFS and CSCM, exactly the same protocol is used. For practical reason (limitation of the device capacity), the maximal load is limited to 10% of the compressive strength for the Mikti composition. For the compositions CBFS and CSCM, it was not possible to start the test before an equivalent age of 30 hours. The slag slows the development of the mechanical properties of concrete. Consequently, when trying to start the test before such age, damage occurs during the preparation of the sample and leads to the failure of the sample.

8.2.1. E-modulus

Results of the E-modulus are already presented in Chapter 6 for the compositions C0.4 and CSCM and in [8] for the composition CBFS. Only E-modulus results of the Mikti composition are modeled in Figure 6 according to the equivalent time and in Figure 7 according to the advancement degree of reaction.

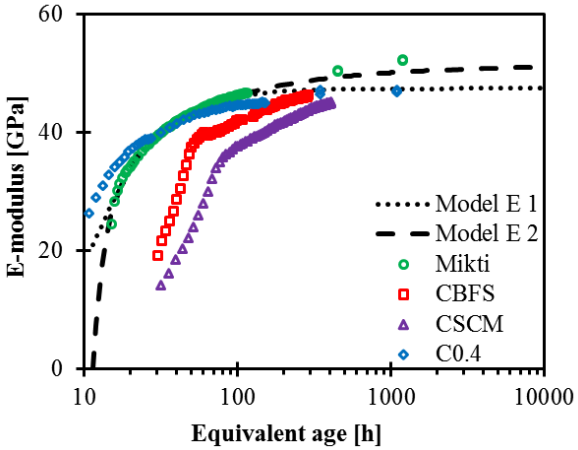

Figure 6 – Evolution of the E-modulus according to the equivalent age

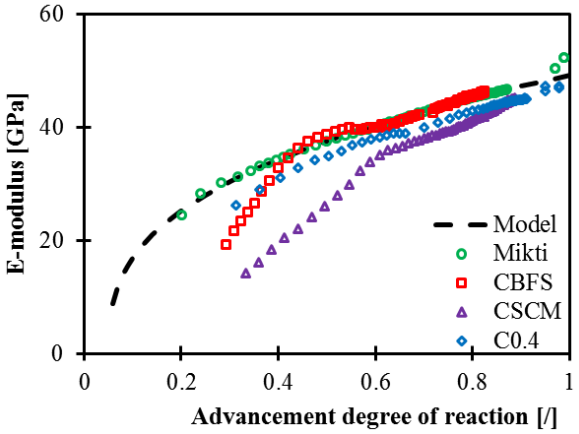

Figure 7 – Evolution of the E-modulus according to the advancement degree of reaction

As in chapter 6, the Equation 4 is used to model the evolution of the E-modulus according to the equivalent time. However, for the Mikti composition, this equation is not able to correctly fit the experimental results as shown in Figure 6 where this equation is called "Model E 1". As for the compressive strength, a new equation considering the delayed of the setting due to the superplasticizer is developed and corresponds to the Equation 5. As shown in Figure 6, this equation is able to correctly model the experimental data. The Equation 6 is used to model the evolution of the E-modulus according to the advancement degree of reaction (Figure 7).

$$E(t_{eq}) = E(t_{eq} = \infty).\exp\left(-\left(\frac{p_E}{t_{eq}}\right)^{r_E}\right) \quad (4)$$

$$E(t_{eq}, t_{eq,f}) = E(t_{eq} = \infty).\exp\left(-\left(\frac{p_E}{t_{eq}-t_{eq,f}}\right)^{r_E}\right) \quad (5)$$

$$E(\alpha, \alpha_0) = E_\alpha.(\alpha - \alpha_0)^{a_f} \quad (6)$$

Values of each parameter are given in Table 3. Equations 5 and 6 well represent the evolution of the E-modulus. The effect of the substitution of cement by slag and limestone filler is very significant in the evolution of the E-modulus especially during early age. The replacement of 75% of cement by slag decreases the evolution of the E-modulus at very early age till an advancement degree of reaction of 0.3. Then the E-modulus is higher with slag. The substitution of slag by limestone filler leads to a general decrease of the E-modulus. Two stages appear in the evolution of the E-modulus of the CBFS and CSCM compositions. The first stage occurs since final setting till an equivalent time of 50 and 70 hours or an advancement degree of reaction of 0.4 and 0.6 for respectively the compositions CBFS and CSCM. During the first stage, the E-modulus evolves according to a power law in equivalent time and according to a linear law in advancement degree of reaction. The second stage starts just after the first stage. During the second stage, the E-modulus evolves according to a logarithmic law in equivalent time and according to a linear law in advancement degree of reaction.

Table 3 – E-modulus parameters for the Mikti composition from Equations 5 and 6.

$E(t_{eq}=\infty)$ [GPa]	p_E [/]	r_E [/]	E_α [GPa]	a_0 [/]
51.4	1.88	0.58	50.1	0.36

8.2.2. Poisson's ratio

For the Poisson's ratio, results of the four compositions are presented in Figure 8 according to the equivalent time and in Figure 9 according to the advancement degree of reaction. The modelling of the Poisson's ratio is performed only for the composition CBFS and Mikti with equations presented in Chapter 6. For the composition CSCM and C0.4, the modelling is already presented in Chapter 7.

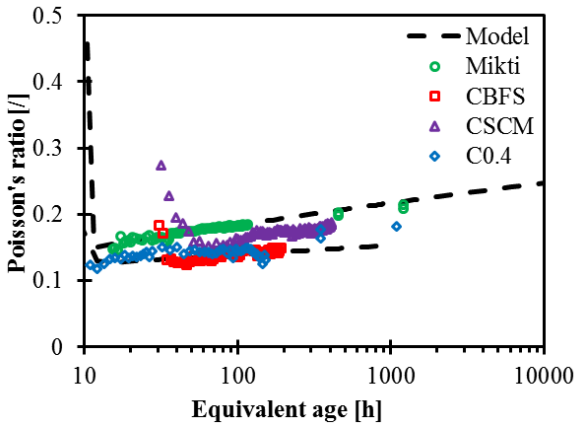

Figure 8 – Evolution of the Poisson's ratio according to the equivalent age

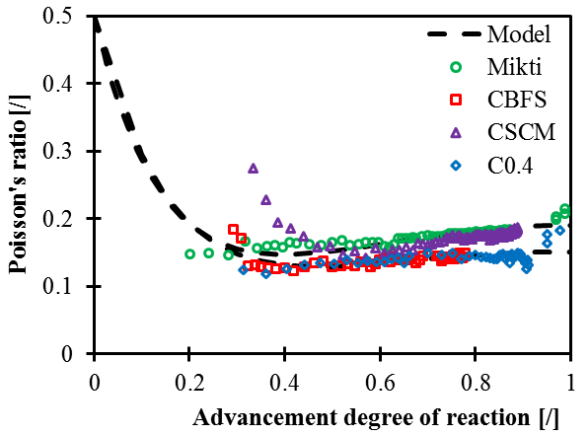

Figure 9 – Evolution of the Poisson's ratio according to the advancement degree of reaction

For both compositions, the equations are able to correctly fit the experimental results with both timescales. Values of each parameter are given in Table 4.

Table 4 – Poisson's ratio parameters for the Mikti and CBFS composition

	$\nu_{t,s}$ [/]	$r_{\nu,s}$ [/]	$\nu_{t,f}$ [/]	$r_{\nu,f}$ [/]	ν_α [/]	c_α [/]
CBFS	1.05	-2.5	0.12	-0.042	6.1	0.15
Mikti	0.40	0.10	0.35	19.5	0.19	6.6

The substitution of 75% of cement by slag seems to not impact in general the evolution of the Poisson's ratio. In contrast, the substitution of 25% of slag by limestone filler changes the evolution of the Poisson's ratio. A general increase of the Poisson's ratio is observed. At very early age, the decrease of the Poisson's ratio seems to occur more slowly for the composition CSCM. According to Bernard, *et al.* [9], the decrease of the Poisson's ratio occurs as long as the water phase is continuous and is due to the consumption of water during the hydration process. It is observed in chapter 6 that the increase in water-cement ratio leads to an increase of the Poisson's ratio and to a lengthening of the time of reduction of the Poisson's ratio. The limestone filler can be considered as an inert product [3] and does not absorbed water. Therefore, a substitution of cement or slag by limestone filler should lead to a higher quantity of water in the cement paste and extends the period during which the water phase is continuous. Between an advancement degree of reaction between 0.5 and 0.7, the evolution of the Poisson's is very similar for compositions C0.4, CBFS and CSCM. Afterwards, the increase of the Poisson's ratio is more significant for the composition CSCM. This increase is due to the solid stiffness evolution according to [9]. This is in agreement with the results of the E-modulus presented in Figure 7. After an advancement degree of reaction of 0.7, the rate evolution of the E-modulus of the composition CSCM is higher than the compositions CBFS and C0.4.

8.2.3. Amplitude creep factor

For each repeated minute-long loading test, a load corresponding to 20% of the compressive strength is applied during 5 minutes. During these 5 minutes-long plateau of stress, the creep coefficient is computed from raw displacement measurements after having removed the free strain from the dummy specimen (thermal and autogenous strain). In Chapter 4 (section 7), basic creep for short duration of loading is modeled with a logarithmic expression inspired from the Model Code 2010 (Equation 7).

$$\varphi_c(t,t') = A(t').\ln\left(1+(e-1).\left(\frac{(t-t')}{t_A}\right)^{K(t')}\right) \qquad 7$$

where $t_A = 0.083h = 300s$, A is the amplitude creep factor which varies according to the age of loading and which corresponds to the value of the creep coefficient after 5 minutes of loading, K is a kinetic parameter

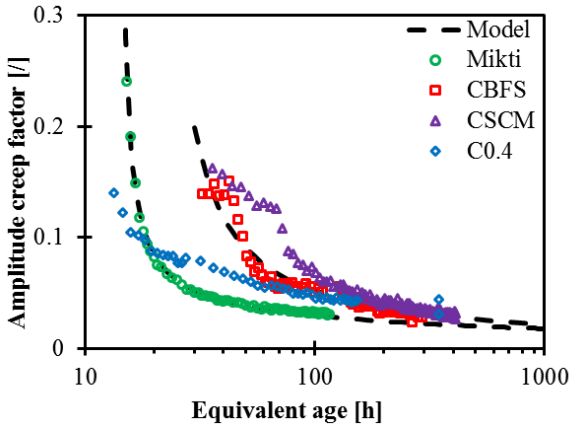

Figure 10 – Evolution of the amplitude creep factor according to the equivalent age

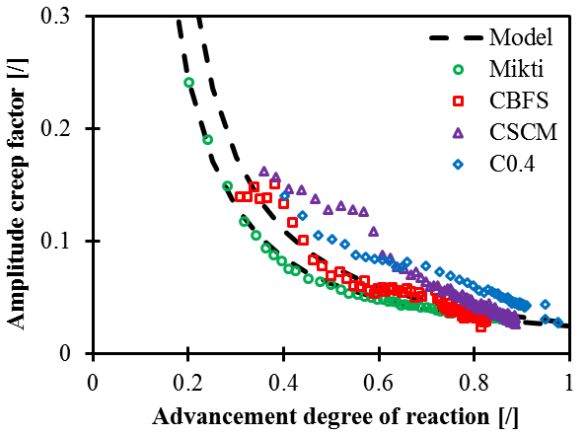

Figure 11 – Evolution of the amplitude creep factor according to the advancement degree of reaction

As in Chapter 6, the amplitude creep factor is modeled with the inverse of a logarithmic law in equivalent time and with a power law in advancement degree of reaction. For the Mikti composition, the consideration of the effect of the retardation of the setting by the superplasticizer is again considered by subtracting the value of the final setting time to the equivalent time as presented in Equation 8.

$$A(t_{eq}, t_{eq,f}) = \frac{1}{A_{t,1}.ln\left(\frac{t_{eq}-t_{eq,f}}{t_A}\right)+A_{t,2}} \quad 8$$

Results of the amplitude creep factor are shown in Figure 10 according to the equivalent time and according to the advancement degree of reaction in Figure 11. Values of each parameter are given in Table 5. A good agreement is observed between model and experimental results for both time-scales. When regarding results according to the equivalent age, it is observed that the main difference in evolution of the amplitude creep factor between C0.4, CBFS and CSCM occurs during the early age period. After an equivalent age of 150 hours, each composition seems to obtain very similar values. Therefore the substitution of cement by slag and limestone filler has a high impact on the short term creep during early age but not for hardened concrete. Thus, it is observed that during early age the microstructure of the binder is strongly different for a same advancement degree of reaction. When slag reacts this difference of microstructure decreases strongly and leads to a similar behaviour in comparison to an ordinary cement paste with an equivalent water-binder ratio. As for the E-modulus, the evolution of the amplitude creep factor follows two stages for the compositions CBFS and CSCM. The separation between both stages occurs at the same time as the E-modulus. During the first stage, the evolution of the amplitude creep factor is low (in the same order than the noise of the measurement) and only few data are available. Therefore it is quite complicated to define correctly the trend occurring during this first stage. However the amplitude creep factor seems to follow a linear law during this period for both time-scales. During the second stage, the trend is clearer and corresponds to the inverse of a logarithmic law in equivalent time and to a power law according to the advancement degree of reaction. Consequently, the evolution of the E-modulus and the amplitude creep factor seem to be correlated.

Table 5 – Amplitude creep factor parameters for the composition CBFS and Mikti.

	$A_{t,1}$ [/]	$A_{t,2}$ [/]	A_α [/]	$a_{A,\alpha}$ [/]
CBFS	11.8	-35.1	0.026	-1.39
Mikti	9.4	-8.46	0.023	-1.23

In Figure 13, the amplitude creep factor is plotted according to the E-modulus for each composition. When concrete reaches an E-modulus of 30 GPa, a very similar evolution is observed for all compositions. For the Mikti mix, it is observed that, for a same E-modulus, the short term creep is higher at very early age than the one of the composition C0.4. This is in agreement with the observations carried out in Chapter 6. On the contrary, for an E-modulus higher than 30 GPa, the inverse trend is observed. For the CBFS and CSCM compositions, curves are nearly superimposed and no relevant difference is observed for all data. Therefore the substitution of 25% of slag by limestone filler has no effect on the relation linking the E-modulus and the amplitude creep factor. A similar observation is carried out when the E-modulus is compared to the compressive strength (Figure 12). A similar evolution is observed since setting time for both compositions. According to the results obtained, the relation between the E-modulus and the compressive strength is independent on the water-cement ratio for concrete (Chapter 6). During very early, the nature of the binder does

not influence the relation between the compressive strength and the E-modulus whereas for an E-modulus higher than 30 GPa this relation is dependent of the nature of the binder. The relation between the E-modulus and the amplitude creep factor seems to be only slightly influenced by the nature of the binder but significantly by the water-binder ratio. Thus it is observed that short term creep is more influenced by the quantity of water in the binder and much less by the nature of the binder itself for such composition. Therefore, for a same water-binder ratio and a same aggregate content, short term creep is mainly governed by the stiffness of the cement paste.

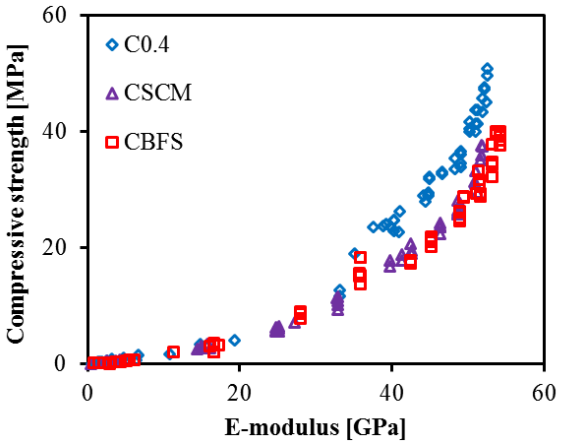

Figure 12 – Compressive strength development as a function of the E-modulus.

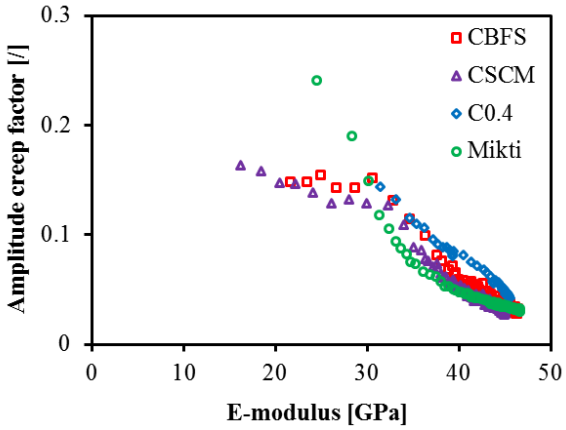

Figure 13 – Amplitude creep factor versus E-modulus.

8.2.4. Kinetic creep factor

The evolution of the kinetic creep factor K is presented in Figure 14 according to the equivalent time and in Figure 15 according to the advancement degree of reaction. For each composition, K decreases during the hydration process. For the Mikti composition, the value of K is higher. In chapter 6, it is observed that K is higher for the compositions with low water-cement ratio. The same observation is carried out with the Mikti mix. For the compositions CBFS, CSCM and C0.4, the results are quite scattered and it is difficult to highlight a clear effect of the slag and the limestone filler on the evolution of the kinetic creep factor.

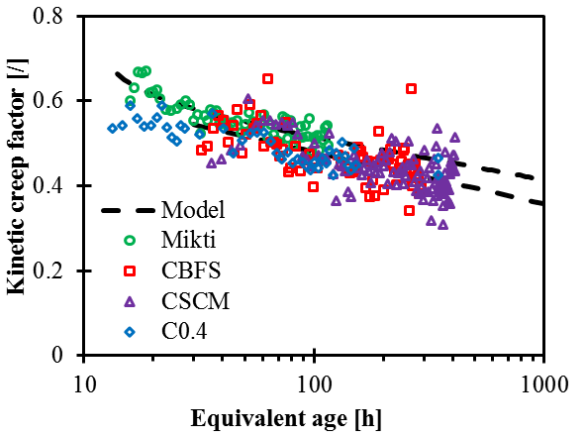

Figure 14 – Evolution of the kinetic creep factor according to the equivalent age

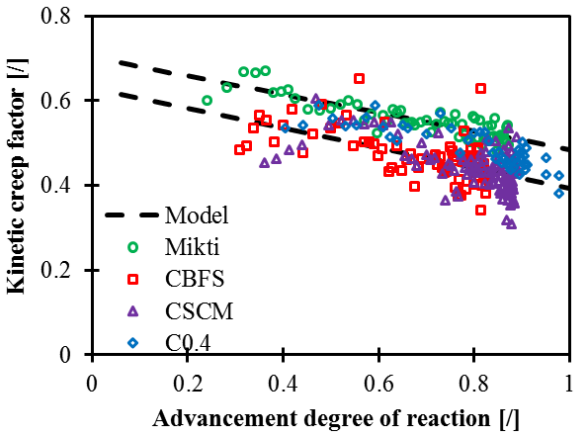

Figure 15 – Evolution of the kinetic creep factor according to the advancement degree of reaction

As it has been observed in Chapter 6, the kinetic creep factor follows a logarithmic trend in equivalent time and a linear trend in advancement degree of reaction. Per consequent, the same equations are used to fit results of the CBFS composition for both timescales. For the Mikti composition, the consideration of the effect of the retardation of the setting by the superplasticizer is again considered by subtracting the value of the final setting time to the equivalent time as presented in Equation 9.

$$K(t_{eq}) = K_{t,1}.\ln(t_{eq} - t_{eq,fs}) + K_{t,2} \quad 9$$

Values of each parameter are given in Table 6.

Table 6 – Kinetic creep factor parameters for compositions CBFS and Mikti.

	$K_{t,1}$ [/]	$K_{t,2}$ [/]	K_α [/]	P [/]
CBFS	-0.053	0.72	-0.24	0.63
Mikti	-0.042	0.70	-0.22	0.70

SECTION 8.3 – LONG DURATION CREEP TESTS

The test protocol used in the sixth section of the Chapter 4 for the long duration creep test is used for the four compositions. For the concretes C0.4, CBFS and CSCM, exactly the same protocol is used. For practical reason (limitation of the device capacity), the maximal load is limited to 20% of the compressive strength for the Mikti composition. Due to technical issues, it was not possible to perform creep tests on the composition C0.4 for an advancement degree of reaction of 0.38 and 0.45 which corresponds respectively to an age after setting of 5 and 8 hours. Therefore tests were performed at an age of 19, 24, 40 and 71 hours corresponding to an advancement degree of reaction of 0.55, 0.62, 0.75 and 0.84 for the composition C0.4. Therefore results of the composition C0.4 will be compared to the compositions CBFS and CSCM with an advancement degree of reaction of 0.6 and 0.7. Results of the specific creep function are presented in Figure 16. Several preliminary observations are carried out:

- For each composition, the effect of the age at loading is strongly marked in the evolution of the specific creep.
- For a same advancement degree of reaction (α=0.45 and 0.6), the specific creep of the Mikti composition is significantly lower than the one of the other compositions.
- The effect of the replacement of 75% of cement by slag does not induce significant effect in the magnitude of the specific creep. The specific creep is slightly higher for the C0.4 composition. This difference seems to increase for higher advancement degrees of hydration. Therefore it is observed that slag decreases the amplitude of the specific creep. This observation was already done by several authors in the past [10–13] and is especially marked at later ages [14]. In term of kinetic, a difference is also observed for the compositions C0.4 and CBFS. The short term creep evolves faster for the CBFS composition whereas the long term creep evolves faster for the C0.4 composition.
- The substitution of 25% of slag by limestone filler increases the magnitude of the specific creep. A factor between 2 and 3 is obtained between the compositions CBFS and CSCM whatever the advancement degree of reaction at loading. The amplitude of the specific creep of the CSCM composition is more than 2 times higher at very early age than the one of the composition C0.4. This factor seems to decrease when the advancement degree of reaction increases.
- It should be also noticed that some unexpected results are obtained with the composition CSCM. For results obtained at an advancement degree of reaction of 0.38 and 0.45, an increase in the amplitude and the kinetic of the specific creep is observed when the advancement degree of reaction increases.

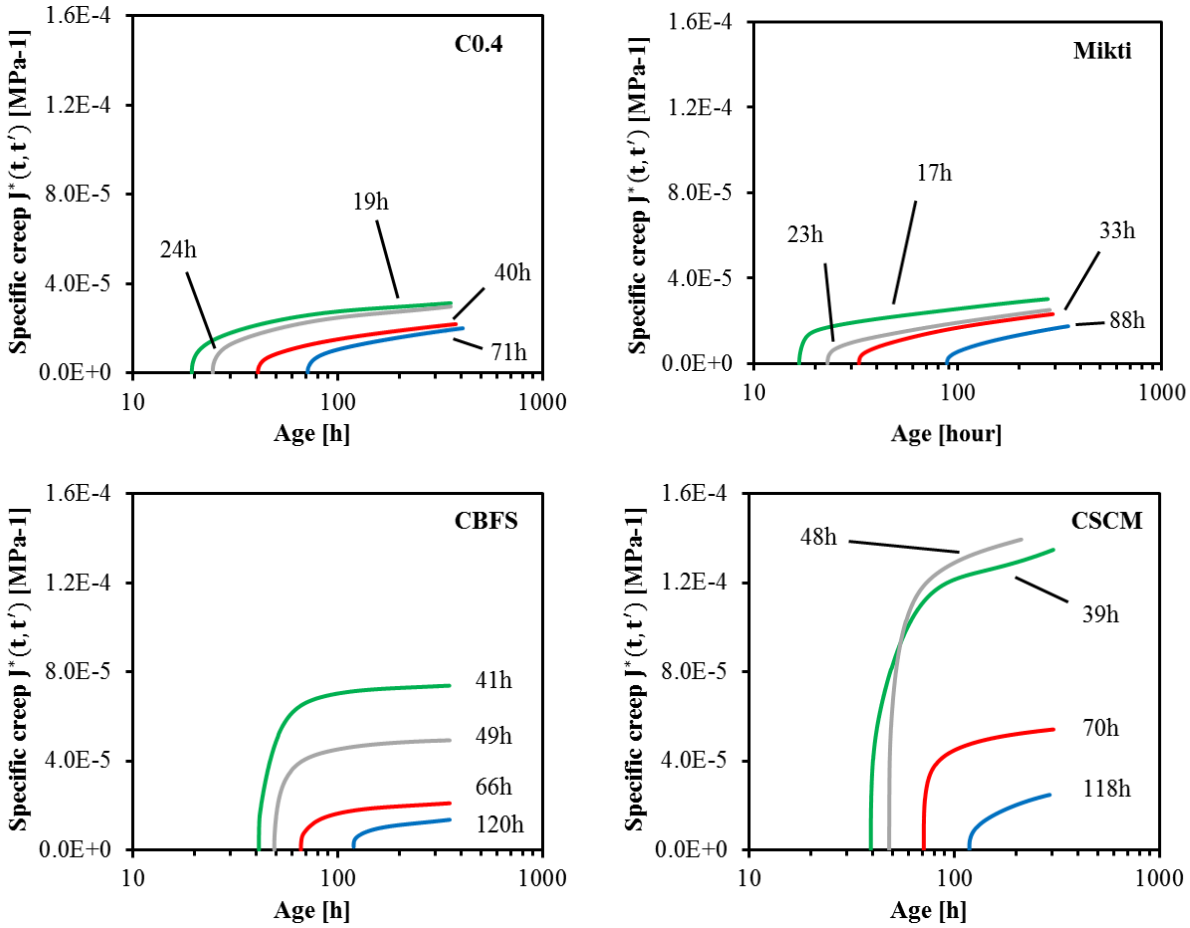

Figure 16 – Evolution of the specific creep function for several ages at loading.

To understand the difference of amplitude between each composition occurring during the first hours after loading, mainly two parameters must be considered: the E-modulus and the amplitude creep factor. Values of both parameters are given in the Table 7 for an advancement degree of reaction corresponding to the time when the long duration creep tests start. When comparing the CBFS and the CSCM compositions, it is observed that the short term creep increases when the E-modulus decreases and when the amplitude creep factor increases. This is coherent because the specific creep corresponds to the ratio between the creep coefficient and the E-modulus at the time of loading. However, this observation cannot explain the difference observed between the compositions C0.4 and CSCM. Indeed, for an advancement degree of reaction of 0.6 and 0.7, the value of the E-modulus and the amplitude creep factor are similar for both compositions. Then it should be expected that results are similar for the short term creep and it is not the case. Therefore, the difference comes from another parameter, not considered in this section but in the next one.

Table 7 – Values of the E-modulus and the amplitude creep factor when the long duration creep tests start.

	α=0.38		α=0.45		α=0.6		α=0.7	
	E [GPa]	A [/]	E [GPa]	A [/]	E [GPa]	A [/]	E [GPa]	A [/]
CBFS	30.5	0.14	37	0.09	40	0.055	42.4	0.05
CSCM	18	0.155	23	0.14	35	0.09	38	0.069
C0.4	-	-	-	-	38.2	0.083	40	0.078
Mikti	-	-	36	0.067	40	0.048	-	-

8.3.1. Three terms model

In order to understand this difference, basic creep is divided in three terms as presented in the Chapter 4, section 7. The first term studied is the long term creep. The long term creep is defined with the evolution of the specific creep rate occurring after one day of loading or more. The specific creep rate is presented in Figure 17 for each composition.

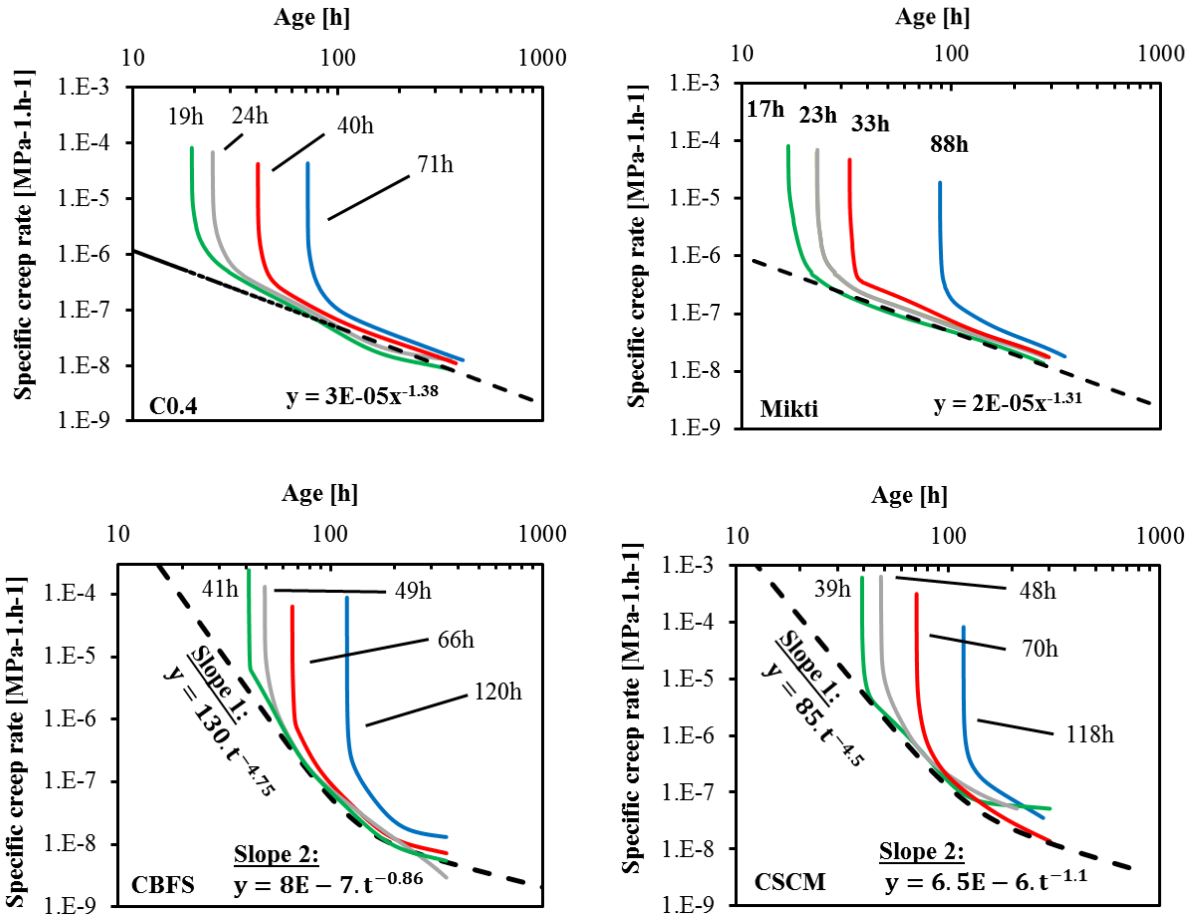

Figure 17 – Evolution of the specific creep rate for several ages at loading and modelling of the long term creep (dashed line).

The long term creep of the compositions C0.4 and Mikti is similar to the results obtained with the OC composition. For very early age loading, long term creep is the main part of the basic creep after only one day of loading. Whereas, when the loading is applied at advancement degree of reaction higher than 0.8, short term creep continues to be significant after duration of loading of one week. This confirms the fact that long term creep can be correctly assessed with a load applied at very early age as observed in the Chapter 4 (section 7) with the OC composition.

For the compositions CBFS and CSCM, the specific creep rate does not follow one asymptote but two (Figure 17). The transition between the first and the second asymptote starts around an age of 100 hours. This age corresponds to the time when the second peak of hydration due to slag ends (Figure 1). Therefore the substitution of cement in high quantity by slag causes a change in the determination and the modelling of the long term creep. For classical concrete, one power expression model correctly the long term creep. When adding mineral additions in the binder a second power expression

is needed for the modelling of the long term creep as expressed in Equation 10. As shown in Figure 17, such expression is able to very accurately fit the results.

$$C_{LT}(t,t') = \frac{f_1}{g_1+1}.(t^{g_1+1} - t'^{g_1+1}) + \frac{f_2}{g_2+1}.(t^{g_2+1} - t'^{g_2+1}) \quad 10$$

In

Figure 18, the modelling of the long term creep rate of each composition is shown. During early age, the long term creep is very significant for the compositions with slag. This is in contrast with the compositions C0.4 and Mikti for which the long term creep rate is quite low whatever the age at loading. Therefore long term creep is a significant phenomenon in the development of the basic creep of early age concrete with high substitution of cement by slag. This effect is even more pronounced when limestone filler is partially used instead of the slag. This explains why the amplitude creep factor and the E-modulus are not sufficient to understand the difference occurring during the development of creep during the very early age. After an age of 100 hours, the long term creep rate has a magnitude of the same order. During this period, limestone filler increases the long term creep and the slag decreases slightly the long term creep. This difference of evolution was also noticed in the evolution of the E-modulus (Figure 6) and the amplitude creep factor (Figure 10). It is during this time window that the behaviour of the CBFS and CSCM becomes close to the evolution of the composition C0.4. As long term creep is linked to the CSH, the knowledge of the development of the CSH (quantity, density…) should help in the microstructural interpretation of this difference of behaviour in the long term creep with the substitution of cement by slag and limestone filler. Such investigation would be of very high interest and could be performed in the future in the frame of a research collaboration with a specialized laboratory in that field.

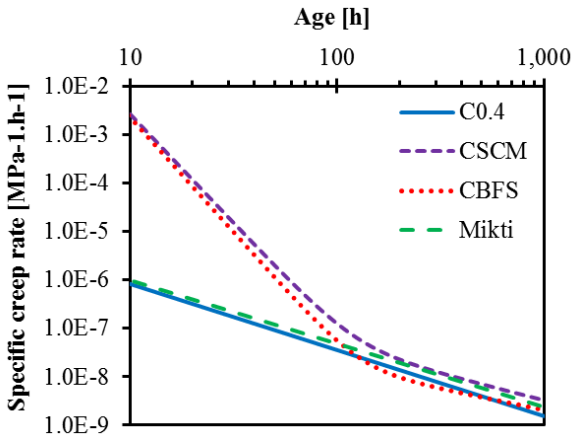

Figure 18 – Modelling of the long term creep rate

Values of each parameter of the Equation 10 are given in Table 8.

Table 8 – Long term creep parameters

	C0.4	CBFS	CSCM	Mikti
f_1	-	130	85	-
g_1	-	-4.75	-4.5	-
f_2	1.92E-5	8.01E-07	6.50E-06	2.02E-05
g_2	-1.37	-0.86	-1.10	-1.31

The second parameter studied is the initial short term creep which is linked to the state of the material when the load is applied and thus to the amplitude creep factor obtained with the repeated minute-long loadings. After removing the long term creep, each curve is normalized by their own value obtained at an age after loading of 1 hour. As expected with results obtained with repeated minute-long loading test, the master curve follows a logarithmic trend. For compositions C0.4, CSCM and Mikti, a same master curve is observed during the first hours after loading. This observation is not true for the composition CBFS for which a difference is observed and depends on the age at loading. For samples loaded at an advancement degree of reaction of 0.38 and 0.45 a same evolution is observed whereas another very similar evolution is obtained for concrete loaded at an advancement degree of reaction of 0.6 and 0.7.

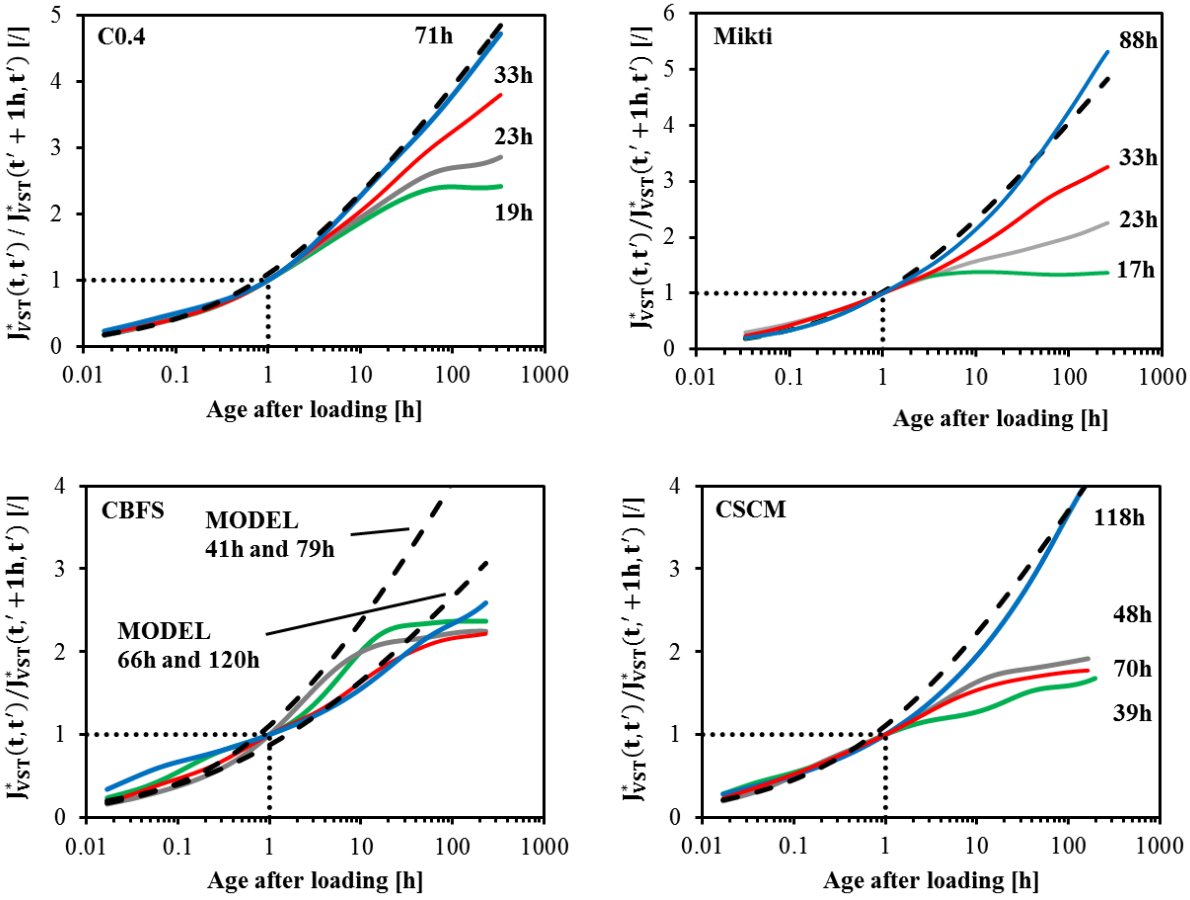

Figure 19 – Normalization of the specific creep at an age after loading of 1 hour after removing long term creep.

This difference in the initial short term creep of the CBFS composition is explained by the evolution of the kinetic creep factor. In Figure 20, a moving average on three points is carried out on the results of the kinetic creep factor. It is highlighted that the kinetic creep factor evolves significantly between an advancement degree of reaction of 0.45 and 0.6 for the CBFS composition. At an advancement degree of reaction of 0.38 and 0.45, the kinetic creep factor is around 0.54 while for an advancement degree of reaction of 0.6 and 0.7, the kinetic creep factor is around 0.45. This change occurs during the same period when a change of trend was observed in the evolution of the E-modulus and the amplitude creep factor of the CBFS composition. However the same phenomenon occurs for the composition CSCM between an advancement degree of reaction of 0.6 and 0.7. A difference is then also expected for this composition but no difference is noticed in the master curve.

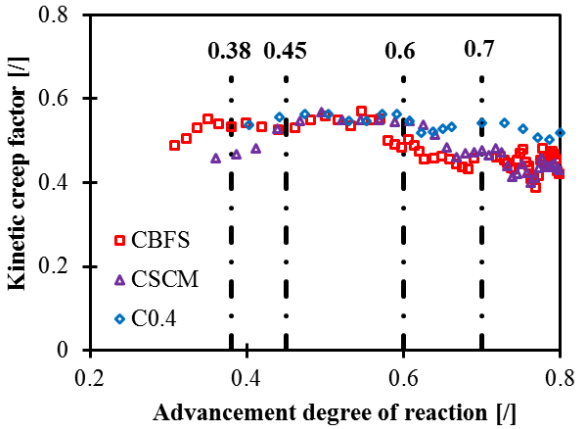

Figure 20 – Moving average on three points of the kinetic creep factor for compositions C0.4, CBFS and CSCM.

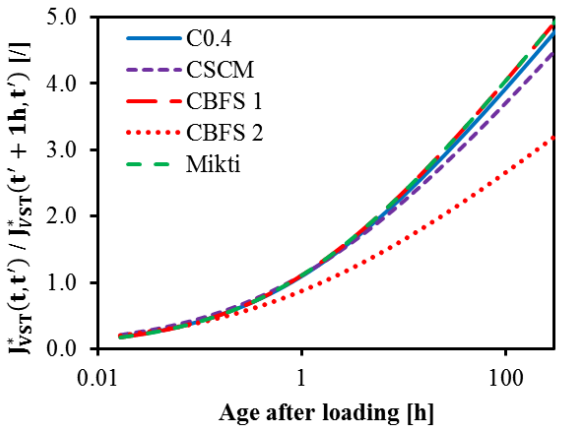

Figure 21 – Evolution of the normalized initial short term creep for each compositions. CBFS 1 refers to loading applied at α=0.38 and 0.45. CBFS 2 refers to loading applied at α=0.6 and 0.7.

The master curves of each composition are compared in Figure 21. A same evolution is observed for each composition except for the composition CBFS for loading applied after an advancement degree of reaction of 0.45. This means that till the time when slag has not reacted, this master curve is the same for the different compositions. Therefore, for an appropriate modelling of this phenomenon for mix with partial substitution of cement by slag, it is necessary to change the master curve according to the advancement of the hydration of the slag. This change is carried out by changing the parameter q_3 and n of the model. Values of the q_3 and n parameters in the model are given in Table 9. Therefore the slag decreases the kinetic of the initial short term creep. This change in the master curve of the initial short term creep can be explained by the microstructural characteristics of the binder. The substitution of cement by slag makes the porosity finer and limits the water movement inside the binder.

Table 9 – Kinetic parameters of the initial short term creep

	C0.4	CSCM	CBFS 1	CBFS 2	Mikti
q_3	1.58	1.6	1.26	1.6	1.6
n	0.52	0.48	0.43	0.53	0.53

For each composition, the value of the initial short term creep coefficient obtained after 1 hour of loading is defined and is plotted according to the amplitude creep factor in Figure 22. For the Mikti and C0.4 compositions, a linear relation is observed and both parameters decreases to zero simultaneously. For the SCM and CBFS compositions, a linear relation is observed for concrete with an advancement degree of reaction higher or equal to 0.45. Before, a strong decrease of the creep coefficient (obtained after 1 hour of loading) is observed. Two reasons can explain this difference.

1. The consideration of the long term creep is done since the time when the load is applied. If the long term creep is not perfectly defined for composition with slag that will lead to a significant error in the determination of the initial short term creep. Indeed, the amplitude of the long term creep was found very significant for the composition with high substitution of cement by slag and limestone filler.
2. Inversely, the long term creep is not considered in the determination of the amplitude creep factor where it is assumed that only one phenomenon occurs during a loading of 5 minutes.

Per consequent, the decoupling between the initial short term creep and the long term creep is complex at very early age for concrete with high substitution of cement by slag or limestone filler. That is why the results obtained during the very early age are difficult to interpret.

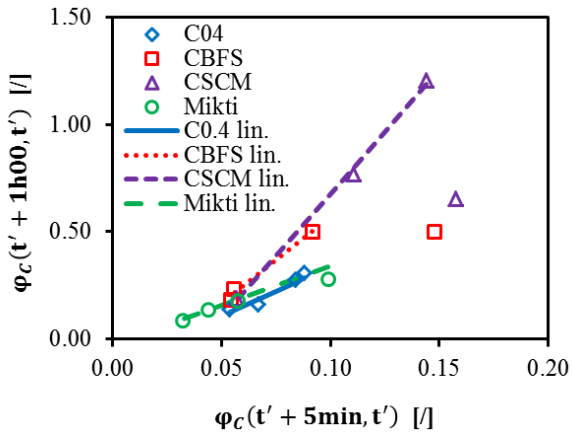

Figure 22 – Relation between the creep coefficient obtained after 1 hour of loading with the creep long duration test and the creep coefficient obtained after 5 minutes of loading with the repeated minute-long loading test.

Results of the modelling of the initial short term creep are presented in the Figure 23. For all compositions and ages at loading, the model can very well fit the experimental results during the first hours or days after loading. When the logarithmic trend is not followed anymore, it is assumed that it represents the effect of the solidification of the material. For specimen loaded at early age, the solidification phenomenon is already marked after few hours of loading (see Figure 23). For concrete loaded at later ages, solidification phenomenon appears after several days.

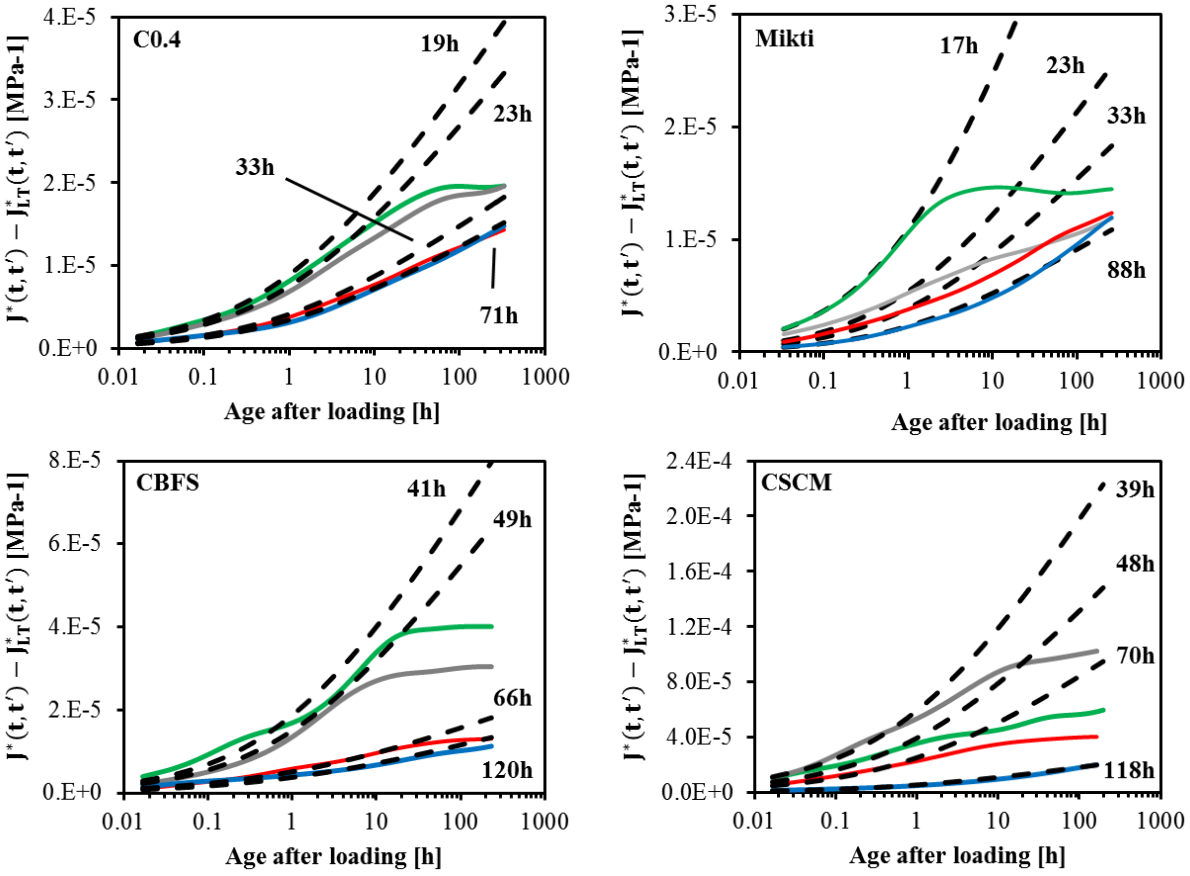

Figure 23 – Evolution of the initial short term creep and modelling (dashed lines)

The third and last parameter studied is the solidification term creep. The amplitude of this parameter is linked to the derivative of the E-modulus (see Chapter 4, section 7). As for the initial short term creep, two operations are needed in order to characterize the solidification term creep. First, the solidification term creep is obtained after removing the long term creep and the initial short term creep from the results. Results of this double subtraction are presented in Figure 24 for each composition. A same global effect of the age at loading is observed in the solidification creep. The solidification creep decreases when the age at loading increases. For early age loading ($\alpha \leq 0.45$), the solidification term creep evolves strongly during the first days after loading and has a high amplitude.

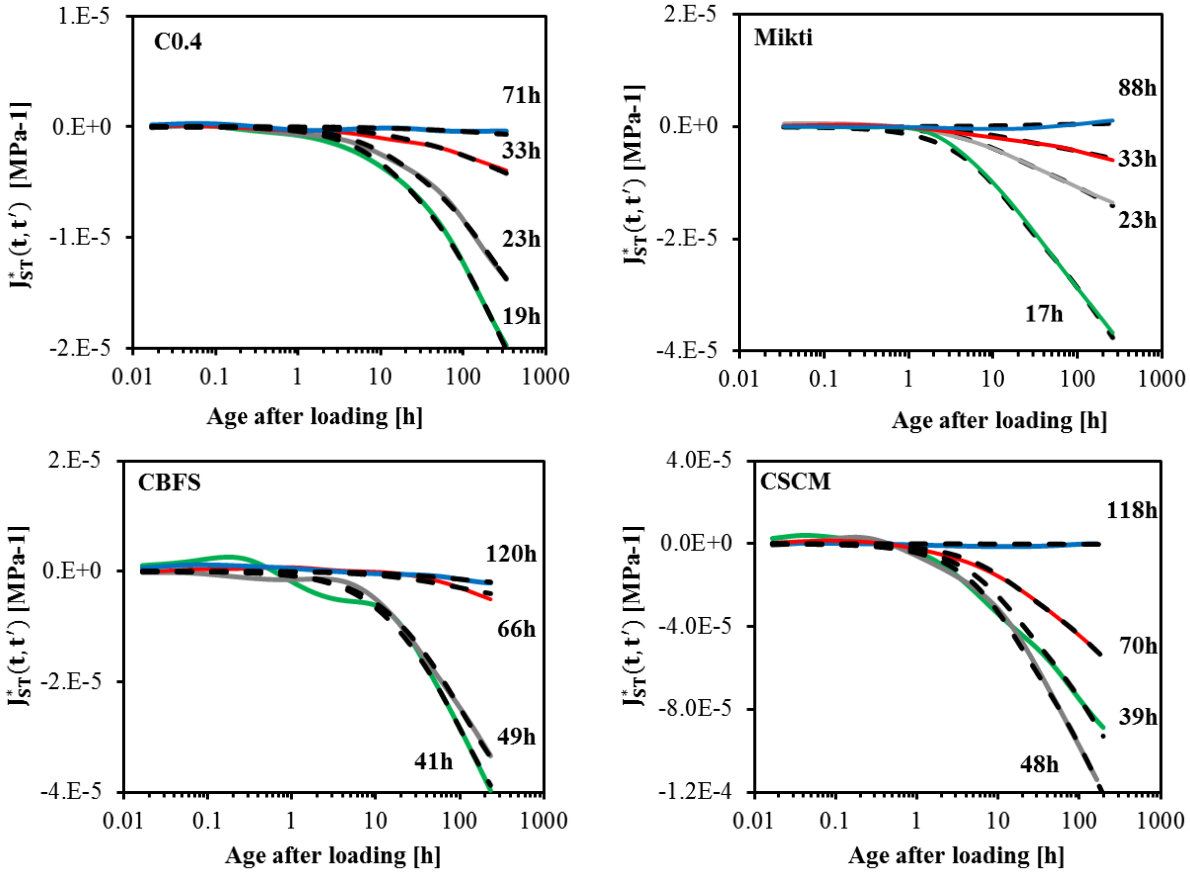

Figure 24 – Evolution of the solidification creep and modelling (dashed lines).

Secondly, each solidification creep functions are normalized by their value obtained after 100 hours of loading. In Figure 25, both operations are carried out for each composition. When normalized, the solidification creep follows a same master curve. For later ages at loading, the amplitude of the solidification phenomenon is very low and therefore is very difficult to assess especially when already two subtractions were already applied to the results. Therefore, only results coming from early age loading are used to define the master kinetic curve of the solidification creep term.

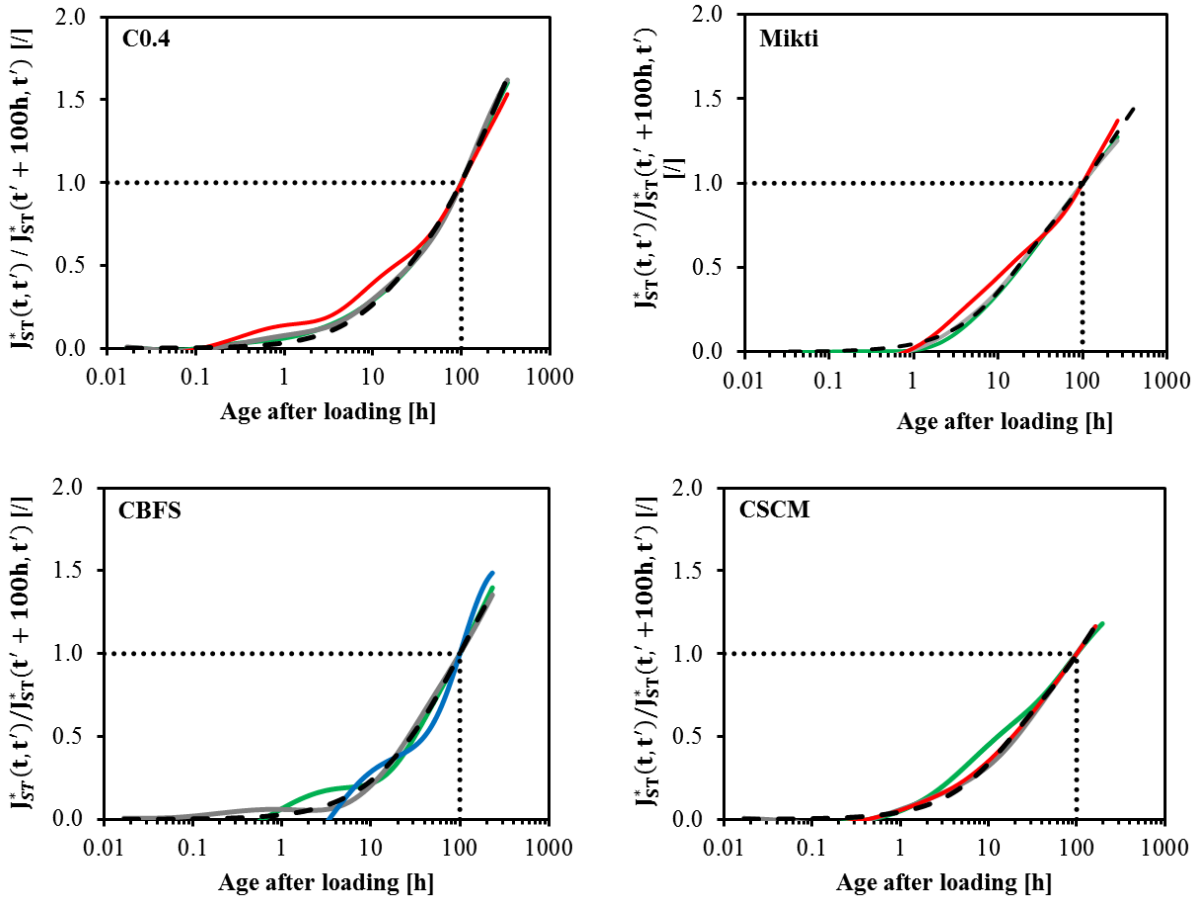

Figure 25 – Normalization of the solidification creep at an age after loading of 100 hours.

The average results obtained from early age loading is presented for the different compositions in Figure 26. No particular effect of the slag and limestone filler is observed on the kinetic of the solidification term creep.

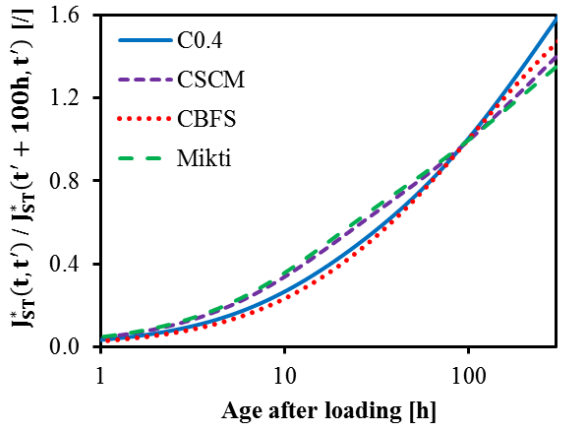

Figure 26 – Evolution of the normalized solidification creep for each composition.

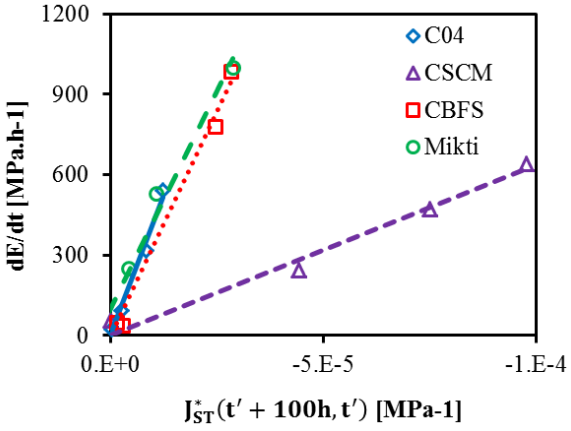

Figure 27 - Amplitude of the solidification creep versus the derivative of the E-modulus obtained at the age of loading

In Figure 27, the amplitude of the solidification term creep (corresponding to the value of the solidification creep function obtained after an age after loading of 100 hours) is compared to the derivative of the E-modulus for each age at loading of each composition. A general same linear

relation is obtained for each composition except the composition CSCM. For a same derivative of the E-modulus, the limestone filler decreases strongly the solidification creep. For all other results, no effect of the slag is detected. It could then be concluded that the relation between the amplitude of the solidification creep and the derivative of the E-modulus is independent on the substitution of cement by slag till 75%.

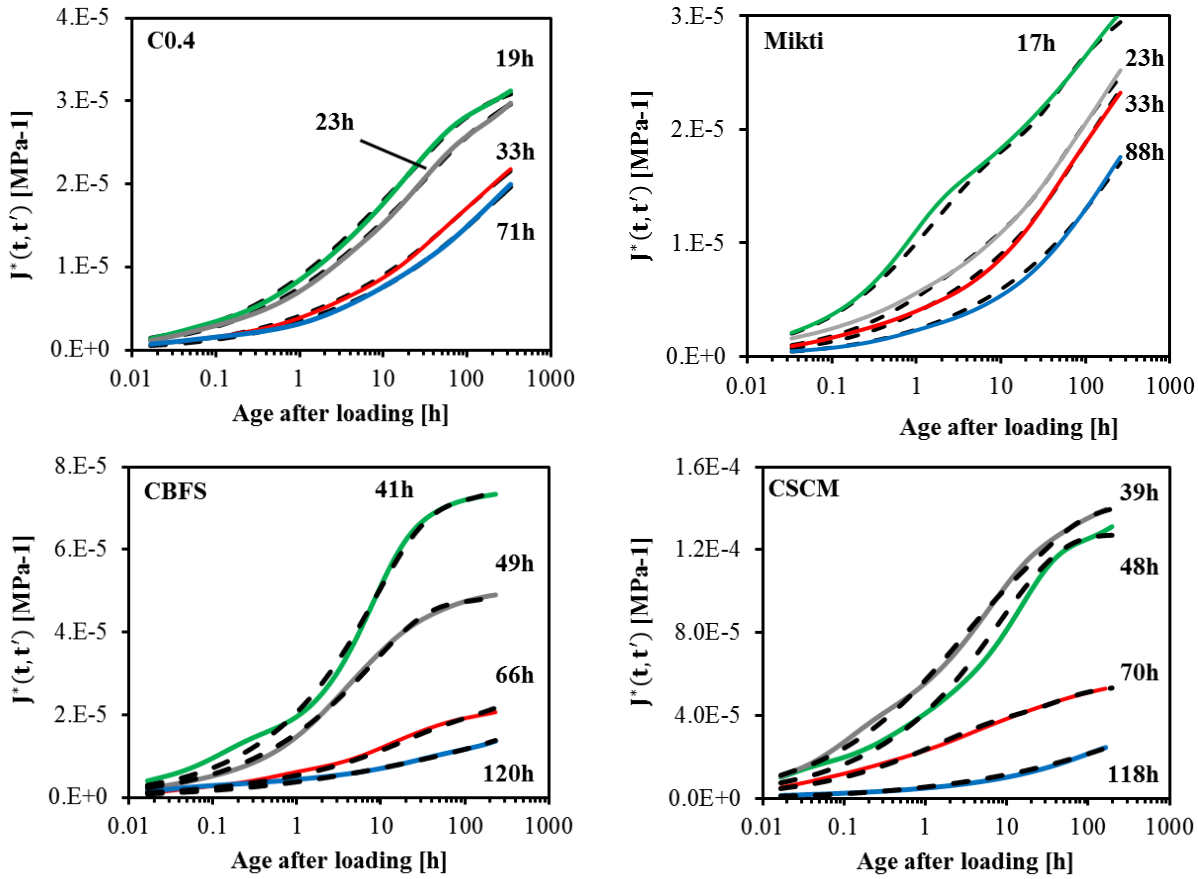

Figure 28 – Evolution of the specific creep and final modelling (dashed lines)

In Figure 28, the contribution of the very short term creep, the solidification term creep and the long term creep are summed and compared to the experimental results. A very good agreement for each age at loading is observed. It is then concluded that the effect of slag and limestone filler can be modelled by splitting the basic creep phenomenon in three terms since very early age.

8.3.2. Adapted Model Code 2010

Another way to model basic creep since very early was presented in the Chapter 4, section 7. This model is an adapted version of the Model Code 2010 (MC2010). As presented in [1,15], MC2010 can be simplified in Equation 11, where the parameter C is related to the general amplitude of the creep, is independent of the age at loading and is expressed in MPa. The parameter τ is only function of the age at loading and is expressed in [d].

$$C(t,t') = \frac{1}{C}.\ln\left(1+\frac{t-t'}{\tau}\right) \qquad 11$$

Results of the modelling with the adapted MC2010 are presented in Figure 29 for the C0.4 and Mikti compositions. A general very good correspondence is obtained between experimental results and the modelling whatever the age at loading.

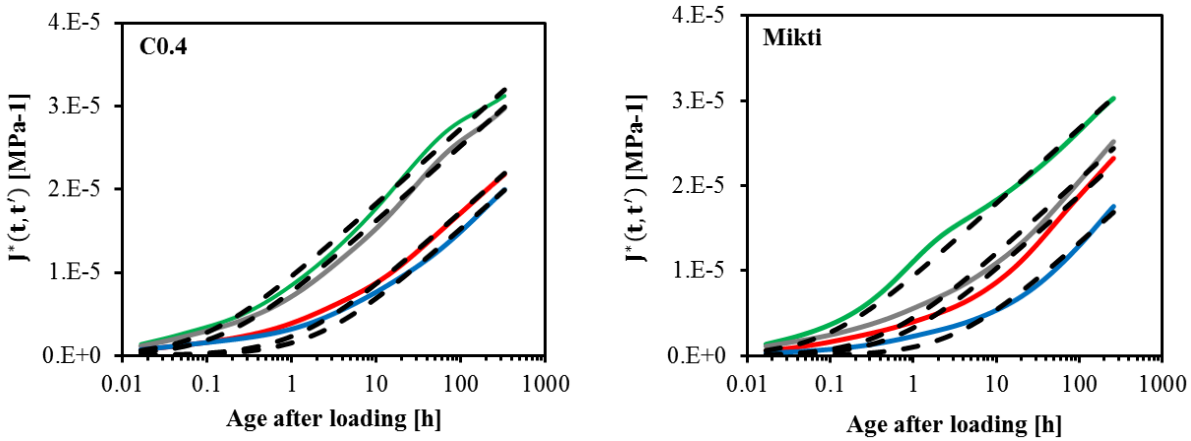

Figure 29 - Specific creep and adapted MC2010 (dashed lines) of the C0.4 and Mikti compositions

Results of the modelling with the adapted MC2010 are presented in Figure 30 for the CBFS and CSCM compositions. In order to improve the modelling, only creep results obtained after one or two days of loading were considered for concrete loaded at very early age (less than or equal to an advancement degree of reaction of 0.45). A very good agreement is obtained between experimental results and the modelling particularly for hardened concrete. For loading applied at an advancement degree of reaction of 0.45 or less, the model is not able to correctly fit in the same time creep occurring during the first days after loading and for long duration of loading. That leads, at very early age, to an overestimation of the creep phenomenon during the first days after loading.

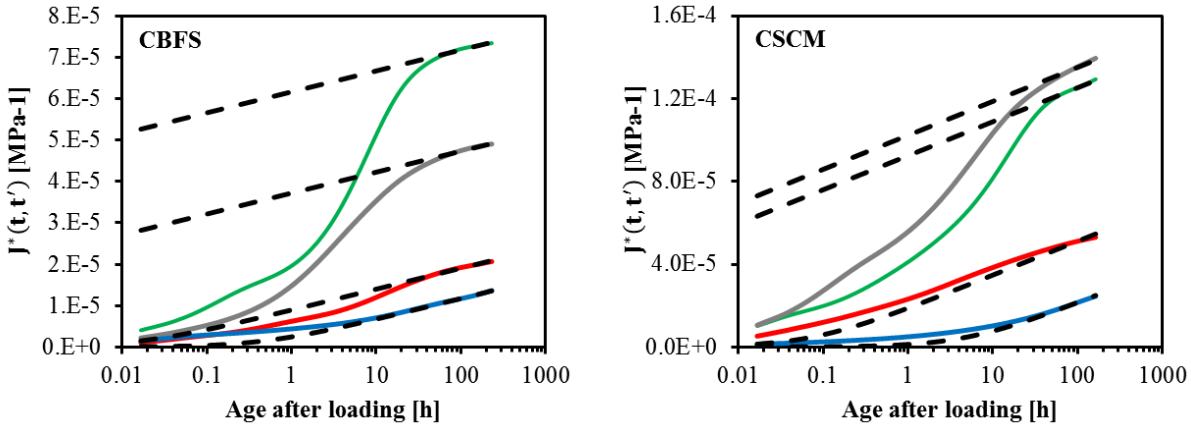

Figure 30 – Specific creep and adapted MC2010 (dashed lines) of the C0.4 and Mikti compositions

The value of the parameter τ is plotted according to the inverse of the derivative of the E-modulus in Figure 31 for each composition. Predictive values obtained with MC2010 are also presented. For the composition C0.4 and Mikti, a very good agreement is obtained between the optimized values fit on the experimental results and the predicted value given by MC2010. For the composition CBFS and CSCM, the results obtained for an advancement degree of reaction of 0.6 and 0.7 are relatively close to the results obtained for the Mikti and C0.4 compositions especially for the composition CSCM. The values of τ obtained for the CBFS are slightly lower. On the other hand, the values of τ obtained for an advancement degree of reaction of 0.38 and 0.45 are strongly lower than the values obtained for

the C0.4 and Mikti compositions. In comparison, results of the ordinary concrete are given in Figure 31. The period, during which there is a divergence between the values of $\boldsymbol{\tau}$ predicted by MC2010 and the optimized values fit with the experimental results, is the same for the compositions CBFS and CSCM and the ordinary concrete. This period stops when the inverse of the derivative of the E-modulus is lower than 0.14 GPa^{-1}.d. As for the ordinary concrete, the relation between the parameter $\boldsymbol{\tau}$ and the inverse of the derivative of the E-modulus follows a power expression. The power expression is given in Equation 12 where q=2.95E+14, p=19.4 and t_E=1d.GPa^{-1}.

$$\tau = q.\left(\frac{dE}{dt}.t_E\right)^p \; if \; \frac{dE}{dt} > 7.1GPa.d^{-1} \qquad 12$$

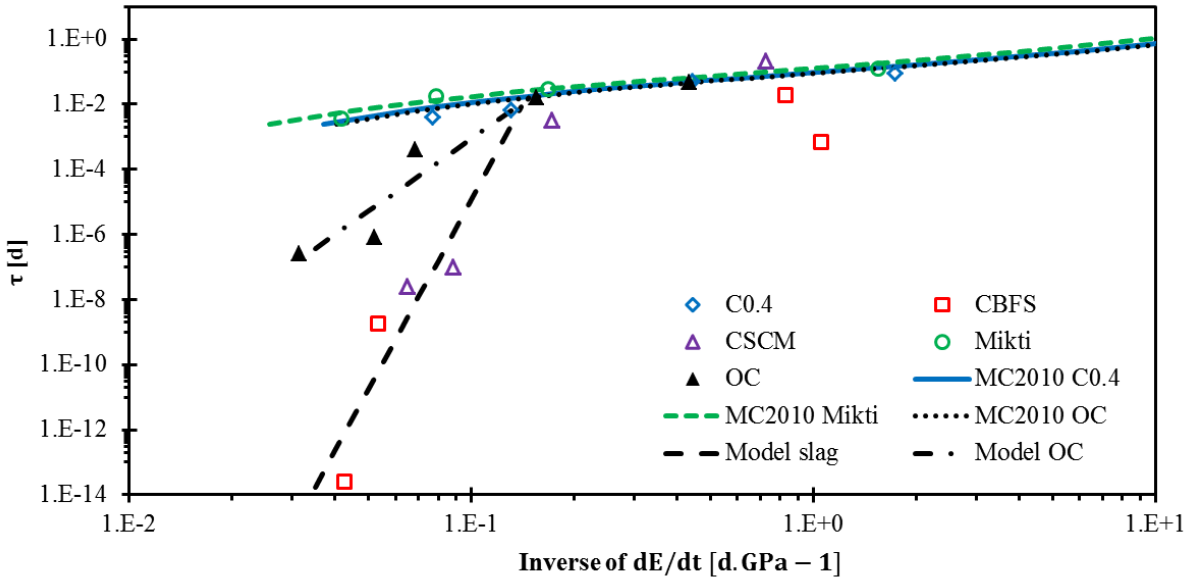

Figure 31 – Relation between the parameter $\boldsymbol{\tau}$ of the adapted MC2010 and the inverse of the E-modulus rate.

The amplitude parameter C of the adapted MC2010 is given in Table 10 for each composition. It is observed that the value of C from the Mikti and C0.4 compositions are very close. These values obtained from experimental results are also compared in this table to the value predicted by the Model Code 2010. A strong difference is observed between both especially for the Mikti composition.

The values obtained from CBFS and CSCM are strongly different. The substitution of 75% of cement by 75% by slag increases the factor C by a factor around 2. Whereas the replacement of cement by slag (50%) and by limestone filler (25%) decreases the parameter C by a factor around 2.

Table 10 – Values of the parameter C predicted by MC2010 and obtained by optimization of each composition (in GPa).

	C0.4	CBFS	CSCM	Mikti
Optimized value	255	455	140	261
Value predicted by MC2010	401	-	-	840

CONCLUSIONS

Repeated minute-long loading tests were applied on four concrete mixtures since very early age. Three compositions were used for the study of the effect of the substitution of cement by slag and limestone filler. The last compositions is an ultra-high performance self-compacting concrete (UHPSCC) which is used in order to confirm that the methodology defined in chapter 4 is able to characterize the mechanical properties of such composition since the setting. The Poisson's ratio, the E-modulus and an amplitude creep factor corresponding to the creep coefficient obtained after 5 minutes of loading are defined. For all the investigated properties, new or existing models are used. Models are expressed in function of the equivalent time and the advancement degree of reaction.

For concrete compositions using slag, it is observed that two stages appear in the evolution of the E-modulus and the amplitude creep factor. The separation between these both stages is related to the hydration of the slag. For an advancement degree of reaction lower than 0.45 (first stage), the slag decreases the E-modulus and the amplitude creep factor. When slag has reacts (second stage), the E-modulus is higher with the incorporation of slag and the amplitude creep factor is still lower. The partial substitution of slag by 25% of limestone filler increases the period during which the first stage occurs till an advancement degree of reaction of 0.6. During this first stage, the adding of limestone filler decreases the E-modulus and increases the amplitude creep factor. During the second stage, the E-modulus is slightly lower but increases faster and the amplitude creep factor is very close to the composition with only slag.

For the Mikti composition, the consideration of the effect of the retardation of the setting due to the high content of superplasticizer is considered by subtracting the value of the final setting time to the equivalent time in the models.

For the study of the long term creep, long duration creep tests were performed at four ages of loading. For compositions with slag, the loadings were applied before, during and after the peak of hydration of the slag. The new modelling presented in Chapter 4 is used for the four concretes. The main observations are:

- Long term creep is significantly influenced by the nature of the binder during very early age. For composition with slag and limestone filler, the long term creep is strongly higher till the time when slag has not reacted. This time corresponds to an advancement degree of reaction of 0.45 for the composition with 75% of cement substituted by slag and an advancement degree of reaction of 0.6 when 25% of slag is substituted by limestone filler. Whereas for a hardened state, long term creep decreases with slag and increases when limestone filler is added instead of the slag. But the long term creep is very similar for both composition to the long term creep of an ordinary concrete with the same water-binder ratio.
- At early age, the kinetic of the initial short term creep is very similar for each composition even for the Mikti composition. But when slag reacts, a decrease of the kinetic is observed. Therefore an aging factor must be applied in the kinetic term for concrete composition with slag. The amplitude of the initial short term creep corresponds to the amplitude creep factor obtained with the repeated minute-long loading test. The linear relation linking both parameters depends on the nature of the binder.
- A same master curve is obtained for the kinetic of the solidification term creep whatever the age at loading and the concrete composition. The amplitude of the solidification is linearly dependent on the derivative of the E-modulus for each composition. This linear relation is very similar for each composition except the one with limestone filler. For a

same derivative of the E-modulus, the limestone filler decreases the amplitude of the solidification term creep.

An adapted version of the Model Code 2010 (MC2010) is also used to model basic creep. It is possible to model accurately the specific creep especially for hardened concrete. For very early age, creep is overestimated during few days after loading for compositions with slag and limestone filler. Results predict by MC2010 are compared. For very early age, an adaptation of the aging factor is proposed for composition with high quantity of slag and limestone filler.

It is generally observed that the high substitution of cement by slag and limestone filler leads to a significant change in the evolution of the viscoelastic properties of concrete till and advancement degree of reaction corresponding to the end of the second peak of hydration due to slag. During this period, concrete with high content of mineral addition behaves differently because of the very low advancement degree of reaction of the slag. After the peak of hydration of the slag, the viscoelastic behaviour is very similar to ordinary concrete with equivalent water-binder ratio.

Therefore, when slag starts to react and when looking only at the mechanical behaviour, the risk of cracking increases for concrete with high substitution of cement by slag. Indeed, the E-modulus increases and the creep and relaxation phenomenon decrease in magnitude. While, when combining slag and limestone filler, the opposite situation is observed which leads to a decrease of the cracking risk for such composition. However for a good consideration of the risk of cracking of a composition, the mechanical behaviour is not sufficient. The simultaneous consideration of the free deformation is needed.

REFERENCES

[1] R. Le Roy, F. Le Maou, J.M. Torrenti, Long term basic creep behavior of high performance concrete: data and modelling, Mater. Struct. 50 (2017) 11. doi:10.1617/s11527-016-0948-8.

[2] R. Le Roy, Déformations instantanées et différées des bétons à hautes performances, PhD thesis, Ecole Nationale des Ponts et Chaussées, Paris, France, 1995.

[3] J. Carette, S. Staquet, Monitoring and modelling the early age and hardening behaviour of eco-concrete through continuous non-destructive measurements: Part I. Hydration and apparent activation energy, Cem. Concr. Compos. 73 (2016) 10–18. doi:10.1016/j.cemconcomp.2016.07.002.

[4] A. Darquennes, Comportement au jeune âge de bétons formulés à base de ciment au laitier de haut fourneau en condition de déformations libre et restreinte, PhD thesis, Université Libre de Bruxelles, 2009.

[5] E. Gruyaert, N. Robeyst, N. De Belie, Study of the hydration of Portland cement blended with blast-furnace slag by calorimetry and thermogravimetry, J. Therm. Anal. Calorim. 102 (2010) 941–951. doi:10.1007/s10973-010-0841-6.

[6] J. Carette, Towards Early Age Characterization of Eco-Concrete containing blast-furnace slag and limestone filler, PhD thesis, ULB-BATir, Brussel, Belgium, 2015.

[7] S. Staquet, L. Lauvin, J.-C. Renaud, S. Dubroca, F. Toutlemonde, Expérimentation sur poutres préfléchies à talon BTHP, Paris, 2005.

[8] J. Carette, S. Staquet, Monitoring and modelling the early age and hardening behaviour of eco-concrete through continuous non-destructive measurements: Part II. Mechanical behaviour, Cem. Concr. Compos. 73 (2016) 1–9. doi:10.1016/j.cemconcomp.2016.07.003.

[9] O. Bernard, F.-J. Ulm, E. Lemarchand, A multiscale micromechanics-hydration model for the early-age elastic properties of cement-based materials, Cem. Concr. Res. 33 (2003) 1293–1309. doi:10.1016/S0008-8846(03)00039-5.

[10] J.J. Brooks, A. Neville, Creep and Shrinkage of Concrete as Affected by Admixtures and Cement replacement materials, Spec. Publ. 135 (1992) 19–36.

[11] J.C. Chern, Y.W. Chan, Deformations of concrete made with blast-furnace slag cement and ordinary Portland cement, ACI Mater. J. 86 (1989) 372–382.

[12] J. Li, Y. Yao, A study on creep and drying shrinkage of high performance concrete, Cem. Concr. Res. 31 (2001) 1203–1206. doi:10.1016/S0008-8846(01)00539-7.

[13] A.Y. E. Tazawa and S. Tanaka., Drying Shrinkage and Creep of Concrete Containing Granulated Blast Furnace Slag, Spec. Publ. 114 (1989) 1325–1344. doi:10.14359/2604.

[14] E. Özbay, M. Erdemir, H.I. Durmuş, Utilization and efficiency of ground granulated blast furnace slag on concrete properties - A review, Constr. Build. Mater. 105 (2016) 423–434. doi:10.1016/j.conbuildmat.2015.12.153.

[15] J.M. Torrenti, R. Le Roy, Analysis and Modelling of Basic Creep, in: S. Dray (Ed.), CONCREEP 10, American Society of Civil Engineers, Reston, VA, 2015: pp. 1400–1409. doi:10.1061/9780784479346.165.

CHAPTER 9:
COMPARISON BETWEEN VISCOELASTIC PROPERTIES IN TENSION AND IN COMPRESSION

The principal load-bearing function of concrete in structures is to carry compressive stresses. On the contrary, steel reinforcement and prestressing tendons carry tensile stresses. For this reason, most investigations were carried out to determine the mechanical properties of concrete in compression. Similarly, most explanations about the mechanical properties are related to the compressive case.

Creep and associated relaxation play an important role in the stress calculation of a concrete structure for which deformation is restrained. This phenomenon occurs particularly during the first days following the casting of concrete. Indeed, in sealed condition, low compressive stresses first develop and then relatively high tensile stresses can occur. These stresses are induced by the restriction of the thermal and autogenous deformation.

Tanks and containments are not always prestressed. Tensile stresses occur in the structure and no cracking has to be ensured. To improve the prediction of the behaviour of the concrete structures and for economic reasons, designers need more information about tensile properties. In concrete structures, internal restraint causes a build up of tensile stresses within the material due to shrinkage whereas tensile creep counteracts the shrinkage as a stress relaxation mechanism. Importance of tensile creep is to be considered for the onset and the prediction of cracking propagation. The study of tensile creep has direct relevance for the design of concrete structures. Time that concrete takes to crack depends on the tensile strength and also the tensile creep and associated relaxation. However, the current data about tensile creep at early age are very scarce.

The purpose of this chapter is to study the difference in tension and compression of the viscoelastic behaviour of concrete at very early age. This chapter is divided in four sections. In the first section, the compositions and devices used are presented. The experimental program is explained in the second section. The third section is related to the experimental results obtained on the E-modulus and the basic creep in tension and compression. The fourth section focuses on the modelling of the tensile creep

SECTION 9.1 – MATERIALS AND METHODS

9.1.1. Materials and mixture

The tests presented here were performed on the ordinary concrete (OC) studied in the chapter 4, the Vercors concrete (V-OC) and the Mikti concrete studied in the chapter 8. A complete description of the composition of three concretes is given in Chapter 3. For all compositions, tests are performed in sealed condition at a constant temperature of 20°C. For each test, concrete is protected from drying by a double layer of self-adhesive aluminum sheet.

9.1.2. Testing E-modulus

- E-modulus in compression

The test protocol developed in the fourth section of the Chapter 4 is used for the monitoring of the elastic properties in compression. The electromechanical testing device presented in Chapter 4 (section 3) is used to perform the test.

- E-modulus in tension

In tension, a similar methodology is used for the monitoring of the E-modulus since setting. Each hour, a load corresponding to 20% of the tensile strength is applied in 10 seconds at a constant force rate. The TSTM device presented in Chapter 4 (section 2) is used to perform the test. In addition, the two electromechanical testing devices presented in Chapter 4 (section 3) are used to perform a test at specific ages of loading.

9.1.3. Assessment of the creep strain

- Creep in compression

SHORT TERM CREEP

The test protocol developed in the sixth section of the Chapter 4 is used for the monitoring of the short term creep in compression by means of repeated minute-long loading test.

CREEP TEST WITH PERMANENT LOADING

The test protocol presented in the sixth section of the Chapter 4 for permanent loading is used for the three compositions. Tests are performed on cylinders with a diameter of 100 mm and a height of 320 mm.

- Creep in tension

In tension, a similar methodology is used to assess the creep strain on long duration. For each test, a load corresponding to 40% of the tensile strength is applied in 10 seconds at a constant force rate. The load is kept constant during one week or more. For each tensile creep test, one or two dummy specimens are casted in order to monitor the free deformation of the concrete during the whole test. The test specimens are cylinders with a diameter of 100 mm and a height of 550 mm. A complete description of the testing device and its associated instrumentation is presented in the third section of the Chapter 4.

SECTION 9.2 – EXPERIMENTAL PROGRAM

A review of the literature was performed in Chapter 2 about the difference of behaviour in tension and in compression of cement based materials. It was highlighted that the E-modulus seems higher in tension than in compression. A higher difference is observed for concrete with low water-cement ratio. This can be associated to the development of microcracks caused by the restrained of the shrinkage of the cement paste by the aggregate. However, no clear evidence of this difference was given in the literature. Another difference between tensile and compressive E-modulus can come from the load magnitude imposed to the concrete sample when testing. For creep, results from the literature are very scarce about the difference of behaviour in tension and in compression especially at early age. From these observations, two experimental campaigns have been defined. A synthesis of the tests performed in this study is given in Table 1.

Table 1 – Experimental program

Composition	Type of test	Stress level [%]	Parameter(s) studied	Beginning of the test
Ordinary concrete	Repeated minute-long loading test	5 -10 - 20 - 40 (C)[1]	E-modulus Amplitude creep factor	12h00
	Tensile creep test	20 (T)	E-modulus	8h00
		20 (T)	E-modulus	9h00
		40 (T)	E-modulus and tensile creep	20h00
				24h00
				40h00
				72h00
	Compressive creep test	40 (C)	Compressive creep	20h00
				24h00
				40h00
				72h00
Mikti	Repeated minute-long loading test	10 (C)	E-modulus Amplitude creep factor	14h00
	Tensile creep test	20 (T)	E-modulus Tensile creep	75h00
	Compressive creep test	10 (C)	Compressive creep	88h00
Vercors	Repeated minute-long loading test	20 (C)	E-modulus Amplitude creep factor	14h00
	Tensile creep test	40 (T)	E-modulus Tensile creep	75h00
	Compressive creep test	40 (C)	Compressive creep	69h00

9.2.1. E-modulus in tension and compression

To define the difference between E-modulus in tension and in compression, several repeated-minute long loading tests were performed since very early age on the ordinary concrete. In compression, tests were performed at different stress level (5 – 10 – 20 – 40 % of the compressive strength). In tension, two repeated minute-long loading test were performed since setting time at a stress level

[1] C is related to compressive test and T is related to tensile test.

corresponding to 20% of the tensile strength and 4 single tests were performed at ages of 20 – 24 – 40 and 72 hours at a stress level corresponding to 40% of the tensile strength on sample never loaded before. In addition, single tests were performed on the Vercors concrete and the Mikti composition at an age of 75 hours.

9.2.2. Basic creep in tension and compression

- Short term creep

An important difference between tensile and compressive creep comes from the magnitude of the load applied. To understand this effect, repeated-minute long loading tests were performed since very early age on the ordinary concrete at different stress levels in compression (5 – 10 – 20 – 40 % of the compressive strength).

- Long duration creep

To compare basic creep in tension and in compression on longer duration, tests were performed at an age of 20 – 24 – 40 and 72 hours on the ordinary concrete for a duration of loading of one week or more at a stress level corresponding to 40% of the strength. In addition, tests were performed on the Vercors concrete and the Mikti composition at an age of 75 hours.

SECTION 9.3 – EXPERIMENTAL RESULTS

9.3.1. Preliminary results

► Setting time

Setting time of the concretes was determined by monitoring of the transmission of the ultrasound P- and S-wave through concrete according to the method developed by Carette, *et al.*[1,2]. Values of the initial and final setting time are given in Chapter 3.

► Tensile strength

Two splitting tensile tests are performed just before launching each tensile creep test in order to define the load to be applied (corresponding to 40% of the tensile strength). It is often considered that the tensile strength f_t is 10% lower than the splitting tensile strength f_{ts}. f_{ts} can be obtained through the following formula which derives from the theory of elasticity, with F the measured peak load [kN], D the sample diameter [cm], and L the length of the specimen [cm]:

$$f_t = 0.9 f_{ts} = 0.9 \frac{20.F}{\pi.D.L} \quad (1)$$

Results of the tensile strength of each composition are presented in Figure 1 for the three compositions.

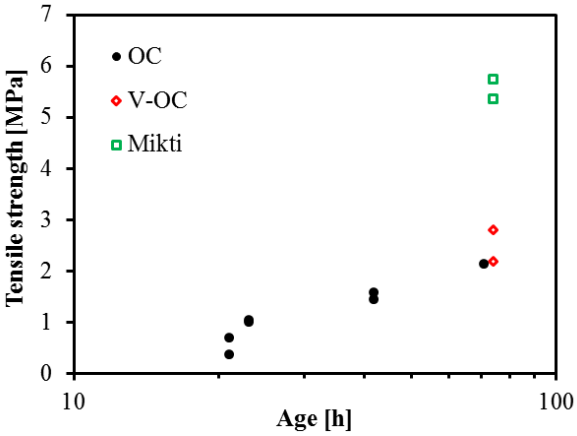

Figure 1 – Evolution of the tensile strength according to the age of the material.

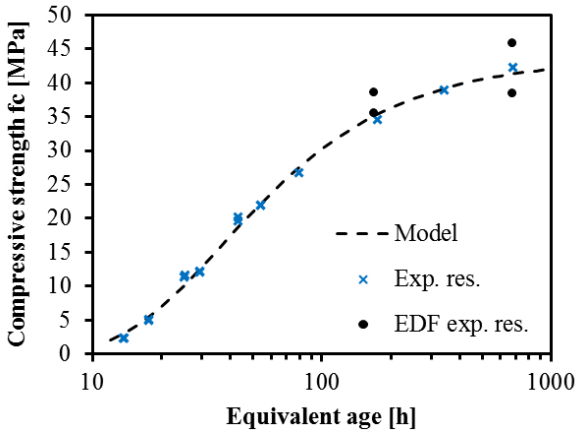

Figure 2 – Evolution of the compressive strength according to the equivalent age of the V-OC composition [3].

► Compressive strength

The compressive strength is defined since few hours after the final setting till 28 days. Results of the compressive strength f_c are given according to the equivalent time t_{eq} in chapter 4 (section 4) for the ordinary concrete, in chapter 8 for the Mikti composition and in [3] for the Vercors composition. Experimental results, (noted "Exp res." in the figure 2) on the Vercors concrete are given in the Figure 2. In comparison, the values of the f_c obtained at 7 and 28 days by EDF (Matériaux et Mécanique des Composants department) on the Vercors concrete are also given in this figure (noted "EDF exp. Res"). Results are in good agreement. The exponential model used to fit the experimental results is the same than in Chapter 6 (Equation 18). The model well represents the evolution of the compressive strength. More information about the material parameters of the Vercors concrete is presented in [3].

9.3.2. E-modulus in tension and compression

For each repeated minute-long loading, the E-modulus is calculated from the set of recordings (load and displacement in the central section) between 30% and 80% of loading (see Chapter 4, Section 4). In each case, the tangent elastic modulus E is computed by least square method. As described in Chapter 4 (section 5), the effect of the stress level on the measurement of the E-modulus is quantified by performing repeated loading tests at four stress levels: 5 – 10 – 20 and 40 % of the compressive strength. The test started a few hours after the setting. These results are already presented and discussed in the fifth section of the Chapter 4. In Figure 3, these results are compared to the E-modulus obtained in tension from repeated loading tests (noted "E T RL" in the legend) and single loading tests (noted "E T S" in the legend). Results in tension from repeated loading test are very close to the results obtained in compression during the first hours after setting. After an age of around 20 hours, a difference in the evolution of the E-modulus in tension and in compression is observed. Lower values of the E-modulus are obtained in tension. This difference increases with the age at loading. In contrast, when no load is applied before, the tensile E-modulus obtained is higher than the one in compression. These results follow very well the evolution of E-modulus in compression in term of kinetic. This difference in the results on the tensile E-modulus can be explained by an accumulation of damage occurring during each tensile loading. Therefore, a strong fatigue effect takes place on concrete when repeated loadings in tension are applied during the early age of concrete. Per consequent, it is observed that repeated loading test cannot be used for the monitoring of the tensile E-modulus even if very small loads (20% of the tensile strength) are applied to the sample. It is also observed that concrete is damaged when several tensile loadings are applied on the sample during very early age. However, such repeated variation does not exist in real case structure during the early age of cement based materials.

When results of the tensile E-modulus obtained from the single loading tests are compared to the E-modulus in compression, it is observed that a significant difference exists in term of amplitude of the E-modulus for each age at loading tested (20 – 24 – 40 and 72 hours). The difference of magnitude between the tensile and compressive loading cannot explain such variation in the amplitude of the E-modulus in tension. It is generally accepted that the tensile strength of ordinary concrete corresponds to around 10% of the compressive strength. In the fourth section of the Chapter 4, results of the compressive and tensile strength are presented. From this results, it is observed that the correlation between f_c and f_t is valid since very early age. Thus the loading applied in compression with a stress-strength ratio of 5% is in the same order of magnitude than the loading applied in tension with a stress-strength ratio of 40%. Per consequent, it is highlighted that the stress level is a first step in the understanding of the difference of behaviour between E-modulus in tension and in compression. But there is still a difference observed which is not explained. In addition, it should be noticed that exactly the same testing device, the same instrumentation and an equivalent protocol of loading are used for tests performed in tension and in compression.

In Figure 4, the E-modulus values of the Vercors concrete are displayed. Measurements on the sample have started 4 hours after setting. The whole test duration is 2 weeks. In comparison, the value of the E-modulus obtained at 28 days by EDF ("Matériaux et Mécanique des Composants" department) is also given in this figure. Experimental results (noted "Exp. res." in the figure) in compression are in very good agreement with results obtained by EDF (noted "EDF res. 28d" in the figure). In addition, results of the tensile E-modulus (noted "E Tension" in the figure) are also displayed. As for the results obtained on the ordinary concrete, the E-modulus in tension is higher than the one in compression for a same age at loading. The exponential model used to fit the experimental results is the same than in

Chapter 6 (Equations 27). The model well represents the evolution of the compressive strength. More information about the material parameter of the Vercors concrete is presented in [3].

For the Mikti composition, results of the E-modulus in compression are already presented in Chapter 8.

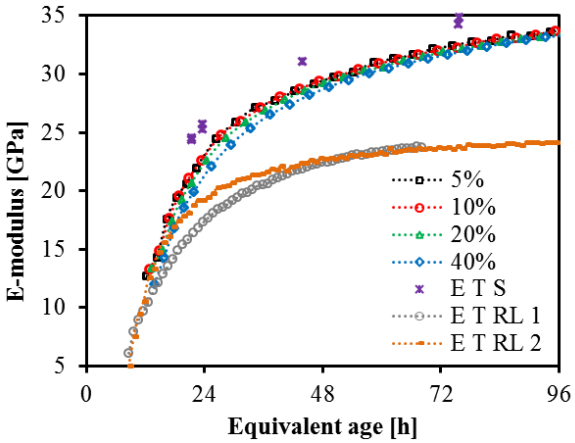

Figure 3 – Evolution of the E-modulus in tension and in compression according to the equivalent time of the ordinary concrete

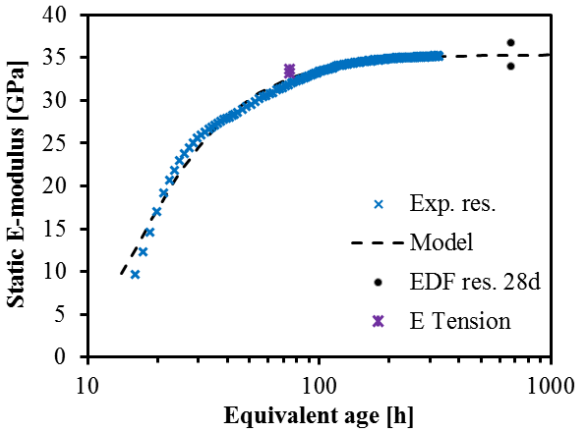

Figure 4 – Evolution of the E-modulus of the Vercors concrete [3].

The evolution of the ratio between the E-modulus in tension and in compression is presented in Figure 5. For the ordinary concrete, this ratio decreases when concrete hardens. For an age of 20 hours (12 hours after the final setting), the tensile E-modulus is 20% higher than the E-modulus in compression. For an age of 72 hours, the tensile E-modulus is 10% higher than the E-modulus in compression. In comparison, the ratio between the E-modulus in tension and in compression obtained with the Mikti and Vercors concrete at an age of 75 hours is around 1.03. Therefore, for each composition the E-modulus is higher in tension.

From these experimental results, it is observed that the amplitude of the ratio between the E-modulus in tension and in compression cannot be directly explained by the development of microcracking caused by the restrained shrinkage of the cement paste by the aggregate. Indeed, for composition with lower water-cement ratio, the difference observed in this ratio must be higher however it is not the case. Moreover, this ratio decreases during early age while it should be expected that this ratio increases if the development of microcracking (due to restrained shrinkage of the cement paste by the aggregate) is the source of the difference between E-modulus in tension and compression. However one parameter is not considered till here: the self-healing of the cement paste due to the formation of new hydrate products. At early age, the mechanical characteristics of the cement matrix (E-modulus, tensile strength…) are low. Therefore, the energy released from the microcrack initialisation and propagation is also low [4]. This leads to a large number of short microcracks with a very small opening. Due to their small dimension, the self-healing process can be very easy and important. This could explain why this ratio decreases with the age of the concrete. However this explanation is just an interpretation of the difference observed. Information about the quantity and the evolution of microcracks are needed in order to prove such affirmation. Moreover, this explanation alone is not sufficient to understand the difference of the E-modulus in tension and in compression. Additional experimental and numerical works are needed to explain this difference.

Even if the ratio between the E-modulus in tension and in compression evolves according to the age at loading, in a first stage it seems reasonable that the E-modulus in tension can be obtained from results in compression multiplied by a constant factor. This factor should depend on the composition.

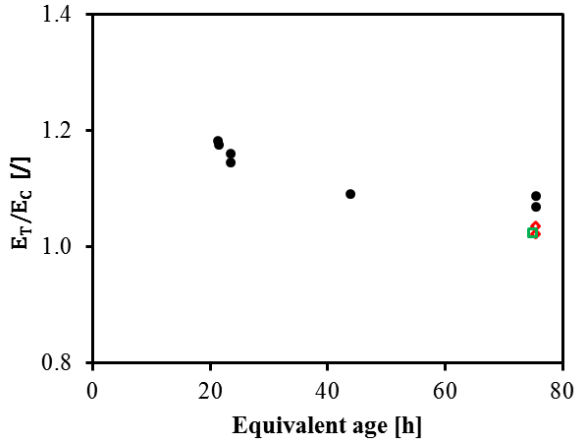

Figure 5 – Evolution of the ratio between the E-modulus in tension and in compression according to the equivalent time.

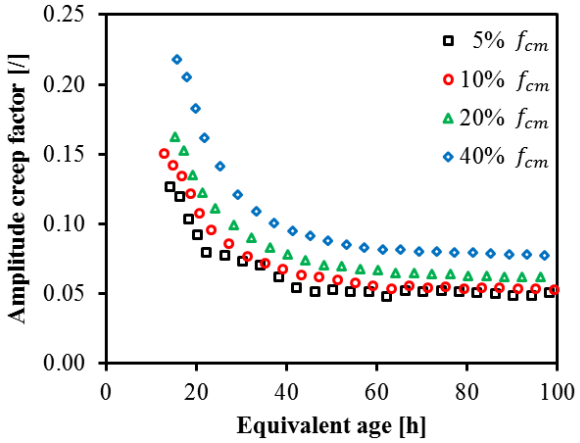

Figure 6 – Evolution of the amplitude creep factor for loading amplitudes of 5 – 10 – 20 – 40 % of the compressive strength of the ordinary concrete

9.3.3. Basic creep in tension and compression

► Effect of the stress level on the compressive short term creep

The amplitude creep factor values corresponding to the variable stress/strength ratio are displayed in Figure 6. It is observed that with the increase of the applied stress, the estimated amplitude creep factor A decreases and this effect progressively decreases as the concrete hardens. On Figure 7, this amplitude effect is quantified. Each point is obtained by linear interpolation of the experimental results. For any given loading age, a non-linear relationship is observed between the loading amplitude and A. This confirms that the stress-strain relationship is in fact non-linear in term of elastic properties (see Chapter 4, section 5) and creep properties.

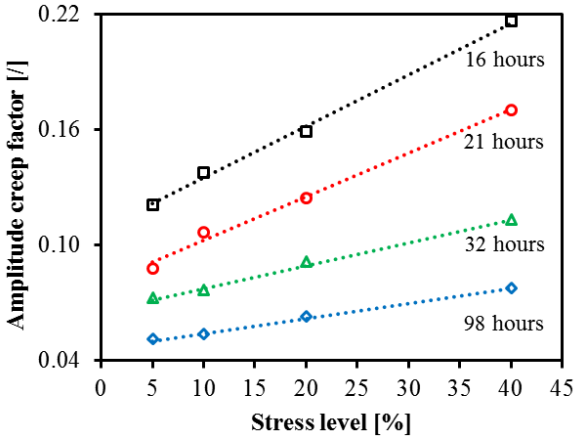

Figure 7 – Evolution of the amplitude creep factor according to the stress level for several ages at loading

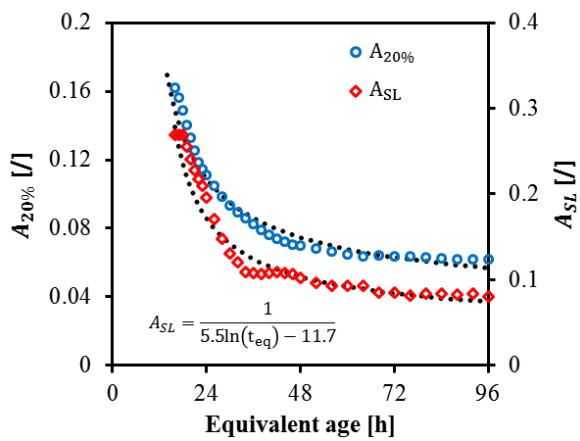

Figure 8 – Evolution of $A_{20\%}$ and A_{SL} determined with one repeated minute-long loading test.

The dependency of A to the stress/strength ratio is described in Equation 2, where σ is the applied stress, f_{cm} is the compressive strength, $A_{20\%}$ is the amplitude creep ratio corresponding to a reference stress/strength ratio of 20 % applied in 10 s, and A_{SL} is a time-dependent amplitude parameter describing the effect of the stress level on the apparent measurement of A.

$$A\left(t_{eq}, \frac{\sigma}{f_{cm}}\right) = A_{20\%}(t_{eq}) + A_{SL}(t_{eq}).\left(\frac{\sigma}{f_{cm}} - 0.2\right) \quad 2$$

$$A_{20\%}(t_{eq}) = \frac{1}{6.1 \ln\left(\frac{t_{eq}}{1h}\right) - 10.2} \quad 3$$

$$A_{SL}(t_{eq}) = \frac{1}{5.5 \ln\left(\frac{t_{eq}}{1h}\right) - 11.7} \quad 4$$

The evolution of parameters $A_{20\%}$ and A_{SL} are shown in Figure 8. The evolution of A_{SL} confirms that the increase of A due to an increase of the loading amplitude is especially strong at very early age, and drops to low values during hardening. The expression of A_{SL} is provided in Equation 4. However the observations carried out here are limited to a stress/strength ratio up to 40%. After this stress/strength ratio, damage should be considered in the evolution of the amplitude creep factor.

► Analysis of tensile and compressive creep with permanent loadings

COMPRESSIVE CREEP

Results from compressive creep tests were already presented and discussed in the sixth section of the Chapter 4 for the ordinary concrete, in the Chapter 8 for the Mikti composition and in [3] for the Vercors composition.

TENSILE CREEP

The experimental results of the strain of the loaded and dummy specimen for creep tests in tension are presented in Figure 9 for one age of loading for each composition. The elastic and creep strain are defined by subtracting the strain of the dummy specimen to the one of the loaded specimen. Furthermore, it is observed that a decrease of the total strain of the loaded specimen occurs during the loading period for each composition. This is explained by the very low amplitude of the tensile creep strain which is in the same order of magnitude than of:

- the free strain (autogenous and thermal strain) of the specimen,
- the strain caused by small thermal variations of the temperature in the room where specimen are tested. It was observed that the localization of the specimen in the air-conditioned room causes relevant change in the strain of the dummy specimen and thus in the determination of the tensile creep strain.

It is therefore well necessary to cast a dummy specimen for each test and to place it close to the sample loaded. In addition, the instrumentation used to measure the displacement of the sample is in Invar© and is exactly the same for the loaded and dummy specimen.

In addition, a loss of water can occur during the test if the sample is not perfectly sealed. Additional drying shrinkage would take place during the test because of this loss of water. In order to understand the scale of the problem, a simple calculation is performed with data from the literature [5]. When an

ordinary concrete sample (prism 7x7x28 cm) is exposed to drying at a relative humidity of 50% and a temperature of 20°C, drying shrinkage reaches a value 220 µm/m in only one week. The loss of water represents 2.5% of the total mass of the sample. If now, the mass loss is only 0.1%, the drying shrinkage stays significant with a value of about 9 µm/m. Such value cannot be neglected in the case of tensile creep. Therefore, special attention was taken in order to assure that no loss of water occurs during the test. Samples were weighted before and after the test. With two layers of self-adhesive aluminium sheet, no change was observed for duration of loading of two weeks.

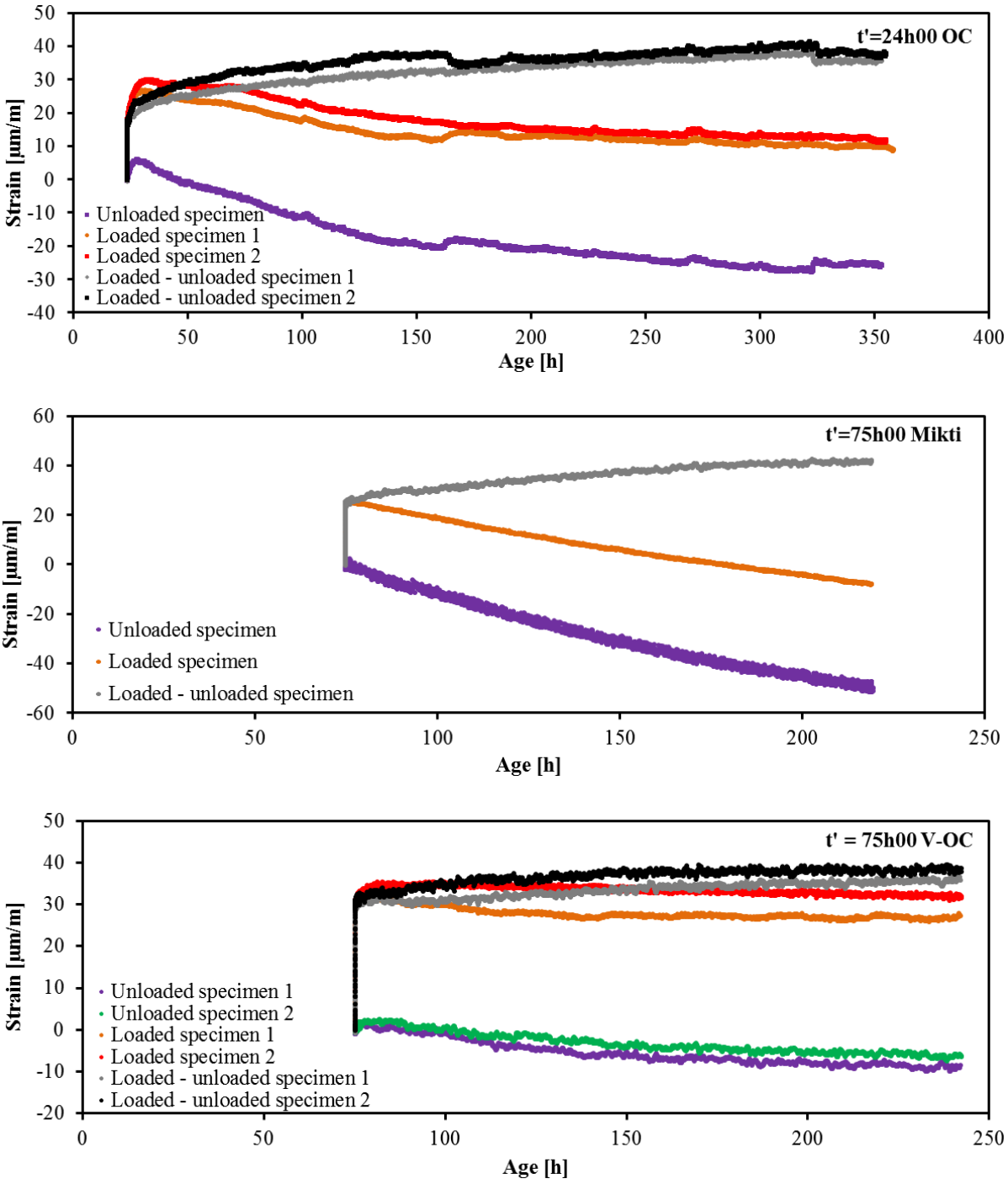

Figure 9 – Evolution of the strain of the loaded, unloaded specimen and the subtraction between both specimens for one age of loading of the ordinary, Mikti and Vercors concretes.

COMPARISON BETWEEN TENSILE AND COMPRESSIVE CREEP

The results of the specific tensile creep function are presented in Figure 10 for each age at loading (20 – 24 – 40 and 72 hours) of the ordinary concrete. Same results are displayed in Figure 11 according to the age after loading. The effect of the age at loading is strongly marked in the evolution of the tensile specific creep. Due to the very low amplitude of the tensile creep strain, the noise measurement is relatively high. From results obtained on the loading applied at an age of 40 hours, it is observed that the beginning of the evolution of the tensile creep function is quite low in comparison with the other tensile creep function. This change of trend can come from a difference in the initial temperature between the loaded and dummy specimen. Indeed, if both samples have a difference of temperature of 0.5 °C at the start of the test and if the coefficient of thermal expansion of the concrete is equal to 12 µm/m/°C, that leads to an error of 6 µm/m in the determination of the tensile creep strain during the beginning of the evolution of the tensile creep strain. However, special attention was taken during the different test in order to minimize this difference. Samples were prepared 1 or 2 hours in advance in order to assure a quasi-equivalent temperature in both samples at the start of the test. However, for very early age testing, such parameters are technically very complex to control. Due to this technical complexity for the determination of the tensile creep strain, only the general trend observed will be discussed.

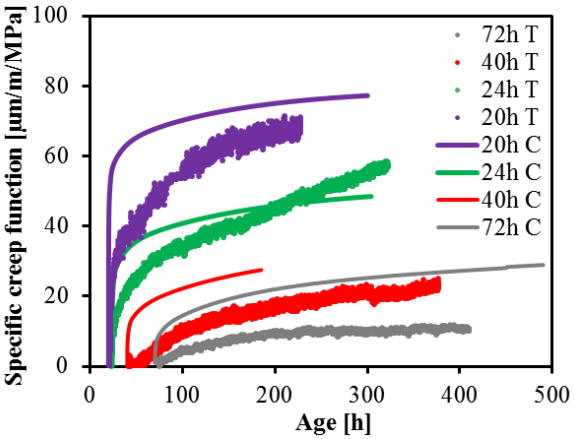

Figure 10 – Specific tensile and compressive creep function according to the age of the material

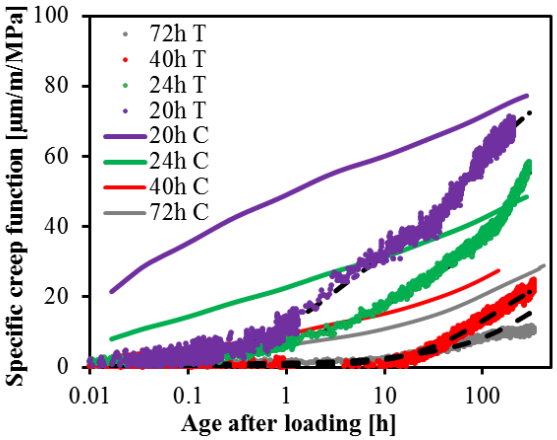

Figure 11 - Specific tensile and compressive creep function according to the age after loading. Dash lines correspond to the fitting of the tensile specific creep function with 6 Kelvin-Voigt chains in series.

In comparison, results from compressive creep tests are also presented in Figure 10 and Figure 11. Two main differences are observed in the evolution of the specific creep function. During the first hours after loading, the specific creep function is lower in tension than in compression whatever the age at loading. Afterwards, the trend changes. The rate evolution of the specific creep is higher in tension than in compression for age at loading of 20 – 24 and 40 hours. From results of the literature, same observations can be carried out with results obtained by Atrushi [6] on high performance concrete and by Ji, *et al.* [7] on concrete with substitution of cement by silica fume, fly ash and slag. A comparison between tensile and compressive creep were performed in [8]. The ratio between basic compressive creep strains and tensile ones according to several authors are plotted in Figure 12 and a very large dispersion can be observed. However, it is generally observed that this ratio decreases according to the age after loading of the material. Therefore the differences of behaviour in tension and in compression of concrete are associated to two periods. The first period occurs on small duration of loading and seems to correspond to the short term creep. The second period occurs on longer duration and seems to be associated to the long term creep. Thus, it could be assumed that the mechanisms related to the short and long term creep depend on the nature (tension or compression) and/or the amplitude of the loading.

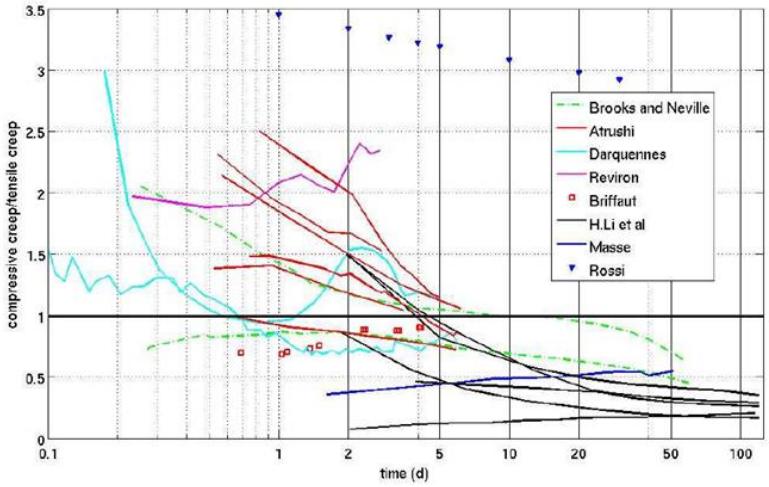

Figure 12 - Ratio of compressive creep to tensile creep [8]

To analyze the difference of behaviour between tensile and compressive specific creep, all tensile specific creep curves were fitted with least and square method by means of 6 Kelvin-Voigt chains in series [9]. Results of the modelling are shown in Figure 11. A very good correspondence is obtained between the fitting and experimental results for ages at loading of 20 – 24 and 40 hours. For results obtained at an age of 72 hours, the evolution of the tensile specific creep function does not follow the global trend of other results after an age after loading of 100 hours. It was then decided to consider only results before an age after loading of 100 hours for the fitting. In Figure 13, tensile specific creep is plotted according to the compressive specific creep. As discussed just before, the difference of behaviour in tension and in compression occurs during two periods. For short duration of loading (few hours), the specific creep is higher in compression especially at very early age. Then, for longer duration of loading, the tensile specific creep develops faster. Results obtained for an age at loading of 72 hours does not follow very well the global trend for long duration of loading. However, for such age at loading, the amplitude of the tensile specific creep is very low. The pertinence of this evolution compared to the other one is therefore questionable. In Figure 14, the same comparison is performed for the Mikti and Vercors concrete at an age of 75 hours and for the ordinary concrete at an age of 72 hours. A similar evolution is observed for the Vercors and ordinary concrete. This is quite coherent because both concrete have a similar composition with an effective water-cement ratio of 0.45 (OC) and 0.52 (V-OC) (see Chapter 3). For the Mikti composition, the difference of behaviour in tension and compression is less marked. While lower evolution of the tensile creep is well observed during the first hours of loading and a higher evolution is observed on longer duration.

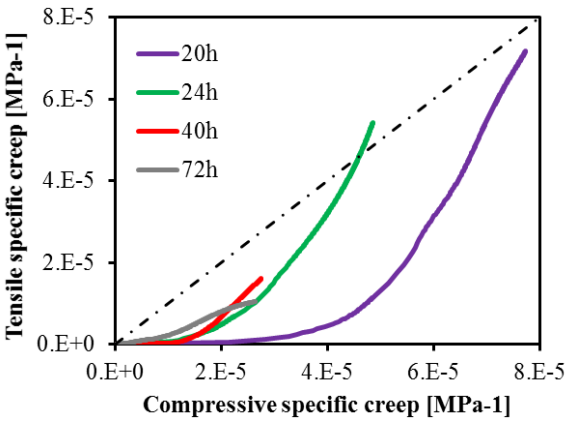

Figure 13 – Tensile versus compressive specific creep function for age at loading of 20 – 24 – 40 and 72 hours on the ordinary concrete.

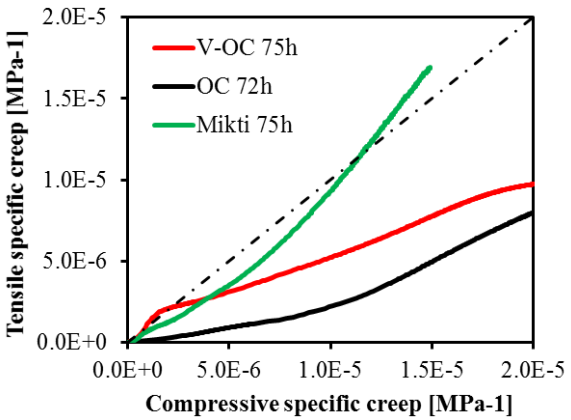

Figure 14 - Tensile versus compressive specific creep function on the ordinary concrete (72h00), the Mikti concrete (75h00) and the Vercors concrete (75h00).

SECTION 9.4 – MODELLING OF TENSILE CREEP

9.4.1. Three terms model

In order to understand the difference between tensile and compressive basic creep, the tensile specific creep is divided in three terms as presented in seventh section of the Chapter 4. The first term studied is the long term creep. The long term creep is defined with the evolution of the specific creep rate occurring after one day of loading or more. The specific creep rate is presented in Figure 15 for each age at loading of the ordinary concrete in tension and in compression. As expected from previous observations, long term creep is higher in tension than in compression. The difference is quite small. As in compression, for very early age loading, long term creep is the main part of the basic creep after only one day of loading. Whereas, when the loading is applied later, it was observed in compression that short term creep continues to be significant after duration of loading of one week. In tension, the duration of the short term creep is largely lower whether at very early age or after.

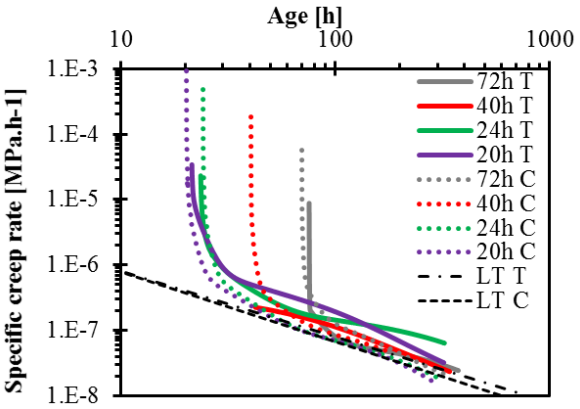

Figure 15 – Specific creep rate in tension and in compression according to the age of the ordinary concrete. Dashed lines correspond to the modelling of the long term creep in compression (LT C) and in tension (LT T).

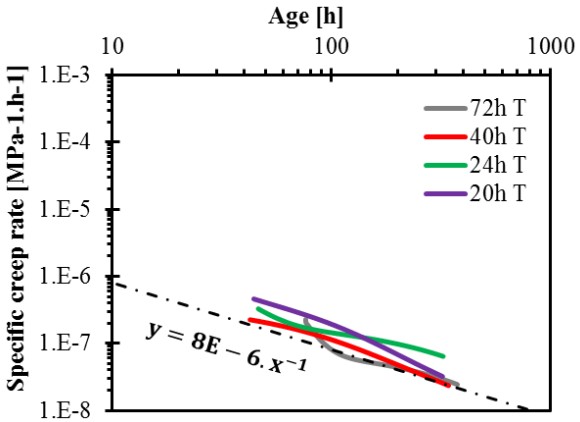

Figure 16 – Specific creep rate in tension corresponding to the long term creep. Dashed line corresponds to the modelling of the long term creep.

The second parameter studied is the initial short term creep which is linked to the state of the material when the load is applied and thus to the amplitude creep factor obtained with the repeated minute-long loadings. In Figure 17, the long term creep is removed from the tensile specific creep function. It is observed that for age at loading of 40 hours or more, long term creep represents the major part of the specific creep in tension. While for very early age loading, a significant evolution of the creep still occurs after the subtraction of the long term creep. After removing the long term creep, each curve is normalized by their own value obtained at an age after loading of 1 hour. A same logarithmic evolution is observed for concrete loaded at an age of loading of 20 and 24 hours. The parameters of the initial short term creep are the parameter q_3 and n which are respectively equal to 0.65 MPa^{-1} and 0.26. A very good correspondence is obtained between the logarithmic expression (dashed lines) and the experimental results. In contrast to results obtained in compression, the logarithmic expression is able to fit the initial short term creep on long duration for very early age loading. This means that the solidification term creep, defined in the case of compressive loading, does not exist in tension.

In Figure 18, the contribution of the very short term creep and the long term creep are summed and compared to the experimental results. A very good agreement for each age at loading is observed. It is then concluded that tensile creep can be modelled by splitting the basic creep phenomenon in two terms since very early age.

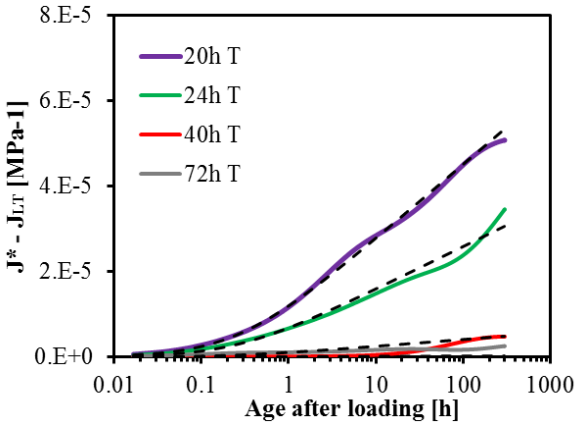

Figure 17 – Evolution of the tensile specific creep after subtraction of the long term creep.

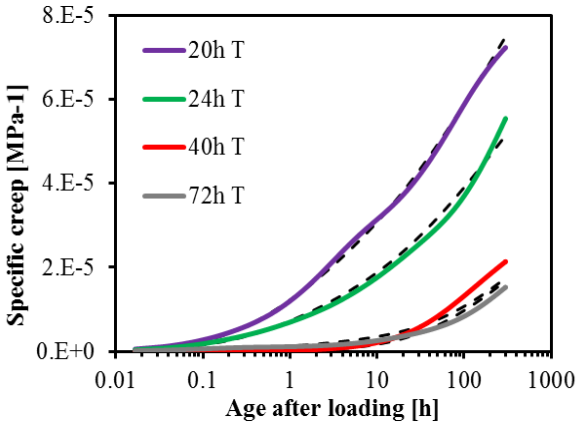

Figure 18 - Evolution of the specific creep and final modelling (dashed lines).

9.4.2. Adapted version of the Model Code 2010

Another way to model basic creep since very early was presented in the seventh section of the Chapter 4. This model is an adapted version of the Model Code 2010 (MC2010). As presented in [10,11], MC2010 can be simplified in Equation 5, where the parameter C is related to the general amplitude of the creep, is independent of the age at loading and is expressed in MPa. The parameter τ is only function of the age at loading and is expressed in [d].

$$C(t,t') = \frac{1}{C}.\ln\left(1+\frac{t-t'}{\tau}\right) \quad 5$$

Results of the modelling with the adapted MC2010 are presented in Figure 19 for the tensile specific creep of the ordinary concrete. A general very good correspondence is obtained between experimental results and the modelling whatever the age at loading. A value of C=80.3 GPa is found whereas a value of 217.8 GPa was found for compressive creep. The value of C is inversely proportional to the amplitude of the long term creep. Therefore, a lower value of C in tension means that the long term creep is higher in tension. This is in agreement with previous observations. The value of the parameter τ for the different age of loading is given in Table 2.

Table 2 - Value of parameter $\boldsymbol{\tau}$ from Equation 5

t′ (h)	20	24	40	72
τ (d)	2.49E-07	8.20E-07	3.90E-04	1.62E-02

The values of the parameter $\boldsymbol{\tau}$ are plotted according to the inverse of the derivative of the E-modulus in Figure 20. Results obtained for compressive creep and predictive values obtained with MC2010 are also presented. The values of $\boldsymbol{\tau}$ for tensile creep are strongly higher than in compression. The relation between the parameter $\boldsymbol{\tau}$ and the inverse of the derivative of the E-modulus follows two power expressions. Both power expression are given in Equations 6 and 7 where q=9E+10, p=-10, t_E=1d.GPa^{-1} and n=12.

$$\begin{cases} \tau = a.\left(\frac{dE}{\quad}.t_E\right)^p & if\ \frac{dE}{\quad} > 12.8\ GPa.d^{-1} \end{cases} \quad 6$$

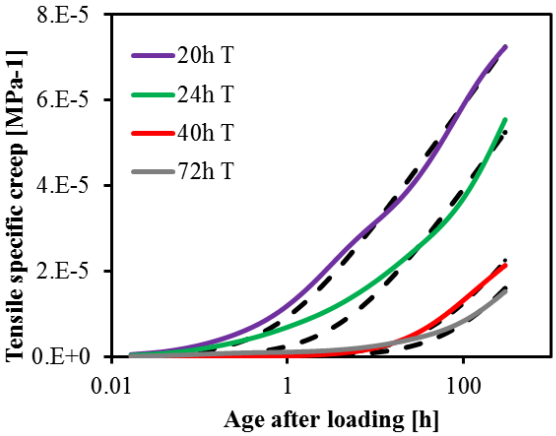

Figure 19 – Tensile specific creep and adapted MC2010 (dashed lines) of the ordinary concrete

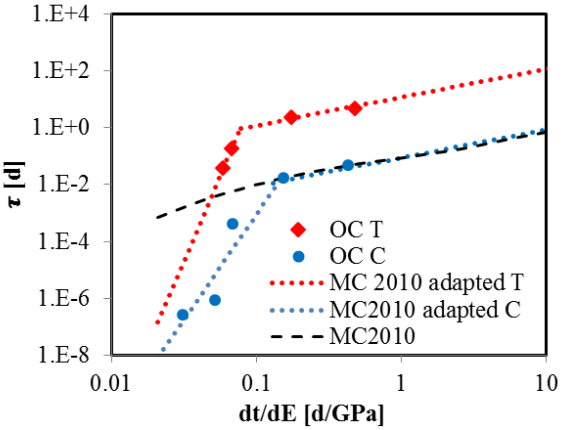

Figure 20 - Relation between the parameter τ of the adapted MC2010 and the inverse of the E-modulus rate.

CONCLUSIONS

Repeated minute-long loading tests and single loading tests were applied in tension. It is observed that values of the repeated minute loading tests are lower than the value of the E-modulus obtained with single loading tests. A strong fatigue effect is observed when tensile loading are applied each hour since setting time. Tensile E-modulus obtained with single loading tests is compared to the results of a repeated minute-long loading tests for which load are applied at four stress levels (5 – 10 – 20 – 40%) in compression since very early age. It is highlighted that the stress level is a first step in the understanding of the difference of behaviour between E-modulus in tension and in compression. But there is still a difference observed which is not explained. It is also observed that the ratio between the tensile and compressive E-modulus decreases along the hydration process. At very early age, the E-modulus is 20% higher in tension while at an age of 72 hours the tensile E-modulus is 10% higher than the one in compression.

From repeated minute-long loading tests applied at four stress levels (5 – 10 – 20 – 40%) in compression, it is observed that the amplitude creep factor increases when the stress level increases especially at very early age.

Tensile and compressive creep tests are performed on an ordinary concrete at several ages at loading (20 – 24 – 40 – 72 hours) with duration of loading of one week or more and a stress/strength ratio of 40%. Differences have been observed between tensile and compressive creep. For short duration of loading, the amplitude of the compressive creep is higher whereas for long duration of loading, tensile creep develops faster. These observations are in agreement with several results from the literature.

Tensile creep is modelled by using the three terms model developed in Chapter 4. It is observed that the long term creep follows a logarithmic expression for which the amplitude is higher than in compression. A logarithmic expression is also used to model the evolution of the initial short term creep. No solidification phenomenon was observed in the evolution of the tensile creep. Therefore tensile creep is modelled with two terms: the long term creep and the initial short term creep.

An adapted version of the Model Code 2010 (MC2010) is also used to model tensile creep. It is possible to model accurately the tensile specific creep especially for hardening and hardened concrete for duration of loading till two weeks. In comparison with results obtained in compression, the amplitude parameter C is lower in tension and the value of the kinetic parameter τ is higher in tension.

REFERENCES

[1] J. Carette, S. Staquet, Monitoring the setting process of eco-binders by ultrasonic P-wave and S-wave transmission velocity measurement: Mortar vs concrete, Constr. Build. Mater. 110 (2016) 32–41. doi:10.1016/j.conbuildmat.2016.02.019.

[2] J. Carette, S. Staquet, Monitoring the setting process of mortars by ultrasonic P and S-wave transmission velocity measurement, Constr. Build. Mater. 94 (2015) 196–208. doi:10.1016/j.conbuildmat.2015.06.054.

[3] B. Delsaute, J.-M. Torrenti, S. Staquet, Monitoring and modeling of the early age properties of the Vercors Concrete, in: TINCE 2016, Paris, 2016: p. 12.

[4] P. Rossi, J.-L. Tailhan, F. Le Maou, Comparison of concrete creep in tension and in compression: Influence of concrete age at loading and drying conditions, Cem. Concr. Res. 51 (2013) 78–84. doi:10.1016/j.cemconres.2013.04.001.

[5] R. Cortas, Nouvelle approche expérimentale pour la maitrise de la fissuration du béton jeune : influence de la nature et de la saturation des granulats, PhD thesis, Ecole centrale de Nantes and Université Libre de Bruxelles, 2012.

[6] D.S. Atrushi, Tensile and Compressive Creep of Early Age Concrete : Testing and Modelling, PhD thesis, The Norwegian University of Sciences and Technology, Trondheim,Norway, 2003.

[7] G.M. Ji, T. Kanstad, Ø. Bjøntegaard, E.J. Sellevold, Tensile and compressive creep deformations of hardening concrete containing mineral additives, Mater. Struct. 46 (2012) 1167–1182. doi:10.1617/s11527-012-9962-7.

[8] F. Benboudjema, M. Briffaut, A. Hilaire, J.M. Torrenti, G. Nahas, Early Age Behavior of Massive Concrete Structures: From Experiments To Numerical Simulations, in: CONCRACK 3-RILEM-JCI Int. Work. Crack Control Mass Concr. Relat. Issues Concern. Early-Age Concr. Struct., 2012: pp. 1–12.

[9] Z.P. Bažant, A. Asghari, Computation of Kelvin chain retardation spectra of aging concrete, Cem. Concr. Res. 4 (1974) 797–806.

[10] R. Le Roy, F. Le Maou, J.M. Torrenti, Long term basic creep behavior of high performance concrete: data and modelling, Mater. Struct. 50 (2017) 11. doi:10.1617/s11527-016-0948-8.

[11] J.M. Torrenti, R. Le Roy, Analysis and Modelling of Basic Creep, in: S. Dray (Ed.), CONCREEP 10, American Society of Civil Engineers, Reston, VA, 2015: pp. 1400–1409. doi:10.1061/9780784479346.165.

CHAPTER 10: GENERAL CONCLUSIONS AND SUGGESTIONS FOR FURTHER WORKS

SUMMARY AND CONCLUSIONS

The study of the development of the properties of cement based materials since setting time was performed in two main phases:

1. The development of a new testing and modelling approach for the characterization of the autogenous strain, the coefficient of thermal expansion, the E-modulus and the creep properties since setting time on an ordinary concrete.
2. The extension of this new approach to the study of relevant parameters which are the water-cement ratio, the restrained effect of aggregate on the cement paste in the development of concrete properties at early age, the substitution of cement by mineral addition and the difference of behaviour in tension and in compression.

Development of a new testing and modelling approach

A new test protocol is defined for the monitoring of the autogenous strain and the coefficient of thermal expansion. Every 130 minutes, thermal variations of 3°C are applied on a concrete sample with the device so-called BTJADE. Thermal and autogenous strains are distinguished by creating a fictive thermal cure at 20°C from the experimental results. A similar strategy is developed for the monitoring of the autogenous deformation and the coefficient of thermal expansion for cement paste and mortar by using the Autoshrink device.

Two new testing devices were developed for the monitoring of the viscoelastic properties of cement based materials since setting time. A revisited TSTM system has been developed. The direct measurement of the creep deformation and the relaxation stresses is possible with the simultaneous use of the TSTM mould and the dummy mould. Several adaptations were performed in order to assess the early age properties of cement based materials since setting time. Two electromechanical testing devices are used for the study of the viscoelastic properties of early age and hardened concrete. The longitudinal and lateral displacement is assessed with extensometers in Invar with elastic anchorages.

Compressive creep tests were performed at different ages of loading (15 – 20 – 24 – 40 – 72 hours) with duration of loading of one week and a stress level of 40%. It is observed that the short term of basic creep can be divided in two terms. The first term occurs just after the loading and has duration of few hours whereas the second term occurs on longer duration of loading. A comparison between the experimental observations and the evolution of the microstructure was done. The short term creep is divided in two mechanisms. The first mechanism is associated to the state of the material (capillarity pores, CSH…) when the load is applied and this mechanism is strongly correlated to the largest diameter pores for which the volume fraction decreases sharply during the very early age. The second mechanism is associated to the solidification of the cement paste during loading which is linked to the evolution of the CSH and ipso facto to the decrease of the capillarity pores. From this observation, a new test protocol was defined and is based on permanent loading tests and one repeated minute-long loadings test. Repeated minute-long loadings are applied every 30 minutes for duration of 5 minutes. For that purpose, a TSTM and a device called BTJASPE were used. With the TSTM, the load is applied in 10 seconds and corresponds to 20% of the strength of the material when the load is applied. With BTJASPE, the load is applied in 50 seconds and corresponds to a strain of 250 µm/m.

It is showed that the autogenous deformation, the Young's modulus and the amplitude of the first term of the short term creep can be determined since setting in only one test. An excellent agreement between the experimental data has been obtained with the BTJASPE and the TSTM device, what demonstrates the reliability of the results and the protocols of loadings with both devices. Results on the E-modulus were also compared to classical extensometry testing, to dynamic response of a system to ambient vibration (EMM-ARM) and to ultrasonic testing methods (FreshCon, BTPULSE and embedded piezoelectric transducers). Results from classical extensometry testing and EMM-ARM are in very good agreement with results obtained with BTJASPE and TSTM whereas values of E-modulus from ultrasonic testing methods are higher. This difference decreases as the concrete hardens. To understand this difference, tests on the effect of the loading stress rate and amplitude were performed. However, results cannot explain the difference obtained between static and dynamic E-modulus.

Two methodologies were used for the modelling of creep. The first model considers that creep is divided in three terms:

- The long term creep is defined with one creep test for which the load is applied at early age during one week or more. After one day or more, the creep compliance rate follows a power law which corresponds to the long term creep.
- The initial short term creep is obtained after having removed the long term creep and corresponds to a logarithmic law. The kinetic is constant and the amplitude depends on the amplitude parameter defined with the minute-long duration loadings test. This term fits well the results obtained during the first hours of loading or more. This term is function of the actual state of the material (capillarity porosity, CSH) when the load is applied. The function is linked to the amplitude term of the minute-long duration loadings test which is strongly correlated to the evolution of the largest diameter pores.
- The solidification creep is obtained after having removed the long term and the initial short term creep. The kinetic is constant and the amplitude depends on the derivative of the elastic modulus at the age of loading.

The Model Code 2010 is used and compared to experimental results. For ages at loading of 40 and 72 hours, the predicted values of MC2010 are quite close to the experimental results. However, for earlier loadings, a significant difference is observed. An adapted version of the Model Code 2010 is proposed. In this version, the effect of the age at loading is considered by using the inverse of the derivative of the elastic modulus.

Ultrasonic testing method was compared to the Vicat test for the determination of the initial and final setting time of cement paste. From results of the literature and results obtained during this thesis, it appears that criteria using threshold values or the maximum of the derivative of a dynamic parameter cannot be used directly on cement paste. The consideration of the air content is needed.

Extension to other parameters

► Autogenous strain and coefficient of thermal expansion (CTE)

The autogenous deformation and the coefficient of thermal expansion are defined for several water-cement ratios and an eco-composition on cement paste, mortar and concrete. New models are proposed for their characterization since setting according to the equivalent time and the advancement degree of reaction for computational purpose. Physical mechanisms are highlighted and considered in the modelling. From the experimental results, a difference of the influence of the water-cement ratio

has been observed on the evolution of the CTE according to the scale of the material. For concrete, the final amplitude of the CTE is higher for low water-cement ratio while for cement paste, the inverse trend is observed. Properties of the cement paste and inclusions (E-modulus, Poisson's ratio, CTE) are important to consider when upscaling the CTE. The Hobb's model and the Rosen-Hashin bounds consider these properties. This methodology allows predicting very accurately the CTE of mortar but not the one of concrete.

It is observed that the autogenous strain and the CTE are linked in terms of mechanisms. When the swelling of the cement paste occurs, a decrease of the CTE is observed. The influence of the water-cement ratio on the amplitude of the variation of the CTE depends on the scale of the material and also on the nature of the binder. On the contrary, the autogenous strain associated to the self-desiccation of the material are linearly linked to the increase of the CTE till a threshold value of the advancement degree of reaction. After this threshold, self-desiccation phenomenon goes on to develop while the CTE stays constant.

Through comparison between the experimental results and the setting time obtained with ultrasonic measurement and penetration resistance test, it is observed that:

- the initial setting time is associated to the moment when the value of the CTE does not correspond anymore to a liquid.
- the final setting time is associated to a minimum of the autogenous strain obtained before the swelling of the concrete. This value corresponds to a zero value of the derivative of the autogenous strain.

► <u>E-modulus and basic creep</u>

Repeated minute-long loading tests were applied on compositions with several water-cement ratios, on different scales of the material (cement paste, mortar and concrete), on compositions with substitution of 75% of cement by slag and/or limestone filler and on Ultra-High Performance Self-Compacting Concrete (UHPSCC). The Poisson's ratio, the E-modulus and an amplitude creep factor corresponding to the creep coefficient obtained after 5 minutes of loading are defined. For all the investigated properties, new or existing models are used. Models are expressed in function of the equivalent time and the advancement degree of reaction for computational modelling purpose. It is generally observed that:

- For effective water-cement ratios between 0.25 and 0.55, linear trends exist between the effective water-cement ratio and the material parameters of several models.
- For composition with high content of superplasticizer, it is necessary to consider the final setting time when using models based on the equivalent time.
- The E-modulus in tension is higher than the one in compression. The stress level is a first step in the understanding of the difference of behaviour between E-modulus in tension and in compression. But there is still a difference observed which is not explained. It is also observed that the ratio between the tensile and compressive E-modulus decreases along the hydration process.
- For concrete compositions using slag, two stages appear in the evolution of the E-modulus and the amplitude creep factor. The separation between these both stages is related to the hydration of the slag. After the peak of hydration of the slag, the viscoelastic behaviour is very similar to an ordinary concrete with equivalent water-binder ratio.

By using homogenization model, it is observed that:

- The model of Bache and Nepper-Christensen, the trisphere model and the Illston model are able to accurately predict the evolution of the E-modulus of concrete since very early age by using cement paste data.
- The presence of sand restrained strongly the development of the cement paste during the very early age whereas the aggregate has a similar restraining effect on the creep strain whatever the age of the material especially for high water-cement ratio.

For the study of the long term creep, long duration creep tests were performed at four ages of loading on compositions with substitution of 75% of cement by slag and/or limestone filler and on Ultra-High Performance Self-Compacting. For the study of the water-cement ratio (range 0.28-0.42), data coming from Robert Le Roy works were used. The modelling of these results were performed with the three terms model and the adapted version of the Model Code 2010. From the modelling carried out with the three terms model, it is observed that:

- The initial short term creep
    - is not influenced by the water-cement ratio,
    - changes of kinetic when slag reacts,
    - is linearly correlated to the value of the amplitude creep factor obtained from repeated minute-long loading test. This linear relation depends on the nature of the binder.
    - Is lower in tension.
- The solidification term creep
    - is not influenced by the water-cement ratio,
    - has a same kinetic whatever the nature of the binder,
    - has an amplitude linearly dependent on the derivative of the E-modulus for each composition. This linear relation is very similar for each composition except the one with limestone filler.
    - Does not exist in tension.
- The long term creep
    - is higher for composition with high water-cement ratio,
    - is significantly influenced by the nature of the binder during very early age. For composition with slag and limestone filler, the long term creep is strongly higher till the time when slag has not reacted.
    - Is higher in tension

The adapted version of the Model Code 2010 is able to model accurately the specific creep especially for hardened concrete. For very early age, creep is overestimated during few days after loading for few classical compositions. For concrete with high quantity of cement substituted by slag, the Model Code 2010 is not able to accurately fit the results till slag has not reacted. For classical composition, tensile basic creep can be modeled by increasing the amplitude parameter C and the kinetic parameter τ.

PERSPECTIVES

The new approach developed in this work has opened the way for various experimental and numerical works and has the advantage to define several parameters with a very limited number of tests. Several parameters could be studied with this methodology such as the substitution of aggregate by recycled aggregate, the total substitution of cement by geopolymer or also the incorporation of new raw materials arriving on the market.

For further study, the evolution of the relative humidity should be measured during the test and considered in the modelling. This will improve the understanding of the mechanisms occurring during the hydration process.

Several creep tests were performed in tension but are limited. The whole database created in compression should be extended to the tensile case.

All tests carried out in the thesis were performed at a constant temperature of 20°C. More sophisticated tests with different histories of temperatures are still needed for computational purposes.

With all the data defined during this work, it will be interesting to perform restrained shrinkage tests with the TSTM device. This test allows comparing the stresses computed with the viscoelastic properties of the concrete and the one from the restrained shrinkage test.

The conclusions are limited to medium stress levels (40 %). A next step of this research is the study of higher stress levels and the coupling between damage and creep at early age. For such study a correct identification of damage is necessary. Acoustic emission and ultrasonic methods can be used to quantify and localize damage. However, for very early age concrete two problems occur. First, during the hydration process, the development of microcracking occurs on unloaded concrete. It is therefore necessary to correctly separate damage associated to the loading applied and damage related to the restriction of the displacement of the cement paste by the aggregate in free condition. Secondly, the energy released on microcrack initiation and the kinetic energy due to microcrack propagation are low. It could be then difficult to assess correctly damage for very early age concrete with acoustic emission.

Direct homogenization methods were used to understand the effect of aggregate on the development of the concrete properties. 3D modelling with the consideration of the properties of the cement paste and aggregate could also help to interpret the restriction of the cement paste due to aggregate.

From a numerical point of view, the specific effect of the age at loading on elastic and creep properties is not well considered in numerical models especially at very early age. Including the developed models in existing finite element software could contribute to the improvement of the prediction of the effect of creep and relaxation on the material and structural properties of a given concrete.

ANNEXE

ANNEXE I – HOMOGENIZATION OF THE E-MODULUS THROUGH SEVERAL EXISTING MODELS

1. Voigt's model

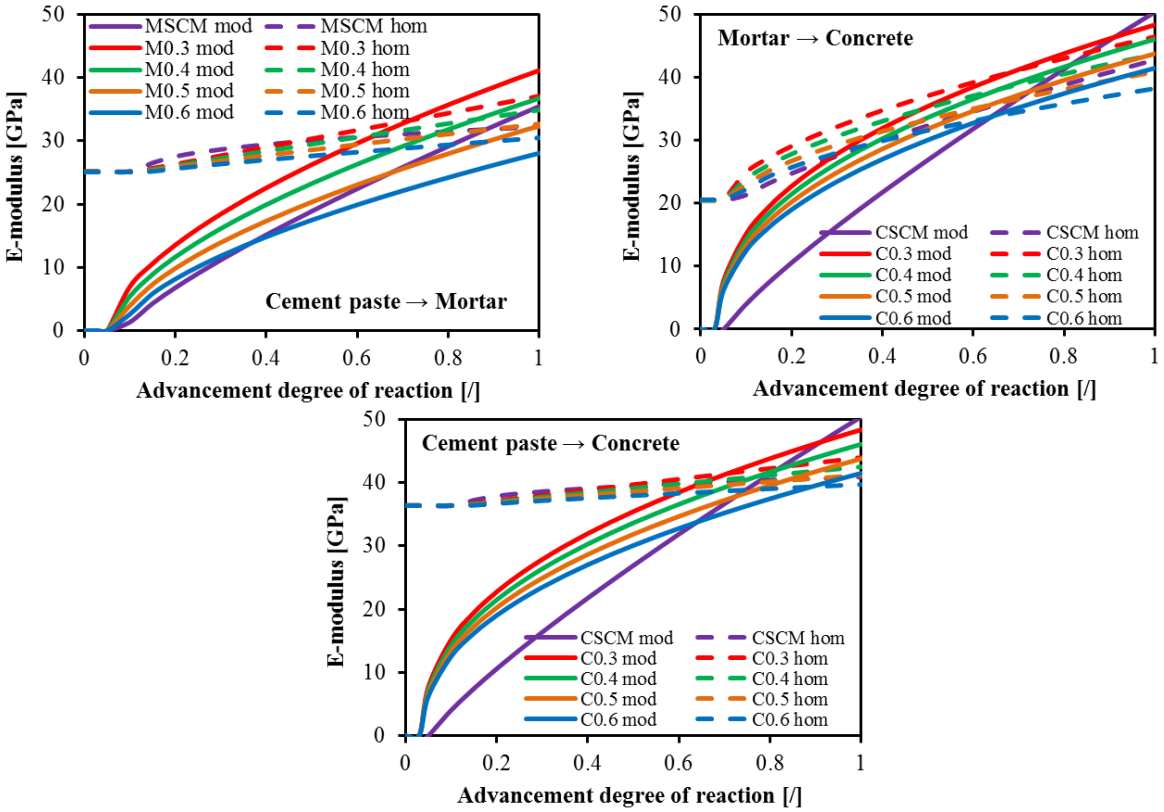

Figure 1 – E-modulus predicted according to Voigt's model

2. Reuss's model

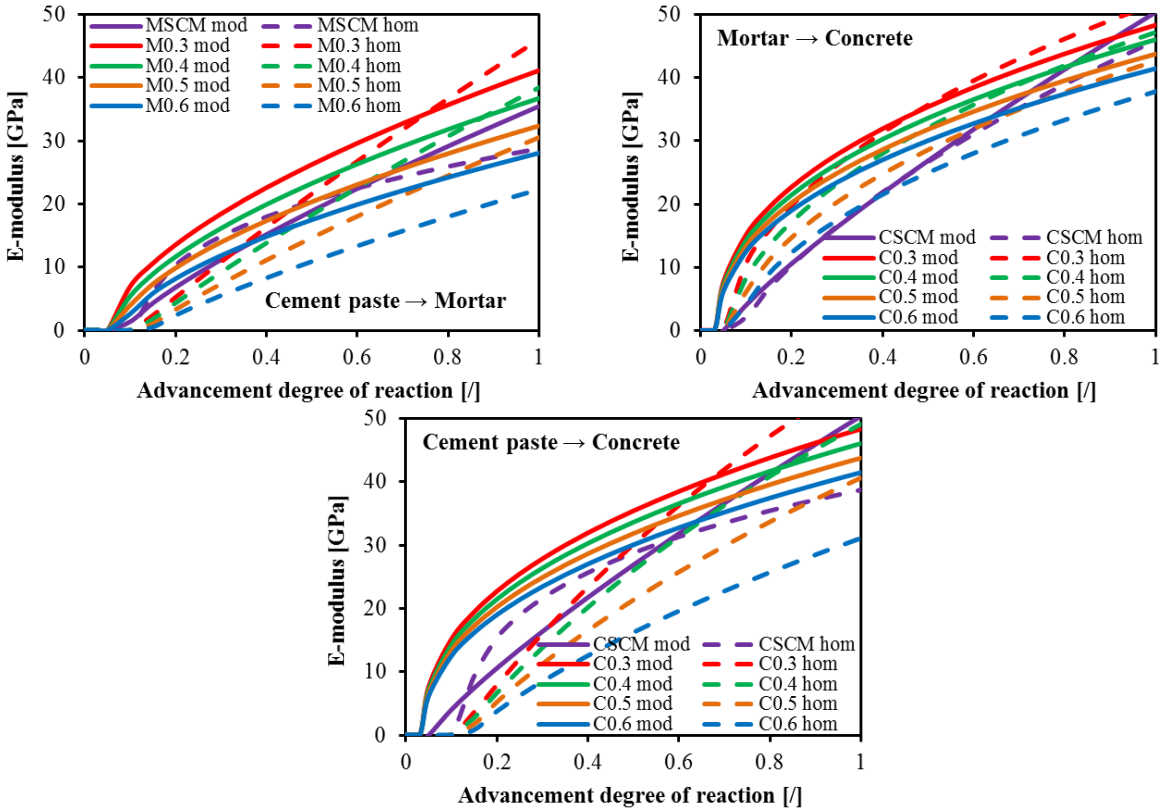

Figure 2 - E-modulus predicted according to Reuss's model

3. Hirsch-Dougill's model

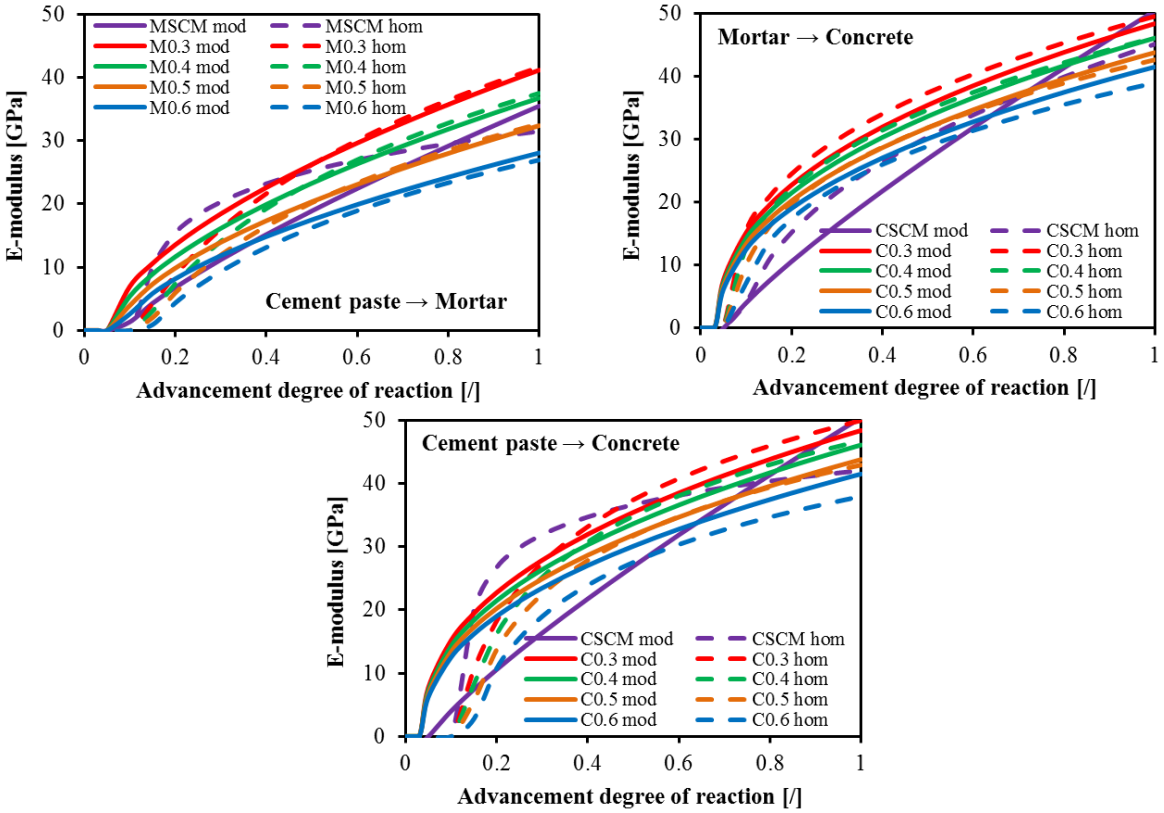

Figure 3 - E-modulus predicted according to Hirsch-Dougill's model

4. Popovics's model

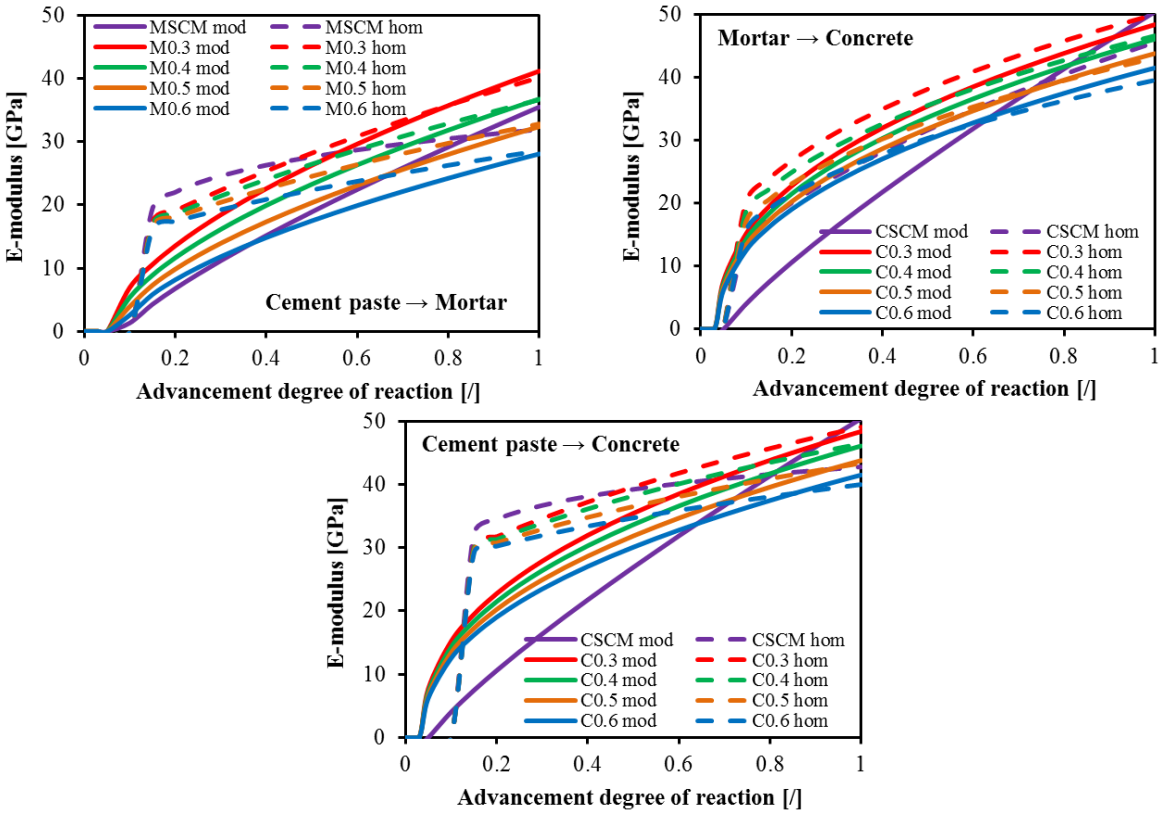

Figure 4 - E-modulus predicted according to Popovics's model

5. Counto's model

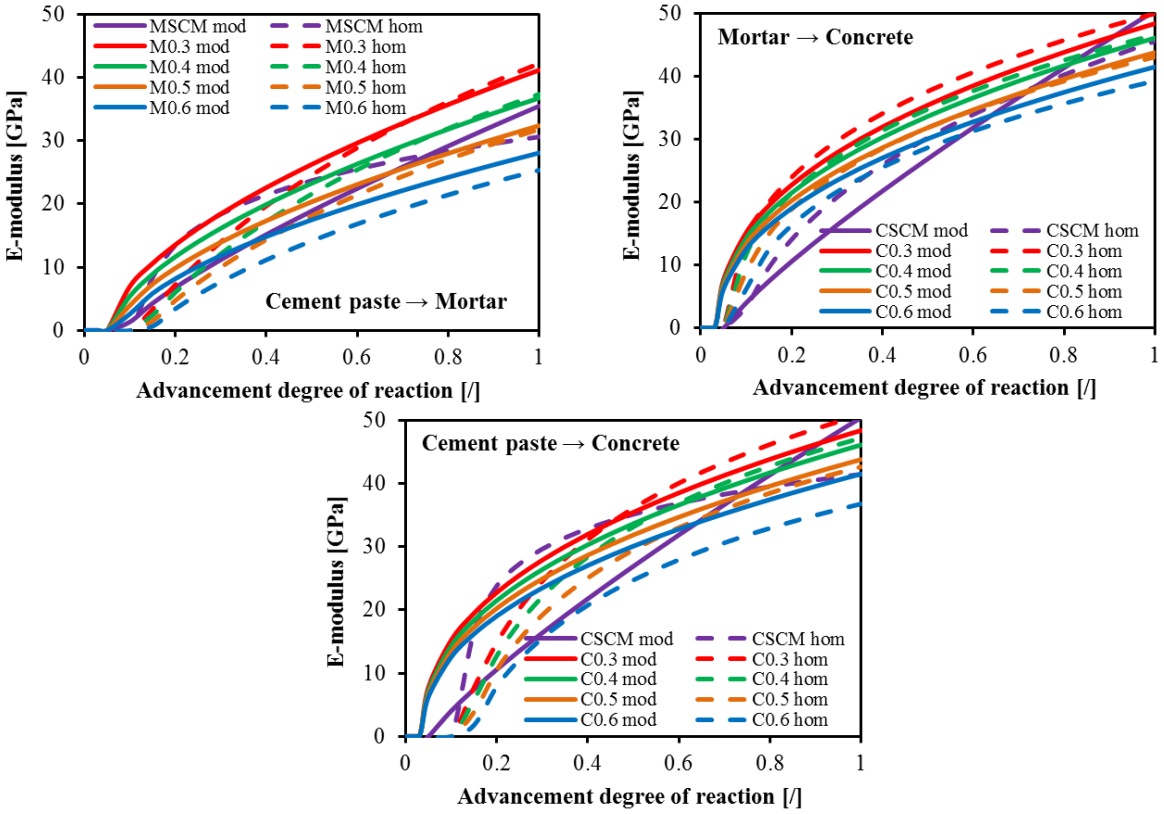

Figure 5 - E-modulus predicted according to Counto's model

6. Hashin's model

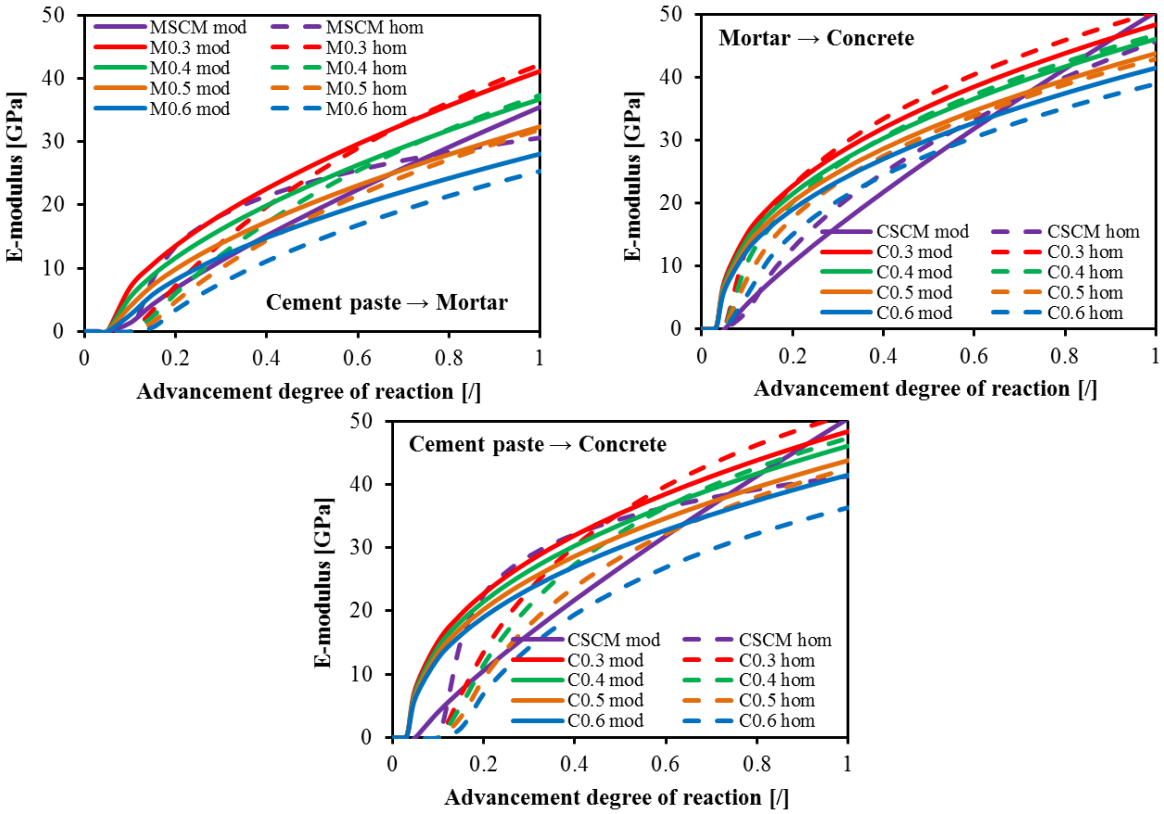

Figure 6 - E-modulus predicted according to Hashin's model

7. Bache and Nepper-Christensen model

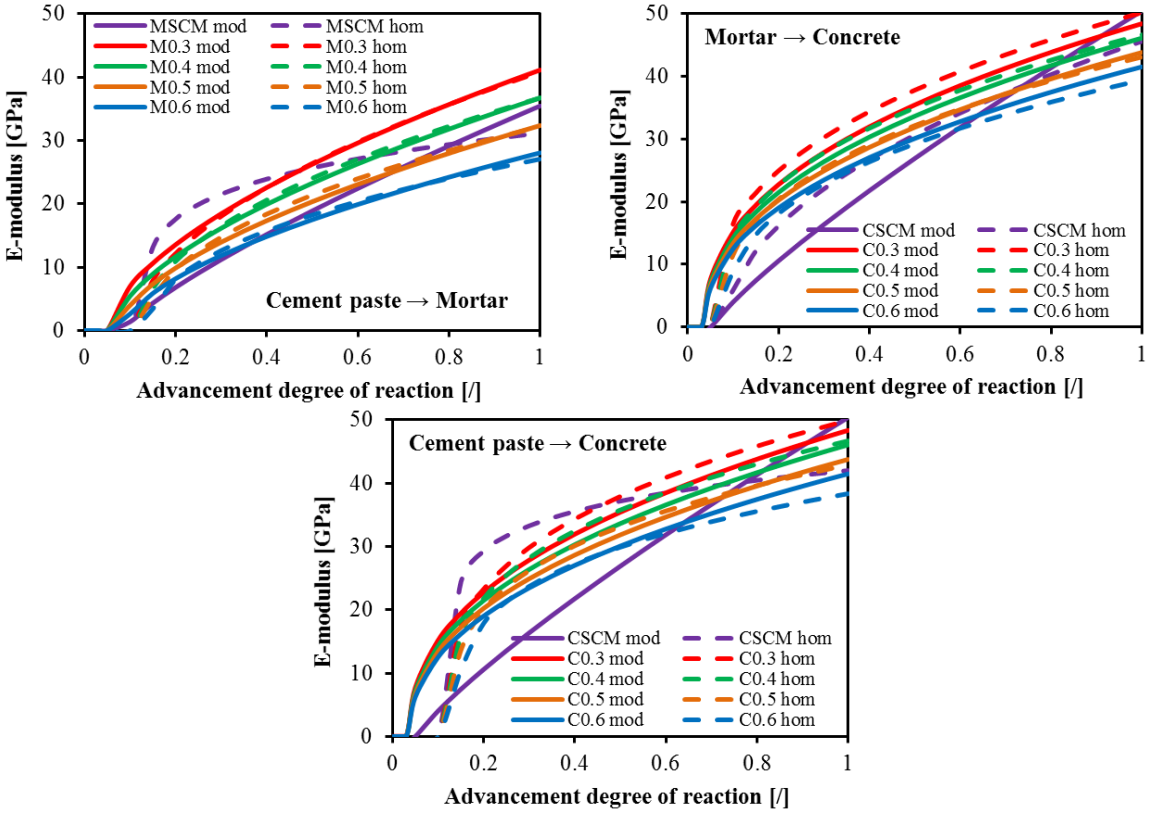

Figure 7 - E-modulus predicted according to Bache and Nepper-Christensen model

8. Mehmed-Kern model

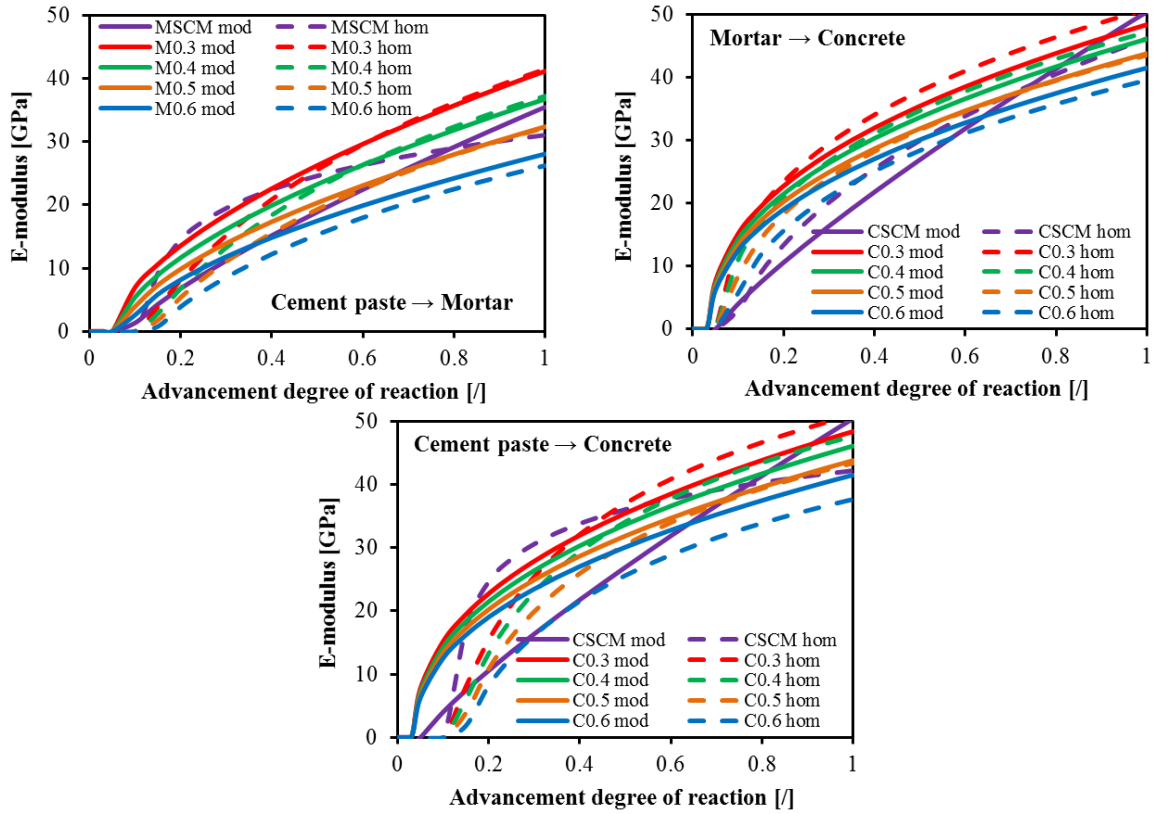

Figure 8 - E-modulus predicted according to Mehmed-Kern's model

9. Illston model

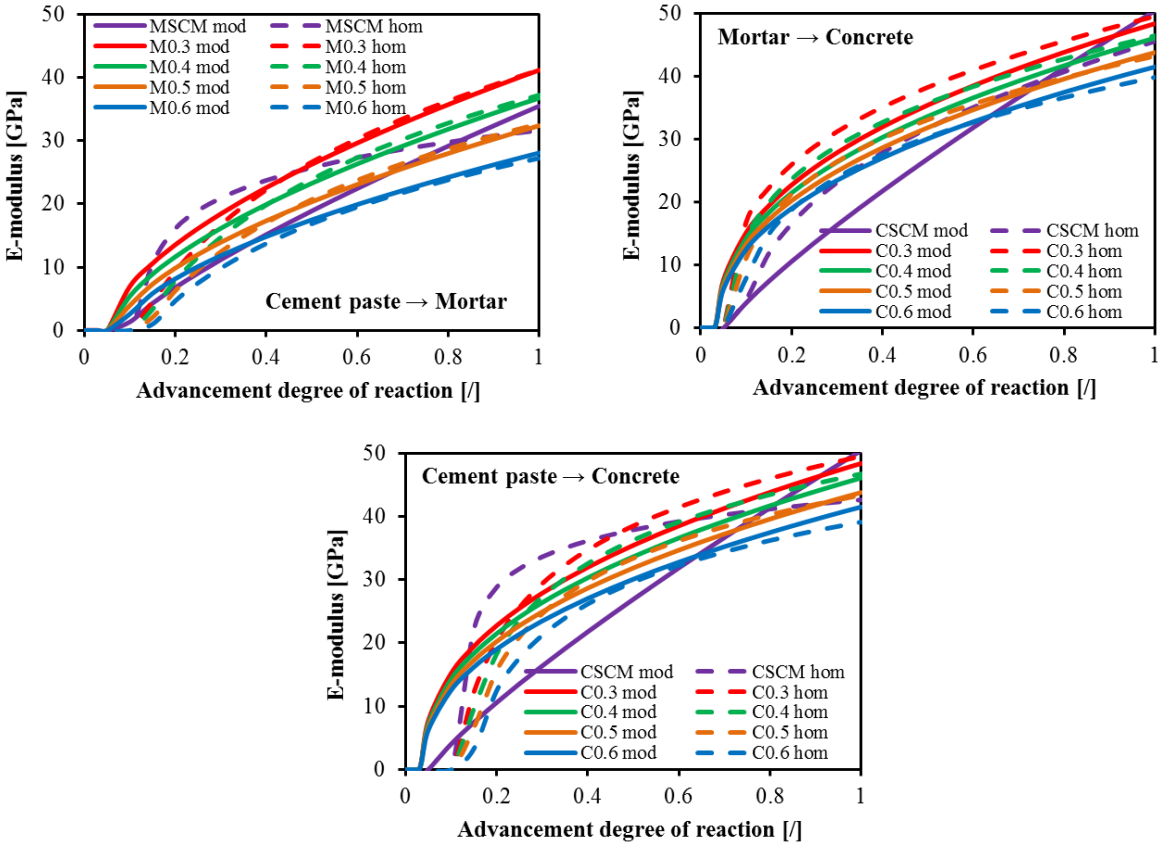

Figure 9 - E-modulus predicted according to Illston's model

10. Maxwell model

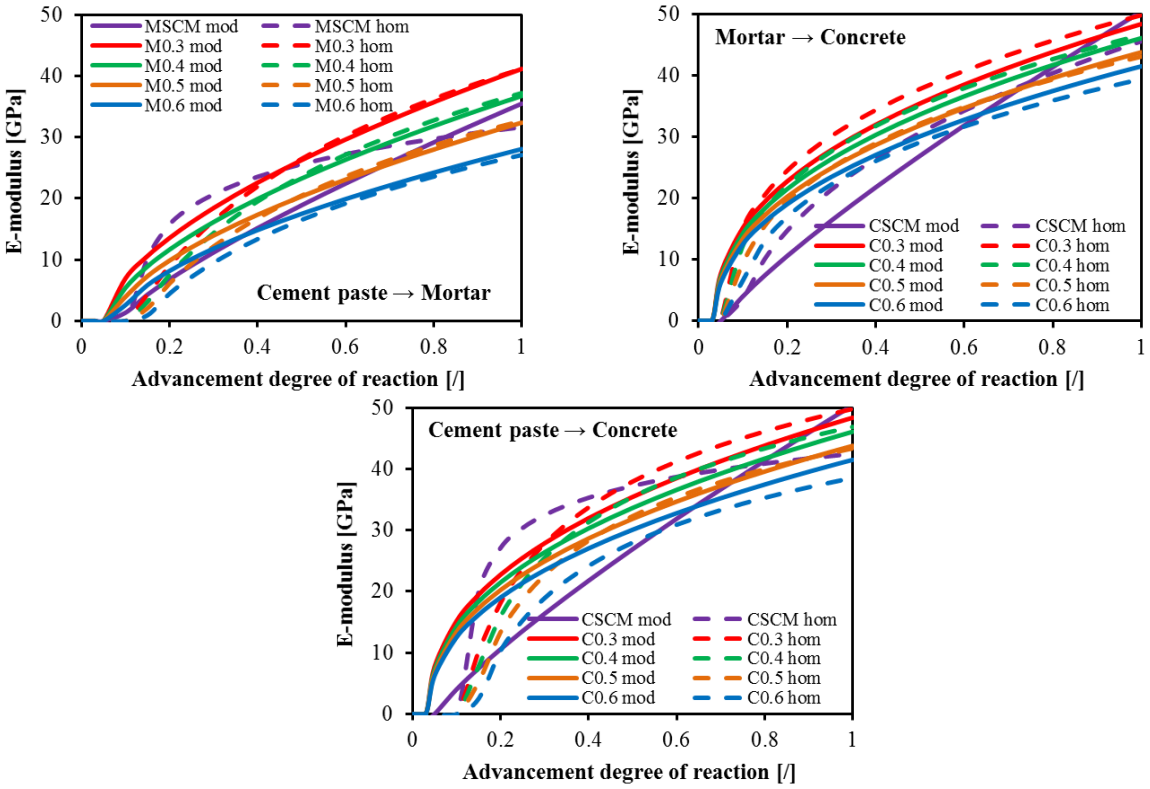

Figure 10 - E-modulus predicted according to Maxwell's model

11. Hobb's model

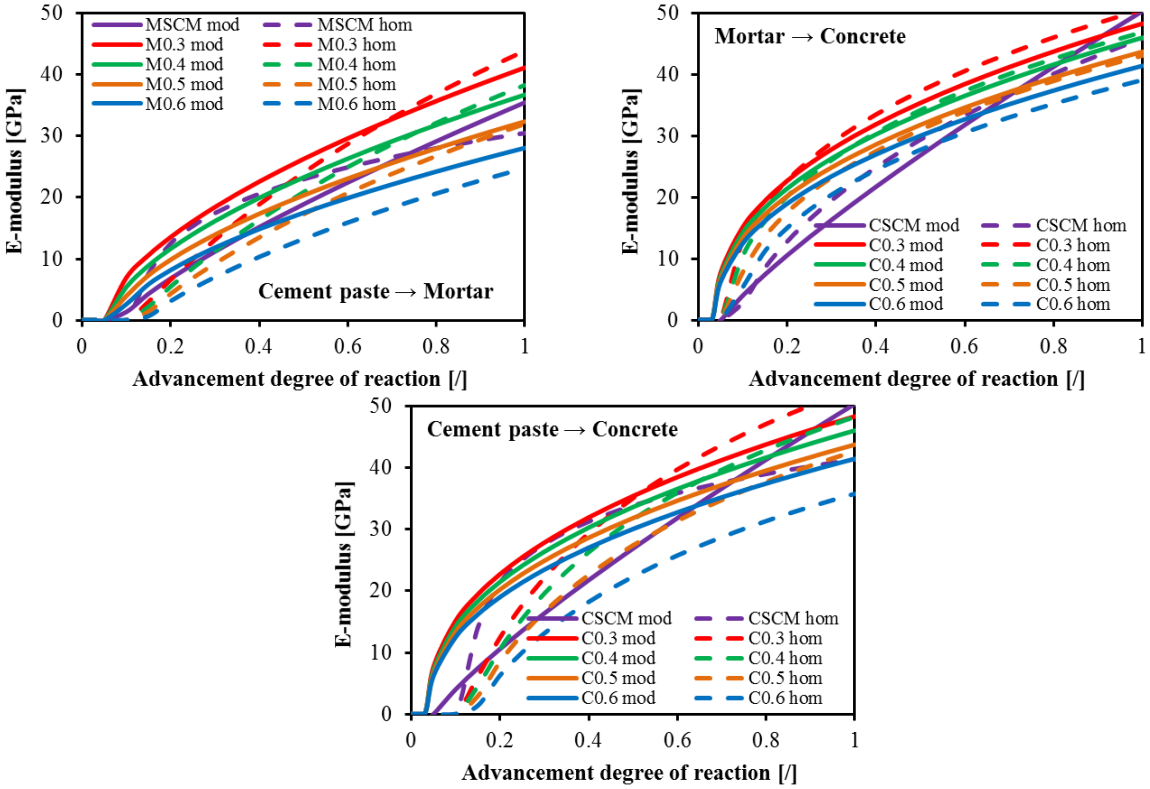

Figure 11 - E-modulus predicted according to Hobb's model